

A B C

Fig. 15-12 ■ Palatal expansion in adolescents requires a rigid framework because of the heavy forces (2 to 4 pounds with slow expansion, 10 to 20 pounds with rapid expansion) that will be encountered. **A,** Haas-type expander with metal framework and plastic shelves contacting the palatal mucosa; **B,** Hyrax expander with metal framework only; **C,** Minn-expander, which incorporates a spring to smooth the force application but still produces heavy force if activated rapidly; although the various expansion appliances look quite different, results with all are very similar. Although the various expansion appliances look quite different, results with all are similar. A bonded expander, retained by bonding to the enamel rather than using bands also can be used (see Fig. 15-13). With this method, the enamel is prepared for bonding only on the facial and lingual, but not the occlusal, surfaces; otherwise removing the appliance is too difficult.

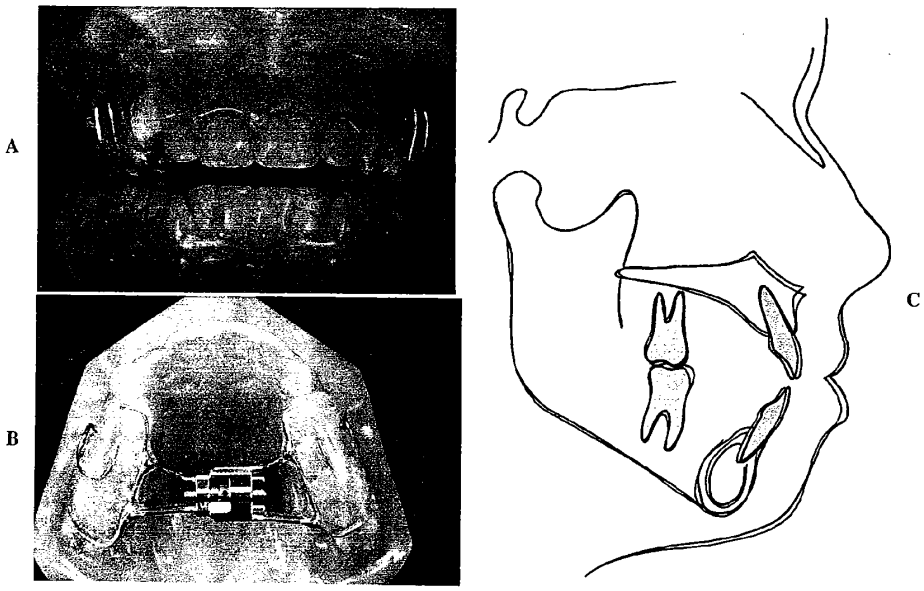


Fig. 15-13 ■ **A** and **B,** Palatal expander with bite blocks. With this design, intrusive pressure against the posterior teeth, created by the elastic rebound of the patient's stretched soft tissues, controls the tendency for bite opening and downward-backward rotation of the mandible that occurs with other designs of palatal expanders. **C,** Cephalometric superimposition before and after expansion, showing the very small mandibular rotation when expansion was done with a device of this type.

ClearCorrect Exhibit 1002, Page 1869 of 3373

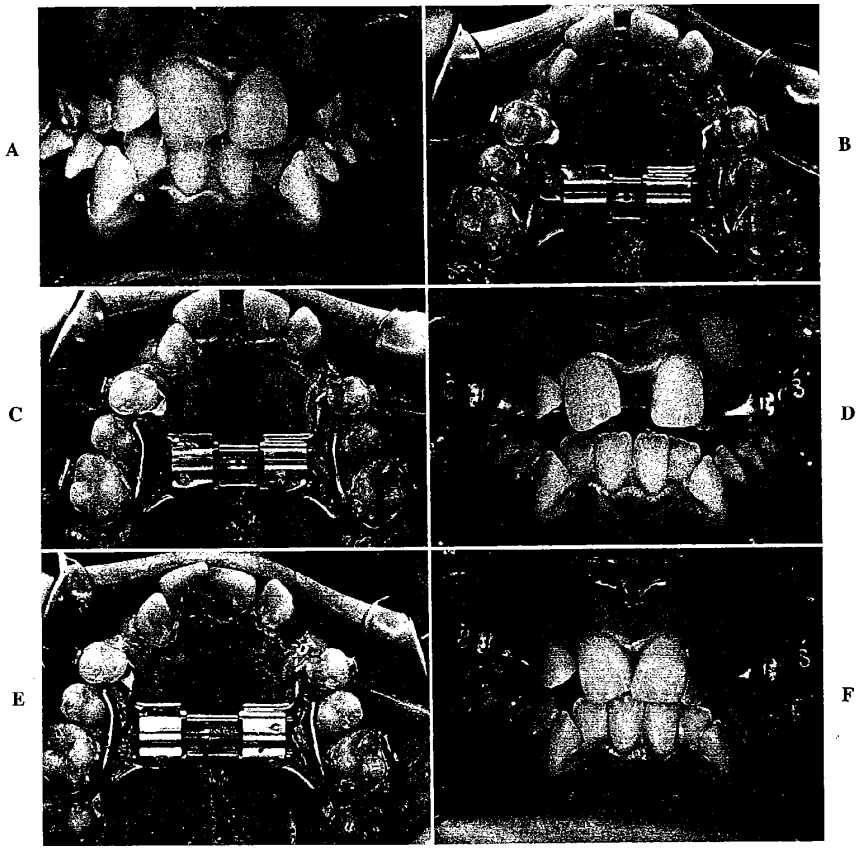


Fig. 15-14 ■ Rapid maxillary expansion with a jackscrew appliance to open the midpalatal suture. **A,** Maxillary constriction and crowding before treatment; **B,** jackscrew appliance in place, soldered to bands on the maxillary first molars and first premolars, with an arm contacting the second premolars. At this point, the appliance has been opened approximately 3 mm. Note the separation between the maxillary central incisors. **C,** Occlusal view after 10 days of separation. Note the wide central diastema. **D,** Labial view after 10 days of separation. A tendency toward anterior open bite is created by contact of the maxillary lingual and mandibular buccal molar cusps. **E,** Occlusal view 3 months after separation was begun and 10 weeks after the screw was stabilized by tying it with brass wire. Note the spontaneous closure of the diastema, which occurs because of a combination of elastic rebound of the gingival fibers that moves the teeth together, and skeletal relapse. **F,** Labial view at 3 months. Overcorrection of the posterior crossbite is being maintained by the stabilized appliance.

months of retention. With slow expansion, approximately 2½ months are needed to obtain the expansion, and the appliance can be removed in another 2 months.

Some degree of relapse can be expected after palatal expansion because of the elasticity of the palatal soft tissue. Therefore it is wise to overcorrect the crossbite initially (see Fig. 15-14). Even if 3 to 4 months of stabilization with the palate-separating device have been provided, additional retention of the crossbite correction is needed when the fixed appliance is removed. A palate-covering removable retainer is satisfactory but may be somewhat awkward in combination with fixed appliances to align the teeth as the first stage of treatment proceeds. An alternative is a heavy labial archwire placed in the headgear tubes, which will maintain the lateral expansion while light resilient archwires are being used to align the teeth (Fig. 15-15), or a lingual arch.

Correction of Dental Crossbites. Three approaches to correction of less severe dental crossbites are feasible: a heavy labial expansion arch, as shown in Fig. 15-15, an

ClearCorrect Exhibit 1002, Page 1870 of 3373

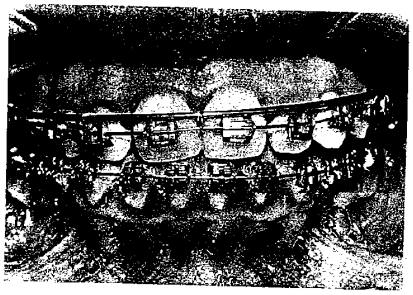


Fig. 15-15 ■ A heavy labial archwire (usually 36 or 40 mil steel) placed in the headgear tubes on first molars can be used to maintain arch width after palatal suture opening while the teeth are being aligned. This is more compatible with fixed-appliance treatment than a removable retainer and does not depend on patient cooperation.

expansion lingual arch, or cross-elastics. Removable appliances, although theoretically possible, are not compatible with comprehensive treatment and should be reserved for the mixed dentition or adjunctive treatment.

The inner bow of a facebow is also, of course, a heavy labial arch, and expansion of this inner bow is a convenient way to expand the upper molars. This expansion is nearly always needed for patients with a Class II molar relationship, whose upper arch is too narrow to accommodate the mandibular arch when it comes forward into the correct relationship. The inner bow is simply adjusted at each appointment to be sure that it is slightly wider than the headgear tubes and must be compressed by the patient when inserting the facebow. If the distal force of a headgear is not desired, a heavy labial auxiliary can provide the expansion effect alone.

A transpalatal lingual arch for expansion must have some springiness and range of action. As a general princi-

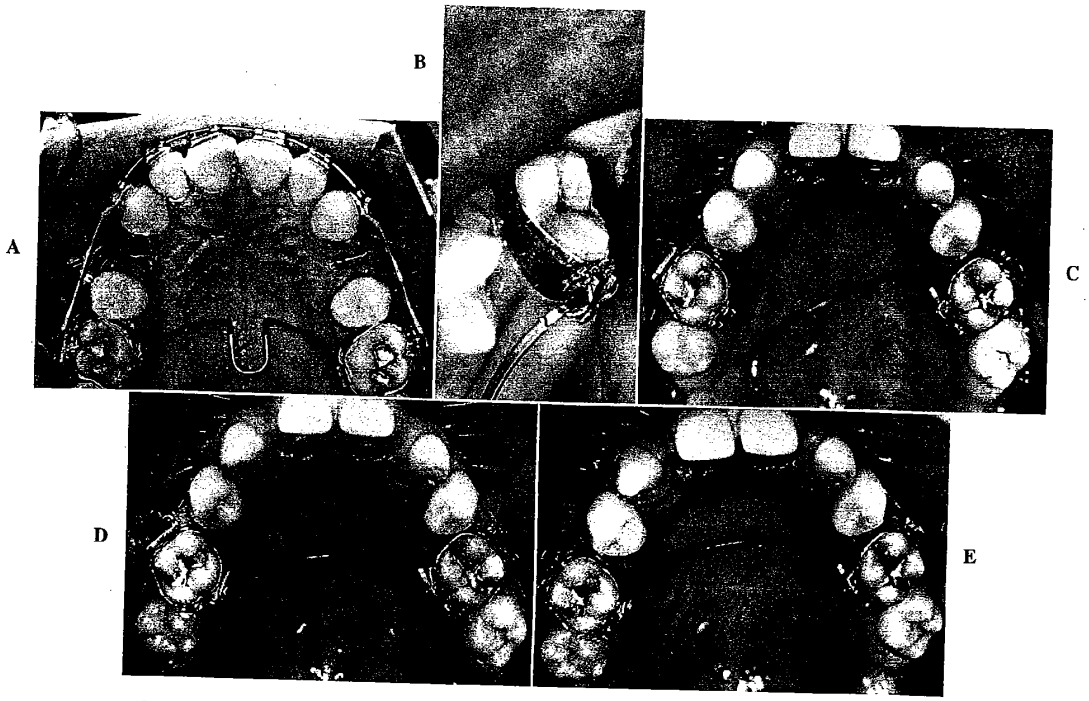


Fig. 15-16 ■ **A,** An expansion lingual arch of this type, using 36 mil steel wire doubled over into a horizontal lingual sheath, is often used for small amounts of expansion in the first stage of comprehensive treatment rather than the more flexible expansion arches shown in Chapter 14, because it also will contribute to stabilization of the posterior segments later, augmenting the posterior anchorage. **B,** A more efficient alternative, especially if more than a small amount of expansion is needed, is to use the new 32 × 32 lingual arch brackets. Then a 32 × 32 TMA lingual arch can be used for the initial tooth movement, and a steel arch of the same size can be placed for the later stabilization. **C,** Activation of a TMA lingual arch (equal on the two sides); **D,** initial and, **E,** follow-up molar positions. (**B** to **E,** Courtesy Dr. CJ Burstone.)

ClearCorrect Exhibit 1002, Page 1871 of 3373

ple, the more flexible a lingual arch is, the less it adds to anchorage stability, which can be an important consideration in adolescent and adult patients. If anchorage is of no concern, a highly flexible lingual arch, like the quad helix design discussed in Chapter 13, is an excellent choice. When the lingual arch is needed for both expansion and anchorage, however, the choices are 36 mil steel wire with an adjustment loop, or the new system that allows the use of 32 × 32 TMA or steel wire (Fig. 15-16) (see Chapter 12).

The third possibility for dental expansion is the use of cross-elastics, typically running from the lingual of the upper molar to the buccal of the lower molar (Fig. 15-17). These elastics are effective, but their strong extrusive component must be kept in mind. As a general rule, adolescent patients can tolerate a short period of cross-elastic wear to correct a simple crossbite, because any extrusion is compensated by vertical growth of the ramus, but cross-elastics should be used with great caution, if at all, in adults. As any posterior crossbite is corrected, interference of the cusps increases posterior vertical dimension and thereby tends to rock the mandible downward and backward, even if cross-elastics are avoided. The elastics accentuate this tendency.

If teeth are tightly locked into a crossbite relationship, a bite plate to separate them vertically can make the correction easier and faster. In children and young adolescents, this is rarely needed. The necessary vertical clearance is achieved by mandibular repositioning of the type that accompanies growth anyway. In older adolescents and adults, however, a bite plate may be necessary.

■ Impacted or Unerupted Teeth

Bringing an impacted or unerupted tooth into the arch creates a set of special problems during alignment, primarily because an unerupted tooth is usually a long way from the line of occlusion. The most frequent problem of this type is an impacted maxillary canine or canines, but it is occasionally necessary to bring other unerupted teeth into the arch, and the same techniques apply for incisors, canines, and premolars. Impacted lower second molars pose a different problem and are discussed separately.

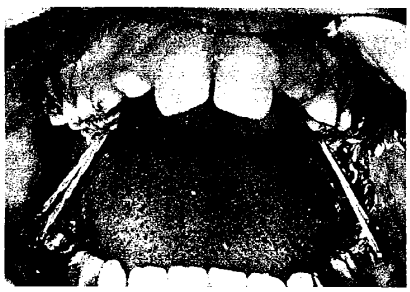


Fig. 15-17 ■ Cross-elastics from the lingual of the upper molars to the buccal of the lower molars. Cross-elastics are an effective way of correcting transverse dental relationships, but they also extrude teeth, and this must be kept in mind.

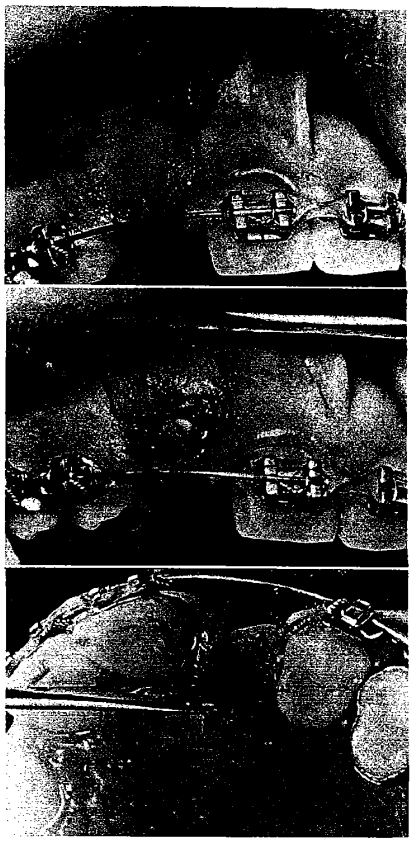


Fig. 15-18 ■ Apically positioned flap for exposure of an unerupted canine. **A,** Initial incision lines; **B,** crown exposed with apical repositioning of the labial tissue; **C,** lingual exposure of the same tooth.

The problems in dealing with an unerupted tooth can be divided into three categories: (1) surgical exposure, (2) attachment to the tooth, and (3) orthodontic mechanics to bring the tooth into the arch.

Surgical Exposure. It is important for a tooth to erupt through the attached gingiva, not through alveolar mucosa, and this must be considered when flaps for exposure of an unerupted tooth are planned. If the unerupted tooth is in the mandibular arch or on the labial side of the maxillary alveolar process, a flap should be reflected from the crest of the alveolus and sutured so that attached gingiva has been transferred to the region where the crown is exposed (Fig. 15-18). If this is not done, and the tooth is brought

ClearCorrect Exhibit 1002, Page 1872 of 3373

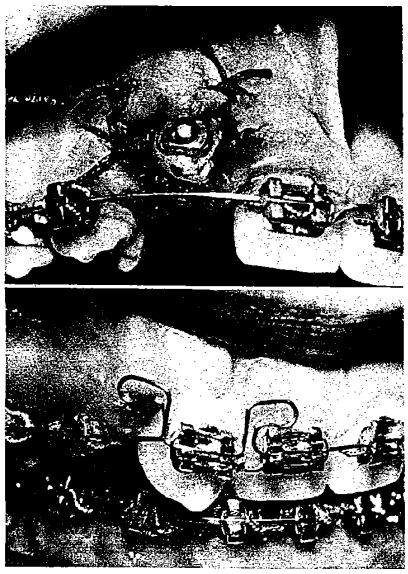


Fig. 15-19 ■ **A,** Attachment bonded to the labial surface of the crown of an unerupted canine (same patient as Fig. 15-18), with the apically repositioned flap sutured in place. An elastomeric attachment from the archwire to the bonded button will be used initially to bring the canine toward the line of occlusion. Later, the button will be replaced with a bonded bracket. **B,** Tooth in position, after placement of a normal bonded bracket and boot loops to complete the repositioning.

through alveolar mucosa, it is quite likely that tissue will strip away from the crown, leaving both an unsightly and periodontally compromised gingival margin.[8] If the unerupted tooth is on the palatal side, similar problems with the heavy palatal mucosa are unlikely, and flap design is less critical.

Occasionally, a tooth will obligingly erupt into its correct position after obstacles to eruption have been removed by surgical exposure, but this is rarely the case after root formation is complete. Even a tooth that is aimed in the right direction usually requires orthodontic force to bring it into position.

Method of Attachment. The least desirable way to obtain attachment is for the surgeon to place a wire ligature around the crown of the impacted tooth. This inevitably results in loss of periodontal attachment, because bone destroyed when the wire is passed around the tooth does not regenerate when it is removed. Occasionally no alternative is practical, but wire ligatures should be avoided whenever possible.

Before the availability of direct bonding, a pin was sometimes placed in a hole prepared in the crown of an unerupted tooth, and in special circumstances, this remains a possible alternative. The best contemporary approach, however, is simply to expose an area on the crown of the tooth and directly bond an attachment of some type to that surface (Fig. 15-19). In many instances, a button or hook is better than a standard bracket because it is smaller. A wire or elastomeric ligature can then be looped around the bonded attachment before the flap is repositioned and sutured into place, so that the ligature extends into the mouth.

Mechanical Approaches for Aligning Unerupted Teeth. Orthodontic traction to pull an unerupted tooth toward the line of the arch should begin as soon as possible after surgery. Ideally, a fixed orthodontic appliance should already be in place before the unerupted tooth is exposed, so that orthodontic force can be applied immediately. If this is not practical, active orthodontic movement should begin no later than 2 or 3 weeks postsurgically.

An unerupted tooth is usually so far from the line of occlusion that it is impossible to tie even the most flexible continuous wire against it. One possible approach is to tie from the impacted tooth to a relatively heavy base archwire, using an elastomeric material (Fig. 15-20) or, even better if space allows, a modern A-NiTi coil spring. A second alternative is to use a special alignment spring, either soldered to a heavy base archwire or bent into a light archwire (Fig. 15-21). Compared with tying with an elastomeric material, this technique has the advantage of a considerably longer range and a more constant force magnitude. When the unerupted tooth has been brought relatively close to the line of occlusion and a standard bracket can be bonded in the proper position, loops in a continuous archwire can be used to complete the alignment. A box loop (Fig. 15-22), usually formed in 14 mil steel wire, is preferred for this purpose. Although a highly flexible archwire like 16 mil A-NiTi could be used, this is another situation in which distortion of arch form could result, and the ability of a loop to concentrate springiness where it is needed makes this approach better.

A third alternative, magnetic force to initiate movement of an unerupted tooth, is becoming increasingly more feasible. The great virtue of this method is that no mechanical connection is required, and problems associated with premature exposure of the unerupted tooth to the oral environment could be avoided. Magnetic attraction between an attachment bonded to the tooth and an intraoral magnet would produce the tooth movement. Recent reports demonstrate that it is possible to bond a small magnet to an unerupted maxillary canine, and use magnetic attraction to a larger magnet contained within a palate-covering removable appliance.[9,10] The attractive force is determined by the distance between the magnets, and so can be controlled with good precision. The direction of the force depends on the orientation of the magnets, which also can be controlled, especially since the magnet within the removable appliance can be positioned almost wherever desired. As magnet technology continues to improve, magnetic attrac-

ClearCorrect Exhibit 1002, Page 1873 of 3373

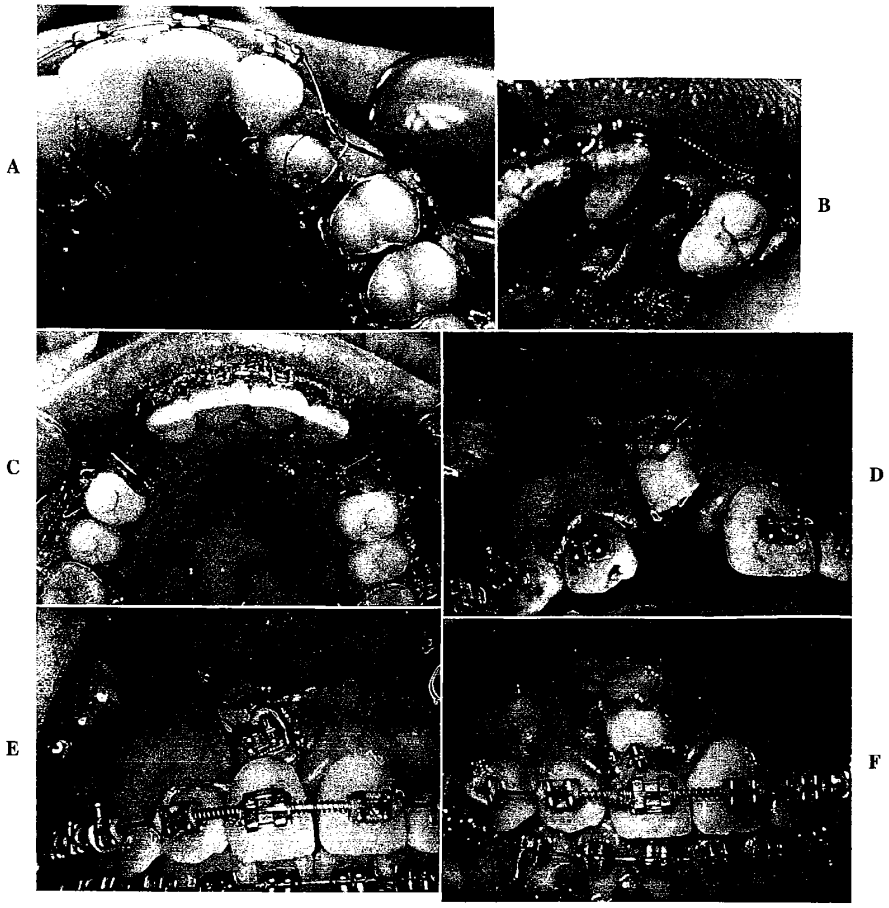


Fig. 15-20 ■ **A,** If an unerupted tooth is not too far out of line, a flexible archwire like 16 A-NiTi can be tied directly to the attachment. **B,** In the more usual situation, a button is bonded to whatever portion of the tooth can be exposed, and **C,** traction is applied via springs or auxiliary attachments. **D,** If the unerupted tooth is labially positioned, it is important to employ an apically repositioned flap so that a gingival attachment is preserved. Then an attachment can be bonded **(E).** An elastomeric chain **(F)** looped around a rigid base archwire often is the best approach for bringing labially positioned incisors into the arch.

tion is likely to become the preferred method for moving deeply embedded teeth.

Ankylosis of an unerupted tooth is always a potential problem. If an area of fusion to the adjacent bone develops, orthodontic movement of the unerupted tooth becomes impossible, and displacement of the anchor teeth will occur. Occasionally, an unerupted tooth will start to move and then will become ankylosed, apparently held by only a small area of fusion. It can sometimes be freed to continue movement by being anesthetized and lightly luxated, breaking the area of ankylosis. If this procedure is done, it is critically important to apply orthodontic force immediately after the luxation, since it is only a matter of time until the tooth re-ankyloses. Nevertheless, this approach can sometimes allow a tooth to be brought into the arch that otherwise would have been impossible to move.

Unlike impaction of most other teeth, which is an obvious problem from the beginning of treatment, impaction of lower second molars usually develops during orthodontic treatment (Fig. 15-23). This occurs when the mesial marginal ridge of the second molar catches against the distal surface of the first molar, so that the second molar progressively tips mesially instead of erupting. Moving the first molar posteriorly during the mixed dentition increases the chance that the second molar will become impacted, and this possibility must be taken into account when pro-

ClearCorrect Exhibit 1002, Page 1874 of 3373

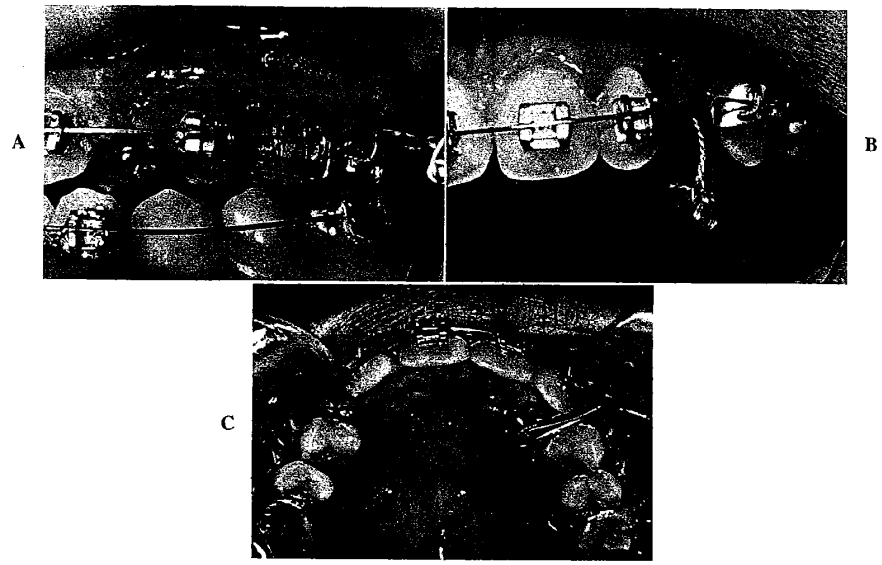


Fig. 15-21 ■ **A,** An auxiliary spring soldered to a base archwire provides a long range of action to bring an unerupted canine facially and occlusally. This is more efficient than elastomeric ties. A spring bent into an archwire also can be employed. **B,** A vertical spring bent into a 14 mil steel archwire to bring down an impacted maxillary canine, before activation; **C,** same spring activated by rotating the loop 90 degrees. A stop against the molars, so that the wire cannot just spin in the molar tubes, is essential. This method is also very effective, providing excellent force characteristics with a long range of action (see also Fig. 15-20, *C*).

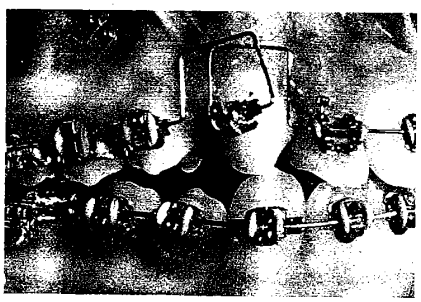


Fig. 15-22 ■ A canine or premolar positioned high in the labial vestibule can be brought into the arch most efficiently by using a box loop in 14 mil steel wire. Initially, the bracket is tied to the loop (note the small V-bend in the bottom of the loop so that the ligature does not slip off when the loop is tied in this way). Eventually, the wire can be tied into the bracket slot.

cedures to increase mandibular arch length are employed.

Correction of an impacted second molar requires that the tooth be moved posteriorly and uprighted. In most cases, if the mesial marginal ridge can be unlocked, the tooth will erupt on its own. When the second molar is not severely tipped, the simplest solution is to place a separator between the two teeth (Fig. 15-24). For a more severe problem, one possibility is to solder an auxiliary spring to an archwire mesial to the first molar and extend it posteriorly into the embrasure between the first and second molars. The long arm of an auxiliary spring of this type gives excellent flexibility and range of action, but also makes it difficult to keep the spring in place and may lead to substantial soft tissue irritation. A better alternative is to surgically expose the second molar, bond a tube to the buccal surface, and then use an auxiliary spring inserted into this tube to upright the second molar (Fig. 15-25).

An auxiliary spring, soldered to a heavy archwire or extending from the first molar auxiliary tube, is often useful to bring both upper and lower second molars into alignment when they erupt late in orthodontic treatment (Fig. 15-26). This allows the use of a flexible wire in the posterior part of the arch, while a heavier and more rigid wire is in place anteriorly.

ClearCorrect Exhibit 1002, Page 1875 of 3373

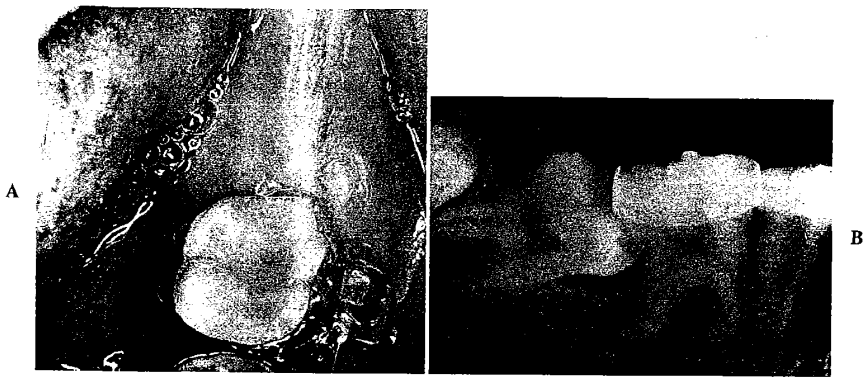


Fig. 15-23 ■ Impacted mandibular second molar in a 14-year-old patient. **A,** Occlusal view; **B,** radiographic view. The clinically exposed cusp is the distobuccal cusp, not the mesiobuccal cusp one would expect to see in this location. (See Fig. 15-25 for treatment of this patient.)

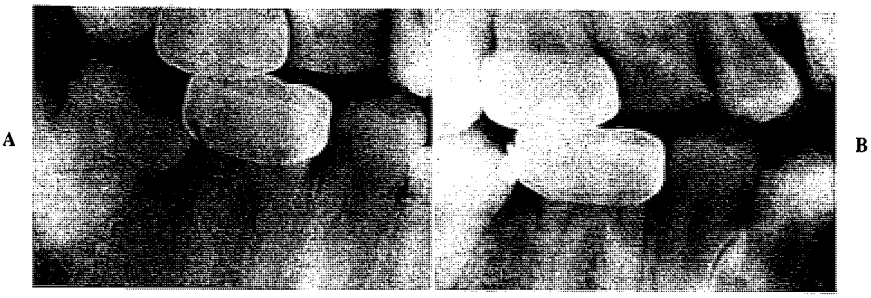


Fig. 15-24 ■ Brass wire separator used to de-impact a mandibular second molar. **A,** Second molar trapped beneath distal bulge of first molar; **B,** uprighting obtained with 20 mil brass wire tightened around the contact. Usually it is necessary to anesthetize the area to place a separating wire of this type. A spring clip can be used in the same way, but both brass wire and spring clips are effective only if the tooth is minimally tipped.



Fig. 15-25 ■ Use of a bonded tube and auxiliary spring to upright a severely impacted mandibular second molar (same patient as Fig 15-23). **A,** Surgical exposure of a portion of the facial surface of the crown; **B,** tube bonded on the distobuccal cusp. *Continued.*

ClearCorrect Exhibit 1002, Page 1876 of 3373

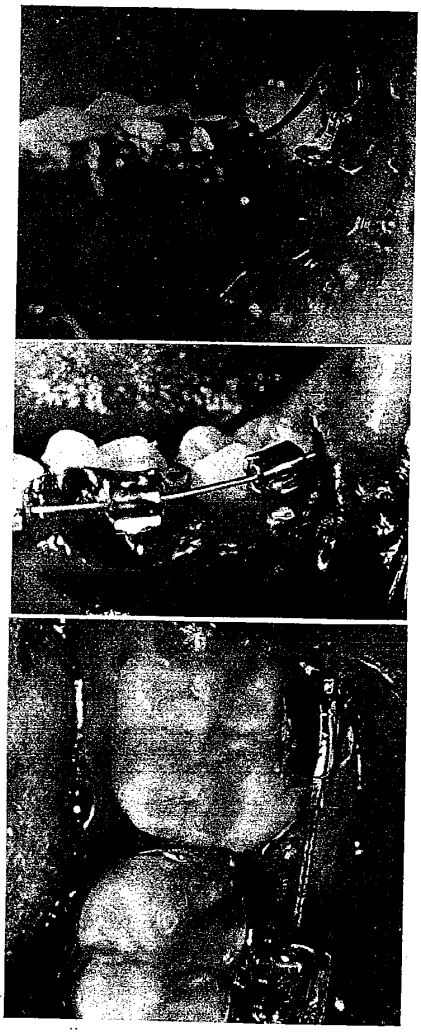


Fig. 15-25—cont'd. ■ C, helical spring from archwire inserted into buccal tube; D, uprighting completed, with the second molar in position for normal banding or bonding; E, occlusal view after uprighting.

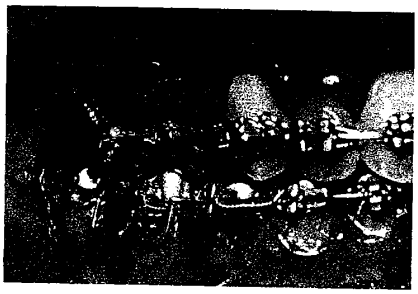


Fig. 15-26 ■ When a second molar is banded relatively late in treatment, a spring soldered to the main archwire and extending beneath the first molar tube as shown here provides excellent flexibility to align the second molar while allowing a heavy archwire to remain in place anteriorly to maintain arch form. If the first molar carries an auxiliary tube, an efficient alternative is to place a segment of rectangular NiTi wire from the first to the second molar.

■ Diastema Closure

A maxillary midline diastema is often complicated by the insertion of the labial frenum into a notch in the alveolar bone, so that a band of heavy fibrous tissue lies between the central incisors. When this is the case, a stable correction of the diastema almost always requires surgery to remove the interdental fibrous tissue and reposition the frenum. The frenectomy must be carried out in a way that will produce a good esthetic result and must be properly coordinated with orthodontic treatment.

It is an error to surgically remove the frenum and then delay orthodontic treatment in the hope that the diastema will close spontaneously. If the frenum is removed while there is still a space between the central incisors, scar tissue forms between the teeth as healing progresses, and a long delay may result in a space that is more difficult to close than it was previously.

It is better to align the teeth before frenectomy. Sliding them together along an archwire is usually better than using a closing loop, because a loop with any vertical height will touch and irritate the frenum. If the diastema is relatively small, it is usually possible to bring the central incisors completely together before surgery (Fig. 15-27). If the space is large and the frenal attachment is thick, it may not be possible to completely close the space before surgical intervention. The space should be closed at least partially, and the orthodontic movement to bring the teeth together should be resumed immediately after the frenectomy, so that the teeth are brought together quickly after the procedure. When this is done, healing occurs with the teeth together, and the inevitable postsurgical scar tissue stabilizes the teeth in their correct position instead of creating obstacles to final closure of the space.

The key to successful surgery is removal of the interdental fibrous tissue. It is unnecessary, and in fact undesir-

ClearCorrect Exhibit 1002, Page 1877 of 3373

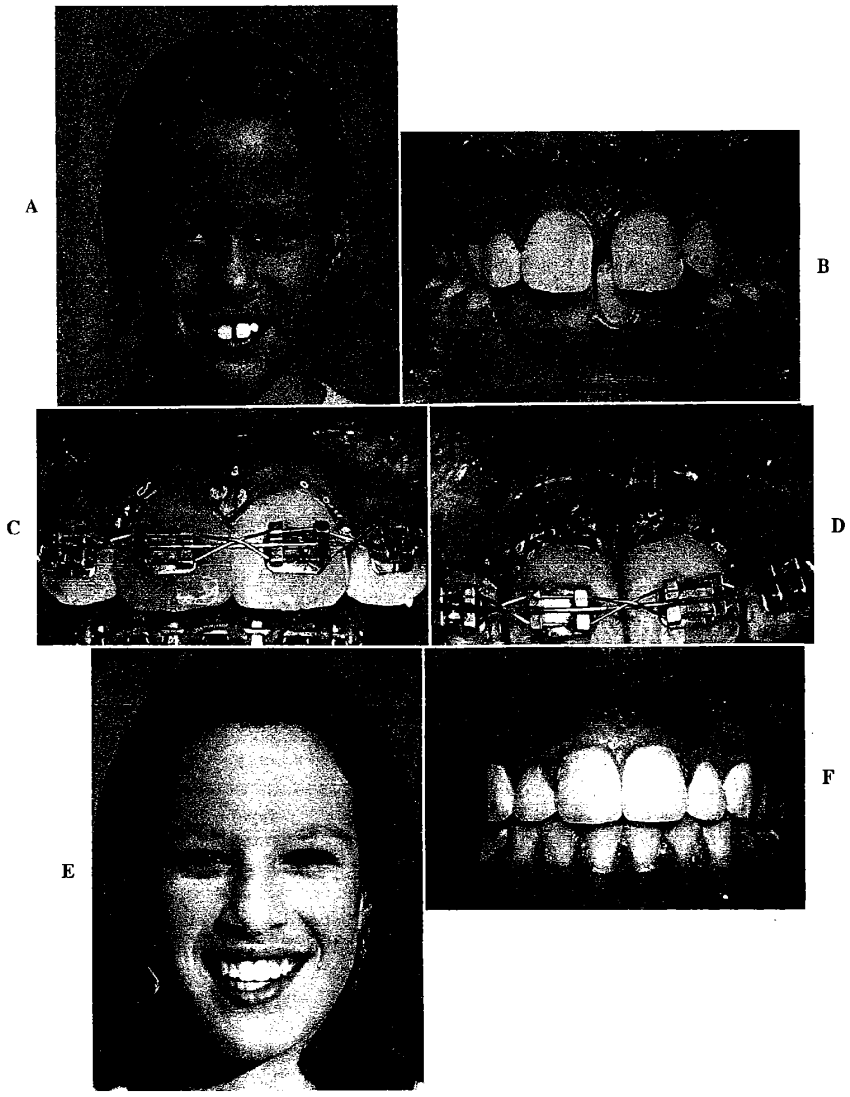


Fig. 15-27 ■ Management of a maxillary midline diastema. **A,** Facial appearance, showing the protuding maxillary incisors caught on the lower lip; **B,** intraoral view before treatment; **C,** teeth aligned and held tightly together with a figure-8 wire ligature, before frenectomy; **D,** appearance immediately after frenectomy, using the conservative technique advocated by Edwards in which a simple incision is used to allow access to the interdental area, the fibrous connection to the bone is removed, and the frenal attachment is sutured at a higher level; **E,** facial appearance 2 years after completion of treatment; **F,** intraoral view 2 years after treatment.

ClearCorrect Exhibit 1002, Page 1878 of 3373

able, to excise a large portion of the frenum itself. Instead, a simple incision is used to allow access to the interdental area, the fibrous connection to the bone is removed, and the frenum is then sutured at a higher level.[11]

A maxillary midline diastema tends to recur, no matter how carefully the space was managed initially. A bonded fixed retainer (see Chapter 18) is recommended.

Leveling

The archwire design for leveling depends on whether there is a need for absolute intrusion of incisors, or whether relative intrusion is satisfactory. This important point is discussed in detail in Chapter 7, and the biomechanical considerations in obtaining intrusion are described in Chapters 9 and 10. The discussion following assumes that an appropriate decision about the type of leveling has been made, and focuses on the rather different techniques for leveling by relative intrusion (which is really differential elongation of premolars, for the most part) as contrasted to leveling by absolute intrusion of incisors (see Fig. 7-5).

■ Leveling by Extrusion (Relative Intrusion)

This type of leveling can be accomplished with continuous archwires, simply by placing an exaggerated curve of Spee in the maxillary archwire and a reverse curve of Spee in the mandibular archwire (Fig. 15-28). For most patients, it is necessary to replace the initial highly resilient alignment arch with a slightly stiffer one to complete the leveling. As with the alignment archwire, the choice of wires for this purpose depends on which type of edgewise appliance is being used.

18-Slot, Narrow Brackets. When preliminary alignment is completed, the second archwire is almost always 16 mil steel, with an exaggerated curve of Spee in the upper arch and a reverse curve in the lower arch. In most instances, this approach is sufficient to complete the leveling. An alternative is to use 16 or 18 mil M-NiTi, preformed by the manufacturer with an extremely exaggerated curve.

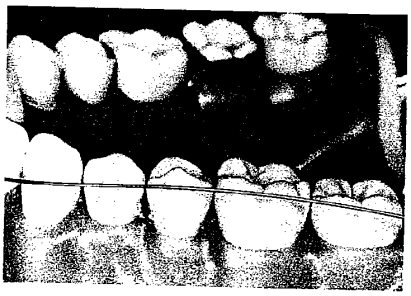


Fig. 15-28 ■ A reverse curve of Spee in the lower archwire, illustrated here alongside a lower arch with which it could be used, is a satisfactory method if vertical growth will occur to compensate for the extrusion that occurs in the premolar region.



Fig. 15-29 ■ An auxiliary leveling arch (usually 17 × 25 steel) extending from the auxiliary tubes on the first molars and tied beneath the base arch anteriorly can be used to augment the leveling ability of continuous archwires. With a continuous base archwire, the effect is primarily premolar extrusion, not the incisor intrusion that a similar auxiliary arch could produce with base arch segments, but this often is what is desired in growing children. (See Fig. 15-36, *D*, for an additional illustration of an auxiliary depressing arch to assist in leveling the lower arch with a continuous base arch.)

In some patients, particularly in nonextraction treatment of older patients who have little if any remaining growth, an archwire heavier than 16 mil steel is needed to complete the leveling of the arches. Rather than use an 18 mil archwire, it is usually quicker and easier to add an auxiliary leveling arch of 17 × 25 mil TMA or steel. This arch inserts into the auxiliary tube on the molar and is tied anteriorly beneath the 16 mil base arch (Fig. 15-29). In essence, this augments the curve in the base arch and results in efficient completion of the leveling.

It is sometimes said, as an argument in favor of the 22-slot appliance, that the wires available for use with the 18-slot appliance are not large enough to accomplish all necessary tooth movements. One of the few situations in which that may be true is in final leveling with continuous archwires, which may require either a continuous 18 mil steel archwire or the auxiliary wire suggested previously.

22-Slot, Wider Brackets. For a typical patient using the 22-slot appliance, initial alignment with a 17.5 mil twist or 16 mil A-NiTi wire is usually followed by a 16 mil steel wire with a reverse or accentuated curve, and then by an 18 mil round wire to complete the leveling. This archwire sequence is nearly always adequate for completion of leveling, and it is rare that 20 mil wire or an auxiliary archwire is required.

■ Leveling by Intrusion

Leveling by intrusion requires a mechanical arrangement other than a continuous archwire attached to each tooth. The key to successful intrusion is light continuous force directed toward the tooth apex. It is necessary to

ClearCorrect Exhibit 1002, Page 1879 of 3373

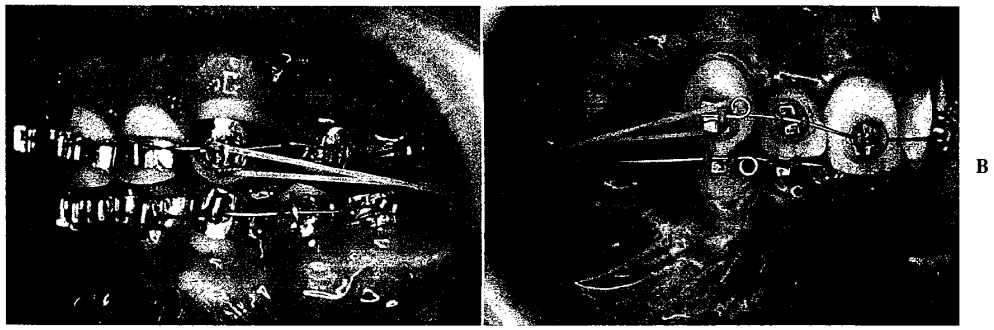


Fig. 15-30 ■ **A,** Illustration of 16 mil steel archwires for leveling in the first stage of Begg technique. An "anchor bend" is placed mesial to the first molar, and the archwire is lightly ligated or clipped as it passes the second premolar, rather than being pinned into the bracket on these teeth. **B,** Similar bends are placed in the initial wires with the modern Begg-edgewise techniques, as here with the TipEdge appliance. **(B,** Courtesy Dr. PC Kesling.)

avoid pitting intrusion of one tooth against extrusion of its neighbor, since in that circumstance, extrusion will dominate. This can be accomplished in two ways: (1) with continuous archwires that bypass the premolar (and frequently the canine) teeth, and (2) with segmented base archwires (so that there is no connection along the arch between the anterior and posterior segments) and an auxiliary depressing arch.

Bypass Arches. This approach to intrusion is most useful for patients who will have some growth (i.e., who are in either the mixed or early permanent dentitions). Three different mechanical arrangements are commonly used, each based on the same mechanical principle: uprighting and distal tipping of the molars are pitted against intrusion of the incisors.

A classic version of this approach to leveling is seen in the first stage of Begg technique, in which the premolar teeth are bypassed and only a loose tie is made to the canine. A 16 mil resilient steel archwire is fabricated as shown in Fig. 15-30, using an "anchor bend" anterior to the first molar. The long span of the archwire anterior to the anchor bend provides a gentle intrusive force on the incisors, while the reaction force on the molar tends to upright it and tip it distally. Light Class II elastic forces are used while this archwire is in place. The result is stabilization of the lower molar against the distal tipping, at the cost of some extrusion of the molar. Hence there is a need for some vertical growth while this treatment is being carried out, to prevent downward and backward rotation of the mandible. The light archwire, however, does intrude the lower incisors. The upper incisors are being pulled downward by the Class II elastic, which counterbalances the intrusion these teeth otherwise might experience.

Exactly the same effect can be produced in exactly the same way using the edgewise appliance, if the premolars and canines are bypassed. Mulligan has advocated just this approach to the fabrication of a leveling archwire, using a 16 mil steel wire with an anchor bend similar to the initial archwire in the Begg technique.[12]

A more flexible variation of the same basic idea is developed in Rickett's utility arch (Fig. 15-31).[13] The utility arch is characterized by step-down bends between the first molar and the lateral incisors, so that the archwire is less likely to be distorted by the forces of occlusion. It is fabricated of 16 × 16 mil wire, used in 18-slot brackets. In most cases, the rectangular wire is placed into the brackets with slight labial root torque to control the inclination of the teeth as the incisors move labially while they intrude.

Successful use of any of these bypass arches for leveling requires that the forces be kept light. This is accomplished in two ways: by selecting a small diameter archwire, and by using a long span between the first molar and the incisors. Wire heavier than 16 mil steel should not be used, and Ricketts recommends a relatively soft 16 × 16 cobalt-chromium wire for utility arches to prevent heavy forces from being developed. Overactivation of the vertical bends

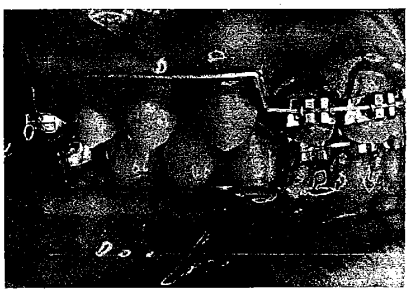


Fig. 15-31 ■ Utility arches for leveling, showing the long span from molars to incisors that makes it possible to produce absolute intrusion.

ClearCorrect Exhibit 1002, Page 1880 of 3373

can cause loss of control of the molars in all three planes of space.

The 16 mil steel wires typically used in bypass arches, though resilient, are too stiff for efficient alignment of severely malposed incisors, even if loops are bent into the wire between adjacent teeth. Small rotations or displacements can be corrected simply by tying to a 16 mil wire and gradually bringing the wire into the bracket slot, particularly if the brackets are narrow so that interbracket span is adequate. Where significant malpositions exist, however, it is better to correct the alignment with a resilient wire, perhaps using only a resilient anterior segment, before tying a round or rectangular bypass arch into the brackets. If intrusion is desired from the beginning, an auxiliary arch for this purpose can be used along with the anterior alignment segment, as described below.

In contrast to leveling with continuous fully engaged archwires, the size of the edgewise bracket slot is largely irrelevant when bypass arches for leveling are used. Whether the appliance is 18- or 22-slot, the bypass arch should not be stiffer than 16 mil steel wire. If preliminary alignment is needed before the bypass arch for leveling is placed, of course, slot size would be a factor and the alignment archwires recommended previously as appropriate for each bracket slot would be the best choices.

Two weaknesses of the bypass arch systems previously described limit the amount of true intrusion that can be obtained. The first is that, except for some applications of the utility arch, only the first molar is available as posterior anchorage. This means that significant extrusion of that tooth may occur. In actively growing patients with a good facial pattern, this is not a major problem, but in nongrowing patients or those with a poor facial pattern in whom molar extrusion should be avoided, the lack of posterior anchorage can compromise the ability to intrude incisors. High-pull headgear to the upper molars can be added with any of the bypass arch systems to improve upper posterior anchorage, and with a utility arch setup, the second molar and second premolar can be incorporated into the posterior segment for better anchorage control.

The second weakness is that the intrusive force against the incisors is applied anterior to the center of resistance, and therefore the incisors tend to tip forward as they intrude (Fig. 15-32). Without an extraction space, forward movement of the incisors is an inevitable consequence of leveling, but often in extraction cases, this result is undesirable. The anchor bend at the molar in the Begg approach creates a space-closing effect that somewhat restrains forward incisor movement (Fig. 15-33), but this also tends to bring the molar forward, straining the posterior anchorage. The same thing happens for the same reason with a Mulligan bypass arch or a utility arch. A utility arch can be activated to keep the incisors from moving forward and has the additional benefit of a rectangular cross-section anteriorly so that tipping can be controlled, but the result is still a strain on posterior anchorage. The segmented arch approach to leveling developed by Burstone, which overcomes these limitations, is recommended for maximum control of the anterior and posterior segments of the dental arch.

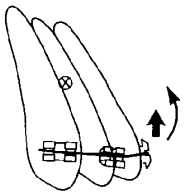


Fig. 15-32 ■ When the incisor segment is viewed from a lateral perspective, the center of resistance can be seen to be lingual to the point at which an archwire attaches to the crown. For this reason, the incisors tend to tip forward when an intrusive force is placed at the central incisor brackets. This tendency toward labial tipping can be controlled either by applying a force to tip the incisors distally as they are being intruded, canceling the mesial tipping, or by applying the intrusive force more posteriorly, as by attaching an intrusion arch to stabilized anterior segment more distally, in the vicinity of the lateral rather than the central incisors, for instance (see Fig. 15-37).

Segmented Archwires for Leveling. The segmented arch approach depends on establishing stabilized posterior segments and controlling the point of force application against an anterior segment. This technique requires auxiliary rectangular tubes on first molars, in addition to the regular bracket or tube. After preliminary alignment if needed, a full dimension rectangular archwire is placed in the bracket slots of teeth in the buccal segment, which typically consists of the second premolar, first molar, and second molar. This connects these teeth into a solid unit. In addition, a heavy lingual arch (36 mil round or 32 × 32 rectangular steel wire) is used to connect the right and left

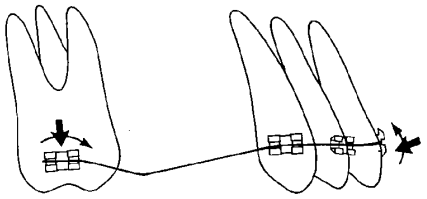


Fig. 15-33 ■ Diagrammatic representation of forces from a leveling archwire that bypasses the premolars, with an anchor bend mesial to the molars. A force system is created that elongates the molars and intrudes the incisors. The wire tends to slide posteriorly through the molar tube, tipping the incisors distally at the expense of bodily mesial movement of the molars. An archwire of this design is used in the first stage of Begg treatment but also can be used in edgewise systems. A long span from the molars to the incisors is essential.

ClearCorrect Exhibit 1002, Page 1881 of 3373

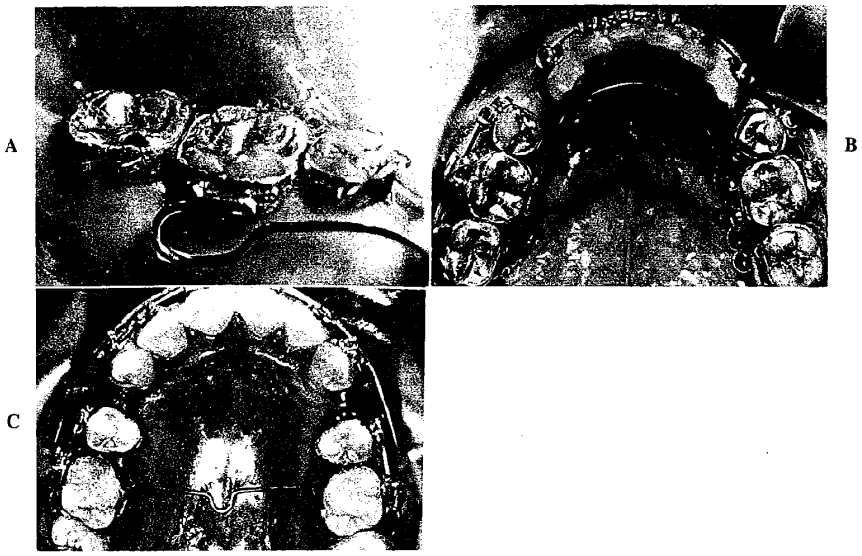


Fig. 15-34 ■ Mandibular stabilizing lingual arch in 36 mil steel wire, used for anchorage control in segmented arch leveling. **A,** Distal insertion into the horizontal tube on the first molar; **B,** the wire must clear the anterior segment, lying lingually and gingivally to these teeth. **C,** Maxillary transpalatal arch for anchorage control during intrusion, soldered to the first molar bands. This is effective for anchorage, but the lingual arch must be removed during finishing, and it can be awkward and difficult to cut it free.

posterior segments, further stabilizing them against undesired movement (Fig. 15-34). A resilient anterior segmental wire is used to align the incisors, while the posterior segments are being stabilized.

For intrusion, an auxiliary depressing arch placed in the auxiliary tube on the first molar is used to apply intrusive force against the anterior segment. This arch should be made of rectangular wire that will not twist in the auxiliary tube. Burstone recommends 18 × 25 steel wire with a 2½-turn helix (Fig. 15-35), or 19 × 25 TMA wire without a helix.[14] This depressing arch is adjusted so that it lies gingival to the incisor teeth when passive and applies a light force (approximately 15 gm per tooth) when it is brought up beneath the brackets of the incisors. It is tied underneath the incisor brackets, but not into the bracket slots, which are occupied by the anterior segment wire.

An auxiliary depressing arch can be placed while a light resilient anterior segment is being used to align malposed incisors, but it is usually better to wait to add the depressing arch until incisor alignment has been achieved and a heavier anterior segment wire has been installed. A braided rectangular steel wire or a rectangular TMA wire is usually the best choice for the anterior segment while active intrusion with an auxiliary depressing arch is being carried out.

Two strategies can be used with segmented arches to prevent forward movement of the incisors as they are intruded. The first is the same as with bypass arches: a space-closing force can be created by tying the depressing arch back against the posterior segments (see Fig. 15-35). Even with stabilized posterior segments, this produces some strain on posterior anchorage.

The second and usually preferable strategy is to vary the point of force application against the incisor segment. If the anterior segment is considered a single unit (which is reasonable when a stiff archwire connects the teeth within the segment), the center of resistance is located as shown in Fig. 15-32. Tying the depressing arch distal to the midline, between the central and lateral incisors, or distal to the laterals (Fig. 15-36), also brings the point of force application more posteriorly so that the force is applied more nearly through the center of resistance (Fig. 15-37). This prevents anterior tipping of the incisor segment without causing anchorage strain.

Even with the control of posterior anchorage obtained by placing rectangular stabilizing segments and an anchorage lingual arch, the reaction to intrusion of incisors is extrusion and distal tipping of the posterior segments. With careful attention to appropriate technique with the segmented arch approach, it is possible to produce approximately 4 times as much incisor intrusion as molar extrusion in nongrowing adults. Although successful intrusion

ClearCorrect Exhibit 1002, Page 1882 of 3373

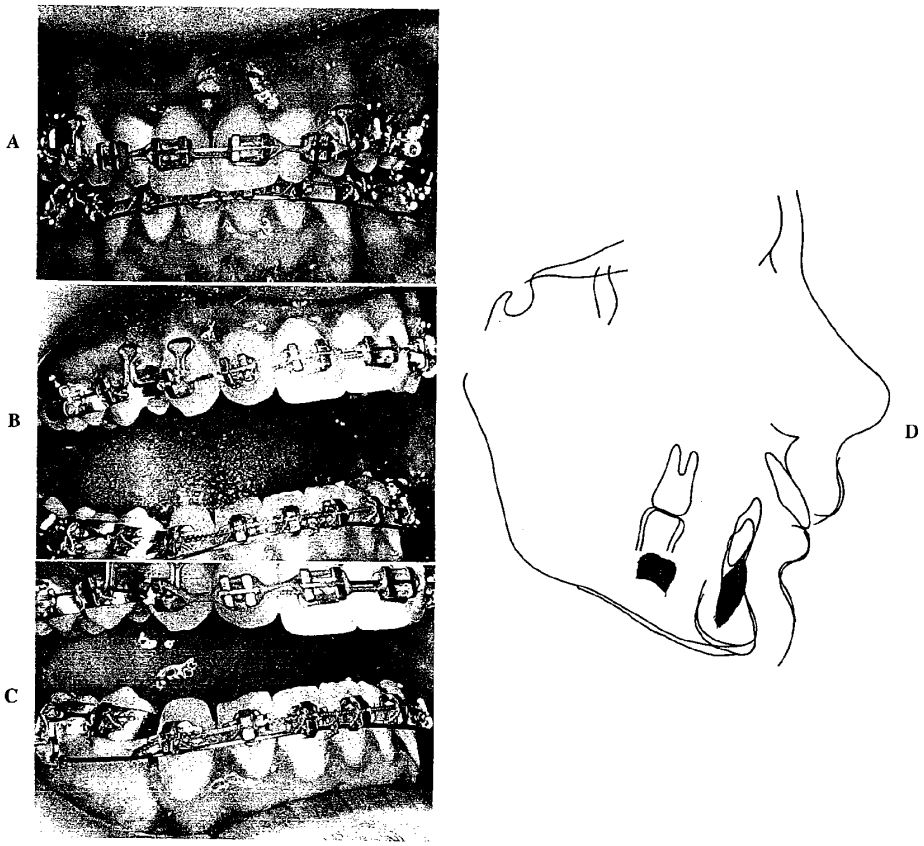


Fig. 15-35 ■ Segmented arch technique for leveling by intrusion of the lower incisors. **A,** After preliminary alignment, an anterior segment of 17 × 25 braided steel wire has been placed in the mandibular anterior segment. Posterior segments are stabilized, and a 17 × 25 steel depressing arch is placed in auxiliary tubes on the first molars and tied beneath the incisor brackets anteriorly; **B,** lateral view of appliance at initial activation; **C,** lateral view, 8 weeks later; **D,** cephalometric superimposition showing the amount of intrusion obtained in 3 months.



Fig. 15-36 ■ Segmented arch application for intrusion of maxillary incisors. **A,** The depressing arch in the vestibule, before activation. It is adjusted so that it provides about 50 gm of force when **B,** it is deflected down to the level of the brackets.

ClearCorrect Exhibit 1002, Page 1883 of 3373



Fig. 15-36—cont'd. ■ **C,** Buccal view showing the 2½ turn helix used in steel wire. For this patient, the depressing arch is tied in the midline because it is desirable for the incisors to tip forward as they depress. **D,** Buccal view of another patient. Note that the intrusion arch is tied between the lateral incisors and canines, moving the point of force application nearer the center of resistance of the anterior segment to prevent labial tipping of the incisors during the intrusion. In this patient, an auxiliary wire also is being used in the lower arch, but to supplement the continuous arch that is in place. The lower leveling will occur largely by elongation of the canine and premolar, rather than by intrusion of the incisors.

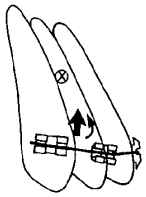


Fig. 15-37 ■ Tying an auxiliary depressing arch distal to the midline, as shown in Fig. 15-36, moves the line of force more posteriorly and therefore closer to the center of resistance of the anterior segment, diminishing or eliminating the moment that causes tipping. Compare this figure to Fig. 15-32.

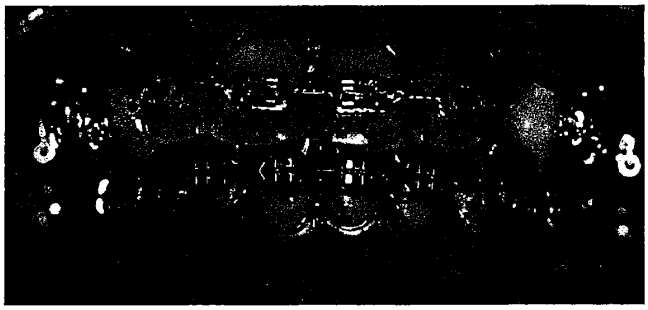


Fig. 15-38 ■ Utility arch inserted in auxiliary tube on molars, to intrude maxillary incisors while alignment loops are used in the buccal segments. Loops like those shown in this utility arch have two purposes: they decrease stiffness, so a larger wire than 16 × 16 steel can be used, and they can be activated to exert a distal or space-closing effect, providing a force to counteract the labial tipping of incisors that otherwise would occur.

ClearCorrect Exhibit 1002, Page 1884 of 3373

can be obtained with round bypass arches, the ratio of anterior intrusion to posterior extrusion is much less favorable. A utility arch can be used in conjunction with stabilized posterior segments, simply by placing the utility arch into an auxiliary tube on the first molar (an arrangement recommended by Ricketts for older patients). With this alteration (Fig. 15-38), the ratio of intrusion to extrusion improves. For adults, however, to control anterior tipping, it is advantageous to tie the depressing arch beneath a separate base archwire anteriorly, rather than tying directly into the incisor brackets as is usually done with a utility arch.

At the conclusion of the first stage of treatment, the arches should be level, and teeth should be aligned to the point that rectangular steel archwires can be placed without generating excessive forces. The duration of the first stage, obviously, will be determined by the severity of both the horizontal and vertical components of the initial malocclusion. For some patients, only a single initial archwire will be required, while for others, several months may be needed for alignment, and several more months for segmental leveling, before the next stage can begin. As a principle of treatment, it is important not to move to the second stage of treatment until both leveling and alignment are adequate.

■ *References*

1. Begg PR, Kesling PC: Begg orthodontic theory and technique, Philadelpia, 1977, WB Saunders.
2. Stoner MM: Wire: clinical considerations. In Graber TM, Swain BF, editors: Current orthodontic concepts and techniques, ed 2, Philadelphia, 1975, WB Saunders.
3. Lew K: A comparison of archwires used for initial alignment in Begg treatment, Aust Orthod J 10:180-182, 1988.
4. Melsen B: Palatal growth studied on human autopsy material, Am J Orthod 68:42-54, 1975.
5. McNamara JA: An orthopedic approach to the treatment of Class III malocclusion in young patients, J Clin Orthod 21:598-608, 1987.
6. Haas AJ: The treatment of maxillary deficiency by opening the midpalatal suture, Angle Orthod 35:200-217, 1965.
7. Sarver DM, Johnston MW: Skeletal changes in vertical and anterior displacement of the maxilla with bonded rapid palatal expansion appliances, Am J Orthod Dentofacial Orthop 95:462-466, 1989.
8. Vanarsdall RL, Corn H: Soft-tissue management of labially positioned unerupted teeth, Am J Orthod 72:53-64, 1977.
9. Sandler JP: An attractive solution to unerupted teeth, Am J Orthod Dentofacial Orthop 100:489-493, 1991.
10. Vardimon AD, Graber TM, Drescher D, Bourauel C: Rare earth magnets and impaction, Am J Orthod Dentofacial Orthop 100:494-512, 1991.
11. Edwards JG: The diastema, the frenum, the frenectomy: a clinical study, Am J Orthod 71:489-508, 1977.
12. Mulligan TF: Common sense mechanics. VI. Clinical application of the diving board concept, J Clin Orthod 14:98-103, 1980.
13. Ricketts RW, et al: Bioprogressive therapy, Denver, 1979, Rocky Mountain Orthodontics.
14. Burstone CJ: Deep overbite correction by intrusion, Am J Orthod 72:1-22, 1977.

ClearCorrect Exhibit 1002, Page 1885 of 3373

Chapter 16

The Second Stage of Comprehensive Treatment: Correction of Molar Relationship and Space Closure

Correction of molar relationship
- Correction of molar relationship by differential growth
- Differential anteroposterior tooth movement, using extraction spaces
- Molar correction with interarch elastics

Closure of extraction spaces
- Moderate anchorage situations
- Maximum incisor retraction (maximum anchorage)
- Minimum incisor retraction

At the beginning of the second stage of treatment, the teeth should be well aligned, and any excessive or reverse curve of Spee should have been eliminated. The objectives of this stage of treatment are to correct molar and buccal segment relationships to provide normal occlusion in the anteroposterior plane of space, and to close extraction spaces or residual spaces in the arches.

Correction of Molar Relationship

Correction of the molar relationship nearly always involves moving from a Class II or partially Class II relationship to Class I, although occasionally the treatment will be aimed at a Class III problem. Excluding surgical repositioning of the jaws, which is especially likely to be required in Class III correction, there are three major possibilities for correcting the molar relationship: (1) differential growth of the jaws, guided by extraoral force or a functional appliance, (2) differential anteroposterior movement of the upper and lower posterior teeth as extraction spaces are closed, and (3) differential anteroposterior movement of all the teeth under the influence of Class II or Class III elastics. These approaches are not mutually exclusive, and in fact some combination of the three is almost always used in the treatment of an individual patient.

■ Correction of Molar Relationship by Differential Growth

The use of extraoral force or functional appliances to influence jaw growth is discussed in some detail in Chapter 14. The different timing of skeletal growth in males and females must be kept in mind when this approach is used. During adolescence, the mandible tends to grow forward more than the maxilla, providing an opportunity to improve a skeletal Class II jaw relationship. Girls mature considerably earlier than boys, and are often beyond the peak of the adolescent growth spurt before the full permanent dentition is available and comprehensive orthodontic treatment can begin. Boys, who mature more slowly and have a more prolonged period of adolescent growth, are much more likely to have a clinically useful amount of anteroposterior growth during comprehensive treatment.

Whether extraoral force or a functional appliance is used to modify growth in Class II patients, a favorable response includes both restraint of maxillary growth and differential mandibular growth. Extraoral force is more compatible with the fixed appliances needed for comprehensive treatment than are functional appliances, and functional appliance therapy alone is unlikely to provide a satisfactory result in the early permanent dentition. In skeletally immature patients with a permanent dentition, there is nothing wrong with using a first phase of functional appliance treatment even though the permanent teeth have erupted, and then using a fixed appliance to obtain detailed occlusal results, but it is likely that the functional appliance therapy will have to be modified or discontinued when the fixed appliance treatment begins. Headgear therapy can be continued quite nicely.

An ideal patient for use of extraoral force in the early permanent dentition is a 12- to 14-year-old boy with a Class II problem, whose skeletal maturity is somewhat behind his stage of dental development, and who has good growth potential (Fig. 16-1). Boys at age 13, it must be remembered, are on the average at the same stage of maturation as girls at 11, and significant skeletal growth is almost always continuing. On the other hand, girls at age 13 are, on the average, at the same developmental stage as boys at 15, and by this time, clinically useful changes in jaw relationship from growth guidance are unlikely.

Although correction of molar relationship is a major goal of the second rather than the first stage of treatment, extraoral force should be applied against the first molars from the beginning in any patient for whom molar correction by differential growth is desired. There is no reason to wait for alignment and leveling to be completed, especially since every passing day decreases the probability of a favorable growth response. The extraoral force can also help control anchorage during alignment.

ClearCorrect Exhibit 1002, Page 1886 of 3373

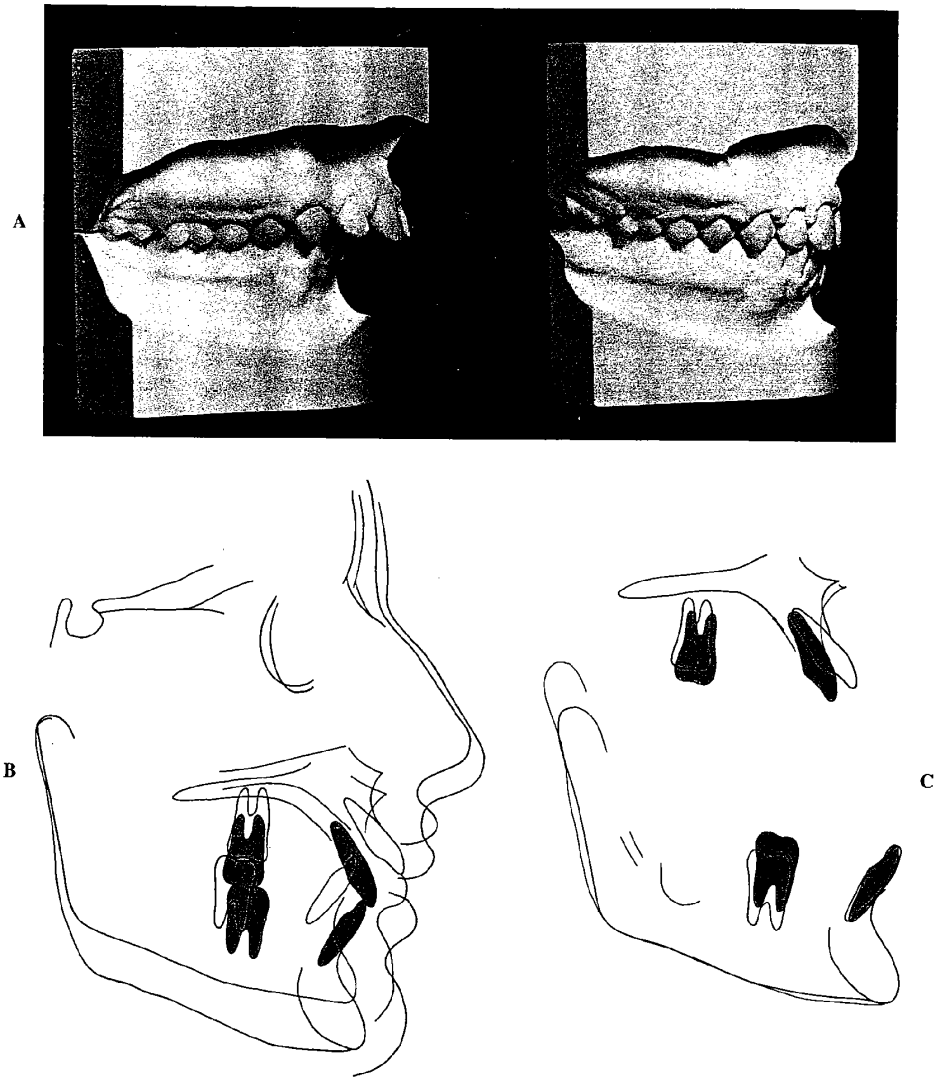


Fig. 16-1 ■ Class II correction in a 13 year-old boy, using extraoral force to the maxilla. **A,** Dental casts before and after treatment; **B** and **C,** cephalometric superimposition showing treatment changes. Note the large amount of vertical growth, which allowed the maxilla and maxillary dentition to be displaced distally as they moved vertically, while the mandible grew downward and forward. As the maxillary and mandibular superimpositions show, overbite was corrected by relative intrusion (i.e., the lower incisors were held at the same vertical level while the molars erupted). There was relatively more eruption of the mandibular than the maxillary molar, reflecting the upward-backward direction of headgear force, and only a small amount of distal driving of the upper molars.

ClearCorrect Exhibit 1002, Page 1887 of 3373

Although the main purpose of extraoral force is growth modification, some tooth movement in all three planes of space inevitably accompanies it. When there is good vertical growth and the maxillary molars are allowed to elongate, the maxillary teeth erupt downward and backward, and spaces may open up in the maxillary arch. Even though the extraoral force is applied against the first molar, it is unusual for space to develop between the first molar and second premolar. Instead, the second and to a lesser degree, the first premolars follow the molars. The result is often a space distal to the canines, along with a partial reduction of overjet as the jaw relationship improves (Fig. 16-2).

When this result occurs, the preferred approach is to consolidate space within the maxillary arch at a single location, using elastomeric chains to bring the canines and incisors into an anterior segment and the molar and premolars into a posterior segment. When the molar relationship has been corrected, the residual overjet is then reduced by retracting the incisors in this nonextraction patient in exactly the same way as in a patient who had a first premolar extraction space (see following). Extraoral force should be continued until an intact maxillary arch has been achieved. Discontinuing it when only the molar relationship has been corrected is unwise, both because the maximum skeletal effect probably has not been obtained at that point, and because the retraction of the incisor teeth requires posterior anchorage, which can be reinforced by the headgear.

■ Differential Anteroposterior Tooth Movement, Using Extraction Spaces

There are two reasons for extracting teeth in orthodontics, as discussed in detail in Chapter 7: (1) to provide space to align crowded incisors without creating excessive protrusion, and (2) to allow camouflage of moderate Class II or Class III jaw relationships when correction by growth modification is not possible. The more extraction space required for alignment, the less there is available for differential movement in camouflage, and vice versa. An important part of treatment planning is deciding which teeth to extract and how the extraction spaces are to be closed (by retraction of incisor teeth, mesial movement of posterior teeth, or some combination). These decisions determine the orthodontic mechanics.

In this section, it will be assumed that appropriate treatment planning decisions have been made, and the orthodontic mechanotherapy necessary to produce different types of tooth movement for molar correction will be described.

Class II Correction by Distal Movement of Maxillary Posterior Teeth: Upper Second Molar Extraction. The concept of "distal driving" of the maxillary posterior teeth has a long orthodontic history. Despite the belief of many practitioners that their usual correction of a Class II molar relationship was obtained by moving the upper molars back, the early cephalometric studies showed that this was not the case. It is now clear that significant distal positioning of the upper posterior teeth relative to the maxilla occurs primarily in patients who have a great deal of vertical growth and elongation of the maxillary teeth (see Fig. 16-1). Without this, it is difficult to produce more than 2 mm of distal movement of the upper molars, unless the upper second molars are extracted. With second molar extraction and good headgear cooperation, the maxillary dental arch can be moved posteriorly even in the absence of growth (Fig. 16-3), but still to only a limited extent.

There are numerous illustrations in the orthodontic literature of Class II malocclusion corrected by using an intraoral appliance to push the upper molars distally, and



Fig. 16-2 ■ Space tends to open up within the maxillary arch when extraoral force to the upper first molars is used and the patient grows well. **A,** Occlusal view before treatment; **B,** same patient after 12 months of treatment with only a headgear. **C,** In patients with Class II malocclusion, the upper molars usually are rotated mesially, and part of the apparent backward movement of the first molar is a distal rotation of the buccal cusps as the tooth rotates around its lingual root. This type of rotation can be produced by a facebow or by a transpalatal lingual arch. In **B,** note the spacing in the premolar area, as gingival fibers produce distal rotation of these teeth also. When a complete fixed appliance is placed at this stage, one of the first steps is consolidation of the space distal to the canines.

ClearCorrect Exhibit 1002, Page 1888 of 3373

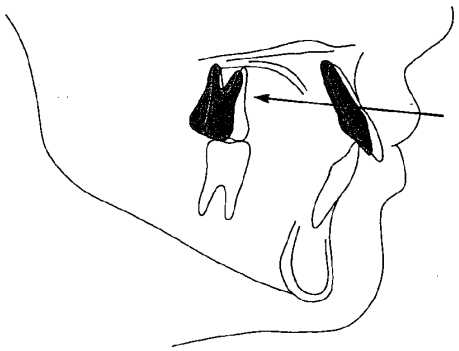


Fig. 16-3 ■ After extraction of maxillary second molars, extraoral force can successfully move the maxillary dentition posteriorly, as this cephalometric superimposition shows. To achieve this effect, extraoral force must be applied nearly full time, to promote efficient tooth movement. The effective limit of movement of this type is 4 to 5 mm. (Retraced from Armstrong MM: Am J Orthod 59:217-243, 1971.)

then retracting the teeth anterior to them. In patients with mild to moderate skeletal Class II malocclusion, the upper molars are likely to have rotated mesially around the lingual root (see Fig. 16-2, *C*), and merely correcting the rotations improves the occlusal relationships. This can be done with a transpalatal lingual arch, an auxiliary labial arch, or the inner bow of a facebow. Sometimes upper molars are so mesially rotated that it is difficult or impossible to insert a facebow until the rotation has been partially corrected with a more flexible appliance. It is an important concept, however, that beyond the rotation correction, significant distal movement of the molars (in the absence of second molar extraction) requires vertical growth. This means that treatment based on distal driving of the molars is less and less likely to succeed as patients become more and more mature.

Extraction of upper second molars to camouflage a skeletal Class II relationship should be considered only when specific indications are present (see Chapter 8). The key to success is a force system that moves the first molars and then the other teeth back, without reciprocal protrusion of the anterior teeth. Extraoral force is an obvious choice in terms of anchorage control, and with this approach, headgear force of moderate intensity with long duration is

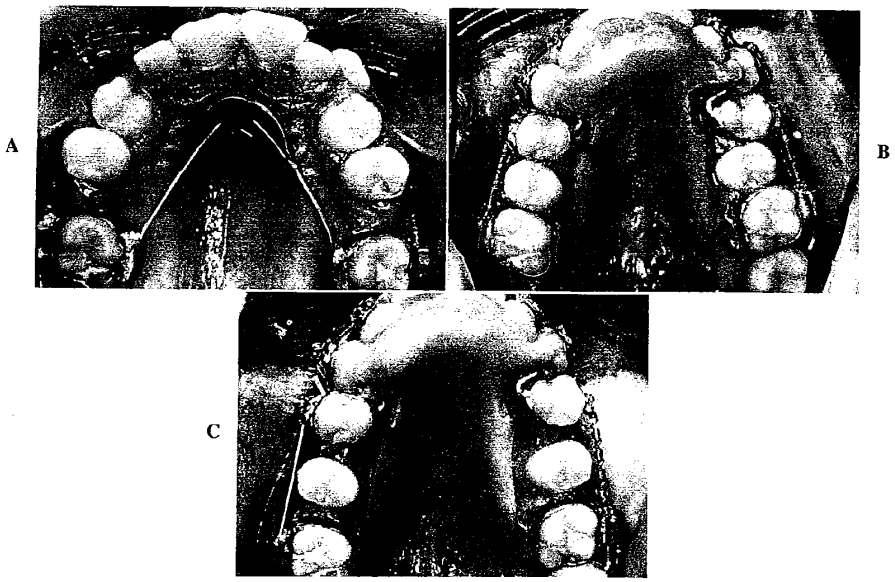


Fig. 16-4 ■ **A**, Maxillary stabilizing lingual arch with palatal button (often called a Nance holding arch), in a patient whose upper molars were tipped distally in a preliminary phase of treatment; **B** and **C**, The stabilizing lingual arch placed across the first premolars incorporates acrylic against the palatal mucosa and also an anterior bite plate, in a patient in whom NiTi coil springs are being used to move the molars distally and gain arch length. (**B** and **C**, Courtesy Dr. A Gianelly.)

ClearCorrect Exhibit 1002, Page 1889 of 3373

needed. Skeletal effects in rapidly growing patients can be achieved with fewer hours per day of headgear wear than are necessary to successfully move teeth. The patient must wear the headgear full time or nearly so to move the maxillary teeth posteriorly. The force magnitude should be large enough to simultaneously reposition all the maxillary teeth, which means that with an archwire tying the teeth together, the force should be approximately 300 gm on each side.

Using the anterior palate for anchorage also is a possibility, and both removable appliances and lingual arches with a button against the anterior palate have been used for this purpose (Fig. 16-4). With a lingual arch and palatal button, A-NiTi coil springs produce an effective and nearly constant force system for the distal movement.[1] Magnets in repulsion also can be used, but the magnetic force decays rapidly as the magnets separate, and the A-NiTi springs have the additional advantage of being less bulky. Contacting the palatal tissue has the potential to cause significant irritation, however, and this type of anchorage is recommended only when cooperation is totally lacking and a commitment to the second molar extraction plan has already been made.

Force from Class II elastics also can be used to position the upper molars distally, but there are two potential problems. First, the elastics have an extrusive component, which means that they should not be used in patients who will not have some vertical growth during the period of treatment. Second, if an intact lower arch is pitted against an intact upper arch, even with upper second molars extracted, there will be considerably more mesial movement of the lower teeth than distal movement of the upper teeth (Fig. 16-5). For this reason, if Class II elastics are used to drive upper molars distally, it is preferable at first to apply the elastic force against the first molars alone, via sliding jigs as illustrated in Fig. 16-6. The upper archwire is reduced in size posteriorly to allow freer sliding, the lower arch is stabilized with a full dimension rectangular archwire, and the force of the elastics is reduced to about 100 gm (3 to 4 oz). This procedure is important not only to impede forward tipping of the mandibular teeth but also to maintain transverse control of the lower arch. Class II elastics tend to widen the lower molars to the point that they can produce a molar crossbite. A heavy rectangular archwire, slightly constricted across the molars, is needed to prevent this complication.

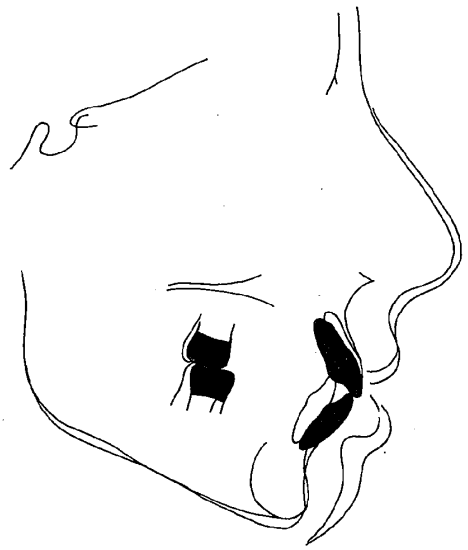


Fig. 16-5 ■ Cephalometric superimposition showing the response to Class II elastics in a girl in whom this was the major method for correcting a Class II malocclusion. Note that with rectangular archwires, some torque of the upper incisors was obtained. The rotational effects often associated with Class II elastics were less apparent for this patient than is sometimes the case (see also Fig. 16-13), but the considerably greater forward displacement of the lower arch than retraction of the upper is typical.

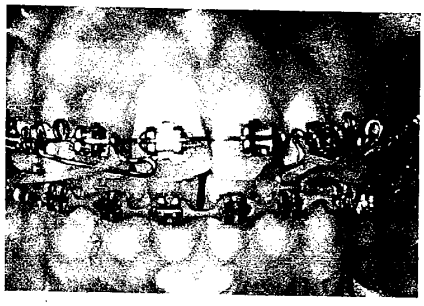
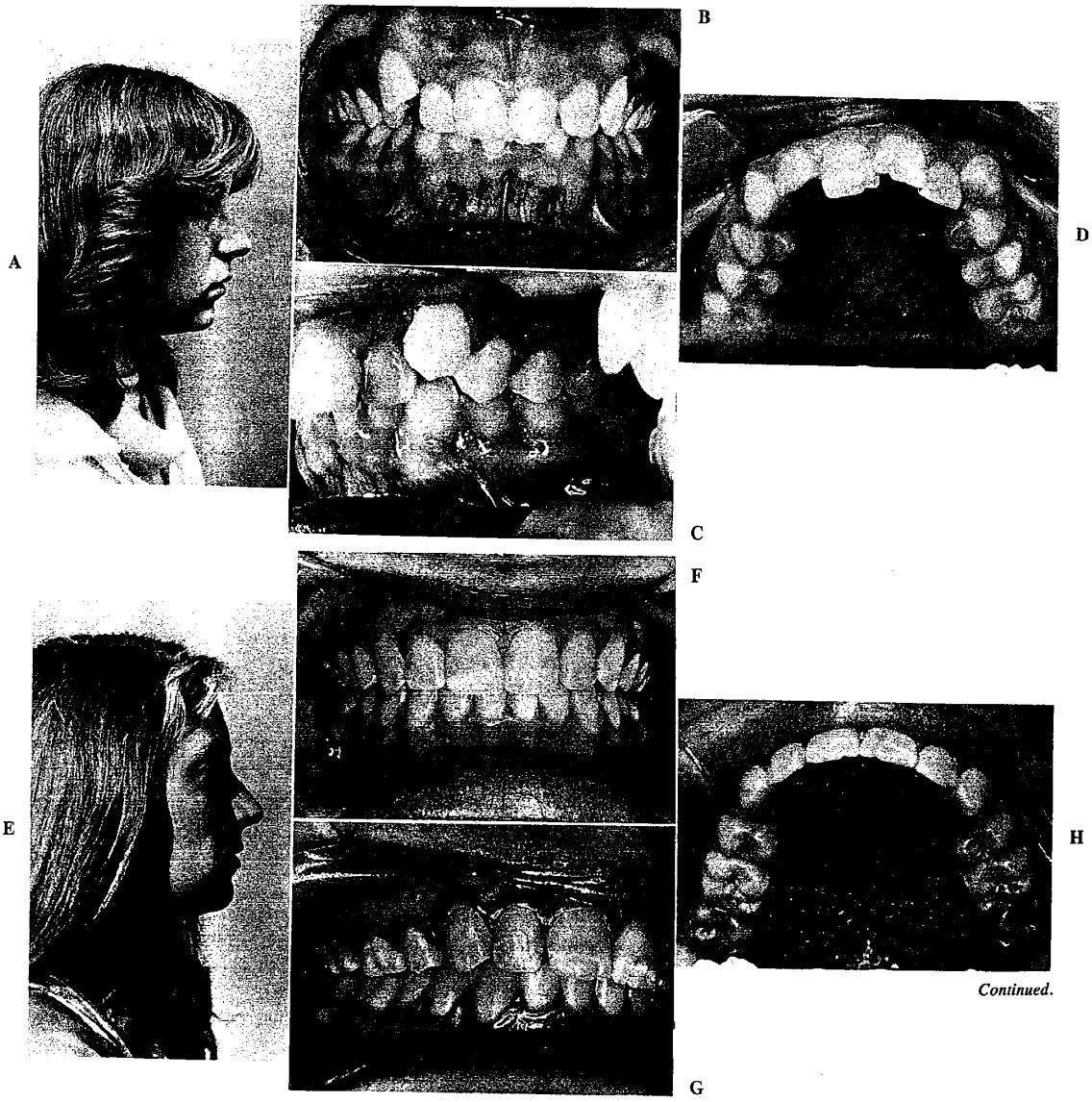


Fig. 16-6 ■ A "sliding jig" as illustrated here can be used to transfer Class II elastic force to the posterior segment of the maxillary arch. Rather than attaching to the maxillary archwire or anterior teeth, the elastic is hooked to the front part of the jig, which contacts the mesial surface of the first molar. In typical use, a jig later is shortened to apply the Class II force to the second premolar.

Once the upper molar has been moved distally into a correct relationship, the jig is altered and force applied against the second premolars. As a final step, Class II elastic force is continued as the space between the first and second premolars is closed. With this approach, the elastic force against the lower arch should not exceed 100 gm per side. Even though this force is distributed over all the lower teeth, some mesial movement of the lower arch is an inevitable side effect.

Class II Camouflage by Extraction of Upper First Premolars. Like upper second molar extraction, extraction of upper first premolars is a deceptively attractive solution to Class II problems and should be adopted only

ClearCorrect Exhibit 1002, Page 1890 of 3373



Continued.

Fig. 16-7 ■ Records of a patient who was treated with extraction of upper first premolars for camouflage of a Class II malocclusion. **A,** Pretreatment profile photograph; **B** to **D,** pretreatment intraoral photographs; **E,** posttreatment profile; **F** to **H,** posttreatment intraoral photograph; **I,** cephalometric superimposition. For this patient, retraction of the maxillary incisors was accomplished with good anchorage control, the esthetic change was quite acceptable, and jaw function was normal.

ClearCorrect Exhibit 1002, Page 1891 of 3373

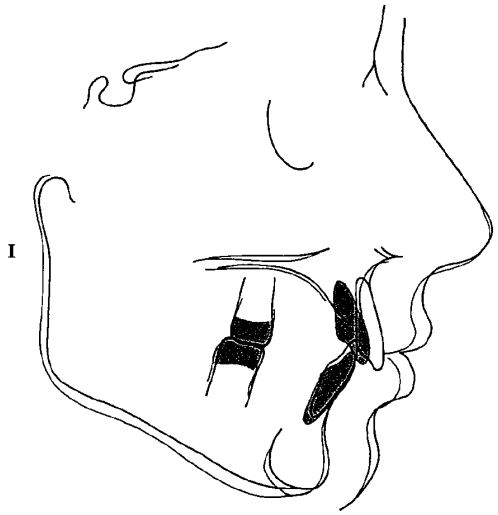


Fig. 16-7—cont'd. ■ For legend see opposite page.

when its specific indications exist (Chapter 8). With this approach, the objective during orthodontic treatment is to maintain the existing Class II molar relationship, closing the first premolar extraction space entirely by retracting the protruding incisor teeth (Fig. 16-7). Maxillary posterior anchorage must be reinforced, but one method, Class II elastics from the lower arch, is specifically contraindicated. The remaining possibilities are extraoral force to the first molars, a stabilizing lingual arch, or retraction of the maxillary anterior segment with extraoral force directly against these teeth.

If retraction springs or closing loops between the maxillary anterior and posterior segments are used, reinforcing the posterior anchorage with both a lingual arch and extraoral force is possible and usually desirable. The advantage of retracting the anterior teeth with springs is that an optimum force system can be placed against the anterior teeth; the disadvantage is that this force system will also tend to displace the maxillary posterior teeth forward.

Excellent reinforcement of posterior anchorage can be obtained with extraoral force, if it is applied consistently and for long durations. The more constant the headgear wear, the less a stabilizing lingual arch will be needed. Conversely, a stabilizing lingual arch augments the posterior anchorage full time, while headgear is likely to be worn a good bit less.

It seems intuitively obvious that a lingual arch with a button against the palatal tissue should be more effective than a straight transpalatal lingual arch, but when first molars are being stabilized, this is not necessarily true. The effect of the lingual arch is primarily to prevent the molars from rotating mesiolingually around their palatal root, and secondarily to prevent them from tipping mesially. A straight transpalatal lingual arch (see Fig. 15-16), however, is as effective as one with a palatal button in preventing rotation, and for most patients, the marginally better stabilization with a palatal button is not worth the cost in tissue irritation. Note that this is true when a lingual arch is used to stabilize molars, but not true when the lingual arch is to stabilize premolars, as in the second molar extraction situation discussed above. When pulled mesially, premolars tip more than they rotate, and a palatal button is needed on a lingual arch to stabilize them.

In addition to headgear and/or lingual arch stabilization, all the strategies described in Chapter 10 for reducing strain on anchorage (avoiding friction, retracting canines individually, etc.) are appropriate with upper first premolar extraction and can be brought into use.

Retracting protruding maxillary anterior teeth with extraoral force (Fig. 16-8) totally avoids strain on the posterior teeth and is extremely attractive from that point of view.[2] This technique has two major disadvantages: (1) The force system applied to the anterior teeth is far from ideal. When extraoral force is applied directly to the anterior segment, it is difficult to keep it from being undesirably heavy, but the force intermittently falls to zero when the headgear is removed. (2) There is significant friction, not only where teeth slide along the archwire but also within the headgear mechanism itself. This makes it difficult to control the amount of force, and more friction on one side than the other may lead to an asymmetric response. In fact, it is unusual if space does not close faster on one side than the other.

Excellent patient cooperation is essential. Only if the headgear is worn nearly full time will efficient tooth movement be obtained, and although it is possible to obtain this level of cooperation, it is unwise to rely on it routinely. Patients for this approach should be selected carefully.

In the late 1980s, it was claimed by some dentists that extraction of upper first premolars would lead to later temporomandibular dysfunction problems. The claim was never supported by any evidence, and recent research data have refuted it.[3] It is important to limit first premolar extraction for camouflage of Class II malocclusion to the appropriate patients, but if this is done, it can be an excellent treatment method.

Extraction of Maxillary and Mandibular Premolars. Correction of Class II buccal segment relationships with extraction of all four first premolars implies that the mandibular posterior segments will be moved anteriorly nearly the width of the extraction space. At the same time, the protruding maxillary anterior teeth will be retracted without forward movement of the maxillary buccal segments. This, in turn, implies (though it does not absolutely require) that Class II elastics will be used to assist in closing the extraction sites.

The Begg technique is a classic illustration of the use of Class II elastics to produce differential movement of the arch segments while correcting the molar relationship. In

ClearCorrect Exhibit 1002, Page 1892 of 3373

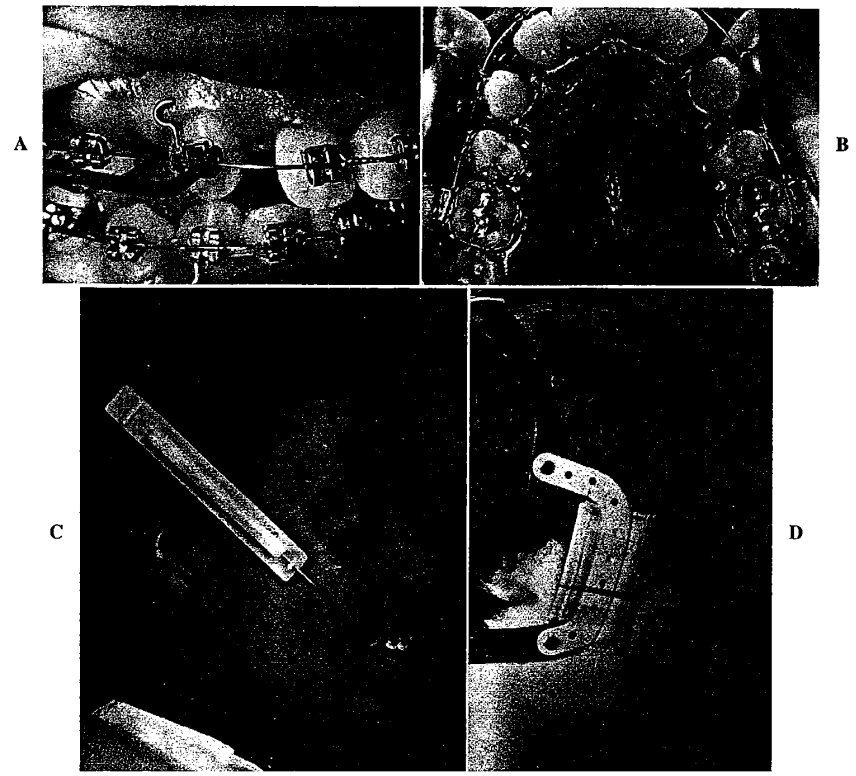


Fig. 16-8 ■ Retraction of the maxillary canines with a J-hook headgear. **A,** The headgear hooks over the archwire mesial to the canine bracket and pushes distally against the bracket. Approximately 200 gm of force on each side should be used; **B,** an occlusal view shows the distal translation of both canines. Note that the response at this stage is greater on one side than the other, which is not uncommon with headgear applied directly to the archwire for tooth movement; **C,** high-pull head cap with J-hooks for canine retraction; **D,** an alternative headcap, providing a more directly posterior force.

the Begg approach, at the beginning of the second stage of treatment, light interarch elastics are added to help close space, while Class II elastics are continued (Fig. 16-9). An anchor bend is placed in the upper archwire so that the maxillary anterior teeth are tipped back in part by the force system associated with the archwire itself (see Fig. 15-30).

In the lower arch, the anchor bend is used to control the amount of mesial tipping of the molars. The Class II elastics reinforce and accentuate the differential tooth movements along the archwires (Fig. 16-10). Friction as the archwires slide through the molar tubes during space closure is minimized by the considerable freedom between the 16 mil base arch and the 25 mil round tube through which it slides. It is extremely important that only light forces be used, so that optimum force levels are reached where tipping is desired while forces for bodily movement remain suboptimum.

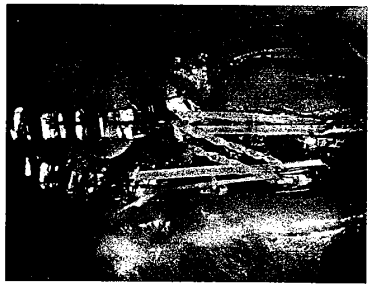


Fig. 16-9 ■ The second stage of Begg treatment, in which intra-arch elastics are used simultaneously with Class II elastics for space closure and correction of molar relationship. This pattern of elastic force is continued until the extraction spaces are closed. The effect is to trade forward movement of the mandibular posterior teeth for retraction of the maxillary anteriors.

ClearCorrect Exhibit 1002, Page 1893 of 3373

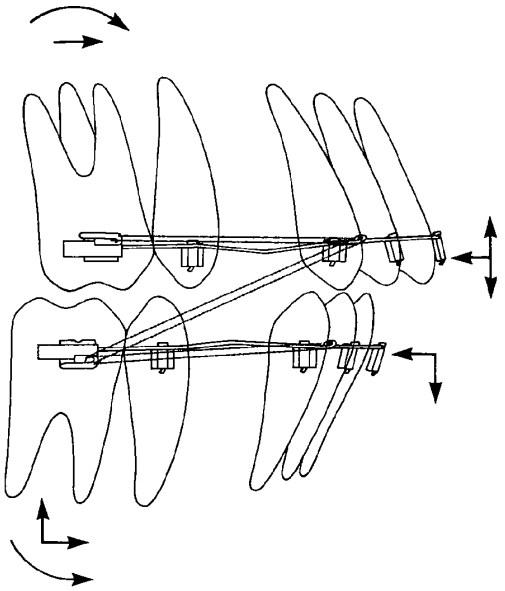


Fig. 16-10 ■ Diagrammatic representation of forces encountered in the second stage of Begg treatment, in which base archwires *(red)* with anchor bends are combined with intra-arch and Class II elastics *(pink)*. The anchor bends produce bodily forward movement of the molars and allow lingual tipping of the incisors, which receive no moments. These bends also depress the incisors and elongate the molars, which is counteracted by the Class II elastics for the upper arch but accentuated by the elastics for the lower.

A similar mechanical arrangement, of course, can be produced with the edgewise appliance. A round wire in an edgewise bracket allows tipping of the incisors in essentially the same way as with the Begg approach, but the mesiodistal width of the canine brackets tends to keep the canine teeth more upright, thereby increasing the strain on posterior anchorage. For this reason, when a Begg-like sliding space closure in both arches is used with the edgewise appliance, reinforcement of maxillary anchorage with headgear is a good idea, and somewhat heavier Class II elastic force is needed.

It is also possible with the edgewise appliance to structure anchorage so that space closure by retraction of the maxillary anterior teeth and protraction of the mandibular posterior segments occurs without the use of Class II elastics. The best control is achieved with segmented arch technique, using space-closing springs in each arch fabricated specifically for the type of space closure desired (see Closure of Extraction Spaces, this chapter).

When differential space closure without interarch elastics is desired, a more common approach with the edgewise appliance is to extract maxillary first but mandibular second premolars, thus altering the anchorage value of the two segments (Fig. 16-11). With this approach, routine space-closing mechanics will move the lower molars forward more than the upper, particularly if maxillary posterior anchorage is reinforced with a stabilizing lingual arch or headgear. This upper first-lower second premolar extraction pattern greatly simplifies the mechanics needed for differential space closure with continuous-arch edgewise technique.

■ Molar Correction with Interarch Elastics

Molar correction with Class II elastics, without extraction spaces as previously described, is produced largely by mesial movement of the mandibular arch, with a small amount of distal positioning of the maxillary arch. The amount of force varies with the amount of tipping allowed in the mandibular arch. Unless tipping is desired, which is rarely the case, Class II elastics should be used only with a well-fitting rectangular wire in the lower arch that is somewhat constricted posteriorly. Large amounts of force must be used (approximately 300 gm per side) to displace one arch relative to the other when both are stabilized with rectangular wires in edgewise brackets. Incorporating the lower second molars in the appliance and attaching the elastics to a mesial hook on this tooth increase the anchorage and give a more horizontal direction of pull than hooking the elastic to the first molar.

It is important to keep in mind that with or without extraction, Class II elastics produce not only anteroposterior and transverse effects but also a vertical force (Fig. 16-12). This force elongates the mandibular molars and the maxillary incisors, rotating the occlusal plane up posteriorly and down anteriorly. If the molars extrude more than the ramus grows vertically, the mandible itself will be rotated downward (see Fig. 16-11). Class II elastics are therefore contraindicated in nongrowing patients who cannot tolerate some downward and backward rotation of the mandible. The rotation of the occlusal plane, in and of itself, facilitates the desired correction of the posterior occlusion (Fig. 16-13), but even if elongation of the lower molars can be tolerated because of good growth, the corresponding extrusion of the maxillary incisors can be unsightly.

Class II elastics, in short, may produce occlusal relationships that look good on dental casts but are less satisfactory when viewed from the perspective of skeletal relationships and facial esthetics (see Fig. 16-5).

Because of their vertical effects, prolonged use of Class II elastics, particularly with heavy forces, is rarely indicated. Using Class II elastics for 3 or 4 months at the completion of treatment of a Class II patient, to obtain good posterior interdigitation, is often acceptable. Applying heavy Class II force for 9 to 12 months as the major method for correcting a Class II malocclusion is rarely good treatment.

Class III elastics also have a significant extrusive component, tending to elongate the upper molars and the lower

ClearCorrect Exhibit 1002, Page 1894 of 3373



Fig. 16-11 ■ Cephalometric superimposition showing the result of treatment with extraction of upper first and lower second premolars. Even with second premolar extraction, some retraction of the mandibular incisors may occur, but most of the space closure will be by mesial movement of the lower molar. This adult patient experienced no growth, and a slight downward and backward rotation of the mandible occurred.

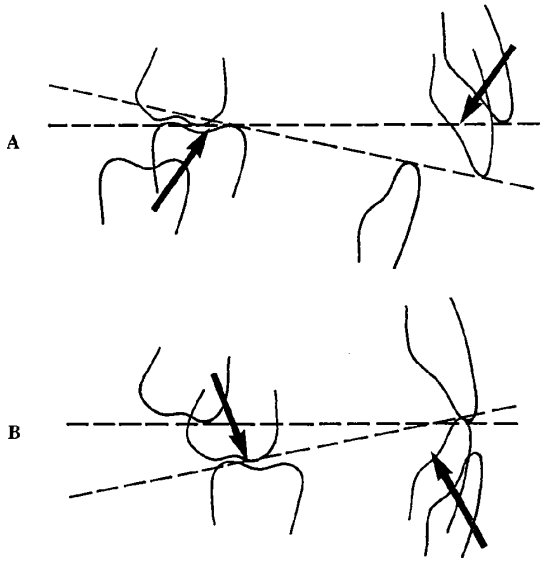


Fig. 16-12 ■ Rotation of the occlusal plane with Class II (**A**) and Class III (**B**) elastics. The rotational pattern helps correct the molar relationship and so is helpful from that point of view, but it can be deleterious in some patients because the elongation of the molars may cause undesirable rotation of the mandible or undesirable tooth-lip relationships.

ClearCorrect Exhibit 1002, Page 1895 of 3373

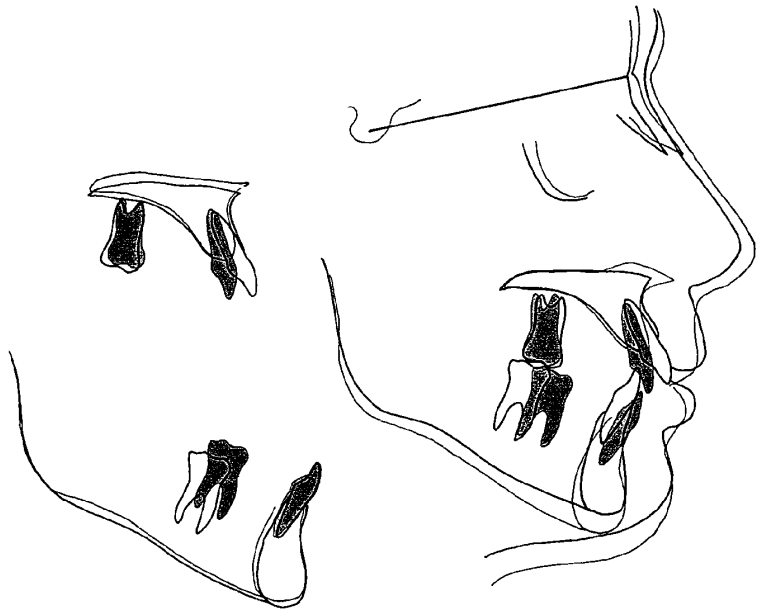


Fig 16-13 ■ Cephalometric superimposition showing the vertical effects of Class II elastics in this patient, who had premolar extractions and so did not have forward movement of the lower incisors despite the forward movement of the lower molars. Note the elevation of the lower molar, extrusion and distal tipping of the upper incisor, rotation of the occlusal plane, and downward and backward rotation of the mandible.

incisors. Elongating the molars enough to rotate the mandible downward and backward is disastrous in Class II treatment, but within limits can help treatment of a Class III problem. If it is desired to use Class III elastics to assist in retracting mandibular incisors (see further discussion following), high-pull headgear to the upper molars worn simultaneously with the elastics can control the amount of elongation of the upper molars. Elongation of the lower incisors, however, still can be anticipated.

Closure of Extraction Spaces

To obtain the desired result in closing spaces within the arch, it is essential to control the amount of incisor retraction versus molar-premolar protraction. Indications for extraction have been discussed in Chapters 6 and 7, and the biomechanical concepts related to control of posterior anchorage and the amount of incisor retraction are described in Chapter 10. In this section, the focus is on contemporary mechanotherapy for space closure with the 18- and 22-slot edgewise appliances.

■ Moderate Anchorage Situations

Most patients fall into the moderate anchorage category, meaning that after alignment of the incisors has been completed, it is desired to close the remainder of the premolar extraction space with a 50:50 or 60:40 ratio of anterior retraction to posterior protraction. The different wire sizes in 18- and 22-slot edgewise appliances require a different approach to mechanotherapy.

Moderate Anchorage Treatment with 18-Slot Edgewise: Closing Loops. Although either sliding or loop mechanics can be used, the 18-slot appliance with single or narrow twin brackets on canines and premolars is ideally suited for use of closing loops in continuous archwires. Appropriate closing loops in a continuous archwire will produce approximately 60:40 closure of the extraction space if only the second premolar and first molar are included in the anchorage unit and some uprighting of the incisors is allowed. Greater retraction will be obtained if the second molar is part of the anchorage unit, less if incisor torque is required.

The spring characteristics of a closing loop, a critical part of its design, are largely determined by two major factors: the size of the archwire, and the distance between points of attachment. This distance in turn is largely determined by the amount of wire incorporated into the loop, but is affected also by the distance between brackets. Closing loop archwires should be fabricated from rectangular wire to prevent the wire from rolling in the bracket slots. Closing loops with equivalent properties can be produced from different sizes of wire, by increasing the amount of wire incorporated into the loop as the size of the wire increases, and vice versa. Wires of smaller cross-sectional

ClearCorrect Exhibit 1002, Page 1896 of 3373

area allow the use of simpler loop designs. The first principle of closing loop design is that the simplest possible loop is preferred because more complex configurations are less comfortable for patients, more difficult to fabricate clinically, and more prone to breakage or distortion.

A second principle is that, to the greatest extent possible, the loop should "fail safe." This means that, although a reasonable range of action is desired from each activation, tooth movement should stop after a prescribed range of movement even if the patient does not return for a scheduled adjustment. Too long a range of action, with too much flexibility, could produce disastrous effects if a distorted spring were combined with a series of broken appointments. The ideal loop design therefore would deliver a continuous, controlled force designed to produce tooth movement at a rate of approximately 1 mm per month, but would not include more than 2 mm of range, so that movement would stop if the patient missed a second consecutive monthly appointment.

Fig. 16-14, taken from the work of Booth,[4] illustrates the effects on the spring characteristics of a steel closing loop from changing wire size, the design of the loop, and the interbracket span (the combination of these latter two parameters, of course, determines the amount of wire in the loop). Note that, as expected, changing the size of the wire produces the largest changes in characteristics but the amount of wire incorporated in the loop is also important.

For closure of a maxillary first premolar extraction space without tipping, pitting the canine and two incisors against the posterior segment, the ideal retraction force would be approximately 250 gm (100 gm for the canine, 75 gm each for the lateral and central incisors). Obviously, this force could vary depending on the size of the teeth and whether the incisors could be allowed to tip slightly or would require total bodily movement; usually it is somewhat less for mandibular space closure because the teeth are smaller and more tipping often can be allowed. A closing loop should produce this amount of force at about 1.5 mm activation and should retain a significant fraction of this force level at least down to 0.5 mm.

From Fig. 16-14, it can be seen that based on these criteria, most of the commonly used steel wires produce far too much force when a simple vertical loop is used. Even 17 × 25 mil wire is too stiff unless additional wire is incorporated, changing the configuration as shown in the lower right part of Fig. 16-14. A 10 mm vertical loop in 16 × 22 mil wire produces force characteristics that reasonably approximate those desired.

To close an extraction space while producing bodily tooth movement, a closing loop must generate not only a closing force, but also appropriate moments to bring the root apices together at the extraction site. As discussed in Chapter 10, a moment-to-force ratio of approximately 10:1 is needed, meaning that a canine tooth being retracted with a 100 gm force must also receive a 1000 gm-mm moment. If the bracket is 1 mm wide, a vertical force of 1000 gm

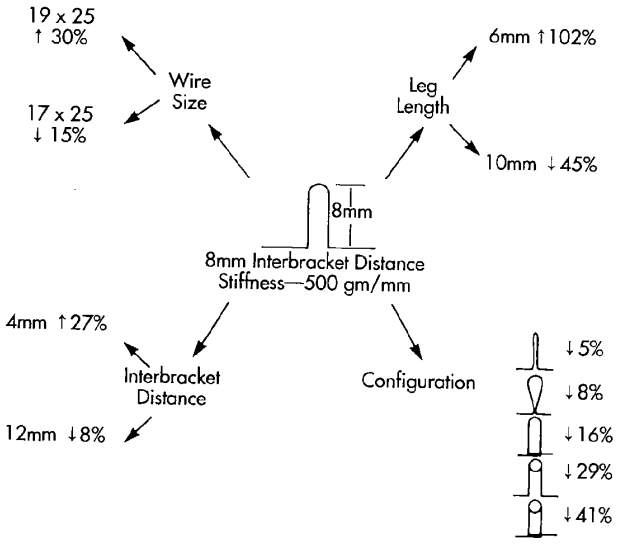


Fig. 16-14 ■ The effect of changing various aspects of a closing loop in an archwire. Note that an 8 mm vertical loop in 18 × 25 wire produces twice as much force as the desired 250 gm/mm. The major possibilities for producing clinically satisfactory loops are reducing wire size or incorporating additional wire by changing leg length, interbracket distance, and/or loop configuration (redrawn from Booth[3]).

ClearCorrect Exhibit 1002, Page 1897 of 3373

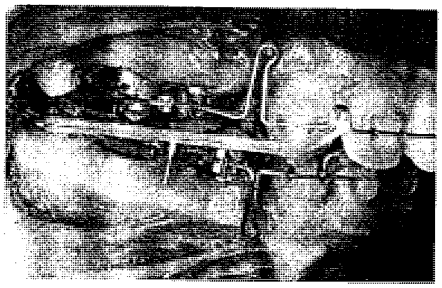


Fig. 16-15 ■ Eight millimeter closing loops in 16 × 22 wire used with Class II elastics in this patient. Note that the maxillary loop has been activated by pulling the wire through the maxillary tube and bending it up. In the mandibular arch, the loop is not active at this time, and the approximation of the legs to create a rigid archwire is apparent. The lower archwire has a tieback mesial to the first molar, so that this loop can be activated by tying a ligature from the posterior teeth to the wire rather than by bending over the end of the wire distal to the molar tube.

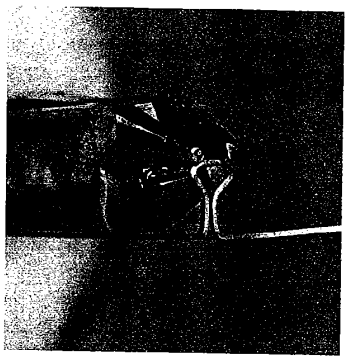


Fig. 16-16 ■ A three-prong plier can be used to bring the vertical legs of a closing loop together if they are separated. The legs should touch lightly before activation of the loop by opening it.

must be produced by the archwire at each side of the bracket.

This factor limits the amount of wire that can be incorporated to make a closing loop springier, because if the loop becomes too flexible, it will be unable to generate the necessary moments even though the retraction force characteristics are satisfactory. Loop design is also affected. Placing some of the wire within the closing loop in a horizontal rather than vertical direction improves its ability to deliver the moments needed to prevent tipping. Both because of this effect and because a vertically tall loop can impinge on soft tissue, using a closing loop only 7 mm tall while incorporating 10 to 12 mm of wire—a delta or T-shaped loop—is preferred.

All other factors being equal, a loop is more effective when it is closed rather than opened during its activation. On the other hand, a loop designed to be opened can be made so that when it closes completely, the vertical legs come into contact, effectively preventing further movement and producing the desired fail-safe effect (Fig. 16-15). A loop activated by closing, in contrast, must have its vertical legs overlap. This creates a transverse step, and the archwire does not develop the same rigidity when it is deactivated. The smaller and more flexible the wire from which a closing loop arch is made, the more important it is that the wire become rigid when the loop is deactivated.

These design considerations indicate that an excellent closing loop for 18-slot edgewise is a delta-shaped loop in 16 × 22 wire that is activated by opening. Such a wire fits tightly enough in an 18 × 25 mil bracket to give good control of root position. With 10 mm of wire in the loop, the force delivery is close to the optimum, and the mechanism fails safe because contact of the vertical legs when the loop is deactivated limits movement between adjustments and makes the archwire more rigid. It is important to activate the upper horizontal portion of a delta or T-loop so that the vertical legs are pressed lightly together when the loop is not activated (Fig. 16-16). This also ensures that the loop will still be active until the legs come into contact.

A second important adjustment of a closing loop archwire is placing a gable bend at the extraction site. This adjustment is necessary to generate the root-paralleling moments. With 16 × 22 wire and a loop of the delta design, a gable bend of approximately 20 degrees on each side is needed (Fig. 16-17). With the same loop in 17 × 25 wire, a smaller gable bend would generate the same moment. With a 16 × 22 closing loop, it is ordinarily necessary to remove the archwire and reactivate the gable bends after 3 to 4 mm of space closure, but is is not necessary to do this at each appointment.

A final factor in the design of a closing loop archwire is the location of the loop. Mechanically, it would be ideal to place the loop in the exact center of the extraction space, but a loop placed in the center of the initial extraction site becomes displaced distally as the space closes, and this is undesirable. The preferred location, therefore, is at the spot that will be the center of the embrasure when the space is closed (Fig. 16-18). This means that, in a first premolar extraction situation, the closing loop should be placed about 5 mm distal to the center of the canine tooth.

A closing loop archwire is activated by pulling the posterior part of the archwire distally through the molar tubes, which activates the closing loop the desired amount (1 to 1.5 mm), and then fastening the wire in that position. The wire slides through the brackets and tubes only when it is being activated. After that, as the closing loop returns to its original configuration, the teeth move with the archwire, not along it. There are two ways to hold the archwire in its activated position. The simplest is by bending the

ClearCorrect Exhibit 1002, Page 1898 of 3373

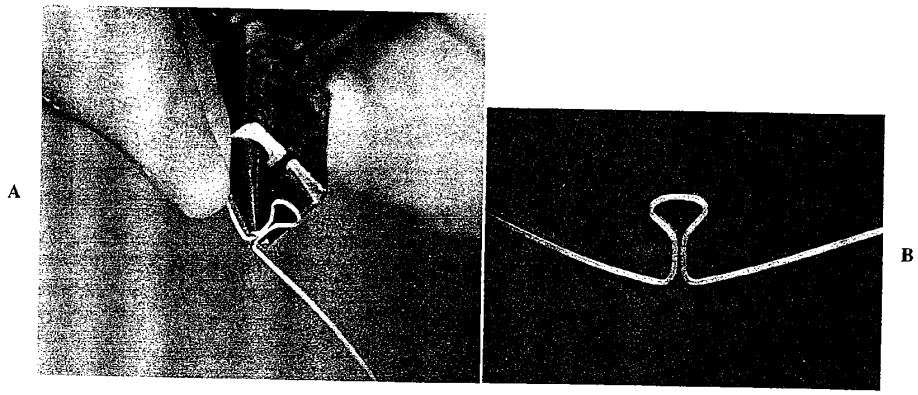


Fig. 16-17 ■ Gable bends for a closing loop archwire. **A,** Gable bends are placed by bending the wire at the base of the loop; **B,** appropriate gable for a 16 × 22 closing loop (40-45 degrees total, half that on each side).

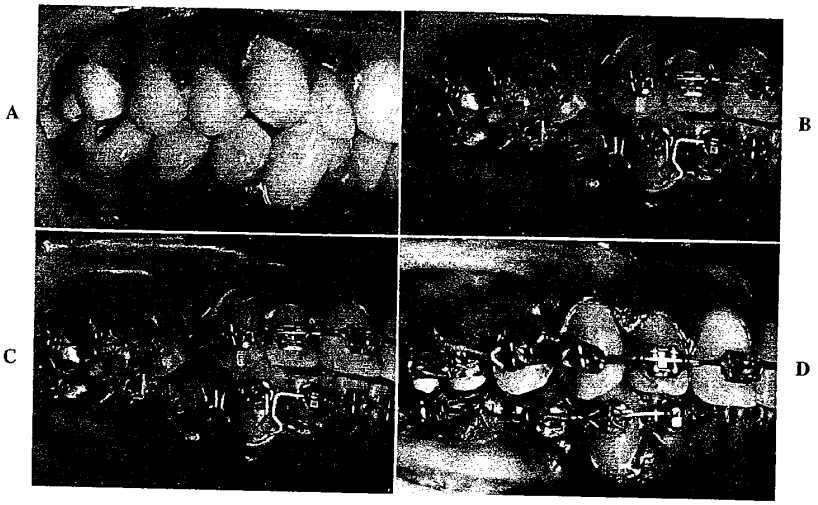


Fig. 16-18 ■ Stages in space closure for a specific patient. **A,** The original malocclusion; **B,** 16 × 22 closing loops at initial activation, after the completion of stage 1 alignment and leveling. Note the soldered tiebacks for activation. **C,** Closing loops later during space closure; **D,** spaces closed and finishing archwire in place.

ClearCorrect Exhibit 1002, Page 1899 of 3373

end of the archwire gingivally behind the last molar tube. The alternative is to place an attachment on the posterior part of the archwire, usually a soldered tieback as shown in Fig. 16-18, so that a ligature can be used to tie the wire in its activated position.

As a general rule, if it is anticipated that a closing loop archwire will not have to be removed for adjustment (the distance to be closed is 4 mm or less), bending the posterior end of the wire is satisfactory. It can be quite difficult to remove an archwire that has been activated by bending over the end, however, and it saves time in the long run to use tiebacks for closing loop archwires that will have to be removed and readjusted.

Specific recommendations for closing loop archwires with the 18-slot appliance and narrow brackets are:

1. 16 × 22 wire, delta or T-shaped loops, 7 mm vertical height, and additional wire incorporated in the loop to make it equivalent to 10 mm of vertical height
2. Gable bends of 40 to 45 degrees total (half on each side of the loop)
3. Loop placement 4 to 5 mm distal to the center of the canine tooth, at the center of the space between the canine and second premolar with the extraction site closed

These recommendations certainly are not the only clinically effective possibilities. The principle should be that if a heavier wire (17 × 25 mil, for instance) is used, the loop design should be altered to incorporate additional wire for better force-deflection characteristics. Also, the gable angulations should be adjusted according to both the springiness of the loop and the width of the brackets. With wide brackets on the canines, for instance, the reduced interbracket span would make any loop somewhat stiffer, and both this and the longer moment arm across the bracket would dictate a smaller gable angle (but the range of the loop would be reduced, which is why wide brackets are not recommended).

Moderate Anchorage Space Closure with 22-Slot Edgewise. As a general rule, space closure in moderate anchorage situations with the 22-slot edgewise appliance is done in two steps, first retracting the canines, usually sliding them along the archwire, and second, retracting the four incisors, usually with a closing loop. This two-step space closure will produce an approximately 60:40 closure of the extraction space, varying somewhat depending on whether second molars are included in posterior anchorage and incisor torque requirement.

A 19 × 25 wire is the largest on which sliding retraction of a canine should be attempted (because clearance in the bracket slot is needed), and 18 × 25 wire also can be used. An archwire with a posterior stop, usually in front of the first molar tube, is needed. This stop has the effect of incorporating all the teeth except the canine into the anchorage unit. The canine retraction can then be carried out with a coil spring, a spring soldered to the base archwire, an intra-arch latex elastic, or an elastomeric material (Fig. 16-19). As a general rule, A-NiTi coil springs are preferred because they produce an almost ideal light constant force.[5] Elastics produce variable and intermittent forces, and both elastomeric chains and steel coil springs produce rapidly decaying interrupted forces.

In addition to its convenience and straightforward design, this type of sliding space closure has the important advantage that it fails safe in two ways: (1) The moments necessary for root paralleling are generated automatically by the twin brackets normally used with the 22-slot appliance. Unless the archwire itself bends, there is no danger that the teeth will tip excessively. (2) The rigid attachment of the canine to the continuous ideal archwire removes the danger that this tooth will be moved far outside its intended path if the patient does not return for scheduled adjustments. For this reason, a long range of action on the retraction springs is not dangerous, as long as the force is not excessive. The ideal force to slide a canine distally is approximately 200 gm, about half of which is used to overcome friction (see Chapter 10). A-NiTi springs that produce this level of force over a wide enough range to close an extraction space with a single activation now are commercially available.

The second stage in the two-stage retraction is usually accomplished with a closing loop, although it is possible to close the space now located mesial to the canines by

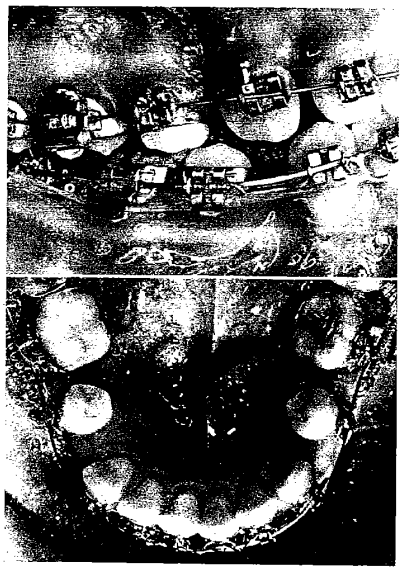


Fig. 16-19 ■ Sliding space closure in 22-slot edgewise. **A,** Elastomeric chain for canine retraction in the mandibular arch, sliding the tooth on an undersized rectangular archwire. **B,** NiTi coil springs for retraction of first premolars in a second premolar extraction case. NiTi springs give much better control of force levels and a much greater range of action, and therefore are preferred.

ClearCorrect Exhibit 1002, Page 1900 of 3373

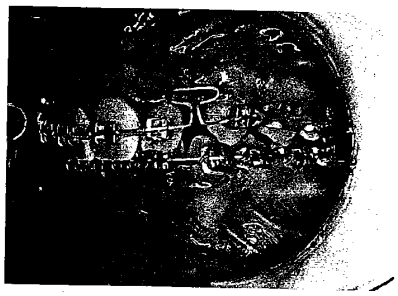


Fig. 16-20 ■ T-shaped loop in 18 × 25 wire, typically used with the 22-slot edgewise appliance to retract the four incisors after independent retraction of the canine.

again sliding the archwire through the posterior brackets. For this stage of incisor retraction, a rectangular wire with its smallest side at least 18 mil is needed—anything smaller rolls in the 22-slot and would allow the incisors to tip while being retracted. An 18 × 25 steel wire with a T-loop, though still too stiff, serves this purpose reasonably well while retaining the fail-safe design (Fig. 16-20). Although loops in a 19 × 25 steel wire also can be used, the better force-deflection characteristics of 18 × 25 wire make it the preferred choice: the 19 × 25 loop either has to give up the fail-safe design, or is much too stiff. A third alternative, in many ways now the preferred approach, is a closing loop in 19 × 25 beta-Ti wire. This provides better properties than 18 × 25 steel (quite close to 16 × 22 steel), at the cost of more difficulty in forming the archwire.

Although the two-step procedure is predictable and has excellent fail-safe characteristics, which explains why it remains commonly used, it takes longer to close space in two steps than one.

It is possible to use a closing loop archwire for one-step (en masse) closure in the 22-slot appliance, as described previously for 18-slot edgewise. In this case, an overlap design in 19 × 25 steel, a T-loop in 18 × 25 steel, or a fail-safe loop in 19 × 25 beta-Ti wire can be considered. The steel wires place a greater strain on anchorage than would be encountered with 18-slot and lighter wires, and all three of the possibilities provide less than ideal torque control during the retraction because they are so much smaller than the bracket slot. If en masse space closure is desired with the 22-slot appliance, a segmented arch technique offers advantages.

The segmented arch approach to space closure is based on incorporating the anterior teeth into a single segment, and both the right and left posterior teeth also into a single segment, with the two sides connected by a stabilizing lingual arch (Fig. 16-21). A retraction spring is used to connect these stable bases, and the activation of the spring is varied to produce the desired pattern of space closure (Figs. 16-22 and 16-23). Because the spring is separate from the wire sections that engage the bracket slots, a wire

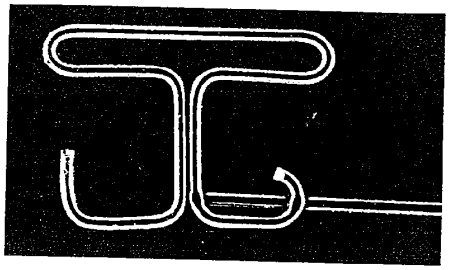


Fig. 16-22 ■ Composite retraction spring designed by Burstone for use with the segmented arch technique, consisting of 18 mil beta-Ti wire (the loop) welded to 17 × 25 beta-Ti. This spring can be used for either en masse retraction of incisors or canine retraction.

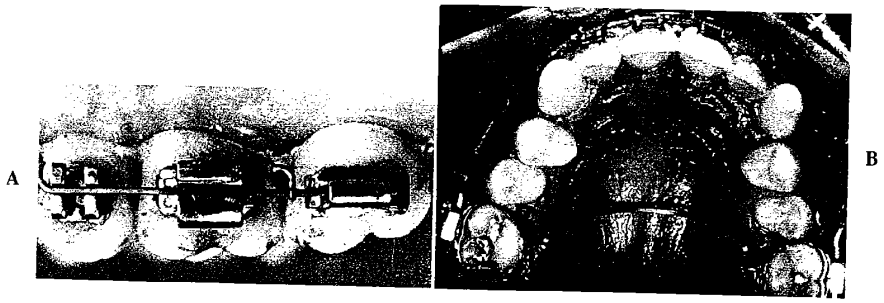


Fig. 16-21 ■ Stabilization of the posterior segments in Burstone's segmented arch technique requires **A,** a 21 × 25 steel wire segment in the bracket slots or tubes of the posterior teeth. Note the soldered tieback mesial to the second molar (courtesy Dr. CJ Burstone); and **B,** a heavy lingual arch. This current design by Burstone uses a rectangular 28 × 28 wire that is tied into a special lingual bracket on the first molars.

ClearCorrect Exhibit 1002, Page 1901 of 3373

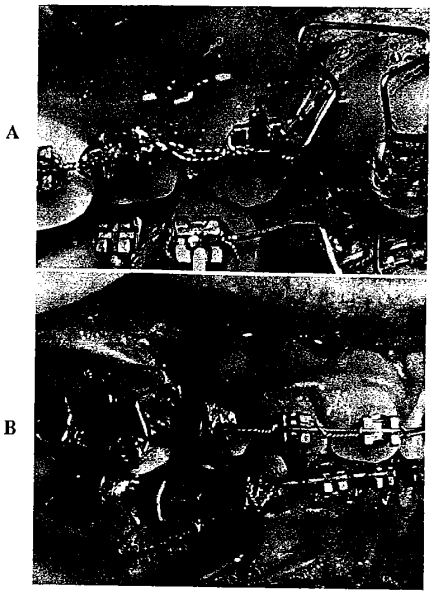


Fig. 16-23 ■ Space closure with the segmented arch technique. **A,** En masse retraction of the anterior maxillary segment and canine retraction in the mandibular arch (see also Fig. 16-29). Note that the retraction springs fit into a vertical tube on the canine bracket. Braided wire in the maxillary anterior area will be replaced by a stabilizing anterior segment. **B,** Upper and lower en masse space closure using beta-Ti T-loops between segments in this patient with extraction of upper first and lower second premolars. (Courtesy Dr. CJ Burstone.)

size and design that produce optimum properties can be used. An auxiliary rectangular tube, usually positioned vertically, is needed on the canine bracket or on the anterior wire segment to provide an attachment for the retraction springs (see Chapter 12). The posterior end of each spring fits into the auxiliary tube on the first molar tooth. With beta-Ti wire, the design of the retraction spring can be greatly simplified over the design necessary with steel wire (Fig. 16-23).[6] These springs are very effective, and with careful initial activation, an impressive range of movement can be produced before reactivation is necessary.

The greatest disadvantage of segmented arch space closure is not its increased complexity, but that it does not fail safe. Without a rigid connection between the anterior and posterior segments, there is nothing to maintain arch form and proper vertical relationships if a retraction spring is distorted or activated incorrectly. For this reason, despite the excellent results usually obtained with segmented arches and retraction springs, it is important to monitor these patients especially carefully and to avoid long intervals without observation.

■ Maximum Incisor Retraction (Maximum Anchorage)

It is not always desirable to retract the anterior teeth as far as possible after premolars have been extracted. In fact, over-retraction of incisors is as much of a potential problem as leaving them too prominent by not maintaining adequate posterior anchorage. When maximum retraction is needed, however, it is vital that the orthodontic mechanotherapy be structured to provide this. Techniques to produce maximum retraction combine two possible approaches. The first is reinforcement of posterior anchorage by appropriate means, including extraoral force, stabilizing lingual arches, and interarch elastics. The second approach involves reduction of strain on the posterior anchorage, which includes any combination of eliminating friction from the retraction system, tipping the incisors before uprighting them, or retracting the canines separately.

Maximum Retraction with the 18-Slot Appliance. With the 18-slot appliance, friction from sliding is usually avoided by employing closing loops and tipping/uprighting is rarely part of the anchorage control strategy. To obtain greater retraction of the anterior teeth, a sequence of steps to augment anchorage and reduce anchorage strain could be as follows:

1. Add stabilizing lingual arches and proceed with en masse space closure. The resulting increase in posterior anchorage, though modest, will change the ratio of anterior retraction to posterior protraction to approximately 2:1.

2. Reinforce maxillary posterior anchorage with extraoral force and (if needed) use Class III elastics from the high-pull headgear to supplement retraction force in the lower arch, while continuing the basic en masse closure approach. Depending on how well the patient cooperates, additional improvement of retraction, perhaps to a 3:1 or 4:1 ratio, can be achieved.

3. Retract the canines independently, preferably using a segmental closing loop, and then retract the incisors with a second closing loop archwire. Used with stabilizing lingual arches (which are needed to control the posterior segments in most patients), this technique will produce a 3:1 retraction ratio. When this procedure is reinforced with headgear, even better ratios are possible.

A more detailed discussion of each of these approaches follows.

Reinforcement with Stabilizing Lingual Arches. Stabilizing lingual arches must be rigid and should be made from 36 mil or 32 × 32 steel wire. These can be soldered to the molar bands, but it is convenient to be able to remove them, and Burstone's designs (see Chapter 12) are preferred.

It is important for a lower stabilizing lingual arch to lie behind and below the lower incisors, so that it does not interfere with their retraction. If 36 mil round wire is used, the lower arch is more conveniently inserted from the distal than from the mesial of the molar tube (see Fig. 15-34).

ClearCorrect Exhibit 1002, Page 1902 of 3373

The maxillary stabilizing lingual arch is a straight transpalatal design. Because maximum rigidity is desired for anchorage reinforcement, an expansion loop in the palatal section of this wire is not recommended unless a specific indication exists for including it.

If lingual arches are needed for anchorage control, they should be present during the first and second stages of treatment, but can and should be removed after space closure is complete. Their presence during the finishing stage of treatment, after extraction spaces have been closed, is usually not helpful and may interfere with final settling of the occlusion.

Reinforcement with Headgear and Interarch Elastics. Extraoral force against the maxillary posterior segments is an obvious and direct method for anchorage reinforcement. It is also possible to place extraoral force against the mandibular posterior segments, but usually more practical to use Class III elastics to transfer the extraoral force from the upper to the lower arch.

Interarch elastics for anchorage reinforcement were a prominent part of the original Tweed method for maximum retraction of protruding anterior teeth. In the Tweed approach to bimaxillary protrusion, lower but not upper premolars were extracted initially, so that an intact upper arch was available to resist the pull of Class III elastics. This step was the first component of the anchorage reinforcement: pitting an intact upper arch against a segmented lower arch (and later, the reverse).

The second part of Tweed anchorage reinforcement was "anchorage preparation," achieved by tipping the molars and premolars distally (Fig. 16-24). Class III elastics were used to maintain lower incisor position while this was done. The distally tipped molars then allowed the incisors to be retracted further than otherwise would have occurred. Only after the lower incisors had been retracted, sliding the canine initially and then using a closing loop, were the upper premolars extracted. At that point, the lower arch was stabilized and Class II elastics were used to prepare anchorage by tipping back the upper molars, before the upper incisors were retracted (Fig. 16-24, *B*).

Although the original Tweed approach can be used with the contemporary 18-slot appliance, it is rarely indicated. Prolonged use of Class II and Class III elastics is extrusive and requires good vertical growth for acceptable results. Distally tipping the molars augments their anchorage value primarily by first moving these teeth distally, then mesially.

Segmented Retraction of the Canines. Segmented retraction of the canines with frictionless springs is an attractive method for reducing the strain on posterior anchorage and is a readily available approach with the modern 18-slot appliance. It is also possible to retract the canines by sliding them on the archwire, but the narrow brackets usually used with the 18-slot appliance and the tight clearance and relatively low strength of a 17 × 25 archwire produce less-than-optimum sliding.

For frictionless retraction of the canines, as in Ricketts' bioprogressive technique,[7] an auxiliary tube on the molar is needed. An auxiliary tube on the canine is unnecessary, because the retraction spring can fit directly into the canine bracket. Instead of stabilizing lingual arches, a base or utility arch from the first molar to the incisors is normally used (Fig. 16-25). Handled correctly, this technique provides efficient space closure with excellent force characteristics.

Segmented canine retraction springs used in bioprogressive technique are shown in Fig. 16-25. These flexible springs require a root-paralleling gable bend of approximately 60 degrees and an antirotation bend of approximately 20 degrees. Closing loops are then used for the second stage of retraction of the incisors (Fig. 16-26).

Segmented canine retraction of this type presents two problems. The first is that it is difficult to control the position of the canine in all three planes of space as it is retracted. If the canine is pulled distally from an attachment on its buccal surface, the point of attachment is not only some distance occlusal but is also buccal to the center of resistance. This means that without appropriate moments,

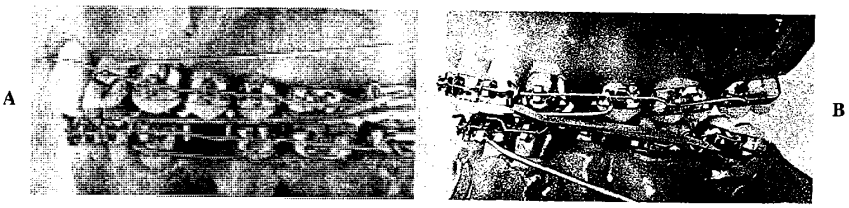


Fig. 16-24 ■ Anchorage preparation in Tweed technique. Class III elastics from a stabilized upper arch reinforced with headgear are being used to tip back the lower posterior teeth. Note the second order (tipback) bends in the lower archwire. **A,** A sliding jig to the second premolar is being used to transfer the Class III elastic force to the posterior segment; **B,** anchorage preparation completed in the lingual arch. Note the distally tipped position of the lower posterior teeth and the use of Class II elastics to accomplish similar distal tipping of the upper posterior teeth. (From Tweed CH: Clinical orthodontics, St Louis, 1966, Mosby–Year Book.)

ClearCorrect Exhibit 1002, Page 1903 of 3373

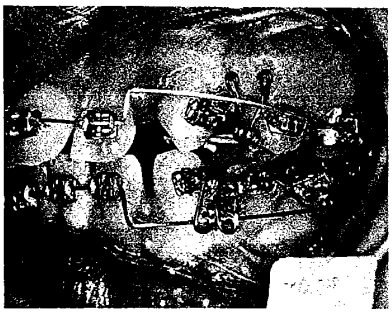


Fig. 16-25 ■ Utility arches from the first molars to the incisor segment used in conjunction with segmented canine retraction springs. This frictionless retraction of the canines reduces the strain on posterior anchorage and produces greater total retraction of the anterior teeth compared with en masse space closure, but careful fabrication and activation of the retraction springs are needed to maintain control of canine position.

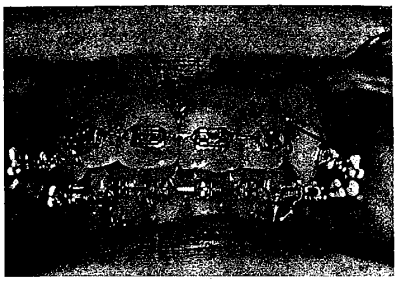


Fig. 16-26 ■ After the canines are retracted with segmental closing loops, the four incisors are retracted. This patient illustrates alternative archwires for retraction of the anterior segment, using 18-slot edgewise and Rickett's bioprogressive technique. In the upper arch, a contraction utility arch with helical loops to increase its anteroposterior flexibility is being used for anterior retraction. In the lower arch, double-delta loops are being used.

the tooth will tip distally and rotate mesiobuccally. Both a root-paralleling moment and an antirotation moment must be obtained by placing gable bends in the spring. Control of the vertical position of the canine, particularly after the gable bends in two planes of space have been placed, can be a significant problem.

Second, much more than with en masse retraction using segmented mechanics, segmental retraction of canines does not fail safe. The canine is free to move in three dimensional space, and there are no stops to prevent excessive movement in the wrong direction if a spring is improperly adjusted or becomes distorted. A missed appointment and a distorted spring can lead to the development of a considerable problem (Fig. 16-27), and patients must be monitored carefully.

Maximum Retraction with the 22-Slot Appliance. The same basic approaches are available with the 22- as with the 18-slot appliance: to increase the amount of incisor retraction, a combination of increased reinforcement of posterior anchorage and decreased strain on that anchorage is needed. All the possible strategies for anchorage control can be used. With a 22-slot appliance in which sliding retraction of canines is the approach to moderate anchorage, the following sequence of steps to increase incisor retraction might be logical:

Reinforcement of Posterior Anchorage with Extraoral Force. Stabilizing the posterior segments with extraoral force while sliding the canine along an archwire significantly increases posterior anchorage. This approach can be especially helpful in the upper arch, where headgear attached to the molars is easily placed, but the same approach can be used in the lower arch. Wearing two facebows to apply force to upper and lower molar teeth at the same time is difficult but not impossible. Reinforcing the upper arch with headgear, with Class III elastics off the headgear to reinforce anchorage for retraction of the lower



Fig. 16-27 ■ Vertical control of this canine was lost during retraction with a segmented retraction spring. A box-loop in 16 × 16 wire is being used to regain the correct vertical level. The greatest problem with segmented retraction springs is that they have no fail-safe component, allowing displacements of this type to occur if a spring is distorted and the patient misses scheduled appointments.

canines, is a more typical arrangement.

Application of Extraoral Force Directly Against the Canines to Slide Them Posteriorly. With this approach, a headgear using four hooks (Fig. 16-28) is normally used.[2] The hooks fit over a base archwire, typically 19 × 25 steel, and approximately a 200 gm force is supplied at each point of attachment to slide the canines posteriorly. It is easier to attach extraoral force to the mandibular anterior than posterior region, and this arrangement is tolerated well by patients, much better than two facebows.

Retracting the canines in this way totally avoids strain on posterior anchorage during the first retraction step. The disadvantages are the same as when protruding maxillary

ClearCorrect Exhibit 1002, Page 1904 of 3373

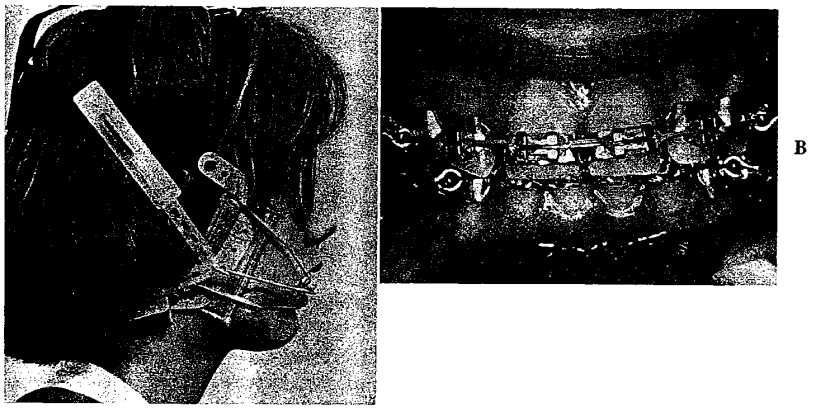


Fig. 16-28 ■ Four-hook headgear being used for retraction of the canines (in a patient who is also wearing a facebow to the molars). **A**, The hooks extend forward from a headcap and, **B**, attach over the upper and lower archwires mesial to the canines. Bands rather than bonded brackets on anterior teeth, particularly the canines, may be needed if headgear is applied directly to the anterior part of the dental arch.

incisors are retracted with headgear: this approach requires excellent cooperation by the patient, who should wear the headgear essentially full time to achieve effective tooth movement. Moreover, friction may cause asymmetric space closure. For cooperative patients, however, this method is quite effective.

The second step, after retraction of the canines, is done with a closing loop as described previously.

Use of Segmented Arch Mechanics for Canine Retraction. As discussed earlier, use of a segmented arch system to retract the canines independently, followed by retraction of the four incisors, is a practical method for conserving anchorage and equally adaptable to 22- and 18-slot appliances (Fig. 16-29). It produces a result approximately equivalent to retracting the canines with headgear, provided that at least a stabilizing lingual arch is used to reinforce posterior anchorage. The problems are also the same as with the 18-slot appliance: the canine can become displaced during its retraction and may become spectacularly malpositioned if something goes wrong, because no fail-safe mechanism is in place.

Segmented Arch Mechanics for Tipping/Uprighting. Rather than independent retraction of the canines, Burstone[6] now recommends two-step space closure in maximum anchorage cases by en masse distal tipping of the anterior teeth, followed by uprighting (see Fig. 17-8). The segmented arch technique is used, but with a differently activated spring assembly from the one needed for space closure in moderate retraction cases. Compared with independent retraction of the canines with loops, the fail-safe characteristics of this approach are much improved (though still not as good as with continuous archwires). Excellent control of anchorage for maximum retraction, without the use of headgear, can be obtained. The segmented arch approach is particularly valuable in treatment of adults (see Chapter 20) but can be used very effectively in adolescents.

■ Minimum Incisor Retraction

As with any problem requiring anchorage control, the approaches to reducing the amount of incisor retraction involve reinforcement of anchorage (the anterior teeth in this situation) and reduction of strain on that anchorage. An obvious strategy, implemented at the treatment planning stage, is to incorporate as many teeth in the anterior anchor unit as possible. Therefore if extraction of teeth is necessary at all, extracting a second premolar or molar, not a first premolar, is desirable. All other factors being



Fig. 16-29 ■ Retraction of upper and lower canines with T-loops in beta-Ti wire, in segmented arch technique with the 22-slot edgewise appliance. (Courtesy Dr. CJ Burstone.)

ClearCorrect Exhibit 1002, Page 1905 of 3373

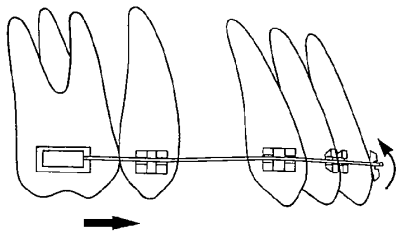


Fig. 16-30 ■ Torque forces against the incisors create a crown-forward as well as a root-backward tendency. Preventing the incisor crowns from tipping forward tends to pull the posterior teeth forward, which can be advantageous if it is desired to close space in this way.

equal, the amount of incisor retraction will be less the further posteriorly in the arch an extraction space is located (see Chapter 8).

A second possibility for reinforcing incisor anchorage is to place active lingual root torque in the incisor section of the archwires, maintaining a more mesial position of the incisor crowns at the expense of somewhat greater retraction of the root apices (Fig. 16-30). When the incisors protrude, some degree of forward tipping of these teeth is usually present, so that when the incisors are retracted, they can be allowed to tip lingually at least slightly. Advantage can be taken of this when incisor retraction is desired. Conversely, in patients in whom it is desired to close extraction sites by moving the posterior teeth forward, the incisors are often already upright, and lingual root torque is likely to be desired for both esthetic reasons and control of anchorage. Burstone's segmented arch technique can be used to particular advantage when this strategy for producing differential forward movement of posterior teeth is used.[6]

A third possibility for maximizing forward movement of posterior teeth is to break down the posterior anchorage, moving the posterior teeth forward one tooth at a time. After extraction of a second premolar, for example, it may be desired to stabilize the eight anterior teeth and to bring the first molars forward independently, creating a space between them and the second molars before bringing the second molars anteriorly. This strategy can readily be combined with the anterior torque approach.

A final possibility for maximizing protraction of posterior teeth is the use of extraoral force, pulling the teeth forward from a facemask or equivalent device (see Chapter 14). This provides the same opportunities and limitations as any other use of extraoral force for tooth movement. If the patient can be persuaded to wear reverse headgear essentially full time, excellent tooth movement can be obtained. With only 10 to 14 hours of wear per day, however, the results are often disappointing. Since a reverse headgear inevitably crosses the face, it is difficult to obtain the same level of cooperation as with a conventional posteriorly placed headgear, particularly in adolescents who are the candidates for comprehensive treatment.

It rarely should be necessary to use involved mechanotherapy to protract posterior teeth. The need for this approach usually arises from an effort to close spaces from congenitally missing teeth, teeth that were lost to decay, or perhaps teeth that should not have been extracted for orthodontic purposes. If the temptation to use first premolars as a routine extraction is avoided, most of the need for minimum retraction mechanotherapy is also avoided.

■ *References*

1. Gianelly AA: Japanese Ni-Ti coils used to move molars distally, Am J Orthod Dentofacial Orthop 99:564-591, 1991.
2. Hickham JH: Direct edgewise orthodontic approach, J Clin Orthod 8:617, 1974.
3. Gianelly AA, Anderson CK, Boffa J: Longitudinal evaluation of condylar position in extraction and nonextraction treatment, Am J Orthod Dentofacial Orthop 100:416-420, 1991.
4. Booth FA: Optimum forces with orthodontic loops, Houston, 1971, MS Thesis, University of Texas Dental Branch.
5. Miura F et al: Studies on the Japanese NiTi alloy coil springs, Am J Orthod Dentofacial Orthop 94:89-96, 1988.
6. Burstone CJ: The segmented arch approach to space closure, Am J Orthod 82:361, 1982.
7. Ricketts RM et al: Bioprogressive therapy, Denver, 1979, Rocky Mountain Orthodontics.

ClearCorrect Exhibit 1002, Page 1906 of 3373

Chapter 17

The Third Stage of Comprehensive Treatment: Finishing

Root paralleling at extraction sites
Torque of incisors
Correction of vertical relationships
  Excessive overbite
  Anterior open bite
Midline discrepancies
Tooth size discrepancies
Final "settling" of teeth
Removal of bands and bonded attachments
Positioners for finishing
Special finishing procedures to avoid relapse
  Control of unfavorable growth
  Control of soft tissue rebound

By the end of the second stage of treatment, the teeth should be well aligned, extraction spaces should be closed, and the teeth in the buccal segments should be in a normal Class I relationship. In the Begg technique, major root movements of both anterior and posterior teeth still remain to obtain root paralleling at extraction sites and proper axial inclination of tipped incisors. With contemporary edgewise techniques, relatively little finishing is required, but minor versions of these same root movements are likely to be required. In addition, most cases require some adjustment of the vertical relationship of incisors as a finishing procedure, either correcting moderately excessive overbite or closing a mild anterior open bite.

Root Paralleling at Extraction Sites

In the Begg technique, extraction spaces are closed by initially tipping the teeth together, and then uprighting them (Fig. 17-1). In the finishing stage, the moments necessary for root uprighting are generated by adding auxiliary springs that fit into the vertical slot of the Begg (ribbon arch) bracket. In most instances, a heavier (20 mil) archwire replaces the 16 mil archwire used as a base arch up to that point, to provide greater stability. Root paralleling is accomplished by placing an uprighting spring in the vertical slot and hooking it beneath the archwire. Since the root-uprighting forces are also crown-separating forces, the crowns must be tied together across the extraction site. The Begg uprighting springs extend only a short distance from the point of insertion into the bracket to the point where they are hooked to the archwire. Therefore it is necessary both to make the uprighting springs from small-diameter wire (usually 14 mil steel) and to increase their length by bending a double helix at the base of the spring.

During space closure with the edgewise appliance, it is almost always a goal of treatment to produce bodily tooth movement during space closure, preventing the crowns from tipping together. If proper moment-to-force ratios have been used, little if any root paralleling will be necessary as a finishing procedure. On the other hand, it is likely that at least a small amount of tipping will occur in some patients, and therefore some degree of root paralleling often will be necessary.

Exactly the same approach used in Begg technique can be employed with the edgewise appliance if it includes a vertical slot behind the edgewise bracket (Fig. 17-2). This allows an uprighting spring to be inserted and hooked beneath a base archwire in the same way as in Begg technique. This approach is reasonably effective with narrow edgewise brackets and an undersized round wire (typically 18 mil) in the 22-slot edgewise appliance, but in contemporary edgewise practice, this method has been almost totally abandoned in favor of angulated bracket slots that produce proper root paralleling when a full-dimension edgewise arch is placed as a finishing archwire.

With the 18-slot appliance, the typical finishing archwire is either 17 × 22 or 17 × 25 steel. These wires are flexible enough to engage narrow brackets even if a moderate degree of tipping has occurred, and the archwire will generate the necesary root paralleling moments. If a greater degree of tipping has occurred, a more flexible full-dimension rectangular archwire is needed. To correct more severe tipping, a beta-titanium (beta-Ti) or even a nickel-titanium (NiTi) 17 × 25 wire might be needed initially, with a steel archwire used to obtain final positioning.

With wider 22-slot brackets on the canines and premolars and with the use of sliding rather than loop mechanics, there is usually even less need for root paralleling as a finishing procedure than with narrow brackets and closing loop archwires. If teeth do tip even slightly into the extraction space, however, a full-dimension steel archwire in a 22-slot bracket is much too stiff to produce the needed root-uprighting moment. Even a 19 × 25 steel wire is undesirably stiff. A 21 × 25 beta-Ti wire is the best choice

ClearCorrect Exhibit 1002, Page 1907 of 3373

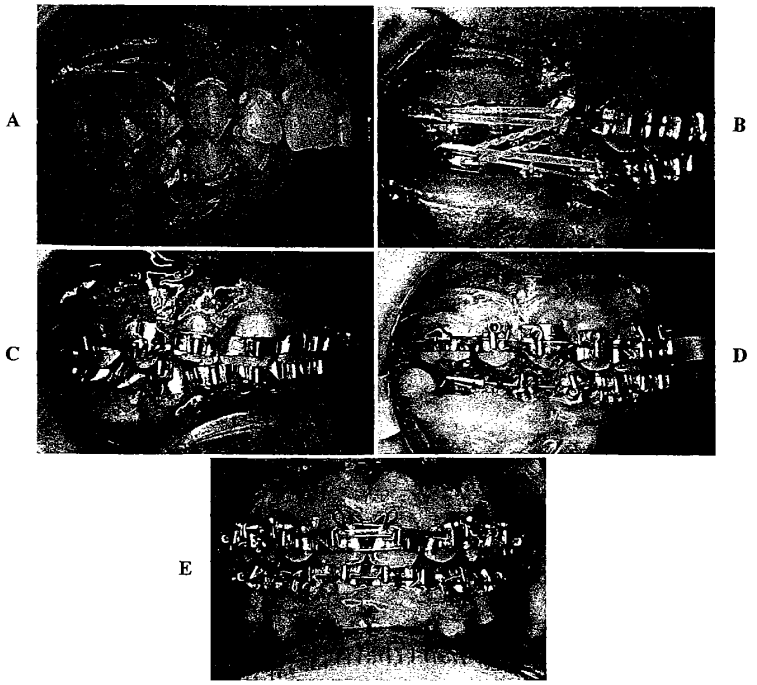


Fig. 17-1 ■ Stages in Begg technique. **A,** The original Class II, division 1 malocclusion; **B,** space closure during stage 2, using intra-arch elastics plus Class II elastics; **C,** tooth positions at the end of stage 2 (note the lingual tipping of incisors and mesiodistal tipping of canines and premolars); **D,** lateral view of the Begg appliance, during stage 3, showing auxiliary root-uprighting springs on second premolars, canines, and lateral incisors. These springs extend into the vertical slot of the Begg bracket and hook beneath the archwire adjacent to the tooth. **E,** Anterior view showing a torquing auxiliary to the maxillary central incisors. This auxiliary archwire is "piggy-backed" over the base arch and hooks beneath the base arch posteriorly.



Fig. 17-2 ■ An auxiliary uprighting spring placed in a vertical slot behind an otherwise standard edgewise bracket, for distal root positioning of the canine tooth. With the introduction of contemporary straight-wire appliances, this use of auxiliary uprighting springs in edgewise technique was almost completely abandoned in favor of preangulated brackets and resilient NiTi or beta-Ti archwires.

for a finishing archwire under most circumstances, and if significant root paralleling is needed, 21 × 25 NiTi should be used first.

Although austenitic NiTi (A-NiTi) wires perform much better than martensitic NiTi (M-NiTi) wires in alignment, there is not that much difference in their performance as rectangular finishing wires. The great advantage of A-NiTi is its very flat load-deflection curve, which gives it a large range. In the finishing stage, however, appropriate stiffness at relatively small deflections, rather than range, is the primary consideration. A-NiTi wires may deliver less force than their M-NiTi counterparts (this will depend on how the manufacturer manipulated the wire—see Chapter 10), and if rectangular A-NiTi is used in the finishing stage, torsional stiffness must be considered in the choice of the wire.

A root-paralleling moment is a crown-separating moment in edgewise technique just as it is in Begg technique, and this effect is important to remember. Either the teeth

ClearCorrect Exhibit 1002, Page 1908 of 3373

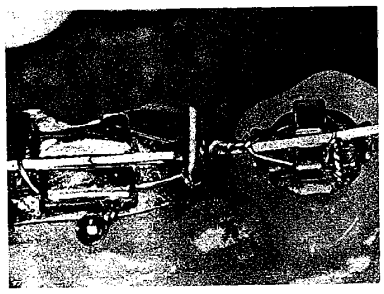


Fig. 17-3 ■ A rectangular archwire that incorporates active root paralleling moments or torque must be tied back against the molar teeth to prevent space from opening within the arch. If the ligature used to tie back the archwire is cabled forward and also used to tie the second premolar, the tieback is less likely to come loose.

must be tied together at the extraction site or the entire archwire must be tied back against the molars (Fig. 17-3) to prevent the extraction site from reopening during finishing.

Occasionally, a severely tipped canine tooth will be encountered, and a longer range of action is needed than can be delivered by even the most flexible continuous archwire. In this situation, there are two options: (1) bending a loop into a rectangular archwire to provide the desired flexibility (see Fig. 16-27), or (2) using an auxiliary root-uprighting spring (Fig. 17-4).

With the 18-slot appliance, the best choice is usually a box loop in 16 × 22 steel wire. The loop is preferred over a very flexible archwire because the malalignment is concentrated at one spot in the arch, and arch form can be distorted by the flexible wire (the same reason that loops are still occasionally indicated for initial alignment). At the same time that the root of the canine tooth is being positioned distally, this loop also can be used to obtain a last bit of space closure.

A similar box loop archwire can be used with the 22-slot appliance, made from 18 × 25 wire (the smallest size that will not twist in a 22-slot bracket). The preferred alternative, however, is to bypass the tipped canine with a rectangular base arch and use an auxiliary root-uprighting spring tied into the canine bracket (see Fig. 17-4). An 18 × 25 box loop almost always is too stiff.

Torque of Incisors

If protruding incisors tipped lingually while they were being retracted, lingual root torque as a finishing procedure may be required. In the Begg technique, the incisors are deliberately tipped back during the second stage of treatment, and lingual root torque is a routine part of the third stage of treatment. Like root paralleling, this is accomplished with an auxiliary appliance that fits over the main or base archwire. The torquing auxiliary is a "piggyback arch" that contacts the labial surface of the incisors near the gingival margin, creating the necessary couple with a moment arm of 4 to 5 mm (see Fig. 17-1). Although these piggyback torquing arches come in a number of designs, the basic principle is the same: the auxiliary arch, bent into a tight circle initially, exerts a force against the roots of the teeth as it is partially straightened out to normal arch form (Fig. 17-5).

A torquing force to move the roots lingually is also, of course, a force to move the crowns labially (see Fig. 16-31). In a typical patient with a Class II malocclusion, anchorage is required to maintain overjet correction while upper incisor roots are torqued lingually. Class II elastics are normally worn during the third stage of Begg treatment to ensure that the maxillary incisor crowns do not become repositioned labially. In addition, the incisors are usually taken to an edge-to-edge relationship during the second stage of Begg treatment, allowing some possibility for the maxillary crowns to move forward during the third stage (see Fig. 17-1). The Class II elastics that reinforce the upper arch, however, further add to the tendency to displace

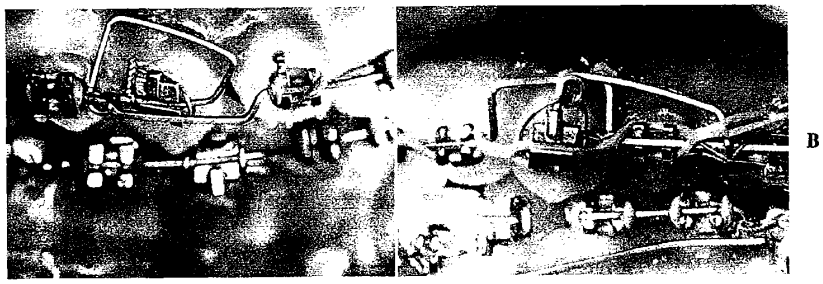


Fig. 17-4 ■ Auxiliary root springs used with the 22-slot appliance. **A,** An auxiliary root spring in TMA wire welded to the base arch that bypasses the canine and tied into the canine edgewise bracket slot. **B,** An auxiliary root spring in steel wire, placed in the vertical tube on a Burstone canine bracket and activated by hooking beneath the base arch posteriorly. Note that the base archwire bypasses the tooth being uprighted. (Courtesy Dr. CJ Burstone.)

ClearCorrect Exhibit 1002, Page 1909 of 3373

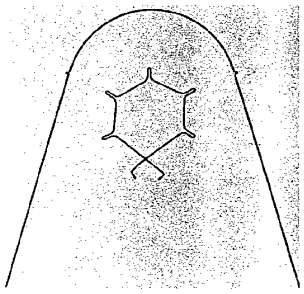


Fig. 17-5 ■ Torquing auxiliary archwires exert their effect when the auxiliary, originally bent into a tight circle as shown, is forced to assume the form of the base archwire over which it will be placed. This tends to distort the base archwire, which therefore should be relatively heavy wire—at least 18 mil steel.

the lower arch mesially, and the inclination of the lower incisors will be improved as much by labial tipping as by lingual root torque.

The torquing auxiliaries normally used in Begg technique not only place lingual force against the incisor roots, they tend to alter the form of the arch itself, because the torquing auxiliary wire tends to constrict the base arch posteriorly. A major reason for using a heavier base archwire in the third stage of treatment is to resist this potential distortion of arch form. Better results are achieved with a 20 mil steel base arch during the third stage than with a 16 mil wire, as originally used by Dr. Begg.

Precise positioning of individual teeth is difficult to obtain with the Begg appliance. The minimal area of contact between the base archwire and the bracket, though helpful in providing for relatively free tipping and sliding movements, makes it impossible to use the base arch to obtain detailed tooth positioning, and the auxiliaries used for root positioning have no fail-safe component at all. They continue to work until disconnected. Tooth positioners (see following) are usually used with the Begg appliance to detail the occlusal relationships, but a positioner is unable to materially affect root position.

For this reason, modifications of the Begg appliance, so that a rectangular archwire in a rectangular slot can be used for finishing purposes, have been proposed repeatedly. This method requires a combination bracket, incorporating an edgewise bracket slot along with the vertically oriented Begg slot, or a modified edgewise bracket that allows tipping in one direction and that incorporates a vertical slot for uprighting springs. Recent versions of combination brackets are shown in Figs. 17-6 and 17-7. With these variations, the first two stages of treatment are carried out largely as in traditional Begg technique. At the finishing stage, root paralleling and torquing are done with Begg-style auxiliary wires, up to a stage of completion ap-

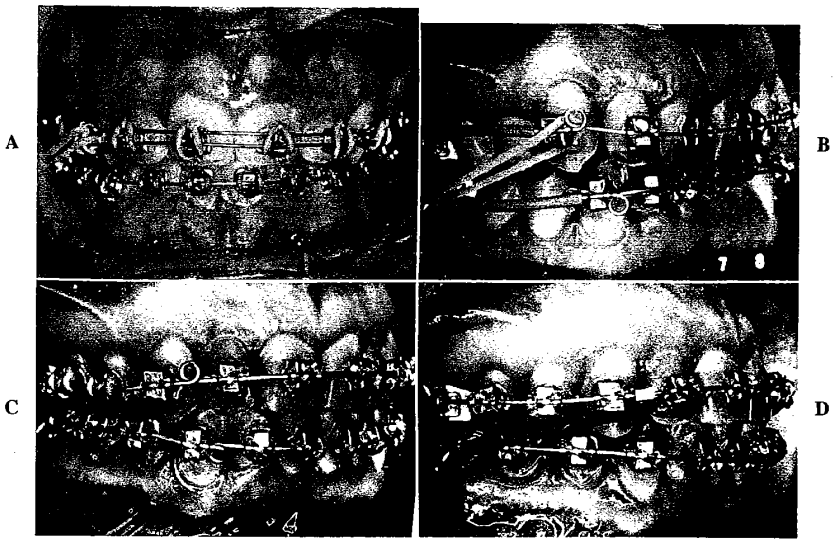


Fig. 17-6 ■ **A,** The CAT (combination anchorage technique) appliance (also shown in Fig. 17-7) uses a combination bracket with both Begg and edgewise slots. A rectangular archwire in the edgewise slot can be used in finishing, either alone as in the lower arch or in conjunction with a wire in the Begg slot, as in the upper arch; **B** to **D,** the Tip-Edge appliance uses a modified adgewise bracket to allow the tipping needed in the initial stages of Begg technique, then employs a rectangular archwire during finishing. (**A,** Courtesy Dr. WJ Thompson; **B** to **D,** courtesy Dr. PC Kesling.)

ClearCorrect Exhibit 1002, Page 1910 of 3373

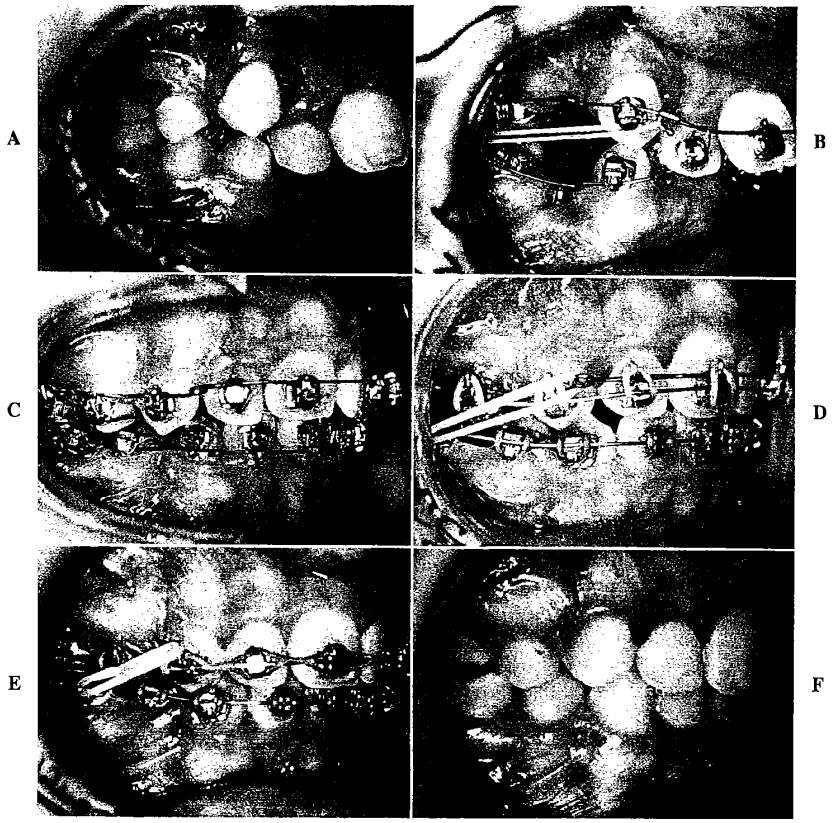


Fig. 17-7 ■ Stages in treatment with the CAT appliance. **A,** The original Class II crowded malocclusion; **B,** stage 1, using dual-flex archwires. The anterior section is 16 mil NiTi, the posterior section 16 steel. In the initial stage of Begg treatment, the rigidity of steel wire is needed for the anchor bends that control molar position. The dual-flex wires allow the normal posterior anchor bends, without the necessity for loops for alignment anteriorly; **C,** completion of stage 2, with 18 mil steel wires in place (compare to Fig. 17-1); **D,** early in stage 3 (finishing), with rectangular NiTi wires in the edgewise slot of both the upper and lower brackets, and an 18 mil steel wire pinned in the Begg slots of the upper brackets for vertical stabilization; **E,** later in finishing, with rectangular NiTi wires alone; **F,** posttreatment occlusion. (Courtesy Dr. WJ Thompson.)

proximately equivalent to that at which patients treated with the current edgewise appliances usually enter the finishing stage. Then a rectangular archwire is used in much the same way that it would be in edgewise treatment.

In edgewise technique, only moderate additional torque should be necessary during the finishing stage, except in the relatively few maximum anchorage patients in 22-slot edgewise for whom tipping/uprighting was chosen as an anchorage conservation technique (see below). With the 18-slot appliance, a 17 × 25 steel archwire has excellent torsion properties, and active torque with the archwire is entirely feasible. Building torque into the bracket slot initially means that it is unnecessary to place torquing bends in the archwire, making the accomplishment of torque as a finishing procedure relatively straightforward.

With the 22-slot appliance, steel full-dimension rectangular wires are far too stiff for effective torquing, and if incisors have been allowed to tip lingually too much, as can happen in the correction of maxillary incisor protrusion, correcting this merely by placing a rectangular steel archwire is not feasible. Torquing auxiliaries similar to those in the Begg appliance were once commonly used with 22-slot standard edgewise technique, and a number of designs have been offered commercially. These piggyback arches are usually used with round rather than rectangular base archwires.

One of the great virtues of pretorqued brackets is that, even in the 22-slot appliance, tipping of incisors can be

ClearCorrect Exhibit 1002, Page 1911 of 3373

largely prevented during retraction and space closure. In addition, full-dimension NiTi or beta-Ti archwires can be used to torque incisors with 22-slot brackets (provided the brackets have torque built in), further reducing any need for auxiliary arches. For these reasons, torquing auxiliaries for 22-slot edgewise have almost disappeared from contemporary use. For torque, the best finishing wire in 22-slot edgewise is 21 × 25 beta-Ti.

When tipping/uprighting is used with edgewise technique, the segmented arch approach is required, and springs connecting the segments are maintained until the stage of uprighting approaches what would usually be observed at the completion of continuous-arch edgewise space closure (Fig. 17-8). At that point, continuous rectangular arches are employed in finishing, as in other edgewise cases discussed in this chapter.[1]

One torquing auxiliary deserves special mention: the Burstone torquing arch (Fig. 17-9). It can be particularly helpful in patients with Class II, division 2 malocclusion whose maxillary central incisors are severely tipped lingually and require a long distance of torquing movement, while the lateral incisors need little if any torque. Because of the long lever arm, this is the most effective torquing auxiliary for use with the edgewise appliance. It is equally effective with the 18- or 22-slot appliance.

Two factors determine the amount of torque that will be expressed by any rectangular archwire in a rectangular slot: the inclination of the bracket slot relative to the archwire, and the tightness of the fit between the archwire and the bracket. The variation in torque prescriptions in contemporary edgewise appliances is shown in Table 12-1. These variations largely reflect different determinations of the average contour of the labial and buccal surfaces of the teeth, but some differences are also related to the expected fit of archwires. With the 18-slot appliance, it is assumed that the rectangular archwires used for finishing will fit tightly in the bracket slot (i.e., that the finishing archwires will have a minimum dimension of 17 or 18 mil). With the 22-slot appliance, on the other hand, some prescriptions have extra built-in torque to compensate for rectangular finishing archwires that will have more clearance. Torque will not be expressed to the same extent with a 19 × 25 wire in a 22-slot bracket as with a 17 × 25 wire in an 18-slot bracket. The difference amounts to several degrees of

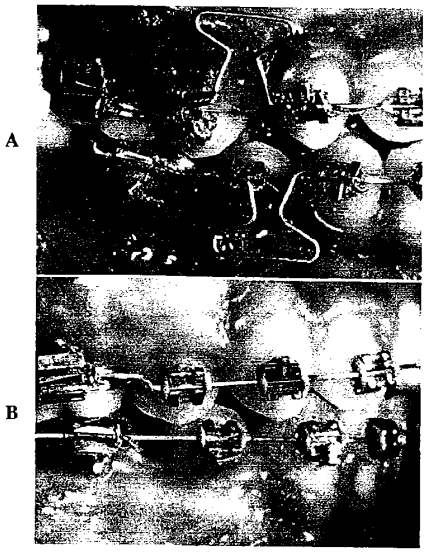


Fig. 17-8 ■ **A,** Use of anterior retraction springs in the segmented arch technique to close a premolar extraction space. Note that the posterior segments are stabilized, and the retraction segments fit into the auxiliary tubes on the first molars. **B,** Rectangular archwires for finishing, later in the same case. (Courtesy Dr. CJ Burstone.)

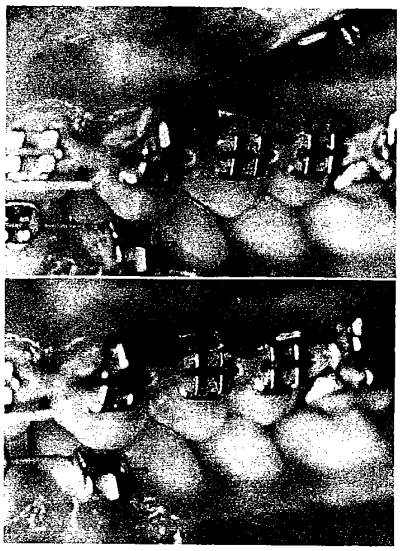


Fig. 17-9 ■ The Burstone torquing auxiliary is particularly useful in Class II, division 2 cases where maxillary central incisors need a large amount of torque. The torquing auxiliary is full-dimension (21 × 25 or 17 × 25, in 22- or 18-slot brackets respectively) steel wire that fits in the brackets only on the central incisors. The base arch (preferably also full-dimension rectangular wire) extends forward from the molars through the lateral incisor brackets, then steps down and rests against the labial surface of the central incisors. When the torquing auxiliary is passive, its long posterior arms are up in the buccal vestibule. It is activated by pulling the arms down and hooking them beneath the base archwire mesial to the first molar. The segment of the base arch that rests against the labial surface of the central incisors prevents the crowns from going forward, and the result is efficient torque of the central incisor roots.

ClearCorrect Exhibit 1002, Page 1912 of 3373

torque. Obviously, when the torque prescription is established, it is important to know what finishing wires are intended.

For full expression of the torque built into brackets in the 22-slot appliance, the best finishing wire usually is 21 × 25 beta-Ti. This wire's torsional stiffness is less than that of 17 × 25 steel (see Fig. 10-11 for a comparison of torsional stiffnesses of different types and sizes of wire). Braided rectangular steel wires are available in a variety of stiffnesses, and the stiffest of these in 21 × 25 dimension also can be useful in 22-slot finishing. A solid 21 × 25 steel wire cannot be recommended because of its stiffness and the resulting extremely high forces and short range of action. If a solid steel wire of this size is used, it should be preceded by 21 × 25 beta-Ti.

Correction of Vertical Relationships

If the first two stages of treatment have been accomplished perfectly, no change in the vertical relationship of incisors will be needed during the finishing stage of treatment. Minor adjustments often are needed, however, and major ones occasionally are required. At this stage, anterior open bite is more likely to be a problem than residual excessive overbite, but either may be encountered.

■ Excessive Overbite

Before attempting to correct excess overbite at the finishing stage of treatment, it is important to carefully assess why the problem exists, and particularly to observe the vertical relationship between the maxillary lip and maxillary incisor. An excessive curve of Spee in the lower arch still may be the cause of overbite, but by this stage of treatment, the problem is often slight elongation of the maxillary incisors. If so, an auxiliary intrusion arch is the preferred solution.

If a rectangular finishing archwire is already in place, the simplest approach may be to cut this archwire distal to the lateral incisors and install an auxiliary intrusion arch (Fig. 17-10). Alternatively, if the patient is still growing and relative rather than absolute intrusion would be satisfactory (see Chapter 15), a light round continuous archwire (16 or 18 mil steel) with an accentuated curve of Spee can be placed, and an auxiliary arch added to it. As a general rule, if an auxiliary depressing arch is added to a continuous base archwire, the base archwire should be a relatively small round wire, whereas if the base arch is segmented, the segments should be rectangular wire.

It is important to remember that when an auxiliary intrusion arch is used, a stabilizing transpalatal lingual arch may be needed to maintain control of transverse relationships and prevent excessive distal tipping of the maxillary molars. The greater the desired vertical change in incisor position, the more important it will be to have a stabilizing lingual arch in place, and vice versa. Small corrections during finishing usually do not require placing a lingual arch.

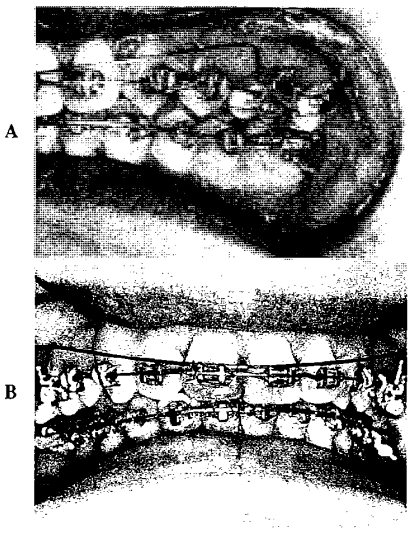


Fig. 17-10 ■ Use of an auxiliary depressing arch at the finishing stage to correct a mildly excessive overbite. **A,** Lateral view; **B,** anterior view. The auxiliary depressing wire is 17 × 25 beta-Ti. Note that the maxillary base arch (17 × 25 steel) is segmented between the canine and second premolar. If intrusion is desired, the base arch must be segmented.

■ Anterior Open Bite

As with deep bite, it is important to analyze the source of the difficulty if an anterior open bite persists at the finishing stage of treatment. Only rarely is a persistent open bite caused by lack of eruption of the upper incisors, and elongating these teeth is usually undesirable. If the open bite results from excessive eruption of posterior teeth, whether from a poor growth pattern or improper use of interarch elastics, correcting it at the finishing stage can be extremely difficult. High-pull headgear to the upper molars is the best approach if excessive vertical development of the posterior maxilla is the basic problem, and this treatment will have to be continued until growth is nearly complete, usually well into the retention period.

If no severe problems with the pattern of facial growth exist, however, a mild open bite at the finishing stage of treatment is usually caused by an excessively level lower arch. This condition is managed best by elongating the lower but not the upper incisors, thereby creating a slight curve of Spee in the lower arch. Because of the stiffness of the rectangular archwires used for finishing, even with 18-slot edgewise, it is futile to use vertical elastics without altering the form of the archwires to provide a curve of Spee in the lower arch. Moreover, it is preferable to replace a heavy rectangular lower archwire with a lighter round wire before using anterior vertical elastics.

The preferred approach is to place a light round wire (16 or 18 mil steel) in the lower arch, with a slight curve of

ClearCorrect Exhibit 1002, Page 1913 of 3373

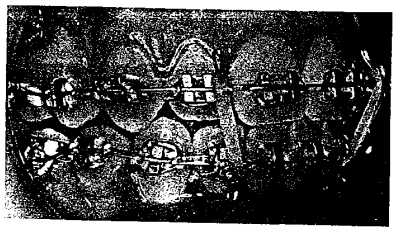


Fig. 17-11 ■ Anterior vertical elastics used with light archwires to close a mild anterior open bite at the end of the treatment. A 16 mil round wire with a curve of Spee is used in the lower arch. For this patient, two small elastics are being used on the right and left sides. An alternative is to use a single larger elastic in an anterior box configuration.

Spee and any vertical steps necessary to correct marginal ridge discrepancies, while retaining a full-dimension rectangular archwire in the upper arch. Posterior marginal ridge discrepancies may also contribute to the open bite and should be eliminated with small vertical steps in the archwires. Light elastic force is then used to augment the action of the archwires, elongating the lower incisors to close the open bite (Fig. 17-11). Elongating lower anterior teeth in this way, of course, is no substitute for controlling posterior vertical development. If carried to an extreme, this will produce an esthetically unacceptable relationship even if proper occlusion is achieved.

Midline Discrepancies

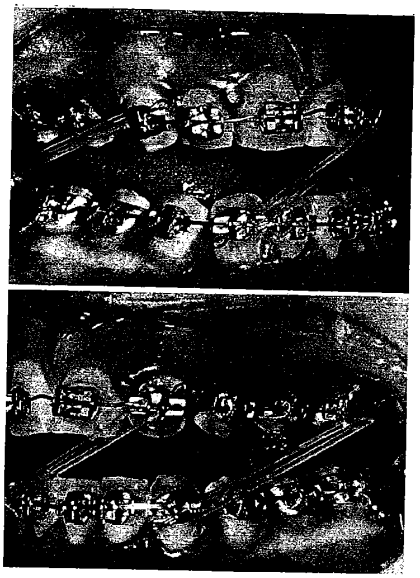
A relatively common problem at the finishing stage of treatment is a discrepancy in the midlines of the dental arches. This condition can result either from a preexisting midline discrepancy that was not completely resolved at an earlier stage of treatment, or an asymmetric closure of spaces within the arch. Minor midline discrepancies at the finishing stage are no great problem, but it is quite difficult to correct large discrepancies after extraction spaces have been closed and occlusal relationships have been nearly established.

As with any discrepancy at the finishing stage, it is important to establish as clearly as possible exactly where the discrepancy arises. Although coincident dental midlines are an important component of functional occlusion—all other things being equal, a midline discrepancy will be reflected in how the posterior teeth fit together—it is undesirable esthetically to displace the maxillary midline, bringing it around to meet a displaced mandibular midline. A correct maxillary midline is important for good facial esthetics, while a small displacement of the mandibular midline creates no esthetic difficulty.

If a midline discrepancy results from a skeletal asymmetry, it may be impossible to correct it orthodontically, and treatment decisions will have to be made in the light of camouflage versus surgical correction (see discussion in Chapter 8). Fortunately, midline discrepancies in the finishing stage are not usually this severe and are caused only by lateral displacements of maxillary or mandibular teeth. Usually, the midline discrepancy is accompanied by a mild Class II or Class III relationship on one side.

In this circumstance, the midline often can be corrected by using asymmetric Class II (or Class III) elastic force. As a general rule, it is more effective to use Class II or Class III elastics bilaterally with heavier force on one side than to place a unilateral elastic. However, if one side is totally corrected while the other is not, the patient usually tolerates a unilateral elastic reasonably well. It is also possible to combine a Class II or Class III elastic on one side with a diagonal elastic anteriorly, to bring the midlines together (Fig. 17-12). Coordinated steps in the archwires also can be used to shift the teeth of one arch more than the other.[2]

An important consideration in dealing with midline discrepancies is the possibility of a mandibular shift contributing to the discrepancy. This can arise easily if a slight discrepancy in the transverse position of posterior teeth is present. For instance, a slightly narrow maxillary right posterior segment can lead to a shift of the mandible to the left on final closure, creating the midline discrepancy. The correction in this instance, obviously, must include some force system (usually careful coordination of the maxillary and mandibular archwires, perhaps reinforced by a posterior cross-elastic) to alter the transverse arch relationships.



A

B

Fig. 17-12 ■ Midline correction can be approached with any combination of asymmetric posterior and anterior diagonal elastics. **A** and **B,** In this patient, a combination of Class II, Class III, and anterior diagonal elastics are being used, with a rectangular archwire in the lower arch and a round wire in the upper arch, attempting to shift the maxillary arch to the right.

ClearCorrect Exhibit 1002, Page 1914 of 3373

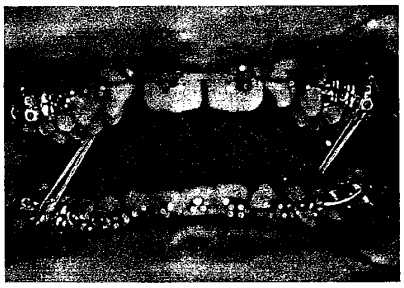


Fig. 17-13 ■ Parallel cross-elastics, used to correct a mild transverse discrepancy leading to a lateral mandibular shift late in treatment.

Occasionally, the entire maxillary arch is slightly displaced transversely relative to the mandibular arch so that with the teeth in occlusion, relationships are excellent, but there is a lateral shift to reach that position. Correction again would involve posterior cross-elastics, but in a parallel pattern as shown in Fig. 17-13.

If a midline discrepancy is from displacement of mandibular teeth more than maxillary teeth, or vice versa, the difference in stability with rectangular versus round wires can be used to help in correcting the situation. If the maxillary midline is correct while the mandibular midline deviates slightly toward one side, and a mild Class II relationship still exists on that side, replacing the rectangular mandibular finishing arch with a 16 or 18 mil round wire while retaining a full-dimension rectangular arch in the upper arch can facilitate correction with a unilateral Class II elastic. This approach should be reserved for small discrepancies, and it is important to carefully observe and control any expansion of the lower molar while a Class II elastic is worn against a light archwire. Prolonged use of Class II or Class III elastics during the finishing stage of treatment should be avoided, but a brief period of interarch elastic force is often necessary to obtain final positioning of teeth.

Tooth Size Discrepancies

Tooth size discrepancy problems must be taken into account when treatment is planned initially (see Chapter 7), but many of the steps to deal with these problems are taken in the finishing stage of treatment. Reduction of interproximal enamel (stripping) is the usual strategy to compensate for discrepancies caused by excess tooth size. When the problem is tooth size deficiency, it is necessary to leave space between some teeth, which may or may not ultimately be closed by restorations.

One of the advantages of a bonded appliance is that interproximal enamel can be removed at any time. When stripping of enamel is part of the original treatment plan, most of the enamel reduction should be done initially, but final stripping can be deferred until the finishing stage. This procedure allows direct observation of the occlusal relationships before the final tooth size adjustments are made. A topical fluoride treatment always is recommended immediately after stripping is done.

Tooth size deficiency problems often are caused by small maxillary lateral incisors. Having a small space distal to the lateral incisor is usually esthetically and functionally acceptable. Addition of composite resins to small teeth is an excellent way to compensate for tooth size problems and is often the best plan for small incisors (Fig. 17-14). It is better to add small amounts of resin on both sides of a small tooth than a large amount on one side. During finishing, segments of coil spring are usually placed on the finishing archwire to precisely position the small tooth. The composite build-ups should be done as soon possible after the patient is in retention, but not until soft tissue inflammation has been resolved.

More generalized small deficiencies can be masked by altering incisor position in any of several ways. To a limited extent, torque of the upper incisors can be used to compensate: leaving the incisors slightly more upright makes them take up less room relative to the lower arch and can be used to mask large upper incisors, while slightly excessive torque can partially compensate for small upper incisors. These adjustments require third-order bends in the finishing archwires. It is also possible to compensate by slightly tipping teeth, or by finishing the orthodontic treatment with mildly excessive overbite or overjet, depending on the individual circumstances.[3]

Final "Settling" of Teeth

At the conclusion of Class II or Class III correction, particularly if interarch elastics have been used, the teeth tend to rebound back toward their initial position despite the presence of rectangular archwires. In addition, it is not uncommon for a full-dimension rectangular archwire, no matter how carefully made, to hold some teeth slightly out of occlusion.

Because of the rebound after Class II or Class III treatment, it is important to slightly overcorrect the occlusal relationships. In a typical Class II anterior deep bite patient, the teeth should be taken to an end-to-end incisor relationship, with both overjet and overbite totally eliminated, before the headgear or elastic forces are discontinued (Fig. 17-15). This provides some latitude for the teeth to rebound or settle into the proper relationship.

No matter what the original malocclusion, a rectangular finishing archwire nearly always requires some first-, second-, or third-order bends to precisely position the teeth. One cannot simply place an ideal rectangular archwire in a straight-wire appliance and assume that the ideal position of each tooth will result. For essentially every patient, variations in tooth morphology and bracket positions will

ClearCorrect Exhibit 1002, Page 1915 of 3373

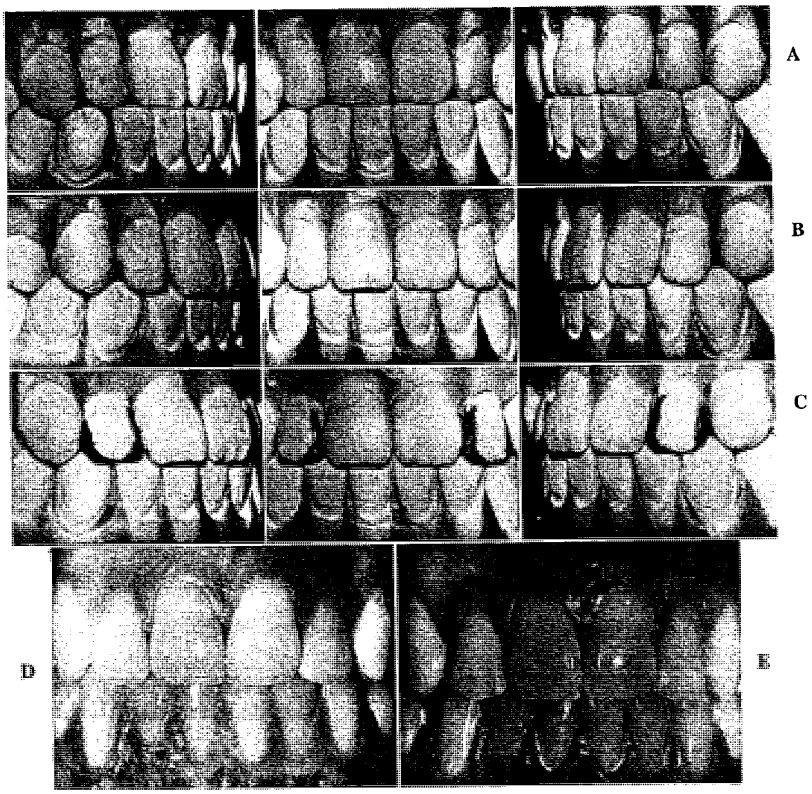


Fig. 17-14 ■ Small maxillary lateral incisors create tooth-size discrepancy problems that may become apparent only late in treatment. **A,** Setup showing anterior edge-to-edge relationship with the upper incisors in proximal contact; **B,** spaces distal to the lateral incisors with proper overjet/overbite relationship. This approach can be a satisfactory solution for some patients. **C,** Wax-up showing possible addition of composite restorative material to build up the small laterals and allow space closure; **D,** clinical photograph of same patient immediately after; **E,** 12 months after composite build-ups of the laterals. (From Fields HW: Am J Orthod 79:176-183, 1981.)

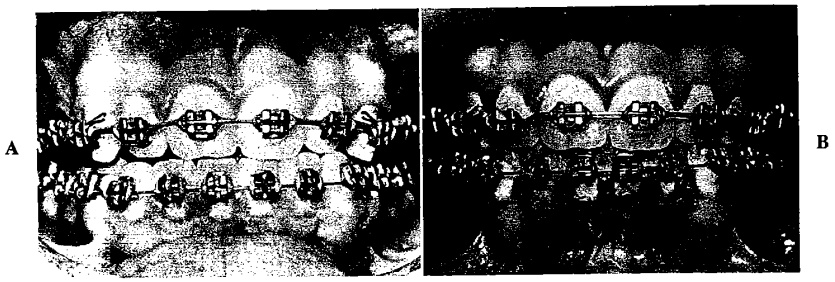


Fig. 17-15 ■ In finishing, overcorrection of Class II or Class III relationships is necessary to compensate for the rebound that occurs when headgear or elastic force is discontinued. **A,** Occlusion at the time Class II elastics were discontinued; **B,** same patient 8 weeks later, without archwire changes or other treatment.

ClearCorrect Exhibit 1002, Page 1916 of 3373

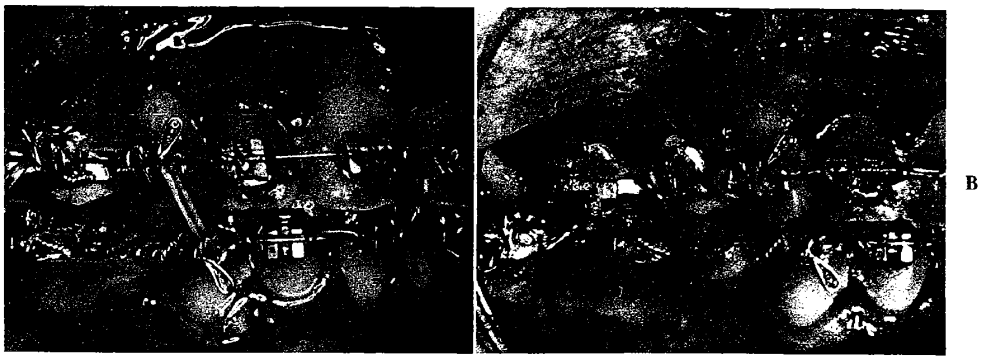


Fig. 17-16 ■ Use of vertical elastics for settling. **A,** Heavy rectangular archwires have been replaced by 16 mil steel, and 3/8-inch light vertical elastics in a box pattern are being worn to bring the teeth into tight occlusion; **B,** 4 weeks later.

require some adjustments in the final rectangular archwires.

The more precisely the archwire fits the brackets and the more bends that it requires, the more likely that some teeth will be almost but not quite in occlusion. This phenomenon was recognized by the pioneers with the edgewise appliance, who coined the term "arch-bound" to describe it. They found that with precisely fitting wires, it was almost impossible to get every tooth into solid occlusion, although one could come close.

These considerations lead to the formulation of two rules in finishing treatment:

1. Interarch elastics and headgear should be discontinued, and the rebound from their use allowed to express itself, 4 to 8 weeks before the orthodontic appliances are removed.

2. As a final step in treatment, the teeth should be brought into a solid occlusal relationship without heavy archwires present.

The final step of finishing therefore is appropriately called "settling," since its purpose is to bring all teeth into a solid occlusal relationship before the patient is placed in retention. There are three ways to settle the occlusion: (1) by replacing the rectangular archwires at the very end of treatment with light round arches that provide some freedom for movement of the teeth (16 mil in the 18-slot appliance, 16 or 18 mil in the 22-slot appliance) and allowing the teeth to find their own occlusal level; (2) with laced posterior vertical elastics after removing the posterior segments of the archwires; or (3) after the bands and brackets have been removed, with the use of a tooth positioner.

Replacing full-dimension rectangular wires with light round wires at the very end of treatment was the original method for settling, recommended by Tweed in the 1940s and perhaps by other edgewise pioneers earlier. These light final arches must include any first- or second-order bends used in the rectangular finishing arches. It is usually unnecessary for the patient to wear light posterior vertical elastics during this settling, but they can be used if needed (Fig. 17-16). These light arches will quickly settle the teeth into final occlusion and should remain in place for only a few weeks at most.

The difficulty with undersized round wires at the end of treatment is that some freedom of movement for settling of posterior teeth is desired, but precise control of anterior teeth is lost as well. It was not until the 1980s that orthodontists realized the advantage of removing only the posterior part of the rectangular finishing wire, leaving the anterior segment (typically canine-to-canine or first premolar-to-first premolar, and using laced elastics to bring the posterior teeth into tight occlusion (Fig. 17-17).[4] This method sacrifices a large degree of control of the posterior teeth, and therefore should not be used in patients who had major rotations or posterior crossbite. For the majority of patients who had well-aligned posterior teeth from the beginning, however, this is a remarkably simple and effective way to settle the teeth into their final occlusion.

The elastics for this settling are laced around the tubes and brackets as shown in Fig. 17-17. A typical arrangement is to use light ¾-inch elastics, with a Class II or Class III direction depending on whether slightly more correction is desired. These elastics should not remain in place for more than 2 weeks, and 1 week usually is enough to accomplish the desired settling. At that point, the fixed appliances should be removed and the retainers placed.

Removal of Bands and Bonded Attachments

Removal of bands is accomplished by simply breaking the cement attachment and then lifting the band off the tooth—which sounds simpler than it is in some instances. For upper molar and premolar teeth, a band-removing plier

ClearCorrect Exhibit 1002, Page 1917 of 3373

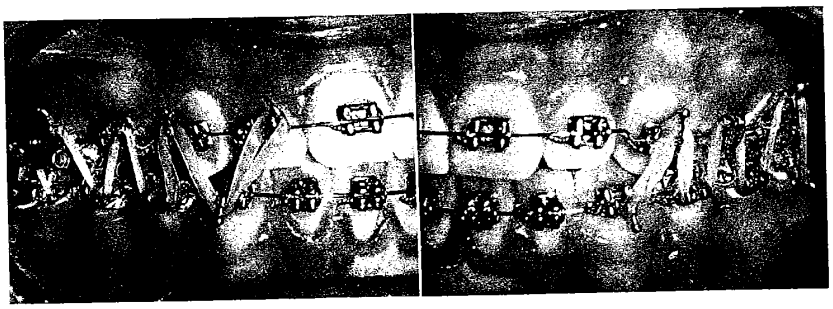


Fig. 17-17 ■ Use of laced elastics for settling the teeth into final occlusion at the end of treatment. The elastics can be used either with light round archwires, or with rectangular segments in the anterior brackets and no wire at all posteriorly.



A **B**

Fig. 17-18 ■ Removal of molar bands with a band-removing plier. **A,** Lower posterior bands are removed primarily with pressure from the buccal surface; **B,** upper posterior bands are removed from the lingual surface, using a lingual attachment welded to the band.

is placed so that first the lingual, then the buccal surface is elevated by the plier (Fig. 17-18). A welded lingual bar is needed on these bands to provide a point of attachment for the plier if lingual hooks or cleats are not a part of the appliance. For the lower posterior teeth, the sequence of force is just the reverse: the band-removing plier is applied first on the buccal, then the lingual surface. Maxillary anterior bands are removed from the labial surface with an anterior band-removing plier, while tightly fitted mandibular anterior bands usually must be slit with a cutting plier to make it possible to take them off. The difficulty of removing anterior bands is another reason for bonding except in special circumstances.

Bonded brackets must be removed, insofar as possible, without damaging the enamel surface. This is done by creating a fracture within the resin bonding material or between the bracket and the resin, and then removing the residual resin from the enamel surface (Fig. 17-19). With metal brackets, applying a cutting plier to the base of the bracket so that the bracket bends has the disadvantage of destroying the bracket, which otherwise could be reused, but this is the safest method.[5]

Enamel damage from debonding metal brackets is rare, but there have been a number of reports of enamel fractures and removal of chunks of enamel when ceramic brackets are debonded (see Chapter 12). It also is easy to fracture a ceramic bracket while attempting to remove it, and if that happens, large pieces of the bracket must be ground away with a diamond stone in a handpiece. These problems arise because ceramic brackets have little or no ability to deform—they are either intact or broken. Shearing stresses are applied to the bracket to remove it, and the necessary force can become alarmingly large, even with the special instruments now offered for this purpose (Fig. 17-20).

There are three approaches to these debonding problems: (1) grind away the brackets, rather than attempting to break them loose. This is time consuming, and there is the risk of enamel damage from the diamond rotary instruments; (2) modify the interface between the bracket and the bonding resin to increase the chance that when force is applied, the failure will occur between the bracket and the bonding material. Chemical bonds between the bonding resin and the bracket can be too good, and most manufac-

ClearCorrect Exhibit 1002, Page 1918 of 3373



Fig. 17-19 ■ Removal of bonded brackets. **A,** A special plier with a wire loop can be used to grasp the one wing of the bracket and apply a shearing force to fracture the bonding resin. This works particularly well with twin brackets. The advantage of this method is that the bracket usually is undamaged; the disadvantage is heavy force that may cause enamel damage; **B,** a cutter can be used to distort the bracket base, which leads to fractures within the bonding resin. The first approach is more compatible with recycling of brackets, but the second is safer.



Fig. 17-20 ■ A number of special instruments have been designed to make removal of ceramic brackets safer and easier. This one creates a torquing force on the bracket. Whatever the special instrument, however, weakening the bond with heat or a chemical agent first probably is needed for maximum effectiveness.

turers now have weakened them or abandoned chemical bonding altogether; (3) use heat to soften the bonding resin, so that the bracket can be removed with lower force. Electrothermal instruments for removing ceramic brackets now are available. There is no doubt that less force is needed when the bracket is heated, and research findings indicate that there is little patient discomfort and minimal risk of pulpal damage.[6,7] Nevertheless, the ideal solution would be to perfect the second approach so that ceramic brackets can be debonded without heating as readily as metal ones.

Cement left on the teeth after debanding can be removed easily by scaling, but residual bonding resin is more difficult to remove. The best results are obtained with a 12-fluted carbide bur at moderate speeds in a dental handpiece (Fig. 17-21).[8] This bur cuts resin readily but has little effect on enamel. Topical fluoride should be applied when the cleanup procedure has been completed, however, since some of the fluoride-rich outer enamel layer may be lost with even the most careful approach.

Positioners for Finishing

An alternative to segmental elastics or light round archwires for final settling is a rubber or plastic tooth positioner. A positioner is most effective if it is placed immediately on removal of the fixed orthodontic appliance. Normally, it is fabricated by removing the archwires 4 to 6 weeks before the planned removal of the appliance, taking impressions of the teeth and a registration of occlusal relationships, and then resetting the teeth in the laboratory, incorporating the minor changes in position of each tooth necessary to produce appropriate settling (Fig. 17-22). All erupted teeth should be included in the positioner, to prevent supereruption. As part of the laboratory procedure, bands and brackets are trimmed away, and any band space is closed.

This indirect approach allows individual tooth positions to be adjusted with considerable precision, bringing each tooth into the desired final relationship. The positioning device is then fabricated by forming either a hard rubber or soft plastic material around the repositioned and articulated casts, producing a device with the inherent elasticity to move the teeth slightly to their final position (Fig. 17-23).

The use of a tooth positioner rather than final settling archwires has two advantages: (1) it allows the fixed appliance to be removed somewhat more quickly than otherwise would have been the case (i.e., some finishing that

ClearCorrect Exhibit 1002, Page 1919 of 3373

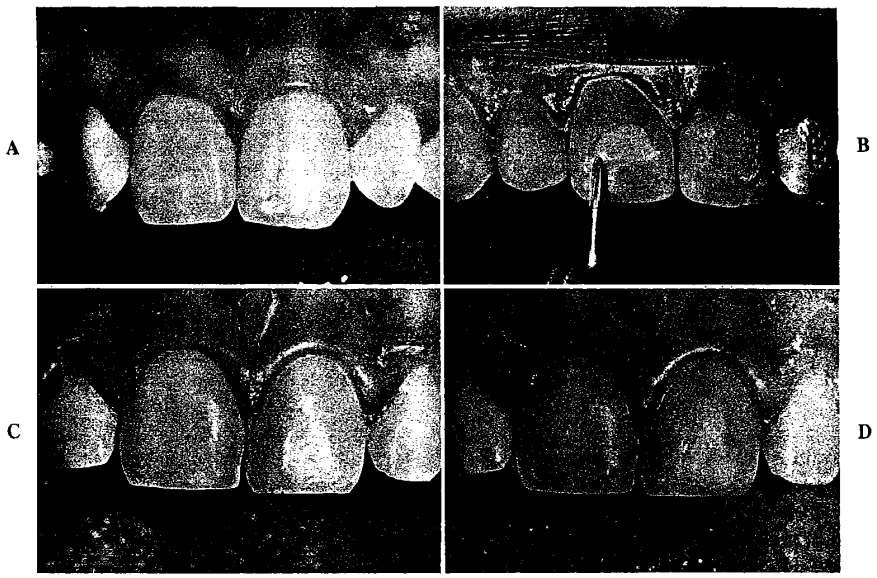


Fig. 17-21 ■ Removing excess bonding resin is best accomplished with a smooth 12-fluted carbide bur, followed by pumicing. **A,** Closeup view of the virgin surface of upper incisors; **B,** excess resin left on the tooth surface after removal of brackets. Upon debonding, the bond failure usually occurs between the base of the bracket and the resin, leaving excess resin on the tooth. The carbide bur is used with a general wiping motion to remove the resin; **C,** tooth surface after the remainder of the resin has been removed with the bur; **D,** tooth surface after final removal of resin (compare to **A**).

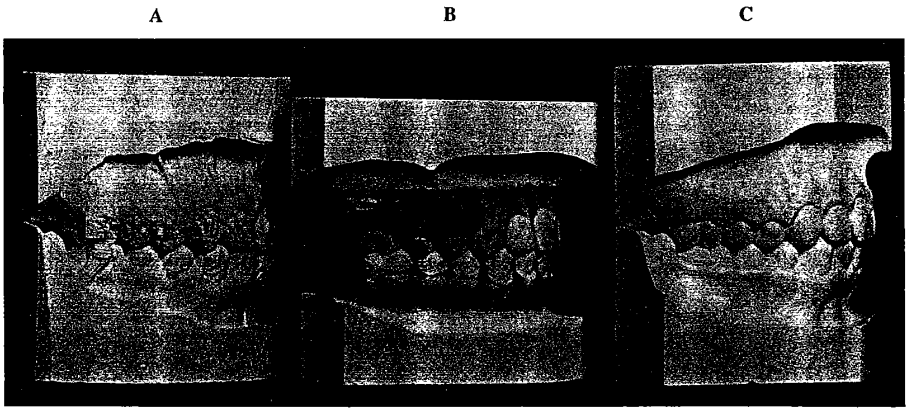


Fig. 17-22 ■ Use of a positioner for finishing. **A,** Casts 1 month before appliance removal, used to fabricate an immediate positioner; **B,** the positioner setup, with bands and brackets carved off the teeth in the laboratory; **C,** casts 2 weeks after appliance removal and placement of the positioner, showing the teeth settled into their finished relationship.

ClearCorrect Exhibit 1002, Page 1920 of 3373



Fig. 17-23 ■ A tooth positioner made from a transparent plastic material, placed in the patient's mouth. The patient bites into the positioner, which creates forces to slightly displace the teeth and also massages the gingiva. A device of this type is most effective in moving teeth if it is placed immediately after the fixed appliance is removed.

could have been done with the final archwires can be left to the positioner), and (2) it serves not only to reposition the teeth but also to massage the gingiva, which is almost always at least slightly inflamed and swollen after comprehensive orthodontic treatment. The gingival stimulation provided by a positioner is an excellent way to promote a rapid return to normal gingival contours (Fig. 17-24).

The use of positioners for finishing also has disadvantages. First of all, these appliances require a considerable amount of laboratory fabrication time, and therefore are expensive. Second, settling with a positioner tends to increase overbite more than the equivalent settling with light elastics. This is a disadvantage in patients who had a deep overbite initially but can be advantageous if the initial problem was an anterior open bite. Third, a positioner does not maintain the correction of rotated teeth well, which means that minor rotations may recur while a positioner is being worn. Finally, good cooperation is essential.

With modern edgewise appliances, the first advantage is not nearly so compelling as it was previously. It is an error to depend on a positioner to accomplish more than minimal settling of the occlusion. Major movements of teeth simply cannot be accomplished with any degree of certainty. At present, therefore, there are two main indications for use of a positioner: (1) a gingival condition with more than the usual degree of inflammation and swelling at the end of active orthodontics, and (2) an open bite tendency, so that settling by mild depression rather than elongation of posterior teeth is needed. Severe malalignment and rotated teeth, a deep bite tendency, and an uncooperative patient are contraindications for positioner use.

A positioner should be worn by the patient at least 4 hours during the day, and during sleep. Since the amount of tooth movement produced by a positioner tends to decline rapidly after a few days of use, an excellent schedule is to remove the orthodontic appliances, clean the teeth and apply a fluoride treatment, and place the positioner immediately, asking the patient to wear it as nearly full time as possible for the first 2 days. After that, it can be worn on the usual night-plus-4 hours schedule.

As a general rule, a tooth positioner in a cooperative patient will produce any changes it is capable of within 3 weeks. Final (posttreatment) records can be taken 2 or 3 weeks after the positioner is placed. Beyond that time, if the positioner is continued, it is serving as a retainer rather than a finishing device (see Chapter 18)—and positioners, as a rule, are not good retainers.

Special Finishing Procedures to Avoid Relapse

Relapse after orthodontic treatment has two major causes: (1) continued growth by the patient in an unfavorable pattern, and (2) tissue rebound after the release of orthodontic force.

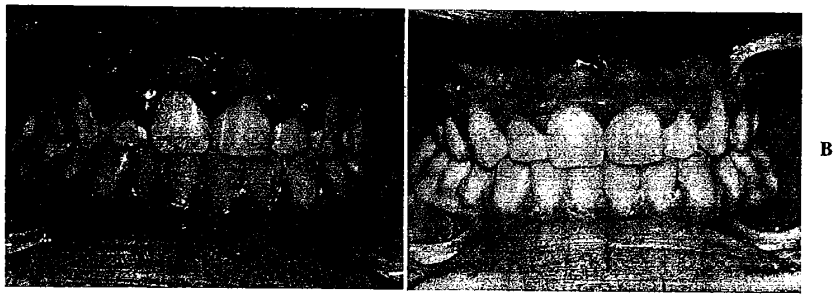


Fig. 17-24 ■ Gingival improvement with positioner wear. **A,** Swollen maxillary papillae immediately after band removal, just before placement of a positioner; **B,** 2 weeks later. This degree of gingival reaction anteriorly is rarely seen, especially with bonded attachments, but when it occurs, a positioner is one of the best means to resolve it.

ClearCorrect Exhibit 1002, Page 1921 of 3373

■ Control of Unfavorable Growth

Changes resulting from continued growth in a Class II, Class III, deep bite, or open bite pattern contribute to a return of the original malocclusion, and so are relapse in that sense. These changes are not attributed to tooth movement alone, however, but to the pattern of skeletal growth. Controlling this type of relapse requires a continuation of active treatment after the fixed appliances have been removed, rather than specific finishing procedures to prevent relapse. For patients with skeletal problems who have undergone orthodontic treatment, this "active retention" takes one of two forms. One possibility is to continue extraoral force in conjunction with orthodontic retainers (high-pull headgear at night, for instance, in a patient with a Class II open bite growth pattern). The other appropriate option is to use a functional appliance rather than a conventional retainer after the completion of fixed appliance therapy. This important subject is discussed in more detail in Chapter 18.

■ Control of Soft Tissue Rebound

A major reason for retention is to hold the teeth until soft tissue remodeling can take place. Even with the best remodeling, however, some rebound from the application of orthodontic forces occurs, and indeed the tendency for rebound after interarch elastics are discontinued has already been discussed. There are two ways to deal with this phenomenon: (1) overtreatment, so that any rebound will only bring the teeth back to their proper position, and (2) adjunctive periodontal surgery to reduce rebound from elastic fibers in the gingiva. In some cases, permanent retention is required to maintain the desired relationships, but this need not be planned if either of the two approaches described here would make it unnecessary.

Overtreatment. Since it can be anticipated that teeth will rebound slightly toward their previous position after orthodontic correction, it is logical to position them at the end of treatment in a somewhat overtreated position. Only a small degree of overtreatment is compatible with precise finishing of orthodontic cases as described previously, but it is nevertheless possible to apply this principle during the finishing phase of treatment. Considering three specific situations:

Correction of Class II or Class III Malocclusion. The rebound or settling after Class II or Class III correction has already been discussed. After headgear or elastics have been discontinued, it can be expected that the teeth will rebound 1 to 2 mm (see Fig. 17-15), so this degree of overtreatment is required. This rebound is entirely different from relapse tendencies caused by continued growth, which take at least several months to become apparent. The rebound from the forces used for Class II or Class III correction occurs relatively quickly, within 3 to 4 weeks.

Crossbite Correction. Whatever the mechanism used to correct crossbite, it should be overcorrected by at least 1 to 2 mm before the force system is released. If the crossbite is corrected during the first stage of treatment, as should be the case, the overcorrection will gradually be lost during succeeding phases of treatment, but this should improve stability when transverse relationships are established precisely during the finishing phase.

Irregular and Rotated Teeth. Just as with crossbites, irregularities and rotations can be overcorrected during the first phase of treatment, carrying a tooth that has been lingually positioned slightly too far labial, for instance, and vice versa. It is wise to hold the teeth in a slightly overcorrected position for at least a few months, during the end of the first stage of treatment and the second stage. As a general rule, however, it is not wise to build this overcorrection into rectangular finishing archwires.

Similarly, a tooth being rotated into position in the arch can be overrotated.[9] Maintaining an overrotated position can be done by adjusting the wings of single brackets, or by pinching shut one of a pair of twin brackets. Maintaining overcorrected labiolingual positions of incisors is done readily with first-order bends in working archwires. Rotated teeth should be maintained in an overcorrected position as long as possible, but even then, these teeth are often candidates for the periodontal procedures described following.

Adjunctive Periodontal Surgery. A major cause of rebound after orthodontic treatment is the network of elastic supracrestal gingival fibers. As teeth are moved to a new position, these fibers tend to stretch, and they remodel very slowly. If the pull of these elastic fibers could be eliminated, a major cause of relapse of previously irregular and rotated teeth should be eliminated. In fact, if the supracrestal fibers are sectioned and allowed to heal while the teeth are held in the proper position, relapse caused by gingival elasticity is greatly reduced.

Surgery to section the supracrestal elastic fibers is a simple procedure that does not require referral to a periodontist. It can be carried out by either of two approaches. The first method, originally developed by Edwards,[10] is called *circumferential supracrestal fibrotomy* (CSF) (Fig. 17-25). After infiltration with a local anesthetic, the procedure consists of inserting the sharp point of a fine blade into the gingival sulcus down to the crest of alveolar bone. Cuts are made interproximally on each side of a rotated tooth and along the labial and lingual gingival margins unless, as is often the case, the labial or lingual gingiva is quite thin, in which case this part of the circumferential cut is omitted. No periodontal pack is necessary, and there is only minor discomfort after the procedure.

An alternative method is to make an incision in the center of each gingival papilla, sparing the margin but separating the papilla from just below the margin to 1 to 2 mm below the height of the bone buccally and lingually (Fig. 17-26).[11] This modification is said to reduce the possibility that height of the gingival attachment will be reduced after the surgery, but there is little if any risk of gingival recession with the CSF unless cuts are made across thin labial

ClearCorrect Exhibit 1002, Page 1922 of 3373

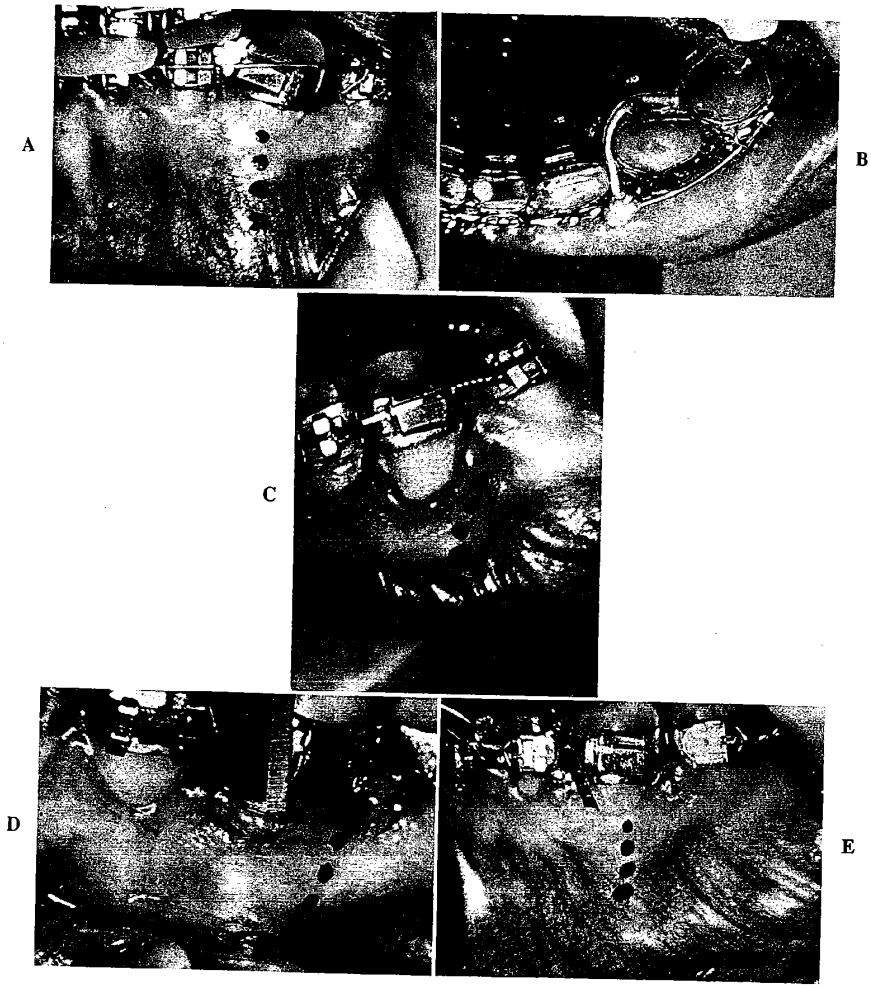


Fig. 17-25 ■ Elastic stretch of the supracrestal gingival fibers and the release of this elastic stretch by fiber section can be demonstrated by placing tattoo marks in the gingiva. **A,** India ink tattoos placed in the vicinity of a rotated maxillary canine before correction of the rotation; **B,** elastic thread used to rotate the tooth into position; **C,** the tooth rotated to its correct position in the arch. Note the displacement of the gingival tissues, as revealed by the deviation of the tattoo marks. **D,** Circumferential incision around the tooth, penetrating to the crest of the alveolar bone; **E,** after the incision, the gingival tissue returns to its original position. Periodontal probing shows a normal sulcus depth after the incision. (From Edwards JG: Am J Orthod 57:35-46, 1970.)

ClearCorrect Exhibit 1002, Page 1923 of 3373

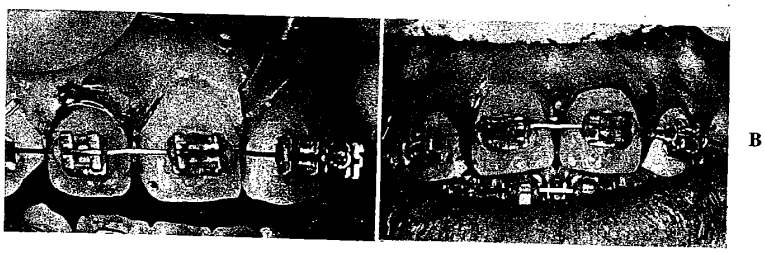


Fig. 17-26 ■ The "papilla split" procedure is an alternative to the CSF approach for sectioning gingival circumferential fibers to improve posttreatment stability. Vertical cuts are made in the gingival papillae without separating the gingival margin at the papilla tip. **A**, The blade inserted to make the vertical cut; **B**, view at completion of the papilla splits. One advantage of this procedure is that it is easier to perform with an orthodontic appliance and archwire in place.

or lingual tissues. From the point of view of improved stability after orthodontic treatment, the surgical procedures appear to be equivalent.

Neither the CSF nor the papilla-dividing procedure should be done until malaligned teeth have been corrected and held in their new position for several months, so this surgery is always done toward the end of the finishing phase of treatment. It is important to hold the teeth in good alignment while gingival healing occurs. This means that either the surgery should be done a few weeks before removal of the orthodontic appliance or, if it is performed at the same time the appliance is removed, a retainer must be inserted almost immediately. It is easier to do the CSF procedure after the orthodontic appliances have been removed, although it can be carried out with appliances in place. An advantage of the papilla-dividing procedure may be that it is easier to perform with the orthodontic appliance still in place. The only problem with placing a retainer immediately after the surgery is that it may be difficult to keep the retainer from contacting soft tissue in a sore area.

Experience has demonstrated that sectioning the gingival fibers is an effective method to control rotational relapse, but does not control the tendency for crowded incisors to again become irregular. The primary indication for gingival surgery therefore is a tooth or teeth that were severely rotated.[12] This surgery is not indicated for patients with crowding without rotations.

■ *References*

1. Burstone CJ: The segmental arch approach to space closure, Am J Orthod 82:361-378, 1982.
2. Gianelly AA: Asymmetric space closure, Am J Orthod Dentofacial Orthop 90:335-341, 1986.
3. Fields HW: Orthodontic-restorative treatment for relative mandibular anterior excess tooth size problems, Am J Orthod 79:176-183, 1981.
4. Steffen JM, Haltom FT: The five-cent tooth positioner, J Clin Orthod 21:528-529, 1987.
5. Bennett CG, Shen C, Waldron JM: The effects of debonding on the enamel surface, J Clin Orthod 18:330-334, 1984.
6. Bishara SE, Trulove TS: Comparisons of different debonding techniques for ceramic brackets: an in vitro study. II. Findings and clinical implications, Am J Orthod Dentofacial Orthop 98:263-273, 1990.
7. Rueggeberg FA, Lockwood P: Thermal debracketing of orthodontic resins, Am J Orthod Dentofacial Orthop 98:56-65, 1990.
8. Rouleau BR, Marshall GW, Cooley RD: Enamel surface evaluation after clinical treatment and removal of orthodontic brackets, Am J Orthod 81:423-426, 1982.
9. Zachrisson BU: On excellence in finishing (interview), J Clin Orthod 20:99-120, 1986.
10. Edwards JG: A surgical procedure to eliminate rotational relapse, Am J Orthod 57:35-46, 1970.
11. Ahrens DG, Shapira Y, Kuftinec MM: An approach to rotational relapse, Am J Orthod 80:83-91, 1981.
12. Edwards JG: A long-term prospective evaluation of the circumferential supracrestal fiberotomy in alleviating orthodontic relapse, Am J Orthod Dentofacial Orthop 93:380-387, 1988.

ClearCorrect Exhibit 1002, Page 1924 of 3373



ClearCorrect Exhibit 1002, Page 1925 of 3373

Dear Doctor,

Raintree Essix™ Inc. is the pioneer in researching and developing plastic products for Essix™ appliances.

Essix™ retainers have proven to be an esthetic method of retaining finished orthodontic cases at a fraction of the cost and frustration of conventional devices. They provide absolute stability and make the teeth appear brilliant. Since they require no adjustment, it is feasible to monitor the majority of retention supervision by phone, affording the clinician significant relief in chair time and administrative detail.

Also, techniques for minor tooth movement, temporary bridges, fluoride trays, night guards and bite splints have been developed that take a fraction of the time and cost to fabricate.

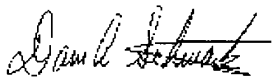
Essix™ appliances are critically dependent on the use of quality materials, and precision instruments. Dr. Jack Sheridan, the originator of Essix™ concepts, is the exclusive consultant of Raintree Essix™ Inc. on technique and materials. He insists that clinicians have a source of materials that are reliable and reasonably priced. He tests all materials that we offer. Only after being satisfied with quality, consistent with price, does he endorse distribution.

We are constantly updating our products. Within the last two years, we have improved, tested, manufactured and marketed additional plastics that are compatible with the clinician's needs. For example, our new Essix™ Type "C" plastic is virtually indestructible and our brilliantly clear Essix™ Type "A" plastic is 20% stronger.

We know our products and are aware of the concerns of the clinician. Raintree Essix™ Inc. is prepared to answer your technical questions, supply literature, and provide tested, reliable products at reasonable prices. We routinely send out updates on technique and products, at no charge to our customers. Also, we have a constantly updated World Wide Web site of the Internet. Our customers can communicate directly with us or Dr. Sheridan, anywhere in the world, at any time!

Feel free to call us at (800) 883-8733 or (504) 488-0080. You don't have to place an order to talk to us or get technical support. We believe in old-fashion customer service. We will continue to provide a complete line of products and services that offers you, our valued customer, the greatest value consistent with quality and dependability.

Very truly yours,



Dann A. Schwartz
President

Contents

Essix™ Appliances: *Fabrication, Application and Rationale*

Mouthguard Techniques

Moving Teeth with Appliances: *How to Create Windows and Divots*™

The Essix™ Machine: *Amplified Vacuum Thermoforming Tips*

Video Reviews

Singe Essix™ Posterior Extension Appliance: *Two Layers of Essix™ Plastic - Reinforced*

Essix™ Technology: *Fabrication of Temporary Anterior Bridges*

The Alpern Invisible *Without the Occlusal Retainer*™

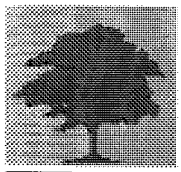
The New Ortholink™ Service

ClearCorrect Exhibit 1002, Page 1926 of 3373

Raintree Essix

Raintree Essix - email: raintree@essix.com
Tel.: (504) 488-0080 - Toll-free: (800) 883-8733 - FAX: (504) 488-2429
Last revised: January 7, 1997.

ClearCorrect Exhibit 1002, Page 1927 of 3373



RAINTREE ESSIX
ESSIX™ & ARS MATERIALS INC.

Essix™ Appliances

Fabrication, Application & Rationale

TABLE OF CONTENTS

I Essix™ Cast Standards

II Essix™ Plastic Sheet
Types "A" and "B"

III Adapting Vacuum
Thermoforming Machines For Essix™

IV Getting the Best Fit on an Essix™ Appliance

V Schedule of Wear for Essix™ Retainers

VI Essix™ Retainer:
3-3 and Full Arch Appliances

VII Open Bite Considerations
with Conventional Essix™ Appliances

VIII Can Essix™ Retainers be Swallowed?

IX Managing the Extraction Site with Essix™ Retainers

X Essix™ Temporary Bridge

XI Letter to Patients Regarding Essix™ Retention

XII Using the Divoter™

XIII Shimming (Reinforcing) the Divot

XIV Other Applications of Essix™ Technology

ClearCorrect Exhibit 1002, Page 1928 of 3373

Full Arch Appliances
Minor Tooth Movement
Bleaching Trays
Bite Planes
Space Maintainers

XV Thermoforming with Essix™ "B" Plastic

XVI Contraindications and Limitations of Essix™ Retainers

For ease of printing, this page is available as one complete document.

Raintree Essix ← Technical Magazine

Raintree Essix - email: raintree@essix.com
Tel.: (504) 488-0080 - Toll-free: (800) 883-8733 - FAX: (504) 488-2429
Last revised: September 4, 1996. BRAY TECHNOLOGIES, INC., Copyright (c) 1995, 96.

ClearCorrect Exhibit 1002, Page 1929 of 3373

Moving Teeth with Essix™ Appliances: Windows & Divots™

by Dr. John J. Sheridan

I. Principles of Essix Tooth Moving Mechanics
II. Range of Tooth Movement and Types of Plastic
III. Types of Tooth Movement: Tip, Differential Bodily Movement, Rotation, and Torque
IV. Creating the Window
V. Creating the Divot
VI. Shimming (Reinforcing) the Divot

For ease of printing, this page is available as one complete document.

Raintree Essix ← Technical Magazine

Raintree Essix - email: raintree@essix.com
Tel.: (504) 488-0080 - Toll-free: (800) 883-8733 - FAX: (504) 488-2429
Last revised: September 4, 1996. **BRAY TECHNOLOGIES, INC., Copyright (c) 1995, 96.**

ClearCorrect Exhibit 1002, Page 1930 of 3373

Raintree Essix Retainers

I. About Essix Retainers

II. Essix Cast Standards

III. Materials for Essix cast fabrication

IV. Essix Copolyester Plastic Sheet

V. Adapting vacuum thermoforming machines for Essix

VI. Getting the Best Fit on an Essix Appliance

VII. Schedule of Wear for Essix Retainers

VIII. Why Essix Retainers are Cuspid-to-cuspid Appliances

IX. Open Bite Considerations with Essix Appliances

X. Can Essix Retainers be Swallowed?

XI. Managing the Extraction Site with Essix Retainers

XII. The Essix Temporary Bridge

XIII. Other applications of Essix Technology

XIV. Contraindications and limitations of Essix Retainers

NOTE: ALL PRODUCTS MENTIONED ON THESE PAGES CAN BE OBTAINED FROM THE RAINTREE ESSIX CORPORATION

Raintree Essix ← Products

Raintree Essix - email: raintree@essix.com
Tel.: (504) 488-0080 - Toll-free: (800) 883-8733 - FAX: (504) 488-2429
Last revised: September 3, 1996. BRAY TECHNOLOGIES, INC., Copyright (c) 1995, 96.

ClearCorrect Exhibit 1002, Page 1931 of 3373

ORTHO BYTES

Clinical implications of digital orthodontics

W. Ronald Redmond, DDS, MS, William J. Redmond, DDS, MS, and M. John Redmond, DDS, MS
Laguna Niguel, Calif

After nearly 30 years of orthodontic practice, I (W.R.R.) have achieved several goals that allow for a total integration of computers and treatment efficiency. First, my 2 sons have elected to join me in the practice of orthodontics, and second, I have arranged what I believe to be the perfect marriage between orthodontic and computer technologies.

As our practice grew to multiple locations, we developed a unique clinical problem, handwritten treatment cards. Patients would frequently make appointments in offices other than the location where their treatment card was stored. We spent a great deal of time faxing copies of treatment cards to outlying locations and had even more trouble making sure the fax copy was re-entered onto the original card. This quickly became a nightmare.

Even though we started using computers for all of the clerical and some of the clinical operations as early as 1985 using Orthotrac software, we didn't realize that our computer system would facilitate our practice growth and ultimately simplify our clinical activities. Orthotrac solved the problem by providing us with electronic treatment cards. This "simplification," however, posed its own set of problems. Computer terminals needed to be placed at each chair and networked. In addition, the satellite offices required high-speed networks to allow a patient's treatment information to be viewed at any location. With the help of Orthotrac and the telephone company, the networking was accomplished. Can you imagine the joy? No longer did we "pull" and "file" patient charts each day. No longer did we fax copies of treatment charts. Best of all, patients were impressed with our high-tech offices.

As our practice continued to grow, we found that our system was still not entirely complete. Patient folders containing examination notes, radiographs, and clinical photographs occasionally were transferred from their original location or taken home by one of the doctors for diagnostic purposes. We found ourselves mired in a morass of lost or misplaced records. When a doctor asked for a panorex or headfilm while the patient was in the chair, the answer was invariably, "Sorry doctor, the records are in another office location."

Several different options were explored that would allow for the digitalization of orthodontic records, but each method presented obstacles that would prove to be cost-ineffective and make data transfer so slow as to be impossible. Once more, we looked to the computer industry and the latest in computer technology to find the answers. I found a digital radiographic system and camera that would allow for storage directly on my hard drive. An automatic back-up system was set up on my server that continuously updates dual hard-drives of all patient radiographic and photographic records. I no longer need to worry about crashes or lost information as a result of the redundancy of the dual drives. A network of computers allows for easy viewing of photos and radiographs that have been transferred quickly and in a cost-effective manner.

Over the last 12 months, we have put in place a new network that incorporates digital photography, digital radiography, and Microsoft terminal server technology. Using a new communications service, Digital Subscriber Line (DSL), which can transmit and receive information up to 1.5 megabits per second, we have established an intranet for our orthodontic practices. Because this intranet is accessible from any Internet connection, we now have the ability to view our examination notes, radiographs, and clinical photographs from practically anywhere.

We are delighted to be able to view our diagnostic records from any practice location and from our homes. No longer are we told that the records are in another office. And, as you might expect, our patients are again impressed by our high-tech capabilities. Best of all, our clinical efficiency is improved because of ready access to pertinent clinical information.

A confluence of opportunities occurred within the past 18 months that made the preceding capabilities possible. Microsoft Windows NT 4.0 with Terminal Server Client was released in 1998. This software is a return to a "server-centered" network. Like the SCO UNIX based system we had been using for our Orthotrac management program, Terminal Server facilitated the transfer of graphic data through a local area network (LAN) or a wide area network (WAN). The programs and the data remain on the server, and the terminals (or PCs) simply provide a viewing screen, keyboard, and mouse. This method of software deployment has been called "thin slice" utilization. Multiple "licensed-users" can access the same program simultaneously. The obvious power of this system is the decrease in data transferred, with the inherent increase in transfer speed, and management of programs through periodic updates only on the server.

Terminal Server Client functions equally well in an intranet or Internet environment, however, each program is accessed by a separate intranet or Internet connection. This proved to be cumbersome and inefficient.

Citrix Metaframe 1.8, also a thin slice software, provides a solution to Microsoft's Terminal Server Client, by transmitting the server desktop to the terminal with all the program

Copyright © 2000 by the American Association of Orthodontists.
0889-5406/2000/$12.00 + 0 8/1/104691

ClearCorrect Exhibit 1002, Page 1932 of 3373

icons available. With a single Internet connection, patient photographic, radiographic, and treatment card information may be accessed. Citrix Metaframe Client can be downloaded from www.citrix.com and installed on practically any PC or terminal, facilitating the addition of "clients" to the network.

Implementation of our system uses digital photography (Olympus D600L), digital radiography (Sirona Digital Pan/Ceph), and the above server software. These technologies coupled with a high speed Internet connection (DSL 1.5 megabits/second) and a static IP (Internet protocol) address allows access to all the data contained on the servers.

All connections to the Internet are susceptible to hackers, and care must be taken to safeguard programs and patient records. Citrix Metaframe 1.8 is designed to function with encryption software to help maintain privacy. The federal guidelines for transmission of patient information over a public venue (Internet) have been established. As of Jan 1, 1999, patient information must be encrypted to prevent public disclosure. The Federal statutes provide an implementation period of 2 years, until Jan 1, 2001, before penalties will be imposed. The penalties are substantial, with up to $50,000 in fines and 10 years in jail. Anyone contemplating the transmission of patient records over the Internet must be aware of this legislation.

The transmission and reception of digital orthodontic records and treatment protocols presents the profession with a unique opportunity. Diagnostic information is always available and on a "real-time" basis. Records taken in New York can be viewed in California immediately. Second opinions and diagnostic help are facilitated. Databases may be established and used for teaching and clinical support. The opportunities are unlimited and, I believe, provide a portal to the new millennium.

ORTHOLINKS

This section of OrthoBytes will present Internet links that are of interest to the orthodontic community. Readers who wish to submit Internet addresses for this section should contact the Editors.
In the November issue of the Journal, there was an error in one of the Ortholinks. The correct links and text are printed below. We apologize for any problems this caused.

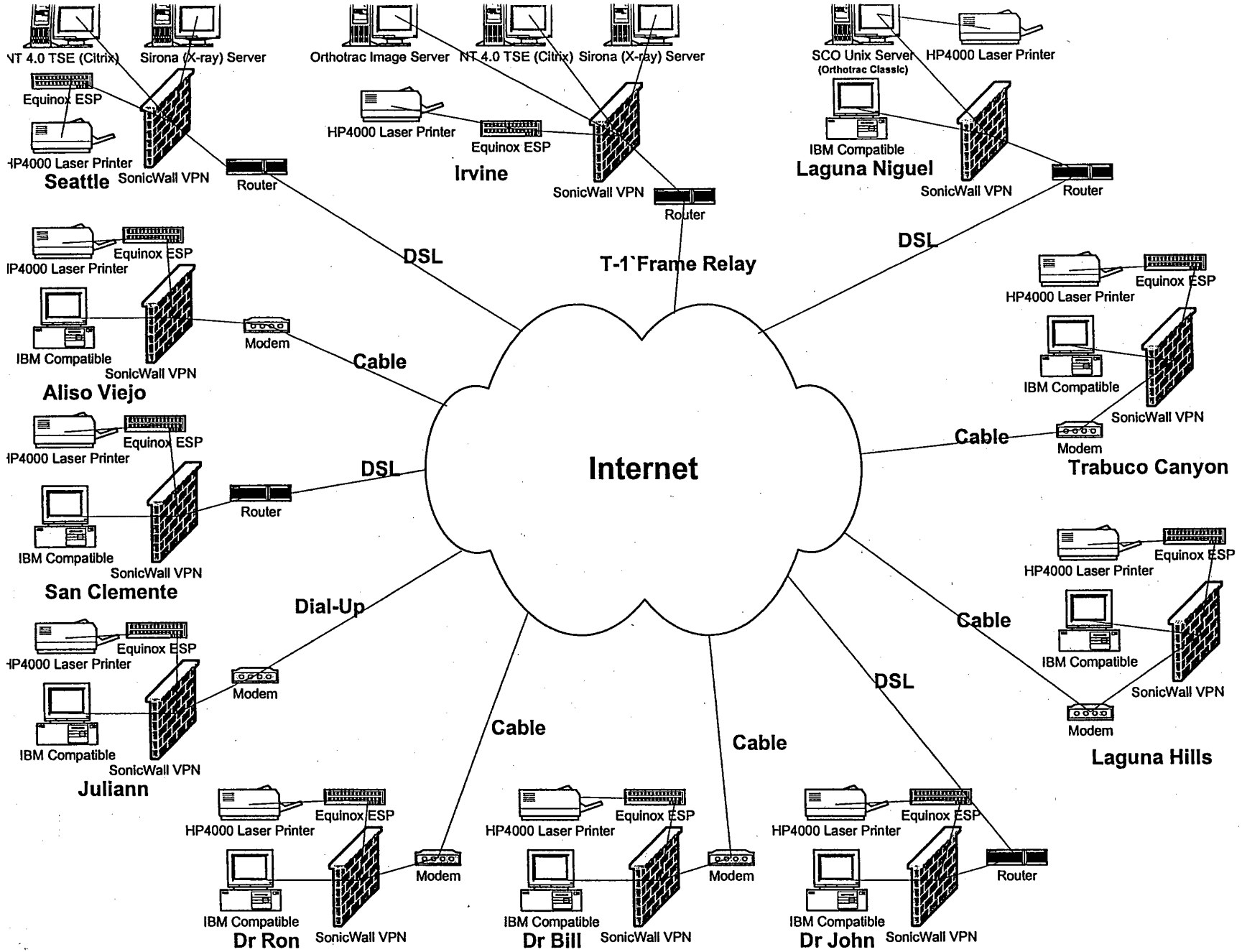
Dr. Potter's Interview in the Orthodontic CYBER Journal and the ToothCam
http://www.oc-j.com/2-99/toothcam.htm
http://www.caltech.edu/~pinelab/TimeLapse/ToothCam/toothcam.html

The Orthodontic CYBERJoumal contains an interview given by Dr Potter, a neurobiologist, who underwent orthodontic treatment as an adult. His experiences may be enlightening to many orthodontists. Although the general impression seems positive, orthodontic technology was described as "prehistoric and barbaric," and diagnosis was considered superficial. Read the whole interview and then visit the ToothCam web site, from where you can download movies of treatment progress made by the patient and read a detailed diary.

Dr. Silverstein's Digital Camera Setup
http://www.orthonj.com/camera.html

This page, from Dr Robert Silverstein's web site, describes his digital camera setup. Dr Silverstein uses an Olympus D-600L with a ring-flash specially made for digital cameras. Useful tips and sample photos are included, as well as a Microsoft Word template for inserting them into letters for the referring dentist. The flash is the SR Electronics RF-50. Ring Flash and a review can be found at http://www.dcresource.com/Ringflash/ringflash_review.html.

ClearCorrect Exhibit 1002, Page 1933 of 3373



ClearCorrect Exhibit 1002, Page 1934 of 3373

CAD/CAM for Dental Restorations—Some of the Curious Challenges

E. Dianne Rekow, Arthur G. Erdman, Donald R. Riley, and Barney Klamecki

Abstract—Computer-aided design and manufacturing for dental restorations has opened a new world of possibilities—some that appeal to engineers and clinicians and some that have created some interesting challenges. The objective of this overview is to briefly describe a system being developed by the Universities of Maryland and Minnesota which is capable of producing dental crowns. Some of the challenges and difficulties that have arisen during the development activities will be addressed. The final focus will be on some of the questions that, because of the new technology, can now be addressed and are presenting new challenges.

Current State of the Art for Production of Dental Restorations

MANY dental restorations are currently produced using the lost-wax casting technique (Table I). A dentist prepares the tooth, removing all decay and creating a design of the remaining tooth structure that will a) support the loads to which the tooth will be subjected during function, b) integrate unique features for the materials from which the restoration will be fabricated, c) maximize the retention of the restoration on the tooth. An impression of the prepared tooth and any adjacent proximal teeth is made, creating a three-dimensional negative of the teeth. Another impression of the opposing, occluding teeth is also made. A temporary restoration is placed on the prepared tooth and the patient leaves the dental office until the final cast restoration is fabricated.

Dental plaster is poured into the impressions, creating a model of the patient's mouth. The portion of the model that duplicates the prepared tooth must be removable so that a wax pattern can be created. To accomplish this; a brass pin is placed in the model below the prepared tooth. A second layer of plaster is added to the model, surrounding the pin. When this second layer of plaster has hardened, two thin cuts are made through the first layer of plaster (which contains the representation of the prepared tooth) just proximal to prepared tooth. The section of the model with the prepared tooth can now be removed from and reinserted into the models. This section is called the die.

When the restoration is seated on the tooth, the edge where the restoration meets the tooth is called the margin. After a die has been made removable from the models, excess plaster below the margin is removed and the margin is marked. Separating medium is placed over the die. A technician then melts and carves wax to create a wax pattern of the required restoration.

The wax pattern is sprued and invested. When the investment material has hardened, the wax pattern is burned out. Molten restorative material is flowed into the investment. The raw casting is recovered, cleaned, and polished. The restoration is now ready to be seated in the patient's mouth.

The patient must now return to the dental office. The temporary restoration is removed and any debris left on the tooth removed. The tooth must be thoroughly dried and the restoration glued to the tooth.

Using typical materials, the minimum time required for these operations is 9 h. Usually, however, a patient will wear a temporary for 1–2 weeks. Temporary restorations seldom fit as accurately as a permanent restoration so tissues around them often become inflamed and the prepared tooth may move slightly. Both of these phenomenon complicate the procedure for placing the restoration. Inflamed tissue is more sensitive and usually more resistant to anesthesia. Movement of the tooth will create problems in fitting the final restoration.

With the CAD/CAM systems, restorations can be produced much more quickly, eliminating the need for temporary restorations. Furthermore, with the automation, consistent quality becomes possible.

TABLE I
Steps of Lost-Wax Technique

1)	Dentist prepares tooth
2)	Take impression
3)	Make temporary and place on patient's tooth
4)	Pour first plaster into impressions
5)	Seat pins in plaster
6)	Pour second plaster as base
7)	Section die
8)	Isolate margins on die
9)	Mark margins
10)	Apply separating medium
11)	Carve wax pattern
12)	Sprue wax pattern
13)	Invest wax pattern
14)	Burn out wax
15)	Cast
16)	Recover casting
17)	Polish casting (ready to seat restoration)
18)	Remove temporary restoration from patient's tooth
19)	Seat cast restoration on patient's tooth

The DentiCAD System

The system being developed at the Universities of Maryland and Minnesota automates the production of dental restorations. The system has three functional components parts: data acquisition, CAD/CAM, and machining. With the automation, the labor intensive processes currently required are eliminated and restorations can be designed and fabricated in less than 1 h.

Manuscript received March 6, 1989.

E. D. Rekow is with the Department of Orthodontics, School of Dentistry, University of Maryland, Baltimore, MD 21201.

A. G. Erdman, D. R. Riley, and B. Klamecki are with the Department of Mechanical Engineering, University of Minnesota, Minneapolis, MN 55455.

IEEE Log Number 9144234.

0018-9294/91/0400-0314$01.00 © 1991 IEEE

ClearCorrect Exhibit 1002, Page 1935 of 3373

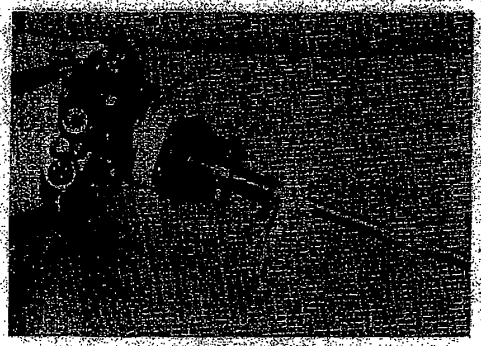


Fig. 1. Camera system for "optical impressions."

Data Acquisition

Two techniques for data acquisition are being developed. With the first, data are acquired from the patient directly through an optical "impression" based on a customized stereophotogrammetric technique. Stereo pairs of images are obtained for the prepared tooth, the proximal teeth, and the opposing teeth. A special lens is used that incorporates a prism so that the distal portion of posterior teeth can be seen (Fig. 1). The lens fits onto a standard 35-mm camera. The images are captured on film and then digitized on a high-resolution (4096 × 4096 pixel) digitizer, providing a data acquisition accuracy of 2.5 μm. (Note: when high-resolution real-time cameras become available, they will be integrated into the design, eliminating the need for a separate digitizing step.)

A set of stereo pairs of images is recorded [Fig. 2(a) and (b)]. In its current configuration, one image is recorded, the camera is moved, and the second half of the stereo pair is recorded. This requires that the object remain stationary throughout the procedure. This is not a realistic constraint in a clinical setting and a stereo lens design is currently underway.

The images are processed. The first operation is to differentiate areas of interest (bounded by the margins of the prepared tooth) from areas of no interest. This is accomplished through customized edge-finding algorithms. Using different threshold values, these same edge-finding algorithms can locate burr scratches on the surface of the tooth, adding apparent features to an otherwise optically flat surface (Fig. 3).

From the stereo pairs, each point in the first half of the image pair is matched with its equivalent in the second half of the image pair. This creates a triplex of x, y, disparity values where x, y are the planar coordinates for a point or feature in the first half of the stereo pair and the disparity value is the shift of that point or feature to its position in the second half of the stereo pair.

From the geometry of the camera used to capture the images and this triplex of x, y, disparity, a three-dimensional reconstruction of the surface of the prepared tooth is created (Fig. 4—the data displayed in this image is identical for all four views; only the viewing angle has changed). Identical operations are used for establishing the 3-D surface map of the proximal edges of adjacent teeth and the opposing teeth.

In the second configuration for data acquisition, optical triangulation is used (Fig. 5). With this alternative, a die must be prepared. Positioning accuracy of the system is ± 10 μm in x, y, and z (Fig. 6). A low-powered laser beam is directed at the die. The reflection of the beam is sensed by a CCD chip. The deflection of the reflected beam from a known position gives the z coordinate. The x and y coordinates are obtained by recording the location of the moving plate onto which the die has been placed. A point by point scan of the surface creates the

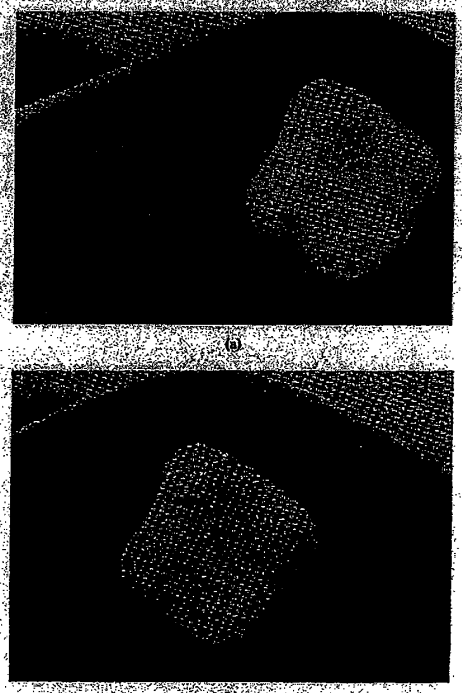


Fig. 2. Right and left halves of a stereo pair of images of a prepared mandibular first molar.

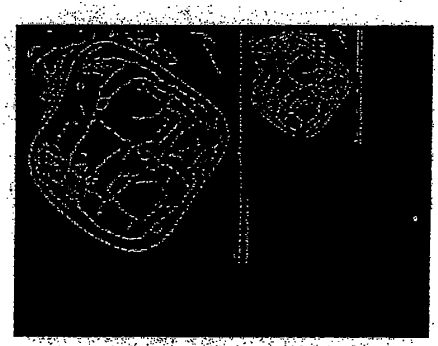


Fig. 3. Edge finding algorithm applied to the left half of the stereo pair shown in Fig. 2.

ClearCorrect Exhibit 1002, Page 1936 of 3373

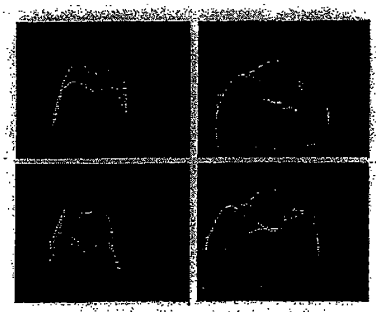


Fig. 4. Reconstructed prepared tooth (from various views).

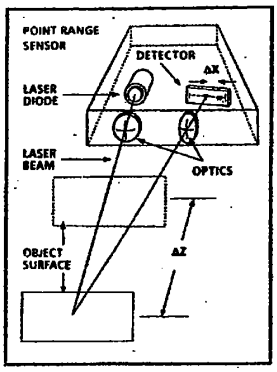


Fig. 5. Principle of optical triangulation.

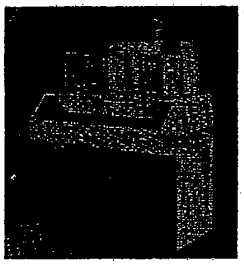


Fig. 6. Triangulation digitizer.

digital x, y, z surface map (Fig. 7 shows the graphical display of a digitized mandibular first molar).

CAD/CAM

The CAD/CAM operations replace the waxing processes of the traditional techniques. Custom software was developed in C language with a Unix operating system on an Iris 4D/50



Fig. 7. Digitized mandibular first molar.

Graphics Workstation (Silicon Graphics, Mountain View, CA). The 3-D data (from either data acquisition technique) is used to calculate the space into which the restoration must fit. This space is defined by the space available with the teeth together as well as their relative positions as they move through the entire range of motion of the jaw.

The design of the restoration creates three surfaces: the internal surface, the external surface to the crest of convexity (this is the portion of the restoration that occludes with opposing teeth and contacts the adjacent teeth), and the external surface of the tooth between the crest of convexity and the margins. The internal surface must mirror the configuration of the prepared tooth. Near the margins it must replicate the shape of the prepared tooth exactly. Away from the margins it needs to be offset by a sufficient amount to permit a gluing agent to be added (to keep the restoration in place on the tooth).

For the external surface above the crest of convexity, the CAD software automatically accesses a database of ideal tooth morphologies. From the calculated available space, a scale factor is generated for the general dimensions of the crown. However, the location of cusp tips and fossae in the occlusal surface must be modified to fit the unique requirements of each patient. The software automatically establishes these relationships, moving reference points to the required positions and blending adjoining surfaces smoothly so that the typical morphology is maintained but the uniqueness for each patient is obtained. The remaining external surface blends the margins (defined by the internal configuration) and the crest of convexity (defined by the other external portion), creating a smooth surface.

The CAM software automatically translates the design created by the CAD portion of the system to tool paths for a micromilling machine (Fig. 8). Offsets are automatically added to the surface to compensate for cutter tool diameters. Antigouging algorithms prevent the cutter from removing material during one cutting path that is part of the required surface in an adjacent area.

Machining

The tool paths are automatically sent to a micromilling machine with positioning accuracy of ± 5 μm (Servo Products, Pasadena, CA). The restoration is fabricated from a single block of material. The internal and external surfaces below the crest of convexity are machined. The restoration is flipped 180° and the external portion above the crest of convexity is fabricated.

ClearCorrect Exhibit 1002, Page 1937 of 3373



Fig. 8. Machine tool paths for CAD/CAM designed restoration.

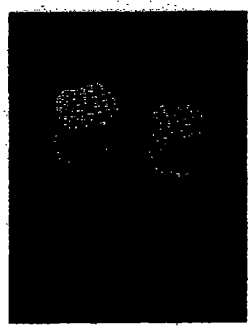


Fig. 9. Machined restorations.

(Fig. 9 shows restorations machined from metal and machinable ceramic.)

Challenges During System Development

A number of interesting—and sometimes frustrating—challenges arose as part of the development process. One of the first was translating clinical criteria into engineering tolerances to produce decision-based design rules for the CAD algorithms. Ideally a restoration should exactly fit the tooth at the margins. Clinical justification for this is twofold. First, with any gap in the fit, an area is created that collects debris and can result in decay and/or inflammation to the gum tissues. The second is that many of the gluing agents used either abrade away or are water soluble and simply wash away over time if there is a misfit between the restoration and the tooth.

Clinically, the test for acceptable fit is that a clinician moving a dental explorer across the tooth-restoration interface cannot feel that interface. There is little agreement in the dental literature about what that tolerance is. Indeed, there is little agreement about exactly what and how measurements should be made to qualitatively determine what the clinician can sense [1]. By translating all of the measurements reported into a single set of geometric relationships, it appears that acceptable cast restorations generally achieve a fit of 40–60 μm at the margins [1]–[5].

Another interesting challenge is how to optically acquire accurate data from real teeth. A prepared tooth may be stained from old restorative materials or caries. It may contain filling materials with coloration substantially different from that of a normal tooth. By using edge finding algorithms these discolorations and other materials act as pseudofeatures, enhancing the point matching for disparity calculations.

Imaging the teeth is not a trivial problem. In many typical prepared teeth, the sides of the remaining tooth structure are quite long. To be clinically successful they must also have nearly parallel and vertical walls. Many of the commercially available imaging systems trade depth of field for resolution [4]—to achieve very high resolution (to the micron level) the depth of field is much less than the height of a typical preparation. For the optical impressions, problems are managed by merging multiple views of capture the entire prepared tooth surface.

For the triangulation digitizer, special modifications of the machine were required. To compensate for the depth of field problem, a number of ranges of depth of field are scanned. A point is recorded only when the reflected light hitting the CCD sensor exceeds a specified light-threshold. If insufficient light is sensed, the z-axis drive shifts the laser-sensor and another measurement is attempted. This process is repeated until sufficient light levels are obtained. To compensate for the near-parallel walls, the die is scanned from an angle, providing the laser with an apparent viewing angle of less than 85°.

Clinical and Materials Questions

While the technology of CAD/CAM has produced some interesting engineering questions and challenges that have already been solved, unquestionably interesting ones remain for the dentist, engineer, and materials investigators.

One of these is the quality of margins that are needed. Should the CAD/CAM technology provide only what is currently average marginal quality or integrity or should the technology be pushed to its limits, providing improved fit as a standard?

Each of the steps of the traditional impression-lost wax-casting process has implicit sources of error. These include distortions in the impression material, plaster, wax pattern, or investment material; changes in water-powder ratios or techniques of the mixing; casting failures; and others. Automation eliminates these but replaces them with different contributions of error. Table II summarizes these contributions for off-the-shelf high resolution component parts [6]. The imaging and digitizing errors are dependent upon the quality of the lenses employed (or the degree to which distortions can be mathematically removed), the resolution of the digitizer, and the density of features on the teeth which can be detected. Surface modeling errors are contributed by curve fitting algorithms and three-dimensional reconstruction techniques. The contribution of errors from CAM comes from two different sources: 1) the positioning accuracy in the milling machine, wear of the cutter, and relative movement, if any, between the cutter and the part being fabricated and 2) scalloping error resulting from cutter paths plus the errors resulting from the cutter being able to move only in straight-line movements from one specified point to the next.

In the worst case, all of these contributions to error can be assumed to be independent so they are additive, yielding a total error contribution from the new technology of 17.8 μm. Even in this worst case, there is the potential for accuracy greater than that currently available with the lost-wax technique. Restorations produced with the lost-wax technique are usually considered to be acceptable with marginal fit of about 40–60 μm. Based on a small sample size, restorations produced with the Minnesota CAD/CAM system can produce margins of 0–49 μm

ClearCorrect Exhibit 1002, Page 1938 of 3373

TABLE II
ERROR CONTRIBUTIONS FROM CAD/CAM

Imaging and Digitizing	2.5 μm
Surface Modeling	10.0 μm
CAD	0.0 μm
CAM:	
Milling	4.8 μm
N/C Path	0.5 μm
	17.8 μm

(average = 23 μm, SD = 23 μm) measured from the margin to 300 μm from the margins in 20 μm increments [7]. Machining operations are more critically controlled very close to the margins. For the first 100 μm, the fit ranged from 0 to 37 μm (average = 12 μm, SD = 15 μm). Should effort be expended to further reduce the errors to reach the theoretical limit? What should be the standard? Stated differently, is there any clinical difference between margins that fit to within 40–60 μm and those that fit to within 20 μm?

Another surprising area of opportunity that has arisen is specification of processing parameters. For any milling operation, it is possible to vary spindle speed, material feed rate, and depth of cut simultaneously. Different materials demand different values for these parameters, yet little has been published concerning this problem. Cutting parameters for dental materials do not appear in the standard machinists' handbook. The size of the cutters used for the geometries produced by dental CAD/CAM systems is much smaller than those used for typical industrial applications. Little work relating materials properties to cutting parameters at the scale required for dentistry has been done. The physics of material removal with small cutters awaits scientific inquiry.

Another question which has arisen relates to surface finish. The American Dental Association specification for the finish of a metal crown requires an 8 μm rms smoothness criterion but says nothing about reflectance or spectral feature. With currently practiced polishing operations, a surface that meets this smoothness criterion is also shiny. With the machining operation, it is possible to obtain this smoothness yet still be able to see the tracks of the tool path. Should a metal crown be smooth, or shiny, or both?

The opportunities and challenges to the dental materials investigators are tremendous. It is now possible to consider an entirely new array of materials—castability or manipulation within the oral cavity is no longer a criterion for selection. The parameters that make a material ideal for a dental restoration are not well quantified. When new materials are possible, questions arise about how the tooth should be prepared to optimize the performance of the tooth-restoration system.

SUMMARY

The DentiCAD system can produce dental restorations that fit at least as well as those that are cast. The system speeds production, eliminates the labor intensive steps currently required, and provides consistent quality. This CAD/CAM technology applied to the dental problem of designing and fabricating restorations, has created some interesting engineering challenges for acquiring data, establishing tolerances for clinical criterion, and managing existing dental materials. The future, however, will be more and more interesting as we learn to ask new and different questions about what new possibilities the automation creates.

REFERENCES

[1] J. R. Holmes, "Marginal fit of castable ceramic (Dicor) crowns," M.S. thesis, Univ. North Carolina, Chapel Hill, NC, 1986.
[2] J. M. McLean *et al.*, "The estimation of cement film thickness by an *in vivo* technique," *Brit. Dental J.*, vol. 131, pp. 107–111, 1971.
[3] U. C. Belser, M. I. MacEntree, and W. A. Richter, "Fit of three porcelain-fused-to-metal marginal design, *in vivo*: A scanning electron microscope study," *J. Pros. Dental.*, vol. 53, pp. 24–34, 1985.
[4] D. N. Allan, "A macroscopic study of filled teeth," *Brit. Dental J.*, vol. 21, pp. 386–390, 1970.
[5] G. J. Christiansen, "Marginal fit of gold inlay castings," *J. Pros. Dental*, pp. 227–231, 1966.
[6] R. Caudell, Univ. Alabama, presentation at Greater NY Dental Meet., Dec. 3, 1987.
[7] E. D. Rekow, V. P. Thompson, and H. S. Yang, "Margin fit of CAD/CAM produced crowns," *J. Dental. Res.*, vol. 70, 1991.



E. Dianne Rekow received the M.S.M.E., D.D.S., and Ph.D. degrees in biomedical engineering from the University of Minnesota, Duluth.

She is currently an Associate Professor in the Department of Orthodontics at the University of Maryland, School of Dentistry, Baltimore. Her research focuses on CAD/CAM in dentistry.

Dr. Rekow is a fellow in the Academy of Dental Materials and a member of ASME, SPIE, IADR, and other professional organizations.

Arthur G. Erdman received the Ph.D. degree in mechanical engineering from Rensselaer Polytechnic Institute, Troy, NY.

He is currently a Professor of Mechanical Engineering at the University of Minnesota, Minneapolis, and Chairman of the Design Division. His major research interests are kinematics and biomedical engineering.

Dr. Erdman is an active member of ASME and a number of other professional organizations.

Donald R. Riley received the Ph.D. degree in mechanical engineering from Purdue University, West Lafayette, IN.

He is currently a Professor of Mechanical Engineering at the University of Minnesota, Minneapolis, and serves as co-Chairman of the University's Productivity Center. His major research interests are CAD/CAM and computer graphics.

Dr. Riley is an active member of ASME and a number of other professional organizations.

Barney Klamecki received the Ph.D. degree in mechanical engineering from the University of Illinois, Chicago.

He is currently a Professor of Mechanical Engineering at the University of Minnesota, Minneapolis. His major research interests are manufacturing and machining operations.

Dr. Klamecki is an active member of ASME, SME, and other professional societies.

ClearCorrect Exhibit 1002, Page 1939 of 3373

CAD/CAM for Dental Restorations—Some of the Curious Challenges

E. Dianne Rekow, Arthur G. Erdman, Donald R. Riley, and Barney Klamecki

Abstract—Computer-aided design and manufacturing for dental restorations has opened a new world of possibilities—some that appeal to engineers and clinicians and some that have created some interesting challenges. The objective of this overview is to briefly describe a system being developed by the Universities of Maryland and Minnesota which is capable of producing dental crowns. Some of the challenges and difficulties that have arisen during the development activities will be addressed. The final focus will be on some of the questions that, because of the new technology, can now be addressed and are presenting new challenges.

Current State of the Art for Production of Dental Restorations

MANY dental restorations are currently produced using the lost-wax casting technique (Table I). A dentist prepares the tooth, removing all decay and creating a design of the remaining tooth structure that will a) support the loads to which the tooth will be subjected during function, b) integrate unique features for the materials from which the restoration will be fabricated, c) maximize the retention of the restoration on the tooth. An impression of the prepared tooth and any adjacent proximal teeth is made, creating a three-dimensional negative of the teeth. Another impression of the opposing, occluding teeth is also made. A temporary restoration is placed on the prepared tooth and the patient leaves the dental office until the final cast restoration is fabricated.

Dental plaster is poured into the impressions, creating a model of the patient's mouth. The portion of the model that duplicates the prepared tooth must be removable so that a wax pattern can be created. To accomplish this; a brass pin is placed in the model below the prepared tooth. A second layer of plaster is added to the model, surrounding the pin. When this second layer of plaster has hardened, two thin cuts are made through the first layer of plaster (which contains the representation of the prepared tooth) just proximal to prepared tooth. The section of the model with the prepared tooth can now be removed from and reinserted into the models. This section is called the die.

When the restoration is seated on the tooth, the edge where the restoration meets the tooth is called the margin. After a die has been made removable from the models, excess plaster below the margin is removed and the margin is marked. Separating medium is placed over the die. A technician then melts and carves wax to create a wax pattern of the required restoration.

The wax pattern is sprued and invested. When the investment material has hardened, the wax pattern is burned out. Molten restorative material is flowed into the investment. The raw casting is recovered, cleaned, and polished. The restoration is now ready to be seated in the patient's mouth.

The patient must now return to the dental office. The temporary restoration is removed and any debris left on the tooth removed. The tooth must be thoroughly dried and the restoration glued to the tooth.

Using typical materials, the minimum time required for these operations is 9 h. Usually, however, a patient will wear a temporary for 1–2 weeks. Temporary restorations seldom fit as accurately as a permanent restoration so tissues around them often become inflamed and the prepared tooth may move slightly. Both of these phenomenon complicate the procedure for placing the restoration. Inflamed tissue is more sensitive and usually more resistant to anesthesia. Movement of the tooth will create problems in fitting the final restoration.

With the CAD/CAM systems, restorations can be produced much more quickly, eliminating the need for temporary restorations. Furthermore, with the automation, consistent quality becomes possible.

TABLE I
Steps of Lost-Wax Technique

1)	Dentist prepares tooth
2)	Take impression
3)	Make temporary and place on patient's tooth
4)	Pour first plaster into impressions
5)	Seat pins in plaster
6)	Pour second plaster as base
7)	Section die
8)	Isolate margins on die
9)	Mark margins
10)	Apply separating medium
11)	Carve wax pattern
12)	Sprue wax pattern
13)	Invest wax pattern
14)	Burn out wax
15)	Cast
16)	Recover casting
17)	Polish casting (ready to seat restoration)
18)	Remove temporary restoration from patient's tooth
19)	Seat cast restoration on patient's tooth

The DentiCAD System

The system being developed at the Universities of Maryland and Minnesota automates the production of dental restorations. The system has three functional components parts: data acquisition, CAD/CAM, and machining. With the automation, the labor intensive processes currently required are eliminated and restorations can be designed and fabricated in less than 1 h.

Manuscript received March 6, 1989.

E. D. Rekow is with the Department of Orthodontics, School of Dentistry, University of Maryland, Baltimore, MD 21201.

A. G. Erdman, D. R. Riley, and B. Klamecki are with the Department of Mechanical Engineering, University of Minnesota, Minneapolis, MN 55455.

IEEE Log Number 9144234.

0018-9294/91/0400-0314$01.00 © 1991 IEEE

ClearCorrect Exhibit 1002, Page 1940 of 3373

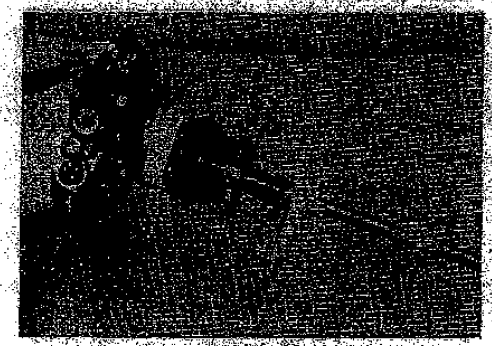


Fig. 1. Camera system for "optical impressions."

Data Acquisition

Two techniques for data acquisition are being developed. With the first, data are acquired from the patient directly through an optical "impression" based on a customized stereophotogrammetric technique. Stereo pairs of images are obtained for the prepared tooth, the proximal teeth, and the opposing teeth. A special lens is used that incorporates a prism so that the distal portion of posterior teeth can be seen (Fig. 1). The lens fits onto a standard 35-mm camera. The images are captured on film and then digitized on a high-resolution (4096 × 4096 pixel) digitizer, providing a data acquisition accuracy of 2.5 μm. (Note: when high-resolution real-time cameras become available, they will be integrated into the design, eliminating the need for a separate digitizing step.)

A set of stereo pairs of images is recorded [Fig. 2(a) and (b)]. In its current configuration, one image is recorded, the camera is moved, and the second half of the stereo pair is recorded. This requires that the object remain stationary throughout the procedure. This is not a realistic constraint in a clinical setting and a stereo lens design is currently underway.

The images are processed. The first operation is to differentiate areas of interest (bounded by the margins of the prepared tooth) from areas of no interest. This is accomplished through customized edge-finding algorithms. Using different threshold values, these same edge-finding algorithms can locate burr scratches on the surface of the tooth, adding apparent features to an otherwise optically flat surface (Fig. 3).

From the stereo pairs, each point in the first half of the image pair is matched with its equivalent in the second half of the image pair. This creates a triplex of x, y, disparity values where x, y are the planar coordinates for a point or feature in the first half of the stereo pair and the disparity value is the shift of that point or feature to its position in the second half of the stereo pair.

From the geometry of the camera used to capture the images and this triplex of x, y, disparity, a three-dimensional reconstruction of the surface of the prepared tooth is created (Fig. 4—the data displayed in this image is identical for all four views; only the viewing angle has changed). Identical operations are used for establishing the 3-D surface map of the proximal edges of adjacent teeth and the opposing teeth.

In the second configuration for data acquisition, optical triangulation is used (Fig. 5). With this alternative, a die must be prepared. Positioning accuracy of the system is ± 10 μm in x, y, and z (Fig. 6). A low-powered laser beam is directed at the die. The reflection of the beam is sensed by a CCD chip. The deflection of the reflected beam from a known position gives the z coordinate. The x and y coordinates are obtained by recording the location of the moving plate onto which the die has been placed. A point by point scan of the surface creates the



Fig. 2. Right and left halves of a stereo pair of images of a prepared mandibular first molar.



Fig. 3. Edge finding algorithm applied to the left half of the stereo pair shown in Fig. 2.

ClearCorrect Exhibit 1002, Page 1941 of 3373

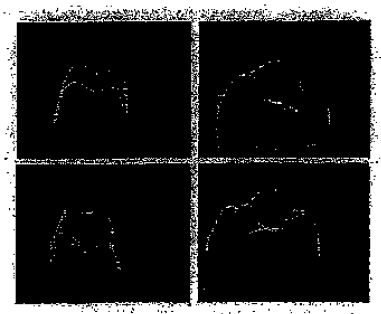


Fig. 4. Reconstructed prepared tooth (from various views).

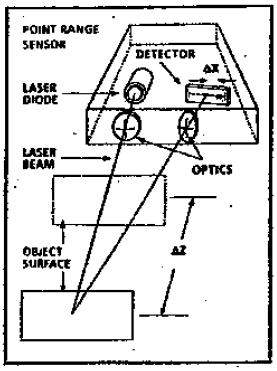


Fig. 5. Principle of optical triangulation.

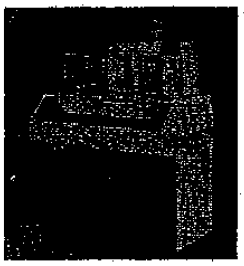


Fig. 6. Triangulation digitizer.

digital x, y, z surface map (Fig. 7 shows the graphical display of a digitized mandibular first molar).

CAD/CAM

The CAD/CAM operations replace the waxing processes of the traditional techniques. Custom software was developed in C language with a Unix operating system on an Iris 4D/50 Graphics Workstation (Silicon Graphics, Mountain View, CA). The 3-D data (from either data acquisition technique) is used to calculate the space into which the restoration must fit. This space is defined by the space available with the teeth together as well as their relative positions as they move through the entire range of motion of the jaw.



Fig. 7. Digitized mandibular first molar.

The design of the restoration creates three surfaces: the internal surface, the external surface to the crest of convexity (this is the portion of the restoration that occludes with opposing teeth and contacts the adjacent teeth), and the external surface of the tooth between the crest of convexity and the margins. The internal surface must mirror the configuration of the prepared tooth. Near the margins it must replicate the shape of the prepared tooth exactly. Away from the margins it needs to be offset by a sufficient amount to permit a gluing agent to be added (to keep the restoration in place on the tooth).

For the external surface above the crest of convexity, the CAD software automatically accesses a database of ideal tooth morphologies. From the calculated available space, a scale factor is generated for the general dimensions of the crown. However, the location of cusp tips and fossae in the occlusal surface must be modified to fit the unique requirements of each patient. The software automatically establishes these relationships, moving reference points to the required positions and blending adjoining surfaces smoothly so that the typical morphology is maintained but the uniqueness for each patient is obtained. The remaining external surface blends the margins (defined by the internal configuration) and the crest of convexity (defined by the other external portion), creating a smooth surface.

The CAM software automatically translates the design created by the CAD portion of the system to tool paths for a micromilling machine (Fig. 8). Offsets are automatically added to the surface to compensate for cutter tool diameters. Antigouging algorithms prevent the cutter from removing material during one cutting path that is part of the required surface in an adjacent area.

Machining

The tool paths are automatically sent to a micromilling machine with positioning accuracy of ± 5 μm (Servo Products, Pasadena, CA). The restoration is fabricated from a single block of material. The internal and external surfaces below the crest of convexity are machined. The restoration is flipped 180° and the external portion above the crest of convexity is fabricated.

ClearCorrect Exhibit 1002, Page 1942 of 3373



Fig. 8. Machine tool paths for CAD/CAM designed restoration.

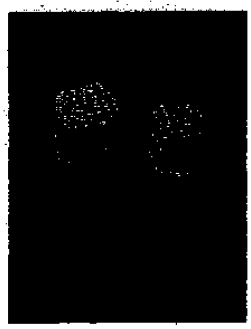


Fig. 9. Machined restorations.

(Fig. 9 shows restorations machined from metal and machinable ceramic.)

Challenges During System Development

A number of interesting—and sometimes frustrating—challenges arose as part of the development process. One of the first was translating clinical criteria into engineering tolerances to produce decision-based design rules for the CAD algorithms. Ideally a restoration should exactly fit the tooth at the margins. Clinical justification for this is twofold. First, with any gap in the fit, an area is created that collects debris and can result in decay and/or inflammation to the gum tissues. The second is that many of the gluing agents used either abrade away or are water soluble and simply wash away over time if there is a misfit between the restoration and the tooth.

Clinically, the test for acceptable fit is that a clinician moving a dental explorer across the tooth-restoration interface cannot feel that interface. There is little agreement in the dental literature about what that tolerance is. Indeed, there is little agreement about exactly what and how measurements should be made to qualitatively determine what the clinician can sense [1]. By translating all of the measurements reported into a single set of geometric relationships, it appears that acceptable cast restorations generally achieve a fit of 40–60 μm at the margins [1]–[5].

Another interesting challenge is how to optically acquire accurate data from real teeth. A prepared tooth may be stained from old restorative materials or caries. It may contain filling materials with coloration substantially different from that of a normal tooth. By using edge finding algorithms these discolorations and other materials act as pseudofeatures, enhancing the point matching for disparity calculations.

Imaging the teeth is not a trivial problem. In many typical prepared teeth, the sides of the remaining tooth structure are quite long. To be clinically successful they must also have nearly parallel and vertical walls. Many of the commercially available imaging systems trade depth of field for resolution [4]—to achieve very high resolution (to the micron level) the depth of field is much less than the height of a typical preparation. For the optical impressions, problems are managed by merging multiple views of capture the entire prepared tooth surface.

For the triangulation digitizer, special modifications of the machine were required. To compensate for the depth of field problem, a number of ranges of depth of field are scanned. A point is recorded only when the reflected light hitting the CCD sensor exceeds a specified light-threshold. If insufficient light is sensed, the z-axis drive shifts the laser-sensor and another measurement is attempted. This process is repeated until sufficient light levels are obtained. To compensate for the near-parallel walls, the die is scanned from an angle, providing the laser with an apparent viewing angle of less than 85°.

Clinical and Materials Questions

While the technology of CAD/CAM has produced some interesting engineering questions and challenges that have already been solved, unquestionably interesting ones remain for the dentist, engineer, and materials investigators.

One of these is the quality of margins that are needed. Should the CAD/CAM technology provide only what is currently average marginal quality or integrity or should the technology be pushed to its limits, providing improved fit as a standard?

Each of the steps of the traditional impression-lost wax-casting process has implicit sources of error. These include distortions in the impression material, plaster, wax pattern, or investment material; changes in water-powder ratios or techniques of the mixing; casting failures; and others. Automation eliminates these but replaces them with different contributions of error. Table II summarizes these contributions for off-the-shelf high resolution component parts [6]. The imaging and digitizing errors are dependent upon the quality of the lenses employed (or the degree to which distortions can be mathematically removed), the resolution of the digitizer, and the density of features on the teeth which can be detected. Surface modeling errors are contributed by curve fitting algorithms and three-dimensional reconstruction techniques. The contribution of errors from CAM comes from two different sources: 1) the positioning accuracy in the milling machine, wear of the cutter, and relative movement, if any, between the cutter and the part being fabricated and 2) scalloping error resulting from cutter paths plus the errors resulting from the cutter being able to move only in straight-line movements from one specified point to the next.

In the worst case, all of these contributions to error can be assumed to be independent so they are additive, yielding a total error contribution from the new technology of 17.8 μm. Even in this worst case, there is the potential for accuracy greater than that currently available with the lost-wax technique. Restorations produced with the lost-wax technique are usually considered to be acceptable with marginal fit of about 40–60 μm. Based on a small sample size, restorations produced with the Minnesota CAD/CAM system can produce margins of 0–49 μm

ClearCorrect Exhibit 1002, Page 1943 of 3373

TABLE II
ERROR CONTRIBUTIONS FROM CAD/CAM

Imaging and Digitizing	2.5 μm
Surface Modeling	10.0 μm
CAD	0.0 μm
CAM:	
Milling	4.8 μm
N/C Path	0.5 μm
	17.8 μm

(average = 23 μm, SD = 23 μm) measured from the margin to 300 μm from the margins in 20 μm increments [7]. Machining operations are more critically controlled very close to the margins. For the first 100 μm, the fit ranged from 0 to 37 μm (average = 12 μm, SD = 15 μm). Should effort be expended to further reduce the errors to reach the theoretical limit? What should be the standard? Stated differently, is there any clinical difference between margins that fit to within 40–60 μm and those that fit to within 20 μm?

Another surprising area of opportunity that has arisen is specification of processing parameters. For any milling operation, it is possible to vary spindle speed, material feed rate, and depth of cut simultaneously. Different materials demand different values for these parameters, yet little has been published concerning this problem. Cutting parameters for dental materials do not appear in the standard machinists' handbook. The size of the cutters used for the geometries produced by dental CAD/CAM systems is much smaller than those used for typical industrial applications. Little work relating materials properties to cutting parameters at the scale required for dentistry has been done. The physics of material removal with small cutters awaits scientific inquiry.

Another question which has arisen relates to surface finish. The American Dental Association specification for the finish of a metal crown requires an 8 μm rms smoothness criterion but says nothing about reflectance or spectral feature. With currently practiced polishing operations, a surface that meets this smoothness criterion is also shiny. With the machining operation, it is possible to obtain this smoothness yet still be able to see the tracks of the tool path. Should a metal crown be smooth, or shiny, or both?

The opportunities and challenges to the dental materials investigators are tremendous. It is now possible to consider an entirely new array of materials—castability or manipulation within the oral cavity is no longer a criterion for selection. The parameters that make a material ideal for a dental restoration are not well quantified. When new materials are possible, questions arise about how the tooth should be prepared to optimize the performance of the tooth-restoration system.

SUMMARY

The DentiCAD system can produce dental restorations that fit at least as well as those that are cast. The system speeds production, eliminates the labor intensive steps currently required, and provides consistent quality. This CAD/CAM technology applied to the dental problem of designing and fabricating restorations, has created some interesting engineering challenges for acquiring data, establishing tolerances for clinical criterion, and managing existing dental materials. The future, however, will be more and more interesting as we learn to ask new and different questions about what new possibilities the automation creates.

REFERENCES

[1] J. R. Holmes, "Marginal fit of castable ceramic (Dicor) crowns," M.S. thesis, Univ. North Carolina, Chapel Hill, NC, 1986.
[2] J. M. McLean *et al.*, "The estimation of cement film thickness by an *in vivo* technique," *Brit. Dental J.*, vol. 131, pp. 107–111, 1971.
[3] U. C. Belser, M. I. MacEntree, and W. A. Richter, "Fit of three porcelain-fused-to-metal marginal design, *in vivo*: A scanning electron microscope study," *J. Pros. Dental.*, vol. 53, pp. 24–34, 1985.
[4] D. N. Allan, "A macroscopic study of filled teeth," *Brit. Dental J.*, vol. 21, pp. 386–390, 1970.
[5] G. J. Christiansen, "Marginal fit of gold inlay castings," *J. Pros. Dental*, pp. 227–231, 1966.
[6] R. Caudell, Univ. Alabama, presentation at Greater NY Dental Meet., Dec. 3, 1987.
[7] E. D. Rekow, V. P. Thompson, and H. S. Yang, "Margin fit of CAD/CAM produced crowns," *J. Dental. Res.*, vol. 70, 1991.



E. Dianne Rekow received the M.S.M.E., D.D.S., and Ph.D. degrees in biomedical engineering from the University of Minnesota, Duluth.

She is currently an Associate Professor in the Department of Orthodontics at the University of Maryland, School of Dentistry, Baltimore. Her research focuses on CAD/CAM in dentistry.

Dr. Rekow is a fellow in the Academy of Dental Materials and a member of ASME, SPIE, IADR, and other professional organizations.

Arthur G. Erdman received the Ph.D. degree in mechanical engineering from Rensselaer Polytechnic Institute, Troy, NY.

He is currently a Professor of Mechanical Engineering at the University of Minnesota, Minneapolis, and Chairman of the Design Division. His major research interests are kinematics and biomedical engineering.

Dr. Erdman is an active member of ASME and a number of other professional organizations.

Donald R. Riley received the Ph.D. degree in mechanical engineering from Purdue University, West Lafayette, IN.

He is currently a Professor of Mechanical Engineering at the University of Minnesota, Minneapolis, and serves as co-Chairman of the University's Productivity Center. His major research interests are CAD/CAM and computer graphics.

Dr. Riley is an active member of ASME and a number of other professional organizations.

Barney Klamecki received the Ph.D. degree in mechanical engineering from the University of Illinois, Chicago.

He is currently a Professor of Mechanical Engineering at the University of Minnesota, Minneapolis. His major research interests are manufacturing and machining operations.

Dr. Klamecki is an active member of ASME, SME, and other professional societies.

ClearCorrect Exhibit 1002, Page 1944 of 3373

Bioengineering in Dentistry
3.2–5

COMPARISON OF THREE DATA ACQUISITION TECHNIQUES FOR 3-D TOOTH SURFACE MAPPING

B. Dianne Rekow
Department of Orthodontics
University of Maryland, Baltimore, MD 21201

MJ McCann, A Nussbaum, S Madirasmi, TC Pong
Departments of Electrical Engineering and Computer Science
University of Minnesota, Minneapolis, MN 55455

ABSTRACT

Three techniques to obtain a high resolution (under 20 micron), complete, 3D surface map of an entire tooth surface are compared. Stereophotogrammetric techniques can provide the required resolution but lens configurations that provide adequate spot size and MTF performance have depth of field substantially less than the length of the tooth. Triangulation digitizing can provide adequate resolution but time for data acquisition is excessive. Miniature mechanical linkages can provide a complete surface map in under 1 minute to a resolution of under 20 microns.

INTRODUCTION

High resolution mapping of an entire tooth surface in three-dimensions is required for the solutions to an array of dental questions. These include determination of complete deformation maps of a tooth under load for finite element modeling, establishing geometries and space available for automated restoration design using expert systems and CAD/CAM, complete characterization of changes resulting from wear, and others.

The objective is to establish a three-dimensional map of the entire surface of any single tooth to a resolution of under 20 microns. This includes complete mapping of the mesial, distal, lingual, and buccal surfaces as well as the occlusal surface. Ideally the data should be acquired quickly with a device that could be used intraorally. Three data acquisition techniques have been investigated: stereophotogrammetry, triangulation optics, and mechanical digitizer.

STEREOPHOTOGRAMMETRY

Investigations into stereophotogrammetric techniques had two phases: (a) lens design for an intraoral lens and (b) 3D reconstruction from 2D images with disparity.

The objective of the lens design was to create a lens system that provided a lateral separation of 10 microns over an object length, width, and depth of 10 mm. This is approximately equivalent to 100 line pairs/mm for points 7 mm away from the axis. To maintain a 35 mm format at the camera, magnification must be less than 2.5x.

Lenses investigated included microscope objectives, cemented triplets, cemented doublet pairs, and a pair of double heliar lenses placed back to back [1]. Lens quality was assessed by both minimum RMS value for the spot diagram and Modulation Transfer Function (MTF). Using either criterion, the heliar system performed best. It had a minimum spot diameter of 26.6 microns (average deviation of 5.9 mm). The MTF stayed above a 1.5% response until approximately 60 line pairs/mm and performs well past 200 line pairs/mm. Off-axis performance was equally good for objects located 3-mm off-axis. Only slight degradation was seen at 7-mm off-axis. Unfortunately, the depth of field was only 200 microns.

Three-dimensional reconstruction from 2D images of tooth models was also investigated. In order to obtain complete disparity mapping, edge finding algorithms were first applied. This permitted first approximation surface reconstructions. Additional resolution was obtained by point matching on images with a random pattern projected onto the surface during image acquisition. For images acquired at a 4000 x 4000 pixel resolution, the theoretical limit in the accuracy of z is 6.2 microns [2]. Work with this technique has been reported previously in greater detail [3] and is continuing.

TRIANGULATION OPTICS

A system using triangulation optics was also investigated. An object is positioned

CH3088-4/91/0000-0344 $01.00 © 1991 IEEE

ClearCorrect Exhibit 1002, Page 1945 of 3373

on a movable table beneath a laser beam. The laser light is reflected from the surface and sensed by a CCD chip. The distance between the reflected and incident light beams is used to calculate the distance between the laser and the object surface, giving the z coordinate of the surface.

The position of the incident laser beam cannot be perpendicular to the long axis of the tooth. In that orientation, much of the axial surfaces would be hidden by the crest of convexity of normal tooth morphology. By orienting the long axis of the tooth approximately 60 degrees from the incident laser beam the hidden surfaces gingival to the convexity can be seen over the entire occlusal-gingival height of the tooth.

The surface map is generated point by point in cylindrical coordinates (b,y,z). The values of b and y are obtained from the position of stepper motors driving the movable stage upon which the tooth is mounted.

Resolution of the system is ± 10 microns in b, y, and z. Rectangular coordinates are obtained from the cylindrical coordinates through normal transformations.

The major limitation of this technique is the time required for data acquisition. Typical scans with 20 micron intervals between points in y and 1 degree increments of rotation require approximately 1.5 hours to obtain a complete surface map.

MECHANICAL DIGITIZER

A miniature mechanical digitizer has been designed [4]. This digitizer is small enough to be used intraorally. A mounting fixture is attached to a tooth away from the tooth to be digitized. The linkage snaps onto the mounting fixture. The opposite end of the linkage includes a small handle and a probe tip. The operator holds the handle and manually passes the probe tip over the surface of interest. Sensors within the links record relative link positions. These positions are used to calculate the location of the probe tip.

Before the complete surface map is obtained, data points at the extremes of the surface are obtained. These define a space of interest, speeding data acquisition. Approximately 10,000 points/second can be digitized; permitting complete surface mapping of the tooth in under 1 minute. There are no constraints in the order that data must be acquired. Precision of the digitizer is under 20 microns.

CONCLUSION

Three techniques have been investigated for obtaining complete three-dimensional maps of a tooth surface. Theoretical calculation of the limits of resolution in z for 3D reconstruction from stereo pairs of images with 4000 x 4000 pixel resolution using point by point disparity mapping meets the design requirement of resolution of under 20 microns. Unfortunately, lens design appears to be a limitation. Lens configurations were found that provide both acceptable RMS values in their spot diagrams and MTF but have a depth of field limited to 200 microns (vs. typical tooth length of 6-10 mm).

Triangulation digitizing provides sufficient resolution but times for data acquisition are excessive.

Miniature mechanical digitizing is feasible, provides the required resolution and access to the entire tooth surface, and can be accomplished quickly.

REFERENCES

[1] MJ McCann, A Nussbaum, Design of an Optical System for the Computer Machining of Dental Replicas, Final Report, EE 5492, University of Minnesota, June 1991.

[2] S Madarasami, University of Minnesota, Department of Computer Science, unpublished results, May 1991.

[3] ED Rekow, AG Erdman, DR Riley, B Klamecki, "CAD/CAM for Dental Restorations - Some of the Curious Challenges", IEEE BIOMED 38(4), 1991.

[4] B Nappi, H Gold, Foster Miller, Inc., "Miniaturized Mechanical Digitizer", US patent application, submitted April 1991.

ADDRESS

E. Dianne Rekow, DDS, PhD
Associate Professor
Department of Orthodontics
University of Maryland at Baltimore
666 West Baltimore Street
Baltimore, Maryland 21201
(301) 328-4429

CH3068-4/91/0000-0345 $01.00 © 1991 IEEE

ClearCorrect Exhibit 1002, Page 1946 of 3373

A review of the developments in dental CAD/CAM systems

E. Dianne Rekow, MSME, DDS, PhD

Baltimore College of Dental Surgery, University of Maryland, Baltimore, Maryland, USA

At least 1000 CAD/CAM (computer-aided design and computer-aided manufacturing) systems for producing restorations are in dental offices. At least nine different systems have been described; the Cerec system (Siemens, Bensheim, FRG) is the best known and most widely used. Clinical results to date suggest that the automated CAD/CAM systems can provide restorations which perform at least as well as cast restorations. There are some technique sensitivities that must be managed with the new technology. The importance of fit at the margins is a controversial issue that remains to be settled. Bond strength of composite-luted restorations is dependent on margin location and luting material properties, and on the combination of silanating, etching, and curing mechanism of the luting composite. Surface finishes equivalent to cast gold and glazed porcelain can be achieved for machinable CAD/CAM materials.

Prosthodontics and Endodontics 1992, 25–33

Dental CAD/CAM (computer-aided design and computer-aided manufacturing) systems have become a reality. At least 1000 systems are already in dental practices. The most widely used is the Cerec system (Siemens, Bensheim, FRG). Others include the Duret (Sopha Bioconcept, Inc., Los Angeles, CA), DentiCAD (BEGO, Bremen, FRG) (Fig. 1), Procera (Nobelpharma, Goteborg, Sweden), DUX (GIM-ALLDENT, Vorel, FRG), and Celay (Mikrona Technologie, Sprietenbach, Switzerland) systems [1•–5•,6–8]. At least three others are being developed in Japan [9•–11•]. Still another system is evolving that will apply CAD/CAM to removable dentures, automatically arranging the teeth and fabricating the occlusal surfaces [12]. Clinical data at 5-year recall exist on some restorations. New, exciting developments are unfolding rapidly.

Some of the systems capitalize on the automation that is available from CAD/CAM techniques (Figs. 2 and 3). Others include copying machines, and reproducing shapes from stone models or wax or acrylic patterns (Fig. 4). The types of restorations produced and materials used for fabrication vary widely. Table 1 provides a brief summary of the component parts of the systems and their capabilities.

Rather than give descriptions of the systems, the objective of this review is to discuss developments reported in the literature during the past year. Specific focus will be placed on clinical results, margin fit, other factors affecting clinical performance, technique sensitivities, and a very brief comparison of new materials created specifically for CAD/CAM systems. The majority of the literature published during this review period (November 1990–November 1991) focuses on the Cerec system, probably related to the International Symposium on Computer Restoration, State of the Art of the Cerec Method, which took place in May of 1991 [13].

Clinical results

Among the first CAD/CAM restorations placed clinically were eight Cerec inlays which were placed in early 1986 [14••]. After 5 years, they were rated using the United States Public Health Service (USPHS) criteria for contour, marginal integrity, marginal discoloration, color match, and recurrent caries. All eight received Alfa ratings for contour, color match, and recurrent caries. Marginal integrity and discoloration were ranked as Alfa for five of the restorations and Bravo for the remaining three.

There are now clinical data on literally thousands of Cerec restorations that have been followed for at least 2 years. Overall, their performance is excellent [15–21]. There appears to be no difference between clinical acceptance or performance for restorations fabricated from either Vita porcelain (Vita Zahnfabrik,

Abbreviations

CAD/CAM—Computer-aided design and computer-aided manufacturing; USPHS—United States Public Health Service.

© 1992 Current Science ISBN 1-870485-41-6 ISSN 1046–0764

ClearCorrect Exhibit 1002, Page 1947 of 3373

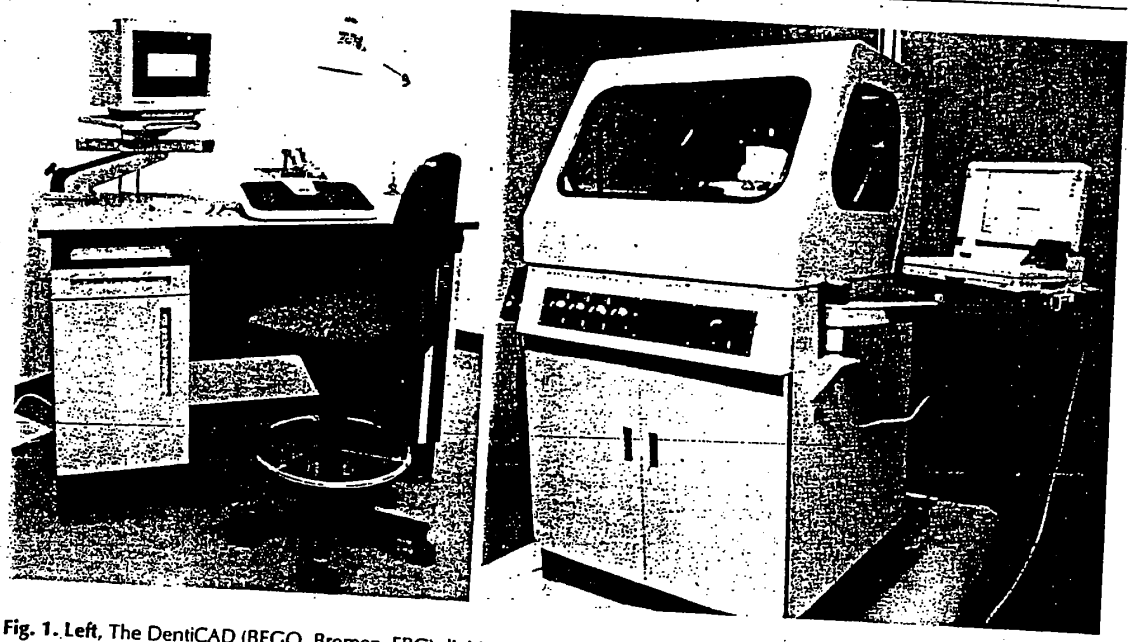


Fig. 1. Left, The DentiCAD (BEGO, Bremen, FRG) digitizer and computer (the laboratory version). **Right,** The DentiCAD milling machine (also the laboratory version of the hardware).

Bad Saeckingen, FRG) or Dicor-MGC (Dentsply, York, PA) [15,22,23]. Teeth restored with Cerec-produced mesiooccl usodistal restorations were shown to be as strong as sound, unrestored teeth [24••].

Problems reported with the Cerec restorations are hypersensitivity [16–18,25••,26–31], fracture at the margins [18,25••,27,30,32], bulk fracture [14••,16,18,27,30,33•], and recurrent caries [30]. Hypersensitivity usually occurs immediately upon placement and may or may not disappear over time. Incidence of the problem is reported in between 1% [25••] and 23% of restorations [26], although most often the rate appears to be approximately 10%. A number of clinical and research results show that gingival margins placed in at least 50% enamel are far superior to those placed in dentin or cementum, with or without the use of dentin bonding agents [34••,35–38,39••]. It is hypothesized that, if postrestorative sensitivity is to be eliminated, the margins must be in a minimum of 50% enamel around the entire periphery of the restoration.

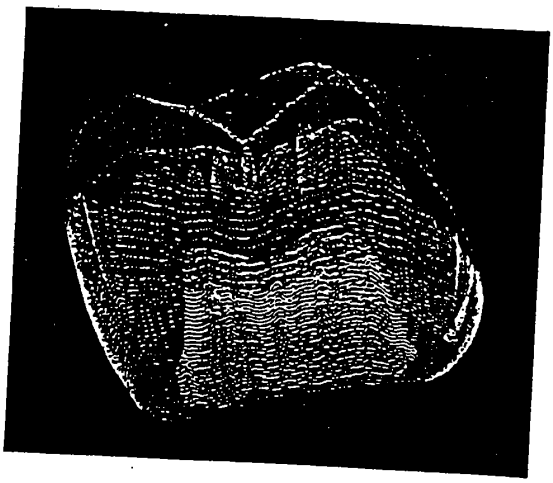


Fig. 2. A wireframe representation of a computer-designed full-coverage crown.

Margin fracture was evident in 0.5% of the restorations [18,25••,27,30,32]. Bulk fractures occurred in approximately 1% to 2.5% of the restorations, generally due to insufficient reduction of the tooth, resulting in a material thickness less than 2 mm at the isthmus [14••,16,18,27,30,33•]. Recurrent caries is rare; in one clinical study it occurred in only two of 831 restorations [30].

For the Procera system, one report of clinical results has been published. At 2 years, margin form ranked excellent or acceptable (using USPHS ratings) in all cases, surface color ranked excellent or acceptable in 90.3% of the cases, and anatomic form was judged excellent or acceptable in 93.4% of the cases [40]. Clinical results for other systems have not been reported.

ClearCorrect Exhibit 1002, Page 1948 of 3373

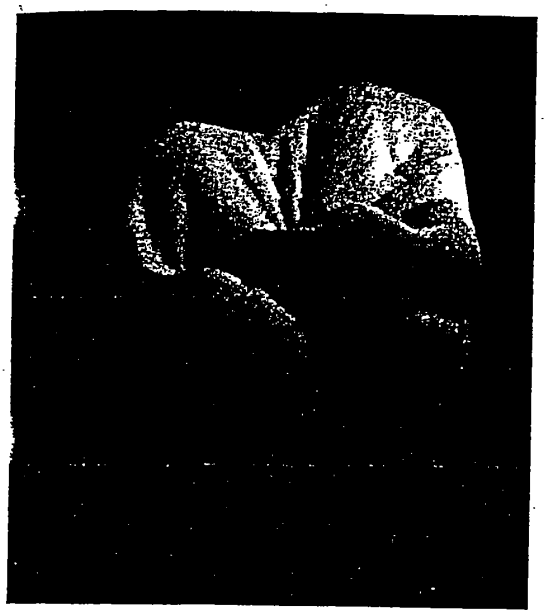


Fig. 3. A computer-generated crown.

Margin fit

Fit at the margins has been reported for Cerec, DentiCAD, and Procera restorations. Cerec restoration fit, without any luting material, averages approximately 100 µm to 150 µm [19,41;42••,43–45]. Comparative studies report marginal gaps averaging 5 µm for direct composites [35], 82 µm [35] to 97 µm [41] for laboratory-produced inlays, 93 µm for indirectly fabricated composite inlays, 139 µm for Cerec Dicor-MGC inlays, and 209 µm for laboratory-produced ceramic inlays [35]. The quality of the fit, however, may or may not be critical since the luting agent offers sealing advantages which may compensate for any inadequacy in fit [45].

The marginal gap is identified as a weakness of the Cerec system, because clinically the resins may result in wash-outs and material collapses over the long run [39••]. Wear at the margins in the composite luting material is reported as ranging from 10 µm at 16 months [45] to 88 µm at the end of the 1st year [33•]. An interesting characteristic of the wear was reported by Isenberg *et al.* [33•]. In their study of 118 restorations, 39 µm of vertical loss of luting material occurred in the first 6 months. By the end of the 1st year, a total of 88 µm had been lost. This value, however, remained constant over the next 12 months; no additional vertical loss was apparent. The authors theorize that the horizontal and vertical wear values reach a maximum and then become constant and that vertical loss of the material in the interfacial region is linear throughout the 1st year, then remains constant.

For Cerec restorations, it is not clear what effect margin space has on the marginal integrity of the inlay restorations. Some investigators [46,47,48••] report that by reducing the amount of composite which is needed for luting, a better marginal quality is obtained because polymerization contraction will play a less-important role in small amounts of composite material than in large bulk [48••]. However, Fett *et al.* [31] and Schmalz *et al.* [48••] found no correlation between margin width of composite and micromorphologic margin quality. In fact, Schmalz *et al.* reported that ceramic inlays with wide luting space showed less disintegration and loss of adhesion at the ceramic or luting composite interface after thermal cycling and mechanical loading than did those with smaller luting spaces. What is important, however, is that the luting cement have the same wear rate as posterior composites [31]. Magne *et al.* [38] suggested that the thicker cement space is better if the restoration fits without friction, permitting deformation of the restorative material or dental tissues during polymerization shrinkage of the luting composite. Schmalz *et al.* [48••] found dye penetration at interproximal margins following thermal cycling combined with mechanical loading to be less for ceramic inlays with wide luting spaces.

Fit at the margins for DUX-produced titanium crowns was reported to average 71 µm, with a range from 20 µm to 150 µm [49••]. For the DentiCAD system, margins of 23 µm ± 23 µm (range from 1 µm to 49 µm) were reported [50]. Demands for fit on margins luted with noncomposite materials may be much higher than for fit for those where a chemical bond can form between the luting and restorative materials. Leakage, as measured by dye penetration following thermal and mechanical loading, is much greater for zinc phosphate cements than for composite materials [35]. Clinical implications of fit for metal CAD/CAM restorations and copings, especially when used with noncomposite luting materials, will probably be nearly equivalent to those for cast restorations.

Perhaps the major implication in poor-fitting margins, with any system, is the potential for overhangs at the

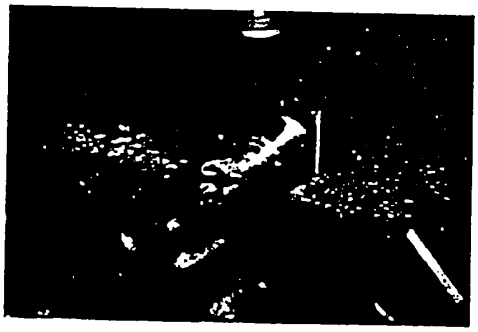


Fig. 4. Machining of a gold crown by a CAD/CAM system. (*From* Uchiyama *et al.* [85]; with permission.)

ClearCorrect Exhibit 1002, Page 1949 of 3373

Table 1. Comparison of features of various CAD/CAM systems*

System	CAD/CAM capability	Data acquisition	Intraoral data	Design	Fabrication	Restoration type	Material choices
Cerec	Full	Optical	Yes	Interactive	Grinding	Inlay, onlay, veneer	Vita porcelain, Dicor-MGC
Duret	Full	Optical	Yes	Interactive or automated	Milling	Inlay, onlay, crowns	Vita porcelain, Dicor-MGC, Ariste, alloys, titanium
DentiCAD	Full	Mechanical	Yes	Automated	Milling	Inlay, onlay, crowns, copings	Vita porcelain, Dicor-MGC, titanium, alloys, composites
Procera	Copying	Mechanical	No	Wax pattern and stone die	Milling and EDM	Copings, crowns.	Titanium
DUX	Copying	Mechanical	No	Automated	Milling	Copings	Titanium
Celay	Copying	Mechanical	No	Acrylic pattern	Milling	Inlay, onlay	Vita porcelain, Dicor-MGC
Osaka	Full	Mechanical	No	Interactive	Milling	Crowns	Unknown
Hyogo	Full	Mechanical	No	Interactive	Milling	Crowns	Unknown
Kyoto	Full	Optical	No	Interactive	Milling	Crowns	Porcelain, ceramics, titanium

*Products and manufacturers are as follows: Cerec, Siemens, Bensheim, FRG; Duret, Sopha Bioconcept Inc., Los Angeles, CA; DentiCAD, BEGO, Bremen, FRG; Procera, Nobelpharma, Goteborg, Sweden; DUX, GIM-ALLDENT, Vorel, FRG; Celay, Mikrona Technologie, Spreitenbach, Switzerland; Osaka, Osaka, Japan; Hyogo, Hyogo, Japan; Kyoto, Kyoto, Japan; Vita porcelain, Vita Zahnfabrik, Bad Saeckingen, FRG; Dicor-MGC, Dentsply, York, PA; Ariste, Spad, Dijon, France.
CAD—computer-aided design; CAM—computer-aided manufacturing; EDM—electric discharge machining (also known as spark erosion machining).

cervical margin. These of course act as plaque retention sites. If the luting material is composite, it may fracture or chip, further exacerbating the problem. Lösche and Roulet [51] found that adding a colored varnish around the margins greatly reduces the danger of inadvertently reducing the enamel during contouring and finishing of the restoration. It also simplifies the finishing operation and reduces the probability of overhangs. Another recommendation for minimizing overhangs is to use dental floss conditioned with glycerin gel to remove excess material before hardening the composite resin [52].

Other factors affecting clinical success

In addition to the fit at the margins, an array of other factors can influence the success of bonded ceramic restoration. These include cementing and bond-enhancement techniques, material properties, surface finish, cement type, and etching time.

For Cerec Dicor-MGC restorations, bond strength is improved by a combination of etching the ceramic, silanating the ceramic, and using a low-viscosity, dual cure resin luting agent [53]. Unquestionably, silanization was seen as the process that uniformly improves the composite-restoration bond [31,53,54]. At least 1 minute's etching time is recommended but longer etching has no effect (enhancing or deteriorating) on bond strength [53,55]. For Vita porcelain, 5% hydrofluoric gel is recommended. For Dicor-MGC, either 5% hydrofluoric gel or 10% ammonium hydrofluoric acid are recommended. The luting composite-dentin interface is best when dentin adhesive systems are used without either bases or liners [19]. Dentin bonding generally enhances the bond but does not preserve the restoration from external or internal leakage, especially when margins are not in enamel [38].

The type of luting material selected can also significantly influence the success of restorations. For the Cerec system, submicron hybrid composites are most desirable [56••]. Dual curing systems are better than light-only or chemical-only curing since resin thicknesses may be fairly large and light may not be able to penetrate the resin thickness or the bulk of the restoration [56••]. Luting-agent viscosity should provide maximum compressive support, marginal integrity, and easy margin molding. Heavy-to-medium viscosity is recommended for restorations under heavy use [56••]. Fine hybrid composites are superior [19]. Submicron composite resins are significantly more wear-resistant than any of their counterparts [44,57,58]. An ultrasonic system, employed as part of the insertion technique, allows the use of highly filled and wear-resistant composite resins as the luting material [59].

Surface finish of Cerec restorations is dependent upon finishing technique. Surfaces at least as smooth as enamel can be obtained using any of six different techniques: 1) fine finishing—(25 μm) high-speed di-

ClearCorrect Exhibit 1002, Page 1950 of 3373

diamond bur with water spray, 2) fine finishing—high-speed diamond followed by GD Baker-Curson bur (Dentsply) with water spray, 3) four sequential grades of aluminum-oxide-impregnated discs (Soflex discs, 3M Dental Products, St. Paul, MN), 4) fine finishing—high-speed diamond with water spray followed by diamond paste (instaglaze, Taub Co., Jersey City, NJ) applied with a rotary bristle brush in an electric motor handpiece, 5) four sequential grades of aluminum-oxide–impregnated discs in an electric motor handpiece with water spray followed by diamond paste applied with a rotary bristle brush mounted in that same handpiece, or 6) fine finishing—high-speed diamond followed by high-speed Baker-Curson bur followed by diamond paste applied with a rotary bristle brush mounted in an electric motor handpiece [60••]. Only the sixth technique produces a finish equivalent to polished gold or glazed porcelain. In another study, either diamond polishing pastes or Diafinish disks (Renfert) produced smoother surfaces than aluminum-oxide discs [61]. However, it was pointed out that the pastes are more likely to damage the bonding resin and are recommended only for extraoral finishing or shaping operations.

The fit of Cerec restorations can be influenced by the grinding wheel. Precision along the mesial-distal direction of the restoration is highly dependent on the number of restorations that have already been cut with that grinding wheel (wear of the diamond or abrading surface of the cutter) as well as on the feed rate of the material into the cutter [62] (precision in the buccal-lingual and vertical dimensions of the restorations is largely independent of the cutter properties [35]). Grinding efficiency for cutting Dicor-MGC glass ceramic is inferior to that for Vita feldspathic porcelain [63]; only one half as many Dicor restorations can be cut before damaging effects are seen on the surface or at the margins [64]. With increasing wear, however, there is less extensive damage to the Dicor than there is to the Vita porcelain [64].

Technique sensitivities

Enough Cerec systems are currently in use that reports of technique sensitivities are beginning to appear. These include powder application (required before the

Table 2. Comparison of various properties of Vita porcelain and Dicor-MGC materials*

Property	Vita porcelain	Dicor-MGC	Study
Biaxial flexure strength, *MPa*			
Fine grit grind	87±10	216±14	Grossmann [75]
Sand blast	74±6	127±19	Grossmann [75]
Flexure strength of machined material, *MPa*			
Control	77.7±8.3	184.2±24.3	Lüthy *et al.* [71]
Etched	73.5±10.3	179.5±33.7	Lüthy *et al.* [71]
Etched or silane treated	75.2±8.1	191.5±18.9	Lüthy *et al.* [71]
Etched or treated with silane or a bonding agent	84.1±11.2	187.9±18.8	Lüthy *et al.* [71]
Fracture toughness, $MPa \cdot m^{1/2}$	1.8	1.5	Grossmann [72••]
Knoop diamond hardness (110-g load)	520±20	330±20	Grossmann [72••]
Wear			
Volume, mm^3	0.0701 (Mk I)	0.0306 (light)	Grossmann [72••]
	0.0869 (Mk II)	0.0379 (dark)	Grossmann [72••]
Vertical, μm	40 (Mk I)	27 (light)	Grossmann [72••], Krejci [76]
	44 (Mk II)	24 (dark)	Grossmann [72••], Krejci [76]
	24.3 (Mk II)	88.0	Grossmann [75], Krejci [76]
Subsurface damage from machining operations, μm	8.2±3.2 (Mk II)	4.1±1.3	Grossmann [75]
	12.4±5.1 (Mk I)		
Groove depth from machining, μm	8.3±1.2 (Mk II)	12.2±7.4	Kelly *et al.* [77••]
	15.5±0.9 (Mk I)		
Shear strength after thermal cycle and mechanical load, *MPa*	43.9–51.1	2.3–31.9	Ueberschär *et al.* [54]

*Vita porcelain is made by Vita Zahnfabrik, Bad Saeckingen, FRG, and Dicor-MGC is made by Dentsply, York, PA, USA.

ClearCorrect Exhibit 1002, Page 1951 of 3373

optical "impression" is captured), cavity design, and finishing the occlusal surface.

Probably the most technique-sensitive process is powder application. Before an optical image can be acquired and processed, a thin layer of opaque powder must be applied to the entire prepared tooth surface. Meyer *et al.* [65] investigated alternative techniques for delivering powder and discovered that, unless care was taken, up to 600 µm of powder could accumulate in some areas. No matter which powder application technique, the cavity floor collects a thicker layer of powder than either the proximal lateral wall or the occlusal margins [65]. An air-flow system was found to deliver an effective powder layer, without any chemical contamination of the room air [66]. Even with that system, however, layer thicknesses were on the order of 20 µm to 56 µm [66]. This layer was incorporated into the image acquired, as if it were the true surface of the preparation (as if a layer of dye spacer had been added to the preparation, including the margins). At least some portion of any misfit of Cerec restorations is a direct result of this powder layer.

Precision is demanded when preparing the cavity preparation. Sharp cavity margins and smooth walls are required to capture the most accurate optical impression possible and to permit milling [7,8,32].

When incomplete seating occurs, the primary areas responsible are usually near the axiopulpal line angle and along the proximal gingival floor [67]. Hickel and Kunzelmann [68] found that by rounding the gingival seat of any proximal box, slight improvement in seating could be achieved.

Approximately 50% of the time required to place a Cerec restoration is involved in adaptation and polishing [4•,26,69]. This is due to the need for the clinician to create and polish the occlusal surface. The technique demands a sound understanding of proper occlusal morphology as well as proper instrumentation [60••,61,70].

Material properties

Two new materials were developed to work with machining and grinding operations of the Dental CAD/CAM systems. Vita porcelain is a feldspathic porcelain; Dicor-MGC is a glass-ceramic. Properties of the two materials are given in Table 2. Both materials are very brittle but Vita porcelain is more brittle than Dicor-MGC [71]. Furthermore, because of its composition, machined Dicor has a lower fracture probability for the same applied force [71,72••]. Surface damage for the porcelain is a network of cracks that could potentially propagate [73] whereas Dicor-MGC contains an array of mica crystals that form cleavable flakes, limiting the propagation of fractures [72••]. Material removal from the feldspathic porcelain appears to be caused by chipping and, in the Dicor-MGC, by crushing [74,77••].

Under thermal cycling and mechanical loading, shear strength of machined Vita is greater than that of Dicor [55]. Failures in shear-strength tests with Vita porcelain had cohesive failure within the composite. For Dicor, failure was at the composite or ceramic interface [55].

Conclusions

The year 1991 was exciting for CAD/CAM developments. The Cerec international symposium drew the attention of the dental community. The findings reported there were very positive—automation can produce restorations whose performance compares favorably with that of traditional cast restorations. The new materials produced for CAD/CAM are performing as expected. In most cases, even though the technology may be expensive to acquire, it appears to be cost-effective in practices in a wide array of countries [28–30,78–82]. While the capabilities of the Cerec system may be limited, some of the limitations are overcome by inventive designs of restoration [79,83,84]. More importantly, an array of other systems with more extensive potential are beginning to appear. Future developments and changes in dentistry and the delivery of dentistry will be very exciting.

References and recommended reading

Papers of particular interest, published within the annual period of review, have been highlighted as:
- • Of special interest
- •• Of outstanding interest

1. • DURET F, PRESTON JD: CAD/CAM imaging in dentistry. *Curr Opin Dent* 1991, 1:150–154.
Summary description of systems and their stage of development plus overview of CAD/CAM technology in general.

2. • REKOW ED: Dental CAD/CAM systems: what is the state of the art? *J Am Dent Assoc* 1991, 122:43–48.
Comparison of systems, their capabilities, and quality of fit at margins.

3. • STACHNISS V, STOLL R: Computer technologies in dentistry: computerized restorations: CEREC and other methods. In Mörmann WH, ed: *Proceedings, International Symposium on Computer Restorations.* Quintessence, 1991, pp 33–49.
System descriptions, and discussion of limitations and problems. Some errors in system descriptions are described.

4. • CRAWFORD PR: CAD/CAM in the dental office: does it work? *Can Dent Assoc J* 1991, 57:121–123.
Brief systems description plus step-by-step timed observation of clinician placing Cerec inlay.

5. • WALTER M, REPPEL PD, BÖNING K: Frästechnik und Funkenerosion eine Aternative zum Titanguss. *Dent Labor* 1991, 31:501–504.
The Procera system is described and a clinical case shown.

6. STOLL R, STACHNISS V: Computerunterstützte Technologien in der Zahnheilkunde. *Dtsch Zahnärztl Z* 1990, 45:314–322.

ClearCorrect Exhibit 1002, Page 1952 of 3373

7. GONZALEZ-CABERZ J: Das CEREC-system: Wege und Gründe zur Zusammenarbeit swischen Zahnarzt und Zahntechniker: I. *Quintessenz Zahntech* 1990, 16:1377–1382.

8. GONZALEZ-CABERZ J: Das CEREC-system: Wege und Gründe zur Zusammenarbeit swischen Zahnarzt und Zahntechniker: II. *Quintessenz Zantech* 1990, 16:1511–1523.

9. • TAKAHASHI J, KAWANAKA M, WANANABE T, KIMURA H: To the development of CAD/CAM system using FGP method. *The Quintessence* 1991; 10:115–121.
One of few reports of Japanese work, in Japanese but with helpful illustrations.

10. • KAWANAKA M: Dental crown made with the CAD/CAM system. *The Quintessence* 1991, 10:155–160.
One of few reports of Japanese work, in Japanese but with helpful illustrations.

11. • TSTUTSUMI S, UMINO K, KANEKO T, KASUGA T, MATSUSHITA T, DO K, EMURA I, OKADA M, MAEDA Y, OKUNO Y: A development of dental CAD/CAM system. *The Quintessence* 1991, 10:135–142.
One of few reports of Japanese work, in Japanese but with helpful illustrations.

12. KAWAHATA N: Application of CAD/CAM to removable denture: arrangement of artificial posterior teeth and duplicating of occlusal surface. *The Quintessence* 1991, 10:115–121.

13. OTT D: International symposium on computer restorations. *Schweiz Monatsschr Zahnmed* 1991, 10:921–924.

14. •• MÖRMANN WH, KREJCI I: Clinical and SEM evaluation of CEREC inlays after 5 years in situ. In Mörmann WH, ed: *Proceedings, International Symposium on Computer Restorations.* Quintessence, 1991, pp 25–23.
Longest-term CAD/CAM inlay data reported in the literature.

15. ISENBERG BP, ESSIG ME, LEINFELDER KF, MUENINGHOFF LA: Clinical evaluation of CEREC CAD/CAM restorations emphasizing marginal integrity [abstract 1345]. *J Dent Res* 1991, 70:434.

16. BIENIEK KW, PETERS A: Clinical evaluation of ceramic restorations machined by a CAD/CAM technique. In Mörmann WH, ed: *Proceedings, International Symposium on Computer Restorations.* Quintessence, 1991, pp 327–336.

17. CONFORTI GP: The CEREC System: twenty months of clinical practice. In Mörmann WH, ed: *Proceedings, International Symposium on Computer Restorations.* Quintessence, 1991, pp 337–338.

18. OTTO T: Clinical evaluation and experience with the CEREC-method in a private practice after two years. In Mörmann WH, ed: *Proceedings, International Symposium on Computer Restorations.* Quintessence, 1991, pp 347–354.

19. BRONWASSER P, MÖRMANN WH, KREJCI I, LUTZ F: Marginal adaptation of adhesive CEREC-Dicor-inlays. In Mörmann WH, ed: *Proceedings, International Symposium on Computer Restorations.* Quintessence, 1991, pp 377–392.

20. BRONWASSER PJ, MÖRMANN WH, KREJCI I, LUTZ F: Marginale Adaptation von CEREC-DICOR-MGC Restaurationen mit Dentinadhäsiven. *Schweiz Monatsschr Zahnmed* 1991, 101:162–169.

21. MAGNUSSON D, ODEN A, KRYSTEK I: Clinical evaluation of CEREC restorations. In Mörmann WH, ed: *Proceedings, International Symposium on Computer Restorations.* Quintessence, 1991, pp 339–346.

22. HOLZ V, BOUILLAGUET S, CIUCCHI B, HOLZ J: In vitro study of proximal adaptation and seal of CEREC inlays. In Mörmann WH, ed: *Proceedings, International Symposium on Computer Restorations.* Quintessence, 1991, pp 405–416.

BAUMANN MA, HEIDEMANN D: Biocompatibility of dental inlay ceramics. In Mörmann WH, ed: *Proceedings, International Symposium on Computer Restorations.* Quintessence, 1991, pp 373–376.

24. •• ROZNOWSKI M, BREMER B, GEURTSEN W: Fracture resistance of human molars restored with various filling materials. In Mörmann WH, ed: *Proceedings, International Symposium on Computer Restorations.* Quintessence, 1991, pp 559–566.
Useful comparison of fracture resistance of teeth with adhesive and nonadhesive restorative materials.

25. •• REISS B, WALTHER W: Uberlebensanalyse and klinische Nachuntersuchungen von zahnfarbenen Einlagefüllungen nach dem CEREC-Ferfahren. *ZWR* 1991, 100:329–332.
Provides breakdown of types of clinical problems with Cerec restorations.

26. BERGMANN M: Swedish experiences with the CEREC-method. In Mörmann WH, ed: *Proceedings, International Symposium on Computer Restorations.* Quintessence, 1991, pp 309–314.

27. MÖRMANN WH, GÖTSCH T, KREJCI I, LUTZ F, BARBAKOW F: Clinical status of 94 CEREC ceramic inlays after 3 year in-situ. In Mörmann WH, ed: *Proceedings, International Symposium on Computer Restorations.* Quintessence, 1991, pp 355–364.

28. GEIGER F: The CEREC-method in a small town private practice. In Mörmann WH, ed: *Proceedings, International Symposium on Computer Restorations.* Quintessence, 1991, pp 173–176.

29. SCHWÄRZLER R: Experience with CEREC restorations in a Zurich private practice. In Mörmann WH, ed: *Proceedings, International Symposium on Computer Restorations.* Quintessence, 1991, pp 177–182.

30. CARLSEN SW: A practice specialized on CEREC-restorations in Denmark. In Mörmann WH, ed: *Proceedings, International Symposium on Computer Restorations.* Quintessence, 1991, pp 183–187.

31. FETT HP, MÖRMANN WH, KREJCI I, LUTZ F: Marginal adaptation of CEREC-MOD inlays in-vitro. In Mörmann WH, ed: *Proceedings, International Symposium on Computer Restorations.* Quintessence, 1991, pp 393–404.

32. PALLESEN V: Clinical performance of CEREC-restorations: restorative procedure and preliminary results. In Mörmann WH, ed: *Proceedings, International Symposium on Computer Restorations.* Quintessence, 1991, pp 285–300.

33. • ISENBERG BP, ESSIG ME, LEINFELDER KF, MUENINGHOFF LA: Clinical evaluation of marginal integrity: two year results. In Mörmann WH, ed: *Proceedings, International Symposium on Computer Restorations.* Quintessence, 1991, pp 163–172.
Good discussion of wear of composite resin luting material around Cerec restorations.

34. •• HALLER B, HOFMANN N: Postrestorative sensitivity: mechanisms and prevention. In Mörmann WH, ed: *Proceedings, International Symposium on Computer Restorations.* Quintessence, 1991, pp 127–140.
Discussion of mechanisms of and techniques for prevention of postrestorative sensitivity. An extensive bibliography is included.

35. SORENSEN JA, AVERA SP, TORRES TJ: A comparison of marginal fidelity and microleakage of posterior restorative systems. In Mörmann WH, ed: *Proceedings, International Symposium on Computer Restorations.* Quintessence, 1991, pp 275–284.

36. ZUELLIG-SINGER R, KREJCI I: Adhesive inlays: effects of cement curing modes on dentin bonding. In Mörmann WH, ed: *Proceedings, International Symposium on Computer Restorations.* Quintessence, 1991, pp 461–468.

37. GOUGOULAKIS A, MÖRMANN WH, BARBAKOW F, LUTZ F: Retention rate and margin adaptation of CEREC veneer in vitro. In Mörmann WH, ed: *Proceedings, International Symposium on Computer Restorations.* Quintessence, 1991, pp 537–546.

38. MAGNE P, DIETSCHI D, HOLZ J: An in vitro evaluation of the marginal and internal seals of CEREC overlays. In Mörmann

ClearCorrect Exhibit 1002, Page 1953 of 3373

WH, ed: *Proceedings, International Symposium on Computer Restorations.* Quintessence, 1991, pp 425–440.

39. •• ROULET FJ, NOACK MJ: Tooth colored conventional and CEREC restorations: claim and reality. In Mörmann WH, ed: *Proceedings, International Symposium on Computer Restorations.* Quintessence, 1991, pp 233–243.
Critique of Cerec system, discussing its strengths and limitations.

40. BESSING B, BESSING C, ERICSON G, LUNDQUIST P, NILSON H, ANDREASEN M: A 2-year follow-up study of titanium crowns. *Acta Odontol Scand* 1990, 48:113–117.

41. THORDRUP M, ISIDOR F, HORSTED-BINDSLEV P: CEREC or laboratory ceramic inlay? In Mörmann WH, ed: *Proceedings, International Symposium on Computer Restorations.* Quintessence, 1991, pp 91–102.

42. •• HAHN R: Experimentelle Untersuchungen zur reproduzierbaren Passgenauigkeit keramischer Einlagefüllungen. *Dtsch Zahnärztl Z* 1990, 45:653–656.
One of the more comprehensive discussions of Cerec margins and their fit as a function of location.

43. ROSE D, PLATZER U, ROTH KKF: Untersuchungen zur Kompositfuge bei computererstellten Keramikinlays. *Dtsch Zahnärztl Z* 1990, 45:677–679.

44. PETERS A, BIENIEK KW: SEM-Examination of the marginal adaptation of computer machined ceramic restorations. In Mörmann WH, ed: *Proceedings, International Symposium on Computer Restorations.* Quintessence, 1991, pp 365–372.

45. WILDER AD: Clinical considerations of CEREC restorations. In Mörmann WH, ed: *Proceedings, International Symposium on Computer Restorations.* Quintessence, 1991, pp 141–150.

46. HICKEL R, KUNZELMANN KH, NKENKE E, PETSCHELT A: Bond strength of five bonding composite resins to CEREC-ceramic. In Mörmann WH, ed: *Proceedings, International Symposium on Computer Restorations.* Quintessence, 1991, pp 567–576.

47. KUNZELMANN KH, HICKEL R, MEISTER C, PETSCHELT A: Curing contraction in thin bonding composite resin layers. In Mörmann WH, ed: *Proceedings, International Symposium on Computer Restorations.* Quintessence, 1991, pp 577–590.

48. •• SCHMALZ G, REICH E, FEDERLIN M: Gap dimension and marginal quality of CEREC inlays in vitro. In Mörmann WH, ed: *Proceedings, International Symposium on Computer Restorations.* Quintessence, 1991, pp 441–452.
Excellent discussion of effect of luting space surrounding restorations on marginal quality, both at the luting composite and enamel interface and at the luting composite and ceramic interface.

49. •• REPPEL PD, BÖNING K, WALTER M: Festsitzender zahnersatz aus gefrastem/funkenerodiertem Titan. *Dtsch Zahnärztl Z* 1991, 46:756–758.
Only article reporting quantitative data on fit of Procera-produced (Nobelpharma, Goteborg, Sweden) restorations.

50. REKOW ED, THOMPSON VP, YANG HS: Margin fit of CAD/CAM produced crowns [abstract 1346]. *J Dent Res* 1991. 70:434.

51. LÖSCHE GM, ROULET JF: A colored varnish to improve the finish of CEREC inlays. In Mörmann WH, ed: *Proceedings, International Symposium on Computer Restorations.* Quintessence, 1991, pp 481–490.

52. KLEIER CW, LÖSCHE GM, ROULET JF: Evaluation of different insertion techniques for CEREC inlays in vitro [abstract 1347]. *J Dent Res* 1991, 70:434.

53. NATHANSON D: Factors in optimizing the strength of bonded ceramic restorations. In Mörmann WH, ed: *Proceedings, International Symposium on Computer Restorations.* Quintessence, 1991, pp 51–60.

54. UEBERSCHÄR M, BIALEK A, GEURTSEN W: Proximal sealing of CEREC-inlays with two different bonding agents. In Mörmann WH, ed: *Proceedings, International Symposium on Computer Restorations.* Quintessence, 1991, pp 453–460.

55. HOFMANN N, HALLER B: Shear strength of composite luted to ceramics: a comparison of three ceramic materials. In Mörmann WH, ed: *Proceedings, International Symposium on Computer Restorations.* Quintessence, 1991, pp 151–162.

56. •• LAMBRECHTS P, INOKOSHI S, VAN MEERBEEK B, VILLEMS G, BRAEM M, VANHERLE G: Classification and potential of composite luting materials. In Mörmann WH, ed: *Proceedings, International Symposium on Computer Restorations.* Quintessence, 1991, pp 61–90.
Excellent discussion of considerations regarding selection of composite luting materials, includes list of available materials, material properties of an array of tooth tissues and restorative materials, and extensive literature citations.

57. ESSIG ME, ISENBERG BP, LEINFELDER KF, MUENINGHOFF LA: An in-vivo evaluation of duo-cured cements with CAD/CAM ceramic inlays [abstract 244]. *J Dent Res* 1991. 70:296.

58. HOFMANN N, KLAIBER B, HENERS M: Okklusale Randschlussqualitat von CEREC-inlays nach mehrmonatiger Tragedauer. *Dtsch Zahnärztl Z* 1990, 45:289–292.

59. NOACK MJ, ROULET FR, BERGMAN P: A new method to lute tooth colored inlays with highly filled composite resins [abstract 1528]. *J Dent Res* 1991, 70:457.

60. •• MARTIN N, JEDYNAKIEWICZ N: Surface analysis of CEREC restorations finished by different techniques. In Mörmann WH, ed: *Proceedings, International Symposium on Computer Restorations.* Quintessence, 1991, pp 469–479.
Careful study of surface finish resulting from various polishing techniques with comparisons to tooth surface and polished gold.

61. KUNZELMANN KH, HICKEL R: Feinpolitur von CEREC-inlays mit Diamontpoliersystem. *Dtsch Zahnärztl Z* 1990. 45:680–682.

62. KUNZELMANN KH, HICKEL R: Zur Präzision des CEREC system: die Schliefeinheit. *Dtsch Zahnärztl Z* 1990. 45:277–280.

63. FEHÉR A, MÖRMANN WH, LUTZ F: Efficiency of CEREC grinding wheels. In Mörmann WH, ed: *Proceedings, International Symposium on Computer Restorations.* Quintessence, 1991. pp 591–602.

64. FEHÉR A, MÖRMANN WH, LUTZ F: Die Standzeit von CEREC-Schleifscheiben. *Schweiz Monatsschr Zahnmed* 1991. 101:857–863.

65. MEYER B, MÖRMANN WH, LUTZ F: Optimizing powder application for CEREC optical impressions. In Mörmann WH, ed: *Proceedings, International Symposium on Computer Restorations.* Quintessence, 1991, pp 511–524.

66. MEYER BJA, MÖRMANN WH, LUTZ F: Optimierung der Puder-Applikation bei der CEREC-methode mit umweltfreund lichen Treibgassystemen. *Schweiz Monatsschr Zahnmed* 1990. 200:1462–1468.

67. STURDEVANT JR, HEYMANN HO, WILDER AD, ROBERSON AR, BAYNE SC: Composite cement thickness of CEREC CAD/CAM ceramic inlays [abstract 245]. *J Dent Res* 1991. 70:296.

68. HICKEL R, KUNZELMANN KH: Der Einfluss der Kavitätenpräparation auf die Randspaltbreite bei CEREC-inlays. *Dtsch Zahnärztl Z* 1990.45:675–677.

69. BESEK M, MÖRMANN WH, LUTZ F: CEREC CAD-chairside assistant: efficacy of trained vs non-trained personnel. In Mörmann WH, ed: *Proceedings, International Symposium on Computer Restorations.* Quintessence, 1991. pp 491–502.

70. STOLL R, STACHNISS V: Adjusting and finishing the occlusal morphology of CEREC restorations using rotating instruments. In Mörmann WH, ed: *Proceedings, International Symposium on Computer Restorations.* Quintessence, 1991. pp 117–126.

ClearCorrect Exhibit 1002, Page 1954 of 3373

71. LÜTHY H, BESEK M, MÖRMANN WH: Influence of surface treatments on flexure strength of computer machined ceramics. In Mörmann WH, ed: *Proceedings, International Symposium on Computer Restorations.* Quintessence, 1991, pp 613–622.

72. •• GROSSMANN DG: Structure and physical properties of DICOR-MGC glass-ceramic. In Mörmann WH, ed: *Proceedings, International Symposium on Computer Restorations.* Quintessence, 1991, pp 103–115.
Excellent description and documentation of material properties of Dicor-MGC.

73. HAHN R, LÖST C: Grinding of ceramic materials. In Mörmann WH, ed: *Proceedings, International Symposium on Computer Restorations.* Quintessence, 1991, pp 623–632.

74. LÜTHY H, GOUGOULAKIS A, LOEFFEL O, MÖRMANN: Flexure strength of computer machined ceramics. In Mörmann WH, ed: *Proceedings, International Symposium on Computer Restorations.* Quintessence, 1991, pp 603–612.

75. GROSSMANN DG: Biaxial flexure strength of CAD/CAM materials [abstract 1341]. *J Dent Res* 1991, 70:433.

76. KREJCI I: Wear of CEREC and other restorative materials. In Mörmann WH, ed: *Proceedings, International Symposium on Computer Restorations.* Quintessence, 1991, pp 245–252.

77. •• KELLY JR, LÜTHY H, GOUGOULAKIS A, POBER RL, MÖRMANN WH: Machining effects on feldspathic porcelain and glass ceramic: fractographic analysis. In Mörmann WH, ed: *Proceedings, International Symposium on Computer Restorations.* Quintessence, 1991, pp 253–273.
Excellent overview of fracture analysis and effects. More complete discussion and background information can be found in Campbell *et al.* (*Int J Prosthodont* 1989, 2:459–466).

78. CARLSEN SW: A practice specialized on CEREC restorations in Denmark. In Mörmann WH, ed: *Proceedings, International Symposium on Computer Restorations.* Quintessence, 1991, pp 183–188.

79. SIERVO S, BANDETTINI B, SIERVO R, VALENTI G: CEREC veneers on natural teeth and prosthetic elements: Italian experiences. In Mörmann WH, ed: *Proceedings, International Symposium on Computer Restorations.* Quintessence, 1991, pp 189–208.

80. LEOBOLD JM: Experience with the CEREC-system in a French private practice. In Mörmann WH, ed: *Proceedings, International Symposium on Computer Restorations.* Quintessence, 1991, pp 209–214.

81. NASH RW: The use of the CEREC in an all-cosmetic practice. In Mörmann WH, ed: *Proceedings, International Symposium on Computer Restorations.* Quintessence, 1991, pp 225–228.

82. BELTTELL JM: The change from gold inlays (metallics) to CEREC ceramics. In Mörmann WH, ed: *Proceedings, International Symposium on Computer Restorations.* Quintessence, 1991, pp 229–232.

83. JEDYNAKIEWICZ N, MARTIN N: Management of complex compound cavities by multi-part CEREC restorations. In Mörmann WH, ed: *Proceedings, International Symposium on Computer Restorations.* Quintessence, 1991, pp 525–546.

84. ESSIG ME, ISENBERG BP, LEINFELDER KF, LIU PR: In vitro evaluation of CEREC veneers utilizing standardized preparation template. In Mörmann WH, ed: *Proceedings, International Symposium on Computer Restorations.* Quintessence, 1991, pp 547–552.

85. UCHIYAMA Y: Production of metal crowns by CAD/CAM. *The Quintessence* 1991, 10:111–117.

E. Dianne Rekow, MSME, DDS, PhD, Baltimore College of Dental Surgery, University of Maryland, Department of Orthodontics, 666 West Baltimore Street, Baltimore, MD 21201-1586, USA.

ClearCorrect Exhibit 1002, Page 1955 of 3373

Specialty Feature

CAD/CAM in Dentistry: A Historical Perspective and View of the Future

E. Dianne Rekow, DDS, PhD

Computer-aided design and manufacturing (CAD/CAM) evolved from the engineering demands of the aerospace and automotive industries. Originally, the two functions were kept separate. CAD was generally used in drafting, while CAM made it possible to program and drive numerically-controlled machine tools.

In the early 1970s, as the technology's ability to increase productivity became apparent, the two functions were merged and combined CAD/CAM systems started to appear commercially.[1] At about the same time, a number of dental groups began investigating the possibility of developing a CAD/CAM system for prosthodontic applications. Each group began their investigations independently, however, and were largely unaware of their counterparts' activities until the mid 1980s.

Altschuler et al. focused on developing a data-acquisition system that could capture data from the mouth quickly, reliably, and with high precision.[2-8] This group's work has evolved into a 3-D surface imaging system. A prototype of the device is now being used by the U.S. Army and the U.S. Air Force.

In Japan, the earliest CAD/CAM research was undertaken by Tsutsumi and his team at Kyoto University. They developed an imaging system that projects multi-stripe coded patterns onto the surface being examined.[9,10] The changes in the patterns that are reflected off this surface (a dental cast, for instance) are then recorded by a video camera, and these data are processed to yield a 3-D surface map of the subject. An interactive CAD/CAM system is used to design a restoration, check for interferences with proximal and occluding teeth, and generate the machine tool paths needed to fabricate the restoration.

Tsutsumi's group is also investigating an array of new, machinable materials that could be used in dental prostheses, and is attempting to establish an index of machinability for materials. Their system is currently in the prototype stage.



Fig. 1: The DentiCAD mechanical digitizer and computer system. (Everything we're doing now is PC based).

Other Japanese teams have also started to develop CAD/CAM systems. At Hyogo and Osaka, Kawanaka and Takahashi are investigating techniques to design and machine crowns.[11,12] Hikito and Uchiyama, working at Hokkaido University, use a coordinate measuring machine to obtain 3-D surface data of a crown form and preparation. CAD software is then used to design a restoration, and CAM commands are generated to fabricate the crown through a combination of spark erosion (also known as electric discharge machining) and milling.[13]

Other groups, lead by Kawabata at Kagoshima University,[14] Mikazaki at Showa University, and Fujita at Kanagawa Dental College, are also developing prototype systems.[15]

The investigations of three other teams, each of which began its work in the early 1970s, have also evolved into modern dental CAD/CAM systems. Mormann and Brandestini's work led to the CEREC System (Siemens); Duret's system is known by his name; and Rekow's group, working at Minnesota, was instrumental in the development of the DentiCAD System.

CEREC Developments

The first CEREC inlay was computer generated from a block of porcelain, at chairside, in September 1985.[16] Today, just seven years later, approximately 1,000 clinicians use the CEREC system in their private practices.[16]

Designed as a direct chairside CAD/CAM restorative method for tooth-colored materials, the CEREC system is restricted to inlays, onlays, and veneers, and relies on a three-dimensional immediate optical impression method. It provides rapid chairside CAD/CAM fabrication and uses adhesive cementation techniques.[17]

The CEREC system consists of a three-dimensional intraoral camera, CAD software (now released in a 2.0 version), and a numerically-controlled grinding unit. A new operating system was released in early 1991, making the system extremely easy to use, much more user friendly, and eliminating the long learning curve that was inherent with the original system.

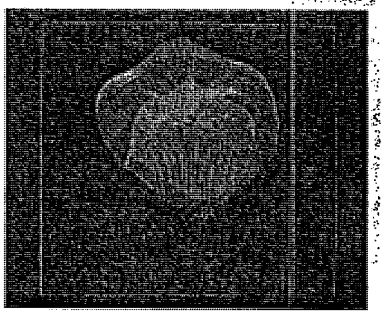


Fig. 2: A DentiCAD designed crown.

Clinical results, both *in vivo* and *in vitro*, were reported in a CEREC symposium held in May 1991.[16] Unquestionably, the system is capable of producing restorations that are clinically acceptable. However, these restorations should be limited to areas of enamel only, since bonds between the bonding composites and dentin are significantly more likely to leak and fail.[18] The major problems reported to date include hypersensitivity (in approximately 10 per cent of the cases), margin fracture over time (.05 per cent), bulk fracture, espe-

ClearCorrect Exhibit 1002, Page 1956 of 3373

cially if the isthmus reduction is insufficient (1.0-2.5 per cent), and recurrent caries (one case out of 831 restorations followed for two years).[19-26]

Duret Developments

The first crown produced with the Duret system was placed during a demonstration at the International Congress of the French Dental Association in Paris in November 1985.[27] Between 3,000 and 4,000 crowns have been produced using this system in France and the United States.[28] It uses an optical impression, an interactive CAD design system, and a micro-milling machine.[29] Currently, work is under way to develop a jaw motion tracker capable of capturing functional motion data that can be incorporated into the occlusal design of the restoration.[28] While this work appears to be progressing, and information concerning the long-term survival of restorations is possible, very little has been published on the performance of the Duret system (clinical survival of the restorations, fit at the margins, etc.).

DentiCAD Developments

The primary design criterion of the DentiCAD system was that the final margin fit should be at least equivalent to that of cast restorations (40-60 microns).[30,31] A number of data acquisition systems, including optically-based stereophotogrammetric and triangulation digitizing were investigated as this system evolved.[32] Unfortunately, these optically-based systems were not satisfactory, as it was impossible to obtain sufficiently high resolution of the data to ensure margins of 40-60 microns. Furthermore, all optical systems demand excellent retraction of the tissue around the margins.

Now, however, the DentiCAD system incorporates a miniature mechanical probe for data acquisition.[33] With this probe, no retraction is necessary, and the technique used for data collection is similar to that used during a clinical exam.

DentiCad is the newest system to become available. The first clinical crowns will be placed this year, with the first public demonstration scheduled for April 1992 at the Cologne Dental Exhibition. The DentiCAD system is capable of producing crowns and copings from titanium, alloys, machinable ceramics and porcelains, or composites. Its design and machining processes are fully automated, providing a crown within 30 minutes of the preparation's completion.

Other Systems

Other systems that employ limited CAD/CAM technology have also become available. These include the Procera, Dux, Celay,[32] and Cicero systems.[34] The Procera, Dux, and Celay systems all require an expert user (dentist or technician) to prepare a pattern of the shape to be fabricated. That shape is then digitized with a mechanical probe, machine tool paths are generated, and the restoration is fabricated. Essentially, these are 3-D versions of the copy milling process used in reproducing keys.

With the Procera System,[35,36] a die is digitized, electrodes are machined, and the internal portion of a crown or coping is produced through electric discharge machining. Then a crown or coping is waxed and placed on the die. The wax pattern is digitized, electrodes are produced, and the restoration is fabricated. One major limitation of this technique is that the material used for the restoration must be electrically conductive. This means that very few dental ceramics and porcelains can be fabricated by this process.

With the DUX system,[37] a mechanical digitizer is used to capture data describing the preparation from stone dies. The software designs a constant-thickness coping. Currently, copings are being produced from titanium, but there appears to be no limitation to the materials that could be used. The greatest limitation of this system is that it does not produce any occlusal surface information; the copings are constant thickness only.

The CELAY system[38] is used to create esthetic inlays and onlays. An acrylic pattern of the restoration is created by the clinician, working directly in the patient's mouth. The acrylic is removed, digitized, and reproduced in machinable ceramic or porcelain. This system's major limitation concerns the extent of restorations that can be fabricated.

The Cicero (Elephant) system is aimed at producing esthetic CAD/CAM restorations.[34] It produces shells of ceramic that are then bonded to another ceramic or metal substructure. An extraoral laser digitizing scanner is used to collect information from a die. CAD software then recreates the mathematical model of the die, generates the occlusal surface, and creates machine tool paths. A refractory die is milled, reproducing the prepared tooth. Powdered metallurgical or porcelain is sintered on the die and milled to the ideal form. Marginal fit is between 22 and 79 microns.

Where Are We Going?

An array of CAD/CAM systems have evolved, but dental CAD/CAM systems are, without question, still in their infancy. Developments are continuing on both existing and new systems. With each iteration, the capabilities of these systems expand, and improvements in technique sensitivities, user friendliness, computing power, and the quality of the restorations are usually evident as well.

But the excitement generated by CAD/CAM is only beginning. Researchers are now focusing on integrating automated techniques for obtaining jaw motion data into the systems, so that functional paths can be incorporated into the occlusal designs. Others are investigating color and esthetic issues that, to date, have remained largely unresolved.

One of the greatest advantages that CAD/CAM offers for the future will probably occur in the development of new materials. Since materials do not need to be cast when CAD/CAM technology is used, different materials become alternatives. The most obvious of these is titanium. While difficult to cast, it can be machined with high precision. New materials are also being developed. Already, a machinable porcelain has been fabricated by Vita and a machinable glass ceramic has been created by Dentsply in collaboration with Corning. Other materials could potentially be engineered to more nearly match the mechanical and esthetic properties of natural teeth.

Another major area for future developments will involve the expansion of the technology to a broader array of restoration types.[39] Inlays, onlays, crowns, and copings have already been demonstrated clinically. Though some groups have been investigating short-span bridges, there have not been any reports in the literature describing their design or clinical success. Little work has been done in addressing the question of how long a span is feasible with a CAD/CAM system. Are the difficulties associated with very long-span one-piece bridges due to distortion in impression materials or due to loading and minute tooth movements during function?

ClearCorrect Exhibit 1002, Page 1957 of 3373

Summary

What can we look forward too? Lots ...with new CAD/CAM systems that ...hance dentistry, providing qual-...storations quickly. The evolution ...f an array of new versions of already ...vailable systems as well as altogether ...ew systems will provide improved ...uality, expanded capabilities, and in-...reasing user friendliness. And new ...aterials will be more esthetic, wear ...ore nearly like enamel, and strong ...nough for full crowns and bridges.

We can also look forward to lots of ...hange. Because of the cost of ...AD/CAM systems, many clinicians are ...ikely to collaborate by sharing a single ...ystem. Laboratories and clinicians ...ay collaborate as well, with data being ...athered in the operatory and sent to a ...aboratory via modem. The fabrication ...would then be done by the laboratory.

Other changes that we cannot even ...redict are likely to occur in dentistry. Exciting times are here. Automation ...hrough dental CAD/CAM systems will, most certainly, change the profession. The impact of that change will only be known in the future. But as the future approaches, the systems and materials available to us will continue to evolve, improve, and enhance dentistry.

...wledgements: *Special thanks to Dave Gipe ...s continuing help in researching our CAD/CAM articles; to a long list of engineers and managers at the University of Minnesota, Foster Miller, and BEGO; and to all the groups who have supported our developments, including NIDR and Digital Dental Systems.*

Dr. Rekow *is associated with the Baltimore College of Dental Surgery at the University of Maryland, Baltimore, Maryland.*

References

1. Erdman, A.G. and Riley, D.R. Computer-Aided Design and Manufacturing – CAD/CAM, in *Mechanical Design and Systems Handbook*, H.A. Rothbard (ed), McGraw Hill, 1985.
2. Altschuler, B.R., Toboada, J., and Segreto, V.A. Intra-Oral Dental Laser Grid Surface Mapping, Applications of Optical Instrumentation in Medicine IV. *SPIE* 70:347-350, 1975.
3. Altschuler, B.R. Applications of Interferometry and Optical Metrology in Dentistry, Applications of Optics in Medicine and Biology. *SPIE* 89:40-46, 1976.
4. Altschuler, B.R., Toboada, J., and Altschuler, M.D. Laser Electro-Optic System for 3-D Topographic Mensurations, Imaging Applications for Automated Industrial Inspection and Assembly. *SPIE* 182:192-196, 1979.
...chuler, M.D., Altschuler, B.R. and Toboada, J. Measuring Surfaces Space-Coded by a Laser-Projected Dot Matrix, Imaging Applications for Automated Industrial Inspection and Assembly. *SPIE* 192:187-191, 1979.
7. Altschuler, M.D., Altschuler, B.R. and Toboada, J. Laser Electro-Optical System for Rapid 3-D Topographic Mapping of Surfaces. *Optical Engineering* 20(6):953-961, 1981.
8. Altschuler, M.D. et al. The Numerical Stereo Camera, 3-D Machine Perception. *SPIE* 283:14-24, 1981.
9. Tsutsumi, S. CAD/CAM in Japan, Proceedings, International Conference on Computers in Clinical Dentistry. Quintessence, J. Preston ed., 1992.
10. Tsutsumi, S., Umino, K. et al. A Development of Dental CAD/CAM System. *The Quintessence (Japanese)* 10(11):135-142, 1991.
11. Takahasi, J., Kawanaka, M., Watanabe, T. et al. To the Development of CAD/CAM System Using FGP Method. *The Quintessence (Japanese)* 10(8):115-121, 1991.
12. Kawanaka, M. Dental Crown Made with the CAD/CAM System. *The Quintessence (Japanese)* 10(9):155-160, 1991.
13. Hikita, K., and Uchiyama, Y. Production of Metal Crowns by CAD/CAM. Unpublished, Hokkaido University, Japan, 1991.
14. Kawahata, N. Application of CAD/CAM to Removable Denture. *The Quintessence (Japanese)* 10(10):115-121, 1991.
15. Presentations at the Japan Society of Artificial Intelligence in Dentistry, Osaka, Japan, February 1991.
16. Proceedings, International Symposium on Computer Restorations, W.H. Mormann ed., Quintessence, 1991.
17. Crawford, P.R. CAD/CAM in the Dental Office: Does it Work? *J Canad Dent Assoc* 57(2):121-123, 1991.
18. Haller, B., and Hofmann, N. Postrestorative Sensitivity: Mechanisms and Prevention. In Mormann ed., Proceedings, International Symposium on Computer Restorations. Quintessence, 127-140, 1991.
19. Mormann, W.H. and Krejci, I. Clinical and SEM Evaluation of CEREC Inlays after 5 Years in situ. In Mormann ed., Proceedings, International Symposium on Computer Restorations. Quintessence, 25-33, 1991.
20. Bieniek, K.W. and Peters, A. Clinical Evaluation of Ceramic Restorations Machined by a CAD/CAM Technique. In Mormann ed., Proceedings, International Symposium on Computer Restorations. Quintessence, 327-336, 1991.
21. Otto, T. Clinical Evaluation and Experience with the CEREC-Method in a Private Practice after Two Years. In Mormann ed., Proceedings, International Symposium on Computer Restorations. Quintessence, 347-354, 1991.
22. Reiss, B., and Walther, W. Uberlebensanalyse und klinische Nachunterscuchungen von zahnfarbenen Einlagefullungen nach dem CEREC-Verfahren. *ZWR* 100(5):329-332, 1991.
23. Mormann, W.H., Gotsch, T., Krejci, I. et al. Clinical Status of 94 CEREC Ceramic Inlays after 3 years In-Situ. In Mormann ed., Proceedings, International Symposium on Computer Restorations. Quintessence, 355-364, 1991.
24. Carlsen, S.W. A Practice Specialized on CEREC-Restorations in Denmark. In Mormann ed., Proceedings, International Symposium on Computer Restorations. Quintessence, 183-187, 1991.
25. Pallesen, V. Clinical Performance of CEREC-Restorations: Restorative Procedure and Preliminary Results. In Mormann ed., Proceedings, International Symposium on Computer Restorations. Quintessence, 285-300, 1991.
26. Isenberg, B.P. Essig, M.E., Leinfelder, K.F. et al. Clinical Evaluation of Marginal Integrity: Two Year Results. In Mormann ed., Proceedings, International Symposium on Computer Restorations. Quintessence, 163-172, 1991.
27. French Company's System Trims Prostheses Production. *Dentist Magazine*, 64:31,November/December, 31, 1986.
28. Duret, F. The Duret System. Proceedings, First International Conference on Computers in Dentistry. J Preston, ed., Quintessence, 1992.
29. Duret, F., Blouin, J.L., and Duret, B. CAD/CAM in Dentistry. *JADA* 117:715-720, 1988.
30. Holmes, J.R. *Marginal Fit of Castable Ceramic (Dicor) Crowns*. MS Thesis, University of North Carolina, 1986.
31. Rekow, E.D., Thompson, V.P. and Yang, H.S. Margin Fit of CAD/CAM Produced Crowns. *IADR* 70(A):Abstract 1349, 1991.
32. Rekow, E.D. Computer-Aided Design and Manufacturing in Dentistry: A Review of the State of the Art. *J Pros Dent* 58:512-520, 1987.
33. Rekow, E.D. Dental CAD/CAM Systems: What is the State of the Art? *JADA* 122:43-48, 1991.
34. Bayne, S.C. What is the Future of CAD/CAM Materials and Techniques? Presentation at the ADA/NIDR Esthetic Restorative Materials Symposium, November 1991.
35. Andresson, M., Bergman, B., et al. Clinical results with Titanium Crowns Fabricated with Machine Duplication and Spark Erosion. *Acta Odontol Scan* 47:269-296, 1989.
36. Reppel, P.D. Boning, K., and Walter, M. Festsitzender zahnersatz aus gefastem/funkenerodiertem Titan. *Dtsch Zahnartztl* 46(11):756-758, 1991.
37. Schlegel, A., Besimo, C., Guggenheim, R. et al. In-Vitro-untersuchung zur Marinalen Passgenäuigkeit von Computergefrasten Titankronen. *Schweiz Monatsschr Zahnmed* 101:1273-1278, 1991.
38. Celay System Product Literature, Microna Technolgie, AG, Spreitenbach, Switzerland.
39. Stachniss, V., and Stoll, R. Computer Technologies in Dentistry Computerized Restorations: CEREC and other Methods. In Mormann ed., Proceedings, International Symposium on Computer Restorations. Quintessence, 33-49, 1991.

ClearCorrect Exhibit 1002, Page 1958 of 3373

MAR-08-00 04:07 PM 2129824782 P.08

THE JOURNAL OF

PROSTHETIC DENTISTRY

EDITOR
Judson C. Hickey
ASSISTANT EDITOR
Ronald P. Desjardins

EDITORIAL COUNCIL
I. Kenneth Adisman, *chairman*
Dale E. Smith, *vice-chairman*
S. Howard Payne, *consultant*
Louis J. Boucher
Thomas A. Curtis
Gerald N. Graser
William A. Jennings
William L. Kydd
Glen P. McGivney
Chester Perry
Kenneth E. Wical

SECTION EDITORS

Fixed prosthodontics and operative dentistry
Samuel E. Guyer
William Lefkowitz
William F. P. Malone
John R. Rhoads
Robert C. Sproull

Removable prosthodontics
Louis Blatterfein
S. Howard Payne

Maxillofacial prosthetics and dental implants
I. Kenneth Adisman
Ronald P. Desjardins

Craniomandibular function and dysfunction
George A. Zarb

Research and education
Louis J. Boucher

Dental technology
Kenneth D. Rudd

EDITORIAL REVIEW BOARD

1988
Charles R. Dufort
Aaron H. Fenton
Gerald N. Graser
L. Frances Greenwood
James B. Lepley
Glen P. McGivney
David L. Moore
Arun Nayyar
Marzban G. Patel
James L. Sandrik
Kenneth A. Turner
Ned B. van Roekel
Samuel P. Weber
Warren Yow

1989
Michael D. Bagby
Charles H. Casey
Thomas A. Curtis
Richard J. Grisius
Howard M. Landesman
Paul J. Mentag
Norman D. Mohl
Robert P. Renner
Jerome U. Shatoff
Sheldon Winkler
Ronald D. Woody
Anthony T. Young

1990
Gerald M. Barrack
Seymour Birnbach
Robert L. DeFranco
Edward S. Duke
Wilmer B. Eames
James A. Fowler, Jr.
John A. Ianzano
William A. Jennings
John D. Jones
David A. Kaiser
David L. Koth
T. Graham Matthews
Lance F. Ortman
Chester K. Perry
James A. Stackhouse
Kenneth L. Stewart
Charles A. Ullo
Gerald D. Woolsey

SPECIAL CONSULTANTS
Paul Barton, *editorial consultant*
P. Kenneth Morse, *statistical consultant*
Ralph W. Phillips, *advisor, dental materials*

EDITORIAL ASSISTANT
Ocie Colleen Ringle

SENIOR MANUSCRIPT EDITOR
Barbara M. Kissane

VOLUME 58
THE C.V. MOSBY COMPANY
DECEMBER
1987
ST. LOUIS

ALN006582

ClearCorrect Exhibit 1002, Page 1959 of 3373

San Diego, Calif.; Ralph P. Felles, D.M.D., M.S., M.P.H., Chief, Dental Service, Jerry L. Pettis Memorial Veterans Hospital, Loma Linda; Associate Professor of Prosthodontics, Loma Linda University School of Dentistry, Loma Linda, Calif.; George W. Carroll, D.D.S., M.S., Chief, Dental Service, VA Medical Center, San Diego, Calif.; Robert A. Wiedlin, D.D.S., M.S., Staff Oral Surgeon, VA Medical Center, Sepulveda; Adjunct Assistant Professor of Oral Surgery, UCLA School of Dentistry, Los Angeles, Calif.; Charles A. Arakaki, D.D.S., Staff Dentist, VA Outpatient Clinic, Los Angeles; Lecturer of Removable Prosthodontics, UCLA School of Dentistry, Los Angeles, Calif.; and Michael A. Perrone, D.D.S., Director of General Practice Residency Program, Jerry L. Pettis Memorial Veterans Hospital, Loma Linda; Assistant Professor of Restorative Dentistry, Loma Linda University, Loma Linda, Calif.

Executive Committee: Krishan K. Kapur, D.M.D., M.S., Chairman; Harry Blechman, D.D.S.; George W. Carroll, D.D.S.; Robert H. Deupree, Ph.D.; Paul Ehrlich, D.D.S.; Robert H. Sprigg, D.D.S.

Operations Committee: Gerald Shklar, D.M.D., M.S., Chairman; Potter Chang, Ph.D.; Richard Toposian, D.D.S.

Biostatistical Staff: Robert H. Deupree, Ph.D., Barbara Komenda, Margaret Lee, Claire Pariidise, Tanya Economou

Research Staff: Angeline Brady, Henry Jones, Armen Melikian, Charlie Minnifield, Alicia Moran, Elizabeth Sambenno, Bill Slagle, and Barbara Villeto

Participating Centers: Veterans Administration Medical Centers at Loma Linda, San Diego, Sepulveda, and West Los Angeles, and Veterans Administration Outpatient Clinic at Los Angeles

Computer-aided design and manufacturing in dentistry: A review of the state of the art

Dianne Rekow, M.S.M.E., D.D.S.*
University of Minnesota, School of Dentistry, Minneapolis, Minn.

Advances in computer-aided design and computer-aided manufacturing (CAD/CAM) are providing a new option for dentistry, creating an alternative technique for producing dental restorations. Three groups are actively engaged in applying CAD/CAM techniques. One group is supported by Hennson International of France. Another is a combined effort between the University of Zurich and Brains, Brandestini Instruments of Switzerland. The third group is at the University of Minnesota; its major sources of support are the U.S. National Institute of Dental Research and the University of Minnesota. Each group has a slightly different philosophy and approach. All three, however, are working toward the common goal of integrating engineering applications of automation in the creation of dental prostheses. This review describes the systems being developed by each of the three groups and identifies similarities and differences between the systems.

*Instructor, Department of Orthodontics and Department of Mechanical Engineering National Institute of Dental Research postdoctoral fellow.

THE FRENCH SYSTEM

The French system uses a laser scanner to produce images of the patient's mouth. Data are processed by shape-recognition software, visualized on a video display, and transferred to a CAD/CAM software package that creates a three-dimensional model of the environment where the prosthesis ultimately will be fitted. The interactive capability of the CAD/CAM software allows the dentist to access a library describing "theoretical teeth," adapt them to the patient's oral environment, and design a three-dimensional model of the prosthesis on the computer screen. The CAD/CAM software computes the instrument paths needed and a micromilling machine cuts the tooth.[1]

A hand-held optical probe measures the three-dimensional coordinates of the tooth prepared for a restoration and of the adjacent teeth.[2] The scanner probe, with a theoretical basis similar to Moire[3] fringe techniques, has a resolution of 20 μm. The probe consists principally of a laser-diode source and a charge-coupled-device (CCD) photoreceptor. A nonreflective substance is applied to the patient's teeth to eliminate spurious reflections. The

ALN006583

ClearCorrect Exhibit 1002, Page 1960 of 3373

probe is passed over the teeth. The signal created by the laser light reflected by the teeth is picked up by the CCD arrays, converted to a digital signal, and relayed to the computer.[4] Data from the signal are then processed and the results are displayed on a video monitor (a process that requires 2 to 4 minutes). A foot pedal permits the image to be fixed for further examination so that it can be accepted or rejected. The probe must pass over the teeth four times and four acceptable images must be obtained. In expert hands, data of the prepared tooth, the adjacent teeth, and the opposing dentition can be acquired in less than 3 minutes.[3]

The CAD/CAM system used is Euclid (Matra Datavision Woburn, Mass.),[4] running on a MicroVAX II (Digital Equipment Corp., Marlboro, Mass.) computer.[4] The Euclid system is used to create a solid model of the surface where the prosthesis will be fitted.[3]

A library of tooth forms has been created. By using routines available in the Euclid unit, the system user can interactively restore the missing teeth on the display.[2] The function of the CAD/CAM system is to generate the prosthesis to fit the unique requirements of the patient being treated. The internal configuration is determined by the dynamics of the flow, thickness, and resistance of the luting agent. The external form and volume depend on contact areas, vestibular and lingual curves, and articulation.[3] The scan recording the required data from the patient's mouth can be made before the preparation has been cut, permitting the existing tooth morphology to be exactly reproduced or, in the case of severely damaged teeth, the morphology of the replacement tooth can be generated from the library of tooth forms. The computer-recording apparatus is capable of recording temporomandibular joint function so that the occlusal surface can be properly formed.[4] Complete modeling on the screen requires 2 to 10 minutes.[3]

When the prosthesis design is complete, the CAM commands in the Euclid software permit the instrument paths for numerical-control (N/C) machining to be generated. A three-axis micromilling machine cuts the prosthesis. The prosthesis can be manufactured to a tolerance of <80 μm.[3] The tooling cycle requires 15 to 20 minutes.[3]

The French system will be capable of creating inlays, onlays, three-quarter crowns, full crowns, three-unit fixed partial dentures, and complete dentures, milled from a solid block. Crowns can be fabricated from gold, composite, nonprecious metals, or ceramic.[4] Complete crowns can be created and seated in a single appointment. On November 30, 1985, at the International Congress of the French Dental Association, Dr. Francois Duret[7] demonstrated the automatic system by producing a posterior crown restoration for his wife in less than 1 hour.[3]

The system can be configured in a variety of ways, from a single stand-alone system to multiple data acquisition and verification monitors in each of several operatories networked to a single computer-milling machine combination.[3] System costs are believed to range from $35,000 to $90,000. Commercial production was scheduled to begin in 1987.[3]

THE SWISS SYSTEM

The Swiss system, trademarked as the CEREC-System (Brains, Brandestini Instruments, Zillikan, Switzerland)[1] also uses an optical topographic scanning procedure and an electronically controlled milling machine.[10] A three-dimensional oral camera has been designed[8] to feed data to an interactive CAD unit. The system is capable of machining porcelain inlays and was demonstrated in Zurich on May 1, 1986.[3]

With the Swiss system, a noncontacting scan head is positioned over a prepared tooth. The scanner incorporates a light-emitting diode and lens system to illuminate the cavity of the tooth. Before reaching the tooth, the light rays are deflected by reflections from a mirror, permitting easy access in a patient's mouth. The rays pass through a set of ruled lines and a lens system. Light passing through the ruled lines casts a pattern of light and dark stripes on the prepared cavity. The light is reflected back to the scan head where it is sensed (at a different angle) by a CCD sensor with resolution of 256 by 256 pixels. The intensity of this reflected light is recorded as voltage values proportional to the intensity of the light reflected back to the CCD chip. The voltage values are recorded in digital form and are transmitted to the computer for subsequent analysis.[6] The scanning of a class II cavity requires only 0.2 seconds.[3]

The vertical dimension of the depth of the cavity is determined by the apparent shift between the incident and reflected light; deeper parts of the cavity exhibit more apparent shift than shallow areas. Although the accuracy of the readings obtained with the scan head are generally adequate, they can be improved by coating the cavity with a layer of white, glare-free substance (such as CAVISON, Svedia Dental Industry, Enkoeping, Sweden). Calibration is required to establish the precise scale for intensity as a function of cavity depth. Calibration can be accomplished by mapping a standard element that can also be mapped with other conventional means (such as a caliper). The total field can be represented in 0.05 mm raster units, covering a total volume of 12.8 by 12.8 by 12.8 mm.[6]

The computer used is a desk-top model (such as an Apple II with two memory boards supplied by Matrox

[8]Moermans WH, Brandestini M. Method and apparatus for the fabrication of custom-shaped implants. U.S. Patent No. 4,575,805. March 11, 1986.

ALN006584

ClearCorrect Exhibit 1002, Page 1961 of 3373

Ltd., Quebec, Canada, Part RGB 256/4). The computer transforms the voltages representing intensity to depth values for each x, y position of the cavity.[8] This system also incorporates a monitor that displays the cavity/inlay data being processed by the system,[9] permitting visual verification of the quality of the data being acquired.[11]

Inlay fabrication is accomplished with a three-axis N/C milling machine.[9] Three translatory platforms are mounted on a supporting frame to provide x, y, and z position control (Micro Control type MR-80.25, part No. 338604, M.C. Corp., Vitry-sur-siene, France). Each platform is moved by a stepper motor (Sigma Instruments mod. No. 20-2220 BD 200, Braintree, Md.) driven by a lead screw that is controlled by the microcomputer. A high-speed turbine (Part No. 464006, Midwest American, Melrose Park, Ill.) powering a diamond bur is rigidly connected to the y-axis platform. The turbine is air driven and coolant is run over the part being milled during the drilling operations.[8]

Inlays are machined from prefabricated rod-shaped blanks of dental porcelain. These blanks measure approximately 9 × 9 × 13 mm and are fabricated by using conventional dental porcelain techniques; Vitadur-353 N (Vita Zahnfabrik, Bad Sackingen, West Germany) frit powder is mixed with distilled water and condensed manually into a 10 × 10 × 15 mm steel die. The condensed frit powder is fired under vacuum and the temperature is increased at a rate of 60° C/min to 950° C and held at that temperature for 1 minute. The porcelain blanks are bonded to a stub, allowing the blanks to be fixed inside the three-axis milling machine. Milling of a class II porcelain inlay requires 5 to 7 minutes.[9]

The inlays are seated with a simultaneously light- and chemical-curing luting agent (Heliobond two-paste system, Espe GmbH, Seefeld, West Germany).[11] The occlusal surfaces are then ground into occlusion by the dentist. Although the milling accuracy of the restoration has not been reported, the marginal integrity of this restoration has been shown to be excellent.[9,11]

THE MINNESOTA SYSTEM

The system at the University of Minnesota is still under development. With this system, data are required in the dental office and sent to another location for processing and machining. This permits system costs to the dentist to be kept at a minimum, well below $5000. The system is being developed to be capable of milling a metal full-coverage crown. When that is possible, other more conservative restorations will be simple modifications. Potentially the system will also be able to mill frameworks for partial dentures and complete denture bases as well as multiunit fixed partial dentures. The major focus on the development of this system is to make it completely automatic, without any interaction by the user.[12,13] To date, no demonstrations have been given with this system. The design criterion for this system, however, is that final crown margins will fit to within 20 μm at the margin.[12]

Data are acquired by using a photographic-based system. In the opinion of this group, tolerances for good fit at the crown margins can only be met with high-resolution data acquisition and digitizing equipment.[12] At that resolution, it is not yet possible to obtain real-time data because no more than 512 × 512 pixels can be written to a computer real time unless extra frame buffers are available, which increases the cost substantially. Data acquired include the surface of the tooth prepared for a crown, the proximal segments of both adjacent teeth, and the surface morphology of the opposing tooth or teeth. The position of the cusp tips of the opposing dentition are obtained relative to the surface of the prepared tooth with the teeth in centric occlusion, working and balancing positions, and protrusion.

Data are acquired with a standard 35 mm camera through a 10 mm diameter single-rod lens magnifying laryngopharyngoscope (Richard Wolf Medical Instruments, Rosemont, Ill.), which attaches to a standard 55 mm lens. A prism system at the distal end of the rod lens permits the field of view to be 90 degrees from the long axis of the lens. Depth of field is essentially infinite. An entire crown preparation can be viewed from a single position approximately 25 mm above the surface of the tooth. A number of views are used, however, to ensure that complete information is obtained and to minimize the likelihood of blur caused by the patient moving. The tooth is illuminated with fiber-optics, which surround the lens. A three-dimensional calibration device is in the field of view of every image, permitting continuous calibration of the image without imposing any constraints on the position of the lens relative to the teeth or in any way constraining the patient's head.[13]

To permit three-dimensional surface reconstruction and reconstruction of the movements of the jaw (at least in the positions where the teeth are in contact), stereo pairs of images are made. The images are recorded on standard film (Ectachrome, ASA 400). The exposed film is developed by commercial processors.

The color slides are digitized by using an Eikonix EC 850 (Eikonix Corp., Bedford, Mass.) digitizing system interfaced with a PDP 11/44 with RSX 11-M-PLUS operating system (Digital Equipment Corp.). The digitizer has a resolution of 4096 × 4096 pixels. The image of the tooth fills the entire field of view of the digitizer, providing a limited resolution of 2.44 μm (for a 10 mm

[8]Moermann WH, Brandestini M. Method and apparatus for the fabrication of custom-shaped implants. U.S. Patent No. 4,575,805, March 11, 1986.

ALN006585

ClearCorrect Exhibit 1002, Page 1962 of 3373

diameter image broken into 4096 pixels by 4096 pixels). Repeatability of the digitizer is 1 pixel. Each pixel has an x,y image address. The digitizer senses the intensity of light passing through each pixel and writes that value, along with the address, to the computer. Images can be analyzed in grey scale as well as in red, blue, and green. Digitizing time is 10 to 90 seconds per slide, depending on the color scale being used.

Two techniques are being investigated for three-dimensional reconstruction. The first is the method of direct linear transformation.[15] Before three-dimensional analysis can begin, each of the points in one stereo image must be matched with its corresponding point in the other half of the stereo pair. To provide original alignment, strong edges (like the margin of the prepared tooth) in each image are found by using algorithms developed by Canny[16] for robot three-dimensional obstacle avoidance and robot vision. The weaker edges (such as bur scratches on the prepared surface) are found by using algorithms devised by Haralich[17] and Marr and Hildreth.[18] Correlation techniques are then used to obtain the most likely relative orientation of the two images. When the correspondence between points has been established, the direct-linear transformation is applied to reconstruct the three-dimensional image. Accuracy with this method is undergoing investigation.

Grimson[19] proposed an alternative technique to the direct-linear transformation. He argued that for any given set of edges (for any image) and intensities, there exists one unique surface. The accuracy of reconstructions with this technique are being evaluated.

Three-dimensional coordinates provide the computer-based equivalent of perfectly mounted casts on an infinitely adjustable articulator. The internal surface of the crown is defined by the reconstructed three-dimensional coordinates of the prepared tooth surface.

When the three-dimensional coordinates from all of the images have been reconstructed, the paths of motion of the opposing dentition as they pass over the prepared tooth are established. This is done using kinematic analysis of the positions of the occluding teeth relative to the prepared tooth.[20] The external surface of the crown is automatically designed. A data base that contains the configuration of each of the tooth forms in their ideal configuration has been created.[20] For any crown designed with this computer system, the ideal form is used, but it is automatically modified to fit the unique requirements of the mesial-distal and buccal-lingual size, margins, and occlusal function of the patient being treated.

The internal and external surfaces of the computer-designed crown are mathematically described by B-spline and/or Bezier surfaces, permitting subsequent machining.[21] The CAD/CAM system used is the ICEM-DDN package (Integrated Computer-Aided Engineering and Machining—Design, Drafting, and Numerical Control, Control Data Corp., Minneapolis, Minn.). The computer-design surfaces are used to generate machine-tool paths for subsequent machining with a five-axis N/C machine.

QUESTIONS FOR COMPARISON OF SYSTEMS

To evaluate the value of any system, a number of questions must be asked. Each dentist must evaluate the advantages and disadvantages that the system brings to his or her practice. In addition, the quality of the CAD/CAM system and the integrity of the restoration that it produces must be carefully considered.

COMPARISONS AND SUMMARY

Three groups are actively engaged in integrating CAD/CAM techniques into the development of automated systems for production of dental restorations. Demonstrations of the French and Swiss systems have been held. Both systems use optical-based real-time data-acquisition devices. Data acquisition with the Minnesota system uses photographs and a high-resolution digitizer.

The Minnesota and French systems are designed to fabricate crowns and to integrate the unique requirements of each patient's occlusal function. The Swiss system is designed to fabricate inlays only and the occlusal surface is created by the dentist after the inlay is seated.

All of these systems use state-of-the-art techniques for designing the restoration. All three mill restorations with commands generated by a CAM package. However, the Swiss and French rely on a three-axis milling machine; the Minnesota system uses a five-axis machine, providing greater freedom in producing required external contours.

Costs of the systems cannot as yet be compared because only the cost of the French system has been published. By limiting the amount of work done in the dental office, the equipment in the office will cost the least with the Minnesota system.

All three systems offer an alternative to the currently practiced impression-die-lost wax-casting technique. Potentially each can save the dentist time by providing restorations that accurately fit the patient without requiring chairside adjustments. In addition, they can provide more consistency in restoration design and open the possibility of a whole array of different restorative materials, including machinable tooth-colored ceramics.

REFERENCES

1. Design International. Machine Design 1986;April:44.
2. Applications. Solid Modeling Today 1984;1:8.

ALN006586

ClearCorrect Exhibit 1002, Page 1963 of 3373

3. Duret F. Vers une prothese informatisee. Tonus 1985;Nov:55-7.
4. Gallagher RT. CAD system turns out dentures in 30 minutes. Electronics 1985;Dec:30.
5. More news on laser scanner. Lab Management Today 1986; Oct:35.
6. Reed D. Addenda for Francois Duret workshop. Phoenix, Ariz: Nuphi International, 1986.
7. Hennson International product literature. The dental CAD/CAM—general description of the project. Vienne, France: Hennson International, 1986.
8. News release. L'un republicain. Vienne, France: Hennson International, 1985.
9. Moermann W, Jans H, Brandestini M, Ferru A, Lutz F. Computer machined adhesive porcelain inlays: margin adaptation after fatigue stress [Abstract]. J Dent Res 1986;65:762.
10. Brandestini M, Moermann W, Lutz F, Krejci I. Computer machined ceramic inlays: in vitro marginal adaptation [Abstract]. J Dent Res 1985;64:208.
11. Moermann W, Brandestini M, Ferru A, Lutz F, Krejci I. Marginale adaptation von adhasiven porcellaninlays in vitro. SSO: Schweiz Monatsschr Zahnmed 1985;95:1118-29.
12. Rekow ED, Erdman AG, Speidel TM. Computer-assisted system to automate production of posterior dental restorations. Biostereometrics 85, SPIE 1985;B602:204-10.
13. Rekow ED, Speidel TM, Erdman AG. Computer-aided system to automate production of posterior dental restorations [Abstract]. J Dent Res 1986;65:317.
14. Rekow ED, Erdman AG. Comparison of techniques for acquiring high-resolution three-dimensional computer-based data directly from the human mouth. Adv in Bioengineering, ASME, 1985;Nov:139-40.
15. Abdel-Aziz YI, Karara HM. Photogrammetric potentials of non-metric cameras. Civil engineering studies, photogrammetry series No. 36. Urbana, Ill: University of Illinois, 1974.
16. Canny JF. Finding edges and lines in images [M.S. thesis]. Boston: Massachusetts Institute of Technology, June 1983.
17. Haralick RM. Digital steps edges from zero-crossings of second directional derivatives. IEEE Trans Pattern Analysis Machine Intelligence 1984;PAMI-6(1):58-68.
18. Marr D, Hildreth E. Theory of edge detection. Proc R Soc Lond [Biol] 1980;207:187-217.
19. Grimson WEL. Computing shape using a theory of human stereo vision [Ph.D. thesis]. Boston: Massachusetts Institute of Technology, 1980.
20. Erdman AG, Rekow ED, Hartzel MA, Chen M. Tools of bioengineering. SOMA: Eng Human Body 1986;1:30-8.

Reprint requests to:
Dr. Dianne Rekow
University of Minnesota
School of Dentistry
Minneapolis, MN 55455

Bound volumes available to subscribers

Bound volumes of the Journal of Prosthetic Dentistry are available to subscribers (only) for the 1987 issues from the publisher at a cost of $42.00 ($51.75 International) for Vol. 57 (January-June) and Vol. 58 (July-December). Shipping charges are included. Each bound volume contains a subject and author index, and all advertising is removed. Copies are shipped within 30 days after publication of the last issue in the volume. The binding is durable buckram with the journal name, volume number, and year stamped in gold on the spine. *Payment must accompany all orders.* Contact The C. V. Mosby Co., Circulation Department, 11830 Westline Industrial Drive, St. Louis, MO 63146, USA; phone (800) 325-4177, ext. 351.

Subscriptions must be in force to qualify. Bound volumes are not available in place of a regular Journal subscription.

ALN006587

ClearCorrect Exhibit 1002, Page 1964 of 3373

DENTAL CAD-CAM SYSTEMS

WHAT IS THE STATE OF THE ART?

ABSTRACT

The author compares six CAD-CAM systems, addressing differences in configuration, capabilities, learning curves to use the system successfully, costs and fit of CAD-CAM-produced restorations.

E. DIANNE REKOW, D.D.S., PH.D.

The advent of interactive computer graphics, computer-aided design and computer-aided manufacturing laid the groundwork for a revolution in engineering—and dentistry. CAD-CAM provides tools to automate design and production, improving productivity and quality.

Dental CAD-CAM systems are being developed to bring this automation to produce dental restorations. Restoration design, whether with the lost wax casting technique or a CAD-CAM system, has three functional components:

- data acquisition;
- restoration design;
- restoration fabrication.

With the CAD-CAM systems, data acquisition (all the steps currently involved in taking an impression and, with some systems, creating models and dies) can be automated. Design, currently the waxing process, is replaced with computer commands supplied either interactively by the user or by special programs called an expert system.

Investing and casting techniques can be replaced by faster fabrication techniques used in modern manufacturing. Varied technologies can accomplish the automation in the dental CAD-CAM systems.

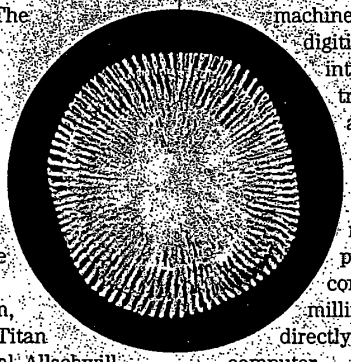
This review describes six dental CAD-CAM systems and offers a framework for establishing their clinical value. Comparisons are made on the basis of system configuration, system capabilities, the learning curve required to use the system successfully, system costs and the fit of CAD-CAM-produced restorations.

COMPARISON OF SYSTEM CONFIGURATIONS

The physical configurations of each of the six different systems are briefly described (references offer more detailed information). The CEREC system,[2-5] manufactured by Siemens Dental Corp. (Benshein, Germany), is one of the best known and widely available. About 1,000 systems are currently in operation. This compact chairside system consists of an optical data acquisition camera, CAD-CAM software and a micromilling machine.

ClearCorrect Exhibit 1002, Page 1965 of 3373

The Duret system is used in 30 dental offices in France and at the University of Southern California. More than 3,000 restorations have been designed and fabricated with this system produced by Sopha (Lyon, France).[9] The Duret CAD-CAM system consists of three discrete units: a camera module for data acquisition, the CAD module used to design the restoration and the milling module.[10]



The DUX system, also known as the Titan system (DCS Dental, Allschwill, Switzerland), consists of a miniature contact digitizer, a central computer and a milling unit.[11,12] The digitizer consists of a table that shifts a die or model beneath a contact stylus. The central computer includes limited CAD capabilities.

The Celay system (Mikrona Technologie, Spreitenbach, Switzerland) is a very small unit consisting of a contact digitizer that "reads" the shape of an acrylic inlay (fabricated directly in the mouth) and directly transfers that shape to a miniature milling machine.[13] The system is similar to a key copying or pantograph machine.

The Procera system[14-16] (Nobelpharma, Inc., Goteborg, Sweden) is a copying and fabrication system using a pantograph and electric discharge machining. The shape of the die and the wax pattern of the restoration are "read" by a pantography stylus that transmits these shapes to a milling machine to produce electrodes in these shapes. These electrodes are used to produce a restoration with EDM.

The DentiCAD system[17,18] (BEGO, Bremen, Germany, and DentiCAD USA, Waltham, Mass.) system consists of miniature robot arm digitizer, CAD-CAM software with an expert system for fully automated design and a milling machine. The robot arm digitizer can be used intraorally or on traditional models and dies. The CAD-CAM software and expert system reside in a personal computer. The milling machine is directly controlled by the computer.

COMPARISON OF SYSTEM CAPABILITIES

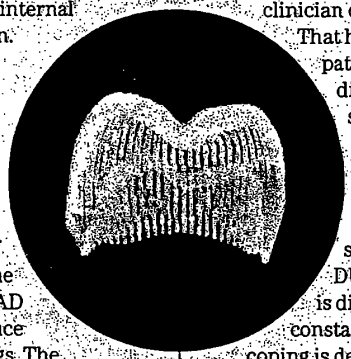
Perhaps the greatest difference among the systems is the type of restorations that can be produced. The CEREC and Celay systems can produce only inlays and a few onlays. The cutting tool used to fabricate restorations with these systems is a flat disk with a diameter of approximately 20 millimeters. It is impossible to have access to the internal portions of a crown.

The DUX and Procera systems produce only copings; they have insufficient CAD capabilities to design the occlusal surface of the restoration. The Duret and DentiCAD systems can produce crowns and copings. The Duret system can also produce inlays (intracoronal restorations and bridges will be available in the DentiCAD system in 1992).

Various materials are available for fabricating CAD-CAM restorations. Many systems, however, can use only a few. The CEREC and Celay systems provide an alternative to amalgams; they produce inlays from ceramic materials. The two most widely used ceramic materials are Machinable Glass Ceramic (Dicor, Dentsply International, York, Pa.) and Vita Porcelain (Vita Zahnfabrik, Bad Sachingen, Germany).

Titanium is another popular choice. It is the preferred material for the DUX and Procera systems. Because the Procera system fabricates restorations with EDM, only electrically conductive materials can be fabricated. The Duret and DentiCAD systems offer a broader range of materials choices, including machinable ceramics, metals (including titanium), and composites. The Duret system also offers an organo-ceramic material (Aristee, Spad Dijon, France).

Another major system difference is the degree of automation. The Celay and Procera systems have very little automation. Each requires a pattern to be produced by a clinician or technician. That human-created pattern is then digitized and simply reproduced by the fabrication methods available for that system. With the DUX system, a die is digitized and a constant thickness coping is designed by the CAD software.



Both the CEREC and Duret systems provide a moderate level of automation; both, however, require the user to be involved interactively with the design of the

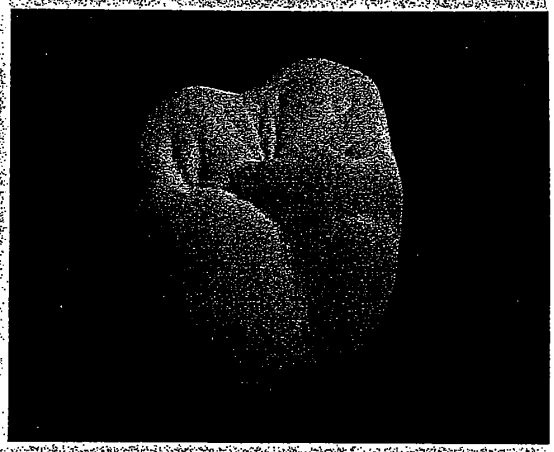
ClearCorrect Exhibit 1002, Page 1966 of 3373

restoration. The user must identify selected points around the margin and provide intelligent input for the restoration design.

The DentiCAD system is the most completely automated; the user need only digitize the teeth required (prepared, opposing and contact areas of the proximal teeth) and load the milling machine. Everything else is done automatically.

The degree of automation has implications in the time required to produce a restoration. The DentiCAD and Duret systems produce similar types of restorations. But with the automation available in the DentiCAD system, the design requires less than three minutes. The Duret system's design requires an expert user who understands occlusion and restoration design and, because so many interactive commands are necessary, the design requires nearly 50 minutes to complete.

One primary advantage provided by CAD-CAM technology is the fast turnaround time for restoration production. Even the slowest systems can produce a restoration easily within three hours (including the time to produce models and a die). The CEREC and Duret systems can produce a restoration within 90 minutes.



Much of the time required with the CEREC system is spent creating the occlusion of the inlay after it has been seated in the patient's mouth (the restoration, in its as-milled form, does not include any occlusal anatomy). Most of the time required by the Duret system is the result of the demands for interactive design of the restoration. The fastest system, the DentiCAD, can produce a full crown in less than 30 minutes.

COMPARISON OF LEARNING CURVES

With any new system, some time is required to learn how to use it. The same is true with the CAD-CAM systems. Major influences in the amount of training required are the number of new technologies—and how those technologies differ from the user's experience or knowledge.



The CEREC and Duret systems both use an optical data acquisition system. Optical "impressions" are at least as difficult to obtain as tradition impressions. Indeed, the optical "impressions" are less forgiving—the margins must absolutely be isolated and visible to capture their entire periphery. The optical systems also require a powder layer placed on the tooth surface (to optimize reflections and color consistency). If that layer is not thin and even, the information captured with the optical systems will include a distortion.

The DUX, Celay and Procera systems all use mechanical pantographic-type digitizers that are easy to use. The DentiCAD digitizer is new technology but easy to learn. The digitizer consists of a linkage and a mounting post. The post is attached, using compound, to a tooth or teeth at any arbitrary position away from the tooth being restored. A probe at the end of the linkage is moved over the areas where data need to be collected (the prepared tooth, for instance).

Contact with the tooth need not be maintained throughout the entire digitizing process. If the probe tip is lifted off the tooth surface, data points are collected only when the two are in contact. There is no need for retraction and

ClearCorrect Exhibit 1002, Page 1967 of 3373

TABLE 1

DENTAL CAD-CAM SYSTEM COMPARISON

	CEREC	DURET	DUX
SYSTEM CONFIGURATION			
Data acquisition	Optical	Optical	Mechanical—on impressions
Fabrication	Milling + hand finish	Milling	Milling
SYSTEM CAPABILITIES			
Restoration type	Inlay, onlay	Crown, inlay, coping	Coping
Material	Dicor, Vita*	Dicor, Aristee†	Titanium
Design automation	Moderate	Moderate	Low
Data acquisition	<5 minutes	5 minutes	15 minutes + model
Restoration design	<10 minutes	50 minutes	5 minutes
Fabrication time	<15 minutes + grind in occlusion	30 minutes	30 minutes
Total time: prep seated in patient	90 minutes	50 minutes	50 minutes + model
LEARNING CURVE—NEW TECHNOLOGIES	Optical impressions, CAD, milling	Optical impressions, CAD, milling	Mechanical digitizer, milling
SYSTEM COSTS			
Initial‡	Mid	High	Low
Operator	Clinician	Clinician	Clinician or technician

*Machinable Glass Ceramic, Denisply International, York, Pa.; Vita Porcelain, Vita Zahnfabrik, Bad Sachingen, Germany.
†Aristee, Spad Dijon, France.
‡Initial costs: low <$50,000; mid $50,000-100,000; high > $100,000.

isolation of the margins. The probe tip is smaller in diameter than burs used to create a preparation so there is no problem with access—the probe can easily obtain data subgingivally. From a clinical perspective, using the probe is similar to examining with an explorer.

The CEREC and Duret systems require the user to become familiar with CAD commands. All systems require the user to learn some fundamentals of milling, though these are similar to concepts currently used with a dental handpiece. Additionally, the Procera system requires familiarity with EDM processing.

COMPARISON OF SYSTEM COSTS

Costs of the various systems range from under $25,000 (Celay) to over $200,000 (Duret). Factors other than initial cost for acquisition also need to be considered. The cost of operating the system may be important. Some systems require an expert user (CEREC and Duret, for instance); only the DentiCAD system can be operated without any special expertise.

The materials cost must be factored into the comparison. At this time, incomplete information is available concerning the materials cost for each restoration for all systems. Another factor is the cost and replacement rate of cutters. Again,

ClearCorrect Exhibit 1002, Page 1968 of 3373

TABLE 1 (CONTINUED)

DENTAL CAD-CAM SYSTEM COMPARISON

CELAY	PROCERA	DENTICAD
Mechanical–direct acrylic	Mechanical–on waxup	Mechanical–direct
Milling	EDM	Milling
Inlay Ceramic	Crown Titanium	Crown, coping Metal, ceramic, composite
Low 15 minutes + model	Low 20 minutes + model + waxup	High <5 minutes
Waxup 5 minutes	Waxup 90 minutes	<3 minutes <20 minutes
20 minutes + waxup	110 minutes + waxup + model	<30 minutes
Milling	EDM, milling, digitizer	Mechanical digitizer milling
Low Clinician	High Clinician, technician	Mid-high No special expertise

incomplete information is available so no fair comparisons can be made.

COMPARISON OF QUALITY OF FIT

There is little agreement concerning the acceptable quality of fit for CAD-CAM restorations. There is little agreement, indeed, about how measurements should be made to determine the quality of fit.[19] For crowns, the fit at the margins (especially subgingival margins) should be better than around an inlay's occlusal periphery since more tissue reaction is likely to occur in those areas.[20,21] Holmes found that excellent full coverage castings typically have a gap between the margin of the preparation and the margin of the restoration of about 40 to 60 microns.[19]

Marginal fit for the CEREC, Duret, Procera and DentiCAD systems are listed separately (values for Celay and DUX are not yet known). Clinical experience with the CEREC inlays—all with supragingival margins—suggests that the 100-μm fit may be adequate for this type of restoration.[22-24] The only clinical data reported to date on the performance of CAD-CAM crowns is from Procera-produced Titanium crowns.[15,16]

Unfortunately, those reports do not quantitate the misfit between the restoration and the preparation at the margins; they report only the tissue response. No clinical data are yet available from the Duret or DentiCAD systems. Laboratory data[25] suggest that the DentiCAD system can provide crowns with marginal fit at least as good as that achieved with excellent castings.

SUMMARY

The advent of computer graphics and CAD-CAM have revolutionized dentistry. It is now possible to provide the equivalent of a cast restoration with a single appointment. Several systems are under development, each providing different characteristics and advantages. Some permit the clinician to be actively involved in the design process; others provide complete automation, freeing the clinician for other tasks.

Some use technologies similar to those already used in dentistry; others draw technologies that are state-of-the-art in engineering or manufacturing but not dentistry. Some aspects, like optical "impressions," are fairly technique sensitive. Others like the DentiCAD digitizer are forgiving and easy to use. Some systems are easy to use; others require expert users. Some are initially expensive; others are relatively less so.

Exciting changes are occurring in producing restorations. CAD-

ClearCorrect Exhibit 1002, Page 1969 of 3373

TABLE 2

FIT OF CAD-CAM RESTORATIONS

SYSTEM	MARGINAL GAP AVERAGE	(MICRONS)	SD RANGE	REFERENCE
DENTICAD	23	28	0-49	22
	12	15	0-37	
CEREC	79	46	(at proximal boxes)	23
	71	16	(at cervical margin)	
	134	16	(at shoulder)	
	88	14	(at occlusal cusp)	
	172	28	(at occlusal fissure)	
PROCERA	Surface color:	90.3% E or A†		15,16
	Anatomic form:	93.4% E or A		
	Marginal index:	100% E or A		
DURET	Average 200			9

* For 100 microns nearest the margin.
† For A-excellent or acceptable, using CDA ratings.

CAM systems are available and more are being introduced continually. Clinicians must decide if and when it is cost effective to integrate this technology into their practice—and which system is the best for their practice. Another, more subtle question needs to be addressed: What happens if you choose not to use CAD-CAM but your competitors do? ■



Dr. Rekow is associate professor, Department of Orthodontics, Baltimore College of Dental Surgery, Dental School, University of Maryland at Baltimore, 666 W. Baltimore St., Baltimore, 21202-1586. Address requests for reprints to the author.

The author thanks NIDR for continuing support under grant R29 DE08455, as well as a huge number of people at BEGO, Foster Miller, the Dental Technology Venture, and the Universities of Maryland and Minnesota.

Information about the manufacturers of the products mentioned in this article may be available from the authors. Publication of the names of products or manufacturers does not imply endorsement by the American Dental Association.

1. Erdman AG, Riley DR. Computer-aided design and manufacturing (CAD-CAM). In: Rothbart HA, ed. Mechanical design and systems handbook. New York: McGraw-Hill;1985.
2. Moermann WH, Brandestini M. Die CEREC computer reconstruction: inlays, onlays, and veneers. Quintessence Verlags GMBH; 1985.
3. Moermann WH, Brandestini M. Method and apparatus for the fabrication of custom-shaped implants. US patent no. 4575805; 1986.
4. Moermann WH, Brandestini M. Chairside computer-aided direct ceramic inlays. Quintessence 1989;20:329-39.
5. Heymann HO. CAD-CAM: exploring the CEREC system. Dent Today.1990;9:6-54.
6. Duret F, Blouin JL, Duret B. CAD-CAM in dentistry. JADA 1988;117:715-20.
7. Duret F, Duret E. Apparatus for taking odontological or medical impressions. US patent no. 4611288, September 1986.
8. Cooks C. CAD-CAM comes to USC. USC Dentistry 1990;14-7.
9. Duret F. Presentation at International Conference on Computers in Dentistry. Houston, September 1991. In press.
10. Duret F, Preston JD. CAD-CAM imaging in dentistry. Current Opinion Dent 1991;1:150-4.
11. Unser DSC Titan system catalog: DSC Dental, 1990.
12. DUX system product literature; GIM-Alldent, Germany.
13. Celay system product literature. Microna Technologie, AG, Spreitenbach, Switzerland.
14. Procera system product literature. Nobelpharma, Nobel Industries, Sweden.
15. Andresson M, Bergman B, et al. Clinical results with titanium crowns fabricated with machine duplication and spark erosion. Acta Odontol Scand 1989;47:279-86.
16. Bergman B, Bessing C, et al. A 2-year follow-up study of titanium crowns. Acta Odontol Scand 1990;48:113-7.
17. DentiCAD product literature. Foster-Miller, Inc., Waltham, Mass.
18. Erdman AG, Rekow ED, Riley DR, Klamecki B, Zhu Y. Automated high-precision fabrication of objects of complex and unique geometry. US patent, filed June 1989.
19. Holmes JR. Marginal fit of castable ceramic (Dicor) crowns. Master's thesis, University of North Carolina, 1986.
20. Loe H, Silness J. Periodontal disease in pregnancy, I. Prevalence and severity. Acta Odontol Scand1963;21:533-51.
21. Silness J, Loe H. Periodontal disease in pregnancy, II. Correlation between oral hygiene and periodontal condition. Acta Odontol Scand 1964;22:122-35.
22. Isenberg BP, Essig ME, Leinfelder KF, Mueninghoff LA. Clinical evaluation of CEREC CAD-CAM restorations emphasizing marginal integrity. IADR Abstract 1345, vol. 70, 1991.
23. Moermann WH, et al. A computer-aided ceramic restorative system. IADR Abstracts 1991; (69); Abstract no. 1855.
24. Moermann WH, ed: Proceedings, International Symposium on Computer Restorations: state of the art of the CEREC method. Chicago: Quintessence; 1991.
25. Rekow ED, Thompson VP, Yang HS. Margin fit of CAD-CAM produced crowns. IADR Abstracts 1991; (70) Abstract no. 1346.

ClearCorrect Exhibit 1002, Page 1970 of 3373

MCS

Elizabeth Diane Rekow

1988

Ph.D. THESIS

Feasibility of an Automated System for Production of Dental Restorations

A Thesis
Submitted to the Faculty of the Graduate School
of the University of Minnesota

by

Elizabeth Dianne Rekow

in partial fulfillment of the requirements
for the degree of
Doctor of Philosopy

November 1988

ClearCorrect Exhibit 1002, Page 1972 of 3373

© Elizabeth Dianne Rekow 1988

Acknowledgements

Few accomplishments are possible without the support of a great array of people. In this endeavor, most significant has been the constant interest, help, and direction from my advisor, Arthur Erdman. Mike Speidel, Chairman of the Department of Orthodontics and also on my committee has been exceptionally helpful as well, carrying an extra share of the departmental load so that this research could continue. The thoughtful comments and time of the other committee members, Darrel Frohrib, Charles Knox, Jack Lewis, and Robert Sorenson, is also greatly appreciated.

My family, of course, has become used to my continued studies and I appreciate their understanding of the time that it has taken from them. Marlin, Chris and Andrew have all continued to be enthusiastic about this research. My parents and Gramma, Clara Miller, have also lent their support through the many years of continuing education.

Equally important has been the enthusiasm and challenges that have been offered by my colleagues in the dental school and in engineering. A vast array of dear friends have often listened to frustrations and offered suggestions along the way and to them I am eternally grateful.

Many thanks to all of you. For with you help I have learned a great deal, met a host of interesting and exciting people, and discovered some exciting things.

- Thank you all -

Abstract

A system capable of automating the production of dental restorations has been created in the investigtations reported here. The significance of an automated system crosses an array of boundaries, offering advantages to the dental patient, clinician, and researchers.

The automated system consists of a data acquisition system, data and image processing functions, and fabrication system. The data acquisition system and image processing is unique, permitting intraoral data to be obtained directly from the patient's mouth to be reconstructed in the computer. Custom designed computer-aided design and manufacturing (CAD/CAM) software then designs a restoration that is morphologically correct yet fits the unique configuration requirements for each patient. The CAD/CAM software generates tool paths, creating a file to drive a micromilling machine. The restoration is milled from a solid block of material.

The system integrates technologies and techniques from stereophotogrammetry, computer and machine vision, image processing, manufacturing, CAD/CAM, material science, and clinical dentistry. It has posed some new questions and has suggested some exciting new research avenues.

Table of Contents

1. Introduction. 1

2. Current Dental Restoration Production Techniques. . . 5

3. Motivation. 10

3.1 French Developments 11

3.2 Swiss Developments. 14

3.3 Other Work in Progress. 16

4. Design Requirements for an Automated System 18

4.1 System Design Requirements. 18

4.2 Restoration Quality 19

5. Alternatives Considered. 23

5.1 Data Acquisition. 23

5.1.1 Techniques. 24

5.1.1.1 Holography. 24

5.1.1.2 Computed Tomography 26

5.1.1.2.1 CT. 26

5.1.1.2.2 MRI 27

5.1.1.3 Ultrasound. 28

5.1.1.4 Contact Digitizers. 28

5.1.1.4 Optical Techniques. 30

5.1.1.5.1 Geometric Range Finding . 30

5.1.1.5.2 Structured Light. 31

5.1.1.5.3 Stereophotogrammetric . . 33

5.1.1.5.4 Moire 33

5.1.1.5.5 Time of Flight. 35
5.1.1.5.6 Interferometry. 36
5.1.1.5.7 Diffraction Range 38
5.1.2 Photographic vs. Real Time Data Acquisition 39
5.2 Data Analysis and Image Processing. 40
5.2.1 Correspondence Solutions. 42
5.2.2 Edge Finding Techniques 49
5.2.3 Surface Reconstruction. 61
5.2.3.1 Direct Linear Transformation. . . . 62
5.2.3.2 Collinearity Equations. 64
5.2.3.3 Grimson Algorithm 65
5.2.3.4 Moire Fringe Technique. 66
5.3 Fabrication Techniques. 67
5.3.1 Electrical Discharge Machining. 68
5.3.2 Laser Beam Machining. 69
5.3.3 Abrasive Jet Machining. 70
5.3.4 Water Jet Cutting 70
5.3.5 Ultrasonic Machining. 71
5.3.6 Stereolithography 71
6. System Decription 73
6.1 Data Acquisition. 75
6.1.1 Data Acquisition System 77
6.1.2 Digitizing. 78
6.2 Data Analysis and Image Processing. 82
6.2.1 Three-Dimensional Surface Reconstruction. . 84
6.2.1.1 Canny Edge Finding. 86
6.2.1.2 Auto-Correspondence and Disparity . 93

ClearCorrect Exhibit 1002, Page 1977 of 3373

6.2.1.3 Surface Reconstruction. 99
6.2.2 Data Base of Ideal Tooth Forms. 100
6.2.3 Artificial Intelligence for Occlusion . . .103
6.3 CAD/CAM 103
6.4 Fabrication 116
6.4.1 Milling 117
6.4.2 Fixturing 119
6.4.3 Materials 120
6.5 System Precision and Accuracy 122
6.5.1 Data Acquisition. 123
6.5.2 Digitizer 125
6.5.2.1 Sensor Linearity. 126
6.5.2.2 System Noise. 128
6.5.2.3 Sensor Stability. 132
6.5.2.4 Array Geometry. 132
6.5.2.5 Lens Distortion 133
6.5.2.6 Overall Digitizer Accuracy. 136
6.5.3 3-D Reconstruction. 136
6.5.4 CAD/CAM 137
6.5.5 Milling 137
6.5.6 Total Automated System. 138
7. Significance of Automated System. 139
8. Unique Contributions. 143
9. Future Investigations 147
9.1 Lens System 147
9.2 Milling Machine 148
9.3 Clinical Trials 148

6.2.1.3 Surface Reconstruction. 99
6.2.2 Data Base of Ideal Tooth Forms. 100
6.2.3 Artificial Intelligence for Occlusion . . .103
6.3 CAD/CAM 103
6.4 Fabrication 116
6.4.1 Milling 117
6.4.2 Fixturing 119
6.4.3 Materials 120
6.5 System Precision and Accuracy 122
6.5.1 Data Acquisition. 123
6.5.2 Digitizer 125
6.5.2.1 Sensor Linearity. 126
6.5.2.2 System Noise. 128
6.5.2.3 Sensor Stability. 132
6.5.2.4 Array Geometry. 132
6.5.2.5 Lens Distortion 133
6.5.2.6 Overall Digitizer Accuracy. 136
6.5.3 3-D Reconstruction. 136
6.5.4 CAD/CAM 137
6.5.5 Milling 137
6.5.6 Total Automated System. 138
7. Significance of Automated System. 139
8. Unique Contributions. 143
9. Future Investigations 147
9.1 Lens System 147
9.2 Milling Machine 148
9.3 Clinical Trials 148

9.4 Data Compression. 150
9.5 Materials 151
9.6 Other Restorations. 152
10.Summary 153
11.Bibliography. 155

Appendix 1. Clinical Criterion for Restoration Fit
Appendix 2. Errors and Quality Restorations

List of Figures

Figure 1. Principles for Triangulation Mensuration
Figure 2. Photographic Image for Test
Figure 3. Raw Digitized Test Image
Figure 4. Edges using Marr-Hildreth Algorithm
Figure 5. Edges using Haralich Algorithm
Figure 6. Edges using Canny Algorithm
Figure 7. Edges using Canny Algorithm with Strong Thresholds
Figure 8. Flow Chart of Processes in Automated System
Figure 9. Data Acquisition System
Figure 10. Tooth Viewed through Lens
Figure 11. Experimental Setup for Data Acquisition
Figure 12. Grating Projected on Tooth - Left View

Figure 13. Grating Projected on Tooth - Right View

Figure 14. Eikonix Digitizer

Figure 15. Close-up of Digitizer Console

Figure 16. Anti-Vibration Device on Digitizer

Figure 17. Edges - from Left View

Figure 18. Edges - from Right View

Figure 19. Camera Model for Disparity Calculation

Figure 20. Flow-Chart of 1:1 Correspondence

Figure 21. Surface Reconstruction

21a. Initial Reconstruction

21b. After 5 Iterations with Smoothing Algorithm

21c. After 10 Iterations

21d. After 15 Iterations

21e. After 20 Iterations

21f. After 25 Iterations

Figure 22. CAMAX Digitizer

Figure 23. Close-up View of CAMAX Digitizer Tip

Figure 24. Example of Tooth Configuration Recreated From Data Base of Tooth Forms

Figure 25. Screen 1 of Occlusal Data Base Program

Figure 26. Screen 2 of Occlusal Data Base Program

Figure 27. Screen 3 of Occlusal Data Base Program

Figure 28. Flow Chart of CAD/CAM Options

Figure 29. Restoration Design Considerations

Figure 30. Dyna Milling Machine

Figure 31. Servo Milling Machine

Figure 32. Milled Restoration

Figure 33. Digitizer Lens Distortion

32a. Line 5

32b. Line 10

32c. Line 40

32d. Line 60

32e. Line 60

32f. Line 70

32g. Line 75

32h. Line 80

32i. Line 100

32j. Line 120

32k. Line 140

32l. Line 147

List of Tables

Table 1. Current Steps for Restoration Production

Table 2. Comparison of Three-Dimensional Data Acquisition Techniques

Table 3. Comparison of Fabrication Techniques

Table 4. Current vs. Automated Restoration Production

Table 5. CAD/CAM Options

Table 6. Error Contribution by Subsystem

Table 7. Gray Level Tests (for Digitizer Sensor Linearity)

Table 8. Digitizer Dark Field Tests (for Systematic Noise)

Table 9. Digitizer Lens Distortion

Chapter 1. Introduction

Dental restorations have been produced since the fifth century B.C. (169). In early times, they were created by metalsmiths. Not until the 1700's did dentists become actively involved in their production. Through this entire time, fabrication techniques have remained essentially unchanged.

With the advent of the new design and fabrication techniques of computer-aided design and manufacturing (CAD/CAM), it seemed reasonable to investigate the possibility of applying those techniques to modernize the production of dental restorations. The particular focus of this investigation is on the feasiblity of automating the production of a single full-coverage posterior cast metal crown.

Applying state-of-the-art CAD/CAM techniques to this dental application has some particularly interesting challenges. First is the problem of access. Posterior teeth are difficult to see; cheeks, tongue, and saliva all impeed a clear view. Additionally, the amount of opening possible is limited. Typically, the maximum clearance between upper and lower posterior teeth is approximately 25 mm. It is also important to remember

that the patient is not delighted about being subjected to the manipulations of the dentist and wiggles with regularity but unpredictably (125).

A tooth needs a restoration for a variety of reasons but the two most prevalent are decay and fracture. A dentist cuts the crown of the tooth, removing decay and creating a configuration which can adequately support a restoration yet provides sufficient bulk of material to prevent distorations and deflections under load during chewing functicns. The resulting configuration will be unique to each patient; no standard, predictable shape can be determined. The size and shape of teeth varies dramatically between patients (and even in contralateral positions in the same mouth). The prepared tooth shape will also depend upon the history of decay, fracture, and previously completed restorative work that has been done on that tooth.

The periphery of the interface between the restoration and the remaining prepared tooth structure is called the margin. The fit of the restoration at the margin is more critical than in any other area. The location of the margin is generally near the gum line, though it can lie beneath the gum line. This position, of course, further complicates the problem of access since not only are tissues potentially in the way, there is often associated bleeding (though minimal) resulting from trauma to the

ClearCorrect Exhibit 1002, Page 1985 of 3373

tissue from the burr during the preparation of the tooth for the restoration.

Another interesting challenge for applying CAD/CAM techniques is the tolerance required for restoration fit. To be clinically acceptable, the gap at the margin between the tooth and the restoration must not exceed 20 microns (44, 101, 103, and 192).

Yet another interesting challenge to automating production of dental restoration relates to the complexity of the configuration. The chewing surface (occlusal surface), especially on posterior teeth, is extremely complex and defies definition by straightforward mathematics. The morphology of the tooth must be restored for function yet the size and specifics of the absolute position of cusp tips and fossae must be unique for each patient. Additionally, the relative orientation of the internal and external surfaces of the restoration must be preserved.

The objective of this investigation is to establish the feasibility of automating the production of dental restorations; particularly a posterior full-coverage metal crown on a mandibular first molar. The techniques currently used to produce restorations are described in Chapter 2. The motivation for automating their production is discussed in Chapter 3. Requirements and design specifications for an automated system are specified in Chapter 4.

ClearCorrect Exhibit 1002, Page 1986 of 3373

Basically, any system to automate the production of dental restorations consists of three subsystems: data acquisition, data analysis and image processing, and fabrication. Alternative technologies considered for each of these subsystems, as well as those ultimately selected, are described in Chapters 5 and 6 respectively. Chapter 6 also discusses the precision and accuracy of the system. The significance of an automated system and unique contributions from this investigation are addressed in Chapters 7 and 8. The final chapter briefly identifies future directions for system development.

ClearCorrect Exhibit 1002, Page 1987 of 3373

Chapter 2. Current Restoration Production Techniques

The current state of the art in the production of dental restorations revolves around the centuries old lost wax casting technique. Table 1 itemizes the steps involved, lists the time required for each, and the level of training required for each.

After a dentist has prepared a tooth for a restoration, removing all the decay and ensuring the integrity of the remaining structure, an impression of the remaining structure and the other teeth in that same dental arch is taken. Usually an impression is also made of the teeth in the opposing dental arch.

The impression is made using an elastomeric material (51). The material is mixed, placed in a mouth-shaped tray to support the material (which has a consistency close to that of mashed potatoes or silly putty), placed in the patient's mouth over the teeth and surrounding tissues and held in place until it "sets". Setting times vary with materials but generally range from 2 to 12 minutes/impression (51). When the material is set, it has a consistency similar to that of modeling clay but retains an elastomeric property so that it can slide past the crest of convexity of normal teeth without being permanently

ClearCorrect Exhibit 1002, Page 1988 of 3373

Table 1. Current Steps for Restoration Production (*)

Step	Time Required (in minutes)	Personnel Required (+)
1. Impression both dental arches	10	D and A
2. Make temporary restoration	10	D and A
3. Pour impression - first pour	5	D or A or L
4. First pour setting time	45	
5. Place pins	5	L
6. Second pour	5	L
7. Second pour setting time	45	
8. Trim die and mark margin	10	L
9. Mount on articulator, plaster set	30 - 45	L
10. Place separating medium	1	L
11. Create wax pattern	20	L
12. Sprue pattern	5	L
13. Invest pattern	10	L
14. Investment setting time	45	
15. Burn out time	60	
16. Cast	10	L
17. Recover casting	10	L
18. Remove sprue, finish, polish	45	L
19. Remove temporary and try in mouth	5	D
20. Modify contacts and occlusion	10 - 30	D
21. Seat permanently	10	D
22. Remove excess cement	5	
23. Final check	5	D

* Assumes full coverage posterior gold restoration being fabricated by experienced technician

\+ D = dentist
A = dental assistant
L = laboratory technician

(refence 78).

ClearCorrect Exhibit 1002, Page 1989 of 3373

distorted. When removed from the mouth, it creates a three-dimensional negative of the teeth and their relative positions to each other.

After the impressions have been made, dental stone (plaster) is poured into the impressions and allowed to harden. The impression material is removed and discarded. The subsequent restoration production techniques may be accomplished in the dental clinic or may be done in a dental laboratory.

Pins are set into the bottom of the arch containing the tooth to be restored in the area of the prepared tooth. A base of plaster is poured over the pins. When this has hardened, the area of stone supporting the prepared tooth is sectioned out. The pins and the holes in the second pour of stone serve as guides, permitting the cast of the prepared tooth (called a die) to be removed and reinserted into the plaster cast.

Excess plaster around the base of the die is removed and the position of the margin of the restoration marked. A separating medium is applied to the die. A wax pattern is then prepared directly on the die.

If jaw interrelationships have been recorded, the models are mounted on an articulator. The articulator is used as a device to represent the relative positions of the dental arches to each other and to represent the motion of the teeth to each other. Rarely do they accomplish this (167, 169).

ClearCorrect Exhibit 1002, Page 1990 of 3373

After the wax pattern is completed, it is sprued and invested for casting. When the investment material has set, the investment and pattern are placed in an oven where the wax is burned away. The remaining cavity in the investment is then filled with molten metal. (Some differences, of course, are necessary for handling materials like cast ceramic.)

The casting is quinched and recovered. The sprue is removed and the casting is finished. Finishing operations involve removing all remaining investment material and polishing the surface. Surface polish is done by hand using an array of burrs and stones of increasingly finer quality. Final finishing is done with rouge on a soft bristle brush or rag wheel. The restoration is now ready for the patient.

The patient returns to the dental office. The temporary restoration is removed and debris from the cementing agent removed. The cast restoration is placed on the tooth and the occlusal, functional, and proximal contacts are checked. The quality of the margins is also evaluated. Clinical criterion for acceptance are given in detail in Appendix 1 but are summarized here:

1. Marginal fit: A dental explorer is passed from restoration to tooth and from tooth to restoration with the tip of the explorer held perpendicular to the surfaces. If the interface between the restoration and tooth can be detected, the restoration should not be permanently seated

ClearCorrect Exhibit 1002, Page 1991 of 3373

but instead should be remade. (Depending on the location of the margin relative to the gum tissue, a gap of 20 to 100 microns can be detected, see reference 44.)

2. Occlusal fit: A mark should be made when the teeth tap together with a piece of occlusal marking paper placed between the teeth. The patient should not detect excessive pressure on that tooth or report any discomfort. All other teeth which contact without the restoration in place must also contact with the restoration in place (55, 135).

3. Interproximal fit: A piece of dental floss should "snap" as it passes between the restoration and the adjacent contact tooth. (None of the dental floss supply companies can provide a measure of the thickness of floss as it distorts and "snaps" through the contact.) (111)

4. Functional fit: As the teeth move through their normal excursions, the restoration should not contact prematurely (88, 165).

The dentist makes whatever modifications are necessary. If the restoration can be modified to pass these acceptance criterion, it is cemented in place. If not, a new impression is made and the process begins again.

ClearCorrect Exhibit 1002, Page 1992 of 3373

Chapter 3. Motivation

The inital motivation for investigating the feasibility of automating the production of dental restorations was simply to modernize an ancient technique. This was further motivated by personal experience (and sometimes frustration) with casting dental restorations as part of the dental training. At times, casting failures resulted in late night marathons to have a restoration ready for a next day patient's appointment. Casting failures could result from inadequacies in the material, inclusions in casting, shrinkage leaving insufficient margins or porosities in the finish (99). Additionally, there was a personal frustration with the labor intensive, slow process of waxing and casting (though finishing the gold is a nice reward).

The feasibility of a CAD/CAM system to automate production of dental restorations has been of interest for years. Some of the earliest published work on acquiring data directly from the mouth was done by Altschuler et.al. (3-7) in the mid 1970's. Curry and Baumrind perplexed about the problem of three-dimensional data acquisition directly from the mouth and created a camera which provided

ClearCorrect Exhibit 1002, Page 1993 of 3373

stereo pairs of photographs from which a three-dimensional computer-based arch could be reconstructed (8).

Developments in automated prosthesis design which occurred during the investigations further strengthened the resolve to succeed (56, 117, and 187, for instance). Advances by investigators in France, Switzerland, and elsewhere have focused on dental applications. At first blush, discovering those activities was depressing but it served as a further impetus to create a system capable of producing excellent dental restorations automatically.

3.1 FRENCH DEVELOPMENTS

A system under development in France is probably the most nearly like the Minnesota system with respect to its overall capabilities (67). It uses a laser scanner to produce images of the patient's mouth (60, 63). This data is processed by shape-recognition software, visualized on a video display, and transferred to a CAD/CAM software package which creates a three-dimensional model of the environment where the restoration ultimately will be placed. The interactive capability of the CAD/CAM software allows the dentist to access a library describing theoretical teeth, adapt them to the patient's oral environment, and design a three-dimensional model of the restoration on the computer screen. The CAD/CAM software

ClearCorrect Exhibit 1002, Page 1994 of 3373

computes the tool paths needed and a micromilling machine cuts the tooth (97).

Before the image is acquired, the tooth must be coated to ensure that the color is uniform. A coating of titanium oxide suspension in a film forming polymer is painted on the tooth. (It is neutralized and removed with ammonium). This coating increases the ratio of light reflected compared with the incident light on the preparation, tending to convert the tooth to a lambertian body (140).

A hand-held optical probe measures the three-dimensisonal coordinates of the tooth prepared for a restoration and of the adjacent teeth (182). The scanner probe uses a modified Moire fringe technique (68) and has a theoretical resolution of 20 microns (61). However, to ensure that the entire preparation is visible, multiple images must be made and the correlation between any two views has a resolution of only 40 to 60 microns (66).

The probe consists principally of a laser-diode source and a charge-coupled-device (CCD) photoreceptor with 256 by 256 pixel resolution (68). The signal created by the laser light reflected by the teeth is picked up by the CCD arrays, converted to a digital signal, and relayed to the computer (62). It is then processed and displayed on a video monitor (a process which requires between 2 and 4 minutes). A foot pedal permits the image to be fixed for further examination so that it can be accepted or rejected. The probe must pass over the teeth four times and four

ClearCorrect Exhibit 1002, Page 1995 of 3373

acceptable images must be obtained. In expert hands, data of the prepared tooth, the adjacent teeth, and the opposing dentition can be acquired in less than 3 minutes (61).

The CAD/CAM system used is built around Euclid, from Matra Datavision (66), running on a Digital Equipment Corporation (DEC) MicroVAX II (62). Euclid is used to create a solid model of the area where the restoration is fitted (182). Precision in the CAD/CAM system is said to be 2.5 microns (66).

A library of tooth forms has been created. Using routines available in Euclid, the system user interactively designs the restoration on the display (182). The scan recording the required data from the patient's mouth can be made before the preparation has been cut, permitting the exiting tooth morphology to be exactly reproduced or, in the case of severely damaged teeth, the morphology of the replacement tooth can be generated from the library of tooth forms. Complete modeling on the screen requires between 2 and 10 minutes (61, 166). The user is required to identify the location of the margin interactively; it is not found automatically with the software (68).

When the restoration design is completed, the CAM commands in Euclid permit the tool paths for numerical controlled machining to be generated. A three and one-half axis micro-milling machine cuts the restoration (68). The accuracy of the machine itself is 20 microns.

ClearCorrect Exhibit 1002, Page 1996 of 3373

Accuracy of the whole process, however, is, at best, the sum of the component errors, which total at least 80 microns. However, a premolar was fabricated using only 400 points distributed in 26 cross-sections. This yields an accuracy of only 200 microns (62). More recent restorations are reported to be precise to approximately 100 microns (68).

3.2 SWISS DEVELOPMENTS

The Swiss system was originally trademarked as the CEREC-System (145) but is now licensed to Siemans Corporation (157). Like the French system, it also uses an optical topographic scanning procedure and electronically controlled milling machine (143). With the system, the tooth must be coated to minimize the effects of discoloration and differential reflection. A three-dimensional mouth camera has been designed (144) to feed data to an interactive computer-aided design unit. The system is capable of machining porcelain inlays only (145).

With this system, a non-contacting scan-head is positioned over a prepared tooth. The scanner incorporates a light-emitting diode and lens system to illuminate the cavity of the tooth. Before reaching the tooth, the light rays are deflected by reflections off a mirror, permitting

ClearCorrect Exhibit 1002, Page 1997 of 3373

easy access in a patient's mouth. The rays pass through a set of ruled lines and a lens system. Light passing through the ruled lines casts a pattern of light and dark stripes on the prepared cavity. The light is reflected back to the scan-head where it is sensed (at a different angle) by a CCD sensor with resolutions of 256 x 256 pixels. Scanning a typical prepared tooth requires only 0.2 seconds (145).

The computer used is a desk-top computer (e.g., an Apple II with two memory boards supplied by Matrox Ltd., Quebec, Canada, Part RGB 206/4). The computer transforms the voltages representing intensity to depth values for each x,y position of the cavity of the prepared tooth (144). This system also incorporates a video monitor which displays the data being processed by the system (145), permitting visual verification of quality of the data being acquired (143). With this system, the user is required to interactively indicate the positions of the margins of the preparation.

Inlay fabrication is accomplished with a three-axis numerically controlled milling machine (145). Three translatory platforms are mounted on a supporting frame to provide x, y and z position control (Micro-Control type MR-80.20, part No. 338404, MC Corp., Vitry-sur-Seine, France). Each platform is moved by a stepper motor (Sigma Instruments mod. 20-1720 BD 200), driven by a lead screw which is controlled by the microcomputer. A high

ClearCorrect Exhibit 1002, Page 1998 of 3373

speed turbine (Midwest American, Melrose Park, Ill., part No. 364006) powering a diamond burr is rigidly connected to the y-axis platform. The turbine is air driven and coolant is run over the part being milled during the drilling operations (144).

Inlays are machined from prefabricated rod-shaped blanks of dental porcelain. These blanks measure approximately 9 x 9 x 13 mm and are fabricated using conventional dental porcelain techniques. The porcelain blanks are bonded to a stub, allowing the blanks to be fixed inside the milling machine. Milling of a typical porcelain inlay requires from 5 to 7 minutes (145). But only the tooth interface side of the restoration is automatically machined.

The inlays are bonded to the tooth with a simultaneously light- and chemically-cured material (143). The occlusal surfaces are then configured by the dentist. While the milling accuracy of the restoration has not been reported in the literature but has been suggested to be between 100 and 200 microns (25, 33, 139).

3.3 OTHER WORK IN PROGRESS

Other preliminary work relating to automating production of dental restorations is underway. Investigations have begun at the University of Alabama, Foster-Miller Corporation in collaboration with Tufts

ClearCorrect Exhibit 1002, Page 1999 of 3373

University, and in Japan.

Work at the University of Alabama has been underway for approximately two years. Reggie Caudell, ME Robotics, and Earl Hydrick, D.D.S., are the two primary investigators (42). To date, much of their work has evolved around quantifying potential sources of error in the CAD/CAM processes. They are beginning investigations into the application of tactile imaging of the surface using a conductive, silicone-based gel (43). They are also investigating optical sensors with accuracy in the 25-micron range.

Foster-Miller Corporation and Tufts University have been working on developing a tactile pencil-type sensor under SBIR grant (127). They have completed phase one; phase two was undergoing evaluation in September 1987. To date, they have profiled a mandibular lower incisor and reproduced it using SDRC software. They have also created a generic tooth using an ARIES solids modeler.

The Dental School at Kanagawa University and the Kanagawa Dental Laboratory have created a CAD/CAM system to create parallel paths on already cast crowns (for partial denture frameworks) (102). Their system is built around the Roland CAMM-3 hardware. It can be used as a point-to-point contact digitizer. There have also been some preliminary developments underway for approximately two years at the Osaka University Dental School. No details about that work are yet available.

ClearCorrect Exhibit 1002, Page 2000 of 3373

Chapter 4. Design Requirements for An Automated System

Design requirements can be specified for both the system itself and for the product produced by the system. Both can significantly impact the technologies selected for system feasibility. Requirements that apply to an automated system relate largely to user interface. Product related requirements are independent of whether it is produced by a casting or an automated system.

4.1 SYSTEM DESIGN REQUIREMENTS

The underlying philosophy in considering a system to automate production of dental restorations is that the system must be reasonable for use in a typical clinical dental practice. This translates into more specific objectives including:

1. Data must be obtained from a patient's mouth. This data includes the shape of a tooth prepared for a restoration, the positions of the adjacent teeth, and the position of the opposing teeth in both static closed position and dynamic positions associated with chewing and speaking.

ClearCorrect Exhibit 1002, Page 2001 of 3373

2. Data must be obtained in no more time than is currently required with impression materials and jaw registration techniques (less than 10 minutes).

3. The system must be simple to use, requiring no special training on the part of the dental staff. This requires that the system be intelligent, fully automated, and essentially fool-proof.

4. The quality of the restoration produced must be at least equivalent to that possible with current clinically practiced state of the art.

4.2 RESTORATION QUALITY

Unquestionably one of the most critical design requirements for the system is that it must produce a product that at least matches the quality of the product produced by the currently practiced impression-lost wax casting technique. This quality relates to fit at the margins, interproximal fit, occlusal fit, and surface finish.

Poor fit at the margins includes cases that are either over-extended or too short (44,111). When the margin is over-extended, debris collects more easily around the periphery of the restoration. This results in increased probability of inflammatory response to the

ClearCorrect Exhibit 1002, Page 2002 of 3373

surrounding soft tissue which can cause severe tissue damage and associated bone loss. In both cases (over-extended and short margins), the margin is not well closed and leakage of saliva (with its full array of microorganisms) occurs. Many dental cements are water-soluble so over time this leakage results in a pooling of salivary products leading to decay beneath the restoration.

If the fit between the restoration and the proximal teeth is not sufficient two things can occur (111). First, the teeth may drift to a new position which provides contact; potentially placing them in a position where the loads of occluslon are not properly supported by the ligaments supporting the teeth and resulting in loss of boney support for the tooth and, in some cases, loss of the tooth itself. Secondly, without proper contact, food is more likely to impact between the teeth. In addition to simply being bothersome, this can lead to increased bacterial growth and concomitant tissue destruction.

The occlusal fit of a restoration is also important (165). If a restoration is excessively high or interferes with opposing teeth during functional movements, trauma to the interferring teeth can result. This trauma can be manifest as discomfort which may be tolerable but it can also lead to some irreversible etiologies. It can result in loss of boney support of the tooth, compromising the strength of the tooth and potentially resulting in loss of the tooth. It can result in endodontitis where the nerve

ClearCorrect Exhibit 1002, Page 2003 of 3373

within the tooth chamber becomes inflammed, causing pressure against the nerve (since the tooth will not expand to compensate for the increased size), requiring the nerve and blood vessels to be removed from the tooth (a root canal treatment) for relief of the pain. Poor occlusal fit has also been implicated as one of the causative agents in temporomandibular joint disease (55).

The surface finish of a restoration is important for both cleanliness and function (47). If the surface finish is excessively rough, bacterial accumulations will increase and increased plaque may form on the restoration. This results in increased probability of tissue inflammation and breakdown in both the tooth itself and the surrounding soft tissues. Additionally, if the surface finish is excessively rough, there is the potential for excessive wear of the opposing teeth.

To quantify these characteristics which are important in the quality of a restoration and its clinical performance, then, the following parameters for restoration quality are used:

1. Fit at the margins: The margins must fit to within 50 microns. The design objective for the development work has been 20 microns; 50 microns would probably be acceptable (44, 70).

2. Interproximal fit: The restoration must contact the adjacent teeth (111).

ClearCorrect Exhibit 1002, Page 2004 of 3373

3. Occlusal fit: The restoration must meet the current clinical tests for occlusal fit: at least one contact mark must appear from the opposing teeth when the teeth are in maximal intercuspation and no interferences must cccur when the teeth move through their excursive functional movements (165).

4. Surface finish: The surface must have an rms surface finish of 8 microns (47).

ClearCorrect Exhibit 1002, Page 2005 of 3373

Chapter 5. Alternatives Considered

Throughout the investigations into the feasibility of automating the production of dental restorations attention has been focused on alternatives to accomplish the tasks of acquiring the data from the mouth, data analysis and image processing, and fabricating the restoration. Each of these areas will be addressed and the feasibility of the alternatives identified. The advantages and disadvantages of each will be addressed and the justification for their not being selected for incorporation into the system design will be identified.

5.1 DATA ACQUISITION

Data acquisition involves both imaging an object and converting that image into a form that is usable for subsequent operations (in this case, digitizing it). An array of different types of data acquisition are described. Both real time and photographic based data acquisition are possibilities; the tradeoffs of the choices is discussed.

ClearCorrect Exhibit 1002, Page 2006 of 3373

5.1.1 Data Acquisition Techniques

Advances in imaging technology have provided an array of possibilities for acquiring three-dimensional data (183). These include: holography, computed tomography (both CT scan and magnetic resonance imaging), ultrasound, contact digitizers (magnetic, servo arm, and force), and optical techniques. Table 2 summarizes these comparisons.

5.1.1.1 HOLOGRAPHY. Holography promises excellent resolution and quick acquisition times (36). Data recording motion can be obtained by pulsing the laser and recording the data with each pulse. Two drawbacks exist, however. First, data acquisition may be reasonable but reduction of the data to a digital form is difficult (153). Secondly, minor movements (as low as 1/4 wavelength) can create distortions (114). For very high precision recordings, isolation from vibration (even those internal to a building) are critical (190). In the clinical setting, such complex elimination of movement when a live patient is involved is unrealistic.

ClearCorrect Exhibit 1002, Page 2007 of 3373

Table 2. Comparison of

Three-Dimensional Data Acquisition Techniques

Technique	Data Resolution	Acquisition Time	Equipment Cost	Operational Problems
Holography	5-50 microns	nonoseconds	Low - Mid	Vibration
CT	375 microns with 1.5 mm slice	seconds	High	Radiation
MRI	600 microns with 1 mm slice	minutes	High	Artifacts
Ultrasound	600 microns	seconds	Mid	Heat
Mechanical Contact Digitizers	1 micron	minutes	Mid - High	Slow
Geometric	microns	seconds	Low	Occluded Views
Structured light	microns	seconds	Low	Ambiguity
Stereophoto-grammetric	2-50 microns	seconds	Low	Comutation Expense
Moire	2-50 microns	seconds	Low	Ambiguity
Time of Flight	2 cm	minutes	Low	Poor SNR
Interferometry	microns	seconds	Low	Ambiguity
Diffraction	mm	seconds	Low	Ambiguity
Shape from Shading	microns	seconds	Low	Light Changes

For further details, see Reference 168.

ClearCorrect Exhibit 1002, Page 2008 of 3373

5.1.1.2 COMPUTED TOMOGRAPHY. Computed tomography (CT) scans and magnetic resonance imaging (MRI) are advancing exceedingly rapidly. Unfortunately, neither offers sufficient resolution for an image representing a prepared tooth and neither are fast enough to permit quantification of the jaw in motion (28, 74). Both of these techniques are expensive and require large, isolated environments for operation.

5.1.1.2.1 CT Scans. Using CT image data, three-dimensional shape information is determined to plan corrective surgery and directly manufacture prostheses (171). Slice thickness are approximately 1.5 mm minimum (171), above the limit permitted by the tolerances of dental restoration fit. A CT scan uses a radiographically obtained image. All of the data required for a restoration is visible, without radiation, however, making radiographic exposure unnecessary and inappropriate.

CT has found one dental application, however, (56). For subperiosteal implants for the mandible, a CT scan is made of the mandible, a model of the mandible is reconstructed and machined from wax, and a custom implant is fabricated to that model. The patient then undergoes surgery for the implantation. Before this technique was devised, preliminary surgery was required to expose and

ClearCorrect Exhibit 1002, Page 2009 of 3373

impression the mandible; a model was then made from the impression, the custom implant fabricated to the model. Then the patient was subjected to a second surgical procedure to implant the prothesis.

5.1.1.2.2 MRI. To obtain an MRI image, a patient is placed in a large magnetic field. That field reorients the nuclei of hydrogen, carbon, nitrogen and phosphorus, placing them all in alignment with the magnetic field. A radio field is applied, altering the alignment. When the radio field is removed, the nuclei shift again to realign with the magneic field. Different tissues realign at different rates, emitting some of the absorbed energy at radio frequency. That energy is used to create computer-generated images (199).

MRI spatial and contrast resolution is better than is possible with CT (128). Current resolution is 0.08 to 0.1 mm with 1 mm between slices. Recent experiments with in-vivo MRI spectroscopy suggest that the ultimate resolution of an image is limited by the signal to noise ratio but approaches 10 microns in all three dimensions (118). Advantages of this technology include absence of any harmful biological effects within current diagnostic ranges, ability to direct image in any plane, and the simultaneous acquisition of multiple tomographic slices (128). With this technology, soft tissues are more easily

ClearCorrect Exhibit 1002, Page 2010 of 3373

imaged than hard tissues; making its value for imaging teeth questionable.

5.1.1.3 ULTRASOUND. Three-dimensional reconstruction in spatial location with ultrasound uses a spark that is discharged in air across a small gap between two electrodes. The spark generates a shock wave the speed of sound. The wave is detected with a microphone. The distance to the spark gap is computed from the transit time of the shock wave and the local speed of sound. Three spark-gaps fixed to a probe of known relationship sequentially fired provide the 3-D position (148).

The resolution with this techniques is 0.3 to 0.5 mm. Real-time 2-D doppler echocardiography has been used to provide information of blood flow from small sample volumes. The ultrasound beam can record on-line velocity profiles along the beam line at discrete time intervals during one cardiac cycle so non-invasive intracardiac blood flow images in real time can be obtained (152). Resolution in ultrasound is still low though it does potentially provide the option of acquring data concerning the jaw as it moves (148). Unfortunately, scattering at interfaces of different tissue types can distort the image. In the mouth, of course, there are a great many different tissue interfaces.

ClearCorrect Exhibit 1002, Page 2011 of 3373

5.1.1.4 CONTACT DIGITIZERS. Of the currently available contact digitizers, including coordinate measurement machines, instrumented linkages, and tactile sensors, only the mechanical type offers sufficient resolution for the precise imaging of prepared teeth (15, 141, 154). Unfortunately, none are able to provide data as the jaw moves. All are very slow; data acquisition would require nearly an hour/tooth for sufficiently high resolution.

Microcontrol Systems (Vernon, CT) has introduced a mechanical contact 3-D digitizer called the Space Tablet and Perceptor. The stylus at the end of the Perceptor's arm is tracked over a solid object. Precision potentiometers housed in the extension arm computes the x, y, z coordinates of each point based on the angle of rotation and the known arm length. Seven points per second can be recorded. Resolution ranges are between 0.1778 and 0.254 mm (0.007 and 0.010 inch).

Polhemus Navigational Sciences Division of McDonnel Douglas (Colchester, VT) has a 3-Space Digitizer. It relies on a set of magnetic transducers for point position measurements. A probe moves freely in space over an object placed on a table. Only nonmetallic objects can be digitized.

ClearCorrect Exhibit 1002, Page 2012 of 3373

5.1.1.5 OPTICAL TECHNIQUES. Optical techniques are among the oldest used to acquire data. There are four basic technologies used: geometric, time of flight, interferometric, and diffraction techniques.

5.1.1.5.1 Geometric Range Measurement. The most common optical techniques utilize geometric range measurement which is a generalization of the triangulation concept. This technique was probably first used by the Egyptians in construction of the pyramids (184).

With this measurement technique, a pair of similar triangles are established – one between an object and the measurement fulcrum and one between the image and measurement fulcrum (see Figure 1). With proper linearization and processing, resolutions of one part/100,000 are possible (122). Measurement range is limited by the detection system. Accuracy is nonuniform and is best for small distances, posing some potential depth of field problems.

Computationally this technique is one of the simplest and most straightforward to implement. It can be scaled over a large range. It does, however, suffer from a generic problem of missing data from occluded views. Furthermore, the data must be acquired one line or point at a time so there are some limitations in potential speed.

ClearCorrect Exhibit 1002, Page 2013 of 3373

Structured (active) light can provide the illumination required with this technique. Alternatively, stereophotogrammetry and Moire also utilize the geometric range measruement principles for measuring depth (from which a three-dimensional surface map can be completed).

5.1.1.5.2 Structured Light. Structured light illumination is one of the simplest applications of geometric range finding techniques. A single point of light is projected on a surface and subsequently imaged on a detector. Displacement of the image point relative to a known reference is proportional to the distance to the object. The projected point scans over the surface (or the surface moves beneath the light) to image the entire surface. Structured light is probably the most commonly used technique for 3-D vision systems because it currently has the greatest potential for fast, accurate, and inexpensive high resolution measurements (110). This is the technology utilized by the Cyber-Optics Systems (54, 110). A Vidicon laser-based system, developed by Cyberware Labs (Pacific Grove, CA), is another. It digitizes objects placed on a stationary platform. An arm that rotates around the platform requires 15 seconds to record 250 points in three dimensions. The imaging device has been shown to be able to image complex surfaces, including the human head.

ClearCorrect Exhibit 1002, Page 2014 of 3373

The most obvious extension of this single-source structured light technqiue is the projection of a single line with line by line detectors. The image of each point on the line is displaced in a direction orthogonal to the line by an amount related to the range (184).

The next extension is to an array of parallel lines (195). This increases the potential data rate but introduces range ambiguity factors since one cannot in general uniquely identify particular projected lines in an image. By imposing constraints, the problems can be avoided or resolved (184). One technique proposed by Altschuler et al. (7), is a form of grid coding which minimizes the number of measurements required and potential ambiguities. The object is illuminated by a grid produced by a series of shutters. A series of illumination patterns uniquely codes each angular position. The detector also ascribes a specific angular coordinate to each object point. Intersection of back projection of these two coordinates gives the 3-D location of the object point.

In triangulation systems, the key parameter is displacement of an image point from a reference point in the detector plane. With structured light illumination, that reference point is a virtual point which is determined by system geometry.

ClearCorrect Exhibit 1002, Page 2015 of 3373

5.1.1.5.3 Stereophotogrammetry. Stereophotogrammetry is a passive technique using ambient lighting. It is more flexible than structured light but creates a greater post-detection processing burden (184). With this technique, stereo-pairs of images are created. The stereo method uses parallax between two images to measure range. Views of the same object by the two cameras will have an apparent translation and objects closer than the parallax intersection will appear to move relative to more distant objects (83, 122, 197).

The main problem associated with this technique is locating matching points in each of the two views. One way to simplify this is to preceed matching with edge detection to reduce the number of points required. Another is a heirarchical approach to first match images at coarse resolutions and then proceed through progressively finer scales.

Stereophotogrammetry was selected for the automated system for production of dental restorations. A detailed description of the technique implemented is given in Chapter 6.

5.1.1.5.4 Moire. An alternative approach to topographic measurement is the Moire technique. In Moire (57, 136), the object is illuminated with grid and a second grid is placed

ClearCorrect Exhibit 1002, Page 2016 of 3373

in the measurement plane. The second grid, in effect, provides a physical set of reference point in the detector plane. Moire generally provides differential range rather than absolute range.

Moire is a full-field, non-contact measurement technique (92, 93). A Moire pattern is made by forming a subject grating (by projecting, shadowing, or contacting) on the object to be measured and comparing this grating with a reference grating (57, 136). This comparison is done by overlapping the two gratings. If the two interfere, a dark interference fringe is formed. What is actually monitored however, is not the phase shift between the two gratings but rather a beat frequency (184). Surface configuration is determined by the number and orientation of the fringes. Each fringe represents a uniform height or distance to the object of interest.

Since Moire is a full-field technique, the contour of the entire visible surface of an object can be mapped at one time. Unfortunately, classical systems have an ambiguity as to the sign of the slopes of the surface contour (89). Without significant apriori knowledge concerning tooth anatomy, especially around the margins, this could pose a substantial problem; a small dip that should be a rise could easily exceed the tolerance limits at the margin.

With the Moire technique, system geometry must be very specific or true contours will not be reproduced.

ClearCorrect Exhibit 1002, Page 2017 of 3373

Recently, to enhance automation of the technique, measurements have been based on phase modulation (89). Using fast Fourier transform analysis to digitially modulate deformed grating images has further enhanced the technique. However, measurement of steep object slopes (like those at the axial walls of a prepared tooth) is one of the limitations with this method.

5.1.1.5.5 Time of Flight. Time of flight range measurements techniques are based on the principal that the signal carrier (either acoustic or optical) travels with known velocity (184). A signal is sent by the measurement system, it is reflected off an object surface, and returns to the measurement system. The elapsed time from signal emission to reception provides distance measurement. To obtain three-dimensional information, the entire scene must be scanned.

One of the difficulties with this technique is that it is not easily scaled to different measurement ranges. It does, however, eliminate the problem of missing points that is implicit in geometric techniques. Uniform sensitivity is available throughout the entire measurement range. It is slow and usually suffers from poor signal to noise ratio. There are some depth of field restrictions.

ClearCorrect Exhibit 1002, Page 2018 of 3373

Within this type of technology, there are two types of signal pulsing techniques. The first is a single pulse technique. Generally, a solid-state laser emits short pulses. Range accuracy is on the order of 1 to 2 cm for a 2.5 to 4 meter field (95 and 119). Alternatively, chirp signals are emitted with a radar or sonar system. The chirp that is transmitted has a frequency which varies linearly over the duration of the transmission. This is the technique used in the Polaroid camera ultrasonic ranging system (184).

5.1.1.5.6 Interfereometry. Range finding using interferometric techniques relies on the fact that waves have a certain fixed wavelength which can, in effect, be used as a measuring device. A signal beam is split into two components (184). One component is sent to the object and reflected back onto the surface. There it is compared with the second component which has tranversed known reference path (serving the function of a local oscillator). The relative shift between the two beams is measured in terms of wavelength. Depth, z, is given by:

$$z = (\lambda/2)\cos[(I-1)/a]$$

where λ is wavelength of the illumination

I is the intensity ready by the detector

a is a constant

ClearCorrect Exhibit 1002, Page 2019 of 3373

since z is a function of light intensity, which is periodic, single measurements are infinitely degenerate. Therefore, this technique is only useful in obtaining absolute range measurements over a finite and small range. Within that range, measurements are extremely accurate.

In typical two-beam interferograms, the fringes represent lines of constant optical path difference between the wavefront under test and the reference wavefront. Adjacent fringes differ in opical path by a constant contour interval. The traditional means of analysis is to digitize the fringe center positions. At these locations, the phase can be determined to be either an even or odd integtral number of pi. The center coordinates along a fringe are assigned an order number which represents the multiple of two-pi phase difference between the wavefronts being tested. Input data from an interferogram consists of triplets of numbers (x, y, m) where m is the fringe order number and x,y are the coordinates of the fringe center (26, 112).

The spatial resolution of the interferogram is determined by the fringes themselves. High sampling resolution is possible along the fringes, but in the direction normal to the fringe, the sampling is limited to one data point per fringe. For general interferograms where noise and variations in intensity (as would likely be the case in a tooth with discoloration or underlying base materials) across the interferogram may exist, it is only

ClearCorrect Exhibit 1002, Page 2020 of 3373

at the fringe centers where the phase value may be confidently determined (112). For an ideal interferogram, several interferograms must be taker for each test and their results averaged to reduce random digitization error as well as the effects of air turbulenece, vibration, and other noise-generation mechanisms present in an individual interferogram (112).

Interferometry has been used for measurements since Michelson's time (77). Accuracies in the range of 1:200 to 1:300 times the fringe period are possible (89). The technique is also significantly (10-100 times) more accurate than fringe counting or simple triangulation. Measurements of 10 microns or better are possible (89). Because the sensitivity of the interferometer is so great however; results can be affected, causing a shift of several fringes, by simply warming the air in the light path of one portion of the instrument (77). lt is not difficult to hypothesize a situation of that sort developing in a human mouth.

5.1.1.5.7 Diffraction Range. If a spot on an object is coherently illuminated, scattered light forms a speckle pattern on a screen. The size of the speckles is a function of the distance between the object and the screen. This technique is easily scaled and has no missing points problem. However, contrast is a periodic function of

ClearCorrect Exhibit 1002, Page 2021 of 3373

depth, so this technique suffers from the same difficulties with potential ambiguities as interferometric techniques. In general, the accuracy possible with this technique is quite low.

5.1.2 Photographic vs. Real Time Data Acquisition

Real-time data acquisition provides a significant advantage over photographic-based systems since it eliminates one step, and thus, one potential for errors to be added. Unfortunately, analog to digital A/D conversion rates are too slow to convert more than 512 x 512 pixels of data in real time without exceeding the limit posed by the Nyquist sampling theorem (48). That theorem states that analog to digital conversion must occur at not less than twice the overall system bandwidth to avoid loss of information and to pervent degredation of harmonic distortion (aliasing).

In current systems, bandwidths fall below 500 kHz. As a rule of thumb, analog to digltal conversion rates should be 1.5 to 2 times the Nyquist rate. For good performance, then, A/D conversion rates of at least 1 Msample/second with 20-16 bit accuracy are the limit. A new 110 Msample/second 8-bit chip has been developed and prototyped, but is not yet commercially available (48).

With the addition of frame buffers, it may be possible to increase real time data acquisiton to 1024 x 1024.

ClearCorrect Exhibit 1002, Page 2022 of 3373

Unfortunately even that is insufficient for image acquisition for high quality restoration fit (for complete discussion of required resolution, see Appendix 2).

5.2 DATA ANALYSIS AND IMAGE PROCESSING

The goal of image analysis is the construction of scene descriptions on the basis of information extracted from images or image sequences (1750. This requires first that features be extracted from the image. Then surface orientation clues can be derived from those features.

The computational theory for recovering scene geometry from images is based on one of four paradigms: stereo, motion, shading, or texture (76). From a mathematical perspective, recovering shape from stereo or motion are essentially equivalent. Motion can be considered a special case of stereo where the separation between cameras (for sequential images) becomes very small. For motion analysis, since separation is small, spatial disparity is small, making any trigonomtric method of depth estimation extremely vulnerable to error. Further scene depth is restricted to pure translation only (76 and 119). It is unlikely that this could be accomplished successfully in the mouth.

Shape from shading techniques provide shape information in one view, by observing the lighting

ClearCorrect Exhibit 1002, Page 2023 of 3373

variations which occur due to the varying angle of incidence that directional lighting has on varying surface slopes. Great care must be taken with this technique to take into account variations in the illumination light and variations in surface reflectivity, both of which can produce erroneous errors (29). The Swiss system capitalizes on this technique and relies on coating the tooth surface to minimize shading variations which naturally occur in teeth (144).

Stereo is a primary method for modelling three-dimensional scene geometry for both humans and machines (76). It requires matching localized features or intensity patches in two images to determine the shift in position between corresponding scene points in each of the images.

There are two central problems in computational stereo. The first is matching corresponding points. The second is obtaining scene depth at image locations where feature matching fails (as in featureless areas).

A modified stereophotogrammetric system was developed for acquiring data in the atuomated system for dental restorations. In order to extract the three-dimensional image from the stereo pairs containing that information, two distinct operations are required. The first relates to solving the correspondence problem. For each point in the left stereo image, the corresponding point in the right image must be identified. To ease the problem of

ClearCorrect Exhibit 1002, Page 2024 of 3373

matching, and to provide a technique for disregrading unnecessary information in the image (gum tissue position, for instance) features are extracted.

The most useful feature is an edge. Surfaces are assumed (and have been shown) to be fairly continuous over their entirety (83, 84, 130). At the edge of any surface, however, light intensity changes dramatically relative to any changes on the surface. Since the margin of the prepared tooth is most critical and since the margin is a well defined edge, edge finding feature extraction algorithms were investigated.

After the correspondence problem has been solved (specifics of how this is accomplished are given in Chapter 6), the reconstruction of the three-dimensional surface coordinates can progress. Alternative techniques investigated for surface reconstruction include stereometric techniques (the direct linear transform, collinearity equations, and an algorithm devised by Grimson) and reconstruction from Moire fringes.

5.2.1 Correspondence Solutions

Correspondence is unquestionably the most difficult step to automate in stereo vision. The existing methods for solving this problem can be grouped into two categories: area-based and feature-based. In area-based

ClearCorrect Exhibit 1002, Page 2025 of 3373

techniques (106, 191, and 193), an area around each point is used to constrain the search for a matching point in the other view that maximizes a correlation function. These techniques rely on the assumption that intensity value over the image is continuous, except at a few discontinuities in depth. The main deficiency of this method is that it fails to find a match in areas with low information content and can be easily confused in ambiguous situations. In addition, it is sensitive to photometric variations since disparity is based only on intensity changes. Unfortunately, intensities often vary from one view to another due to lighting conditions of the scene, and reflectivity of objects which may change from one image to the next.

In the feature-based techniques (29, 84, 137, 138, and161), features representing meaningful properties of the scene (edges, corners, lines, or regions, for instance) in the two views are found. An attempt is made to match corresponding features based on their properties. One advantage provided by feature-based methods over area-based methods is that they work on fewer elements (since there are less features in images than total pixels). Thus, the feature-based methods generally produce faster algorithms. They are aiso generally less sensitive to photometric variations since features are extracted based on geometric properties rather than lighting conditions. These techniques, however do not produce the full disparity maps

ClearCorrect Exhibit 1002, Page 2026 of 3373

that are possible with area-based techniques. Full disparity, however, can be obtained by interpolation techniques.

Most of the methods currently used for solving the correspondence problem are feature-based. One of these was suggested by Price and Reddy (163) where matching is performed over regions. A similarity measure based on characteristics of the regions (size, location, orientation, color) is used. Each characteristic is normalized by a predetermined weight so that the contribution to the similarity function of each characteristic is of the same scale.

Barnard and Thompson (21) propose a matching technique by first selecting candidate points from two views. These are selected by the Moravec interest operator which computes the minimal directional variance taken in four directions over a small window. Matching points from the two candidate sets are determined, assuming a maximum disparity value, giving an initial probability based on the heuristic that matching neighborhoods of points are similar. Next, the probabilities are updated in a relaxation scheme. Consistent disparities within a neighborhood are given higher probabilities. Good matches have high probabilities and incorrect matches have low probability values. The process continues until a certain threshold of acceptable probabilities is reached.

ClearCorrect Exhibit 1002, Page 2027 of 3373

Marr and Poggio (130) suggest a computational theory of the human stereo vision. They match selected points located at the zero crossings of the Laplacian of a Gaussian operator filtered images. Their theory works only on random-dot stereograms. Modified versions of the algorithm have been suggested. One of these is proposed by Grimson (83). He notes that most incorrect matches in the original method occur at discontinuities in depth (like occluding boundaries). He associates this to the continuity of the disparity over an area imposed in the original algorithm. His algorithm imposes the continuity of the disparity along contours. He also allows for small vertical disparities and uses a coarse to fine filtering approach in convolving the images. His method works on some images but fails in complex scenes. Unfortunately, both bad and good matches propogate from the lower resolutions to the higher resolutions.

Medioni and Nevatia (137) match lines representing connected edge points with similar orientations and strength. Matching segments are assumed to lie within a parallelogram window centered at the segment. Two of the parallelogram sides are parallel to the segment orientation. The other two are horizontal and of length twice the maximum allowed disparity. In addition, they must have similar orientation and strength. Matches are evaluated by a minimal differential disparity function that represents the consistency of a match with respect to those

ClearCorrect Exhibit 1002, Page 2028 of 3373

of its neighborhood. The disparity used is the average of the disparities over overlapping points in the matching segments. The process is repeated iteratively, and during each iteration, matches are reevaluated. The match with the lowest differential disparity is selected.

Webb and Aggarwall (193) suggest a shape-directed area based algorithm. They assume a starting match point, and use this information to estimate the shape (surface normal) at this point. The shape is then used to guide the matching process for adjacent points, until the entire image is matched. The method "deals reasonably" (193) with low contrast regions but the overall results are insufficient.

The image registration system designed by Goshtasby (81) uses gradient information in region extraction, and a probabilistic relaxation scheme in matching regions. Regions in one image are assumed objects and regions in the other image are assumed labels. A similarity measure derived from the geometric shape of regions is used in this technique.

The stereo system proposed by Arnold (16-18) matches edges using a modified Viterbi dynamic programming algorithm adapted to stereo. Constraints on occluding edges, intervals between adjacent edges, and angles of edges are inciuded. The algorithm basically matches edges along epipolar lines (horizontal reference lines in each half of a stereo pair, used for horizontal alignment for

ClearCorrect Exhibit 1002, Page 2029 of 3373

matching points) by finding a path of miximum cost, where the cost is a similarity measure derived from edge properties.

Herman and Kanade (98) use stereo and monocular analysis to extract three-dimensional information from a scene. They use lines and junctions as primitives in matching.

Gool et. al. (80) propose an algorithm to describe a polyhedral scene. They extract edges and verticies and perform matching on these features.

Waxman and Duncan (191) proposed a combined motion-stereo analysis with one fixed camera and one moving camera. Motion is used first, allowing for gross correspondence between analytic flow regions. Next a correlation between binocular difference flow (flow difference in the two views) and stereo disparity is used to establish correspondence between previous unmatched features. The ratio of the rate of change of the disparity value plays an important role in this method.

Two similar three-view stereo techniques were developed by Ito and Ashii (106) and Pietikainen and Harwood (158). Three-view stereo uses three images of the scene, with the matching performed over two combinations of two images. In Ito and Ashii's technique, matching of edges from image 1 is done over image 2 along epipolar lines. For each candidate from image 2, a corresponding point in image 3 is derived analytically at the

ClearCorrect Exhibit 1002, Page 2030 of 3373

intersection of epipolar lines defined by the candidate point and the original point in image 3. These later points are correllated with the original point in the first image to select the best match. Ideally, corresponding points (from image 1 and 3) have similar neighborhoods.

In the other three-view stereo technique (158), the three images must be coplanar. The horizontal and vertical images are equidistant from and aligned parallel to the base image. This geometry allows for corresponding points in the base-horizontal and base-vertical images to have the same disparity. Edge points are used in the matching. An edge point from the base image is selected and based on its orientation (closer to horizontal vertical) a search is made in the vertical or horizontal image respectively. Next, another search is carried out in the third image to select the corresponding edge. The resulting triplets constitute a preliminary set of matchings. Final matches are determined from the local properties (orientation and gray level on both sides of the edge). Finally, a contour connectivity procedure is used to eliminate false matches.

Stereo correspondence is one of the most studied problems in computer vision. The many feature-based methods that have been developed use different basic primitives as tokens for match. These range from point features (corners and edges) to linear features (lines,

ClearCorrect Exhibit 1002, Page 2031 of 3373

curves, junctions), to area features (regions). The methods vary in the way the features are extraced. They all integrate the fundamental problems in computer vision of edge detection and image segmentation techniques.

5.2.2 Edge-Finding Techniques

For both biologic systems and machines, vision begins with a huge array of measurements of light in an environment. The goal of vision (either for man or machine) is to recover information about an object. Many steps are required to accomplish this. One of the first clues about physical properties is provided by the changes of intensities in an image (100).

Intensities change quickly at edges. Physical edges are one of the most important properties of objects since they correspond to object boundaries or changes in surface orientation or material properties (185). Edge detection serves to simplify the analysis of images by drastically reducing the amount of data to be processed, while at the same time preserving useful structural information about the object boundaries (40).

A vast array of edge finding techniques have been developed (see reference 173). Generally, the intensity value of adjacent pixels jumps dramatically at an edge (45). The direction of that jump (low to high or vice

ClearCorrect Exhibit 1002, Page 2032 of 3373

versa) depends upon the image and the direction of the scan.

Rosenfeld (174) and Schowengerdt (177) point out that most common class of edge detection is based on the application of local difference operators (a gradient) at every pixel. An edge is detected by a sudden change in gray level from one pixel to the next when the magnitude of a gradient exceeds a threshold (150). Many operators take the differences of gray levels in two orthogonal directions and use either root mean square or maximum absolute value as an estimate of edge steepness and the inverse tangent of the change in x divided by the change in y as an estimate of edge direction.

Differences taken at every pixel are convolution operators. With them, magnitude and direction are determined (by a non-linear process of multiplication and division to find the tangent). Early edge detectors generally embodied a specific edge model designed to locate step edges or intensity gradients. These operators were usually of fixed size (often 2 by 2 or 3 by 3) and failed to address the issues of edge width or resolution. The Roberts, Sobel, and Laplacian operators fall into this category. For the Roberts operator, the image is convolved with:

$$\begin{matrix} 0 & 1 \\ -1 & 0 \end{matrix} \quad \text{and} \quad \begin{matrix} 1 & 0 \\ 0 & -1 \end{matrix}$$

and the 3 by 3 Sobel operator where the image is convolved

ClearCorrect Exhibit 1002, Page 2033 of 3373

with:

$$\begin{matrix} -1 & 0 & 1 \\ -2 & 0 & 2 \\ -1 & 0 & -1 \end{matrix} \qquad \text{and} \qquad \begin{matrix} 1 & 2 & 1 \\ 0 & 0 & 0 \\ -1 & -2 & -1 \end{matrix}$$

The Sobel operator corresponds to edges in two positions. It is less sensitive to noise than the Roberts because it combines differencing across the edge with averaging along the edge.

The Laplacian operator can be used as a difference operator but it responds more strongly to isolated points than it does to lines or edges. The digital version of the Laplacian convolves the image with:

$$\begin{matrix} 0 & -1 & 0 \\ -1 & 4 & -1 \\ 0 & -1 & 0 \end{matrix}$$

It is not a good choice if the image is noisey. If the edge is represented by a ramp function of gray levels, the Laplacian operator yields non-zero magnitude at the top and bottom but is zero along the ramp itself.

An alternative technique proposed by Rosenfeld (174) is to define a difference operator by fitting polynomial surfaces to gray levels in the neighborhood of a given pixel and take the gradient of the polynomial as an estimate of the image gradient. The parital derivates with respect to x and y of the polynomial can be expressed directly in terms of gray levels, precluding the necessity of actual surface fitting. If a plane is fit by least squares to a 2 x 2 neighborhood, the magnitude of the gradient of that plane turns out to be the same as the

ClearCorrect Exhibit 1002, Page 2034 of 3373

magnitude of the Roberts operator. If a quadratic surface is fit to a 3 x 3 neighborhood, the x and y partial derivates are proportional to the results of convolving the image with the Prewitt operator:

$$\begin{array}{ccc} -1 & 0 & 1 \\ -1 & 0 & 1 \\ -1 & 0 & 1 \end{array} \quad \text{and} \quad \begin{array}{ccc} 1 & 1 & 1 \\ 0 & 0 & 0 \\ -1 & -1 & -1 \end{array}$$

Still another technique is template matching. In this approach, the image is convolved with a set of patterns (masks) representing step edges in the principal directions. The maximum of the magnitude of the results at a given pixel is then taken as the edge magnitude and the orientation of the mask giving this maximum defined the edge direction. This template matching approach is described in detail by Yakimovsky and Cunningham (108, 197). Their masks are specially configured (rays and concentric diamonds) rather than rectangular windows. The major application of the masks, however, is for finding correlations for point matching.

The choice of mask size is important. A large mask averages more noise so lower contrast edges can be detected. The "cost" however, is in lower precision in locating the position of the edge and greater computational overhead (150).

Another method for detecting intensity changes capitalizes on derivatives. It incorporates three essential elements: smoothing, differentiating, and feature extraction (100). Smoothing serves two functions.

ClearCorrect Exhibit 1002, Page 2035 of 3373

First it reduces the effects of noise. Secondly, it establishes the resolution or scale at which the changes are to be detected.

The resolution for detecting edges can substantially alter the subsequent interpretation of the image. Hildreth (100) uses an example of an image of a leapord. At fine resolution, rapid intensity changes might delineate individual hairs in its coat; at a coarser resolution they might delineate its spots. Changes from one resolution to another can be detected by smoothing image intensities by different amounts.

Differentiation accentuates intensity changes. It transforms the image into a form from which properties can be extracted more readily. A substantial image change gives rise to a peak in the first derivative and a zero-crossing in the second. A zero-crossing an easily be detected. The detection and description of these features in the smoothed and differentiated surface provides a compact representation, capturing meaningful information in the image. Marr refers to this representation as the primal sketch of the image (132). This primal sketch is a primitive but rich description of the gray-level changes present in an image (129-132). This description is based on a vocabulary of kinds of intensity chages, including edges and modifying parameters specifying position, orientation, termination points, contrast, size, and fuzziness.

ClearCorrect Exhibit 1002, Page 2036 of 3373

From this basis, Marr and Hildreth (131), created another theory of edge detection. In their analysis, intensity changes are detected separately at different scales to detect the wide range of scales of changes which occur in natural images. No single filter can be optimal simultaneously at all scales. By taking local averages of the image at various resolutions and then detecting the changes in intensity that occur in each one, more nearly ideal edge finding can be accomplished. This necessitates determination of an optimal smoothing fiiter and detection of intensity changes as a function of scale.

There are two physical considerations that combine to determine the appropriate smoothing fiiter. First, the motivation for filtering the image is to reduce the range of scales over which intensity changes take place. The filter's spectrum should be smooth and roughly band-limited in the frequency domain. Secondly, there must be a constraint of spatial localization. Things that give rise to intensity changes (illumination changes, changes in orientation, surface reflectance, edges, etc.) are spatially localized. The consequence of this is that the contribution to each point of the filtered image should arise from a smooth average of nearby points rather than from an average of widely scattered points. The only distribution that optimizes the relationship of these two localization requirements is the Gaussian.

ClearCorrect Exhibit 1002, Page 2037 of 3373

The Gaussian, convolved with the intensities of the images on a point by point basis gives a measure of correlation between the central point and a specified size of an adjacent area (called the kernel of the Gaussian). Grimson (83) reports that four kernel sizes, corresponding to four octaves, are needed.

Whenever an intensity change occurs as an edge is crossed, for instance, there is a corresonding peak in the first directional derivatlve (or equivalently a zero-crossing in the second directional derivative of the intensity). So the task of detecting intensity changes is reduced to finding the zero-crossings of the second derivates of intensity. To avoid computational expensive checks of all orientations, the Laplacian (∇^2 were $\nabla^2 = \partial^2/\partial x^2 + \partial^2/\partial y^2$) can be convolved with a two-dimensional Gaussian operator. Intensity changes for a given scale (kernel size), then are best detected by finding the zero values of $\nabla^2 G(x,y) * I(x,y)$ for image I(x,y) where G(x,y) is a two-dimensional Gaussian distribution and ∇^2 is the Laplacian. The intensity changes established by each kernel is represented by oriented primitives called zero-crossing segments. Even with these concerns about computation efficiency, processing is very slow. With the Marr-Hildreth theory, calculation of coarse zero-crossings for a 512 x 512 image took three hours on the MIT Lisp machine (108). (With special customized hardware, the calculations were repeated in 0.25 seconds, however!)

ClearCorrect Exhibit 1002, Page 2038 of 3373

Shanmugami, Dickey, and Green (178a) derived an optimal frequency filter domain for detecting changes based on the following criterion: The operator must (1) have maximum energy in the vicinity of an edge, (2) be limited in frequency bandwidth, (3) have small output when input is constant or slowly varying, and (4) be an even function in space. When step changes of intensity are detected, this operator, though devised to be an optimal frequency domain filter, is essentially equivalent to a spatial derivative (the second derivative of a Gaussian) (100). This detector performs poorly on localization. It also has the intrinsic feature of giving two maxima in the output of the response to an edge, yielding an ambiguous result (185).

Another approach to smoothing is to find an anaytic function which best models or approximates the local intensity pattern. One of the first approaches to this type was the Hueckel operator (100). Surface fitting methods use a variety of basis functions (including planar and quadratic functions) as the operator. The surface is approximated by expansion into the first nine coefficients of a radial Fourier series. This operator was quite popular in the 1970's but subsequent analysis has found serious deficiencies in the Fourier approximation (150).

More recently, Haralich (90 and 91) used the discrete Chebychev polynomial to approximate image intensities with a facet model. With the Haralick operator, edges are detected by locating the local maximum in the image

ClearCorrect Exhibit 1002, Page 2039 of 3373

gradient. The gradient is estimated by fitting a series of polynomial basis functions. This analytically models a patch of the intensity surface and deduces the presence of edges from the coefficients of the model (76). In the one dimensional case, this is equivalent to convolving the image with a filter whose shape is described by a cubic polynomial and which resembles the first derivative of a Gaussian (185). The Haralick algorithm convolves:

$$A\ (1-k\ \frac{r^2+c^2}{\sigma^2}\ )\ \exp[\frac{-(r^2+c^2)}{2\sigma^2}]$$

with the image. (A is an arbitrary scale factor, is kernel size). The Marr-Hildreth algorithm convolves:

$$\frac{x^2+y^2-2\sigma^2}{\sigma^4}\ \exp\ \frac{-(x^2+y^2)}{2\sigma^2}$$

with the image. If k = 0.5 and σ = 1.4, the two are equivalent (for an 11 x 11 non-zero kernel). At σ = 5, the Marr-Hildreth has a non-zero support diameter of 49 pixels.

A smoothing operator derived from regularization theory of mathematical physics has also been proposed (159). It begins with the hypthesis that numerical differentiation of an image is a mathematically ill-posed problem since its solution does not depend continuously on input intensities (the equivalent of saying that the solution is not robust against noise) (100). The smoothing regularizes the image, permitting well-posed differentiation.

The operator is given by S(x) where s(x) minimizes:

ClearCorrect Exhibit 1002, Page 2040 of 3373

$$\sum_{k=1}^{n}(I(x_k) - S(x_k))^2 + \lambda \cdot \int |S''(x)|^2 \, dx$$

The first term is a measure of how well S(x) fits the sampled intensities. The second term measures the smoothness of S(x). The constant λ controls the relative weight of each of the terms (100). Pogglo et.al. (159) showed that the solution of this minimization is equivalent to the convolution of the image intensities with a cubic spline that is very similar to a Gaussian.

Shen and Castan (41 and 197) argue that in general, derivates are sensitive to noise so some low-pass preprocessing is often necessary. The problem of edge finding is further complicated by the fact that derivates and their functions are local features of the image so, when applied to three-dimensional image reconstruction, for one pixel in an image there may exist more than one candidate in the other image which has similar local distributions of gray levels.

This problem was also addressed by Marr and Canny and is the problem of ambiguities and false positives. Ideally, when three-dimensional reconstructions are done, characteristics of points which are relatively stable and insensitive to noise are needed. These points can be established by contours (the application for which Canny developed his techniques), zero-crossings of Laplacians (the Marr-Hildreth solution, for instance), and characteristic points found by use of the Moravec operator (146 and 147). With the Moravec operator, interesting

ClearCorrect Exhibit 1002, Page 2041 of 3373

pixels are often limited to isolated points, making it difficult to find three-dimensional information of the whole scene from disparities of isolated points.

The contour and Laplacian zero-crossing techniques usually locate some continuous lines or curves, making three-dimensional reconstruction easier. However, the gradient thresholding used in edge detection often causes some missed contour points so contours which are found are often broken into several discontinuous parts, creating difficulties in matching. The zero-crossing technique avoids this problem. Unfortunately, by itself, the Laplacian of gray levels is sensitive to noise so a band-limited Laplacian, such as a Lapiacian of a Gaussian is more useful since it eliminates the noise sensitivity. Because of the contradiction between insensitivity to noise and precision of localization of zero-crossings with a Gaussian filter, different Gaussian channels should be used (as proposed by Marr and Hildreth). But that technique requires long computation times.

Shen and Castan (179) have created an algorithm for detecting band-limited Laplacian zero-crossings with precision. For them, a binary Laplacian image is created which enhances subsequent stereo reconstructions. Band-limited Laplacian zero-crossings are sparse, corresponding to pixels with important changes in gray level (like an edge or boundary). The binary Laplacian image (BLI) is formed by defining: if a pixel has a positive Laplacian

ClearCorrect Exhibit 1002, Page 2042 of 3373

value, the BLI value is equal to 1. If the Laplacian is zero or negative, the BLI value is equal to 0. The precision of the algorithm results from the precision of algorithm results from the precision of the Gaussian. There is less noise with this filter, giving increasing precision in localization of zero-crossings. Further, the computational complexity is low since the algorithm requires only four multiplications and nine additions for each pixel.

Even with this technique, at the BLI Level some noise remains. To suppress that noise, before three-dimensional reconstruction is attempted, spatial continuity is used to suppress isolated zones of small surfaces. This process is called area size thresholding. Zones in the BLI are relatively independent of gray level of surfaces, a fact that may be important for the relatively flat color differences observed in imaging the teeth.

There has been considerable energy expended in developing suitable edge-finding algorithms. Many of these investigations (both theoretical and applied) have addressed the question of which operators are most appropriate for performing the required operations. Certainly a better understanding of the advantages and disadvantages of various operators is emerging (100, 123, and 124).

It is unlikely, however, that a single method is the most appropriate for all tasks. Mastin (133) shows some interesting results emphasizing this point. A composite

ClearCorrect Exhibit 1002, Page 2043 of 3373

image, consisting of four parital images (which are dramatically different types - lines, continuous tone, solid gray, and text), was subjected to six different smoothing filters. Results of different algorthims are dramatically different for different types of images. Because of this, a number of edge-finding algorithms were applied to images of the teeth. The relatively simple Roberts and Sobel operators give no useful information. Even looking at the edges found with the operators and knowing what the original image looked like provided no useful information. Adding and subtracting the edge image from the original image provided no useful information.

Figure 2 is an original image. Figure 3 is the raw digitized image at resolution of 480 lines with 640 pixels/line. Figure 4 is the edges found with the Marr-Hildreth algorithm. Figure 5 gives the edges found with the Haralick algorithm. Figure 6 is with the Canny edge finding algorithm and Figure 7 is the same image with a strong edge criterion applied to the Canny operator. Because of its significantly improved performance compared with the others, the Canny edge finding algorithm was selected for use with the automated system. It is described in Chapter 6.

5.2.3 Surface Reconstruction

ClearCorrect Exhibit 1002, Page 2044 of 3373

The major goal in imaging is to establish the three-dimensional coordinates describing the object of interest. A number of techniques have been devised. Some come from photogrammetric applications (see references 1, 125, and 126 general discussion), others have been derived from image processing (see reference 83, for instance), others have come from applications in robotics and artificial intelligence (see reference 31 for instance). The techniques associated with the direct linear transformation (DLT), the Collinearity Condition, the Grimson algorithms, and Moire reconstruction were considered as feasible alternatives for incorporation into the automated system for production of dental restorations.

5.2.3.1 DIRECT LINEAR TRANSFORMATION. The direct linear transformation (DLT) technique is based on the principles of the projective transformation. Given an arbitrary X,Y,Z object coordinate system, the x,y and z image space coordinate system can be found using basic linear transformations (1). Transformations from one arbitrary coordinate system to another are made through a finite series of rotations and translations which include perspective by the following equations:.

$$[X, Y, Z, 1] \begin{vmatrix} L1 & L5 & R1 & L9 \\ L2 & L6 & R2 & L10 \\ L3 & L7 & R3 & L11 \\ L4 & L8 & R4 & L12 \end{vmatrix} = s * [x, y, z, 1]$$

ClearCorrect Exhibit 1002, Page 2045 of 3373

where X,Y,Z represents the coordinates of a point in the object coordinate system (an actual point in space to be digitized). The coordinates x, y, z represent the coordinates of that same point in the image plane (the photograph). L9, L10, and L11 contain the information for s, the perspective scaling. L4, L8, and R4 represent translations. The upper left 3 x 3 matrix contains the concatinated rotations required to align the arbitary axis of the image and object coordinate systems. When the image plane is flat (as in a photograph), z = 0 for all X,Y, Z and R1 = R2 = R3 = R4 = 0. By rearranging, the standard form of the DLT is obtained:

$$x = (L1 * X + L2 * Y + L3 * Z + L4)/s$$

$$y = (L5 * x + L6 * Y + L7 * Z + L8)/s$$

where:

$$s = (L9 * X + L10 * Y + L11 * Z + 1.0)$$

The L's, called the calibration coefficients, incorporate information about the geometry of the image acquisition, the internal configuration of the camera system, including orientation parameters of the camera to the object space (distance from the object, rotation of the camera/film coordinate axis to the coordinate axis of the object space), orientation of the internal parameters of the camera (focal length of the lens, orientation of the film coordinate axis), parameters modeling lens distoration, and parameters modeling film distoration (1, 14, 189, and 196).

ClearCorrect Exhibit 1002, Page 2046 of 3373

The elegance of this technique, however, is that the equations can be solved without apriori knowledge of this array of variables. Instead, if the object coordinates and image coordinates of at least six points (on a calibration devices of some sort usually) are known, the values of the L's can be found. These same L's are then used to solve for the object coordinates of unknown points.

From work that has been done using this technique in tl Department of Orthodontics at the University of Minnesota, resolution is insufficient to meet the strict requirements for imaging the teeth. Resolution with this reconstruction has been shown to be on the order of 1/2 mm 94, 113, 116, and 156); sufficient for the applications for which it was developed but inadequate for automated restorations.

5.2.3.2 COLLINEARITY CONDITION. Three-dimensional coordinates from planar stereo pairs of information can be obtained using the collinearity condition equations for rays, developed by Anderson (14) and Brown (35). The collinearity condition can be expressed as:

$$x_{ij} = -c[(X_j - X_{oi})r_{11} + (Y_j - Y_{oi})r_{21} + (Z_j - Z_{oi})r_{31}]/[(X_j - X_{oi})r_{13} + (Y_j - Y_{oi})r_{23} + (Z_j - Z_{oi})r_{33}]$$

and

$$y_{ij} = -c[(X_j - X_{oi})r_{12} + (Y_j - Y_{oi})r_{22} + (Z_j - Z_{oi})r_{32}]/[(X_j - X_{oi})r_{13} + (Y_j - Y_{oi})r_{23} + (Z_j - Z_{oi})r_{33}]$$

ClearCorrect Exhibit 1002, Page 2047 of 3373

where:

x_{ij}, y_{ij} = image coordinate points i on photo j

c = calibrated focal length

$(X,Y,Z)_j$ = object coordinates of point j

$(X,Y,Z)_{oi}$ = camera station coordinates of photo i

$\begin{vmatrix} r_{11} & r_{12} & r_{13} \\ r_{21} & r_{22} & r_{23} \\ r_{31} & r_{32} & r_{33} \end{vmatrix}$ = rotation matrix R

Curry (53) uses this technique in his work creating a point location and tracking system using digital images for biostereometrics. It requires that information about camera station parameters, camera calibration (principal distance, principal point location, coefficients for symmetric radial lens distortion) be included. It does, however, yield accuracies of 0.2 to 0.3 mm in x, y, and z coordinates (24). Unfortunately, these are not substantially improved over those found using the DLT.

5.2.3.3 GRIMSON ALGORITHM. The Grimson algorithm (83) uses the Laplacian of the Gaussian (G) convolved with the image to determine three-dimensional coordinates of the positions on the object at which the zero-crossings occur. This technique provides information where ever edges occur. However, it gives no explicit information about the remainder of the surface. By capitalizing on the physical constraint of surface consistency, he derives an

ClearCorrect Exhibit 1002, Page 2048 of 3373

interpolation algorithm to complete the surface representation.

The interpolation algorithm relies on the basic hypothesis that in order for a surface to be consistent with a given set of zero-crossings, not only must it give rise to a zero-crossing in the convolved irradiances at those points, but it must also not give rise to zero-crossings elsewhere. He states and proves a surface consistency theorem, describing the probability of a zero-crossing as a function of the shape of the surface. The importance of this theory is that it leads to a method for measuring the probability of a particular surface being inconsistent with the zero-crossing information; yielding a technique for determining the best possible surface to fit the known information.

5.2.3.4 MOIRE FRINGE TECHNIQUE. From Moire fringe information, a surface reconstruction can be accomplished. Each fringe represents an equal height on the surface. Thus, the third dimension (z) for each point on the image (x,y) can be calculated (120):

$$z = A/B$$

where:

$$A = a_m[P_g x_m(x_{op}k_1 - y_{op}k_2 + z_{op}k_3) - a_p P_m(x_{op}k_4 + y_{op}K_5 + z_{op}K_6)]$$

$$B = P_g[x_m(x_o k_1 - y_o k_2 + a_m k_3) - a_p P_m(x_o k_4 + y_o K_5 + a_m K_6)]$$

ClearCorrect Exhibit 1002, Page 2049 of 3373

wnere:

a = lens - film distance in imaging camera

P = period of grid (lines/mm)

P = period of film image grid (lines/mm)

a = grid-lens distance in projection system

$k_1 = \cos\theta\sin\phi$

$k_2 = \sin\theta$

$k_3 = \cos\theta\cos\phi$

$k_4 = \cos\theta\cos\beta + \sin\theta\sin\phi\sin\beta$

$k_5 = \cos\theta\sin\beta$

$k_6 = \sin\theta\cos\phi\sinB - \sin\theta\cos\beta$

θ = viewing angle

ϕ = angie of grid projection to image projection

β = rotation of grid relative to film piane

$(x,y,z)_g$ = grid coodinates

$(x,y,z)_m$ = film coordinates

5.3 FABRICATION TECHNIQUES

Both traditional and non-traditional techniques for fabricating the restoration were investigated. Two factors play heavily into any selection, however. First, the intent is that the automated system should be feasible for installation in a typical dental office. Secondly, only one shaping technique should be used for the entire process. It is possible that additional techniques could complement each other; bringing advantages in time of

ClearCorrect Exhibit 1002, Page 2050 of 3373

production, for instance. However, in an attempt to keep system design as simple as possible, the shaping technique selected must be able to produce both internal and external surface geometry of a dental restoration. Traditional milling provides this capability and is described in Chapter 6. Other techniques investigated include electric discharge machining, laser beam machining, abrasive jet machining, water jet cutting, stereolithography, and ultrasonic machining. Table 3 compares various parameters relating to the alternative techniques.

5.3.1 Electrical Discharge Machining

Electrical Discharge Machining (EDM) dates back to the 1940's. Material is removed by thermal energy generating a spark (194). A dielectric fluid provides a path for discharge of the fluid between the electrode tool and the workpiece. When sufficient voltage is applied, the dielectric ionizes, passing current. The discharge area is focused, creating a local temperature above the melting point of the metal workpiece. A heat-affected layer of 2 to 130 microns remains after EDM. The part may or may not show evidence of any metallurgical changes. Tool wear is an important consideration and in order to control tolerances and minimize cost, material removal rates must be kept low (51).

ClearCorrect Exhibit 1002, Page 2051 of 3373

Table 3. Comparison of Fabrication Techniques

Technique	Material Removal		Tolerances		RMS Surface		Possible Damage Depth		Comments
	cu.in/hr	cu.cm/hr	in	microns	microin.	micron	in	mm	
Conventional Machining	250	4097	0.002	0.050*	20-200	0.5-5.1	0.001	0.03	
Electrical Discharge Machining	3-12	49-197	0.0006-0.005	0.015-0.13	10-500	0.3-12.7	0.005-0.015	0.13-0.38	Conductive materials only
Laser Beam Machining	0.0004	0.007	0.001	0.03	20-50	0.5-1.3	0.005	0.03	No sharp edges
Abrasive Jet Machining	0.06	1.0	0.002	0.05	6-60	0.2-1.5	0.0001	0.003	
Water Jet Cutting									
Ultrasonic Machining	1.2	19.7	0.0003	0.008	10-20	0.3-0.5	0.001	0.03	Best for hard, brittle materials
Stereolithography	N/A	N/A	+	+	+	+	N/A	N/A	

* 4340 steel, stagger tooth milling
\+ no details available at this time
reference 194 for further details

ClearCorrect Exhibit 1002, Page 2052 of 3373

Because thermal energy is utilized, hardness is irrelevant for cutting capabilities. However, only electrically conductive materials can be machined by EDM. Therefore, it is not a reasonable choice for the production of dental retorations which often are fabricated from ceramic, porcelain, and composite materials.

5.3.2 Laser Beam Machining

Laser beam machining has been used for high precision fabrication of complex geometries with high tolerance (104). Basically it is a high-speed ablation process (194). The workpiece is heated, causing surface melting. Evaporation occurs in the small focus area of the laser beam. Cutting is further enhanced by liquid material flowing from the area. While the heat-affected zone is shallow, very high thermal stresses may be applied and residual stresses may result. Sharp corners (like margins of restorations) may create some problems. Usually this technique is not employed for mass material removal. It will cut hard, soft, tough, brittle, stiff and resilient materials.

In most applications, cuts are made all the way through plates of material; it is difficult to precisely control the depth of a cut. Since depth of cut is

ClearCorrect Exhibit 1002, Page 2053 of 3373

critical for both the internal and external surfaces of a dental restoration, this technique is not indicated.

5.3.3 Abrasive Jet Machining

Abrasive jet machining removes material by abrasive particles in a high-velocity gas stream impinging on the workpiece. This differs from conventional sandblasting since it uses finer process parameters and cutting actions are more carefully controlled. Hard brittle materials, including glass and ceramic, can be cut. Diamonds have been cut using diamond abrasives (194). It is not recommended for mass material removal processes, and thus, is not optimal for the dental restoration application where a rather large bulk of material must be removed from the area into which the prepared tooth will fit.

5.3.4 Water Jet Cutting

Water jet cutting was first patented in 1961. Water pressure, at 60,000 psi, is accelerated through an orifice to create a stream traveling at more then twice the speed of sound (96). This high velocity, high pressure water jet cuts the material. Numerically controlled systems do exist. With this jet it is possible to cut graphite, glass, epoxy and other non-metals. It is also possible to

ClearCorrect Exhibit 1002, Page 2054 of 3373

cut highly brittle materials. Unfortunately, workpiece material removal rates are minimal and depth of the cuts are difficult to control (194).

5.3.5 Ultrasonic Machining

Ultrasonic machining is performed by a cutting tool which oscillates at high frequency, typically 20,000 cpm, in an abrasive slurry. The shape of the tool corresponds to the shape to be produced by the workpiece (a custom tool would have to be fabricated before beginning material removal). High speed reciprocal motion of the tool drives abrasive grains across a gap into the workpiece, mechanically removing the material. Soft and ductile materials are easier to cut; hard and brittle materials, including ceramics (155), are possible. It is probably the best alternative for hard and brittle materials (23). The first patent for ultrasonic machining was issued in 1945 (194). This technique can produce complex shapes but it does not compete with conventional material removal operations of the basis of stock removal rates.

5.3.6 Stereolithography

Stereolithography is a new technique and the basis of a newly formed company called 3-D Systems (34). With this

ClearCorrect Exhibit 1002, Page 2055 of 3373

technique, a precisely focused beam of UV-light scans a pool of liquid plastic, solidifying the material and building up complex shapes, layer by layer or point by point.

The method is not capable of producing parts from materials other than UV cured plastics. Few, if any, of the currently used dental materials fall into this category. In the future, however, new materials or different light sources could feasibly be useful with this technqiue. In the near term, however, it is not appropriate for further consideration. This technique may be excessively restricting.

ClearCorrect Exhibit 1002, Page 2056 of 3373

Chapter 6. System Description

The system to automate production of dental restorations acquires data directly from a patient's mouth, reconstructs a true three-dimensional model of that data, designs a restoration which fits the unique requirements of the shape and size for the patient while preserving the important morphological characteristics of the tooth being restored, and then produces a milled restoration. Understandably, a number of elements are required to accomplish this. These include the techniques involved and required to acquire the data, to convert the data into digital form, and then to recreate the three-dimensional surfaces representing the teeth. Table 4 compares current and automated processes. A data base was created to establish the ideal morphology of each of the teeth in the human mouth. A CAD/CAM package has been developed to create the design of the restoration and to generate the milling machine commands to produce it. Special filtering algorithms have ben developed to represent the teeth in a form which is compatible with the CAD/CAM software requirements. Special fixturing has been created to permit restorations to be created. Each of these elements, as well as with a discussion of materials from which

ClearCorrect Exhibit 1002, Page 2057 of 3373

Table 4. Current vs. Automated Restoraton Production

	Current Technique	Automated System
DATA ACQUISITION	• Impressions	• Stereo pairs of images
	• Hinge axis location	• Digitizing
	• Face bow transfer	
DATA PROCESSING AND ANLYSIS	• Pour models	• Edge finding
	• Place pins	• 1:1 correspondence
	• Pour base	• Disparity
	• Mount in articulator	• 3-D reconstruction
	• Trim dies	
	• Mark margins	
FABRICATION	• Wax pattern	• CAD/CAM
	• Sprue	• Mill
	• Invest	
	• Burnout	
	• Cast	
	• Polish	

ClearCorrect Exhibit 1002, Page 2058 of 3373

restoration have been fabricated, will be covered. Figure 8 summarizes the activities involved in an automated system to fabricate dental restorations.

6.1 DATA ACQUISITION

Data acquisition is the first step in restoration production - with either an automated or traditional system. Each patient presents with a unique set of characteristic shapes and sizes of teeth; a restoration will have a unique form, depending upon the history of decay and/or fracture that necessitates that the restoration be placed. The data required includes: (1) the configuration of the tooth prepared by the dentist to receive the restoration, (2) the shape of the proximal surfaces and heights of the adjacent teeth, (3) the surface configuration of the opposing teeth with which the restoration must occlude, and (4) motion of the mandible relative to the maxilla during function (in the areas where any of the teeth remain in contact and therefore guide the motion of the jaws). In general terms, some technique must be devised to create a representation of the teeth.

It is important to remember that the data must be obtained from a living patient who is unconstrained. They wiggle and have only a limited amount of opening possible

ClearCorrect Exhibit 1002, Page 2059 of 3373

between their teeth (usually on the order of 40 to 60 mm between their front teeth but only 25 to 30 mm in the posterior regions of their mouth). They also have cheeks, saliva, and tongues that are often in the way. The oral environment is essentially at 100 percent humidity.

For the automated system investigated, a film-based stereophotogrammetric system has been developed. The film-based system was selected for two major reasons. First, it permits quick data acquisition for the information required for shape reconstruction of the prepared tooth, minimizing the effects of any patient movement. Perhaps more importantly, the intent is to create a system which is feasible for use in a normal dental office. Thus, the cost of the in-office system must be reasonable low and it must be able to be operated with only minimal training.

The data acquisition system created is unique. Teeth are relatively featureless, providing little color variation and long horizontal and vertical areas of nearly flat profile. This creates substantial difficulties for subsequent image processing. In order to alleviate this problem, the data acquisition system design synthesizes structured light and conventional stereophotogrammetry. Data is acquired so that advantages from both techniques can be utilized for subsequent image processing and data analysis. Developments for the data acquisition system are the basis for a patent application now in process.

ClearCorrect Exhibit 1002, Page 2060 of 3373

Because of potential difficulties resulting from disclosure, an in-depth description of the system cannot be provided here. Instead, the general principles and approaches are outlined.

6.1.1 Data Acquisition System

The data acquisition system, in its current configuration, consists of a standard Nikon N2000 35-mm camera body with a special rod lens (Figure 9). The lens is a combination of 100-mm Vivitar 11 Macro telephoto lens (Part 22702350) to which is attached magnifying larygngo-pharynogoscope by V. Stuckard (Richard Wolf Medical Instruments Corp. part number 4450.47 attached with quick-mount stepdown ring part number 5220.00). The laryngo-pharynogoscope (an endoscope) lens is a 5.85 mm diameter rod lens with prism system mounted at the distal end, permitting the field of view to be at 90 degrees to the long axis of the lens. A total distance of 25 mm between the top of the surface being imaged and the top of the lens is required. Depth of field is essentially infinite. Figure 10 is a view of the teeth as seen through this lens.

To obtain three-dimensional data from planar photographs, stereo pairs of images are required. The stereo pairs have been made by moving the camera from one

ClearCorrect Exhibit 1002, Page 2061 of 3373

position to another. Images have been recorded using standard Kodachrome KM 135 film with ASA 400. Development has been done by commercial processors (Black Photography or National Camera Exchange, Minneapolis, MN).

Data was acquired through the experimental setup shown in Figure 11. Light source (1) illuminates a Ronchi grating (2) with 500 cycles/inch (Rolyn Optics Part No. 70.3010). Lens 3 focuses the grating onto the tooth (4). The image is recorded by camera (5) with a standard 100-mm lens plus endoscope. Figures 12 and 13 are views of the resulting image pairs. The dark line crossing the tooth serves as an epipolar line for alignment of scan lines (to be discussed in sections 6.2.1.2 and 6.2.1.3 on auto-correspondence and surface reconstruction).

6.1.2 Digitizing

To convert the photographic images to digital images, an Eikonix EC-850 digitizer (Eikonix Corporation, Waltham, MA) has been used (see Figure 14 and reference 72). The resolution of this digitizer is 4096 by 4096 pixels. The system uses a linear CCD array to acquire each row of data and a high-resolution stepper motor to move from one row to the next. The digitizing work station includes the CCD-camera mounted on a column which permits the camera to be raised or lowered relative to the working table top.

ClearCorrect Exhibit 1002, Page 2062 of 3373

This, combined with the lenses, permits different sizes of film and objects to be digitized.

The primary device of the system is a linear array of 4096 photodetectors. Center to center diode separation is 7.5 microns (72). During a scan, the array is stepped repeatedly in a direction at right angles to its length. Each step is 7 microns.

Each photodiodes is connnected across a capacitor which is initially charged by the scanning circuits. Each time the photodiodes are accessed by the scanning circuits, the capacitors discharge through the photodiode at a rate which is determined by four factors; (1) average light intensity of the light focused on the photodiode, (2) time between scans, (3) dark current of the photodetector, and (4) individual gain of the photodiodes (72).

The time between scans is the sum of two factors: (1) active time to scan the accuracy (fixed by clock rate) and (2) integration time (a pause time) (72). Integration time is controlled by exposure time which can be set at the console (see Figure 15).

Each time a photodetector cell is accessed by the scanning circuits, its output, which is the remaining charge on its capacitor, is fed as voltage to an analog sample and hold circuit. The capacitor is recharged for the next period. When all cells have been read, the pause period is taken before a new scan can begin. At the start of a pause period, during a normal scan, the stage carrying

ClearCorrect Exhibit 1002, Page 2063 of 3373

the array shifts one or more steps, depending upon software commands.

The sample and hold circuit contents (the output of each cell) are clocked into an A/D converter. The output is a digital representation of the gray (or color) levels sensed.

Both transmissive and reflected light sources are available so transparent films, photographs, or solid objects can be digitized. The transmissive light source uses filters to provide red, blue, and green light in addition to a white light source. The intensity of the transmissive light can be manually adjusted to optimize integration time (the time allowed for light to impinge on a given CCD sensor cell). Camera signals are monitored through an oscilloscope which provides instanteous histogram plots of light intensity. The histogram is useful in establishing proper light intensity. Both optical (the equivalent of through the lens viewing in 35-mm cameras) and electronic (maximum intensity levels) focusing are possible (but cannot be achieved simultaneously).

The digitizer can sense up to eight bits of color and can digitize in levels of gray, red, green, or blue. Scan times vary from 4 to 30 seconds/frame of film, depending on the color being digitized. Blue is the slowest due to idiosynchrocies of CCD-chip technology (75). Scan times

ClearCorrect Exhibit 1002, Page 2064 of 3373

are further slowed by filtering the data at input to the computer rather than recording all of the input.

The digitizer hardware drive and the camera control software were both obtained from Eikonix Corporation. Additional programs for camera control were developed by the Department of Orthodontics at the University of Minnesota.

The digitizer precision is within 1/20 pixel (0.37 microns) between pixels and better than 1 pixel (7.5 microns) across the full diagonal (72). Its repeatability has been shown to be $\pm$ 1/2 pixel. For a 10-mm diameter image, a typical large tooth size, the 4096 x 4096 resolution gives a limiting image acquisition resolution of 2.44 microns. (Appendix 2 gives a discussion of errors, sources of errors, and the implications of those errors on probability of producing quality restcrations.)

Experiments conducted with 16-mm film format used a lens system consisting of a Tamron MC Teleconverter (2x), 120 mm of extender tubes, and a Micrc-Nikkor 105 mm lens (2:2.8). An optical grid with 1-mm by 1- mm spacing (Rolyn Optics part 70.0275) was placed in the field of view. With this lens system, a total of 382 pixels between grid markers was measured, yielding a total of 2.6 microns of actual movements in space, essentially varifying the theoretical resolution.

Some special problems are related to digitizing at very high resolutions. The first relates to vibration and

ClearCorrect Exhibit 1002, Page 2065 of 3373

movement of the camera as it moves form one scan line to the next, especially when a very long lens arrangement is required. Without any modification, pixel positions varied dramatically for repeated scans of the same frame of film (by up to 10 pixels). By adding a fixture which ties the lens system to the camera support column, the variation is reduced to 1/2 pixel (see Figure 16).

Another problem (blooming) is implicit in CCD camera technology. Blooming is defined as a phenomenon whereby streaks fan out in the image around an area of intense illumination. Blooming occurs when excess charge in a sensor cell overflows into neighborlng CCD registers (38). This phenomenon is particulary bothersome in areas of high contrast, which, unfortunately, occurs most often around edges.

6.2 DATA ANALYSIS AND IMAGE PROCESSING

After data has been acquired and digitized, it must be manipulated, creating a restoration design which can then be fabricated. This process requires first that the stereophotogrammetric data be analyzed to reconstruct the three-dimensional surface information defining the teeth.

A patient needs a restoration because normal tooth structure has been destroyed (through decay or fracture usually). It is unlikely, then, that sufficient surface

ClearCorrect Exhibit 1002, Page 2066 of 3373

data about the original morphology of the tooth needing the restoration remains when the patient arrives in the dental office. Yet restorations that are placed must preserve the original anatomy of the tooth, providing cusps, grooves, and fossae in their original relative positions. That is, all mandibular first molar full crown restorations, for instance, have five cusps, three buccal and two lingual, a central groove which crosses both the mesial and distal marginal ridges, etc. Since it is unlikely that this morphology data will always be available directly from the patient, a data base of ideal tooth forms was created. It contains the ideal morphology. Specifics for cusp height and contour, width, and depth of fossae must be determined from data unique for each patient and extracted from the stereo images.

First the three-dimensional surface must be reconstructed. This requires that edges be found and that the auto correspondence and disparity problem be solved. A data base of ideal tooth forms has been found, forming the foundation of the design for the final unique tooth form. An artificial intelligence program contains the required tooth to tooth relationships. That data, together with the ideal tooth forms is used by the CAD/CAM software to design the restoration. When the design is complete, fabrication begins. Each of these elements is discussed separately in the next sections.

ClearCorrect Exhibit 1002, Page 2067 of 3373

6.2.1 Three-Dimensional Surface Reconstruction

After the stereo pairs have been digitized, a three-dimensional representation of the surface imaged in those pairs can be reconstructed. The photographic basis for stereoscopy can be found in the principles of image displacement and stereoscopic parallax (73). The change in position of an image from one photograph to another caused by motion of the camera (or object) is defined as stereoscopic parallax or disparity. It is the apparent displacement of the position of an object, with respect to a frame of reference, caused by a shift in the position of the observer (in this case a camera). Differential disparity is the element that is used to determine elevations of surfaces (see reference 83 for a detailed description). If corresponding points in the images can be found and image acquisition geometry is known, the depth of the points can be determined. When combined with planar x,y coordinates, the depth map provides a complete three-dimensional representation of the surface.

Matching performance is improved if features are used to establish the matches rather than itensity values over the whole surface (176). One approach to automate stereomapping is based on applying a set of edge operators, having a range of sizes, to the image; matching first coarse and then progressively finer resolutions (83).

ClearCorrect Exhibit 1002, Page 2068 of 3373

After matching has been completed, the stereo reconstruction can begin. For the automated system for dental restorations, a unique combination of stereophotogrammetry and structured light have been integrated into the data acquisition system. With this combination, two images are essentially contained in each stereo view. The structured light (and the projected grid) add apparent features to the images. Additionally, the underlying image can also be detected. The traditional stereo image information is used to extract information about the margin. Because the margin is continuous, without interruption in the image, it can be reconstructed with high precision.

The structured light image is used to extract data defining the remaining surfaces, away from the margins. These require less precise reconstruction, without compromising the quality of the final restoration fit. In both cases, data is extracted by first filtering the raw data to find the edges (either the margins directly or the grid pattern). The edges are found using the Canny algorithm which is described in detail in the next section. The descriptions of auto-correspondence and disparity algorithms and of the surface reconstruction then follow.

ClearCorrect Exhibit 1002, Page 2069 of 3373

6.2.1.1 CANNY EDGE FINDING. Both smoothed local symmetries and the computation of three-dimensional shape from two-dimensional contours depend on the availability of good edge data. An early implementation of smoothed local symmetries used the difference of Gaussians operator proposed by Marr and Hildreth (131). That algorithm, however, is highly susceptible to noise. The set of zero-crossings varies considerable with noise as does the contour tangent directions determined by it.

Canny (39 and 40) made noise a central concern in his investigation of edge finding. He has created what is generally proported to be one of the best performing variations of the many proposed zero-cossing implementations (76). He uses the calculus of variations to derive an operator from a precise formulation of detection and localization; finding that the optimal shape is (approximately) the first derivative of a Gaussian (30). The edge finder is directional. In one dimension, it optimizes the product of a measure of detectability of an edge (signal to noise ratio and the requirement of a single response to a single step) and a measure of localization (the variance in the position of a zero crossing). Specifically, Canny sets the following criterion:

ClearCorrect Exhibit 1002, Page 2070 of 3373

1. Good detection (no false positives or negatives): There should be a low probability of failing to detect a real edge point, and low probability of falsely marking an edge point. This criterion corresponds to maximizing signal to noise ratio (SNR).

2. Good localization: The points marked as edges by the operator must be as close as possible to the center of the true edge.

3. One response to one edge: This is implicitly captured in the first criterion since when two nearby operators respond to the same edge one of them must be considered to have marked a false positive.

Signal to noise is frequently used as the design criterion for an optimal detector. However, the ability of the edge detector to localize an edge is often either ignored or only indirectly treated (30). Canny's derivation consists of three steps. First, the design is restricted to one-dimensional linear operators. A closed form solution is found to the variational problem of finding a filter "f" that maximizes the product of measures of detection and localization. The optimal filter is approximated by (but is not exactly) the first derivative of a Gaussian. Second, the optimal iinear operators are combined non-linearly in a way that is again optimal with respect to the criteria of detection and localization.

ClearCorrect Exhibit 1002, Page 2071 of 3373

Finally, the edge points output from the non-linear detector are processed by a line-following procedure which assigns labels to the segments of contour and to each segment a set of parameters that describe the type of edge transition (amplitude of the step, uncertainty in amplitude, and uncertainty in position).

The impulse response of the desired operator can be represented by the function f(x). Attention is restricted to antisymmetric functions "f". This is because an arbitrary function can always be split into symmetric and antisymmetric components. The symmetric component adds nothing to detector or localization; it does contribute to the noise components that affect both.

The amplitude of a step can be given by A and the amplitude has a mean-squared noise of n_o^2. The input signal I(x), then, can be represented by (39):

$$I(x) = A\, u\,(x) + n(x)$$

with $n_o^2 = \langle n^2(x) \rangle$ for all x. Then the output of the convolution of the signal with f is given by the convolution integral:

$$\int I(\tau)\ f(x - \tau)\ d$$

The output SNR Ξ is defined as the quotient of the output due solely to the step input and the root mean squared response to the noise component of the signal:

$$\Xi = \frac{A \int_{-\infty}^{0} f(x)\, dx}{n_o \left[\int_{-\infty}^{\infty} f^2(x)\, dx\right]^{1/2}}$$

To formulate a localization criterion, the uncertainty

ClearCorrect Exhibit 1002, Page 2072 of 3373

in the position of the edge is defined to be the standard deviation in the distance of the position of the output maximum from the origin (the true position of the edge). At the maximum, there is a corresponding zero-crossing in the derivative of the output. By the derivative theorem for convolutions, the position x of the zero-crossing corresponds to the position of the zero-crossing in the output of the convolution of the signal with their first derivative f' of the function f(x). The variance of the zero-crossing is given by:

$$\langle x_o^2 \rangle = \frac{\int_{-\infty}^{\infty} n_o^2 f'(x)^2 dx}{A^2 f'(o)^2} \cdot (\delta x_o^2)$$

Since localization improves as the variance of x decreases, the localization criterion is defined as the reciprocal of δx_o:

$$\Gamma = \frac{A \quad f'(o)}{n_o [\int_{-\infty}^{\infty} f'(x) \, dx \,]^{1/2}}$$

Having developed criteria for detection and localization, the problem arises of combining them. Canny elects to use the product of the two. This choice is somewhat arbitrary, but has the property of being invariant under changes of scale or amplitude. The product is given by:

$$\Xi \Gamma = \frac{A \int_{-\infty}^{0} f(x)dx}{n_o [\int_{-\infty}^{\infty} f^2(x)dx]^{1/2}} \frac{A \quad f'(o)}{n_o [\int_{-\infty}^{\infty} f'(x)dx]^{1/2}}$$

If x is replaced by x/w (a change of scale), where w is a space constant which describes the "width" of the

ClearCorrect Exhibit 1002, Page 2073 of 3373

function f, there is no affect in the value of the expression for $\Xi\Gamma$. But the relative contributions from SNR and localization does change. The width of the operator determines the tradeoff in output SNR versus localization. A narrow operator gives better localization but poorer SNR. To handle variations in the SNR in the image, operators of several widths are used. Where several operators respond to the same edge, the operator with the lowest width is selected, giving the best localization while preserving an acceptable SNR.

The problem of maximizing the product $\Xi\Gamma$ can be posed as a variational problem with general solution of the form:

$$f(x) = a_1 \exp(\alpha x) \sin \omega x + a_2 \exp(\alpha x) \cos \omega x + a_3 \exp(-\alpha x) \sin \omega x + a_4 \exp(-\alpha x) \cos \omega x + c$$

subject to the boundary conditions:

$$f(0) = 0 \qquad f(-W) = 0 \qquad f''(0) = s \qquad \text{and } f''(-W) = 0$$

where s is an unknown constant equal to the slope of the function "f" at the origin. The form of this function suggests that is could be approximated by a first derivative of a Gaussian (G') where:

$$G(x) = \exp[-x^2 / 2\sigma^2]$$

The major reason for this approximation is the efficient ways to compute the two dimensonal extension of the filter if it can be represented as some derivative of a Gaussian.

ClearCorrect Exhibit 1002, Page 2074 of 3373

The automatic switching between operators requires local estimation of the noise energy in the operator outputs. This is difficult because there is little information available at the operator outputs to indicate whether a response is due to an edge or to noise. Canny has developed a scheme that uses a model of an edge to predict the response of each operator. He then removes responses of this type to leave the response due to noise only. The noise estimation is done from the outputs of the operators rather than directly from the image.

In two dimensions, an edge also has an orientation which is normal to the contour that the edge defines in two dimensions. To detect edges of a particular orientation, a two-dimensional mask for this orientation is created by convolving a linear edge operator aligned with the edge direction with a projection operator normal to the edge direction. A substantial savings in computational effort is possible if the projection operator is a Gaussian and the same as the Gaussian used in the edge direction. It is possible to create such operators by first convolving the image with a symmetric two-dimensional Gaussian and then differentiating in the direction of the edge.

After the image has been convolved with a symmetric Gaussian, the edge direction is estimated from the gradient of the smoothed image intensity surface. The gradient magnitude is then non-maximum suppressed in that direction. The directional non-maximum suppression is

ClearCorrect Exhibit 1002, Page 2075 of 3373

equivalent to the application of the following non-linear differential operator:

$$\nabla f \cdot \nabla(\nabla f \cdot \nabla f) = 0$$

This operator locates zero-crossings in the second derivative in the edge direction. The dot product of the second term with f gives the component of the second term in the gradient direction. The second term is the gradient of the squared slope. The zero value implies a maximum or minimum in the slope itself.

It is interesting to compare the performance of the Canny operator with the Laplacian. The two-dimensional Laplacian can be decomposed into components of second derivatives in two arbitrary orthogonal directions. If one of the derivatives is in the direction of the principal gradient, the operator output will contain one contribution that is essentially the same as the operator described above, and also one from a detector that is aligned with the direction of the edge contour. The second component contributes nothing to localization or detection and is worse by $\sqrt{2}$ in localization and detection than the Canny operator.

Stereo pairs of digital images were subjected to the Canny edge finding algorithm (installed in the Sun Workstation in the Artifical Intelligence Laboratory of the Department of Computer Science at the University of

ClearCorrect Exhibit 1002, Page 2076 of 3373

Minnesota). Filter width of 2, space constant sigma of 2.5, and threshold of 1.0 where used. Only a single width has been applied since Canny has shown that most features are detected at the finest scale and relatively few are added from coarser scales (39). Figures 12 and 13 are the original stereo pairs. Figures 17 and 18 are the set of images after the Canny edge finding algorithm is applied. Since only edges are found (in this case grating lines and preparation margins), the image is binary.

After edges have been identified, a stereo pair of binary images exists. These images are then used to recreate the surface of the thooth. The first step in that process is to automatically solve the 1:1 correspondence problem and then to establish the disparity between points in the two halves of the stereo pair.

6.2.1.1 AUTO CORRESPONDENCE AND DISPARITY. One of the major challenges in all stereo reconstruction techniques is to establish unambiguous, accurate correspondence between points in the two halves of the stereo paris of images. A number of attempts have recently been made to solve this problem. Smoothness has been used as an important matching constraint. Smoothness suggests the continuity rule which stipulates that image points that are near to each other are projections of three-dimensional points that are close to each other (162). Since depth usually varies smoothly

ClearCorrect Exhibit 1002, Page 2077 of 3373

across a surface, the disparity given by correct matches should also vary smoothly except at surface boundaries or edges (79,130). This general property has been translated into a number of specific constraints used in matching algorithms, including continuity (130), figural continuity (16, 134), disparity gradient limit (17, 37, 115), stereo correspondence equation systems (46) and coherence (162).

The technique integrated into the system to automate production of dental restorations capitalizes on two basic principles: smoothness and analyticity. The two are somewhat similar. Smoothness or continuity suggest that depth changes smoothly over a surface and is discontinuous at edges. Analyticity suggests that any line describing the surface is fairly well behaved and derivatives, at least to second order, exist over the surface (81). Unfortunately, rarely will images provide views of surfaces which meet these criterion over the entire image.

The principal of coherence, as defined by Prazdny (162) states: "A discontinuous disparity field may be a superimposition of several interlaced continuous disparity fields, each corresponding to a piecewise smooth surface." That is, disparity (and therefore depth) can be modeled as overlapping analytic regions with singularities at opaque occluding boundaries or sharp changes in orientation. This property of piecewise analyticity of disparity permits examination of a small neighborhood of an image point.

ClearCorrect Exhibit 1002, Page 2078 of 3373

Thus, the disparity field can be represented as pieces. The piecewise analyticity of disparity permits description of the transformation of a neighborhood in one image into its corresponding neighborhood in the other half of the stereo pair. If one defines neighborhoods which are sufficiently small, any surface can be considered to be locally planar. The disparity, then, can also be modeled as locally planar.

The objective is to define the disparity for small neighborhoods in the left image of a stereo pair and to relate to local image deformations and underlying surface structure. The images are obtained with a parallel optic axis and coincident images planes (see Figure 19). The focal point of the left camera (with center at x_L, y_L) is at the origin; the right camera (with center at x_R, y_R) is displaced (along the x axis) by an amount B. (Upper case variables represent world coordinates; lower case is used for image coordinates.)

A single point in (X,Y,Z) coordinates projects to:.

$$(x_L, y_L) = (X/Z, Y/Z) \qquad (x_R, y_R) = ([X + B]/Z, Y/Z)$$

This yields equations for horizontal and vertical disparity (relative to the left image coordinates) of:

$$\text{disparity} = (x_R - x_L) = B/[Z\,(x_L - y_L)]$$

Because of the geometry from which the images are obtained, there can be no shift in the vertical plane of the image. The coordinates of the centers of the two

ClearCorrect Exhibit 1002, Page 2079 of 3373

images can only shift along the horizontal axis. That is, the epipolar alignment is preserved. The importance of this alignment is that it reduces the search required to find matching points from a two-dimensional problem to a one-dimensional problem. Thus, to find a match for a point along one epipolar line in one image it is only necessary to search along the corresponding epipolar line in the other image (27). Furthermore, it ensures that for any given point in one image, we can determine a line segment in the other that must contain the point (unless it is occluded from view by other points on the three-dimensional scan line.

Each neighborhood independently undergoes a search for the disparity that best fits a subset of the zero-crossing matches in the neighborhood. A neighborhood in the left image is positioned over the right image at each possible disparity offset, and those zero-crossing matches that are closest to this constant disparity, and do not differ from the constant disparity by more than a threshold, are accepted.

A square window is selected in one half of the image pair (the left half). The window size is set interactively; current values is set at 5 x 5 pixels with an image resolution of 256 x 256 pixels. The initial position of the window is set at address (0,0) at the upper left hand corner of the window. A second window is set in the right half of the stereo pair. It is of identical size

ClearCorrect Exhibit 1002, Page 2080 of 3373

to the window in the left half. The values and patterns of the light intensity with the windows are compared. If they match, the windows in the left image advances by 1 pixel in the horizontal direction and the process begins again.

If the values of the light intensity do not match, the right window advances sequentially one pixel at a time. At each position, the match of the light intensities is checked. When a match is found, the left window advances by 1 pixel in the horizontal direction and the process begins again. (Figure 20 gives a flow chart of the steps in the matching process.)

Two attributes are used to evaluate the existance and quality of a match: angle threshold and maximum disparity. The edge pixels within each window are used to form a best fit line. The angle of that line should be similar in both halves of the image pair. If the angle between the two lines being considered as a potential match is above a specified threshold, no match is defined to have occurred. The current threshold is set at 30 degrees.

The second criterion (maximum disparity) is also imposed to ensure that a valid match has occurred. Since the images now consist of binary images of edges (the grid and the margin of the prepared tooth) and non-edges, the nth edge marker in the right half of the pair should be the displaced equivalent of the nth edge mark in the left half of the image pair. Furthermore, the disparity from one half of the image to the other should be within a threshold

ClearCorrect Exhibit 1002, Page 2081 of 3373

limit (because the surface is continuous). If it exceeds that threshold, it is defined to not be a match. The current theshold for disparity shift maximum is 9 pixels.

If a match is not found, the right window advances sequentially one pixel at a time. At each position, the possibilities of matches is checked. When a match is found, the left window shifts and the process begins again.

The output of this stage is a disparity map D(i,j) where shift of the contour line/gird line from the left image to the right image is defined as disparity. It, in fact, gives right side edge position in left side coordinates. Since the epipolar constraint has been applied, the only shift/disparity that can occur is in the horizontal direction.

Since surfaces are assumed to be smooth, except at discontinuities, the configuration of the tooth surface which lies between grid lines is assumed to be smooth. The expection (in keeping with piecewise analyticity in neighborhoods assumption and shown by Duncan in (59)) is that the surface change is linear. Thus, the disparity between grid lines is calculated using the slope between the two proximal grid lines, giving:

$$D(l,m) = (l-i)[D(i+1,j)-D(i,j)]/n$$

where:

l,m are pixel addresses where grids do not fall

i,j are x,y position of adjacent grid lines

ClearCorrect Exhibit 1002, Page 2082 of 3373

n is the number of pixels between proximal grid lines $n = x(j+1) - x(j)$

The margins are the most critical element of the restoration, requiring the greatest degree of precision in data and three-dimensional reconstruction. The margins are found with the Canny edge finding algorithms then reconstructed separately for each pixel.

6.2.1.3 3-D SURFACE RECONSTRUCTION. Based on the geometry from which stereo image pairs are obtained, depth is proportional to the inverse of the disparity. Thus:

$$z = H - k/D = H - (B\ f)/D$$

where H is the distance from the object to the focal point of the lens system of the data acquisition device, k is a function of the lens focal length (f) and (B), the separation of the images along the baseline between the two camera positions. D is the disparity value obtained from the 1:1 correspondence solution technique described in the previous section.

The values of H, B, and f are known for the data acquisition system. So the entire surface can be reconstructed. The x,y values are the values in the left image pair. For each x,y, the associated z value is obtained from the disparity value.

ClearCorrect Exhibit 1002, Page 2083 of 3373

As expected, the output of the reconstruction contains noise. The noise can be filtered out, again calling upon the assumptions of a smooth surface. The smoothing algorithm applied assumes that within the surface area there will be no sudden changes in surface height. Thus, if the depth of the image at any pixel is greater than some theshold value different from that of its eight surrounding neighboring pixels, the depth value is replaced with the average value of the neighboring pixels. The filtering process is iterative and continues until no depth difference is greater than the threshold value or 25 iterations have been performed. For current development, a threshold of three units has been used.

Figure 21a is the noisey 3-D surface reconstructed from the images is Figure 17 and 18. After successive iterations, the smooth surface can be retrieved (see Figures 21b-f).

6.2.2 Data Base of Ideal Tooth Forms

A data base containing the ideal morphology of each tooth has been created. Each of the fourteen unique tooth forms were digitized. The tooth forms used were plaster models used to teach dental morphology to first year dental students at the University of Minnesota. They were created by and are available from Dr. Fred Nobel, Department of

ClearCorrect Exhibit 1002, Page 2084 of 3373

Operative Dentistry, University of Minnesota. Third molars (wisdom teeth) were not digitized or included since they (1) are often congenitally missing, (2) often are extracted, and (3) are rarely in occlusion and, hence, do not contribute to normal function and are only rarely restorated.

A mechanical contact digitizer was used to create the data base. Models of each tooth (at 2.5 times scale) were digitized with a three-dimensional surface digitizer (CAMSCAN) made available by CAMAX Corporation (Minneapolis, MN). (See Figures 22 and 23.) The three-dimensional coordinates of each point were recorded to 0.0002 inch (0.005 mm) accuracy and written to a PDP 11/23 computer and then to magnetic tape.

The raw data files were converted to a format acceptable to the computers and graphic equipment available in the Mechanical Engineering Department at the University of Minnesota. The data base coordinates were transferred to a VAX 11/70. The data files were filtered using Fortran programs for the Vax in conjunction with the Evans and Sutherland PS300 to remove obviously noisey points, usually resulting from difficulty in controlling the pointer of the digitizer as it crossed from the top to the sides of the teeth. Subsequent filtering was also done to eliminate unncessary points; when three points lie on a straight line, for instance, the middle one can be eliminated without loosing any data. Filtering was also

ClearCorrect Exhibit 1002, Page 2085 of 3373

done to eliminate points which doubled back on themselves or created excessively sharp peaks.

Bicubic uniform B-splines with multiple knots for the boundaries are used to approximate the surface (22 and 198). This provides a number of possibilities. First, the B-spline geometry ensures continuity of the surface without sudden changes (to second order derivatives). This property is important from two aspects. It ensures aesthetics and facilitates subsequent machining. Traditionally produced dental restorations are smooth and continuous. All external surfaces can be polished with round burrs (they are blended surfaces). Thus, there are no sharp points on the surface. These aesthetics are preserved with the B-spline representation.

When machining begins, it is important to avoid sudden accelerations. Otherwise machine tools are damaged or broken, workpiece materials are gouged or torn, or the machine can be damaged. By ensuring continuity to second order derivatives over the entire surface, these problems can be eliminated.

The data files defining the configuration of the mandibular first molar concisors are described by just over 6,000 data points. Lower central incisors contain approximately 4,000 data points. Figure 24 is an example of the configuration of a tooth as recorded in the data base.

ClearCorrect Exhibit 1002, Page 2086 of 3373

6.2.3 Artificial Intelligence for Occlusion

Static and dynamic occlusal contact relationships (centric occlusion, working and balancing occlusion, and protrusion) were incorporated into a data base for an expert system for occlusion. The data base was created with TurboProlog on an IBM-PC-AT with 20 MBytes memory. Contact points between teeth and paths of motion of contacting cusps as they move in funciton are included in the data. When queried, the system identifies all contacts and motion paths for any specified tooth and motion combination. To date, no graphical output has yet been included nor has it yet been integrated into the sofware of the CAD/CAM system. Figure 25 - 27 show examples of the sequential screen responses to menu-selected options.

6.3 CAD/CAM

After three-dimensional surface reconstruction of the patient data is complete, the restoration design process can begin. The CAD/CAM software manipulates the surfaces, creating a restoration which fits into the space available. The internal configuration of the restoration is determined directly from the three-dimensional configuration of the prepared tooth. The external surface is manipulated to

ClearCorrect Exhibit 1002, Page 2087 of 3373

meet the space available in the patient's mouth. Each surface can be described as a series of points on a scan or profile line plus a series of profile lines at different increments. Thus, each scan line functions as a planar projection of the three-dimensional surface.

When the surface is complete, it is divided into segments so that undercuts (and their associated interferences) can be avoided. Three segments are defined: (1) the prepared tooth , (2) the external occlusal surface and sides of the restoration to the crests of convexity (the two maximum horizontal points in any given scan line), and (3) the external surface below the crest of convexity and the internal surface.

The CAD/CAM package selected for early development was CAMAX's CAMAND program which was installed and operating on a Silicon Graphics 1R1S 2400 in the Department of Mechanical Engineering at the University of Minnesota. This software was selected because of it availability and its capability of managing complex surfaces.

As work progressed, however, limitations were found for the dental application. In particular, the commands to offset the cutter were not capable of handling the scale and thinness of the dental restoration margins and would cut parts of them away as subsequent areas were cut.

A custom CAD/CAM package was developed. Work was done on a Silicone Graphics 2400 Turbo Iris Workstation. Figure 28 is a flow chart summarizing the capabilities of

ClearCorrect Exhibit 1002, Page 2088 of 3373

the software; Table 5 is a compilation of CAD/CAM options.

The CAD/CAM system is interactive system with pop-down menues. It consists of a main menu as well as an editor, surface generator, and shading routines. Commands can be entered with either by keyboard or mouse. The software can directly access data files with raw surface data points given as x, y, z coordinates with format of the following form:

P 1.234e01, 2.345e-01, 3.456e03

L 1.000e00, 2.000e00, 2.341e-01

were P indicates the beginning of a new profile line and L indicates a point within the profile line. Each profile line must have the same number of data point in each scan line.

Surface patches are created using uniform B-spline parametric curves in two directions (22 and 198). Offset for the machine tool and tool diameter is set interactively. Gouging checks are made automatically. An output file readable by a milling machine is created by the system. The cutter path command files are stored on floppy discs. Those files are transferred from the Mechanic Engineering Vax to an IBM PC driving the mill.

ClearCorrect Exhibit 1002, Page 2089 of 3373

Table 5. CAD/CAM Options

Options	Comments
Main Menu	
Surface	
B-spline surface	
Uniform	Uniform distance between points multiple knots or periodic basis function
Non-uniform	Not yet implemented
Non-uniform rational	Not yet implemented
Multiple knots	Multiple knots for boundary conditions
Periodic basis function	Normalized basis function applied to entire surface
No. of u direction interpoiated patches	Patches in horizontal of surface control vertices
No. of v direction interpolated patches	Patches in vertical of surface control vertices
Reverse	
Add symmetrical vertices	Adds symmetrical vertices at ends of control vertices (passed via periodic basis function)
Free ends with multiple knots	
Given tangent with multiple knots	Enter tangent values at ends
Hermite Surface	
Free end condition	
Parabolic end condition	
No. of u direction interpolated patches	
No. of v direction interpolated patches	
Offset	
Normal vector	Offset in direction of normal vector
Shifting	Shift tool in z-direction to prevent gouging
Return	
Miscellaneous	
Clock off	Toggle clock on/off
Alarm off	Toggle alarm on/off
Digital on	Toggle digital clock on/off
Reshape clock	Change clock position and size
Bell off	Toggle bell sound on/off
Text port on	Toggle Iris test port on/off

ClearCorrect Exhibit 1002, Page 2090 of 3373

Table 5. CAD/CAM Options - continued

Options	Comments
Window	
Zoom in	Uses mouse to change scale on screen
Zoom out	Uses mouse to change scale on screen
Pan	Pick center of new screen
View	
Rotate X-axis	Rotation angle entered interactively
Rotate Y-axis	Rotation angle entered interactively
Rotate Z-axis	Rctation angle entered interactively
X-view	View looking into +x axis
Y-view	View looking into +y axis
Z-view	View looking into +z axis
Status	
All data file	All data activated including data to be deleted (pink) and hidden (blue)
Current data file	All data except that to be deleted or that is hidden
Include deleted data	Activates deleted data
Include hidden data	Activates hidden data
Points on	Toggles data points on/off -
Grid on	Toggles display grid on/off, perpendicular to locked axis - useful for entering and grid size entered interactively
Lock x-axis	Locks x-axis, permitting editing of displayed data points with 2-D curser
Lock y-axis	Locks y-axis, see above
Lock z-axis	Lccks z-axis, see above
Hide	
Point	
Object	
Group	
Recover Point	Requires hidden data option be selected
Recover Object	Requires hidden data option be selected

ClearCorrect Exhibit 1002, Page 2091 of 3373

Table 5. CAD/CAM Options - continued

Options		Comments
	Recover Group	Requires hidden data option be selected
	Recover all points in group	Recovers all hidden points of group
	Recover all groups in object	Recovers all hidden groups of object
Delete		
	Point	
	Object	
	Group	
	Delete Point	Requires delete data option be selected
	Delete Object	Requires delete data option be selected
	Delete Group	Requires delete data option be selected
	Delete all points in group	Deletes all delete points of group
	Delete all groups in object	Deletes all delete groups of object
Repaint		
	Current status	Redraws the data
	Points	Draws data points (with polnts option in status in either
Grids		
	Clear screen	
Shade		
Miscellaneous		
	Ciock off	Toggle clock on/off
	Alarm off	Toggle alarm on/off
	Digital on	Toggle digital clock on/off
	Reshape clock	Change clock position and size
	Bell off	Toggle bell sound on/off
	Text port on	Toggle lris test port on/off
la		Constant controlling shading
ll		Constant controlling shading

ClearCorrect Exhibit 1002, Page 2092 of 3373

Table 5. CAD/CAM Options - continued

Options		Comments
	d	Constant controlling shading
	K	Constant controlling shading
	Ks	Constant controlling shading
	n	Constant controlling shading
	Kd	Constant controlling shading
	Ka	Constant controlling shading
	Lowest light intensity	Values between 0.0 and 1.0 permitted, 0.35 recommended
	Sight	Display current unit vector of sight, interactively supply coordinates of eye position relative to origin
	Light	Display current unit vector of light, interactively supply coordinates of light position relative to origin
	Save	Save coordinates of light source and look-up table values
	Shade	
	Return	
Edit		for editing current data
	Mlscellaneous	
	Clock off	Toggle clock on/off
	Alarm off	Toggle alarm on/off
	Digital on	Toggle digital clock on/off
	Reshape clock	Change clock position and size
	Text port on	Toggle iris test port on/off
	Window	
	Zoom in	Uses mouse to change scale on screen
	Zoom out	Uses mouse to change scale on screen
	Pan	Pick center of new screen
	View	
	Rotate X-axis	Rotation angle entered interactlvely
	Rotate Y-axis	Rotation angle entered interactively

ClearCorrect Exhibit 1002, Page 2093 of 3373

Table 5. CAD/CAM Options - continued

Options		Comments
	Rotate Z-axis	Rotation angle entered interactively
	X-view	View looking into +x axis
	Y-view	View looking into +y axis
	Z-view	View looking into +z axis
Status		
	All data fiie	All data activated including data to be deleted (plnk) and hidden (blue)
	Current data file	All data except that to be deleted or that is hidden
	lnclude deleted data	Activates deleted data
	lnclude hidden data	Activates hidden data
	Points on	Toggles data points on/off - data points shown in white
	Grid on	Toggles display grid on/off, perpendicular to locked axis - useful for entering data points. Seed point and grid size entered interactively
	Lock x-axis	Locks x-axis, permitting editing of displayed data points with 2-D curser
	Lock y-axis	Locks y-axis, see above
	Lock z-axis	Locks z-axis, see above
Hide		
	Point	
	Object	
	Group	
	Recover Point	Requires hidden data option be selected
	Recover Object	Requires hidden data option be selected
	Recover Group	Requires hidden data option be selected
	Recover all points in group	Recovers all hidden points of group

ClearCorrect Exhibit 1002, Page 2094 of 3373

Table 5. CAD/CAM Options - continued

Options	Comments
Delete	
Point	
Object	
Group	
Delete Point	Requires delete data option be selected
Delete Object	Requires delete data option be selected
Delete Group	Requires delete data option be selected
Delete all points in group	Deletes all delete points of group
Recover all groups in object	Recovers all delete groups of object
Repaint	
Current status	Redraws the data
Points	Draws data points (with points option in status in either toggle position - see above)
Grids	
Clear screen	
Edit	
Move point	Maximum of 30 successive positions can be saved
Recover moved point	Recovers most recent position
Append point	Append current data point
Append points after	Appends until menu is terminated, Grid must be turned ON
Copy point	
Break line	Separates group into two groups
Data	
Squeeze	All deleted data cleared from memory buffer, cannot recover after squeeze actively
Average y	Average y coordinate value for selected group
Scale	Permanently changes data
Translate	Permanently changes data coords
Rotate	Permanently changes data coords
Return	Return to main menu

ClearCorrect Exhibit 1002, Page 2095 of 3373

Table 5. CAD/CAM Options - continued

Options	Comments
Quit	
Save data	Requires Output file is open
Divide data	Save data in file after current object is divided into two parts. Requires Output file be open
Discard Data	Quit without saveing current data
File	
Input data	Opens lnput file
Output data	Opens Output file
Dyna input data	Opens Dyna machine code input file
Dyna output data	Opens Dyna machine code output file

The design of the restoration incorporates information from the three-dimensional reconstruction and form the data base of tooth forms. The internal surface of the restoration is a negative of the prepared tooth and is calculated directly from the reconstruction.

The external three-dimensional surface design is more complicated. The restoration must contact the adjacent teeth. To acocmplish this, the ideal form is scaled so that the mesial-distal distance between proximal teeth matches the distance between contact points of the tooth form in the data base. The scale factor used is simply the ratio of acual mesial-distal length over the mesial-distal length of the ideal form.

The data base contains a local coordinate system, based on maximum height (in the occlusal plane) of the cusp tips. (It also contains the positions of the proximal contacts relative to that local coordinate system.) If a mark is placed on the prepared tooth, a local coordinate system, relative to the prepared tooth can be calculated. Since the two restoration contact point must match the two contact points on the proximal teeth, a transformation from "ideal data base" coordinates to restoration coordinates can be made. With this transformation, the scaled ideal design is superimposed on the prepared tooth configuration.

So the process is:

ClearCorrect Exhibit 1002, Page 2097 of 3373

1. Define C = A X B = A B sin AB for the prepared tooth

$$= \begin{matrix} i & j & k \\ Ax & Ay & Az \\ Bx & By & Bz \end{matrix}$$

$$= (Ay\ Bz - By\ Az)\ i + (Az\ Bx - Bz\ Ax)\ j + (Ax\ By - Bx\ Ay)\ k$$

giving:

$$Cx = Ay\ Bz - By\ Az$$

$$Cy = Az\ Bx - Bz\ Ax$$

$$Cz = Ax\ By - Bx\ Ay$$

2. Define : D = B X C

giving:

$$Dx = By\ Cz - Cy\ Bz$$

$$Dy = Bz\ Cx - Cz\ Bx$$

$$Dz = Bx\ Cy - Cy\ By$$

where A,C,D form a mutually perpendicular right handed coordinate system.

3. Compute the origin:

$$O = (P_1 + P_2 + P_3)/3$$

4. Transform data base tooth (world) coordinates into prepared tooth (local) coordinates:

$$\text{let } r = P_{world} - O$$

then

$$X_t = r \cdot X_{db}$$

$$Y_t = r \cdot Y_{db}$$

$$Z_t = r \cdot Z_{db}$$

$$P_t = [\ x_t\ (P_{t\,db} - O),\ y_t\ (P_{t\,db} - O),\ z_t\ (P_{t\,db} - O)]$$

ClearCorrect Exhibit 1002, Page 2098 of 3373

The ideal tooth form can be truncated at its maximum x dimension (with profile lines aligned with the y axis) (the equivalent of truncating at the crest of convexity). The lower external portion of the restortion can then be designed by taking the perpendicular to the curvature of the internal surface at the margin (in the occlusal direction) and blending that line with the external ideal design (see Figure 29).

When surface design is completed, the surface is divided into three files: (1) fixture, (2) external occlusal surface to the crests of convexity, and (3) external surface below the crests of convexity and the internal surface (including the margins). Cutter paths are generated, based on interactively supplied tool diameter, desired effect, and feed rates (determined by material properties).

Gouging is a potential problem during fabrication of any complex geometry. As a cutter moves, creating a surface, it removes material. It is directed to move through a specified point. However, it has a finite radius in all three dimensions. A vertical offset ensures that the tip removes only the material at the selected point beneath it. However, its radius is operating in a plane parallel to the feed table. If the surface of the workpiece raises faster than the diameter of the cutter diminishes, that material will be removed. If that

ClearCorrect Exhibit 1002, Page 2099 of 3373

material is required to fully describe the surface, its removal is called gouging. In simpler terms, then, gouging is simply an interference between the cutter and the designed part geometry.

In its current configuration, gouging is checked before the cutter paths are used to create command files for the mill. A tool center position of each surface patch is defined. With the tool at that point, the adjacent patches are checked to ensure that no interference with cutter diameter occurs. If interferences exist, the cutter is shifted vertically to eliminate the gouging. This will alter the surface. However, it has been found to be required only on the occlusal surface.

After the gouging check, commands for the milling machine are automatically generated. Specific requirements for the data format and file length are automatically accomplished. The files are then ready for transfer and immediate use with the milling machine.

6.4 FABRICATION

Machining a dental restoration is both a demanding and unique challenge. The goal is to demonstrate that acceptable restorations can routinely be produced by machining in a clinical setting. This goal raises two dental issues: (1) the overall machine tool concept and design must be appropriate for use by dental personnel, and

ClearCorrect Exhibit 1002, Page 2100 of 3373

(2) specific details of operations must assure high quality restorations. The milling process is discussed in the next section. Then details of fixturing and materials investigated are given.

6.4.1 Milling

While the program to control the milling machine is generated automatically by the CAD/CAM system, seemingly mundane tasks like positioning the material to be machined, cutter tool wear, and replacement, and assessing operation performance during machining are also critical to product quality. The machine tool must be easy to set and changes in its performance must be observable and obvious. A typical milling machine configuration was selected for these investigations. In this configuration, the cutting tool position is fixed and the workpiece moves as directed to produce the required geometry. The major advantage of this type is the rigidity of the machine-cutting tool workpiece system, making precision positioning and small tolerances achieveable. The cutter tools are similar to those already in use in general dental practices.

For the feasibility studies, milling is being done on a three-axis Dyna Myte 2000 milling machine (69) driven by an IBM-PC (Figure 30). Because only 900 lines of command code can be uploaded to the Dyna at one time (and each x, y, z position requires three lines of code), the cutter tool

ClearCorrect Exhibit 1002, Page 2101 of 3373

path is broken into a number of separate data files. Each file is written to a floppy disc, and uploaded to the Dyna one file at a time. At this time, it requires approximately 1 hour to cut a restoration and its fixture from wax or aluminum. Of that hour, approximately only 10 minutes is spent in actual cutting; the remainder is upload and data transfer time.

In its current configuration, the precision of the Dyna is not adequate for producing high-quality restorations. The backlash on the feed bed is on the order of 15 to 25 microns in both the x and y directions. It may be possible to substantially improve this value by replacing the servo positioning drives with zero-backlash screw drives.

Servo Systems, Inc. (178) has proposed that their system is substantially more accurate (2.5 microns in positioning repeatability) (See Figure 31.) One of their systems has just arrived in our laboratory; the post processor for the CAD/CAM system (to generate machine controlling files) is currently being developed.

End cutting tools are being used for all cutting. For bulk material removal in areas away from the final restoration, layers of material are removed sequentially. The restoration and its fixturing jig surface are both cut with only a single cut (no rough followed by finishing cuts).

ClearCorrect Exhibit 1002, Page 2102 of 3373

6.4.2 Fixturing

Fixturing is quite simple. A modified vise is attached to the bed of the milling machine to hold the materials. A solid block of material is held with the vise. A special fixture is milled, representing the configuration of the prepared tooth (similar to a die in the lost-wax technique). Then the internal surface of the restoration and the external surface to the heights of contour are milled from another solid block of material.

The partially fabricated restoration is removed from the vise, placed onto the fixture. This preserves the relative orientation between the internal and external surfaces when the final occlusal surface is machined. The partially fabricated restoration is held in place with either dental sticky wax or epoxy. The fixture is held with the vise while the remaining portion of the external surface is cut.

The fixture can also serve as a holding device and can be used during shipping from the lab to the dentist as protection for the margins. This protection is probably not critical for metal crowns but may be very practical for ceramics which are brittle and more susceptible to fracture and cracking.

ClearCorrect Exhibit 1002, Page 2103 of 3373

6.4.3 Materials

An array of materials which have been accepted for use in the human mouth (9-13 and 51) can be machined. These include metals (like gold and semi-precious alloys), ceramics, porcelains, and composites. Preliminary investigations focused on wax and aluminum, simply because of the associated cost factors.

Other materials investigated include K-metal, Dicor and Macor. K-metal, also called technique metal, was developed in 1932 as an alternative to gold for restorations created during the pre-clinical dental technique training program (51). Its material properties are like those of casting gold so the expectation is that it will also machine like gold. It is substantially less expensive than gold. Since it corrodes easily, however, it is not possible to use it for actual restorations but only for refining machining parameters before cutting gold.

Dicor is a dental version of Macor. Macor is a glass-ceramic which lends itself to conventional machining tools and equipment (86). It is different from other ceramics due to its microsructure which consists of an interlocked array of plate-like mica crystals dispersed throughout a glassey matrix. It consists of primarily of silica, magnesium, and aluminum oxides (49).

ClearCorrect Exhibit 1002, Page 2104 of 3373

188. 3M Product Literature, Experimental Laboratory Data specifications for partially stabilized zirconia, Ceramic Materials Department, 3M, St. Paul, MN, June 1985.

189. A.K.I. Torlegard, "State of the Art of Close-Range Photogrammetry" Photogrammetric Engineering and Remote Sensing, 76.

190. J. Unterseher, J. Hansen, B. Schlesinger, Holography Handbook, Ross Books, 1982.

191. A.M. Waxman and J.H. Duncan, "Binocular Image Flows: Steps Toward Stereo-Motion Fusion", IEEE Transactions on PAMI, 8(6), 715-729, 1986.

192. D.J. Wanserski, K.P. Sobszak, J.G. Monaco, G.P. Mcgivney, "An Analysis of Marginal Adapatation of All-Porcelain Facial Margin Ceramo-metal Crowns", Journal of Prosthetic Dentistry, 56(3), 289-291, September 1986.

193. J.A. Webb and J.K. Aggarwal, "Shape and Correspondance, CVGIP, 21, 145-160, 1983.

194. E.J. Weller (ed), Nontraditional Machining Processes Society of Manufacturing Engineers, 1984.

195. P. M. Will and K. S. Pennington, Proceedings, IEEE, 60, 669, 1972.

196. K. W. Wong, "Mathematical Formulation and Digital Analysis in Close Range Photogrammetry", Photogrammetric Engineering and Remote Sensing, 41(11), 1355-1373, November 1975.

197. Y. Yakimovsky and R. Cunningham, "A System for Extracting Three-Dimensional Measurements from a Stereo Pair of TV Cameras", Computer Graphics and Image Processing, 7, 195-210, 1978.

198. X. Xhu, Computer Graphics Notes, University of Minnesota, Summer 1985.

199. G.P. Zientara and L.J. Neuringer, "Medical Imaging for the 21st Century", Perspectives in Computing, 81, 14-24, Spring 1988.

ClearCorrect Exhibit 1002, Page 2105 of 3373

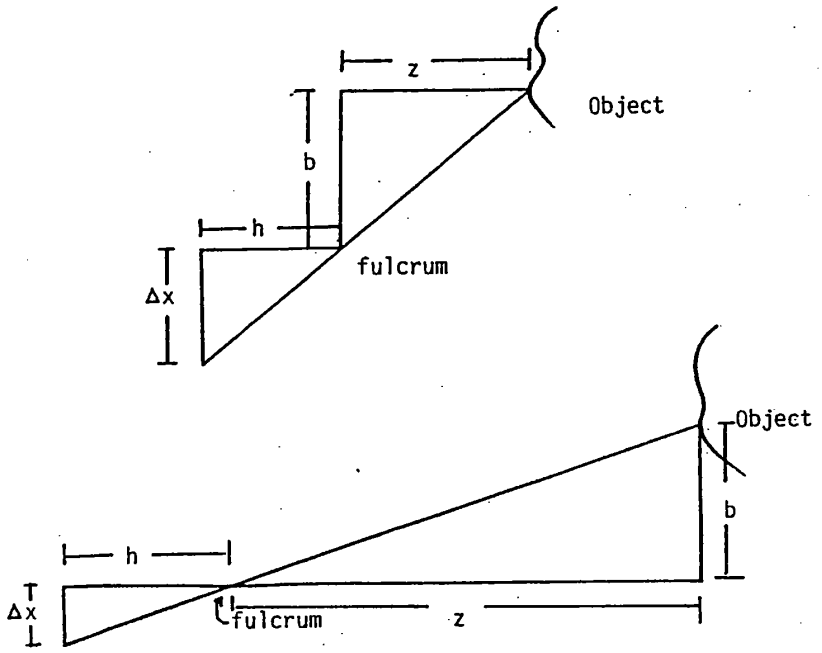


Figure 1. Principles for Triangulation Mensuration

Figure 2. Photographic Image for Test

Figure 3. Raw Digitized Test Image

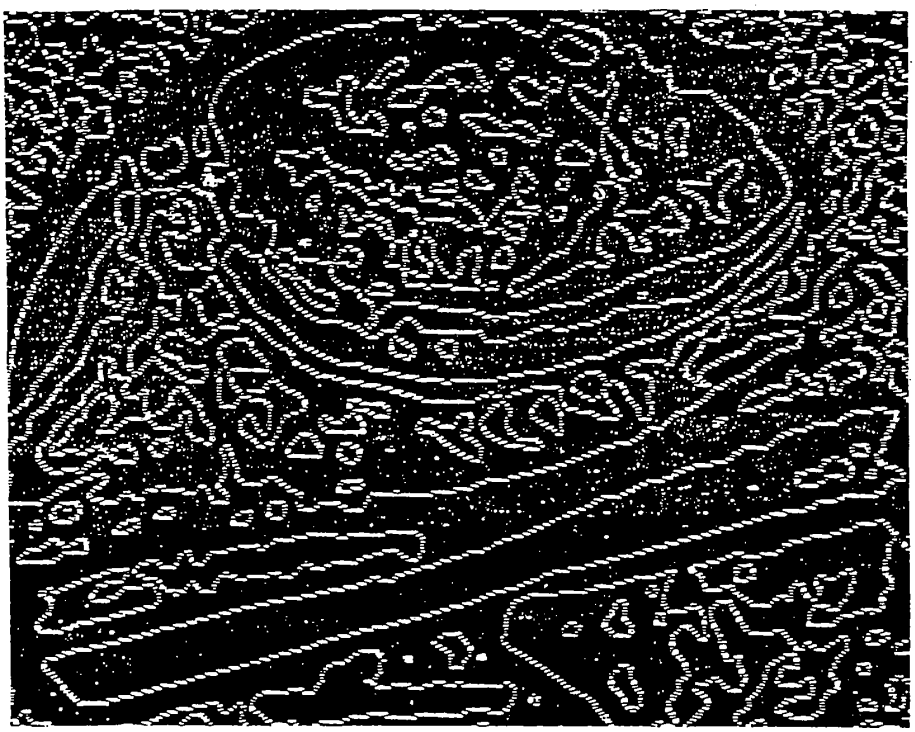


Figure 4. Edges using Marr-Hildreth Algorithm

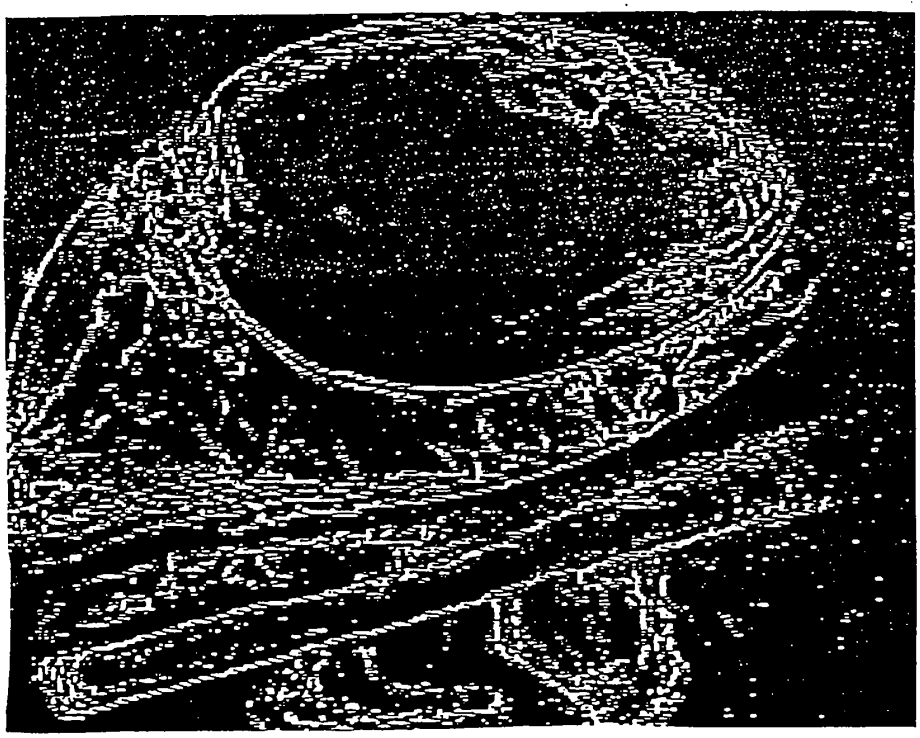


Figure 5. Edges using Haralich Algorithm

The highly interlocked microstructure is the key to Macor's machinability. During machining, as the tool tears its way through the glass-ceramic stock, the interlocking intersections of the randomly oriented crystals stop the microscopic fractures that, in mass, make up the material, stopping the actual cut from propogating through the matrix outside of the localized cutting area. The microscopic fractures are repeately deflected, branched, and blunted - in effect, turned around and arrested.

Since the fractures are localized, Macor glass-ceramic does not sacrifice stength or hardness for the sake of its machinability. Macor's machining characteristics are similar to those of many common metals. It is, however, not a metal and there are special considerations that must be kept in mind when it is subjected to the bite of a tool. It is important that both material and tool be kept cool. In addition to cooling the workpiece, fluid is used to improve the cutting action and trap and wash away the loose powder produced during machining. The powder generated by machining is abrasive so equipment maintenance and cleanliness are important. Because Macor is not resilient, special care must be taken to ensure that loads of fixtures or clamps are evenly distributed.

Macor can be machined to tolerances of 0.0005 inch (49) and polished to 2 microinches (50). Typical machining data includes a cutting speed of 20-35 sfm with spindle speed of 50-60 rpm, chip load of 0.002 inch/tooth, and

ClearCorrect Exhibit 1002, Page 2111 of 3373

depth of cut of 0.150 to 0.200 inch (85). When compared to other materials, it has a machinability index of 25, making it easier to machine than brass (index of 36), more difficult than Teflon (index of 2.5), and much easier than 204 stainless steel (index 229).

Figure 32 is a photograph of a molar restoration fabricated from aluminum. Total cutting time for both the fixture and restoration was just under ten minutes.

6.5 SYSTEM PRECISION AND ACCURACY

System precision and accuracy can be measured directly, establishing the correspondence between an object whose surface configuration has been measured with high precision and one that has been produced by the automated system. Unfortunately, that is a very difficult task to achieve. Further, it produces little insight into the relative magnitudes of errors contributed by component subsystems.

Alternatively, two techniques are possible. One is simply to apply the clinical tests for fit of a restoration produced by the automated system. While this is critical for ultimate successful clincial acceptance of the system and the restorations it produces, it, like the technique proposed above, does not add any insight into error contributions.

ClearCorrect Exhibit 1002, Page 2112 of 3373

A more useful technique is to establish the degree of error of all subsystem components. Since errors are likely to be independent, they will be additive (a worst-case situation). With this data, most likely sources of improvement of product quality become obvious. Based on this argument, the precision and accuracy of each component subsystem was evalutated. Table 6 summarizes the error contribution by subsystem.

Unfortunately the Department of Orthodontics computer system (a DEC 11/44) had a fatal crash before some error contributions could be established. A more modern system is being acquired and installed. This poses some difficulty, however. The Eikonix digitizer interface hardware is peculiar to that hardware. By changing computers, a new driver is needed. Because of changes in Eikonix's interface design, a new digitizer must also be acquired. Consequently, some of the values presented as error contributions are only estimates of actual contributions with the new equipent. Actual contributions will be measured when the new system components are installed.

6.5.1 Data Acquisition

The data acquisition system includes the lens system and the film on which the images are recorded. The lens distortion cannot be evaluated directly since it is

ClearCorrect Exhibit 1002, Page 2113 of 3373

Table 6. Error Contribution by Subsystem

Component Subsystem	Error Contribution (in microns)
Data Acquisition	
Lens System	5 - 25
Film Distortion	3.5 (0.01%)
Digitizer	
Sensor Linearity	0
System Noise	0
Sensor Stability	0
Array Geometry	0.375
Lens Distortion	5 - 25
Overall	2.75
3-D Reconstruction	10
CAD/CAM	0
Milling	
Positioning Error	2.5
NC Module (surface, scalloping)	20
TOTAL:	46 -86 microns

ClearCorrect Exhibit 1002, Page 2114 of 3373

impossible to image directly through the lens to the digitizer. It is possible, however, to look at the total data acquisition-digitizer error. If errors are assumed to be independent (and therefore additive) the contributions from all but the lens can be established and the lens contribution taken as the remainder of that total.

The total lens-film-digitizer error was not established before the computer failed. Lens distoration is assumed to be approximately equivalent to that found with the digitizer lens system (see section 6.5.2.2).

Film distortion values were obtained from Kodak's product literature. Maximum distoration is assumed to be 0.01% (3.5 microns for 35 mm film).

6.5.2 Digitizer

Digitizer precision and accuracy can be broken into radiometric and geometric components. Both are important and may be interconneced (87). For example, nonlinearity in detector response or high levels of system noise, could affect investigations into sensor linearity, noise, and sensor stability. Geometric tests include the array geometry, lens distoration, and overall digitizer performance.

ClearCorrect Exhibit 1002, Page 2115 of 3373

6.5.2.1 SENSOR LINEARITY. In a CCD, pixel illumination is converted to an output voltage by an array of photodiodes and capacitors. The voltage is then converted to a digital value in the range of 0 (black) to 255 (white) by an analog to digital converter. Ideally, the entire conversion process should be linear.

To test this linearity, a Kodak Gray Step Card (log linear to approximately 0.5%) should be imaged under a number of different lighting conditions with a number of different integration times. In the dental application, transmissive lighting is used for digiting, so the gray card should be in slide form. Unfortunately, no slide form exists and it was not possible to locate a Kodak Gray Step Card. In an effort to investigate this linearity, however, a standard gray card (reflectance of 18%, Kodak part No.152-7795) was photographed using a copy stand with Kodak Kodachrome ASA 64 slide film. The slide was processed by a commercial processor (Black's Photos, Minneapolis, MN).

Two test protocals were used. In the first, a number of selected single lines were read at resolution of 4096 by 1 pixels with different exposure levels (integration rates). Additionally, the entire image field was digitized at a 32 times reduction (a resolution of 128 by 128 pixels where every 32nd point and every 32nd line were read). Results fo both are given in Table 7.

ClearCorrect Exhibit 1002, Page 2116 of 3373

Table 7. Gray Level Tests

for Digitizer Sensor Linearity

Exposure Time	Line No.	Gray Level Range min	Gray Level Range max	Max between adjacent pixels
Resolution of 4096 x 1:				
Average	500	5	7	2
	1000	5	8	2
	1500	5	8	2
	2000	6	8	2
	2048	6	8	2
	2500	6	8	2
	3000	6	8	2
	3500	6	10	3
High	500	8	12	3
	3000	9	13	3
Resolution of 256 x 256:				
High		9	13	4
Average		9	12	3
Low		9	14	5

ClearCorrect Exhibit 1002, Page 2117 of 3373

Gray level changes were not substantial for any exposure time. A gray level change of 1 unit is equivalent to a 0.39% change in light intensity. For resolutions of 4096 x 1 pixel, there was never any more than a three unit change (1.17%) between any two adjacent pixel addresses. Over the entire image field, the greatest variation was four units (1.56%). It is reasonable to conclude, therefore, that the sensor is linear within better than 2%. Since subsequent operations find zero crossings of edges where intensity changes vary rather dramatically (yielding a binary image), it is unlikely that these minimal sensor nonlinearities contribute to the quality of the image obtained.

It may be of interest to note, however, that the maximum intensity always occurred in the same position, independent of line number. This suggests that there may be one photodiode or its associated capacitor that is non-linear. Should errors from this source be considered as likely causes of otherwise unexplainable problems. The light intensity from that address could be ignored and the average of an adjacent neighborhood used in its place.

6.5.2.2 SYSTEM NOISE. System noise is defined as fluctuations in pixel gray levels caused by random and systematic perturbations in the CCD sensor and/or the A/D

ClearCorrect Exhibit 1002, Page 2118 of 3373

converter. Systematic noise can be removed by subtracting an image of the noise from each image; random noise must be reduced by more ingenious techniques.

Systematic noise is seen as a repeated spurious resonse by a sensor element. A spurious response is usually defined as one with output of more than 10 percent of the saturation voltage in comparison with the pixels nearest neighbors. The saturation voltage is the maximum usable signal output voltage from the sensor. Blemished pixels can be determined by running the digitizer in the dark (integration time and an exponential function of the temperature (75). Responses above the dark current are spurious and must be rejected from subsequent images if the response cannot be corrected.

Table 8 gives results of running the digitizer with the lens cap on. Selected lines were read with resolution of 4096. The test was run repeatedly, immediately after the system was turned on for the first time that day and again after 10, 36, and 84 minutes of operation. In no case were any variations greater than 4 pixels (1.56%).

There were variations in absolute magnitude over time, however and they are discussed as part of sensor stability in the next section. Because the variations in background are so minimal, they probably do not contribute to the results.

Signal to noise ratio is always of interest. It can be defined as the ratio of maximum signal to noise

ClearCorrect Exhibit 1002, Page 2119 of 3373

Digitizer Dark Field Tests

(for System Noise)

Time from Start of Test (minutes)		Line Number	Gray Level Min	Gray Level Max
	0	1	0	0
	1	500	0	1
	2	1000	0	1
	3	1500	0	1
	4	2048	0	2
	5	2500	0	3
	6	3000	0	3
	7	3500	1	4
	8	4000	1	4
	9	4096	2	4
10 +	0	1	3	5
	1	2048	3	6
	2	4096	3	6
36 +	0	1	7	12
	1	2048	8	12
	2	4096	8	11
84 +	0	1	10	14
	1	2048	10	15
	2	4096	10	14

ClearCorrect Exhibit 1002, Page 2120 of 3373

envelope in the dark. This RMS noise can be established by reading the detector in the dark over a large number of samples and calculating the standard deviation of the samples. Another way of measuring the SNR is by using peak to peak noise, which is merely the range of dark signal noise. This can be statistically shown to be approximately six times the standard deviation of the RMS noise (72). From the above tests, six times the standard devision is 4 gray levls, giving an RMS standard deviation of 0.66 gray levels. This is sufficiently low to be considered inconsequential.

Random noise can result from imperfections in sensor manufacture, electronic leakage between sensor photo sites, variations in the A/D converter, and other factors. Levels of random noise can be approximately quanitified by running the digitizer at various integration times while viewing a neutral gray surface (such as the ""Kodak Gray Card'' slide). Under perfect conditions, with a repeatable sensor and A/D converter, all images should compare perfectly, pixel by pixel. Using this technique, the most ideal integration time should be able to be established (53). As seen in Table 8, the variations are stable with average or extreme high and low exposure setting (integration time). With average (midpoint) exposure setting, the variation between adjacent pixels is minimized. Thus, is is recommended that that value be used. However, it should be noted that the oscilloscope readout aids in establishing

ClearCorrect Exhibit 1002, Page 2121 of 3373

the maximum separate between high and low intensities in the image. The light level passing through the slide containing the image is determined by setting the exposure time at the digitizer counsole (see Figure 15). The value yielding that maximum distribution is the near equivalent of a histogram equilization operator and should be the setting selected.

6.5.2.3 SENSOR STABILITY. After the digitizer and associated electronics are turned on, the sensors and controlls undergo thermal and other changes. To check the internal stability, the background level was checked a number of times including immediately upon turning the system on and after 10 minutes, 36 minutes, and 84 minutes of operation. Ambient temperatures were permitted to fluctuate normally in the environment of the digitizer room. There is some shift immediately after initial powerup but beyond some time the results appear to be stable (see Table 8). The system should be turned on at least 30 minutes before digitizing operations begin.

6.5.2.4 ARRAY GEOMETRY. The CCD array is fabricated as a semiconductor device with pixel centers 7.5 microns apart. The pixels exist as electron wells in a silicone substrate, and as such are not entirely discrete elements. The masks

ClearCorrect Exhibit 1002, Page 2122 of 3373

used in the sensor manufacture are computer-generated at large scale and photographically reduced before being applied to the silicone chip. Manufacturing tolerances are extremely high (0.375 microns center to center and 7.5 microns maximum diagonal across the entire array) (72). Photon indeterminancy error may be more significant than pixel boundary uncertainty error (27). It may be important to conside this calibration in some detail but probably not as first priority.

6.5.2.5 LENS DISTORTION. Lens distoration in any system expected to operate at extremely high precision is always of concern. For these tests, a Ronchi grating (with precision of 1% error in any line pair) was placed under the viewing area of the digitizer. The image was acquired at f8 through a Tamron MC Teleconverter (2x), 120 mm of extender tubes, and a Micor-Nikkor 105 mm lens (2:2.8).

A total of 148 grid lines were placed in the field of view. Of those, 14 were digitized (lines 5, 6, 10, 40, 60, 70, 75, 80, 100, 120, 140, 145, 146, and 147). These represented lines near the edges as well as near the center of the lens.

The pixel address of the centers of each line were measured for 40 different digitizer scan lines evenly distributed through to 4096 pixel range. Table 9 summarizes the results which are also presented graphically

ClearCorrect Exhibit 1002, Page 2123 of 3373

Table 9. Digitizer Lens Distortion

line no.	2-40 slope	2-10 slope	11-20 slope	21-30 slope	31-40 slope
5	0.0036	0.0173	0.0086	-0.001	-0.01147
6	0.0036	0.0172	0.0089	-0.0014	-0.0112
10	0.0036	0.0163	0.0087	-0.00089	-0.0113
40	0.0035	0.0098	0.0065	0.00056	-0.00466
60	0.0034	0.0661	0.0046	0.0022	-0.00163
70	0.0034	0.0043	0.0037	0.0031	0.00075
75	0.0035	0.0032	0.0038	0.00356	0.0016
80	0.0034	0.00194	0.003		0.0029
100	0.0034	-0.0214	0.0014	0.0056	0.0061
120	0.0034	-0.0634	-0.0001	0.0066	0.0107
140	0.0034	-0.0105	-0.001	0.0081	0.0137
145	0.0034	-0.0118	-0.0019	0.0082	0.0147
146	0.0034	-0.0115	-0.0015	0.0089	0.0151
147	0.0034	-0.0115	-0.0017	0.0086	0.0155

line no.	intercept	2-10 int.	11-20 int.	21-30 int.	31-40 int.
5	117	102	112	133	168
6	144	130	140	162	195
10	255	242	252	272	307
40	1081	1075	1079	1092	1110
60	1628	1625	1627	1632	1645
70	1900	1899	1900	1901	1910
75	2036	2036	2036	2035	2043
80	2172	2173	2172		2174
100	2717	2723	2719	2709	2709
120	3266	3276	3269	3254	3242
140	3820	3835	3824?	3803	3787
145	3960	3976	3965	3943	3923
146	3988	4004	3992	3969	3950
147	4016	4032	4021	3998	3976

ClearCorrect Exhibit 1002, Page 2124 of 3373

in Figures 33 a-l (note change of scale between the two axes - it is only for ease of viewing).

When the grid lines are considered throughout their entire range, there is little variation in slope between any two lines (range is 0.0034 to 0.0036 = 5.9%). The grating is rated to 1% accuracy/linearity.

Each line was also considered as four segments (top, top-middle, middle-bottom, and bottom). Within those segments, the lines lying near the periphery of the lens show substantially more variation in slope per segment than those lying near the center of the lens system. In line 5, for instance, slope varies from -0.01147 to 0.0173. In line 75, however, the variation is only 0.0016 to 0.0038. The configuration of the vaiation at the edges confirms the suspicion that barrel distortion is occurring.

For lines near the center, greatest variation from the average is approximately 2 or less pixels (approximately 5 microns). At lines at the periphery, greatest variation is about 10 pixels (25 microns). For high precision results, this distortion will have to be "unmapped" by creating an image pre-processor that can unwarp the image mathematically. Since the digitizer will be replaced, data of the type presented here will have to be acquired to the new system and the pre-processor mathematical unwarping map created for that system. It is anticipated, however, that

ClearCorrect Exhibit 1002, Page 2125 of 3373

the magnitude and distribution of the distortion will be similar to that presented here.

6.5.2.5 OVERALL DIGITIZER ACCURACY. The precision of the digitizing process was studied to optimize tradeoffs in light intensity, depth of field, and operating characteristics of the camera. Accuracy varies with f-stop. At f8, digitizing the same frame of film 10 times reproduced all the point (diode) locations to within 1.147 pixels. At f2.8, however, digitizing the same frame of film 10 times, some point locations could only be reproduced to within 14.765 pixels. At f11, the reproduceability was only slightly improved over that at f8, but there was noticeable reduction in light intensity at the CCD sensor.

6.5.3 3-D Reconstruction

To date no measures of 3-D reconstruction accuracies have been measured. Like the data acquisition lens system, it will be difficult to isolate this variable. It can be established, however, by imaging known shapes, machining the part, and measuring the total tolerance difference between the machined and designed part. If machining

ClearCorrect Exhibit 1002, Page 2126 of 3373

tolerances are known, the 3-D reconstrution error can be inferred from that total. For estimates now the value of 10 microns proposed by R. Caudell (see Appendix 2) is used.

6.5.4 CAD/CAM

The contribution to errors from the CAD/CAM system are assumed to be trivial. This assumption is based upon the fact that the B-spline surface representations are generated from spline curves that are determined by the points on the surface (vs. by using the points to describe a polygon enclosing them). The errors will be on the order of magnitude of the accuracy of the computer and are, therefore, considered to be trivial for overall system error.

6.5.5 Milling

The fabrication of any part on a milling machine has two potential sources of error: positioning error and numerical control module error. Positioning error is dependent upon the quality of the feed beds. For the Dyna mill, it is as high as 25 microns. For the Servo mill, the positioning accuracy in their product specifications is 2.5 microns.

ClearCorrect Exhibit 1002, Page 2127 of 3373

The error contribution from the numerically controlled module is dependent upon the material being cut, feed and spindle rates, cutter diamters, etc. Basically it relates to the surface finish of the part, particularly the scalloped surface that results from multiple paths with a round end cutter. From scans performed over the surface of one crown machined on the Servo system using a Cyber-Optics scanner (54), surface scalloping was seen to be on the order of 203 microns in one area. In another area, where gouging had occurred, the scalloping effect was reduced to 86 microns. With proper cutting instruments and more cutter paths, these effects can be substantially minimized.

6.5.6 Total System Error

Total system error at this point is excessive, ranging from between 46 and 86 microns (see Table 6). The major contributors are the lenses and the numerical control module. Lens distortion can be "unmapped" to minimize its effect. The numerical control errors can be minimized by increasing the number of cutter paths and decreasing the size of the cutter end geometry. Further tests are needed to establish the overall maximum system error. It appears, however, that while the 20 microns limit will be difficult, it is not an impossible objective.

ClearCorrect Exhibit 1002, Page 2128 of 3373

Chapter 7. Significance of an Automated System

Why bother to automate a technique that, obviously, is functional? Over 30 million crowns are piaced each year in the U.S. (9). Obviously they are acceptable; just what advantages are possible, if any, with an alternative technique?

The most exciting possibility with an automated system is the possibility of producing a "cast" restoration in an hour (compared with the minimum of 9 hours turnaround time required with the lost-wax technique). By dramatically shortening the turnaround time from preparation to final restoration placement a number of advantages are available to both the patient and clinician. First, no temporary restoration is needed. Unless a temporary is fit very carefully (a rather time-consuming process), proximal soft tissues will become inflammed, making the patient uncomfortable and final placement of the restoration more difficult. Additionally, unless there are excellent proximal and occlusal contacts provided by the restoration, there is a great probability that the adjacent tooth, prepared tooth, or opposing tooth may shift. Any movement of the teeth, of course, will make final fit of even a

ClearCorrect Exhibit 1002, Page 2129 of 3373

carefully made restoration more difficult, requiring adjustments when the restoration is tried in before final cementation.

When a restoration is placed, the underlying tooth structure may be very sensitive. With some cementation agents it is necessary to acid etch and dry the tooth - a potentially painful operation that generally demands anesthesia. If a one to three hour turnaround time were possible, the anesthesia used during tooth preparation would still be effective so a second set of injections would be unnecessary.

With an automated system of the type described here, data is obtained from the mouth optically. This precludes the need to an impression to be taken. There are few patients who would object to eliminating this step. Further, there are probably few clinicians who would object either. There is a fair amount of difficulty involved in getting accurate, complete, distortion free data, even with the newest and most expensive impression materials available (82).

From a research perspective, the possiblity of eliminating the technique sensitive element of restoration production is appealling. Perhaps it would be possible, then, to begin a set of investigations that can eliminate some of the confusion and ambiguity about which occlusal schemes are more physiologic and cause the least amount of etiologic difficulties (55).

ClearCorrect Exhibit 1002, Page 2130 of 3373

Another very exciting possibility is the potential for a new array of materials to be used for dental restorations. Titanium is one that comes to mind quickly; it can be machined, has been proven to be biocompatible, and is stronger than dental gold alloys. Another possibitity is to use stainless steels. Currently, stainless steel crowns are routinely used for children, especially on baby teeth. However, in their current usage, a stainless steel shell is filled with a plastic filler material which is trimmed to approximate the configuration of tooth. The fit is rarely ideal. With an autcmated system, however, excellent fit could be achieved.

Additionally, an array of ceramics, porcelains, and composite materials may be reasonable choices for dental restorations. They may be less expensive. They can be tooth colored and provide good esthetics. Many are stronger and less brittle than materials currently used - which must be cast.

So, the proposed automated system can provide advantages to the patient - in one-appointment restorations without impressions and less anesthesia as well as elimination of physiologic responses to temporaries by eliminating the possibility of tooth movement and tissue inflammation. It can provide advantages to the clinician - saving time by eliminating temporary restoration fabrication and precluding the need for adjustments to

ClearCorrect Exhibit 1002, Page 2131 of 3373

correct for changes in tooth position. And it creates an array of possible research activities into material possibilities and occlusal schemes.

ClearCorrect Exhibit 1002, Page 2132 of 3373

Chapter 8. Unique Contributions

The primary unique contribution resulting from these investigations is the creation of a system to automate production of high quality dental restorations. The system integrates an array of technologies, including machine vision, stereophotogrammetry, CAD/CAM, and clinical dentistry.

Additionally, never before has there been a data base of ideal tooth forms. There are also unique elements in the acquisition of data, image processing and surface reconstruction, and CAD/CAM components of the system. Machining operations, especially as they relate to the scale of dental restorations, have also proven to be unique.

The data acquisition subsystem configuration is unique. It permits optical access to the posterior regions of the human mouth. In that region, space, patient movement, and high humidity are realities and difficulties which have to be overcome.

The data acquisition system combines techniques from both structured and unstructured light, capitalizing on the advantages available from both lighting sources. This is

ClearCorrect Exhibit 1002, Page 2133 of 3373

especially valuable for relatively featureless surfaces like prepared teeth.

The image processing which permits three-dimensional reconstruction of the data from the mouth is unique. The technique employed uses edge finding algorithms. This is advantageous since it capitalizes on naturally occurring phenomenon which would otherwise be troublesome for image processing. For instance, it is quite common for the teeth requiring restoration to be stainied (from previous filling materials or decay) or to contain a base filling material (a cement base or dowel and core, for instance). With the edge extraction component of the image processing, these phenomenon become additional "features", providing additional data points for solving the 1:1 correspondence problem.

The 1:1 correspondence solution was developed for this particular application. By combining features obtained with structured lighting (the grid superimposed on the surface) and unstructured light (margins and natural features) with stereo, maximum data can be extracted, ensuring good quality, high resolution surface representations can be obtained.

The combination of data acquisition subsystem, image processing, and solution of the 1:1 correspondence problem are the basis for a patent application which is currently being prepared.

ClearCorrect Exhibit 1002, Page 2134 of 3373

The CAD/CAM system developed contains some unique features as well. The primary one is its ability to manage complex, irregular, small components. Another uniqueness is its ability to manipulate and ultimately machine very thin sections (margins) and to create and machine its own fixturing.

Fixturing design is simple yet unique. By first machining the form of the prepared tooth, relative positions of the internal and external surfaces of the restoration are ensured. This, of course, is critical for the clinical success of any restoration.

Machining investigation have also been unique. While standard dental materials and cutting instruments have been used, very small scale cutters in automated milling equipment has not previously been reported.

The development of this system combined with enthusiasm for the possibilities of automation from clinicians and dental laboratories has led to the formation of a company (Digital Dental Systems, Inc.) to generate a marketable product. The NIDR has been enthusiastic in its support as well and we have recently received approval and funding for a five-year continuation of our investigations.

Additionally, the three-dimensional image acquisition and processing capabilities of this system permit investigations into other clinical problem with higher accuracy than has been possible. One of the most obvious has been investigations of wear in restorations, especially

ClearCorrect Exhibit 1002, Page 2135 of 3373

in-vivo long-term wear of various material tyeps as well as patterns of wear and how and where the wear patterns develop and change over time.

ClearCorrect Exhibit 1002, Page 2136 of 3373

Chapter 9. Future Investigations

The feasiblity of automating the creation of dental restorations has been shown. There is, however, further development required, especially to integrate system components into a single system which could feasibly operate in a dental clinical setting. These include improvements in the lens system, and milling machine. Clinical trails need to be undertaken. Data compression techniques need to be implemented. Materials opportunities need to be pursued. The possibility of producing other restoration types in addition to full coverage crowns needs to be explored.

9.1 LENS SYSTEM

One of the remaining devlopements is for a camera system for use in a clinical setting. A dual lens system capable of simultaneously recording the two halves of the stereo pairs of images must be developed. Different lighting and grid sizes and patterns need to be investigated to optimize performance of the edge finding and reconstructions algorithms. The effect of different film types must also be established. Ultimately, when

ClearCorrect Exhibit 1002, Page 2137 of 3373

they become available, high resolution digital data equipment must be directly integrated into system design.

9.2 MILLING MACHINE

Local interactions between the cutting edges and the material being worked have direct influence on final quality of the restoration. Relevant factors of cutting conditions must be identified and built into the system control software to assure production of restorations with acceptable surface finish and surface properties. Surface defects and subsurface variations in structure and/or properties can serve as material failure initiation sites, especially during cyclic loading.

Many tests remain relating to cutting various materials. These include feed rate, spindle speeds, cutter types, and assessment of various fixturing and material types. The dental laboratories and the American Fund for Dental Health have expressed interest in funding at least a substantial portion of these tests.

9.3 CLINICAL TRIALS

Clinical trails are a necessary part of development of the system. Human subjects approval has already been obtained for any clinical investigations relating to the

ClearCorrect Exhibit 1002, Page 2138 of 3373

automated system. Crowns will be fabricated with the system for at least 10 patients. Patients who present for treatment at the University of Minnesota, School of Dentistry, Department of Graudate Operative Dentistry, and, upon clinical examination, are in need of a full crown, will be given the option of choosing to have the crown fabricated by the conventional impression-lost wax casting technique or with the automated system. Type III dental gold will be used for crowns fabricated by either technique.

For patients choosing the automated fabrication, a cast crown will also be fabricated. This fabrication will be done by Hermanson Dental Laboratory, a quality dental laboratory in St. Paul, MN (99). Both crowns will be judged for quality by a panel of three independent clinicans using the criterion used in clinical practical exams at the University of Minnesota School of Dentistry and specified in Appendix 1. The crowns will be judged for marginal integrity, occlusal fit, and interproximal fit both before and after cementation. If the milled crown is not judged to be acceptable, the cast crown will be evaluated and, if accceptable, seated. All crowns will be seated with zinc phosphate cement (142).

For all milled crowns seated, the patient will be recalled at annual intervals for at least three years for re-evaluation. At each recall, the same acceptance criterion as used at original placement will be applied.

ClearCorrect Exhibit 1002, Page 2139 of 3373

In addition, both the plaque and gingival indices will be measured using the protocol described by Loe and Silness (121 and 181).

The only potential risk that may be implicit in seating a milled crown (especially if it is fabricated at the same appointment as the restoration is cut) is an irritation response of the tooth to the combination of drilling and the acidity of the zinc phoshate cement. This risk, however, is thought to be lcw since zinc phosphate is often used at the preparation appointment as an agent to build up areas of the tooth beneath the crown so that less gold is required for the restoration.

9.4 DATA COMPRESSION

The amount of data acquired from a set of stereo pairs digitized with high resolution is impressive. Some technique is required to minimize the amount of data that needs to be stored without compromising the quality of the data. One technique may be to first perform a low-resolution scan to determine the borders in which useful information (the tooth of interest) is included. One way to do this would be to use a Canny edge finding with strong edges criterion to find the limit of the margin of the prepared tooth. Then, a high resolution scan could be performed only in the enclosed area.

ClearCorrect Exhibit 1002, Page 2140 of 3373

9.5 MATERIALS

The feasiblity of creating machined restorations from ceramics or other tooth-colored composite materials is needed. To do so, the properties of existing machinable ceramics available for both dental and non-dental applications must be determined. These matrials include a new machinable version of Dicor (58) currently under development by Corning and Dentsply, a new material (paritally stabilized zirconia), being developed by 3M (188), ceramics being used for opthalmic scalpals (104), and others to be identified through conversations with dental companies (including Caulk and Johnson and Johnson), other universities (including MIT) (109), and a comprehensive review of the literature.

Other, non-castable metals must also be considered and a list of possiblities compiled. When the list is completed, their properties can be determined from the literature. Then, those that are most likely to (1) withstand the forces of occlusion, (2) offer adequate color options, (3) be biocompatible in the oral environment, and (4) can be machined, will be determined. Finite element studies should be performed for crowns fabricated from these materiais. Those that show the most promise for success could be fabricated and evaluated for fit, surface finish, and cinically tested. Additionally, materials

ClearCorrect Exhibit 1002, Page 2141 of 3373

properties are likely to influence the way in which a preparation should be designed for that material (like the differences in margins for gold vs ceramic crowns). These differences need to be modelled and studied.

Of more immediate interest, however, is evaluation of spindle speed and feed rates for different materials as well as the need for cooling either the part or the cutting tool. The problem of chip recovery, especially for precious metal, also needs to be addressed.

9.6 OTHER RESTORATIONS

System capabilities should be expanded so that other restorations, iincluding inlays, partial coverage crowns, and bridges can be fabricated. Beyond that, the feasiblity of expanding system capabilities to permit fabrication of partial denture frameworks and denture bases must be investigated. The addition of inlays, partial crowns, and bridges should be relatively straightforward. Software changes will be needed to alter the configuration designed by the CAD/CAM package. A menu will be needed to permit selection of the desired restoration type. When the software changes have been made, restorations should be preparations made in green teeth. The margins, occlusal fit, and interproximal fit must be evaluated.

ClearCorrect Exhibit 1002, Page 2142 of 3373

Chapter 10. Summary

It is possible to automate the production of dental restorations that now require lost-wax castings. An array of technologies have been investigated and integrated into a system. They include technologies from optics, stereophotogrammetry, robot or machine vision, image processing, three-dimensional surface reconstruction, CAD/CAM, high precision machining, material science, and clinical dentistry.

Definition of system design parameters was a difficult yet critical first step in the design process. Establishing a translation from clinical test and acceptance into engineering tolerances proved to be a non-trivial task and has resulted in creating a new awareness of definition of the problem, especially in the minds of the clinicians. It has also raised some new questions for the clinicians to address. For instance, the ADA specification for gold crowns gives an rms surface finish value. It does not specify spectral quality though all clinicians expect that a smooth crown will necessarily also be shiney. Some changes and additions in the specifications will be required in the future.

ClearCorrect Exhibit 1002, Page 2143 of 3373

The automated system provides substantial advantages to the patient, clinician, and researcher. Time savings are possible for the patient and clinician alike. Resotration production times are dramatically reduced, making one-appointment "cast" restorations a possibility. With that, problematic physiological responses to temporary restorations can be eliminated. Additionally, the automated system permits a whole array of new materials to be considered for restorations.

A number of unique contributions have been made with these investigations. In addition to the creation of the system itself, there have been contributions made to data acquisition techniques, three-dimensional image processing and surface reconstruction, CAD/CAM, micromilling, and the creation of a data base of ideal tooth morphologies.

It is indeed feasible to automate the production of dental restorations. This automation provides some exciting challenges and possibilities for the future.

ClearCorrect Exhibit 1002, Page 2144 of 3373

Chapter 11. Bibliography

1. Y.I. Abdel-Azia and H.M. Karara, Photogrammetric Potentials of Non-Metric Cameras, Civil Engineering Studies, Phtogrammetry Series No.36, University of Illinois, Urbana, llllnois, March 974.

2. G.J. Agin and T.O. Binford, Proceedings, International Conference on Artificial Intelligence,629-640, Stanford, 1973.

3. B.R. Altschuler, J. Toboada, V.A. Segreto, "Intra-Oral Dental Laser Grid Surface Mapping", Applications of Optical Instrumentation in Medicine IV, SPlE, vol. 70, 347-350, 1975.

4. B.R. Altschuler, "Applications of lnterferometry and Optical Metrology in Dentistry", Applications of Optics in Medicine and Biology, SPIE, vol. 89, 40-46, 1976.

5. B.R. Altschuler, J. Toboada, M.D. Altschuler, "Laser Electro-Optic System for 3-D Topographic Mensurations", Imaging Applications for Automated Industrial Inspection and Assembly, SPIE, vol 182, 192-196, 1979.

6. M.D. Altschuler, B.R. Altschuler, J. Toboada, "Measuring Surfaces Space-Coded by a Laser-Projected Dot Matrix'', Imaging Applications for Automated Industrial Inspecation and Assembly,, SPlE Vol. 192, 187-191, 1979.

7. M.D. Altschuler, B.R. Altschuler, J. Toboada, "Laser Electro-Optic System for Rapid 3-D Topographic Mapping of Surfaces", Optical Engineering, 20(6), 953-961, 1981.

8. M.D. Altschuler, et.al., "The Numerical Stereo Camera", 3-D Machine Perception, SPlE, vol. 283, 14-24, 1981.

9. American Dental Association, Beureau of Economic and Behavior Research, 1979 Survey of Dental Services Rendered, Estimated Total and per Capita Number of Dental Services.

10. American Dental Association, Specification No. 5 for Gold Dental Casting Gold Alloy, ADA, April 1968.

ClearCorrect Exhibit 1002, Page 2145 of 3373

11. American Dental Association, Specification No. 8 for Zinc Phosphate Cement, ADA, December 1977.

12. American Dental Association, Specification No. 9, Dental Silicate Cement, ADA, December 1963.

13. American Dental Association, Specification No. 21, Dental Zinc Silico-Phosphate Cement, ADA, December 1969.

14. J.M. Anderson, et. al., Analytical Calibration of Aerial and Terrestrial Camera Systems, Final Technical Report, University of California, Berkeley, 1975.

15. R.H. Anderson, C.W. Gillard, C.C. Huang, Robotics and Industrial Inspection, D.P. Casasent, ed, Proceedings, SPIE vol. 360, 207, 1983.

16. R.D. Arnold, "Local Context in Matching Edges for Stereo Vision", Proceedings, Image Understanding Workshop, 64-72, 1978.

17. R.D. Arnold and T.O. Binford, "Geometric Constraints in Stereo Vision", Proceedings, SPIE, vol. 238, 281-292, 1980.

18. R.D. Arnold, "Automated Stereo Perception", Ph.D. Dissertation, Stanford University, March 1983.

19. R.J. Bartrum Jr. and H.E. Crow, Real-Time Ultrasound: A Manual for Physicians and Technical Personnel (second edition), W.B. Saunders, 1983.

20. D.H. Ballard and C.M. Brown, Computer Vision, Prentice Hall, 1982.

21. S.T. Barnard and W.B. Thompson, "Disparity Analysis of Images", IEEE Transactions on Pattern Analysis and Machine Intelligence, PAMI-2, 333-340, 1980.

22. B. Barsky, "B-Spline Curves, Computer Graphics and Image Processing,

23. T. Baumeister (ed), Marks' Standard Handbook for Mechanical Engineers, McGraw Hill, 1979.

24. Discussions with S. Baumrind and S. Cury, November 1987.

25. Discussions with S. Bayne, July 1988.

26. A.J. Boehnlein, K.G. Harding, "Adaptation of a Parallel Architechture Computer to Phase Shifted Moire Interferometry", Optics, Illumination and Image Sensing for Machine Vision, SPIE vol. 728, 183-194, 1986.

ClearCorrect Exhibit 1002, Page 2146 of 3373

27. R.C. Bolles, H.H. Bakes, "Epipolar-Plane Image Analysis: A Technique for Analyzing Motion Sequences", M.A. Fischler and O. Firschein (ed.), Readings in Computer Vision: Issues, Problems, Principles and Paradigms, Morgan Kaufmann, 26-36, 1987.

28. E. Boskamp, "Application of Surface Coils in MR Imagaing", Medicamundi, vol 29(2), 1984.

29. B. Boucheham, "Multiresolution Stereo Matching Using Topographic Structures", MS Thesis, University of Minnesota, November 1987.

30. M. Brady, "Representing Shape", Nato ASI Series Vol. F11, Robotics and AI, edited by M. Brady et.al., Springer-Verlag, 279-300, 1984.

31. M. Brady and R. Paul (ed.), Robotics Research: The First International Symposium, MIT Press, 1984.

32. M. Brady, J. Ponce, A. Yuille, H. Asade, "Describing Surfaces", Computer Graphics and Image Processing, 32, 1-28, 1985.

33. B. Brandestini, W. Moermann, F. Lutz, I. Krejci, "Computer Machined Ceramic Inlays: In Vitro Marginal Adaptation", IADR/AADR Abstracts, Vol. 64, p. 208, March 1985.

34. H. Brody, "3-D Systems: Plastic Models from CAD Programs", High Technology, 63, July 1987.

35. D. Brown, Advanced Methods for Calibration of Metric Cameras, ASP Symposium on Computational Photogrammetry, Syracuse, NY, 1969.

36. C.J. Burstone, "Holographic Measurement of Incisor Extrusion", American Journal of Orthodontics, 82(1), 1-9, 1982.

37. P. Burt and B. Julesz, "A Disparity Gradient Limit for Binocular Fusion", Science, 208, 615-617, 1980.

38. "Microbytes", Byte, vol. 12(1), 10, January 1987.

39. J. F. Canny, "Finding Edges and Lines in Images", M.S. Thesis, MIT, June 1983.

40. J.F. Canny, "A Computational Approach to Edge Detection", M.A. Fischler and O. Firschein (ed.), Readings in Computer Vision: Issues, Problems, Principles and Paradigms, Morgan Kaufmann, 184-203, 1987.

ClearCorrect Exhibit 1002, Page 2147 of 3373

41. S. Castan and J. Shen, "A Stereo Vision Algorithm Taking into Account the Perspective Distortions", Proceedings, 7th Int. Conf. Pattern Recognition, 441-443, 1984.

42. R. Caudell, presentation at Greater New York Dental Meeting, New York, December 3, 1987.

43. Discussions with R. Caudell, March 17 and 18, 1988.

44. G.J. Christiansen, "Marginal Fit of Gold Inlay Castings", Journal of Prosthetic Dentistry, 227-231, 1966.

45. E. Charniak and D. McDermott, Introduction to Artificial Intelligence, Addison-Wesley, 1985.

46. J.J. Clark and P.D. Lawrence, "A Theoretical Basis for Difference Stereo", Computer Vision, Graphics, and Image Processing, 35, 1-9, 1986.

47. J. Clayton and E. Green, "Roughness of Pontic Materials and Dental Plaque", Journal of Prosthetic Dentistry, 23, 407, 1970.

48. D. Cormier, "Analog to Digital Conversion in a Flash", ESD: THE Electronic System Design Magazine, 18(5), 38-43, May 1988.

49. Corning Glass Works, Technical Bulliten: Macor Material Characteristics, 1-R79.

50. Corning Glass Works, Technical Bulliten: Macor product literature.

51. R.G. Craig (ed), Restorative Dental Materials, Mosby, 1980.

52. S. Curry, F. Moffitt, D. Symes, S. Baumrind, "Family of Calibrated Stereometric Cameras for Direct Intra-Oral Use", SPIE Vol. 361, Biostereometrics '82, Robin E. Herron (ed), August 1982.

53. S. Curry, "A Point Location and Tracking System Employing Digital Images for Use in Biostereometrics", Ph.D. Thesis, University of California, Berkeley, 1985.

54. Cyber-Optics Product Literature, Cyber-Optics, Corp., Minneapolis, MN.

55. P.E. Dawson, Evaluation, Dignosis and Treatment of Occlusal Problems, C.V. Mosby, 1974.

ClearCorrect Exhibit 1002, Page 2148 of 3373

56. E.P. DeGarmo, Materials and Processes in Manufacturing, McMillan, 1969.

56a. P. Dev, L.L. Fellingham, et.al., "3-D Graphics for Interactive Surgical Simulation and Imprint Design", Processing and Display of Three-Dimensional Data II, SPIE vol. 507, J.J. Peason (ed), 52-57, 1984.

57. J.L. Doty, Optical Society of America, 73, 366, 1983.

58. Dicor Product Literature, Dentsply/York Division - Lab Products, Dentsply International, York, PA.

59. J.P. Duncan and S.G. Mair, Sculptured Surfaces in Engineering and Medicine, Cambridge University Press, 1983.

60. F. Duret, Procede de Realisation D'Une Prosthese Dentaire, French Patent 2536654, June 1984.

61. F. Duret, "Vers un Nouveau Symbolisme Pour la Realisation de not Pieces Prosthetiques", Les Cahiers de Prothese, vol. 50, p. 65-71, June 1985.

62. F. Duret, J. Blouin, L. Hanmani, "Principles de Fontionement et Applications Techniques de l'Empreinte Optique Dans l'Exercise de Cabinet", Les Cahiers de Prosthese, Vol. 50, p. 73-110, June 1985.

63. F. Duret, "Vers une Prothese Informatsee", Tonus, TD 73-15.11.1985, p. 55-57, November 1985.

64. F. Duret and Blouin, "De l-Empreinte Optique a la Conception et la Fabrication Assistees per Ordinateur d'une Couronne Dentaire", Journal Dentaire du Quebec, vol 23, p. 177-180, April 1986.

65. F. Duret, E. Duret, Apparatus for Taking Odontological or Medical Impressions, U.S. Patent 4611288, September 1986.

66. Francois Duret Semiar, sponsored by Napili International, Phoenix, Arizona, Seminar held in New York, NY December 5-6, 1986.

67. F. Duret, "Method of and Apparatus for Making a Prosthesis, Especially a Dental Prosthesis", U.S. Patent 4663720, May 5, 1987.

68. Discussions with F. Duret, March 17 and 18, 1988.

69. Dyna Mechtronics, Inc. Santa Clara, CA 95051 (1986).

ClearCorrect Exhibit 1002, Page 2149 of 3373

70. G.T. Eden, et.al., "Fit of Porcelain Fused-to-Metal Crown and Bridge Castings", Journal of Dental Research, 58(12), 2360-2368, December 1979.

71. R.D. Eastman and A.M. Waxman, "Using Disparity Functionals for Stereo Correspondence and Surface Reconstruction", Computer Vision, Graphics, and Image Processing, 39, 73-101, 1987.

72. Eikonix Scan Model 78/79 EC850 Image Digitizer User's Manual, Eikonix Corporation, 23 Cosby Drive, Bedford, MA 01730, 1984.

73. J.E. Estes et.al., "Fundamentals of Image Analysis: Analysis of Visible and Thermal Infrared Data", Manual of Remote Sensing, R.N. Colwell, (ed), American Society of Photogrammetry, 987-1124, 1983.

74. R. Ethier and D. Melanson, "High-Resolution Computed Tomography and Conventional Tomography", Sectional Imaging Methods: A Comparison, (J.T. Littleton, M.L. Durizch, ed.), University Park Press, 1983.

75. Fairchild CCD Imagaing, CCD - The Solid State Imaging Technology, Fairchild Camera and Instrument Corporation, 1982.

76. M.A. Fischler and O. Firschein (ed), Readings in Computer Vision: Issues, Problems, Principles and Paradigms, Morgan Kaufmann, 1987.

77. G.D. Freier, University Physics, Appleton-Century Crofts, 502-503, 1965.

78. Discussions with Dr. Ron Geistfeld and Dr. Marlin Rekow, Febuary 1988.

79. J.J. Gibson, The Perception of the Visual World, Houghton-Mifflin, Boston, 1950.

80. B.V. Gool, "The Creation of Line Drawings as a Basis for Feature Based Stereo Vision", Journal of Robotic Systems, 1, 251-262, 1984.

81. A. Gostasby, "A Symbolically Assisted Approach to Digital Images Registration with Application in Computer Vision", Technical Report 83-013, Department of Computer Science, Michigan State University, 1983.

82. Discussions with Josh Green, July 1988.

83. W.E.L. Grimson, From Images to Surfaces: A Computational Study of the Human Early Visual System, MIT Press, 1981.

ClearCorrect Exhibit 1002, Page 2150 of 3373

84. W.E. Grimson and E.C. Hildreth, "Comments on Digital Step Edges from Zero Crossings of Second Directional Derivatives", [response to the Haralick paper, reference 91], IEEE Transactions on Pattern Analysis and Machine Intelligence, PAMI-7(1), 121-127, January 1985.

85. D.G. Grossman, "Machining a Machinable Glass Ceramic", American Machinist, May 1978.

86. D.G. Grossman and D.L. Taylor, "Machinability Studies on Macor Glass-Ceramic", Science of Ceramic Machining and Surface Finishings II, B.J. Hockey and R.W. Rice (ed), National Bureau of Standards, Special Publication 562, 1979.

87. A.W. Gruen, A Test Strategy for High Resolution Image Scanners", Report No. 350, Ohio State University, October 1983.

88. N.F. Giuchet, Occlusion: A Teaching Manual, distributed by Denar Corporation, 1970.

89. A.M. Halioua, H.C. Liu, "Optical Sensing Techniques for 3-D Machine Vision", in SPIE Vol 665, Optical Techniques for Industrial Inspection, p. 150-160, 1986.

90. R.M. Haralick, "Digital Step Edges from Zero-Crossings of Second Directional Derivatives", IEEE Transactions on Pattern Analysis and Machine Intelligence, PAMI-6(1), 58-68, January 1984.

91. R.M. Haralick, "Authors Reply" [to Grimson and Hildreth, see reference 86], IEEE Transactions on Pattern Analysis and Machine Intelligence, PAMI-7(1), 127-129, January 1985.

92. K. Harding, "Moire Interferometry for Industrial Inspection", Lasers and Applications, 73, 1983.

93. K. Harding and R. Tail, "Moire Techniques Applied to Automated Inspection of Machined Parts", SME Vision '86 Conference, Detroit, Michigan, May 1986.

94. M. Hartfel, et.al., "A System for Three Dimensional Representation of Human Jaw Motion Using Finite Screw Axis Approximations", 1987 Biomechancs Symposium, ASME AMD vol. 84, D.L. Butler and P.A Torzilli (ed), 137-140, June 1987.

95. T. Heikkenen, R. Ahola, et.al., Recent Results of the Performance Analysis of a 3-D Sensor Based on Time of Flight Measurements, in SPIE Vol 665, Optical Techniques for Industrial Inspection, p. 168-173, 1986.

ClearCorrect Exhibit 1002, Page 2151 of 3373

96. S.J. Henry and N.L. Harris, "Abrasive Waterjet CAD/CAM Technology: Is it the Shape of Things to Come in Cutting Glass?", U.S. Glass, Metal, and Glazing, December 1986.

97. Hennson lnternational Product Literature, "The Dental CAD/CAM - General Description of the Project", Hennson International, Chateau de Malissol, F-38200 Vienne, France, January 1986.

98. M. Heman and T. Kanade, "The 3-D Mosaic Understanding System: Incremental Reconstruction of 3-D Scene from Complex lmages", Technical Report, Department of Computer Science, Carnegie Mellon University, February 1984.

99. Discussion with Tom Hermanson, owner, Hermanson Dental Laboratory, 1988.

100. E.C. Hildreth, Edge Detection, Artificial Intelligence Laboratory, AI Memo No. 858, MIT, September 1985.

101. J. R. Holmes, "Marginal Fit of Castable Ceramic (Dicor) Crowns", M.S. Thesis, University of North Carolina, 1986.

102. Discussions with Human Performance Institute, Atomi, Japan, February 1987.

103. A. Ishikeriama, et.al., "Influence of Some Factors on the Fit of Cemented Crowns", Journal of Prosthetic Dentistry, 45(4), 400-404, April 1981.

104. Discussions with R.C. Isphording, Genral Sales Manager, Astro Met Associates, Inc., Cincinnati, Ohio, March 1987.

105. M. Haleous and H.C. Liu, "Optical Sensing Techniques for 3-D Machine Vision", Optical Techniques for Industrial Inspection, SPIE vol. 665, 150-161, 1986.

106. M. Ito and A. Ashii,"Three View Stereo Analysis", IEEE Transactions, Pattern Analysis Machine Intelligence, PAMI-8(4), 524-531, July 1986.

107. R.A. Jarvis, IEEE Transactions, Pattern Analysis Machine Intelligence, PAMI-5, 122, 1983.

ClearCorrect Exhibit 1002, Page 2152 of 3373

108. R.A. Jarvis, "A Perspective on Range Finding Techniques for Computer Vision", Digital Image Processing and Analysis: Vol. 2, Digital Image Analysis, R. Challappa and A.A. Sawchuk, ed., IEEE Computer Society Press, 569-586, 1985.

109. Discussions with Chris Jansen, Technology Licensing Officer, MIT, January 1988.

110. J.A. Jalkio, R.C. Kim, S.K. Case, "Three-Dimensiona Inspection using Multistripe Structured Light", Optical Engineering, 24(6), 966-974, Nov/Dec, 1985.

111. G.R. Jernberg, "The Relationship Between Proximal Tooth Open Contacts and Periodontal Disease'', M.S. Thesis, University of Minnesota, 1980.

112. C.L. Koliopoulis, "Fringe Analysis of Interferograms", Lasers and Optronics, 7(5), 65-73, May 1988.

113. M. Keefe, "A Computer-Assisted Tool to Semi-Automatically Generate Three-Dimensional Facial Soft-Tissue lnformation", Ph.D. Thesis, University of Minnesota, June 1985.

114. H. Kiemle, "Holographic Micro-Images for Industrial Applications", The Engineering Uses of Holography, J.M. Harvey(ed), Cambridge University Press, 1970.

115. J.J. Koenderink and A.J. vanDoorn, "Geometry of Binocular Vision and a Model for Stereopsis", Biology Cybernetics, 21, 29-35, 1976.

116. L. R. Koenig, "Assessment of Clinical Feasibility of A Three Diemnsional Stereophotogrammetrical System", M.S. Thesis, University of Minnesota, 1985.

117. T.A. Krauskop, D.R. Doughterty, D.J. Winningham, "Automated Fabrication of Lower Extremity Prosthetic Sockets", 1987 Advances in Bioengineering, 11-12, ASME BED vol. 3, 1987.

118. P.C. Lauterbur, " New Techniques in NMR Zeugmatographic Imaging", in Biomedical Imaging, O. Hayaishi and K. Torizuka (ed), 97-106, 1986.

119. D.T. Lawton, "Processing Translation Motion Sequences", Computer Graphics and Image Processing, 22(1), 116-144, April 1983.

120. Calculations by H. Li, unpublished, October 1987.

ClearCorrect Exhibit 1002, Page 2153 of 3373

121. H. Loe and J. Silness, "Periodontal Disease in Pregangcy, I: Prevaence and Severity", Acta. Odontologica Scandinavia, 21(2), 533-551, 1963.

122. R.M. Lougheed, R.E. Sampson, "3-D Imaging Systems and High Speed Processing for Robot Control", Machine Vision and Applications, 41-57, 1988.

123. W.H.H.J. Lunscher, M.P. Beddoes, "Optimal Edge Detector Design I: Paramter Selection and Noise Effects", IEEE PAMI-8(2), 164-177, March 1986.

124. W.H.H.J. Lunscher, M.P. Beddoes, "Optimal Edge Detetor Design II: Coefficient Quantification", IEEE PAMI-8(2), 178-187, March 1986.

125. Manual of Photogrammetry, 4th edition, CC. Slama (ed), American Sciety of Photogrammetry, Falls Chruch, Virginia, 1980.

126. Manual of Remote Sensing, Volumes 1 and 2, R.N. Colwell (ed), American Society of Photogrammetry, 1983.

127. Discussions with Paul Marinaccio, Foster Miller, Inc., Waltham, MA, September 1987.

128. A.R. Margulis and B. Demas, The Present Status of Clinical Magnetic Resonance Imaging and its Future Directions", in Biomedical Imaging, O. Hayaishi and K. Torizuka (ed), 145-157, 1986.

129. D. Marr, "Early Processing of Visual Information", Phil. Trans. Royal Society of London, Series V, 275, 483-524, 1976.

130. D. Marr and T. Poggio, "A Computational Theory of Human Stereo Vision", Proceedings, Royal Society of London, Series B, 204, 301-328, 1979.

131. D. Marr and E. Hildreth, "Theory of Edge Detection", Proceedings, Royal Society of London, Series B, 207, 187-217, 1980.

132. D. Marr, Vision, W.H. Freeman, 1982.

133. G.A. Mastin, "Adaptive Filters for Digital Image Noise Smoothing: An Evaluation", Computer Vision, Graphics, and Image Processing, 31, 103-121, 1985.

134. J.E.W. Mayhew and J.P Frissy, "Computational and Psychological Studies Towards a Theory of Human Stereoposis", Artificial Intelligence, 17, 349-385, 1981.

ClearCorrect Exhibit 1002, Page 2154 of 3373

135. B.B. McCollum, C.E. Stuart, "A Research Report: Basic Text for Post Grad Course in Gnathology", Scientific Press, 1955.

136. D.M. Meadows, W.O. Johnson, J.B. Allen, Applied Optics, 9, 942, 1970.

137. G.G. Medioni and R. Nevatia, "Segment Based Stereo Matching", ISG Report 104, 38-54, University of Southern California, October 1983.

138. G. Medioni and R. Nevatia, "Segment-Based Stereo Matching", Computer Vision, Graphics, and Image Processing, 31, 2-18, 1985.

139. Discussions with Georg Meyer, July 1988.

140. M. Mezi, B. Duret, F. Duret, Procede d'ameiioration de l'albedo d'elements vivants pour ieur an aiyse optique tridimensionneiie, French patent 2594320, August 1987.

141. Micro Control Systems product literature, PERCEPTOR 3-D Graphics Digitizer and Data Acquisition Device, Micro Control Systems, Inc., 27 Hartford Tpke, Vernon, Conn, 060066.

142. Mizzy Product Literature, Fleck's Powder and Liquid, Mizzy, Inc., Clifton Forge, VA.

143. W. Moermann, M. Brandestini, A. Ferru, F. Lutz, I. Krejci, "Marginale Adaptation von Adhaesiven Porzelian Inlays in Vitro", SSO; Schwiezerishce Monatsscrift fur Zahnmedizin, vol. 95, 1118-1129, December 1985.

144. W.H. Moermann, B. Brandestitni, "Method and Apparatus for the Fabrication of Custom-Shaped implants", U.S. Patent number 4,575,805, March 11, 1986.

145. W. Moermann, H. Jans, M. Brandestini, A. Ferru, F. Lutz, "Computer Machined Adhesive Porcelain Inalays: Margin Adaptation After Fatigue Stress", paper accompanying abstract number 339, IADR Abstracts, vol. 65, 762, June 1986.

146. H.P. Moravec, "Toward Automatic Visual Obstacle Avoidance", Fifth International Joint Conference on Artificial Intelligence, Cambridge, 1977.

147. H.P.Moravec, "Visual Mapping by a Robot Rover", Sixth International Joint Conference on Artificial Intelligence, Tokyo, 598-600, 1979.

ClearCorrect Exhibit 1002, Page 2155 of 3373

148. W.E. Mioritz, P.L. Shreve, L.E. Mace, "Analysis of Ultrasonic Spatial Locating System", IEEE Transacttions on Instrumentation and Measurement, 25(1), 42-50, 1976.

149. V.S. Nativa and T.O. Binford, "On Detecting Edges", IEEE PAMI-8(6), 699-71 (42b).

150. R. Nevatia, "Image Segmentation", T.Y. Young and K.S. Fu(ed), Handbook of Pattern Recognition and Image Processing, Academic Press, 1986.

151. New Release, "L'Est Republicain", 5 bis, avenue Fech, 54042, Nancy Cedex, 24 December 1985, provided by Hennson International.

152. R. Omoto, "Recent Progress of Ultrasound Diagnostic Imaging in Cardiovascular Disease: Development of Real Time Two-Dimensioal Doppler Echocardiograph", in Biomedical Imaging, O. Hayaishi and K. Torizuka (ed), 83-93, 1986.

153. L Onural, P.D. Scott, "Digital Decoding the in-line Holograms", Optical Engineer, 26(11), 1124-1132, November 1987.

154. K.J. Overton and T.D. Williams, "Tactile Sensation for Robots: Overview and Experience", ASME Computers in Engineering, 2, 115-123, 1983.

155. Discussion with T. Pedersen, Altenburg-Strlsunder Spielkarten Fabriken AG, January 22, 1988.

156. S.W. Peterson, "Measurement and Analysis of Human Joint Motion", Ph.D. Thesis, University of Minnestoa, 1985.

157. Dicussions with Dr. E. Pheiffer, Siemans Corp. March 9, 1988.

158. M. Pietikainen and D.Harwood, "Depth from Three Camera Stereo", Proceedings on Computer Vision and Image Processing , 2-8, Maimi Beach, Fl, June 1986.

159. T. Poggio, H. Voorhees, A.L. Yuille, "A Regularization Solution to Edge Detection", Artificial Intelligence Laboratory, AI Memo 773, MIT, 1984.

160. T. Poggio, "Early Vision: From Computational Structure to Algorithms and Parallel Hardware, Computer Vision, Graphics, and Image Processing, 31, 139-155, 1985.

161. T.C. Pong, L. G. Shapiro, R.M. Haralick, "Stereo Matching Using Topographic Structures", Technical Report, University of Minnesota, Department of Computer and Information Sciences, 1984

ClearCorrect Exhibit 1002, Page 2156 of 3373

162. K. Praxdny, "Detection of Binocular Disparities", Biology and Cybernetics, 52, 93-99, 1985.

163. K.Price and R. Reddy, "Maching Segments of Images", IEEE Transactions on PAMI, 1, 110-116, 1979.

164. L.H. Quam, "Heirarchial Warp Stereo", in M.A. Fischler and O. Firschein (ed), Reading in Computer Vision: Issues, Problems, Principles and Paradigms, Morgan Kaufmann, 80-86, 1987.

165. S.P. Ramfjord and M.M. Ash, Occlusion, Saunders, 1971.

166. O. Reed, "Addenda for Francois Duret Workshop - December 5-6, 1986", Napili International, 4515 North 32nd St, Phoenix, Arizona 85018, August 5, 1986.

167. E.D. Rekow, "Applications of Planar Kinematics in Orthodontics", M.S. Thesis, University of Minnesota, 1982.

168. E.D. Rekow, A.G.Erdman, "Comparison of Techniques for Acquiring High-Precision Three-Dimensional Computer-Based Data Directly from the Human Mouth", Advances in Biomedical Engineering, ASME Winter Annual Meeting, Miami, Fl, November 1985.

169. E. D. Rekow, F.W. Worms, A.G. Erdman, T.M. Speidel, "Treatment Induced Errors in Occlusion Following Orthognathic Surgery", American Journal of Orthodontics, 88(5), 425-432, November 1985.

170. M.E.Ring, Dentistry: An Illustrated History, Mosby, 1985.

171. M.L. Rhodes, "Computed Tomography and its Modern Applications", Diagnostic Imaging Applications, SPIE vol 516, kE. Bechenback (ed), 28-51, October 1984.

172. D.F. Rogers and J. A. Adams, Mathematical Elements for Computer Graphics, McGraw Hill, 1976.

173. A. Rosenfeld, "Survey - Picture Processing: 1984", Computer Vision, Graphics, and Image Processing, 30, 189-242, 1984.

174. A. Rosenfeld, "Image Analysis", Digital Image Processing Techniques, M.P. Ekstrom (ed), Academic Press, 257-288, 1984.

ClearCorrect Exhibit 1002, Page 2157 of 3373

175. A. Rosenfeld, "Image Analysis: Problems, Progress, and Prospects", Readings in Computer Vision: Issues, Problems, Principles and Paradigms, M.A. Fischler and o. Firschein (ed), Morgan Kaufmann, 3-12, 1987.

176. A. Rosenfeld, "Computer Vision", Handbook of Pattern Recognition and Image Processing, T.Y. Young and K.S. Fu (ed), 355-368, Academic Press, 1986.

177. R. A. Schowengerdt, Techniques for Image Processing and Classification in Remote Sensing, Academic Press, 1983.

178. Servo Systems, Inc, Pasadena, California.

178a. K.S. Shanmugan, F.M. Dickey, J.A. Green, "On Optimal Frequency Domain Filters for Edge Detection in Digital Pictures", IEEE Transactions, PAMI-1, 37-49, 1979.

179. J. Shen and S. Castan, "A New Fast Algorithm for Stereo Vision", Computer Vision for Robots, SPIE vol 595, December 1985.

180. H.T. Shillingburg, S. Hobo, L, Whitsett, Fundaments of Fixed Prosthodontics, Quintessence, 1987.

181. J.Silness, H. Loe, "Periodontal Disease in Pregnancy, II: Correlation between Oral Hygiene and Periodontal Condition", Acta Odontologial Scandanavia, 22(9), 122-135, 1964.

182. "Applications", Solid Modeling Today, 1(10), 6, May 1986.

183. H. Sochurek, "Medicine's New Vision", National Geographic, 171(10), 2-41, January 1987.

184. T.C. Strand, "Optical 3-D Sensing for Machine Vision", Optical Engineering, 24(1), 33-40, Jan/Feb, 1985.

185. V. Torre and T.A. Poggio, "On Edge Detection", IEEE Transactions on Pattern Analysis and Machine Intelligence, PAMI-82, 147-163, March 1986.

186. D. Terzopoulos, "Multiresolution Computational Processes for Visual Surface Reconstruction", Computer Vision, Graphics, and Image Processing, 24, 52-96, 1983.

187. B.A. Toth, D.S. Ellis, B.S. Steward, Computer Designed Prostheses for Orbiocranial Reocnstruction, Plastic and Reconstructive Surgery, 8193, 315-322, March 1988.

ClearCorrect Exhibit 1002, Page 2158 of 3373

188. 3M Product Literature, Experimental Laboratory Data specifications for partially stabilized zirconia, Ceramic Materials Department, 3M, St. Paul, MN, June 1985.

189. A.K.I. Torlegard, "State of the Art of Close-Range Photogrammetry" Photogrammetric Engineering and Remote Sensing, 76.

190. J. Unterseher, J. Hansen, B. Schlesinger, Holography Handbook, Ross Books, 1982.

191. A.M. Waxman and J.H. Duncan, "Binocular Image Flows: Steps Toward Stereo-Motion Fusion", IEEE Transactions on PAMI, 8(6), 715-729, 1986.

192. D.J. Wanserski, K.P. Sobszak, J.G. Monaco, G.P. Mcgivney, "An Analysis of Marginal Adapatation of All-Porcelain Facial Margin Ceramo-metal Crowns", Journal of Prosthetic Dentistry, 56(3), 289-291, September 1986.

193. J.A. Webb and J.K. Aggarwal, "Shape and Correspondance, CVGIP, 21, 145-160, 1983.

194. E.J. Weller (ed), Nontraditional Machining Processes Society of Manufacturing Engineers, 1984.

195. P. M. Will and K. S. Pennington, Proceedings, IEEE, 60, 669, 1972.

196. K. W. Wong, "Mathematical Formulation and Digital Analysis in Close Range Photogrammetry", Photogrammetric Engineering and Remote Sensing, 41(11), 1355-1373, November 1975.

197. Y. Yakimovsky and R. Cunningham, "A System for Extracting Three-Dimensional Measurements from a Stereo Pair of TV Cameras", Computer Graphics and Image Processing, 7, 195-210, 1978.

198. X. Xhu, Computer Graphics Notes, University of Minnesota, Summer 1985.

199. G.P. Zientara and L.J. Neuringer, "Medical Imaging for the 21st Century", Perspectives in Computing, 81, 14-24, Spring 1988.

ClearCorrect Exhibit 1002, Page 2159 of 3373

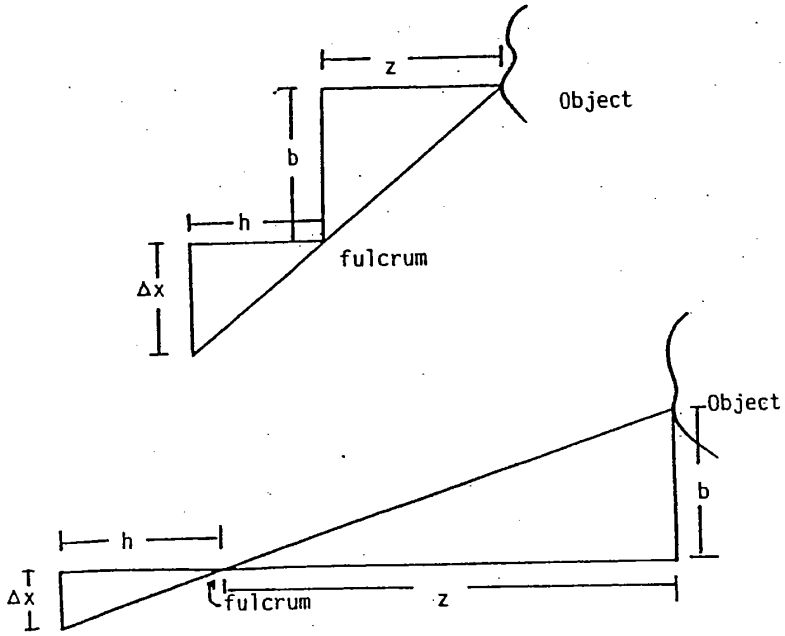


Figure 1. Principles for Triangulation Mensuration

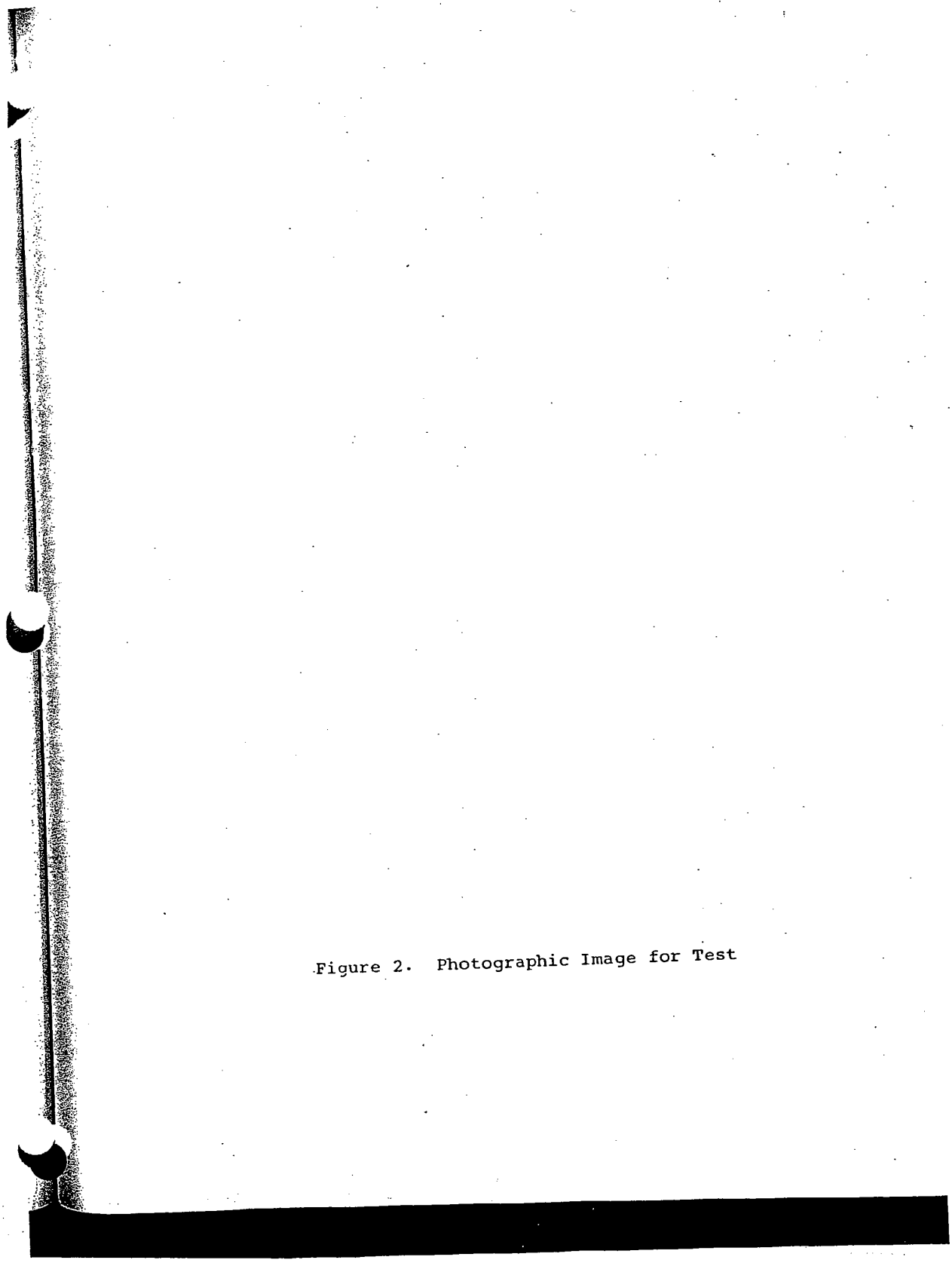


Figure 2. Photographic Image for Test

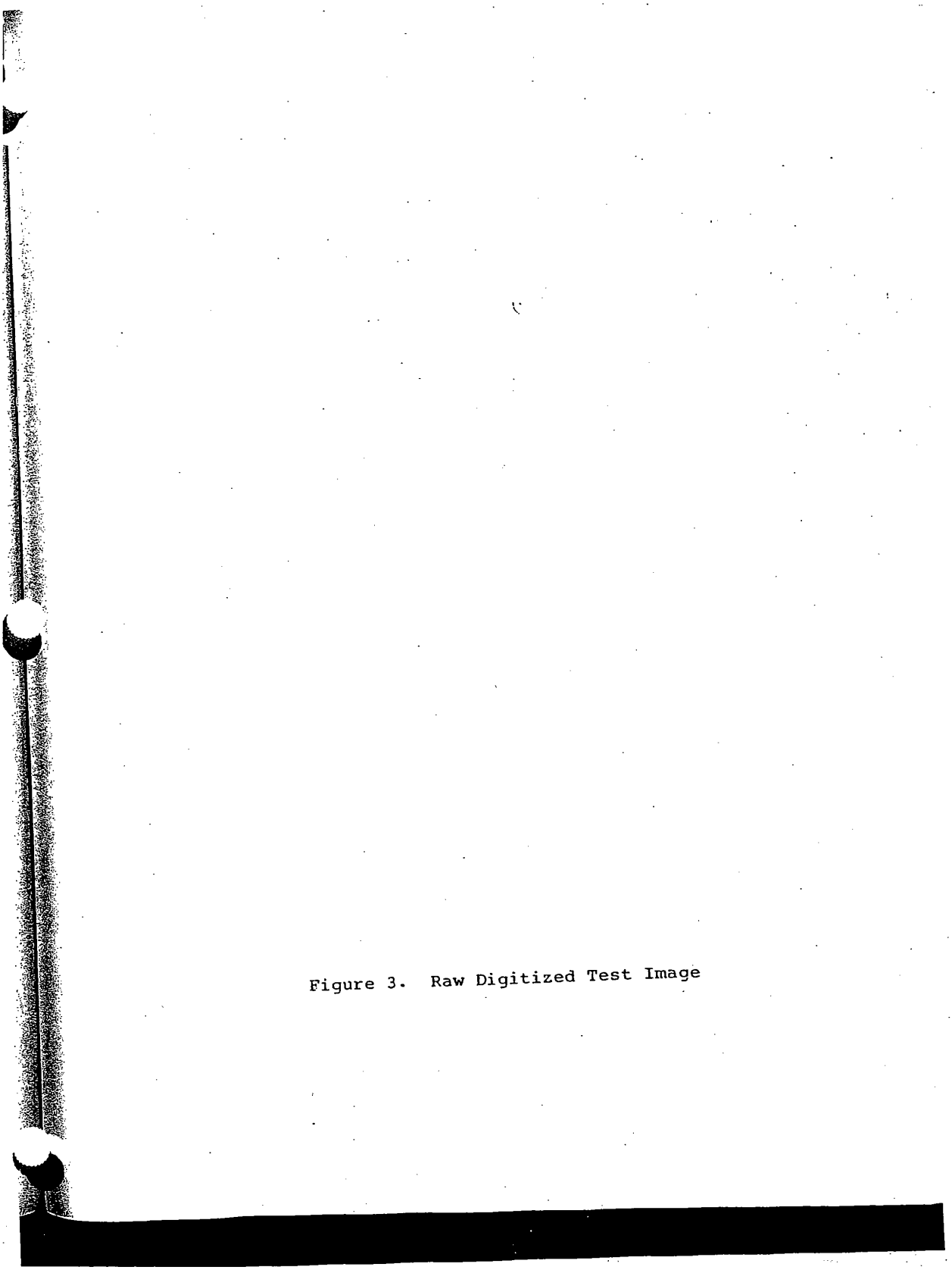


Figure 3. Raw Digitized Test Image

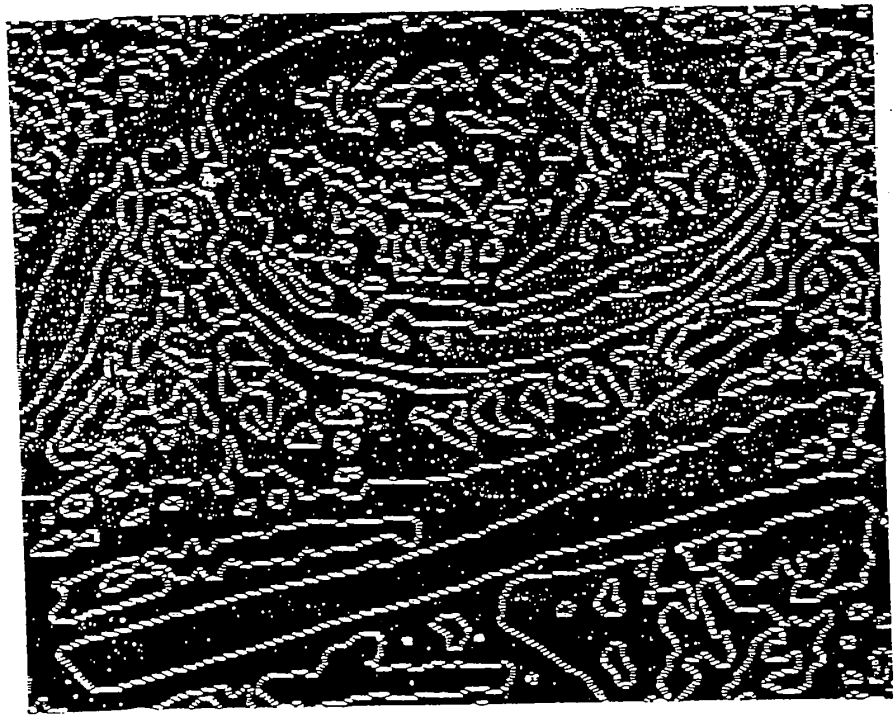


Figure 4. Edges using Marr-Hildreth Algorithm

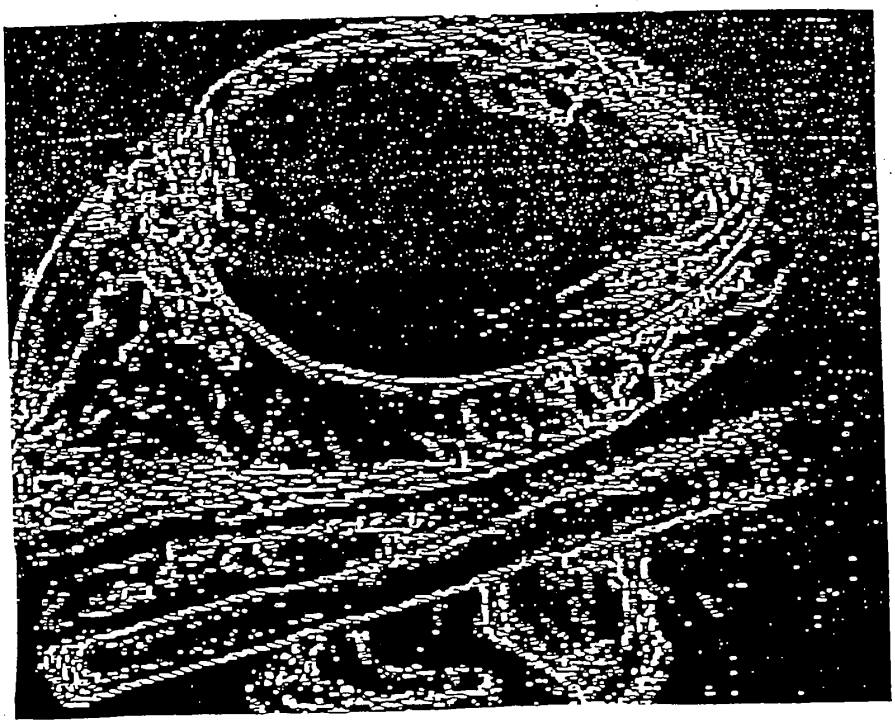


Figure 5. Edges using Haralich Algorithm

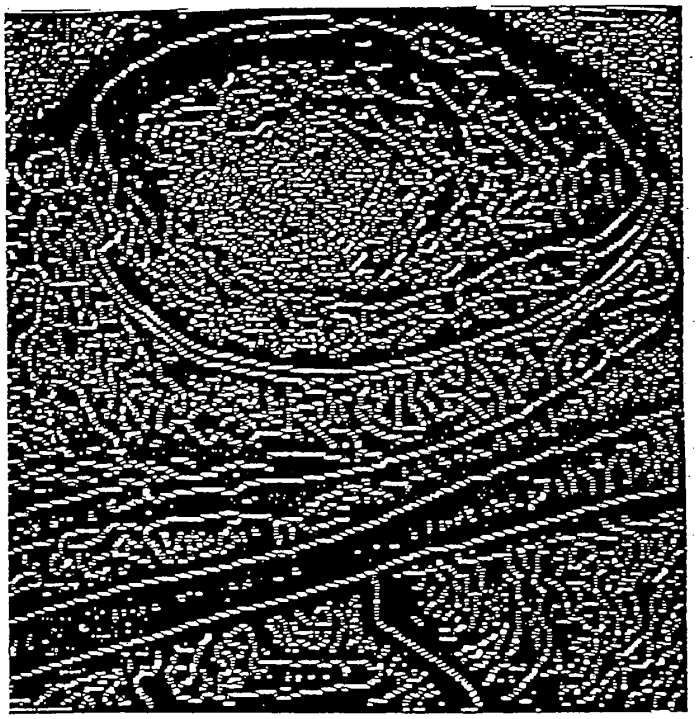


Figure 6. Edges using Canny Algorithm

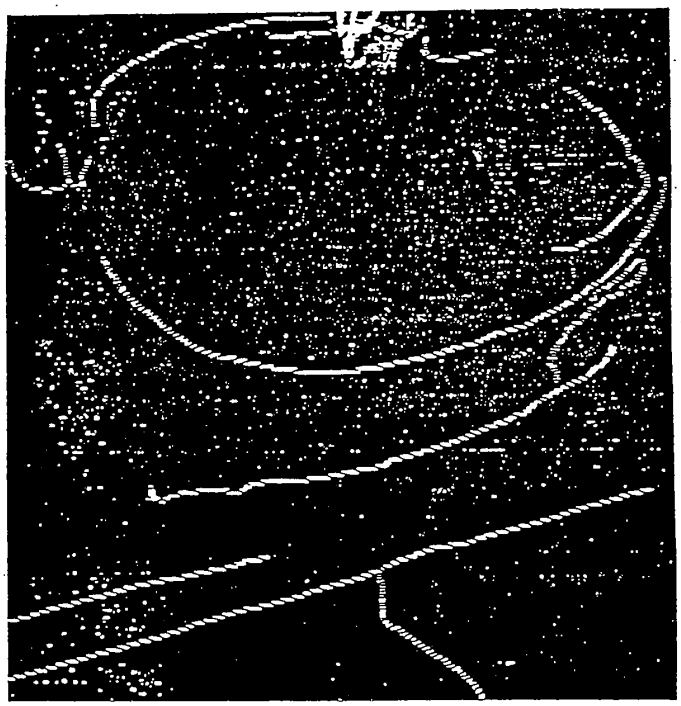


Figure 7. Edges using Canny Algorithm with Strong Thesholds

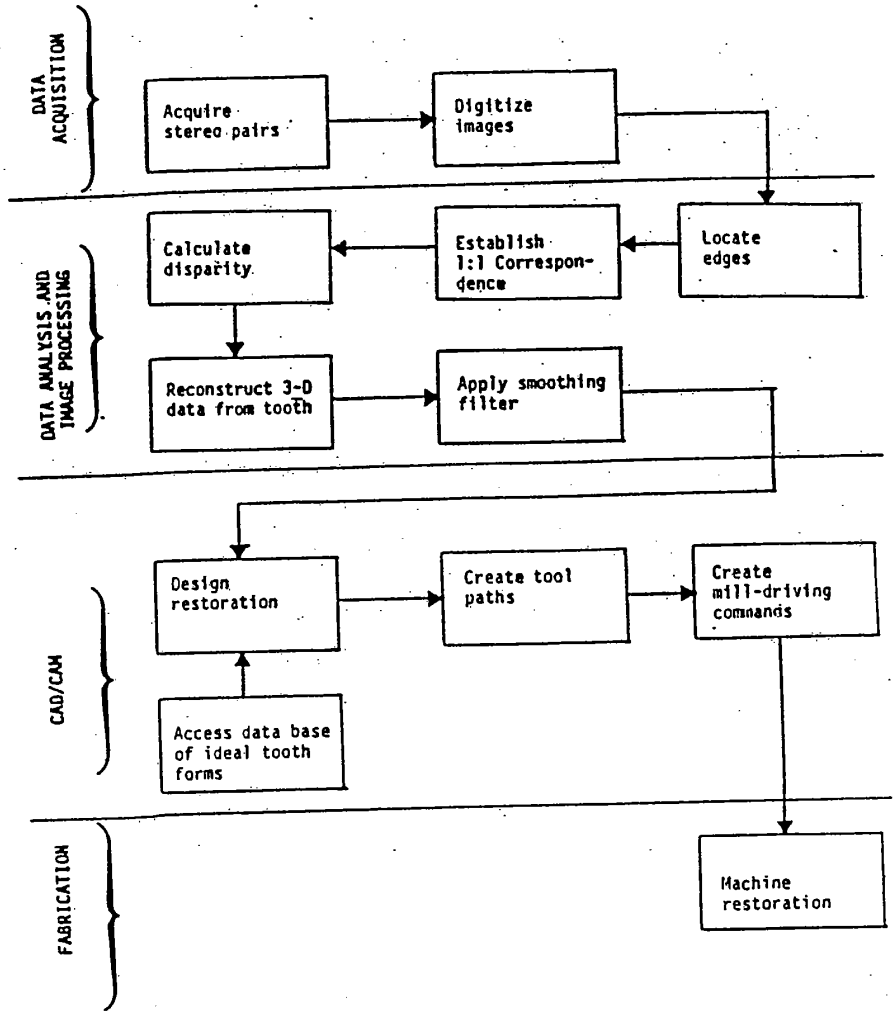


Figure 8. Flow Chart of Processes in Automated System

Figure 9. Data Acquisition System

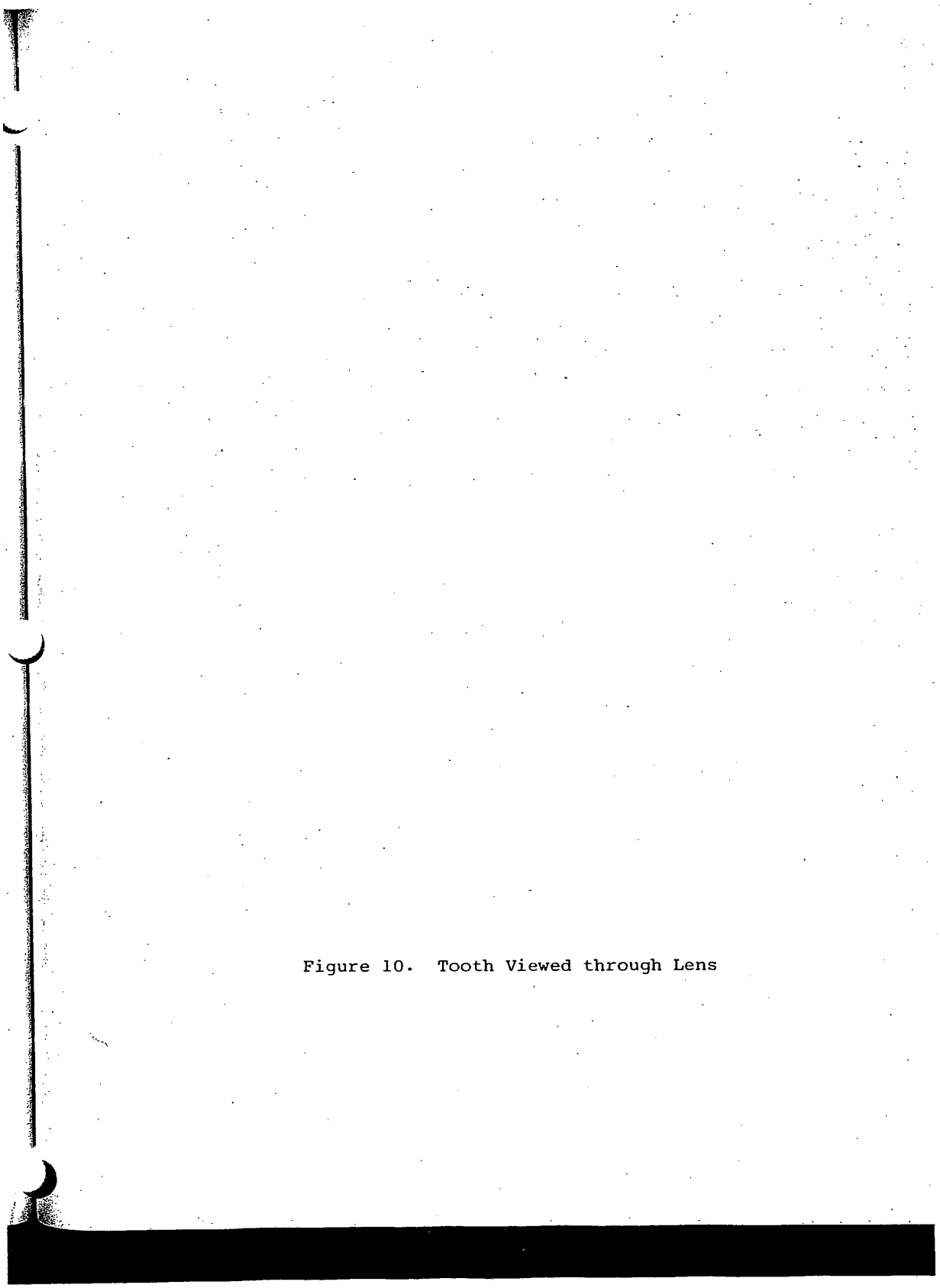


Figure 10. Tooth Viewed through Lens

Figure 11. Experimental Setup forData Acquisition

Figure 12. Grating Projected on Tooth - Left View

Figure 13. Grating Projected on Tooth - Right View

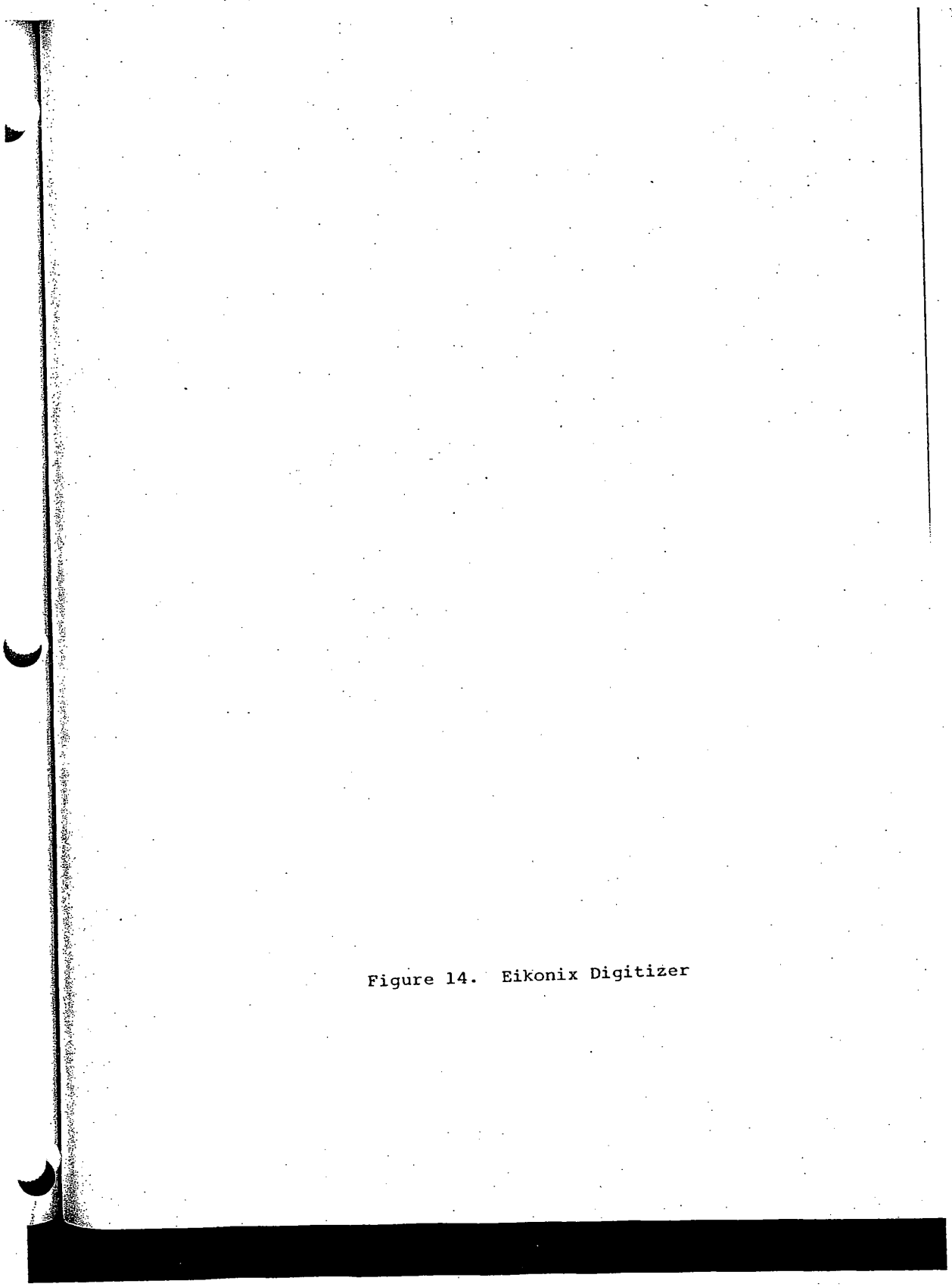


Figure 14. Eikonix Digitizer

Figure 15. Close-up of Digitizer Console

Figure 16. Anti-Vibration Device on Digitizer

Figure 17. Edges - from Left View

Figure 18. Edges - from Right View

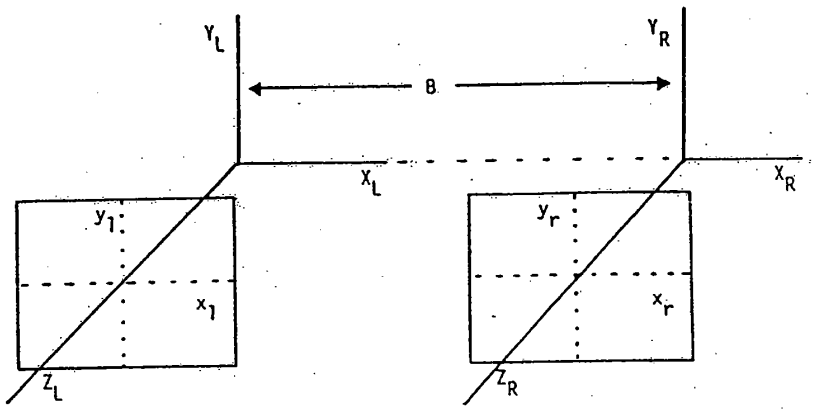


Figure 19. Camera Model for Disparity Calculation

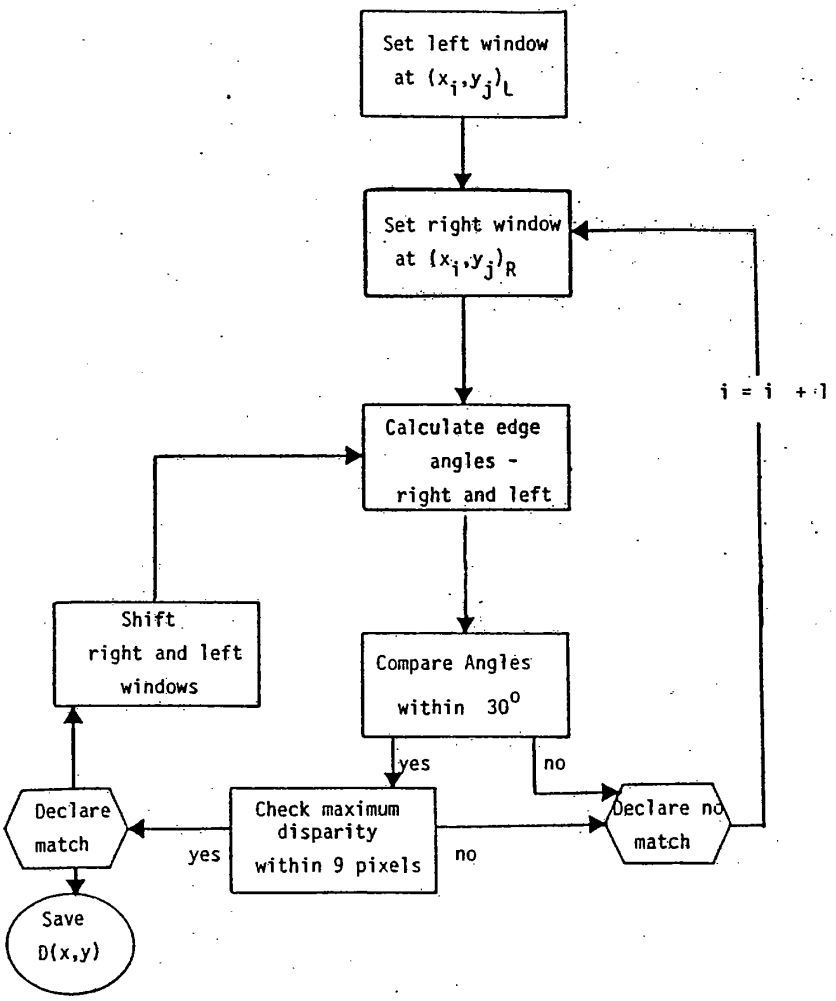


Figure 20. Flow-Chart of 1:1 Correspondence

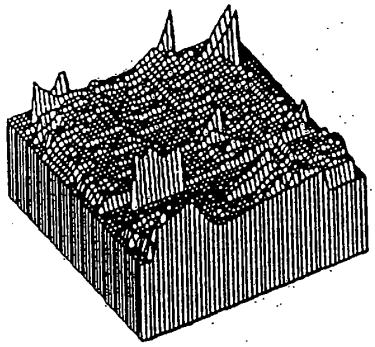


Figure 21a. Surface Reconstruction -
Initial Reconstruction

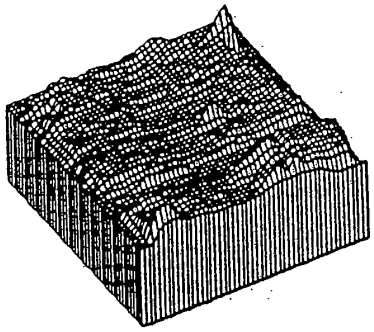


Figure 21b. Surface Reconstruction -
After 5 Iterations with Smoothing Algorithm

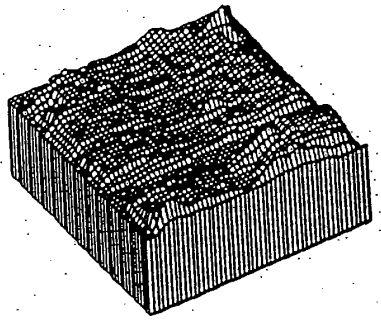


Figure 21c. Surface Reconstruction -
After 10 Iterations

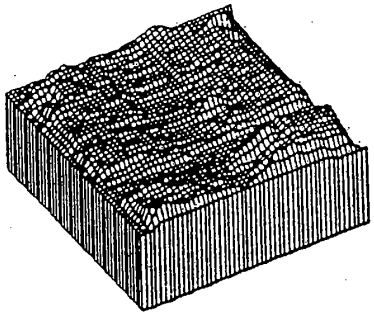


Figure 21d. Surface Reconstruction -
After 15 Iterations

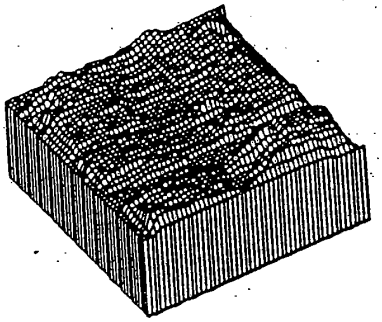


Figure 21e. Surface Reconstruction - After 20 Iterations

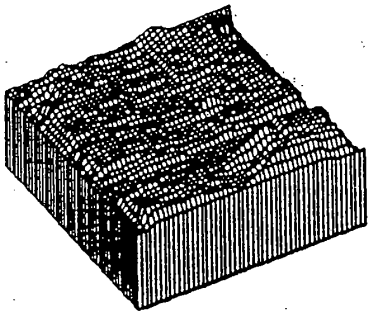


Figure 21f. Surface Reconstruction - After 25 Iterations

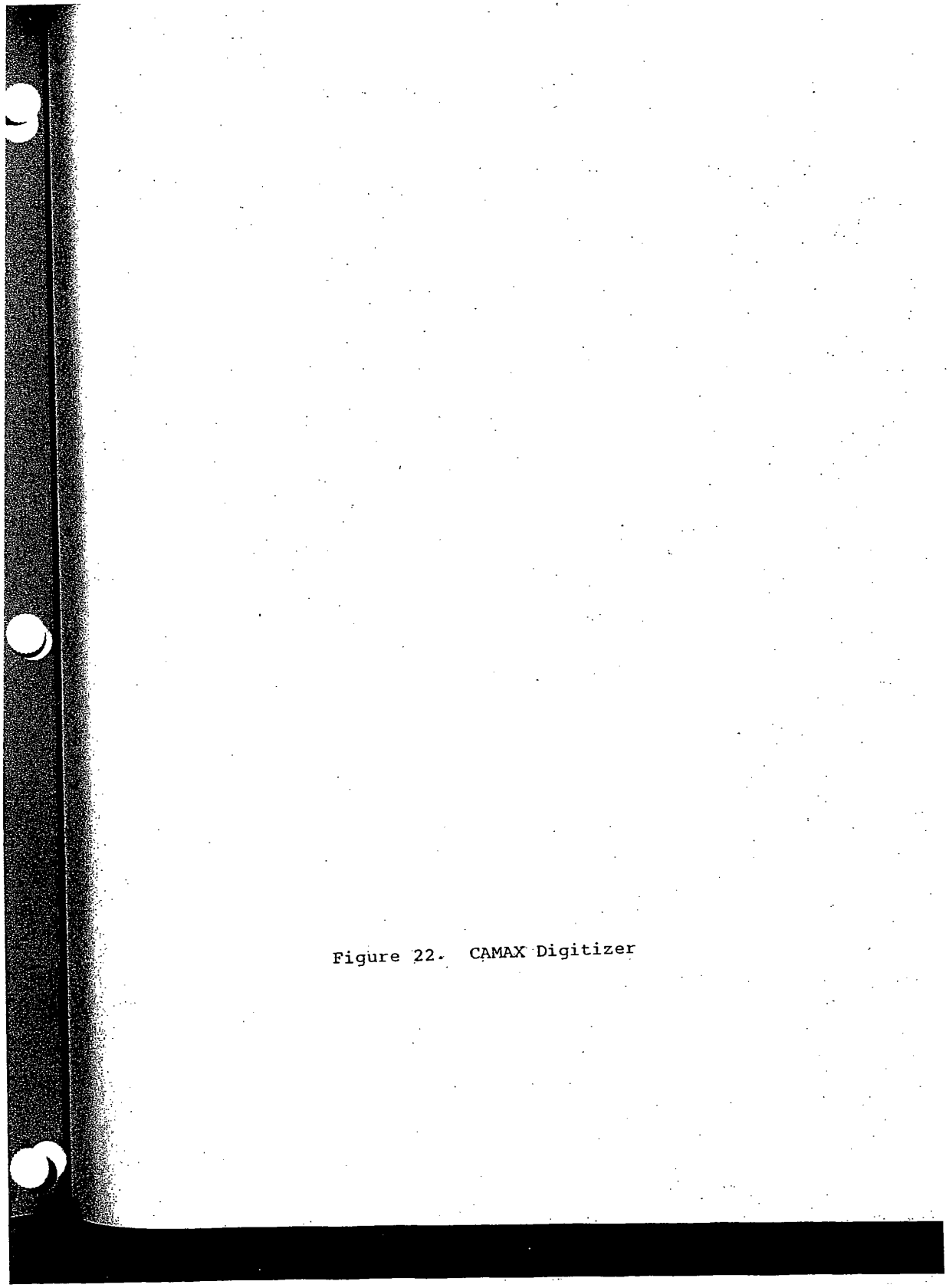


Figure 22. CAMAX Digitizer

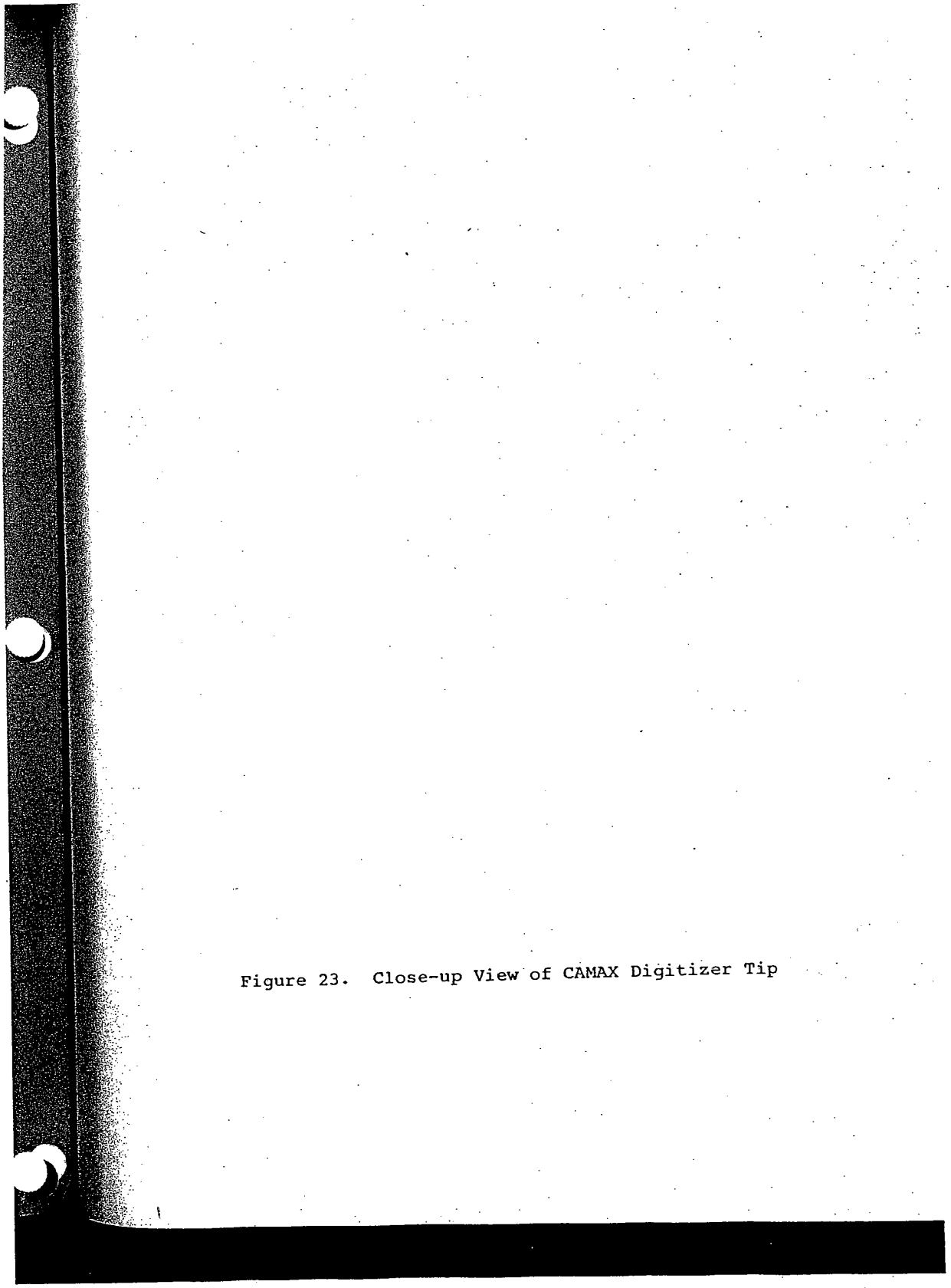


Figure 23. Close-up View of CAMAX Digitizer Tip

Figure 24. Exampled of Tooth Configuration Recreated from Data Base of Tooth Forms

Figure 25. Screen 1 of Occlusal Data Base Program

Figure 26. Screen 2 of Occlusal Data Base Program

Figure 27. Screen 3 of Occlusal Data Base Program.

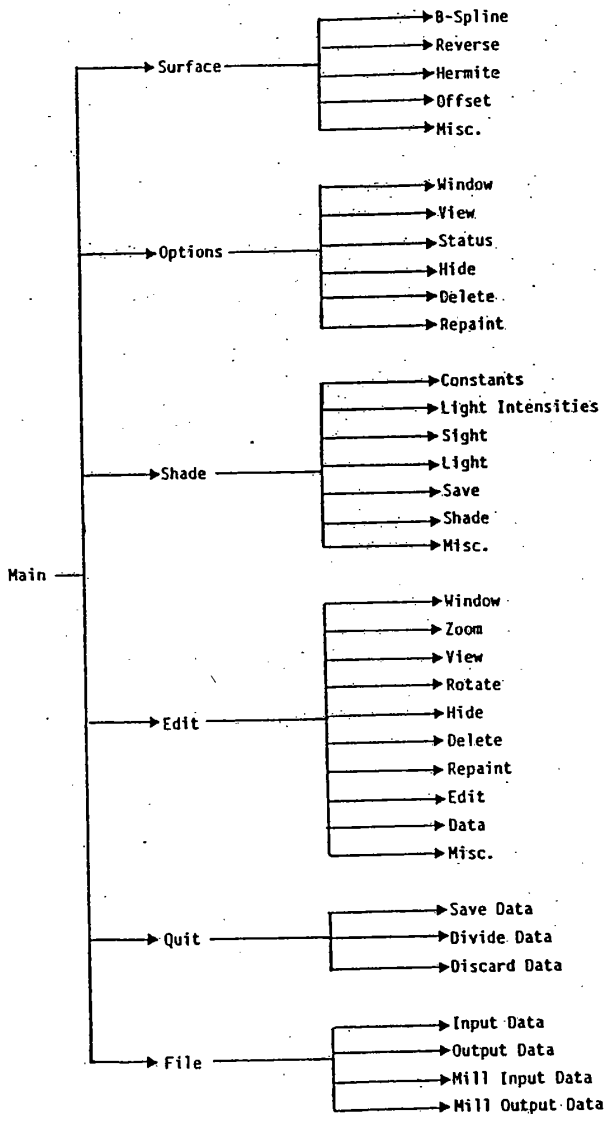


Figure 28. Flow Chart of Primary CAD/CAM Options (See Table 5 for Details)

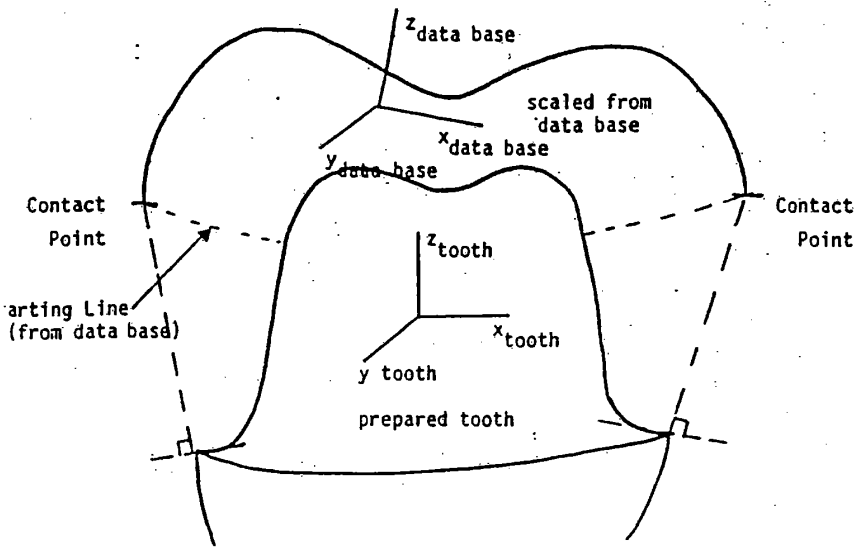


Figure 29. Restoration Design Considerations

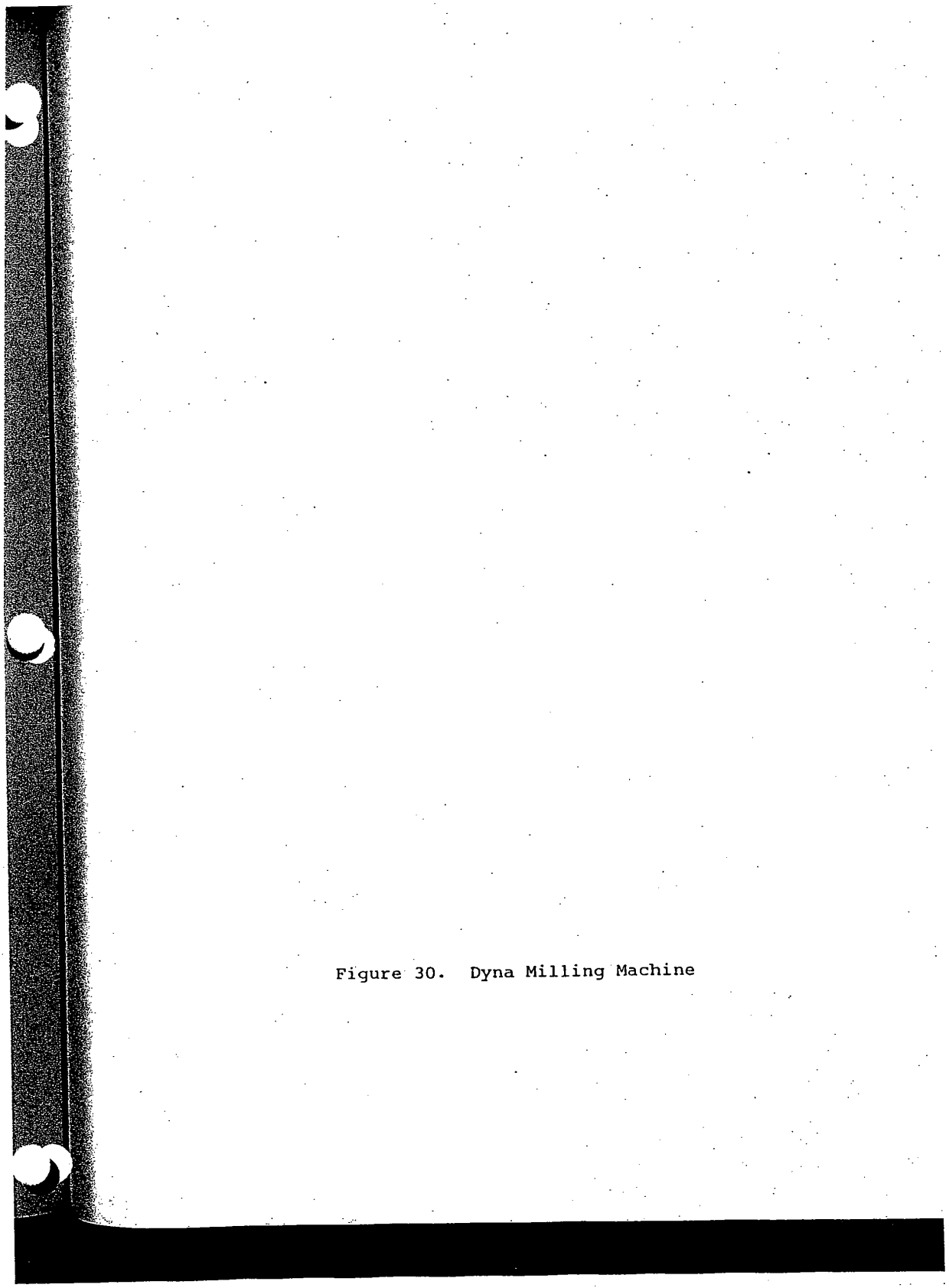


Figure 30. Dyna Milling Machine

Figure 31. Servo Milling Machine

Figure 32. Milled Restoration

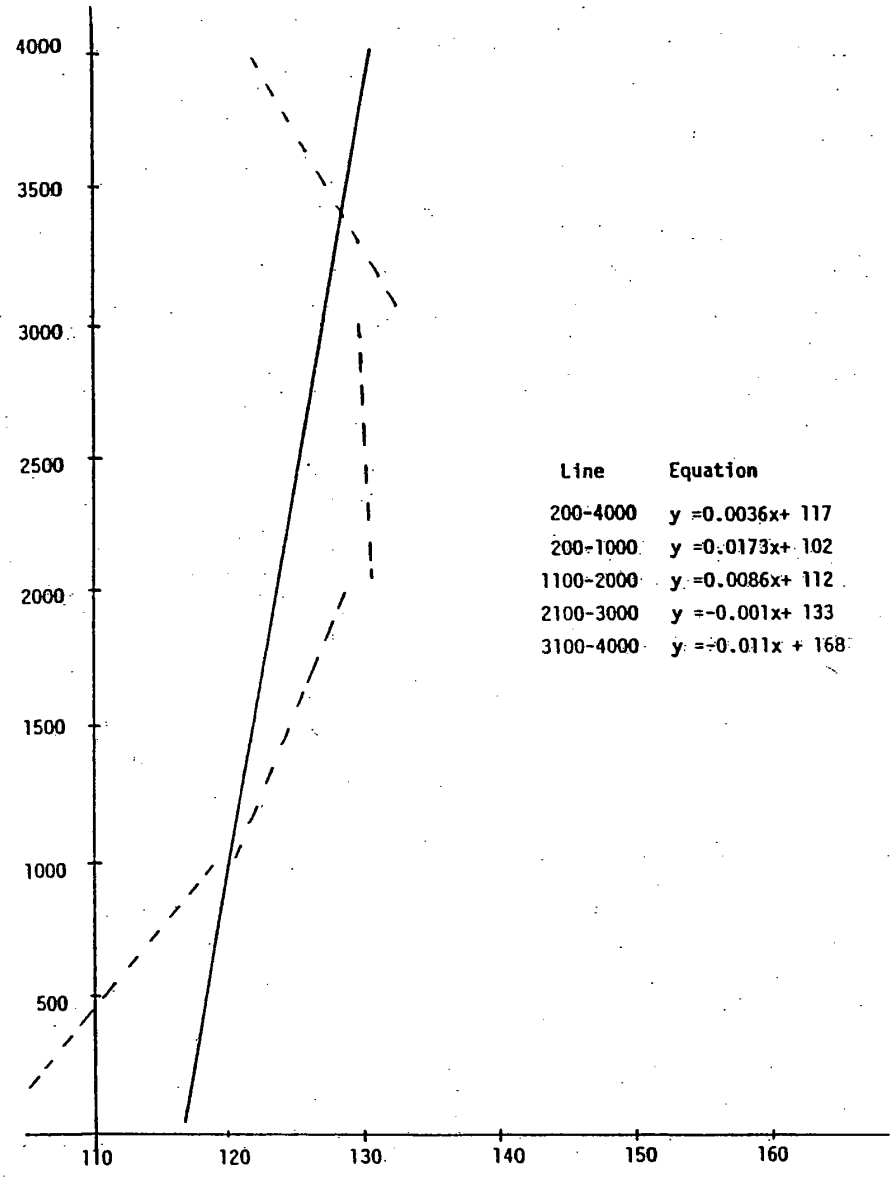


Figure 33a. Digitizer Lens Distortion - Line 5

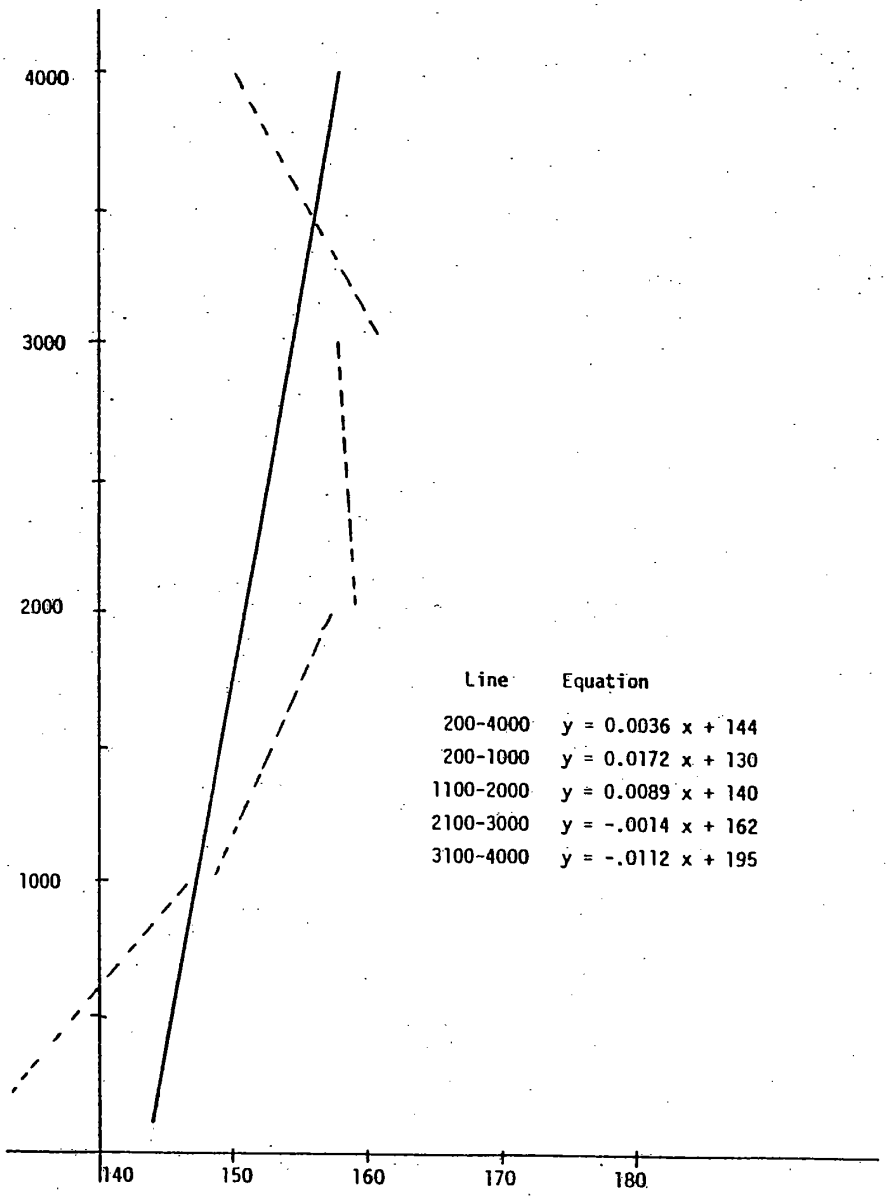


Figure 33b. Digitizer Lens Distortion - Line 6

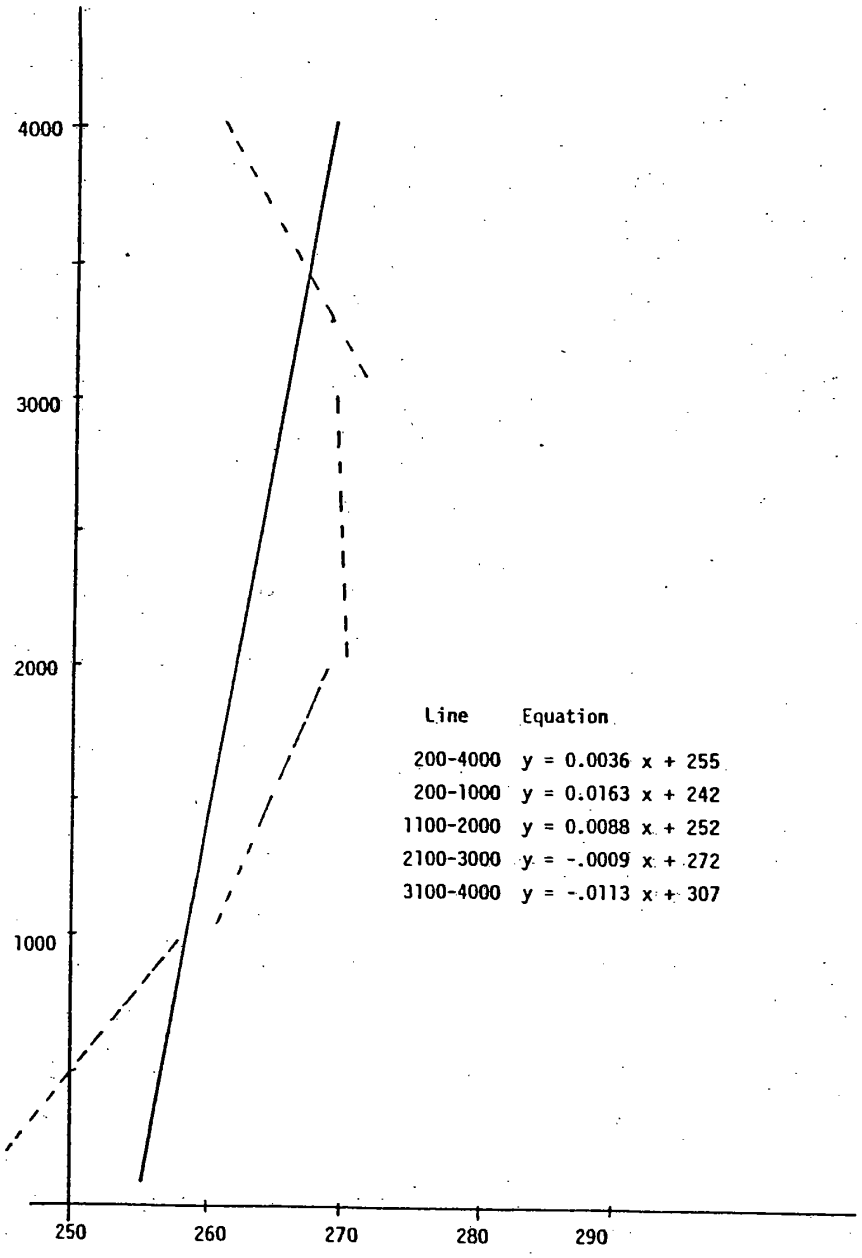


Figure 33c. Digitizer Lens Distortion - Line 10

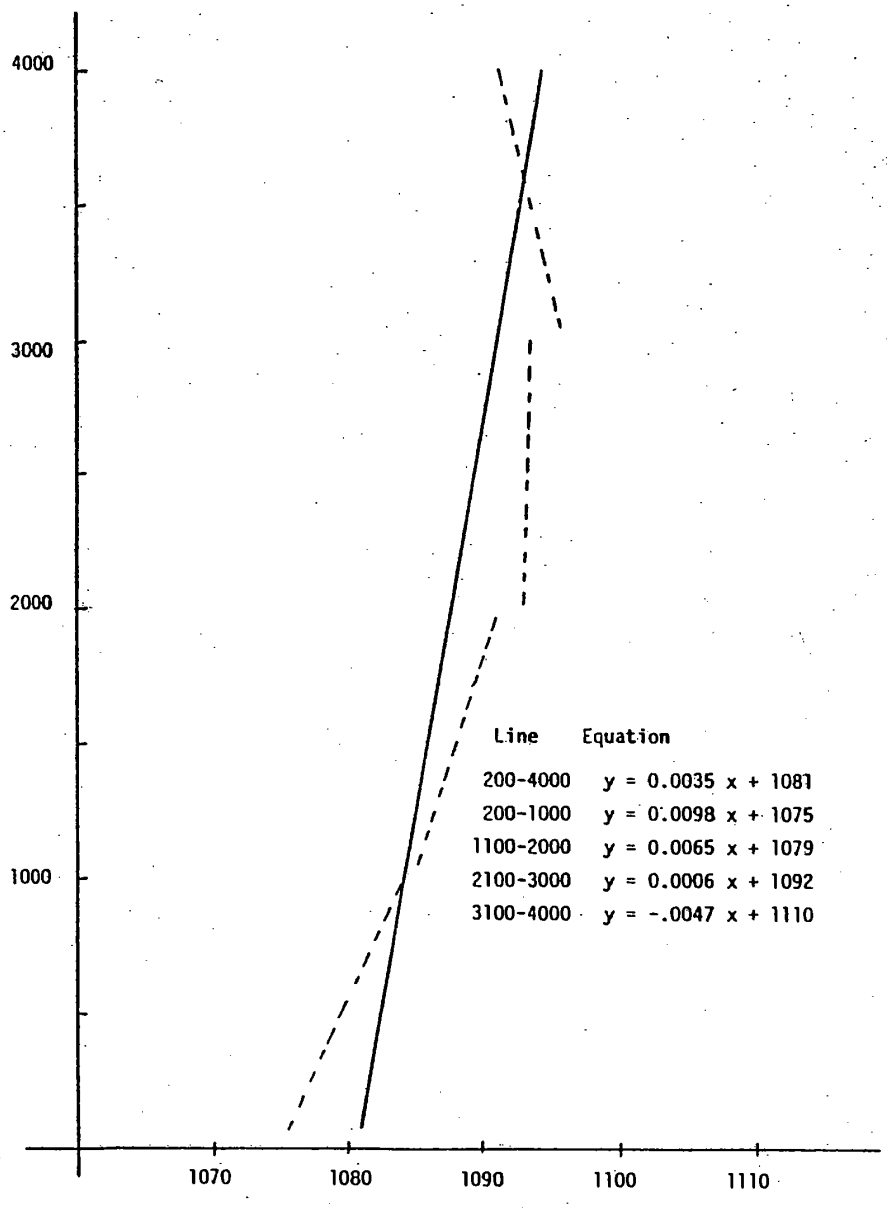


Figure 33d. Digitizer Lens Distortion - Line 40

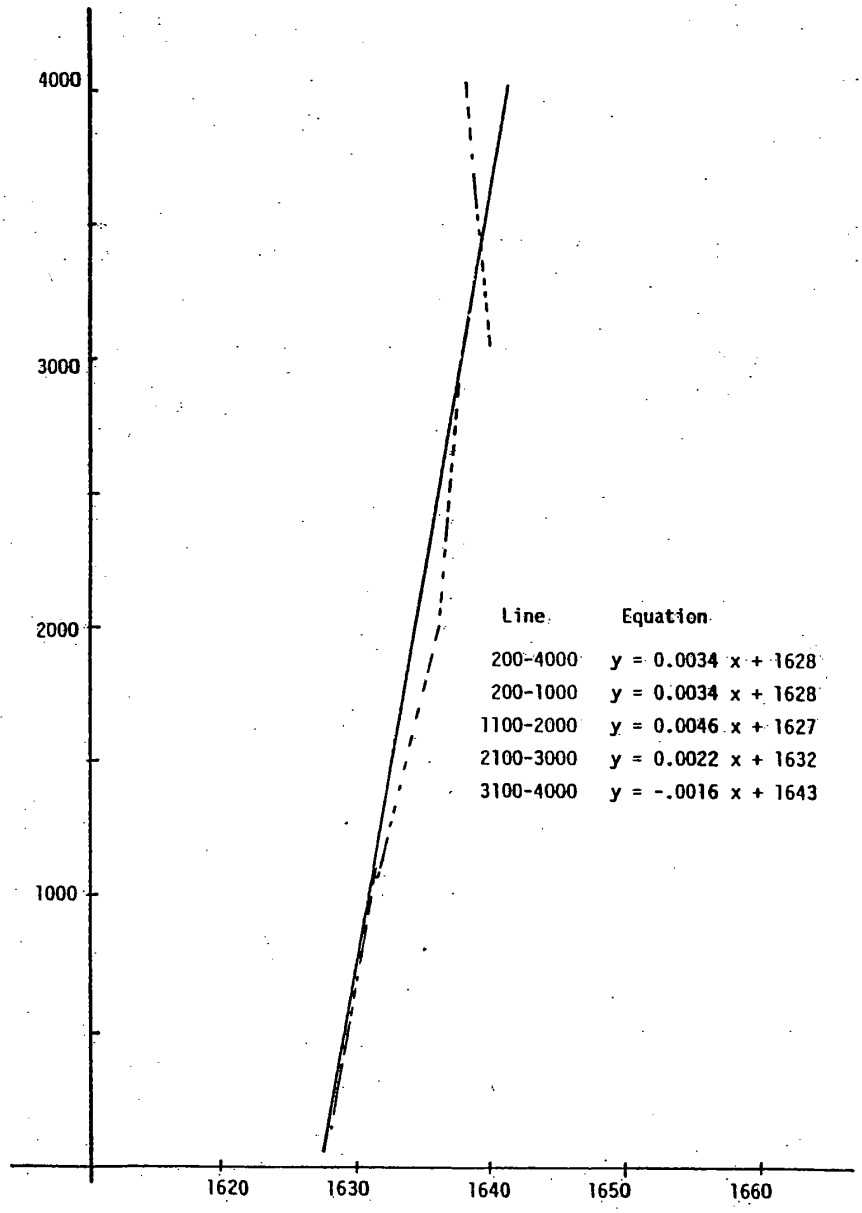


Figure 33e. Digitizer Lens Distortion - Line 60

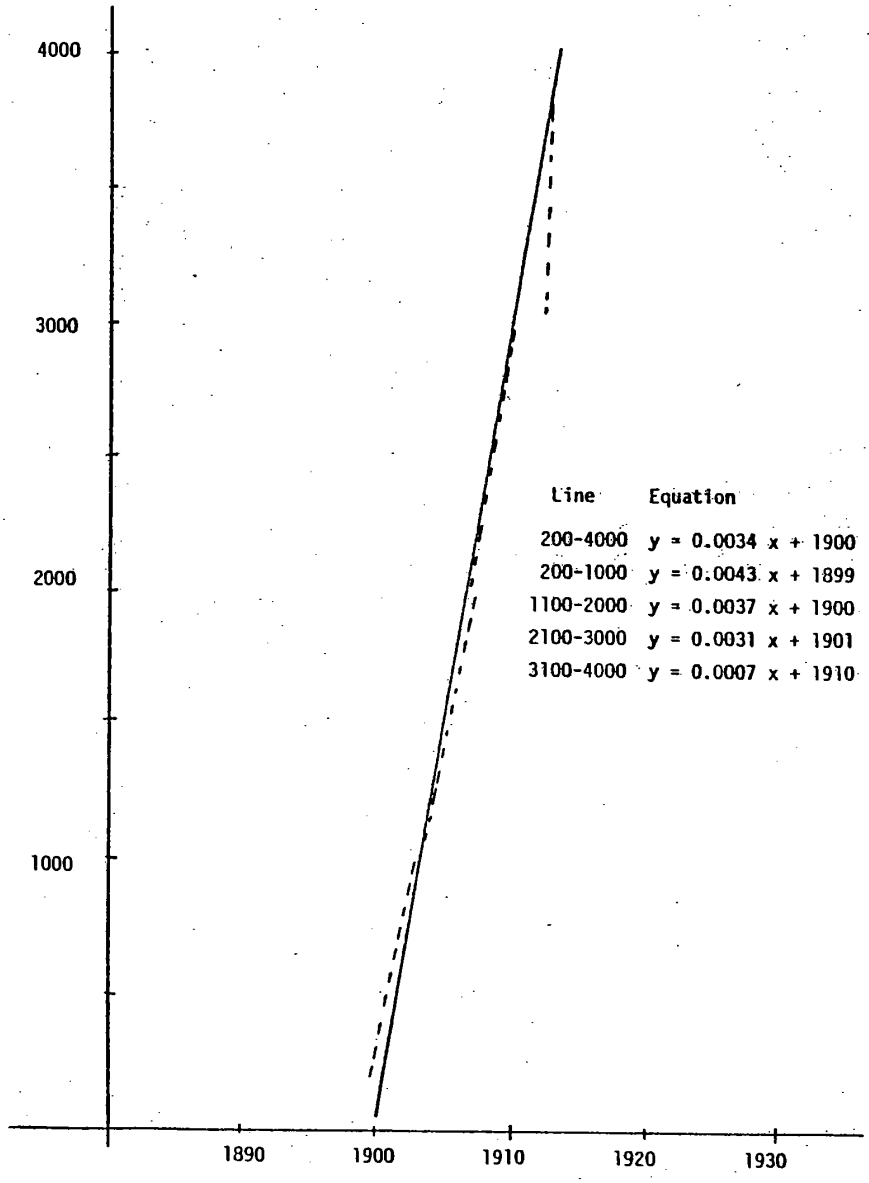


Figure 33f. Digitizer Lens Distortion - Line 70

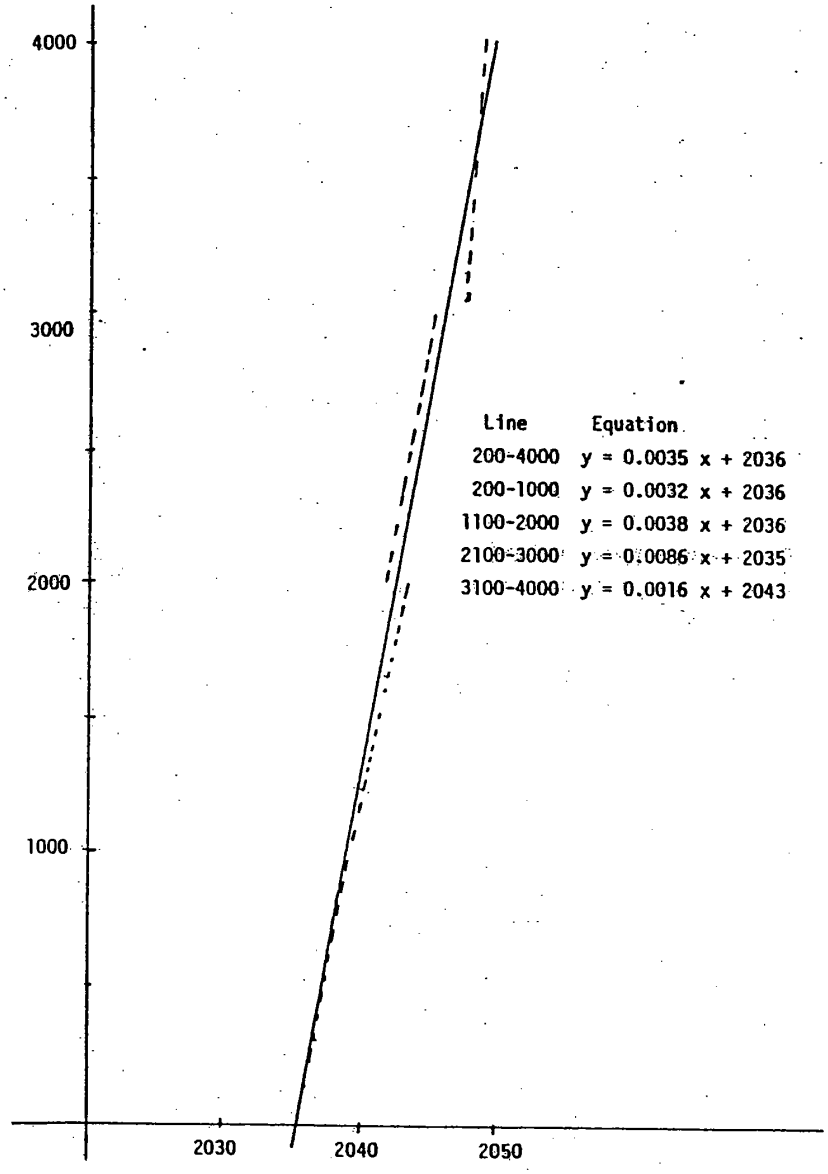


Figure 33g. Digitizer Lens Distortion - Line 75

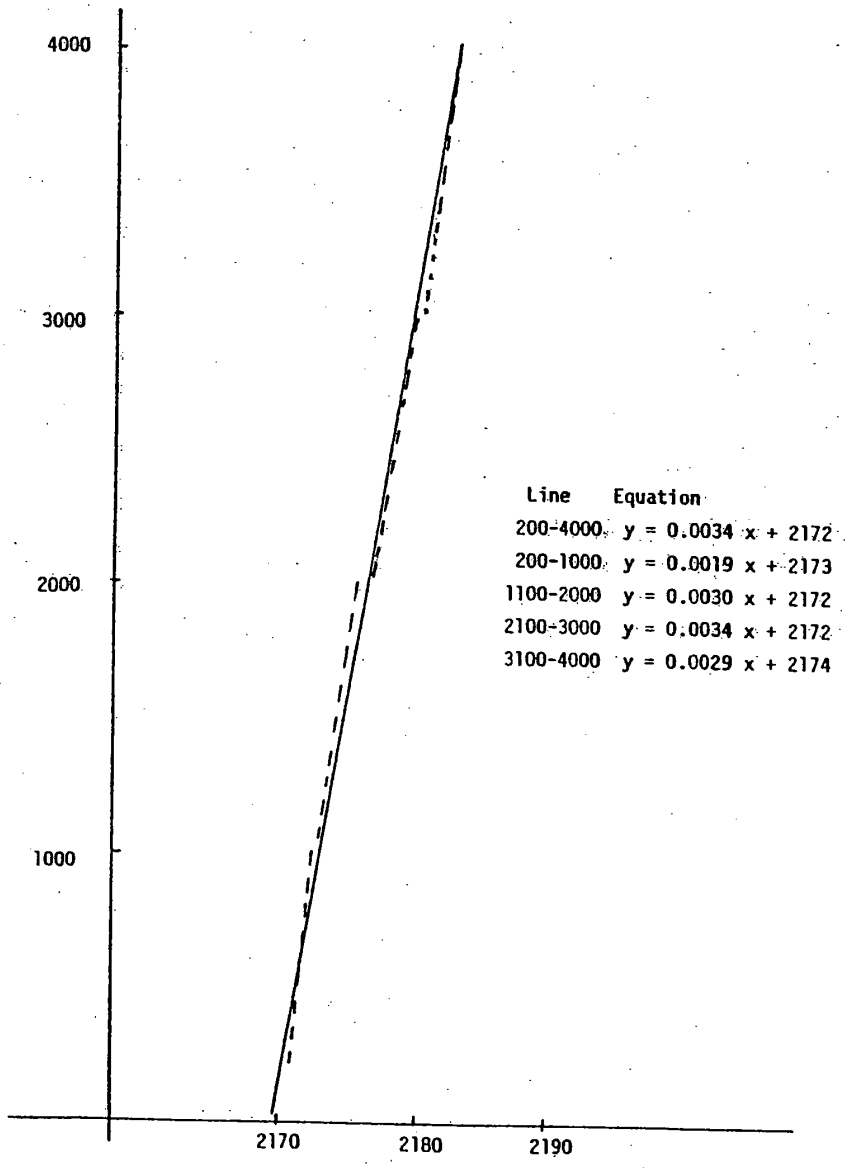


Figure 33h. Digitizer Lens Distortion - Line 80

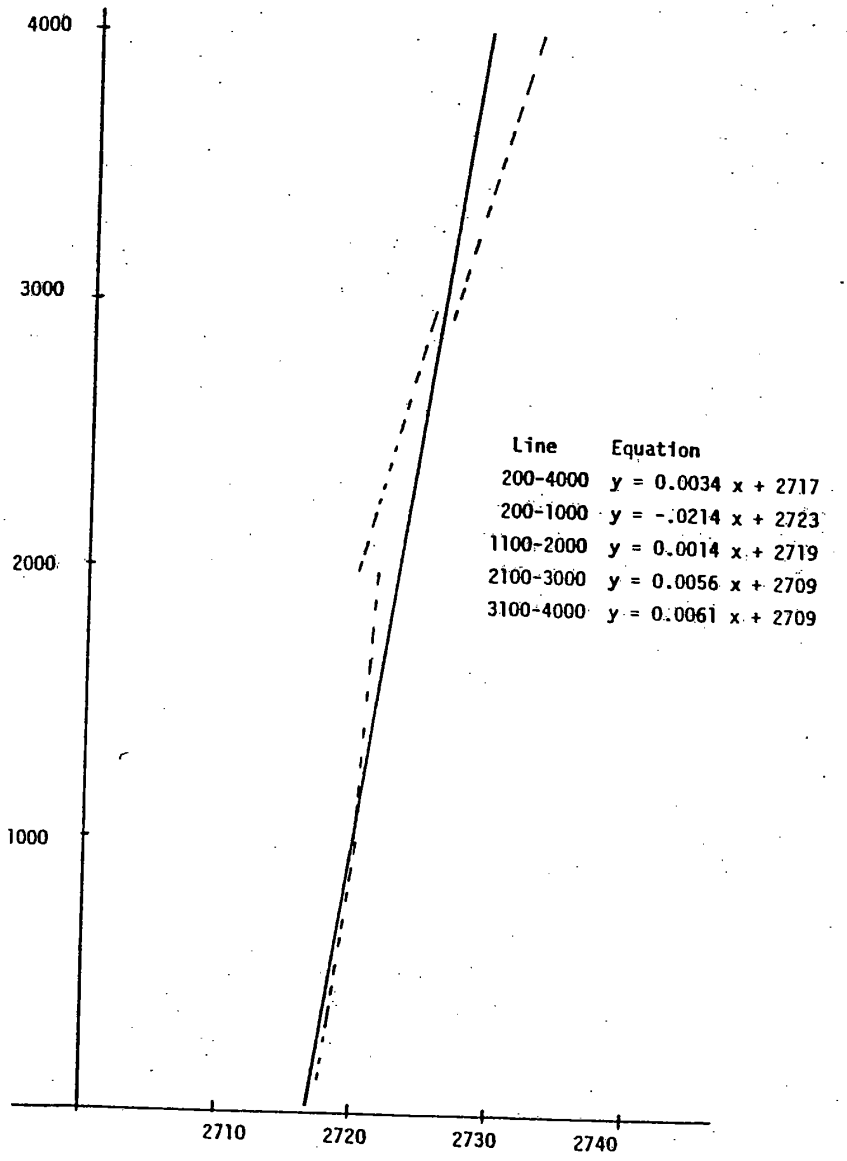


Figure 33i. Digitizer Lens Distortion - Line 100

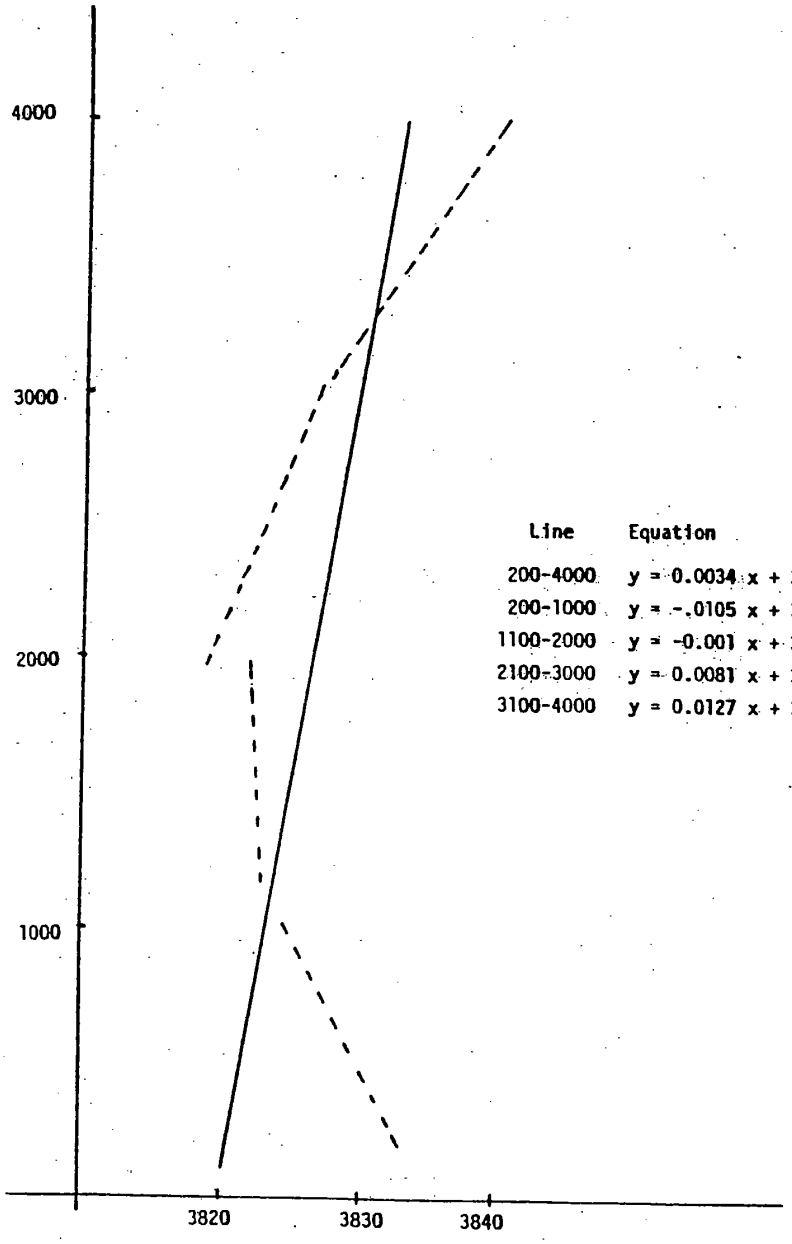


Figure 33k. Digitizer Lens Distortion - Line 140

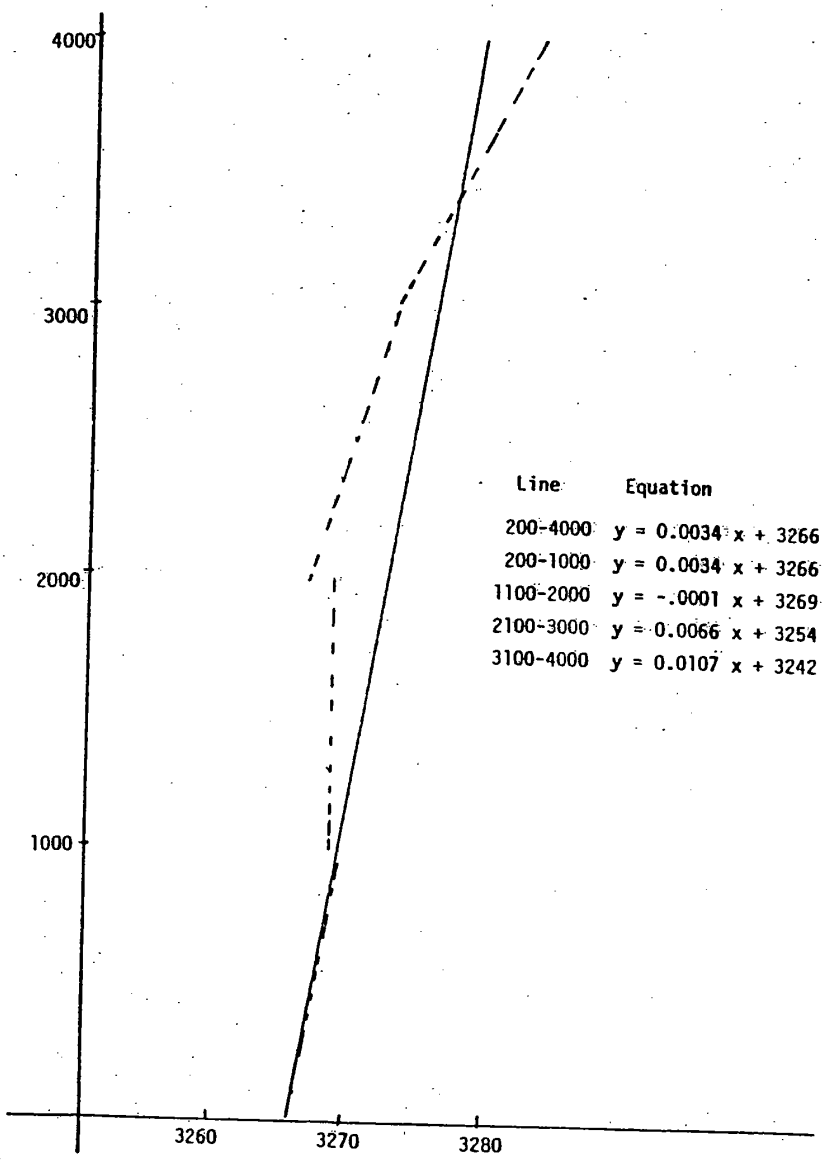


Figure 33j. Digitizer Lens Distortion - Line 120

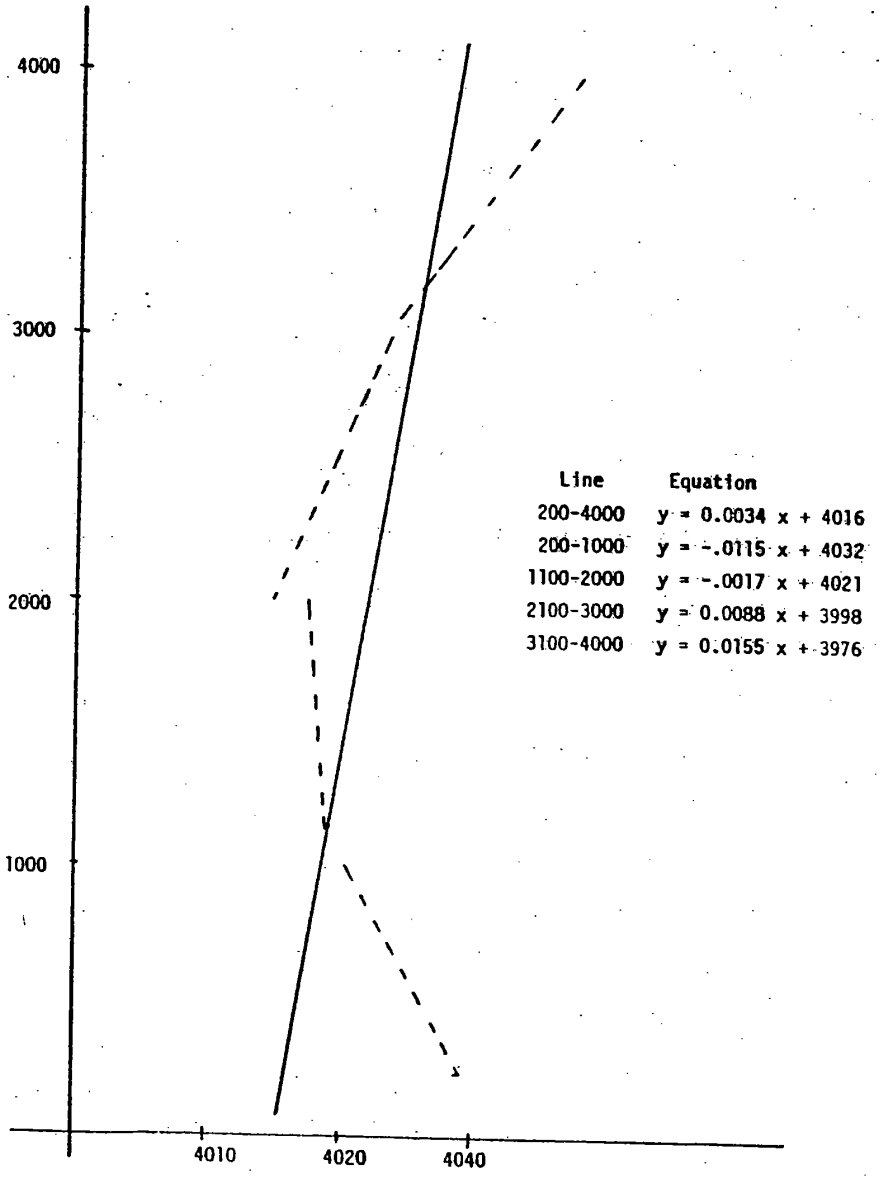


Figure 331. Digitizer Lens Distortion - Line 147

Appendix 1. Clinical Criterion for Restoration Acceptance

Appendix I. Clinical Criterion for Restoration Fit

Evaluation of clinical performance is a difficult issue (4 and 1). In 1973 the House of Delegates of the California Dental Association authorized a task force to "define the standards of quality of dental care and necessary measures or procedures which shall be utilized by any agency who participates in a dental quality control program" (5). The system developed by that agency created a yes-, maybe-, probably no-, no-system of grading the quality of restorations (3). Specific criterion are itemized for each type of restoration. Those restorations judged to be yes or maybe were clinical acceptable; the others are not. Restorations receiving a maybe judgement are to be re-evaluated and re-judged in one year. The criterion developed at the University of Minnesota, School of Dentistry are given in Tables I and II and are very similar to those itemized in the California guidelines. Since these Minnesota criterion have been in place for some years, examiners are familiar with the criterion and reproducability is good (2).

The following criterion are based on the California and Minnesota guidelines and will be applied for rating the automatically produced restorations. The dentists will make independent evaluations. Each dentist will evaluate each characteristeristic (see Table I) of the restoration. An overall grade will be assigned for the restoration. For clinical practical examinations, grades used are:

N - Ideal

S - Clinically satisfactory but not ideal. No compromise to performance. (Eg. a minor surface flaw away from the gingiva.)

M - Not clinically satisfactory but with some modification (without requiring recasting) could be clinically acceptable. (Eg. Heavy occlusal contact.)

E - Clinically unsatisfactory and critical (critical errors are identified in Table II). (Eg. An open interproximal contact.)

If any characteristic is not clinically acceptable, the reason must be explictly stated. If there is disagreement in the judged quality, the restoration will be judged to be clinically acceptable if two of the three judges rate it as acceptable and no judge has assigned a grade of E; it will be unacceptable if two or more judges rate it as unacceptable. All restorations will be judged both before and after cementation. If the automatically produced restoration is judged to be clinically unacceptable at any stage, the patient will be provided the option of having it remade (at no cost to the patient) by either traditional or automatic processes.

References:

1. Symposium on Quality Assessment, R.P. Burakoff, N.A. Demby (ed.), Dental Clinics of North America, vol. 29(3), July 1985.

2. G.L. Hill, M.J. Bebeau, M. Luxenberg, "Improving the Objectivity, Reliability, and Efficiency of Preclinical Evaluation", accepted for publication, J. Dent. Educ., January 1987.

3. "Quality Evaluation for Dental Care: Guidelines for the Assessment of Clinical Quality and Professional Performance", California Dental Association, 1977.

4. G. Ryge, M. Snyder, "Evaluating the Clinical Quality of Restorations", JADA, vol. 87, p. 369-377, August 1983.

5. G. Ryge, "Evaluation of Clinical Quality and Professional Performance", Journal of Dental Education, vol. 39(9), p. 582-3, September 1975.

Table I.
University of Minnesota School of Dentistry
Preclinical Fixed Prosthodontics

MANDIBULAR FULL VENEER CAST GOLD CROWN

Student_____ Bench #____

Preparation (Final)		Critical Error	3	2	1	0	3	2	1	0
Occlusal reduction	(9)	Clearance Occlusal form Relationship with opposing teeth								
Axial reduction	(9)	Convergence Amount of axial reduction Proximal line angles								
Finishing lines	(6)	Chamfer too heavy/light Position relative to gingival margin Maximum points: 24								

Instructor signature _____ Date_____ Total Points_____ Student eval._____

Wax Pattern		Critical Error	3	2	1	0	3	2	1	0
Axial contours	(3)	Facial/lingual surfaces Proximal surfaces								
Proximal contacts	(3)	Facial/lingual width Occlusal/gingival height Contact with adjacent teeth								
Occlusal function	(3)	Centric contacts Eccentric contacts								
Occlusal surface	(3)	Occlusal form Marginal ridges Ridge/groove location Supplemental anatomy								
Margins	(3)	Over/underwaxed Open Internal adaptation								
Surface finish	(3)	Uneven, not smooth Excess lubricant on surface Maximum points: 18								

Instructor_____ Date_____ Total points_____ Student eval._____

Scoring:
- 3 = Meets the standard perfectly
- 2 = Minor deviation from the standard
- 1 = Major deviation from the standard but clinically acceptable
- 0 = Clinically unacceptable

Table I (Continued)

Student_____Bench #_____

Unfinished Casting (with sprue attached)		Critical Error	3 2 1 0	3 2 1 0
Fit on die	(3)	Loose/tight		
Margins	(3)	Short/Long or Open		
Proximal contacts	(3)	Open		
Surface	(3)	Pits/rough/porosity		
		Maximum points: 12		

Instructor signature_____Date_____Total points_____Student eval._____

Finished Casting		Critical Error	3 2 1 0	3 2 1 0
Centric contacts	(3)	Too heavy/light Location		
Occlusal function	(3)	Working/non-working interference		
Proximal contacts	(3)	Location Contour Open/too tight		
Margins	(3)	Short/long or Open		
Surface finish	(3)	Rough/overpolished anatomy		
		Maximum points: 15		

Instructor _____Date_____Total points_____Student eval._____

Contact Soldered		Critical Error	3 2 1 0	3 2 1 0
Contact w/adjacent tooth	(3)	Open/too tight		
Contour	(3)	Bucco-lingual/occluso-gingival		
Finish	(3)	Rough/pits		
		Maximum points: 9		

Instructor_____Date_____Total points_____Student eval._____

Cementation		Critical Error	3 2 1 0	3 2 1 0
Margins	(3)	Open/short		
Occlusion	(3)	High		
		Maximum points: 6		

Instructor_____Date_____Total points_____Student eval._____

Sum total for project (maximum points = 84)_____Student_____

Table II.

EVALUATION CRITERIA - CAST RESTORATION FINISH

Definition	Errors	Rationale
OCCLUSAL ANATOMY		
The occlusal surface of the polished inlay restoration must be functional, i.e. the cusp planes and marginal ridge are continuous with existing tooth form following the slopes of the cusps with distinct grooves, fissures, pits and fossae.	Developmental grooves and fossae are: a) missing or lacking definition; b) improperly positioned so that they interfere with function.	Missing or improperly placed grooves may interfere with the flow of food off the occlusal table resulting in food impaction.
	Occlusal contacts are: a) missing (i.e. more than that due to polishing alone) where they should exist; b) too heavy relative to contacts on adjacent teeth; c) misplaced, i.e. balancing interferences.	Occlusal contacts are important factors in: a) the maintenance of a stabilized occlusion, mastication and distribution of stresses) b) prevention of T.M.J. disturbance and traumatic occlusion.
	Marginal ridge errors: a) The ridge is placed occlusally or cervically to adjacent marginal ridge. N.B. In cases of an irregular plane of occlusion the placement of the marginal ridge will vary; b) The contour of the marginal ridge does not reproduce the existing dentition.	To prevent food impaction interproximally and permit the formation of an adequate occlusal embrasure to provide a sluice way for the escape of food from the occlusal table. The marginal ridge does not allow proper contour and placement of the proximal contact area.

ClearCorrect Exhibit 1002, Page 2211 of 3373

Table II (continued)

Definition	Errors	Rationale
AXIAL CONTOUR AND PROXIMAL CONTACT		
The axial contour of the polished cast restoration must: a) be contoured to protect the surrounding tissue during mastication; b) allow for a proper size of and placement of the contact area with respect to the interdental papillae; c) allow embrasures which are anatomically symmetrical with the adjacent teeth; d) contact the adjacent tooth.	Proximal contour does not adequately reproduce contour of the natural tooth structure--either too full or too flat.	Maintain healthy gingival tissue by: a) minimizing stagnant areas of saliva and food debris accumulation which leads to plaque accumulation; b) allowing adequate room for interdental papillae; c) preventing food impaction.
	Shape and/or location of the contact area does not reproduce the pattern present in the remaining dentition or account for local conditions, e.g. rotations or tipping, associated with that specific tooth and the adjacent teeth.	Proper proximal contact enhances stability of the dentition.
	Embrasures which are inadequate, i.e. as a result of over or under contouring axial surfaces or lacking anatomical symmetry between the mesial half and distal half of an embrasure.	Important in maintaining soft tissue health and providing proper sluice ways for food during mastication.
	▶ Contact is not visually closed and does not offer sufficient resistance to pulled POH unwaxed dental floss so that there is a detectable snap as it passes through the contact area.	Prevent food impaction and resulting trauma to interdental tissue. Maintain arch stability.
	Shredding of POH unwaxed dental floss as it is drawn through the contacts due to roughness or heaviness of contact.	Facilitate oral hygiene procedures.

▶ = critical error

ClearCorrect Exhibit 1002, Page 2212 of 3373

Table II (continued)

Definition	Errors	Rationale
SURFACE QUALITY		
The surface must be smooth, without surface irregularities including ripples or scratches, and be sufficiently dense so as to be free of porosity.	Pitting and voids are visually in evidence on surface areas.*	Pitting and other surface irregularities cause the restoration to be more susceptible to plaque retention.
	The surface is not as smooth as a whiting polish.	A smooth surface enhances esthetics and oral hygiene efforts.
An adequate surface quality and acceptable level of polish (luster) will be impossible if the proper attention has not been given to the casting process as well as proper use of finishing burs.		
MARGIN INTEGRITY		
Margin integrity implies good adaptation of the cast restoration and the absence of marginal deficiencies due to: a) poor casting technique; b) over polishing; c) under polishing; d) poor impressioning technique; e) poor wax-up; f) inadequate cleansing of the cavity.	▶Open margin, pits or voids at the cavosurface margin (the transition from the cast restoration to tooth structure is detectable with a #5 explorer).	Minimize: a) microleakage phenomenon; b) recurrent decay; c) irritation to periodontal tissue; d) dissolution of cement.
The tooth-restoration junction must be sharp and well-defined (no marginal excess flash or overhang present).	▶Excess gold is detectable beyond the margin either visually or with a #5 explorer (due to poor carving technique or excessive expansion).	Prevent fracture of casting flash which results in increased margination or "ditching" (especially at occlusal cavosurface).
	▶Underextended gold at cavosurface margin is detectable either visually or with a #5 explorer (due to over-carving wax, overpolishing gold or inaccurate impression).	Minimize: a) recurrent decay; b) irritation to periodontal tissues; c) dissolution of cement.

▶ = critical error

ClearCorrect Exhibit 1002, Page 2213 of 3373

Table II (continued)

Definition	Errors	Rationale
INTERNAL ADAPTATION OF CASTING		
The casting should be smooth internally and conform to the cavity preparation in detail.	Voids internally along retentive wall.	Reduced retention. Reduced thickness of cement or chance of air entrapment during cementation.
INTEGRITY OF ADJACENT TISSUE		
Minimum soft tissue trauma.	▶ Gingival tissue traumatized.	Maintain periodontal integrity and minimize post-operative discomfort.
Adjacent tooth structure, teeth and restoration must remain undamaged.	▶ Nicks in adjacent tooth structure or restorations. ▶ Alteration of adjacent tooth structure in compensation for a defective restoration.	Maintain integrity of adjacent tooth structure and restorations.
FINAL CEMENTATION		
Casting seated completely.	▶ Visible cement line.	Cement exposed to oral fluids will dissol more rapidly.
Cement removed from gingival sulcus and surrounding tooth structure.	Excess cement remaining subgingivally or on the casting and adjacent tooth structure.	Unseated castings may interfere with occlusal harmony. May cause periodontal irritation.

▶ = critical error

ClearCorrect Exhibit 1002, Page 2214 of 3373

Table II (continued)

CAST RESTORATION FINISH

Occlusal Anatomy	Margin Integrity	Axial Contour	Proximal Contact
☐ Occlusal Grooves	▶☐ Open Margin	☐ Over/Under Contour	▶☐ No Contact
☐ Occlusal Contacts	☐ Flash	☐ Embrasures	☐ Shape or Location
☐ Marginal Ridge	☐ Short Margins (not open)		

Surface Quality	Internal Adaptation	Tissue Considerations	Final Cementation
☐ Pitting and Voids	☐ Voids Internally	☐ Soft Tissue	▶☐ Visible Cement Line
		☐ Adjacent Teeth, Restorations	☐ Excess Sub-gingivally

CRITERIA IN PROCEDURE EXAM: Finishing Cementation

	Step	Definition	Exception	Rationale
.	Verification of casting and check occlusion without dam	Proper contour; all cavo-surfaces closed	None	Work efficiency
∴	Rubber dam	Finishing procedure carried out under dam	None	Work efficiency
3.	Pulp protection	Bases in place; all exposed dentin protected with copyl resin varnish	None	Maintain pulp vitality and less pulpal trauma
4.	Precementation	Perfect contours and contact; smooth (unpolished) surfaces; good anatomical form; perfect margins; dam in place	None	Allow cement to set in moistur free environment
5.	Finish	Restore contour; smooth surfaces	None	Prevent tissue irritation; produce physiological environ.

ClearCorrect Exhibit 1002, Page 2215 of 3373

Appendix 2. Errors and Quality Restorations

Errors and Quality Restorations

In any CAD/CAM system, there are an array of sources from which errors could arise. These include the imaging element selected, the surface model used, the CAD system, the quality of the NC milling machine, and peculiarities of of machining. These elements are listed in Table 1. Also listed are values for errors (means and standard deviations) presented by Dr. Reggie Caudell of the University of Alabama based on some preliminary work they have underway.

It is reasonable to assume that all of the errors are independent. Thus, total system error become an arithmetic sum of all the component erorrs.

Restoration quality is a critical issue for the success of any CAD/CAM system. Also critical is the probability of successfully creating a quality restoration, especially when costly raw materials are being machined. One way to assess the erorrs that can be tolerated in the data acquisition or image formation stage is to look at a summary of reliability allocation. Tables 2 and 3 summarize this information. If there is no surface modeling error and a crown with 25 micron marginal fit is required, there is a 95% probability of success in meeting this tolerance if imaging errors are less than 5.5 microns and 90% probability if imaging errors are less than 7 microns. If 50 micron margins are acceptable, the imaging errors can rise to 15 microns for 95% success and 18 microns for 90% success.

Table 1. Error Contributions

Mean (in microns)	Standard Deviation	Source
See Table A-2		Imaging
10	15	Surface Modeling (Curve fitting)
0	0	CAD
4.8	2.8	NC Milling (Includes positioning error, fourth-axis rotational error, etc.)
0.5	0.3	NC Module (Includes scallop error of surface between cutter path increments, tolerance error from straight line cut between points, etc.)

Source: Dr. Reggie Caudell, University of Alabama, presentation at the Greater New York Dental Meeting, December 3, 1987.

Table 2. Reliability Allocation

Error in Image (in microns) Marginal fit:	Probability of Acceptance 10-micron model error 25 micron	50 micron	No model error 25 micron	50 micron
0	70	97	99+	99+
5	59	90	97	99+
10	50	82	73	99+
15		73	61	95
20		66	50	86
25		59		75
30		54		66
35		50		59
40				53

Source: Dr. Reggie Caudell, University of Alabama, presentation at the Greater New York Dental Meeting, December 3, 1987.

Table 3. Summary

With no surface model error:

Probability of Success	Permitted Image Error	
	25 micron margins	50 micron margins
95	5.5	15
90	7	18

Source: Dr. Reggie Caudell, University of Alabama, presentation at the Greater New York Dental Meeting, December 3, 1987.

BRITISH JOURNAL OF ORTHODONTICS

Incorporating *The Orthodontist* and the *Transactions of the British Society for the Study of Orthodontics*

Volume 13 Number 1 January 1986

Contents

Editorial ii

On the Aetiology of Malocclusion: The Northcroft Lecture, 1985
W. R. Proffit 1

A Preliminary Craniofacial Profile Evaluation of Normo-, Micro- and Macro-Cephalics
C. L. B. Lavelle 13

An Analysis of Complete and Incomplete Overbite in Class II Division 1 Malocclusions (An Analysis of Overbite Incompleteness)
P. A. Banks 23

Lower Incisor Position in Treatment Planning
P. Williams 33

Orthodontic Screening of Nine-Year-Old Children
J. J. Crabb and W. P. Rock 43

Recurrent Swelling of the Upper Lip. A Case Report
A. P. Howat and P. G. J. Rout 49

Research Reports 53

Report of Annual Conference 57

Announcements 59

Book Reviews 60

Letter to the Editor 61

ISSN 0301 228X

ClearCorrect Exhibit 1002, Page 2221 of 3373

Research Reports

The Development of a 3D Cast Analysis System

S. Richmond and M. L. Jones, *UWCM, Cardiff*

The Reflex metrograph was described. The accuracy of the equipment showed favourable results when compared to other three-dimensional techniques (< 0·3 mm). With the basis of an accurate measuring system a quantitative analysis was developed to assess study casts, in order to fulfil the practical need to record the characteristics of a given malocclusion.

The analysis involves the recording of one hundred and ten points. The variables recorded were:

i overjet
ii overbite
iii mesial contact points of central incisors to constructed centreline
iv individual upper and lower mesio-distal widths
v overall mesio-distal widths
vi anterior mesio-distal widths
vii inter canine and inter molar distances
viii three dimensional inter-incisal angles
ix two-dimensional antero-posterior incisal angles
x overall discrepancy
xi anterior discrepancy
xii length of fitted parabolic curve
xiii length of discrepancy of fitted parabolic curve (length of parabolic curve minus mesio-distal widths)

No significant differences were found for intra- and inter-observer errors for twelve cases ($p > 0·1$).

The analysis has many applications but primarily it can provide a consistent and readily available analysis of a set of dental casts. The data recorded may be stored on disc and possibly alleviate the problems of storing study casts.

The effect of anterior mandibular displacement on the proliferative and metabolic activity of the rat condyle

D. H. T. K. Tewson*, J. K. Heath and M. C. Meikle, *Institute of Dental Surgery, London and Strangeways Research Laboratory, Cambridge.*

Functional appliances used in the correction of Class II division 1 malocclusions are designed to produce forward displacement of the mandible, which is believed by many clinicians to stimulate condylar growth. The objective of this investigation was to study the effect of anterior mandibular displacement (AMD) on cell proliferation and matrix formation in the rat condyle using a removable inclined plane. Experimental animals were subjected to AMD of 10 hours/day for 1, 3, 7, 11 or 14 days. After sacrifice, condyles were removed and the explants pulsed in vitro for 6 hours with either [^{3}H]-thymidine, [^{3}H]-proline or $^{35}SO_4^{2-}$. The specific activity of radioisotope incorporation was expressed as dpm/μgDNA, dpm/mg protein, dpm/μg sulphated glycosaminoglycans (GAGS). Cell proliferation was also quantified in a 14-day experiment using [^{3}H]-thymidine autoradiography and a radioactive index (labelled cells/1000 cells counted) established for the anterior, middle and posterior regions of the condyle. There was no significant alteration in cell proliferation (dpm/μg DNA or radioactive index) or matrix formation (dpm/μg GAGS or dpm/mg protein) following anterior mandibular displacement at any point in the time-scale. Some autoradiographic and histological data indicated that the condyle does remodel, but there was no convincing evidence to support the hypothesis that functional mandibular displacement stimulates condylar growth.

Natural Head Position, Posture and Prognathism

S. C. Cole, *Institute of Dental Surgery, London WC1*

Natural head position (NHPn) and natural head posture (NHPr) are terms which have been used synonymously to describe the spatial relationships of the head with reference to the true vertical, the cervical column or both. This is confusing and it would seem logical to ascribe one term to one reference and consider the phenomena separately.

For the purposes of this prospective cephalometric survey NHPn will describe the relationship of the head to the true vertical, while NHPr will describe the relationship of the head to the cervical column.

In order to investigate these two relationships of

ClearCorrect Exhibit 1002, Page 2222 of 3373

the head. five groups were formed, three representing horizontal discrepancies selected on ANB differences (Class I, II and III dental base relationship) and two representing vertical discrepancies selected on Bjork's posterior angles ('high angle' and 'low angle' groups).

Despite the marked differences in 'skeletal' pattern shown between the five groups, the 'Saddle angles' showed no significant difference. However, NHPn and NHPr were significantly different ($p \cdot < 01$) indicating that cranial base orientation alone may have a bearing on both horizontal and vertical 'skeletal' abnormalities. NHPn appeared to affect maxillary prognathism, whilst NHPr affected mandibular prognathism.

These phenomena may help to explain an apparent Class II or Class III tendency in a case where the 'Saddle angle' is normal.

A Comparison of Craniofacial Growth Between The Sexes in Cleft Lip and Palate

J. E. Whitehead, *Cheltenham and District H.A., formerly of Institute of Dental Surgery, London, WC1.*

The aim of this study was to investigate the craniofacial growth in children with repaired complete unilateral cleft lip and palate. The sample examined was composed of experimental groups of twenty male and twenty female cleft children, and control groups of twenty male and twenty female individuals with a normal occlusion and jaw relationship. The cleft groups were compared to each other and to their respective control groups by examining retrospectively lateral cephalometric radiographs taken at mean ages eleven years, fourteen years and seventeen years.

The cranial base, the maxilla, the mandible, the facial profile, the facial heights, anterior and posterior, and the dentoalveolar structures, were investigated, with particular attention given to the changes taking place over the period of study.

The maxilla in the cleft groups was found to be located in a more posterior position relative to the cranial base, with the female clefts in particular showing a concave facial profile at eleven years becoming worse with age. This concavity of facial profile did not become apparent in the male cleft group until fourteen years.

The cleft mandible was reduced in length and ramal height which in combination with an enlarged gonial angle and increased lower face height resulted in the male and female cleft groups exhibiting a backward mandibular rotation. The upper anterior face height was found to be smaller in both cleft groups, but with the lower anterior face height significantly greater, particularly in the male clefts. When the total heights were considered, there was little difference between the groups in this study, it being the relative contributions of the component parts to the whole which varied.

The Performance and Use of a 3D Cast Analysis System

M. L. Jones and S. Richmond, *UWCM, Cardiff*

Using the records of a patient as an illustration, a program was described for the three dimensional measurement of study casts. This program was developed to make maximum use of a Reflex metrograph linked to a Series 35 HP computer. One hundred and ten observations or plots were recorded of the casts in closed and open configuration being stored on disc. Another program was then used to access the data for the necessary measurements and calculations. The detail and development of the program is described in an adjoining paper.

The measurements were derived from the stored data together with intra-observer errors for 20 good quality casts, and made after transformation and orientation to the Functional Occlusal Plane (no teeth were premarked): (1) A residual transformation/observer error (S.D. = $\pm$0·12 mm); (2) Right and left overjet (S.D. = $\pm$0·64 mm); and overbite (S.D. = $\pm$0·73 mm); (3) Mesial incisor edge to derived centre line U/L (S.D. = $\pm$0·33 mm); (4) Anatomic mesio-distal widths of teeth range from $\underline{3}$ S.D. = $\pm$0·1 mm to $\overline{5}$ S.D. = $\pm$0·4 mm; (5) 3D interincisal angle (S.D. = 2·0°); (6) 2D incisal angles to F.O.P. (S.D. = $\pm$2·3°); (7) U/L arch crowding on parabola fit (S.D. = $\pm$1·4 mm); (8) Anterior and overall arch discrepancy (3-3 S.D. = $\pm$0·9 mm, 6-6 S.D. = $\pm$1·5 mm); (9) Intercanine and intermolar width (S.D. = $\pm$0·3 mm). The uses of such measurements were described with the aid of a Class II division 2 case with particular contrast being drawn between the metrograph and radiographic interpretation of incisal angles (inter observer error for casts = S.D. $\pm$2·7°, for radiograph = $\pm$3·5°). The reflex plotter linked to the development of such software should prove a useful tool in future study cast research.

Observations on velocity changes of the standing height during the pubertal growth spurt.

J. Crisp, *Southend Hospital Southend.*

Standing height is generally accepted as one indicator of skeletal maturation.

ClearCorrect Exhibit 1002, Page 2223 of 3373

ja J, Ridell A 1979 Surgical
ognathism by the oblique
ian Journal of Plastic and
3–460

Swift J Q, Markowitz N R
g mandibular advancement
of Oral and Maxillofacial

relapse after mandibular
al of Oral Surgery 36:

I, Tanabe H 1987 Skeletal
se. American Journal of
Orthopedics 92: 412–421

atistics for dentistry and
leston, Virginia

Steinbrenner K, Bent D H
social sciences. McGraw-

982 A comparative study
ne screws in the treatment
Oral Surgery 54: 2–6

Long term follow-up of
or correction of mandib-
Maxillo-Facial Surgery 6:

rgical orthodontic treat-

al changes after surgical
athism. Journal of Oral

985 Displacement of the
fixation after oblique
tric and cephalometric
Maxillofacial Surgery 13:

986 Displacement of the
intermaxillary fixation
my. Journal of Maxillo-

osture and craniofacial
Physical Anthropology

1986 Patterns and etiol-
Class III open bite via
nternational Journal of
athic Surgery 1: 91–99

rrection of dentofacial
w. Journal of Oral and
149

989 Changes in head
vay following surgical
ism. European Journal

Waite D E 1980 Post-
orthognathic surgery.

European Journal of Orthodontics 14 (1992) 125–139

© 1992 European Orthodontic Society

The development of the PAR Index (Peer Assessment Rating): reliability and validity

S. Richmond, W. C. Shaw, K. D. O'Brien, I. B. Buchanan, R. Jones, C. D. Stephens,* C. T. Roberts, and M. Andrews

Department of Oral Health and Development, University of Manchester, and *Department of Child Dental Health, Bristol Dental Hospital, Bristol

SUMMARY The PAR Index has been developed to provide a single summary score for all the occlusal anomalies which may be found in a malocclusion. The score provides an estimate of how far a case deviates from normal alignment and occlusion. The difference in scores between the pre- and post-treatment cases reflects the degree of improvement and, therefore, the success of treatment. Excellent reliability was exhibited within and between examiners (Intraclass Correlation Coefficient, $R > 0.91$). The components of the PAR Index have been weighted to reflect current British orthodontic opinion and is flexible in that the weightings could be changed to reflect future standards and standards currently being achieved in other countries.

The PAR Index offers uniformity and standardization in assessing the outcome of orthodontic treatment.

Introduction

The grading of orthodontic treatment results at study group meetings has been practised for a long time. The idea of individuals grading their own treatment results can be a self-teaching device and improve the quality of future treatment (Hickham, 1975). Unfortunately, the variation in criteria used by different orthodontists makes it difficult to compare results of treatment and the same applies to comprehensive studies which are not limited to the evaluation of specific measurements. Several indices have been developed specifically to assess the success of treatment (Eismann, 1974, 1980; Gottlieb, 1975; Berg, 1979). These indices compare pre- and post-treatment records to register the outcome of orthodontic care. However, the reliability and validity of these indices have never been evaluated. A treatment need index, the Occlusal Index (Summers, 1971) has been used by several authors to assess the outcome of treatment (Pickering and Vig, 1975; Elderton and Clark, 1983, 1984).

The use of indices should ensure uniform interpretation and application of criteria. Although numerous indices have been developed none as yet has been accepted universally. The use of precise criteria is essential, requiring a quantitative objective method of measuring malocclusion and efficacy of treatment.

To fulfil these criteria the PAR Index (Peer Assessment Rating) was developed to record the malocclusion at any stage of treatment. The index was formulated over a series of six meetings in 1987 with a group of 10 experienced orthodontists (British Orthodontic Standards Working Party). Over two-hundred dental casts representing developmental as well as pre-and post-treatment stages were examined and discussed until agreement was reached regarding the individual features which would be assessed in obtaining an estimate of alignment of occlusion. The working party is shown (Fig. 1) assessing a particular case which has been projected onto four screens allowing all members of the working party to view the same case at one time. The scores derived were directly recorded on a computer database to facilitate rapid multiple examiner comparisons.

Section 1: The PAR Index (Peer Assessment Rating)—description and reliability

The concept is to assign a score to various occlusal traits which make up a malocclusion. The individual scores are summed to obtain an

ClearCorrect Exhibit 1002, Page 2224 of 3373

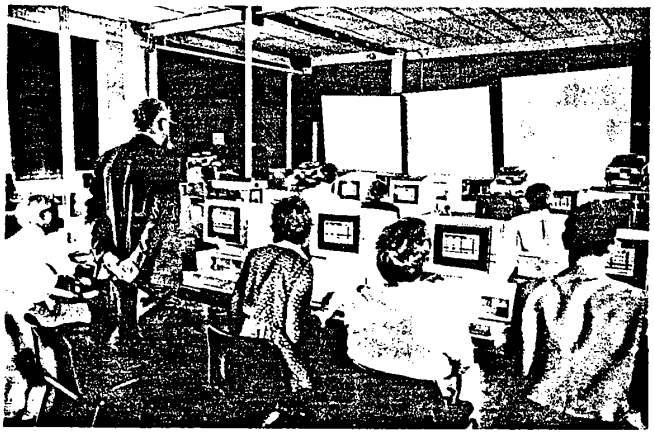


Figure 1 The British Orthodontic Standards Working Party assessing cases projected on four screens, the results were directly entered onto computer to facilitate intra- and inter-examiner error.

overall total, representing the degree a case deviates from normal alignment and occlusion.[1] The score of zero would indicate good alignment and higher scores (rarely beyond 50) indicating increased levels of irregularity. The overall score is recorded on the pre- and post-treatment dental casts. The difference between these scores represents the degree of improvement as a result of orthodontic intervention and active treatment.

There are 11 components of the PAR Index (Table 1).

Table 1 Components of the PAR Index.

1.	Upper right segment
2.	Upper anterior segment
3.	Upper left segment
4.	Lower right segment
5.	Lower anterior segment
6.	Lower left segment
7.	Right buccal occlusion
8.	Overjet
9.	Overbite
10.	Centreline
11.	Left buccal occlusion

[1]Normal occlusion and alignment is defined as all anatomical contact points being adjacent, with a good intercuspal mesh between upper and lower buccal teeth, non-excessive overjet and overbite.

Buccal and anterior segments

The dental arch is divided into three recording segments, left buccal, right buccal and anterior (Fig. 2). Scores are recorded for both upper and lower arches.

Buccal segments. The recording zone is from the mesial anatomical contact point of the first permanent molar to the distal anatomical contact point of the canine.

Anterior segment. The recording zone is from the mesial anatomical contact point of the canine on one side to the mesial anatomical contact point of the canine on the opposite side.

The occlusal features recorded are crowding, spacing, and impacted teeth. Displacements are recorded as the shortest distance between contact points of adjacent teeth parallel to the occlusal plane. The greater the displacement the greater the PAR score. The displacements between first, second, and third molars are not recorded as these contacts are so broad and are extremely variable within the normal range.

An impacted tooth is recorded when the space for this tooth is less than or equal to 4 mm. Impacted canines are recorded in the anterior segment.

Scores for the displacements and impactions are added to give an overall score for each recording zone. The scores for the discrepancies are shown in Table 2.

Figure 2 Division of the

Table 2 Displacement

Score	I
0	0
1	1
2	2
3	4
4	g
5	h

If there is potent
dentition, average n
to calculate the spa

Buccal occlusion

The buccal occlusic
and right sides. Th
with respect to the
recording zone is fi
molar, either first, s
ancies are recorde
occlusion.

The antero-poste
irregularities are sur
sion (Table 4).

Ta
di

U

L

ClearCorrect Exhibit 1002, Page 2225 of 3373

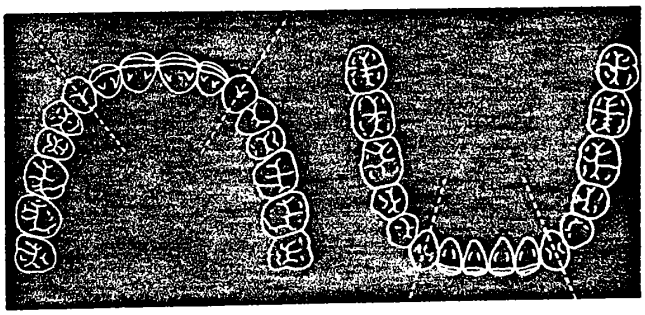


Figure 2 Division of the dental arches into three recording zones: anterior, left, and right.

Table 2 Displacement scores.

Score	Discrepancy
0	0 mm to 1 mm
1	1.1 mm to 2 mm
2	2.1 mm to 4 mm
3	4.1 mm to 8 mm
4	greater than 8 mm
5	impacted teeth

If there is potential crowding in the mixed dentition, average mesio-distal widths are used to calculate the space deficiency (Table 3).

Buccal occlusion

The buccal occlusion is recorded for both left and right sides. The fit of the teeth is scored with respect to the three planes of space. The recording zone is from the canine to the last molar, either first, second, or third. All discrepancies are recorded when the teeth are in occlusion.

The antero-posterior, vertical and transverse irregularities are summed for each buccal occlusion (Table 4).

Overjet

Positive overjet as well as teeth in cross-bite are recorded (Table 5). The recording zone is from the left to right lateral incisors. The most prominent aspect of any one incisor is recorded. When recording the overjet the ruler is held parallel to the occlusal plane and radial to the line of the arch. It is not uncommon to see two upper laterals in cross-bite as well as an increased overjet on the central incisors. In this situation if the overjet were 4 mm, the score would be 3 for the cross-bite and 1 for the positive overjet (4 in total).

Overbite

Records the vertical overlap or open bite of the anterior teeth. Overbite is recorded in relation to the coverage of the lower incisors or the degree of open bite (Table 6). The recording zone includes the lateral incisors. The tooth with the greatest overlap is recorded.

Centreline

Records the centreline discrepancy in relation to the lower central incisors (Table 7). If a lower

Table 3 Mixed dentition crowding assessment using average mesio-distal widths.

Upper		
canine	8 mm	
1st premolar	7 mm	Total = 22 mm (impaction < = 18 mm)
2nd premolar	7 mm	
Lower		
canine	7 mm	
1st premolar	7 mm	Total = 21 mm (impaction < = 17 mm)
2nd premolar	7 mm	

ClearCorrect Exhibit 1002, Page 2226 of 3373

Table 4 Buccal occlusion assessments. (Temporary developmental stages and submerging deciduous teeth are excluded.)

Score	Discrepancy
Antero-posterior	
0	Good interdigitation Class I, II and III
1	Less than half unit discrepancy
2	Half a unit discrepancy (cusp to cusp)
Vertical	
0	No discrepancy in intercuspation
1	Lateral open bite on at least two teeth greater than 2 mm
Transverse	
0	No cross-bite
1	Cross-bite tendency
2	Single tooth in cross-bite
3	More than one tooth in cross-bite
4	More than one tooth in scissor bite

Table 5 Overjet measurements.

Score	Discrepancy
Overjet	
0	0–3 mm
1	3.1–5 mm
2	5.1–7 mm
3	7.1–9 mm
4	greater than 9 mm
Anterior cross-bites	
0	No discrepancy
1	One or more teeth edge to edge
2	One single tooth in cross-bite
3	Two teeth in cross-bite
4	More than two teeth in cross-bite

central incisor has been extracted the measurement is not recorded.

The PAR ruler

A ruler has been designed to make measurement easier (Fig. 3). The information briefly summarizes the recording features of the index and facilitates quick assessments, and allows contact points to be viewed through the ruler.

The ruler is shown recording the displacement between the mesial contact points of the incisors (Fig. 4). The line designated 2 is slightly short of the contact points; therefore, the next longer line would be used and the contact point score between the central incisors would be 3. Figure 5

Table 6 Overbite measurements. Cross-bites including the canines are recorded in the anterior segment.

Score	Discrepancy
Open bite	
0	No open bite
1	Open bite less than and equal to 1 mm
2	Open bite 1.1–2 mm
3	Open bite 2.1–3 mm
4	Open bite greater than or equal to 4 mm
Overbite	
0	Less than or equal to one third coverage of the lower incisor
1	Greater than one-third, but less than two-thirds coverage of the lower incisor
2	Greater than two-thirds coverage of the lower incisor
3	Greater than or equal to full tooth coverage

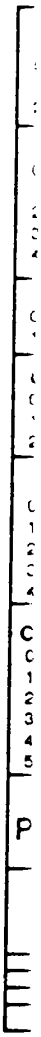


Figure 3 The PAR r

ClearCorrect Exhibit 1002, Page 2227 of 3373

Table 7 Centreline assessments.

Score	Discrepancy
0	Coincident and up to one-quarter lower incisor width
1	One-quarter to one-half lower incisor width
2	Greater than one-half lower incisor width

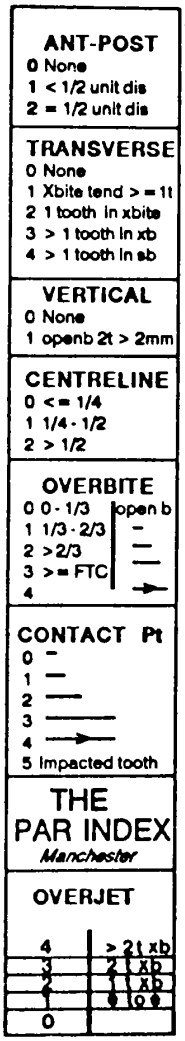


Figure 3 The PAR ruler.

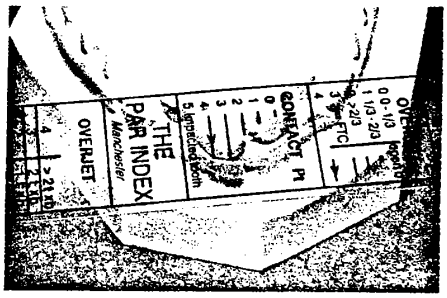


Figure 4 The PAR ruler being used to record the displacement of contact points between the central incisors.

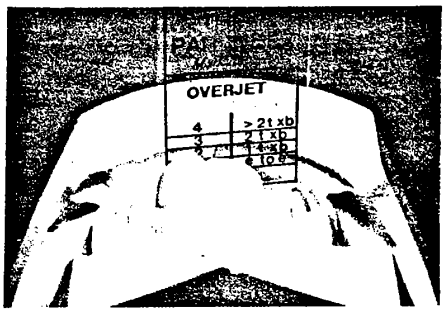


Figure 5 The PAR ruler being used to assess overjet: the overjet recorded would score 2.

shows the ruler being used to record the overjet and in this case would score 2.

Conventions

A series of conventions have been drafted to standardize the approach in assessing occlusions (Appendix 1).

Case analysis

To illustrate the use of the PAR Index, pre- and post-treatment dental casts are shown in Fig. 6;

ClearCorrect Exhibit 1002, Page 2228 of 3373

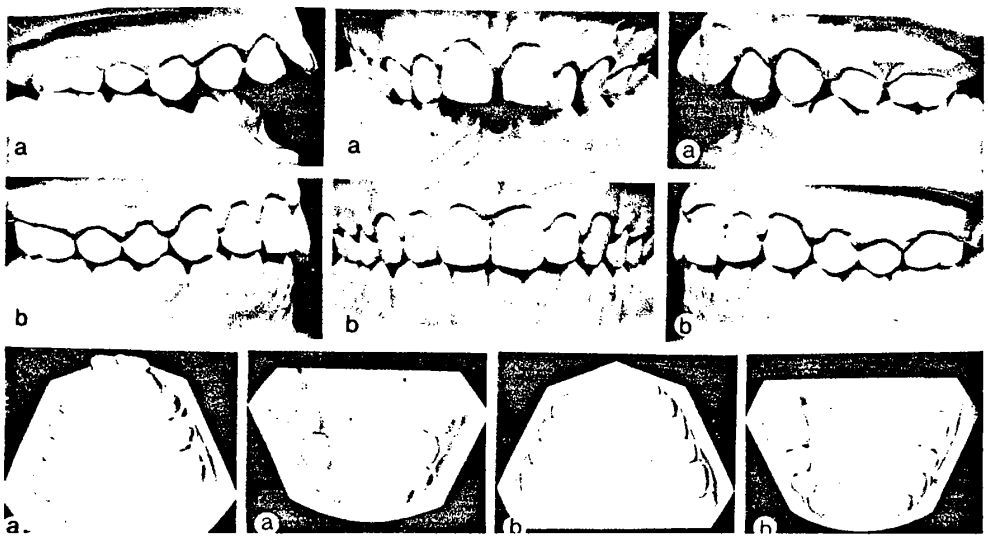


Figure 6 Cases analysis: (a) pre-treatment and (b) post-treatment dental casts illustrate the reduction in PAR score from 21 to 3.

the derivation of the individual component scores are recorded in Table 8. The initial score of 21 has been reduced to 3, a reduction of 18 points.

The case illustrated is a Class II, division 1 malocclusion with an increased overjet greater than 10 mm, and an increased and complete overbite. The molar relationship is half a unit Class II on the right and more than a full unit Class II on the left side. The upper left second premolar is impacted.

As a result of orthodontic treatment the overjet and overbite have been reduced to less than 3 mm. The impacted second premolar has been accommodated. The buccal segments have been improved although the buccal teeth are

Table 8 Derivation of PAR scores (Fig. 6).

PAR components	Before treatment	Total	After treatment	Total
Upper right segment	(6–5),0, (5–4),0, (4–3),0	0	(6–5),0, (5–4),0, (4–3),1	1
Upper anterior segment	(3–2),0, (2–1),2, (1–1),1, (1–2),2, (2–3),0	5	(3–2),0, (2–1),0, (1–1),0, (1–2),0, (2–3),0	0
Upper left segment	(6–5),0, (5–4),0,(4–3),1, and (impaction 3)5	6	(6–5),0, (5–4),0, (4–3),0	0
Lower right segment	(6–5),0, (5–4),0 (4–3),0	0	(6–5),0, (5–4),0, (4–3),0	0
Lower anterior segment	(3–2),0, (2–1),1, (1–1)0, (1–2),0, (2–3),0	1	(3–2),0 (2–1),0, (1–1),0, (1–2),0, (2–3),0	0
Lower left segment	(6–5),0, (5–4),0, (4–3),0	0	(6–5),0, (5–4),0, (4–3),0	0
Right buccal occlusion	Cusp to cusp	2	Less than 1/2 unit Class II	1
Overjet	Overjet greater than 10 mm	4	Overjet within 3 mm	0
Overbite	Overbite within the normal range	0	Normal overbite	0
Centreline	Centreline >1/4 width of lower incisor	1	Centreline within 1/4 width	0
Left buccal occlusion	Cusp to cusp	2	Less than 1/2 unit Class II	1
Total		21		3

Notation of teeth in brackets, followed by the PAR score for each contact point.

not intercuspating fu
has been improved a
upper right canine
compared to the upp

A single score has
and post-treatment de
deviation from norm
in PAR score reflects t
and success of treatm

Reliability

Four examiners (two
and two postgraduate
the use of the PAR
meetings.

In order to determi
a stratified subsample
from a random sam
untreated cases. The d
on two occasions 8 w
measurements were es
Intraclass Correlation
This provides a singl
based on a comparis
comparison between
Fleiss *et al.*, 1979; F
statistics were calculat
iners separately and a

Results

Table 9 shows exce
($R>0.95$) and betwe

Table 9 Calibration exc
and inter-examiner

Component
Upper right
Upper anterior
Upper left
Lower right
Lower anterior
Lower left
Right buccal occlusion
Overjet
Overbite
Centreline
Left buccal occlusion
Total score
Lower 95 per cent confiden

ClearCorrect Exhibit 1002, Page 2229 of 3373







ion in PAR score from

re than a full unit
upper left second

tic treatment the
en reduced to less
ond premolar has
cal segments have
buccal teeth are

	Total
3),1	1
1),0,	0
3),0	0
3),0	0
),0,	0
3),0	0
lass II	1
	0
	0
width	0
lass II	1
	3

not intercuspating fully. The overall alignment has been improved although the distal of the upper right canine is slightly more buccal compared to the upper left canine.

A single score has been derived for the pre- and post-treatment dental casts representing the deviation from normal. The size of reduction in PAR score reflects the degree of improvement and success of treatment.

Reliability

Four examiners (two orthodontically qualified and two postgraduate students) were trained in the use of the PAR Index over a series of meetings.

In order to determine the examiner reliability a stratified subsample of 38 cases was selected from a random sample of 2000 treated and untreated cases. The dental casts were measured on two occasions 8 weeks apart. Differences in measurements were estimated by calculating the Intraclass Correlation Coefficient of Reliability. This provides a single summary of reliability based on a comparison between ratings and comparison between subjects (Barkto, 1966; Fleiss *et al.*, 1979; Fleiss, 1981, 1986). These statistics were calculated between the four examiners separately and as a group.

Results

Table 9 shows excellent reliability within ($R > 0.95$) and between examiners ($R = 0.91$). The intra-examiner lower 95 per cent confidence limits are generally greater than 0.93 and for inter-examiner, 0.87. The paired *t*-test was used to examine for bias. Examiners 2 and 3 both indicated bias between first and second recordings. However, the differences between the means were less than 1.6 PAR points (means: Examiner 2—21.90, 22.97; Examiner 3—19.05, 20.58). An analysis of variance detected bias between the four examiners, Examiner 3, scoring the lowest and Examiner 4 the highest. The difference in the means being first recording, 3.66 and for the second recording 2.81 PAR points. The reliability coefficient and confidence limits were high indicating excellent reliability. The measure of reliability is large and the effect of bias would mean that little damage is done to the precision of measurement.

Discussion

In general, the PAR Index indicated excellent intra- and inter-examiner agreement. Lower levels of agreement were achieved for some of the individual PAR components, particularly the upper left and right buccal segments ($R = 0.76$) compared to the corresponding segments in the lower arch. This may be due to the increased size and the differing morphology of the maxillary teeth, which result in broad contact points and make accurate displacement measurements more difficult than in the lower arch.

It is not surprising that the left and right

Table 9 Calibration exercise: Intraclass Correlation Coefficient of Reliability for the four examiners. Intra- and inter-examiner

	Intra-examiner				Inter-examiner
Component	1	2	3	4	
Upper right	0.88	0.92	0.93	0.90	0.76
Upper anterior	0.94	0.98	0.98	0.95	0.90
Upper left	0.84	0.87	0.84	0.87	0.76
Lower right	0.93	0.95	0.93	0.92	0.87
Lower anterior	0.83	0.96	0.97	0.91	0.87
Lower left	0.96	0.97	0.91	0.86	0.84
Right buccal occlusion	0.79	0.89	0.87	0.89	0.75
Overjet	0.95	0.99	0.87	0.94	0.91
Overbite	0.74	1.00	0.82	0.89	0.77
Centreline	0.76	0.89	0.90	0.83	0.81
Left buccal occlusion	0.83	0.91	0.96	0.77	0.75
Total score	0.96	0.98	0.96	0.95	0.91
Lower 95 per cent confidence limit	0.94	0.97	0.94	0.93	0.87

ClearCorrect Exhibit 1002, Page 2230 of 3373

buccal occlusions also show lower measures of agreement ($R=0.75$) as this depends on the correct registration of the models which can easily 'move' in the hand, and that the line of the buccal occlusion forms a curve and the recording depends on the angle to which the models are viewed.

However, the overall inter-examiner agreement of $R=0.91$ is excellent and compares very favourably to caries calibration exercises (Mitropoulos and Downer, 1987). The use of the ruler with a brief summary contained within, eliminates cross-references to notes of complicated criteria.

Timing trials have been undertaken on 10 sets of mixed and permanent dentitions (Buchanan, 1990). The average time taken to record the overall PAR score for pre- and post-treatment models is 6 minutes. Direct computer entry tends to reduce this time even further.

The difference between the pre- and post-treatment scores reflects the success or degree of improvement. As the score tends towards 0, the deviation from normal is less. Obviously, a score of 0 is not always achievable because of the complexity of the case, but generally a measure of 10 or less indicates an acceptable alignment and occlusion, and 5 or less suggests an almost ideal occlusion.

The case illustrated (Fig. 6) recorded a change in PAR score of 18 and indicates substantial improvement. However, not all cases achieve this degree of improvement.

Section II: The PAR Index—validation

Evaluation of the validity of an index involves enquiring into whether the index measures what it purports to measure. Many studies have used consensus of several experienced orthodontists in order to compare with the results of the index (Salzmann, 1968; Summers, 1971; Malmgren, 1980; Jenny *et al.*, 1983). In general, the process of validation involves the comparison of a subjective measure against a more objective measure of the characteristic.

The primary objective of the validation exercise was to compare a definitive measure of malocclusion using the indices with mean subjective dental opinion, in terms of deviation from normal for a representative sample of pre- and post-treated cases.

The PAR Index is made up of a number of sub-components, each measuring distinct occlusal traits. Perhaps of primary contention amongst the profession would be the importance that should be attributed to any one component relative to another. For example, is an open bite equivalent in importance to a cross-bite or overjet? The validation study provides an opportunity to determine the relative weight that should be applied to each component.

Design of the validation study

The examiners. Seventy-four dentists were invited to participate, representing the various groups carrying out orthodontic treatment in England and Wales, 22 Consultant orthodontists, 22 specialist practitioners, two members of staff employed by the Dental Practice Board of England and Wales and two junior hospital staff members, all possessing specialist orthodontic qualifications, and 15 general dental practitioners and 11 community dentists without orthodontic qualifications.

Each member of the panel of 74 examiners was asked to assess a representative sample of dental casts with respect to deviation from normal occlusion on a nine point scale (Fig. 7). For each dental cast a mean score was obtained from the panel of 74 examiners representing consensus opinion.

The representative sample. A broad range of cases was collected representing treatments undertaken within the general dental and hospital services in England Wales. In all 272 cases were collected consisting of 68 cases from each of the following sources:

1. non-prior approval cases from the Dental Practice Board (one upper removable appliance treatment);
2. prior approval cases from the Dental Practice Board (more than one removable appliance or fixed appliances);
3. treated cases from Manchester and Bristol Dental Hospitals;
4. untreated cases selected from a study of 1000 Cardiff school children taken over a 4-year period 1981–1984 (Shaw *et al.*, 1986).

The dental casts were divided into four groups (A, B, C, and D) consisting of 40 pre- and post-treatment pairs of dental casts including 16 cases which were randomly selected from the four sources and dupli be added to each gro reliability assessments t of the four groups was ized stratified sampl twenty dental casts we order bias, four sequ enable the dental casts session (Table 10). Freq ized to reduce fatigue. and issued in sequence of readings would be study days were arran Bristol.

Assessment of the indices. The four trai iners each scored one Index.

Relationship between ings of the panel of 74 Index. For every den for the panel of 74 ex deviation from norma an index to be valid between it and the me be large. If this is so, valid substitute for the panel of 74 examiners of their mean scores.

None
|
0

Table 10 Design of the

	Sessio
	1st
Time	9.30–1
	Numb
	32 pa
Booklet 1	B
Booklet 2	D
Booklet 3	C
Booklet 4	A

ClearCorrect Exhibit 1002, Page 2231 of 3373

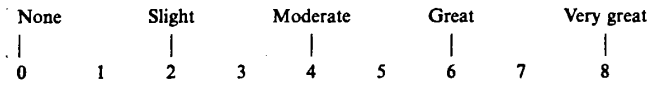


Figure 7 Nine-point scale to assess deviation from normal.

four sources and duplicated to allow them to be added to each group to enable examiner reliability assessments to be undertaken. Each of the four groups was presented as a randomized stratified sample. Three-hundred-and-twenty dental casts were examined. To reduce order bias, four sequences were devised to enable the dental casts to be examined in each session (Table 10). Frequent breaks were organized to reduce fatigue. Booklets were devised and issued in sequence so that an equal number of readings would be collected. Six validation study days were arranged in Manchester and Bristol.

Assessment of the dental casts using the indices. The four trained and calibrated examiners each scored one group using the PAR Index.

Relationship between the mean subjective ratings of the panel of 74 examiners and the PAR Index. For every dental cast the mean scores for the panel of 74 examiners were derived for deviation from normal occlusion. In order for an index to be valid the linear correlation, *r*, between it and the mean subjective score must be large. If this is so, the index will provide a valid substitute for the average opinion for the panel of 74 examiners, being a good predictor of their mean scores.

Results

The PAR Index. The raw total of the PAR components had a correlation, *r*, of 0.74 with the panel of 74 examiners mean subjective scores for deviation from normal occlusion. Direct summing of the sub-components might not provide the best index, as the profession might place greater importance on certain aspects. In order to determine the weights that should be placed on each component to best predict average opinion, multiple regression of the sub-components of PAR against the panel's mean score was carried out. Variables (components of PAR) were added using a forward stepwise procedure, provided a significant improvement in fit was achieved at each stage. The regression coefficients provided weights for each of the components. These were multiplied by a suitable constant and rounded to integers for the convenience of the user. The regression coefficients were derived on one half of the sample (by taking alternate cases) and the PAR components were multiplied in the same ratio as their partial regression coefficients and applied to the other half of the sample. Some of the components did not appear to have any predictive power and consequently were excluded from the weighted PAR Index (Table 11). The Pearson Correlation Coefficient, *r*, was 0.87 for the regression model and 0.85 for the weighted PAR

Table 10 Design of the validation study.

	Session				
	1st	2nd	3rd	4th	5th
Time	9.30–10.15	10.30–11.45	12.00–13.15	14.00–15.15	15.30–16.45
	Number of models				
	32 pairs	40	40	40	40
Booklet 1	B	A1–40	A41–80	B1–40	B41–80
Booklet 2	D	C1–40	C41–80	D1–40	D41–80
Booklet 3	C	B41–80	B1–40	C40–80	C1–40
Booklet 4	A	D41–80	D1–40	A41–80	A1–40

ClearCorrect Exhibit 1002, Page 2232 of 3373

Table 11 Partial regression coefficients, unweighted and weighted integers for individual PAR components.

PAR components	Unweighted	Partial reg. coeff	Weighted
Buccal segments	1	0	0
Upper anterior	1	0.15	1
Lower anterior	1	0.11	1
R and L buccal occlusion	1	0.13	1
Overjet	1	0.65	6
Overbite	1	0.24	2
Centreline	1	0.47	4
r^2	0.47	0.75	0.72
r	0.68	0.87	0.85

Index). There were no significant differences between the correlation values for the regression model and the corresponding weighted index ($P>0.1$). The weighted version gave a statistically significant higher correlation with the mean deviation from normal occlusion than the unweighted PAR ($P<0.001$). The weighted regression line is shown in Fig. 8. The coefficient of determination, r^2, the measure of prediction accuracy and strength of linear association was 0.72 for the weighted index.

Differences in weightings were noticed between the four groups (Table 12). The weightings for the centre line were much greater for consultants and general dental practitioners than for specialist practitioners and community dentists. The buccal segments (displacement measurements) were not weighted for any of the four groups of examiners. The weighting for upper anteriors was 2 for the specialists and 1 for the other groups.

The mean weightings were taken to represent the collective opinion of the panel of the 74 dentists.

Reliability of the weighted PAR Index. The inter-examiner Intraclass Correlation Coefficient of Reliability for the total score for the four examiners on the 38 cases was 0.93 with the lower 95 per cent confidence limit of 0.90. The weighted index shows a slight improvement over the unweighted version (unweighted $R=0.91$, lower 95 per cent confidence limit 0.87).

Case analysis. A case is shown in Fig. 9 and the unweighted and weighted PAR scores presented in Table 13. The case is a Class II

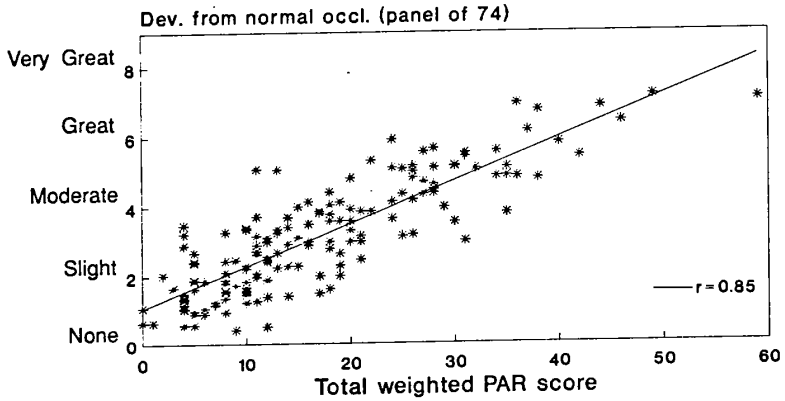


Figure 8 Correlation between the panel of 74 examiners mean subjective scores for deviation from normal and the weighted PAR Index.

Table 12 Weightings der

	PAR co
	Upper anterio
Consultants	1
Specialists	2
G.D.P.	1
Community	1
All	1

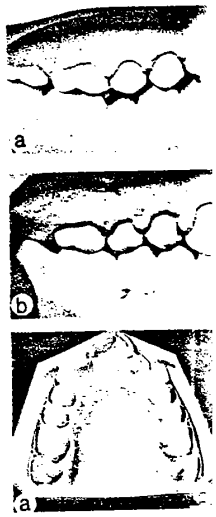


Figure 9 Case analysis: pr 45 to 2.

division 1 malocclusio lower incisor crowdin over 10 mm, and the complete. The mol quarter Class II on th Class II on the left premolars are in lingu

The post-treated c and overbite have be cal occlusions have buccal segments are Good alignment ha arches. The PAR sc treatment and 2 for casts. The weightings

ClearCorrect Exhibit 1002, Page 2233 of 3373

Table 12 Weightings derived for each of the groups of examiners.

	PAR components					
	Upper anterior	Lower anterior	Buccal occlusion	Overjet	Overbite	Centreline
Consultants	1	1	1	5	3	6
Specialists	2	1	1	4	1	−0.54
G.D.P.	1	1	1	5	2	4
Community	1	1	1	4	2	−0.25
All	1	1	1	6	2	4

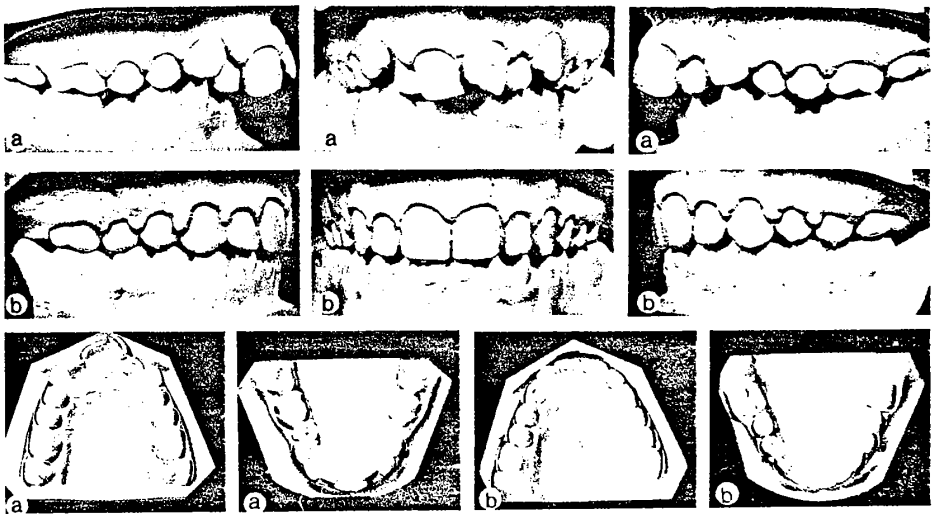


Figure 9 Case analysis: pre-treatment (a) and post-treatment (b) dental casts illustrate the reduction in PAR score from 45 to 2.

division 1 malocclusion with marked upper and lower incisor crowding. The overjet is increased over 10 mm, and the overbite is increased and complete. The molar relationship is three-quarter Class II on the right side and a quarter Class II on the left side. The lower second premolars are in lingual cross-bite.

The post-treated case shows that the overjet and overbite have been fully reduced. The buccal occlusions have been improved, but the buccal segments are not interdigitating fully. Good alignment has been achieved in both arches. The PAR scores were 36 for the pre-treatment and 2 for the post-treatment dental casts. The weightings have increased the initial score by 5 to 41, but the finished score stays at 2. The major contribution to the initial weighted PAR score was from the overjet.

In the previous case (Fig. 6) the PAR score when weighted rose by 17 to 38 for the pre-treatment model and reduced by 1 to 2 for the post-treatment models.

The reduction in weighted PAR scores for the case in Fig. 6 (36 PAR points) and Fig. 9 (43 PAR points) represents the degree of improvement and the success of treatment.

Reliability of the panel of 74 examiners. Reliability within and between the panel of 74 examiners was tested on 16 sets of dental casts

ClearCorrect Exhibit 1002, Page 2234 of 3373

Table 13 Derivation of PAR scores (Fig. 9).

PAR components	Before treatment	Total UN	Total W	After treatment	Total UN	Total W
Upper right segment	(6–5),0, (5–4),0, (4–3),2	2	–	(6–5),0, (5–4),0, (4–3),0	0	–
Upper anterior segment	(3–2),2, (2–1),1, (1–1),2, (1–2),0, (2–3),1	6	6	(3–2),0, (2–1),0, (1–1),0, (1–2),0, (2–3),0	0	0
Upper left segment	(6–5),0, (5–4),1, (4–3),1	2	–	(6–5),0, (5–4),0, (4–3),0	0	–
Lower right segment	(6–5),2, (5–4),2, (4–3),0	4	–	(6–5),0, (5–4),0, (4–3),0	0	–
Lower anterior segment	(3–2),1, (2–1),1, (1–1),0, (1–2),1, (2–3),1	4	4	(3–2),0, (2–1),0, (1–1),0, (1–2),0, (2–3),0	0	0
Lower left segment	(6–5),2, (5–4),3, (4–3),0	5	–	(6–5),0, (5–4),0, (4–3),0	0	–
Right buccal occlusion	Crossbite 45 and < cusp to cusp	3	3	Less than cusp to cusp	1	1
Overjet	Overjet greater than 10 mm	4	24	Overjet within 3 mm	0	0
Overbite	Overbite greater than 2/3	2	4	Normal overbite	0	0
Centreline	Centreline with 1/4 width of lower incisor	0	0	Centreline within 1/4 width	0	0
Left buccal occlusion	Cross-bite, cusp to cusp	4	4	Less than cusp to cusp	1	1
Total		36	45		2	2

UN—unweighted; W—weighted. Tooth notation in brackets, followed by the PAR score.

which had been duplicated and randomized within the groups. The chance corrected measure of agreement was used (O'Connell and Dobson, 1984).

Intra-examiner: There was a poor level of agreement between the panel of 74 examiners when assessing deviation from normal occlusion (Kappa Statistic: 0.39–0.87; Fig. 10).

Inter-examiner: Agreement between examiners in the five practitioner groupings was assessed using the Kappa Statistic (Table 14). There was only moderate agreement between examiners when assessing deviation from normal occlusion indicating a division in assessments between examiners. The decisions of the general dental practitioners and the community

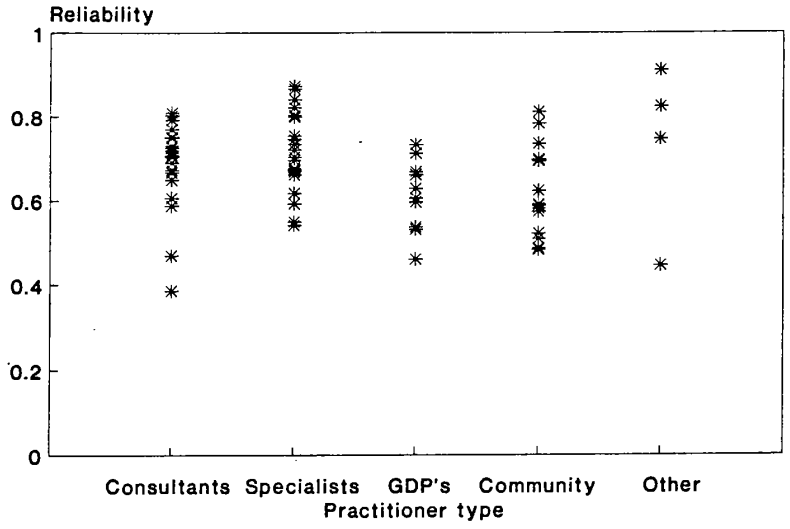


Figure 10 Intra-examiner reliability for the panel of 74 examiners deviation from normal occlusion ratings.

Table 14 Inter-examine

Deviation from normal

dentists showed the
other practitioners in

Discussion

The primary objective
Index. Two-hundred-
casts were assessed by
representing all inter
scores were obtained
examiners to reflect c
opinion.

The components o
weighted statistically t
ion. Several of the indi
not included in the we
not have any predicti
explanation for the e
segments (i.e. spacing
tions) may be that the
the buccal teeth were so
ment of a tooth was s
result and, therefore, b
left or right buccal oc
were a small number
premolars and it could
dentists missed these i
were too few cases t
contribution. Premolar
be recorded in the
although impacted can
scored in the anterior s

Residual extraction s
be accepted in the U
(Elderton and Clark, 19
that the panel of 74 ex
accept extraction spaces

The overjet, overbite,
ancy were weighted high
ively). The weighted f
appears high. An overj
a PAR score of 2, and
of 12. In fact, the overj
overjet in millimetres m
2. The range of weighti
weighting for an overjet
in Table 15. The overjet
in cross-bite.

ClearCorrect Exhibit 1002, Page 2235 of 3373

	Total	
	UN	W
-3),0	0	–
-1),0,	0	0
-3),0	0	–
-3),0	0	–
-1),0,	0	0
-3),0	0	–
usp	1	1
n	0	0
	0	0
4 width	0	0
usp	1	1
	2	2

nt between examner groupings was Statistic (Table 14). agreement between leviation from nordivision in assess- The decisions of the and the community

ratings.

Table 14 Inter-examiner agreement for the five groups of practitioners (Kappa statistic).

	Consultants	Specialists	GDP's	Community	Other
Deviation from normal	0.52	0.57	0.50	0.44	0.59

dentists showed the poorest agreement with other practitioners in their respective groups.

Discussion

The primary objective was to validate the PAR Index. Two-hundred-and-seventy-two dental casts were assessed by a panel of 74 examiners representing all interested parties. The mean scores were obtained from the panel of 74 examiners to reflect contemporary orthodontic opinion.

The components of the PAR Index were weighted statistically to reflect consensus opinion. Several of the individual components were not included in the weighted index as they did not have any predictive power. One possible explanation for the exclusion of the buccal segments (i.e. spacing, crowding, and impactions) may be that the contact points between the buccal teeth were so variable. If the displacement of a tooth was severe, a cross-bite would result and, therefore, be recorded in a score for left or right buccal occlusion. However, there were a small number of cases with impacted premolars and it could be that the panel of 74 dentists missed these impactions or that there were too few cases to produce a significant contribution. Premolar impactions would not be recorded in the weighted PAR Index although impacted canines would, as these are scored in the anterior segment.

Residual extraction spaces are more likely to be accepted in the U.K. than in America (Elderton and Clark, 1983) and it may be argued that the panel of 74 examiners was willing to accept extraction spaces.

The overjet, overbite, and centreline discrepancy were weighted highly (6, 2, and 4, respectively). The weighted factor of 6 for overjet appears high. An overjet of 6 mm would have a PAR score of 2, and a weighted PAR score of 12. In fact, the overjet score is similar to the overjet in millimetres multiplied by a factor of 2. The range of weightings and the equivalent weighting for an overjet in millimetres is shown in Table 15. The overjet score also includes teeth in cross-bite.

Table 15 Comparison of weighted PAR scores for overjet with the equivalent weighting for the overjet in mm.

Overjet (mm)	PAR score	Weighted PAR score	Equivalent weighting for overjet (mm)
0	0	0	0.0
1	0	0	0.0
2	0	0	0.0
3	0	0	0.0
4	1	6	1.5
5	1	6	1.2
6	2	12	2.0
7	2	12	1.7
8	3	18	2.3
9	3	18	2.0
10	4	24	2.4
11	4	24	2.2
12	4	24	2.0
13	4	24	1.9
14	4	24	1.7
15	4	24	1.6

The weighting for centreline discrepancy was higher for consultants and general dental practitioners than the specialist and community dentists. It would seem that the consultants and general dental practitioners were more likely to notice differences in the centrelines.

There was a poor level of agreement between the panel of the 74 examiners when assessing deviation from normal. This division highlights the need for an objective and reliable index.

The weightings which have been derived reflect current British orthodontic opinion. The PAR Index is flexible in that the weightings could be changed to reflect future standards and the standards that are currently being achieved in other countries.

Conclusions

The PAR Index provides a single summary score for all the occlusal anomalies and may be used for all types of malocclusions, treatment modalities and extraction/non-extraction cases. The score provides an estimate of how far a case deviates from normal and the difference in

ClearCorrect Exhibit 1002, Page 2236 of 3373

scores for pre- and post-treated cases reflects the perceived degree of improvement and therefore the success of treatment.

Excellent reliability within and between four trained examiners has been demonstrated using the PAR Index. The PAR Index offers uniformity and standardisation in assessing the outcome of orthodontic treatment. The components of the PAR Index have been weighted to reflect current British dental opinion more closely.

Address for correspondence

Dr Stephen Richmond
Department of Oral Health and Development
Coupland III Building
University of Manchester
Higher Cambridge Street
Manchester M15 6FH

Acknowledgements

The authors are grateful to the British Orthodontic Standards Working Party whose members were actively involved in developing the PAR Index and for the Panel of 74 examiners who gave up their valuable time to record the 320 dental casts. The authors would also like to acknowledge the financial support of the Dental Practice Board.

References

Barkto J J 1966 The intraclass correlation coefficient as a measure of reliability. Psychology Report 19: 3–11

Berg R 1979 Post-retention analysis of treatment problems and failures in 264 consecutively treated cases. European Journal of Orthodontics 1: 55–68

Buchanan I D 1990 The PAR versus the Summers index. Presentation at the British Orthodontic Conference, Torquay 1990

Eismann D 1974 A method of evaluating efficiency of orthodontic treatment. Transactions of the European Orthodontic Society, 223–232

Eismann D 1980 Reliable assessment of morphological changes results from orthodontic treatment. European Journal of Orthodontics 2: 19–25

Elderton R J, Clark J D 1983 Orthodontic treatment in general dental service assessed by the occlusal index. British Journal of Orthodontics 10: 178–186

Elderton R J, Clark J D 1984 An investigation of treatment in the General Dental Service for patients with Class II division 1 malocclusions. British Journal of Orthodontics 11: 2–8

Fleiss J L 1981 Statistical methods for rates and proportions, 2nd ed. Wiley, London

Fleiss J L 1986 The design and analysis of clinical experiments. Wiley, London

Fleiss J L, Slakter M J, Fischmann S L, Park M H, Chilton N W 1979 Inter examiner reliability in caries trials Journal of Dental Research 58: 604–609

Gottlieb E L 1975 Grading your orthodontic treatment results. Journal of Clinical Orthodontics IX: 156–161

Hickham J H 1975 Directional edgewise orthodontic approach. Journal of Clinical Orthodontics IX: 143–154

Jenny J, Cons N C, Kohout F J 1983 Comparison of SASOC, a measure of dental aesthetics, with three orthodontic indices and orthodontic judgement. Community Dentistry and Oral Epidemiology 11: 236–241

Malmgren O 1980 Studies on the need and demand for orthodontic treatment. Swedish Dental Journal Supplement 6

Mitropoulos C M, Downer M C 1987 Inter-examiner agreement in the diagnosis of dental caries among officers of the reference service. British Dental Journal 162: 227–229

O'Connell D L, Dobson A J 1984 General observer agreement measures on individual subjects and groups of subjects. Biometrics 40: 973–983

Pickering E A, Vig P 1975 The occlusal index used in assessing orthodontic treatment. British Journal of Orthodontics 2: 47–51

Salzmann J A 1968 Handicapping malocclusion assessment to establish treatment priority. American Journal of Orthodontics 54: 749–765

Shaw W C, Addy M, Dummer P M H, Rayner C 1986 Dental and social effects of malocclusion and effectiveness of orthodontic treatment: a strategy for investigation. Community Dentistry and Oral Epidemiology 14: 60–64

Summers C J 1971 The occlusal index: a system for identifying and scoring occlusal disorders. American Journal of Orthodontics 59: 552–566

Appendix 1: Conventions for the PAR Index

General

1. All scoring is accumulative.
2. There is no maximal cut-off level.
3. The occlusion should be scored [illegible] functional displacement [illegible] determined from dental casts [illegible]
4. The contact points between [illegible] third molars are not recorded. The [illegible] points between molars are [illegible] however, severe deviations [illegible] cross-bite, and will be noted [illegible] occlusions.
5. If the contact point displacement [illegible] result of poor restorative [illegible] tions or crowns), the displacement [illegible] recorded.
6. Contact points bet[illegible] not recorded.
7. Extraction spaces [illegible] patient is to rece[illegible] ment. However, if [illegible] the distance betw[illegible] be noted.

Canines

Where there are n[illegible] ments resulting fr[illegible] the mesial contac[illegible] molar and the dis[illegible] should be recorde[illegible]

Canine cross-bites s[illegible] overjet section.

Contact points betw[illegible] molars are scored[illegible] contact point of th[illegible] on the mesial surf[illegible] molar. (These cor[illegible] ible. When untre[illegible] were assessed this[illegible] be the most accep[illegible]

[illegible]

[illegible] is unerupted [illegible] of the arch eith[illegible]

ClearCorrect Exhibit 1002, Page 2237 of 3373

ınd analysis of clinical experi-

mann S L, Park M H, Chilton
:r reliability in caries trials.
h 58: 604–609

your orthodontic treatment
Orthodontics IX: 156–161

ional edgewise orthodontic
:al Orthodontics IX: 143–154

ı F J 1983 Comparison of
ıl aesthetics, with three ortho-
ıntic judgement. Community
iology 11: 236–241

ı the need and demand for
dish Dental Journal Supple-

C 1987 Inter-examiner agree-
ntal caries among officers of
Dental Journal 162: 227–228

984 General observer agree-
ıal subjects and groups of
-983

occlusal index used to assess
sh Journal of Orthodontics

ing malocclusion assessment
rity. American Journal of

r P M H, Ray C, Frude N
s of malocclusion and effect-
nent: a strategy for investi-
and Oral Epidemiology 14:

index: a system for identify-
rders. American Journal of

for the PAR Index

ıtive.

ut-off level.

e scored disregarding
ent (this cannot be
tal casts alone).

een first, second, and
ecorded. The contact
ırs are so variable.
ıtions will produce a
noted in the buccal

lisplacement is as a
ative work (restora-
displacement is not

6. Contact points between deciduous teeth are not recorded.
7. Extraction spaces are not recorded if the patient is to receive a prosthetic replacement. However, if space closure is intended, the distance between adjacent teeth should be noted.

Canines

1. Where there are missing canines, displacements resulting from discrepancies between the mesial contact point to the first premolar and the distal of the lateral incisor should be recorded in the anterior segment.
2. Canine cross-bites should be recorded in the overjet section.
3. Contact points between the canines and premolars are scored as follows: the distal contact point of the canine to the midpoint on the mesial surface of the adjacent premolar. (These contact points are so variable. When untreated normal occlusions were assessed this relationship seemed to be the most acceptable.)

Impactions

If a tooth is unerupted and displaced from the line of the arch either buccally or palatally due to insufficient space, this is regarded as an impaction. However, if the tooth is erupted and displaced, the displacement score is recorded.

Incisors

1. If there is agenesis of the upper incisor or the tooth has been lost due to trauma or caries the procedure is as follows:
   (a) if the space is maintained (for a prosthesis), the distance between adjacent teeth is not recorded;
   (b) if the space is to be closed, the distance between adjacent teeth is recorded.
2. When recording an overjet, if the tooth falls on the line the lower grade is recorded.
3. If a lower incisor has been extracted or is missing, the centreline is not recorded.

Molars

1. Contact points between first and second molars are not recorded.
2. If the first molars have been extracted, the contact point of the second molar is recorded.

ClearCorrect Exhibit 1002, Page 2238 of 3373

Recording the dental cast in three dimensions

S. Richmond, B.D.S., D. Orth., R.C.S., M.Sc.D., F.D.S.R.C.S (Edinburgh)*
Heath Park, Cardiff, Wales

A method is described to record the three-dimensional relationship of the teeth within the dental arches. (AM J ORTHOD DENTOFAC ORTHOP 1987;92:199-206.)

There have been many techniques described to quantify the characteristics of a malocclusion. It has been only recently with the advent of new technology that the dental cast can be readily measured and recorded in three dimensions. This facility allows a realistic reconstruction of the dental cast, which would prove useful in research. It is with the research aspect in mind that a quantitative analysis has been devised.

MATERIALS AND METHODS

It is important to design an analysis that has features a clinician would use. The variables used are described and defined below.

1. *Overjet and overbite*

   Overjet and overbite are measurements the clinician uses frequently during, before, and after treatment. The usual technique is to use a ruler or vernier calipers to the labial aspect of the lower incisors to the incisal edge of the upper incisors. With this technique, two different landmarks are used. In the proposed analysis, similar landmarks are chosen on the upper and lower central incisors using the mesial incisal edges.

   Overbite

   Overbite is the distance of the upper central incisors from the lower incisors measured in relation to a perpendicular to the occlusal plane using the same points as those for overjet. This measurement would be difficult to make on dental casts using a ruler or vernier calipers.

2. *Center-line discrepancy*

   The center line is an important assessment because it shows the symmetry of the arches. A shift in the center line would suggest differing molar positions or discrepancy between the tooth diameters of the upper and lower teeth. The center line is constructed using the midpoints between the canines and molars on the lower model because the clinician usually assesses the lower model first and fits the upper model to the lower. This facility enables the operator to determine whether the center lines of the incisors are coincident or how far they deviate from each other and from the constructed center line. Although the construction of the center line may not coincide with the midline of the face, a useful indication of discrepancy in center lines can be determined. In the case of mandibular asymmetry, a gross reading in center-line discrepancy may be noted that would warrant further investigation with radiographs to assess the skeletal symmetry.

3. *Mesiodistal widths*

   Tooth size plays an important part in malocclusions, particularly in space requirements. In this analysis the three dimensional measurement is determined across the anatomic contact points. Results are determined for the anterior (3-3) and overall (6-6) mesiodistal widths.

   In the event of unerupted teeth, the mesiodistal width of its antimere can be used. In the case of both teeth being unerupted, an average mesiodistal width for that particular tooth can be substituted (Table I).

4. *Three- and two-dimensional intercanine and incisal angles*

   The traditional method of assessing intercanine and incisal angles has been by the use of the lateral skull radiograph. A significant difference has been shown between two-dimensional and three-dimensional interincisor assessment on the lateral skull radiograph and dental cast, respectively.[1] This would suggest a difference between the crown and crown/root angulation measuring techniques. However, the authors also noted that the results for the dental cast assessment of the crown angulation were more consistent and reproducible than the assessments for the crown/root angulations on the lateral skull radiograph.

*Department of Orthodontics, University Dental Hospital of Manchester, and Turner Dental School, Manchester, England.

ClearCorrect Exhibit 1002, Page 2239 of 3373

Am. J. Orthod. Dentofac. Orthop.
September 1987

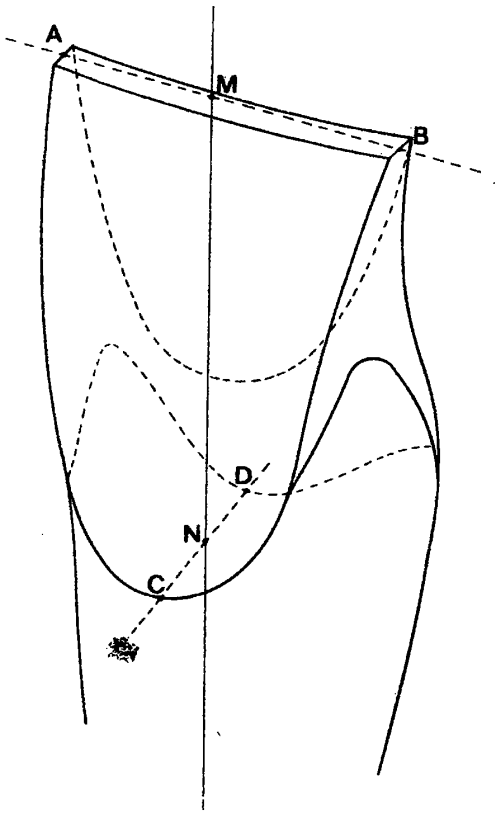


Fig. 1. Interincisal and canine crown angulations. The central axis of the crown is constructed using points A and B defined by the mesioincisal edge and the corresponding point on the distal surface. C–D relate to the points that bisect the crown at the gingival margin when the dental cast is viewed occlusally.

The central axis of the crown is constructed by the midpoints of the incisal edges (A and B) and gingival margin (C and D). The midpoints M and N define the central axis (Fig. 1).

The analysis determines only the axial inclinations of the crowns of the teeth and does not relate to the crown root angle. However, the orthodontist is mainly concerned with the crowns of the teeth unless the crown root angle is acute and torquing will adversely position the root apex.

Two-dimensional angles can be determined by projecting the central axis onto the anteroposterior plane (Fig. 2).

5. *Occlusal plane construction*
The occlusal plane is constructed using the buccal cusp tips of the lower premolars and the mesiobuccal cusp tip of the lower molar (Fig. 3). This is comparable to the functional occlusal plane.[2] The plane is constructed to the best fit of these six points. However, only three points are required to form a plane; therefore, a full complement of teeth is unnecessary.

Table I. Average mesiodistal widths used when the individual teeth are unerupted or missing

	Tooth no.	*Upper (mm)*	*Lower (mm)*
Central incisor	1	8.79	5.5
Lateral incisor	2	6.83	5.98
Canine	3	7.74	6.77
First premolar	4	6.68	6.84
Second premolar	5	6.59	7.145
First permanent molar	6	10.38	10.5

6. *Intercanine and intermolar distances*
It is important during treatment to monitor intercanine and intermolar distances. In certain cases it will be necessary to expand the upper or lower intercanine distance if the arch is excessively narrow and crowded. The distance measured is between the occlusal tips of the canines and the points of the buccal groove of the molars where the buccal surface meets the occlusal surface.

7. *Parabolic curve length*
Several investigators have concluded that there is no consistency in nature and the shape of the dental arch varies so widely among individuals that geometric comparisons are impossible.[3,4] Hawley[5] proposed a geometric method for predetermining the dental arches for orthodontic purposes using the ideas of Bonwill,[6] although Hawley[5] and Chuck[7] advised against strict use of this. The ellipse[8-10] and catenary curve[11] have also been suggested.

The polynominal equation of the fourth degree was proposed by Lu.[12] Hechter[13] found that the parabola had a high "goodness of fit" to the middle curve of teeth when compared with other generated curves.

The parabola has also been suggested by other investigators.[4,9,10,14,15] Richmond[16] concluded that it was doubtful whether the ideal arch form ever exists, but in order to treat a malocclusion, it is necessary to align the teeth and to know the severity of crowding to a given arch form. The parabolic curve was chosen in this analysis because several authors have shown it to be the best fit; it was also selected for its ease in mathematic application.

The parabolic curve is constructed to the best fit

ClearCorrect Exhibit 1002, Page 2240 of 3373

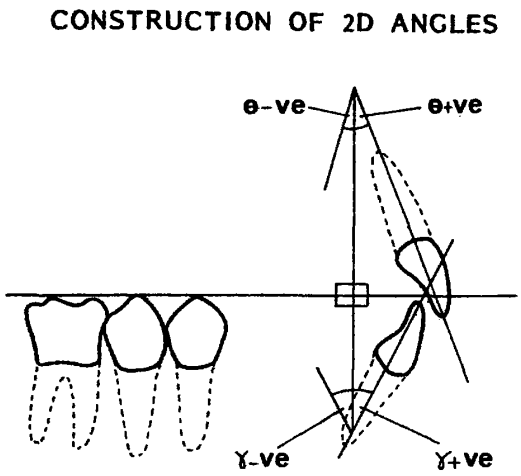


Fig. 2. Construction of two-dimensional angles. Positive angles are produced when the teeth are proclined relative to the perpendicular raised to the occlusal plane.

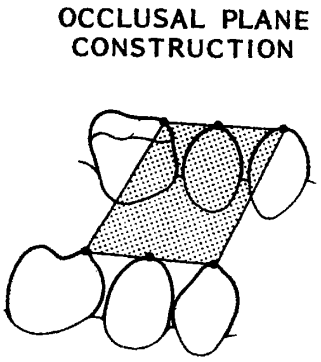


Fig. 3. Occlusal plane points. In three dimensions, three points are required to fit a plane. The occlusal plane is established using the buccal cusp tips of the lower premolars and the mesiobuccal cusp of the molars. The plane is constructed as the best fit using the six points.

of the mesiodistal anatomic contact points ending distal to the first molar (Fig. 4). The curve is constructed to each individual case rather than fitting the case to a preselected arch form. The length of the parabolic curve is noted.

8. *Discrepancy measurements*

A discrepancy measurement is a useful indication of the crowding or spacing within the dental arches that will determine an extraction or nonextraction approach.

Two types of discrepancy measurements are used.

a. *Arch discrepancy*

This discrepancy measurement provides a guideline for how far the anatomic contact points are from the corresponding contact point on the adjacent teeth in relation to the occlusal plane (Fig. 5). Therefore, this measurement attempts to quantify the discrepancy between the contact points in two dimensions.

The distance a–b when projected onto the occlusal plane c–d produces the two-dimensional discrepancy. These distances represent the movement required to align the dental arches to form a flat occlusal plane.

b. *Parabolic curve discrepancy*

The length of the parabolic curve and the overall mesiodistal widths are known; therefore, by subtracting one from the other, the discrepancy can be determined, noting whether the arch is spaced or crowded.

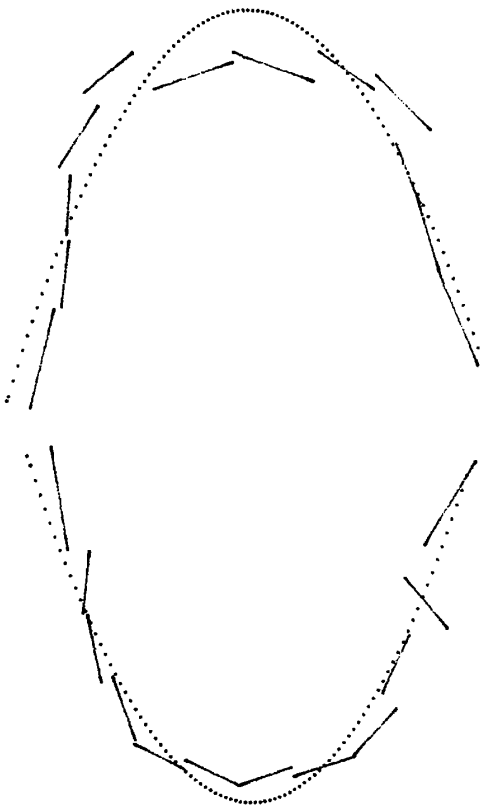


Fig. 4. Parabolic curve length. A parabola was constructed to the best fit of the mesiodistal anatomic contact points ending distal to the first molar (plotted from Fig. 7).

ClearCorrect Exhibit 1002, Page 2241 of 3373

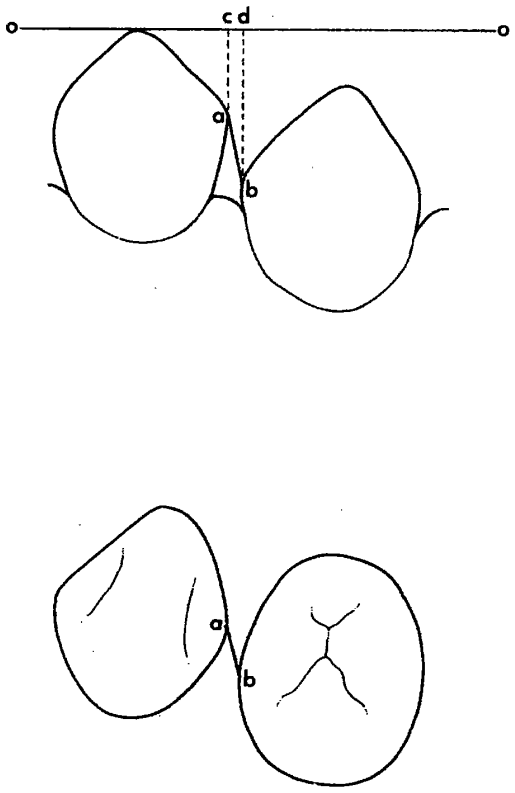


Fig. 5. Discrepancy measurement. The distance a–b is the three-dimensional distance between the anatomic contact points. When the points a–b are projected onto the occlusal plane o–o, the distance is now c–d. This "correction factor" provides a more reliable discrepancy reading and is related to the need for flattening the occlusal plane.

Sample

To test the accuracy and reproducibility of the analysis, 12 sets of dental casts were randomly selected from 150 patients, first checking to validate the occlusal relationships. It was essential that the dental casts be stable when positioned on their heels—together and independently.

Procedure

Eight crossed lines were marked around the land area for each in the upper and lower dental casts (the fiducial points). The intersection of the two lines was used to orientate the dental casts so that when they were in occlusion, the spatial arrangement was noted; therefore, when the casts were moved apart to digitize the occlusal surfaces, all the points could be reorientated to the occluded position by re-recording the fiducial points.

Instrument

The points were recorded by means of the Reflex Metrograph,* which is capable of measuring objects in three dimensions (Fig. 6). This instrument basically consists of a semireflecting mirror; therefore, an object standing in front of the mirror has its image at an equal distance behind the mirror. Working on this principle, a moving light source connected to a three-dimensional (X–Y–Z) slide system behind the mirror can be used to record points corresponding to the image of the object.

Movement of this slide system operates rotary encoders, which translate movement into electrical impulses that can be transmitted to a computer. With the aid of a computer program, this information can be accepted and measurements performed. One of the qualities of the Reflex Metrograph is that the 0.3-mm diameter light source can move into interproximal spaces and contact areas where a pair of dividers could not.

The accuracy of the Reflex Metrograph has been tested by Richmond[16] and the error found to be less than 0.27 mm (<0.3%) with an angular error of less than 0.76%. This compares favorably with other authors.[17-19]

One hundred ten points were recorded. It takes an experienced operator less than 20 minutes to record 110 points.

To illustrate the analysis, a Class II, Division 2 malocclusion is shown in Fig. 7. The following analysis shows a deep overbite of 6 mm and an overjet of 3 mm. The center lines are almost coincident, the mesial edges all being to the right of the constructed center line by approximately 1.5 mm. The distances for the mesiodistal widths are shown.

CLASS II, DIVISION 2 MALOCCLUSION

	Left	*Right*
Overjet	3.05 mm	3.35 mm
Overbite	5.73 mm	5.78 mm

Center-line discrepancy

Mesial edge of upper left central incisor, 1.51 mm right of center line

Mesial edge of upper right central incisor, 1.65 mm right of center line

Mesial edge of lower left central incisor, 1.42 mm right of center line

Mesial edge of right central incisor, 1.19 mm right of center line

*H. F. Ross, Ross Instruments Ltd., Salisbury, Wiltshire, England.

ClearCorrect Exhibit 1002, Page 2242 of 3373

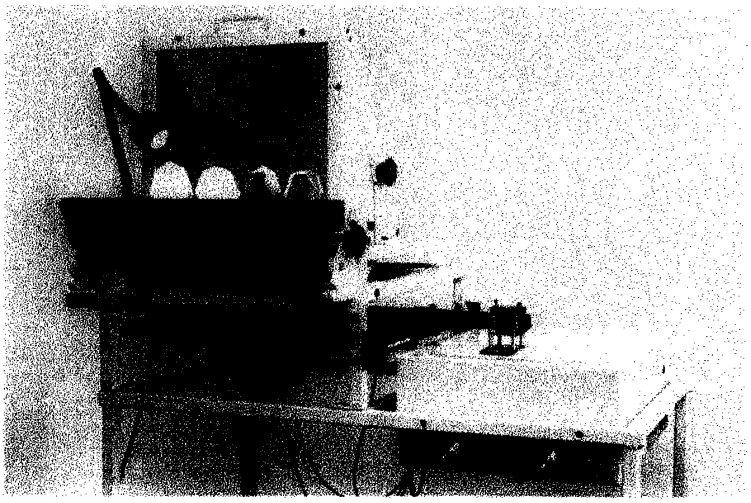


Fig. 6. Reflex Metrograph.

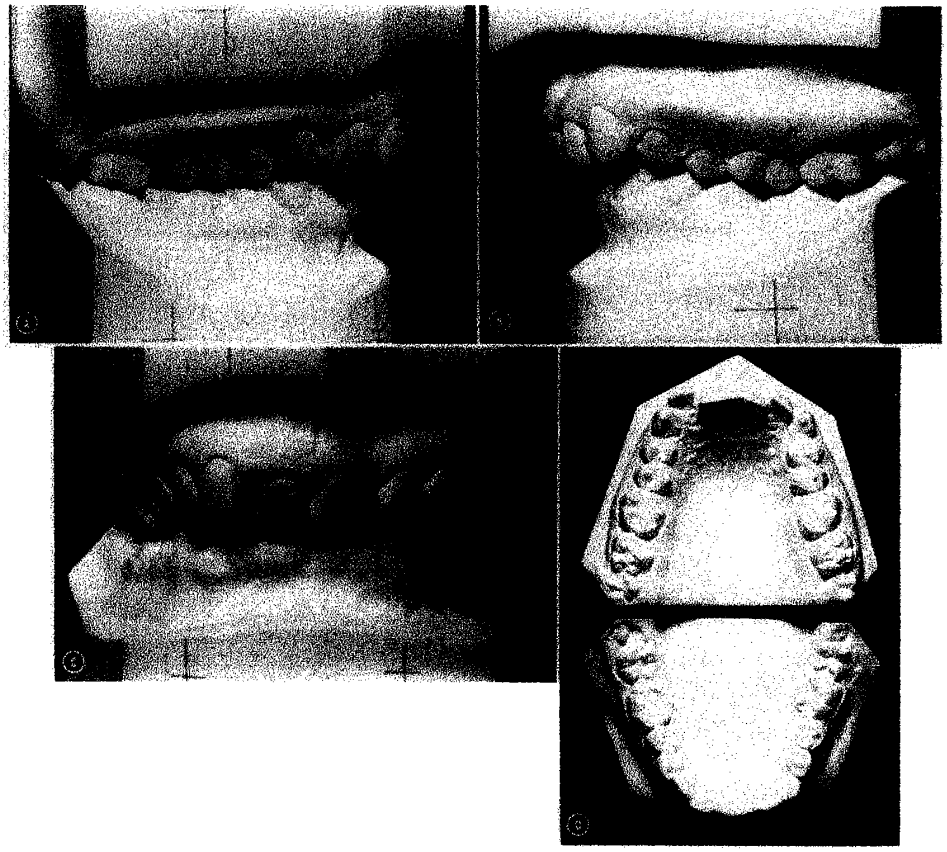


Fig. 7. A through D, Dental casts of Class II, Division 2 malocclusion. (For analysis, see text.)

ClearCorrect Exhibit 1002, Page 2243 of 3373

Table II. Intra- and interobserver errors

		Intraobserver error			*Interobserver error*		
	n	*Mean*	*SD*	*RMS*	*Mean*	*SD*	*RMS*
Overjet	24	0.04	0.32	0.31	0.17	0.49	0.49
Overbite	24	0.13	0.64	0.63	0.16	0.82	0.85
Mesial contact points of central incisors to center line	48	−0.12	0.49	0.49	−0.17	0.63	0.64
Upper mesiodistal widths	44	0.05	0.26	0.27	0.34	0.35	0.48*
Lower mesiodistal widths	144	0.15	0.27	0.32	0.25	0.34	0.43
Three-dimensional angles, incisors	24	0.24	2.12	2.04	0.89	2.34	2.7
Three-dimensional angles, canines	19	0.44	5.82	5.5	−2.48	5.7	5.27
Upper two-dimensional angles	67	−0.18	3.54	3.48	1.65	5.24	5.37*
Lower two-dimensional angles	67	0.69	3.05	3.08	−1.55	3.79	4.03
Overall mesiodistal widths	24	1.06	1.37	1.70	3.45	1.49	3.74*
Anterior mesiodistal widths	24	0.27	0.97	1.01	0.66	1.18	1.32
Overall discrepancy	24	0.24	1.92	1.87	0.1	2.74	3.32*
Anterior discrepancy	24	0.11	1.43	1.39	−0.77	2.06	2.11*
Intercanine distance	20	0.12	0.52	0.52	−0.08	0.56	0.54
Intermolar distance	21	0.03	0.40	0.38	0.01	0.45	0.43
Length of fitted parabola	24	0.44	0.93	1.01	1.36	1.27	1.93*
Length of discrepancy of fitted parabola	24	−0.71	1.57	1.72	−2.01	1.55	2.55

OBSERVER ERRORS: Intraobserver—significant difference $P > 0.5$; interobserver—significant difference $P > 0.5$ except "*" when $0.5 > P > 0.1$.

Mesiodistal widths	*Upper (mm)*	*Lower (mm)*
Left first permanent molar	10.09	10.13
Left second premolar	6.48	6.55
Left first premolar	6.23	6.33
Left canine	7.66	6.34
Left lateral incisor	6.6	6.39
Left central incisor	8.8	5.52
Right central incisor	8.39	5.83
Right lateral incisor	6.27	5.61
Right canine	7.39	6.61
Right first premolar	5.89	6.8
Right second premolar	6.6	6.28
Right permanent molar	10.27	10.52

CANINE AND INCISOR ANGULATIONS

	Three-dimensional angle (°)	*Two-dimensional angle (°)*	
		Upper	*Lower*
Left canine	133.70	1.29	22.74
Left lateral incisor	148.61	−1.68	23.63
Left central incisor	167.42	−12.73	22.82
Right central incisor	167.45	−14.89	25.80
Right lateral incisor	129.60	13.48	28.71
Right canine	158.80	−7.09	12.83

	Upper (mm)	*Lower (mm)*
Overall mesiodistal widths (6-6)	90.67	82.91
Anterior mesiodistal widths (3-3)	45.11	36.30
Intercanine distance	35.34	27.36
Intermolar distance	48.58	44.16
Length of fitted parabola	91.50	85.22

Discrepancy measurements		
1. Arch discrepancy		
Anterior (3-3)	10.22	3.84
Overall (6-6)	14.24	13.83
2. Parabola length minus Mesiodistal widths	1.13	2.31

The canine and incisal angulations are measured in three and in two dimensions. The results suggest that the upper central incisors are retroclined to a perpendicular by 12° to 14°. This is supported by the three-dimensional angle of 167° indicating a high interincisal angle.

Looking at the lateral incisors, it is noted that the upper right lateral incisor is proclined 14° more than the upper left lateral incisor. Therefore, by looking at the results, these would indicate a Class II, Division 2 incisor relationship.

Looking at the arch discrepancy measurement, the upper anterior discrepancy is 10.22 mm and overall 14.24 mm. This would suggest that most of the discrepancy is in the incisor region caused mainly by the retroclination of the upper central incisors.

In the lower arch, there appears to be minimal crowding in the anterior region (3.84 mm), but the overall reading is 13.83 mm. This is mainly due to the rotation of the lower left second pre-

ClearCorrect Exhibit 1002, Page 2244 of 3373

molar and insufficient space for the lower right second premolar. The rotations are indicated on the plot of the dental arches (Fig. 4).

The parabolic-curve discrepancy shows minimal crowding in the upper arch; the parabolic curve suggests retroclination of the upper central incisors and a proclination of the upper right labial incisor. In the lower arch, minimal crowding is also noted; the parabolic curve suggests retroclination of the lower incisors.

RESULTS

The root mean squares (RMS) and standard deviations (SD) are shown for the recorded measurements in Table II.

The inter- and intraobserver errors were acceptable and no significant differences were found, the *P* value being greater than 0.5 for intraobserver and generally greater than 0.1 for interobserver readings. The results would indicate that the measurements undertaken were consistent and reproducible.

The intercanine and incisal angulation readings have been grouped together. Richmond[16] has previously shown that the accuracy of the incisal angulations is generally better than that of the canine angulations. This is due to the distance between the midpoints m–n, which is generally less in canines than incisors, and because the morphology of the canines is slightly unfavorable since the defined points are not always readily identified.

The interobserver error was not significant, which suggests that a technician could be trained to use the analysis to produce a series of readings upon which to build a data base that would be useful in research.

CONCLUSIONS

Freer, Grew, and Little[20] reported that a difference exists between the subjective assessment and diagnosis of orthodontists.

It would be desirable to make consistent assessments of orthodontic cases; by using the above-described analysis, a consistent approach to diagnosis and treatment planning is possible.

All the landmarks were recorded directly on the dental casts. Using the points recorded, planes can be constructed to assess positions of teeth in the three planes of space. Therefore, planes can be directly produced on the dental casts; this offers an advantage over radiographically derived planes as the latter may be subjected to rotational errors and magnification problems.

It is important to remember that the analysis is a recent development and has not as yet been calibrated. This would best be achieved by mensurating ideal occlusions to attain standard values.

Although the full analysis is described, it is possible to measure individual variables alone without digitizing the 110 points. It is also possible to construct other planes and angles if so desired.

In conclusion, this analysis can illustrate and quantify the characteristics of a given malocclusion; it is both consistent and reproducible. The analysis may prove useful to the orthodontist in the clinical setting or for use as a research tool. The analysis can describe the dental cast in the three planes of space and could be useful as a record of the dental cast to alleviate the problems of storage.

I wish to thank Dr. P. J. Scott for his contribution to the preparation of the software for three-dimensional cast measurement and Mr. M. L. Jones for measuring the dental casts to attain the interobserver error. The illustrative work was prepared by the Cardiff Audio-Visual Aids Department and Mrs. L. Lowe, who typed the manuscript.

REFERENCES

1. Richmond S, Jones ML. A comparison of two and three dimensional incisor angles. Br J Orthod 1985;12:90-6.
2. Jacobson A. The "Wits" appraisal of jaw disharmony. AM J ORTHOD 1975;67:125-38.
3. Hellman M. Dimensions versus form in teeth and their bearing on the morphology of the dental arch. Int J Orthod 1919; 5:615-51.
4. Wheeler RC. A textbook of dental anatomy and physiology. 2nd ed. Philadelphia: WB Saunders Co, 1950:196-215, 352-406.
5. Hawley CA. Determination of the normal arch and its application to orthodontics. Dent Cosmos 1905;47:541-57.
6. Bonwill WGA. Geometrical and mechanical laws of articulation. Trans Odont Soc Penn 1884-1885:119-33.
7. Chuck GC. Labial arch form. Angle Orthod 1934;4:312-27.
8. Black GV. Descriptive anatomy of the human teeth. 5th ed. Philadelphia: S.S. White Mfg. Co., 1902.
9. Izard G. New method for the determination of the normal arch by the function of the face. Int J Orthod 1927;13:582-95.
10. Sicher H. Oral anatomy. 2nd ed. St. Louis: The C. V. Mosby Company, 1952:262-3.
11. MacConnaill MA, Scher EA. The ideal form of the human dental arcade with some prosthetic application. Dent Rec 1949;69: 285-302.
12. Lu KH. Analysis of dental arch symmetry [Abstract]. J Dent Res 1964;43:780.
13. Hechter FJ. Symmetry and dental arch form of orthodontically treated patients. J Can Dent Assoc 1978;44:173-84.
14. Broomwell IN. Anatomy and histology of the mouth and teeth. 2nd ed. Philadelphia: P. Blakistone Sons & Co, 1902:99.
15. Currier JH. A computerized geometric analysis of human dental arch form. AM J ORTHOD 1969;56:164-79.
16. Richmond S. The feasibility of categorising orthodontic treatment difficulty—The use of three dimensional plotting [M.Sc.D. thesis]. Cardiff, Wales: University of Wales, 1984.

ClearCorrect Exhibit 1002, Page 2245 of 3373

17. Butcher GW, Stephens CD. The reflex optical plotter. A preliminary report. Br Dent J 1981;151(9):304-5.
18. Scott PJ. The reflex plotters: Measurement without photographs. Photogrammetric Rec 1981;10:435-46.
19. Takada K, Lowe AA, De Cou R. Operational performance of the Reflex Metrograph and its applicability to the three-dimensional analysis of dental casts. AM J ORTHOD 1983;83:195-9.
20. Freer FJ, Grew JM, Little RM. Agreement among the subjective severity assessment of 10 orthodontists. Angle Orthod 1973; 43:185-90.

Reprint requests to:
Dr. Stephen Richmond
Department of Orthodontics
Dental Hospital of Manchester and Turner Dental School
Higher Cambridge St.
Manchester MI5 6FH England

BOUND VOLUMES AVAILABLE TO SUBSCRIBERS

Bound volumes of the AMERICAN JOURNAL OF ORTHODONTICS AND DENTOFACIAL ORTHOPEDICS are available to subscribers (only) for the 1987 issues from the Publisher, at a cost of $40.00 ($50.00 international) for Vol. 91 (January-June) and Vol. 92 (July-December). Shipping charges are included. Each bound volume contains a subject and author index and all advertising is removed. Copies are shipped within 60 days after publication of the last issue in the volume. The binding is durable buckram with the journal name, volume number, and year stamped in gold on the spine. *Payment must accompany all orders*. Contact The C. V. Mosby Company, Circulation Department, 11830 Westline Industrial Drive, St. Louis, Missouri 63146, USA; phone (800) 325-4177, ext. 351.

Subscriptions must be in force to qualify. Bound volumes are not available in place of a regular Journal subscription.

European Journal of Orthodontics

Contents

Volume 3 Number 4

227 A comparison of various facial and occlusal characteristics in mature individuals, with vertical and horizontal growth direction expressed at the chin
A. Lundström (Sweden) and D. G. Woodside (Canada)

237 Cephalometric guidance for the positioning of the incisors
I. Janson and A. Hasund (Germany)

241 Cephalometric analysis as a tool for treatment planning and evaluation
F. V. Tenti (Italy)

247 Skeletal and soft tissue response to activator treatment
Carl-Magnus Forsberg and Lars Odenrick (Sweden)

255 Gingival width in orthdontic clinical diagnosis
G. R. J. Mazeland (The Netherlands)

263 The control mechanism of tooth eruption. An experimental study in adult monkeys
Olav Slagsvold and Kjell Karlsen (Norway)

273 How different social classes benefit from the subsidized orthodontic services in Norway
Reidar Sivertsen (Norway)

279 Dental arch analysis; arch form. A review of the literature
S. J. Rudge (England)

285 Intermaxillary tooth-width ratio analysis
A. Lundström (Sweden)

289 A classification of open bites
Andrew Richardson (Northern Ireland)

297 Editorial

298 Forthcoming events

299 Index to volume 3

ISSN 0141 5387

European Journal of Orthodontics 3 (1981) 279–284
© 1981 European Orthodontic Society
0141–5387/81/00940279/$02.00

Dental arch analysis: arch form
A review of the literature

S. J. Rudge
Chester, England.

Summary. The literature of dental arch analysis is reviewed outlining the methods that have been used to evaluate dental arch form. The theory, practical applications and problems of these methods are described.

Many orthodontists have sought to find a universal, ideal arch form and although most studies have used similar material—a collection of untreated ideal occlusions—there has been very little agreement about the natural shape of this ideal arch.

A review of the literature shows, however, that several assumptions are made:—

There must be an algebraic or geometric formula which explains ideal arch form.

All ideal arches are the same shape and differ only in size.

Every ideal arch is considered to be symmetrical.

One of the earliest descriptions was provided by Hawley (1905) based on the earlier work of Bonwill (1885). Hawley described the ideal arch as being constructed upon an equilateral triangle with slight modifications. The six anterior teeth were thought to be arranged on the arc of a circle whose radius was determined by the combined width of the incisors and canines, with the premolars and first permanent molars arranged in a straight line and the second and third molars turning in towards the midline. The base of the equilateral triangle was thought to represent the intercondylar width. Arch forms provided by supply companies are generally of the Bonwill-Hawley type.

Black (1894) described the upper teeth as being arranged in a semi-ellipse, but Angle (1907) in a detailed discussion of the "line of occlusion" maintained that this line represented a parabolic curve. He considered Hawley's method of arch prediction to be useful only as an approximate guide to occlusion. The interpretation of Angle's use of the line of occlusion, however, has become confused; some orthodontists believe that Angle referred to a line through the contact points, while others think that the line passed through the centres of the crowns or across the middle of the buccal surfaces.

Williams (1917) described the anterior teeth as lying on the arc of a circle with its centre midway between the buccal grooves of the first molars. In an investigation based on the skulls of apes and humans, Hellman (1919) was unable to find any relation between the size of the teeth and the form of the dental arches and he rejected the theories of arch predetermination based on measurements of specific teeth. Hellman criticised Bonwill's equilateral triangle and concluded that the mathematical method of establishing dental arch form was unsatisfactory. This view was also taken by Stanton (1922) and Izard (1927) who found a variance of arch form, represented by an ellipse in 75%, a parabola in 20% and a 'U' or square shape in 5%.

Chuck (1934) suggested that the Bonwill–

ClearCorrect Exhibit 1002, Page 2248 of 3373

Hawley method should be used to construct symmetrical archwires which should then be altered to fit the patient.

McConnail and Scher (1949) suggested that the ideal curve would correspond to a catenary curve—that is one formed when a fine chain is suspended at both ends. Scott (1957) and Musich and Ackerman (1973) claimed that a catenary curve best represented a good average fit for arch forms and that any variation from this form was a consequence of alveolar-process growth beyond the normal range. Musich and Ackerman (1973) described a hanging chain catenometer which permitted estimation of the arch shape and length, the shape of the curve being related to the length of the chain and the vertical distance from the apex of the curve to the horizontal between the attachment points of the chain.

Wheeler (1950) maintained that biological forms could not be reproduced with exactitude and Sicher (1952) supported this view having found considerable variation in the shape of the dental arch, the upper arch being elliptical and the lower parabolic.

Baz (1958) determined normal arch size by a "geometric construction" based on measurements taken directly on the patient's face. This was a development of Hawley's method of arch predetermination.

Remsden (1964) studied various methods of predetermination by comparing them with arches of a sample of "normal" occlusions. He found inaccuracies in all methods but concluded that a parabola best represents the anterior curvature of the dental arch, although an arch that fitted a precise pattern was to be regarded as an exception rather than a rule.

Kato (1964) examined the relative positions of teeth and average arch form by establishing landmarks on the teeth on study models. The landmarks were projected onto a glass plane and plotted on a co-ordinate system. Kato examined upper and lower dental arches of both sexes and concluded that there was no great disparity between the arches. He also pointed out that description of arch shape is largely subjective and that the same arch may be classified differently by different workers.

More recent work has used computer analysis of occlusion and Lu (1964) claimed that the dental arch could be satisfactorily described by a polynomial equation of the 4th degree. Currier (1969) tried to evaluate the arch shape of satisfactory occlusions in a selected sample by comparing them with several geometric curves using mathematical analyses and electronic data processing equipment. He found that the buccal surfaces of the maxillary arch conform more closely to an ellipse than to a parabola but that neither ellipse nor parabola exhibited a significant fit to the lingual curves of the arches.

Sanin (1970) investigated the size and shape of ideal arches by measuring two-dimensional co-ordinates of the mesial and distal points of teeth on 160 sets of study models. He stated that the length and shape of the curve could be determined by mathematical functions such as exponential, logarithmic, elliptical, parabolic, hyperbolic or polynomial. Computer analysis of point co-ordinates obtained, showed that the fit of a curve through the points was best described through a mathematical function and that the 4th degree polynomial was among the easiest curves to fit while still adequately describing the dental arch, thus confirming the earlier views of Lu. Sanin also found that by using two easily obtained linear measurements in a simple formula, an estimate of arch length could be calculated that was close to the estimate obtained by fitting a 4th degree polynominal curve.

The regression equation derived was:—

$$\text{Arch length} = \text{Arch width} \times 0.504 - \text{arch length} \times 1.525 + 14.856 \text{ mms.}$$

where arch width was the distance between the buccal cusps of the first deciduous molars or premolars; arch length was the minimum distance from a point midway between the mesio-incisal angle of the central incisors and a line connecting the distal landmarks of the deciduous second molars or second premolars.

The standard error of the estimate was 1.532 mms.

ClearCorrect Exhibit 1002, Page 2249 of 3373

Brader (1972) stated that dental arch form represents an equilibrium between the forces of the tongue and the circumoral musculature, and thought that the geometry of the arch was best approximated by a closed curve with the curvilinear properties inherent in the trifocal ellipse (generated from 3 internal foci, and comprising a closed, compound elliptical curve) with the teeth occupying only a portion of the total curve at its constricted end. As the tissue forces in the resting state were considered to be the primary determinants of arch form morphology, the geometry of the curve was related to the resting forces of the tongue so that PR=C where P=pressure per unit area; R=radius of curvature at a point along the compound curve corresponding exactly with the pressure site and C is a constant, exhibiting a variation in magnitude between individuals and variation in the same individual at different physiological ages. The arch form becomes stabilized and dental equilibrium attained where C=T (the tension of the circumoral tissues). That is to say, there is an inverse relation between the magnitude of the pressure and the radius of curvature at each side.

Further work by Proffit (1978) has shown that this is not the case in all patients and that tongue morphology is important but that the pressure exerted on the dentition varies.

Trifocal elliptical arch forms are used in archwire fabrication (Brader, 1972; White, 1977) where the selection of the arch is based on the arch width at the buccolingual surfaces of the second premolars. Brader arch forms are adapted to the labial surfaces of the teeth and are of the same shape, differing only in premolar arch width. The maxillary arch selected is one size larger than the mandibular arch so that arch co-ordination is greatly simplified but often leads to a severe reduction in intercanine width (White, 1978).

A geometric approach to arch analysis is provided by the arcogramme technique (Herren et al., 1973). The arcogramme is an open polygon drawn, using a binocular microscope, to join landmarks of the mesial and distal aspects of the crowns of the teeth directly, on study models or on photographs. The real contact points are connected by straight lines to produce the open polygon. Herren and his colleagues believe that the production of a polygon by interpolation of small straight lines gives a better expression of arch shape as it follows the normal dental arch and determines the length and shape of the dental arch more accurately than does the ellipse.

Several authors have described the use of an X–Y digitizer and computer programme to analyse 1 : 1 photographs of study models (Pepe, 1975; Marcotte, 1976; Burstone, 1979). Pepe analysed a sample of only 7 models of normal occlusion by digitization of a full-size occlusal photograph to cartesian co-ordinates which were then compared with mathematically derived curves by computer. Of all the curve generating equations studied in this manner, the catenary was found to be the least descriptive of the arch forms. In more than 75% of the arches studied the catenary curve was found to be inferior even to the quadratic curve fit. However, the polynomial curve was still not a good fit and Pepe concluded that although this curve may be used to describe arch form it is not sufficiently accurate to use for archwire construction.

Computer derived arch forms, now in common use in practice, are produced from measurements of intermolar width, intercanine width and arch depth from the labial surface of the central incisor to the last standing molar. The computer is programmed with the cartesian X–Y co-ordinates necessary for a two-dimensional computer-derived formula. From clinical data, Schulof (1975) designed a biparameter catenary curve from the lower arch to estimate individual arch form, based on anterior tooth size, arch width at the molars, denture position and individual facial angle.

White (1978) attempted to analyse arch shape in 24 ideal occlusions in terms of the usual descriptions of arches—ellipse, parabola, trifocal ellipse and catenary. Overlays of arch shapes were constructed from tracings of the teeth and were then superimposed.

ClearCorrect Exhibit 1002, Page 2250 of 3373

Subjective assessment of the close fit was made. 8% of Bonwill–Hawley designs were found to be good and 52% poor while 12.5% of Brader arch forms and 27% of catenary curves were found to be good. The Rocky Mountain Data System arch forms showed none of poor fit, two of good fit and 95% moderately good, but analysis was only made of mandibular arches. Rocky Mountain have now altered the computer programme to recognise asymmetry and use different mathematical curves for each side, which may well be important because of the 48 arches tested by White only 6% were found to be symmetrical. White concludes, as have others, that no generalized universal arch form seems to be applicable to the individual and that algebraic and geometric formulae provide symmetry which does not account for individual variations.

Faber et al. (1978) pointed to the use of computerized cephalometric study model analysis, stating that predermination of arch form permits the teeth to be arranged along the curve, and arch length or available space to be calculated. The drawback of this type of simulation is that the mathematical curve shape fitted to X–Y co-ordinates is usually either parabolic or a trifocal ellipse and no major study has yet shown that ideal arch form actually approaches these mathematically derived curves.

Burstone (1979) described a procedure for case analysis by digitizing points on a 1 : 1 occlusal photograph of study models to give measurements and tooth position on a visual display unit. Ideal arch forms are then constructed by the computer, taking account of the orthodontist's instructions on incisor inclination, extractions etc., to give a parabolic curve which Burstone believes, by using enough control points in arch form, can be individualized for each patient. The computer stores midline position and calculates space inadequacy. Different visual displays are provided for differing treatment plans provided by the orthodontist and the computer co-ordinates upper and lower arches with a given overbite and overjet together with estimates of anchorage loss.

Discussion

The use of computers in diagnosis and clinical management has increased considerably in recent years and will doubtless continue to do so with the progressive reduction in the cost of computer equipment but a review of the literature illustrates many divergent views on arch shape and analysis.

Two opposing views have been stated on the development of dental arch and jaw shape; on one hand that the position is solely determined by the pressure of lips and tongue (Tomes, 1873) and on the other that arch form is determined prior to muscular development and is independent of functional activity of the oral musculature (Scott, 1967).

It is now generally believed, however, that occlusion and arch shape are determined by an interplay between genetic factors and many varied external environmental factors. Proffit (1978) and Moss (1980) thought that the primary factors involved in the determination of final tooth position are resting pressures of the lips, cheeks and tongue, and the force produced by metabolic activity within the periodontal membrane. These in turn are influenced by secondary factors such as postural position of the head, the jaw and the tongue, alterations in the eruptive mechanism and the morphology of the crowns of the teeth.

Clinicians should therefore be cautious when treating individuals to a mathematically derived ideal and when making archwires to specific "ideal" shapes since studies have not yet determined conclusively what that shape might be or, indeed, whether the very many varying soft tissue factors affecting tooth position are such that any specific arch form can be applied to the individual.

Address for correspondence

S. J. Rudge,
Orthodontic Department,
Chester Royal Infirmary,
St Martins Way,
Chester CH1 2AZ, England.

ClearCorrect Exhibit 1002, Page 2251 of 3373

References

Angle, E. H. (1907). Treatment of malocclusion of the teeth. 7th Edition. S. S. White & Co., Philadelphia.

Baz, D. (1958). Analysis of dental arch form *International Dental Journal*, 8: 291–294.

Black, G. V. (1894). *Descriptive anatomy of the human teeth.* 3rd Edition. Wilmington Dental Manufacturing Co., Philadelphia.

Bonwill, W. G. A. (1885). Geometrical and mechanical laws of articulation. *Transactions of the odontological society of Pennsylvania*: 119–133.

Brader, A. C. (1972). Dental arch form related to intraoral forces: PR=C. *American Journal of Orthodontics*, 61: 541–561.

Burstone, C. J. (1979). Uses of the computer in orthodontic practice. *Journal of Clinical Orthodontics*, 13: 442–453. 539–551.

Chuck, G. C. (1934). Ideal arch form. *Angle Orthodontist*, 4: 312–327.

Currier, J. H. (1969). Human dental arch form. *American Journal of Orthodontics*, 56: 164–179.

Faber, R. D., Burstone, C. J. and Solonche. D. J. (1978). Computerized interactive orthodontic treatment planning. *American Journal of Orthodontics*, 73: 36–46.

Hawley, C. A. (1905). Determination of the normal arch and its application to orthodontia. *Dental Cosmos*, 47: 541–552.

Hellman, M. (1919). Dimensions vs. form in teeth and their bearing on the morphology of the dental arch. International Journal of Orthodontia, 5: 615–651.

Herren, P., Schmoker, R. and Jordi, Th. (1973). Arch shape and space balance determined by the arcogramme technique *Transactions of the European Orthodontic Society*, 49: 61–73.

Izard, G. (1927). New method for the determination of the normal arch by the function of the face. *International Journal of Orthodontia*, 13: 582–595.

Kato, S., Kubota, K., Hashimoto, T., Wada, K., Araki, S. and Lee, S. F. (1964). Study on the positions of teeth and the average form of the dental arch. *Journal of the Nihon University School of Dentistry*, 6: 111–121.

Lu, K. H. (1964). Analysis of dental arch symmetry (Abst.). *Journal of Dental Research*, 43: 780.

Marcotte, M. R. (1976). The use of the occlusogram in planning orthodontic treatment. *American Journal of Orthodontics*-69: 655–667.

McConnail, M. A. and Scher, E. A. (1949). The ideal arch form of the human dental arcade with some prosthetic application. *Dental Record*, 69: 285–302.

Moss, J. P. (1980). The soft tissue environment of the teeth and jaws. An experimental and clinical study. *British Journal of Orthodontics*, 7: 127–137, 205–216.

Musich, D. R. and Ackerman, J. L. (1973). The catenometer, a reliable device for estimating dental arch perimeter. *American Journal of Orthodontics*, 63: 366–375.

Pepe, S. H. (1975). Polynomial and catenary curve fits to human dental arches. *Journal of Dental Research*, 54: 1124–1132.

Proffit, W. R. (1978). Equilibrium theory revisited. Factors influencing position of the teeth, *Angle Orthodontist*, 48: 175–186.

Remsden, W. H. (1964). Co-ordinated arches. An investigation into the form and interrelationship of orthodontic arch wires. Masters Thesis. Temple University School of Dentistry, June: 27–29.

Sanin, C., Savara, B. S., Thomas, D. R., Clarkson, Q. D. (1970). Arc length of the dental arch estimated by multiple regression. *Journal of Dental Research*, 49: 885.

Scott, J. H. (1967). *Dento-facial development and growth.* Pergamon Press: Oxford.

Scott, J. H. (1957). The shape of the dental arches. *Journal of Dental Research*, 36: 996–1003.

Shulof, R. (1975). Data-Bits, Rocky Mountain data systems. 3.

Sicher, H. (1952). *Oral anatomy.* 2nd Edition. C. V. Mosby Co.,

Stanton, F. L. (1922). Arch predetermination and a method of relating the predetermined arch to the malocclusion to show the minimum tooth movement. *International Journal Orthodontia*, 8: 757–778.

ClearCorrect Exhibit 1002, Page 2252 of 3373

Tomes, C. (1873). The bearing of the development of the jaws on irregularities. *Dental Cosmos*, 15: 292–296.

Wheeler, R. C. (1950). A textbook of dental anatomy and physiology, 2nd edition, W. B. Saunders Company, Philadelphia, 196–215, 352–406.

White, L. W. (1977). Accurate arch discrepancy measurements. *American Journal of Orthodontics*, 72: 303–308.

White, L. W. (1978). Individual ideal arches. *Journal of Clinical Orthodontics*, 12: 779–787.

Williams, P. N. (1917). Determining the shape of the normal arch. *Dental Cosmos*, 59: 695–708.

ClearCorrect Exhibit 1002, Page 2253 of 3373

Integrated information-processing system in clinical orthodontics: An approach with use of a computer network system

Mamoru Sakuda, DDS, DDSc, Kazuo Tanne, DDS, DDSc, Kenmi Yoshida, DDS, MS, DDSc, Hiroyuki Inoue, DDS, DDSc, Hiroaki Ohmae, DDS, DDSc, Masafumi Tsuchiya, DDS, DDSc, Satoshi Adachi, DDS, DDSc, Koichi Nakagawa, DDS, DDSc, and Yasuko Inoue, DDS, DDSc
Osaka, Japan

A computer network system has been developed in the Orthodontic Clinic, Osaka University Dental Hospital, to improve treatment efficiency and patient service. The system consists of a 32-bit host computer, its peripheral units, and personal computers connected to the host computer by data-transmission circuits, making up a local area network (LAN). It is possible in this system to integrate various types of data, such as the patient's basic information, treatment records, image data, and diagnostic analysis results to construct a relational database. It has been shown that the computer system developed in the orthodontic clinic has various clinical advantages. (AM J ORTHOD DENTOFAC ORTHOP 1992;101:210-20.)

In recent years, medical information-processing systems[1-4] have been developed in response to advances in computer technology. Applications of information-processing computers are found in patient administration, ordering systems, and integration of patient information, including treatment records and computer-aided diagnosis. However, it has been difficult to integrate all of these data in a computer network system.

In the Orthodontic Clinic of Osaka University Dental Hospital, an integrated computer network system has been designed and is available for clinical use. This system makes it possible to integrate treatment records and diagnostic materials, including x-ray films and color slides, and to reduce chairside time by retrieving images and analyzed data of models and lateral cephalograms at the chairside terminals.

The primary object of this article is to describe the system and to explain its technical features.

DESCRIPTION OF SYSTEM

System configuration

Fig. 1 shows a schematic representation of the system. The main part of the system consists of a 32-bit host computer (ACOS system 3300/model 6, 16 MB; NEC Corp., Tokyo, Japan), magnetic disk drives (3630 MB), an optical disk library (48 GB), magnetic tape drives, a line printer, a center console, and an engineering work station (EWS4800, 8 MB), as shown in Fig. 2, A. In the clinic and laboratories, 25 personal computers (PC-9801UX41, 640

ClearCorrect Exhibit 1002, Page 2254 of 3373

KB) are connected to the host computer by data-transmission circuits, making up the local area network (LAN) system. Fig. 2, B shows a terminal computer installed beside each dental chair.

The main features of the system[5] are summarized as follows:

1. Integration of patient information
2. Efficient administration of patients for making appointments and charging treatment fees
3. Electronic filing of various data, including treatment records
4. Image processing for color slides and various x-ray films
5. Analyses of models and lateral cephalograms for diagnostic purposes
6. Construction of a relational database, comprising character, code, image, and analytic numerical data, and the retrieval of information from the database

All programs for executing these tasks were originally developed, using COBOL/S for the host computer system and C-language for the terminal computer system. Each of the features of the system is explained below.

Integration of patient's basic information

These data include the Dental Hospital identification card number and the Orthodontic Clinic patient's serial number, name, sex, birth date, zip code, address, type of malocclusion, and orthodontist's name (Fig. 3, A). Most of the data are processed with a code system designed for efficient data input on the keyboard. Each patient data file is stored in a master file.

Patient information is retrieved by means of the patient's card number or name (Fig. 3, B).

Efficient administration of patients

Fig. 4, A shows a card reader and a CRT monitor. When a patient puts his or her identification card into the card reader, arrival of the patient is indicated on the CRT monitors in the clinic and the laboratories (Fig. 4, B and C). When a doctor assigns a patient to a vacant chair among 14 dental chairs in the clinic (Fig. 4, C, *4 and *5), all the patient data are transmitted from the host computer to the chairside terminal.

Electronic filing of treatment data

ClearCorrect Exhibit 1002, Page 2255 of 3373

Each electronic file includes treatment records, dental chart, medical and dental histories, growth curve of body height, image data (intraoral and facial photographs and various x-ray films), and diagnostic analyzed data of dental models and lateral cephalograms. These data are quickly reviewed on the CRT display of the chairside terminal (Fig. 5).

Analyses of dental models and lateral cephalograms

For diagnosis and treatment planning, analyses of dental models and lateral cephalograms are needed. Both analyses are available with use of the personal computers with peripheral devices in the laboratory (Fig. 6).

For data input of dental model analysis, digital calipers (Digimatic Calipers, Mitsutoyo Co., Tokyo, Japan) are used (Fig. 6). Model analysis is executed by measuring mesiodistal width of teeth and width of dental arches. A sum total of mesiodistal widths of unerupted lateral teeth from the canine to the second premolar can be predicted with multiple regression. Available arch lengths are entered into the computer on the keyboard. On the basis of the input data, arch length discrepancy and tooth size ratios (Bolton index) are calculated. Results are graphically displayed (Fig. 7). Further, some results of the model analyses are used for cephalometric analyses.

For data input and output of cephalometric analysis, a digitizer (Mediagraph), a printer, and a plotter (Miplot III, Graphtec, Tokyo, Japan) are connected to the personal computers in the laboratory (Fig. 6). Landmarks on the tracing of a lateral cephalogram are entered with a digitizer, and coordinates of these points are then processed to calculate measurements. In our department, an analysis technique[6] for lateral cephalograms was developed by modifying the Downs, Northwestern, and Wylie analyses. In addition, the Tweed,[7] Steiner,[8] and Ricketts[9] analyses are available in the system. Results are graphically displayed on the CRT display and the plotter (Fig. 8).

These results are used for aiding diagnosis and determining treatment plans.

Image data processing for x-ray films and color slides

Image data are stored with a charge-coupled (CCD) camera (Fotovix II, Tamuron, Saitama, Japan) and an image processor (VP-150) (Fig. 9). An image is taken by the CCD camera as analog data, which are converted to digital data by the VP-150. All the data processed are compressed to 1/6 to 1/4 times the original data by means of a data compression technique (Table I) and transmitted to the host computer. For the review of the image on the CRT display, digital data accumulated in the host computer are converted again to analog data. Image data in electronic files can be viewed on each terminal in the clinic and the laboratories (Fig. 10).

ClearCorrect Exhibit 1002, Page 2256 of 3373

Electronic filing of treatment records

After treatment on each day, treatment records are stored into the computer memory (Fig. 5, A). Most items for describing the treatment are coded. Thus data input may be done quickly and easily at each chairside terminal by means of cursor keys only.

Comments and illustrations about treatment may also be entered with a keyboard and a pen digitizer (Fig. 2, B).

Management for treatment fee charge and appointment

There are two types of cost system for orthodontic treatment in Japan. One is for cleft lip and palate patients, who are covered by public health insurance, and the other is the responsibility of the patient. For both systems, items needed for the charge are selected with the cursor keys.Fig. 11 shows a list of items for treatment fee. Input data for treatment fee are automatically transmitted to a computer in the cashier's office of the Dental Hospital.

For making an appointment, the patient's identification card number or orthodontic clinic's serial number is entered, and then the date and the time are chosen. This process is available at all the terminal computers in the clinic and the laboratories. Fig. 12 shows the scheduled table for a month and a week.

Construction of database and information retrieval

Various types of data are stored on magnetic and optical disks, constructing a relational database.

For management of the database, RIQS (Relational Information Query System) is used, and DS/TQF (Decision Support/Table Oriented Query Facility) is applied for information retrieval. In this system, the retrieval of information, or multiaspect searches, is available. Information retrieval is useful for orthodontists who have many patients in the clinic and are involved in research.

DISCUSSION

Computer science has advanced in both hardware and software. With technologic innovation, computers have been applied for information processing in medicine[1-4] and dentistry.[5,6,10,11] In the field of orthodontics, computers are employed mainly for various analytic and measuring systems to investigate craniofacial structure and function.[12-14] These applications are useful for clinical orthodontics. Nevertheless, computer applications for information processing in dentistry or orthodontics are relatively few.

ClearCorrect Exhibit 1002, Page 2257 of 3373

To develop an integrated computer system for clinical use, there have been several technical problems: (1) integration of various types of information, including treatment records, (2) image data processing,[15,16] (3) quick data transmission within a computer network, (4) development of an analytic method for diagnostic aid and (5) construction of a database[1] consisting of different types of information. These points are discussed in the following paragraphs.

The present system includes large amounts of patient information, most of which are entered into the computer daily to reduce chairside time. An efficient data input procedure is indispensable. In this system, most of the character data are converted to codes, so that an operator can select items with corresponding codes by using the cursor keys. This makes data input convenient.

Our coding system was designed for electronic data processing . In medicine, various code systems,[17-20] such as ICD (International Classification of Diseases), SND (Standard Nomenclature of Diagnosis), and ICPC (International Classification of Primary Care), have been developed and are available for worldwide computerization of various diseases and treatments. A standardization of nomenclature in dentistry is needed to develop universal information-processing and communication systems.

Recently, an image-processing system or PACS (Picture Archiving and Communication System)[15,16] has been designed in association with computerized radiography. Since images such as pictures and radiograms are categorized as analog data, a technique to convert data from analog to digital or vice versa is necessary. In the present system, an image processor was installed for this purpose and is capable of compressing data. Data-compressing techniques[15,16,21] are classified into two methods, reversible and irreversible compressions. These methods have both advantages and disadvantages, but an irreversible technique that allows a higher compression rate was employed to achieve a rapid transmission of image data from the host computer to the terminal computers.[16] With respect to the image produced by the irreversible compression technique, the CRT display was examined in comparison with the actual image. It was confirmed that an image compressed to 1/6 to 1/4 times the original data is clinically acceptable.

The present system deals with large amounts of data, including image data. Efficient search and display of these data are necessary to improve treatment efficiency. Currently, a data-transmission circuit of 4 Mb/second speed is used for the network, and retrieval of various clinical data is achieved within a reasonable time. An optical cable circuit will be installed to achieve more rapid data transmission in the future.

The computer network system provides various advantages in comparison with a stand-alone application. Data can be entered into the host computer from all the terminal

ClearCorrect Exhibit 1002, Page 2258 of 3373

computers and viewed on any CRT. Information for treatment fees is quickly sent to the computer of the cashier in the Dental Hospital office. Further, all the staff members and students in the orthodontic clinic can make and change patients' appointments not only in the clinic but also in the laboratories. This system also makes it possible to announce a patient's arrival on all the CRT displays in the laboratories. Patient service has been significantly improved by the computer network system.

Electronic filing of treatment records, modification, and deletion of accumulated data is a serious problem. It is also very important to protect a patient's privacy.[22,23] To eliminate these problems, a user's identification number with a secret password is defined in this system for each doctor in the clinic. When a doctor or an auxiliary who is not in charge enters his or her identification number to access a patient's records, the electronic files are not open to the doctor. New data input and correction of the most recent record are allowed only after the doctor's identification number has been checked. Treatment records before the most recent one can never be altered by any doctor.

For diagnosis and treatment planning, various analyses have been developed in clinical orthodontics. In particular, cephalometric analysis is an important tool to evaluate craniofacial structure. In this system, two types of cephalometric analysis were designed. A technique designed in our department compares patient data with longitudinal standard values for the Japanese population. The Tweed, Steiner, and Ricketts methods are used for determining a treatment plan for a patient. Both types of analysis are integrated into the system for aiding diagnosis and determining treatment plans.

It has been shown that the computer network system is very useful for the large orthodontic clinic, and it may also be applicable to smaller private offices. A personal computer-based network system simulating the present system is now being designed, so various advantages produced by the system will be available to the private orthodontic clinics. In daily work, each orthodontist deals with a large amount of information that is beyond his or her memory. An approach to accumulate and retrieve various patient data will be significant in terms of improving the quality of orthodontic treatment.

Mamoru Sakuda

 Professor and Chairman, Department of Orthodontics.

ClearCorrect Exhibit 1002, Page 2259 of 3373

Kazuo Tanne



References

1. Budd JR, Warwick WJ, Wielinski CC. A medical information relational database system (MIRDS). Comput Biomed Res 1988;21:419-33.

2. Drazen EL, Moore NL. Use of computerized information systems in U.S. health maintenance organizations and hospitals. Computer Programs Biomed 1986;22:105-10.

3. Gremy F. The future of information processing in medicine and public health. Computer Programs Biomed 1980;11:71-80.

4. Gremy F. Strategies for the use of computers in health care. Computer Programs Biomed 1988;27:95-100.

5. Tanne K, Kitai N, Yamagata Y, et al. Integrated orthodontic information system by computer network. Proceedings of the 8th Joint Conference on Medical Informatics, 1988:299-302.

6. Sakuda M, Yamagata Y, Tanne K, Yasuda Y, Yoshida K. Database management system for clinical orthodontics. J Jpn Orthod Soc 1985;44:537-48.

7. Tweed CH. Clinical orthodontics, Vol. 1 and 2. St. Louis: CV Mosby 1966.

8. Steiner CC. Cephalometrics for you and me. AM J ORTHOD 1953;39:729-55.

9. Ricketts RM, Bench RW, Hilgers JJ, Schulhof R. An overview of computerized cephalometrics. AM J ORTHOD 1972;61:1-28.

10. Finkelson MW, Johnson LA, Lilly GE. Interactive videodisc patient simulations of oral diseases. J Pub Health Dent 1988;52:217-20.

11. Hikage K. Integrated orthodontic management system for virtual three dimensional computer graphic simulation and optical video image database: supported system for diagnosis and treatment planning. J Jpn Orthod Soc 1987;46:248-69.

12. Currier JH. A computerized geometric analysis of human dental arch form. AM J ORTHOD 1969;56:164-79.

ClearCorrect Exhibit 1002, Page 2260 of 3373

13. Biggerstaff RH. Computerized diagnostic setups and simulations. Angle Orthod 1970;40:28-36.

14. Savara BS. The role of computers in dentofacial research and the development of diagnosis aids. AM J ORTHOD 1972;61:231-45.

15. Leavitt MB, Newell JB. An image filing system for the implementation of image processing algorithms in a research environment. Comput Biomed Res 1988;21:174-85.

16. Tanne K, Inoue H, Ohmae H, et al. An application of PACS to clinical orthodontics. Proceedings of the 20th Joint Conference on Imaging Technology 1989:327-330.

17. American Medical Association. Standard nomenclature of diseases and operations, 5th ed. New York: McGraw-Hill Book, 1961.

18. Cote AR. International classification for health and diseases: the expandable common concept. Med Inform 1983;8:5-16.

19. Satomura Y. Data standardization for medical records. Jpn J Med Inform 1985;5:4-13.

20. World Health Organization. International Classification of Diseases. 1975 Revision, 1977.

21. Rhodes ML, Quinn JF, Rosner B. Data compression techniques for CT image archiving. J Comput Assist Tomogr 1983;7:1124-6.

22. Nishi S. Privacy problems on the standardization of medical records. Jpn J Med Inform 1985;5:75-80.

23. Scholz RP. Letters to the editor. Computerized patient records: potential risk. AM J ORTHOD DENTOFAC ORTHOP 1989;95:42A-4A.

ClearCorrect Exhibit 1002, Page 2261 of 3373

TABLES

Table I

Table I. Data compression for image processing

Modality of image	*Data compression rate*	*Amount of digital data (KB)*	*Total dot number for CRT display*
Color slide	1/6-1/4	20-30	170 × 106
Cephalogram	1/6	200	400 × 400 (PA) 500 × 400 (Lat)
Hand wrist	1/6	200	300 × 300
Panorama	1/6	200	640 × 250
Occlusal	1/6	50	200 × 250
TMJ	1/6	200	640 × 250
Dental	1/6	25-30	170 × 106
Tracing	1/5-1/6	150	400 × 400

ClearCorrect Exhibit 1002, Page 2262 of 3373

FIGURES

Fig. 1

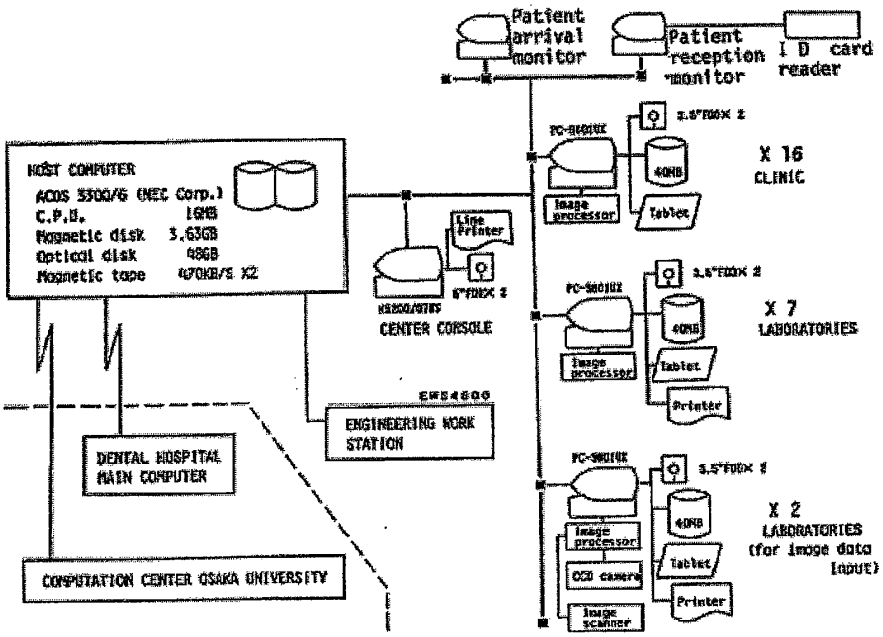


Fig. 1. Block diagram of the integrated computer network system.

ClearCorrect Exhibit 1002, Page 2263 of 3373

Fig. 2



Fig. 2. A, Host computer and its peripheral devices, *1,* host computer; *2,* magnetic disk drives; *3,* optical disk library; *4,* line printer; *5,* magnetic tape drives; *6,* center console; *7,* engineering work station. **B**, Personal computer in the clinic, *1,* CRT; *2,* keyboard; *3,* stylus pen digitizer (for free illustration); *4,* image processor; *5,* CPU; *6,* hard disk drive.

Fig. 3

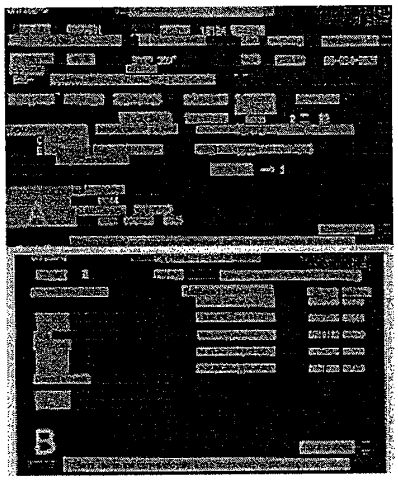


Fig. 3. A, Patient's basic information. **B,** Retrieval of a patient based on the card number or name.

ClearCorrect Exhibit 1002, Page 2264 of 3373

Fig. 4

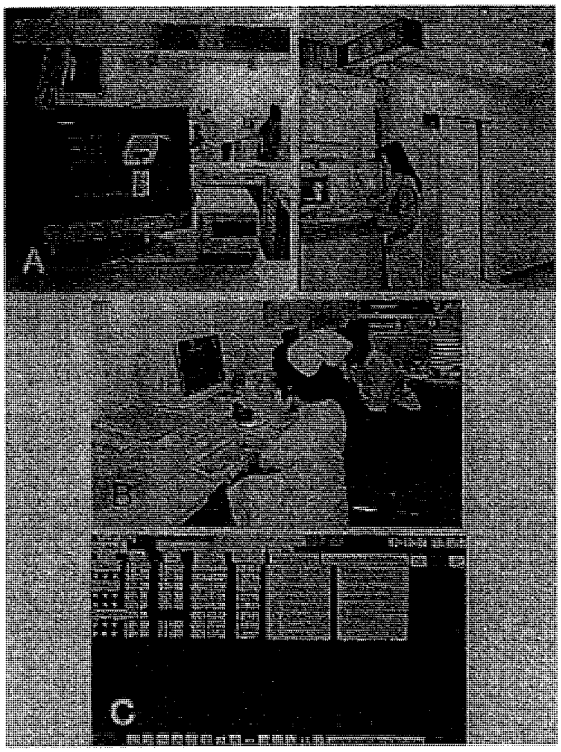


Fig. 4. A, Card reader at the reception center of the clinic; **B**, patient arrival monitor; **C**, patient arrival information, *1, classification of patient's visit; ••• indicates usual treatment with appointment; *2, arrival time; *3, appointment time; *4, approval of patient's arrival by doctor in charge; *5, dental chair number to be assigned.

ClearCorrect Exhibit 1002, Page 2265 of 3373

Fig. 5

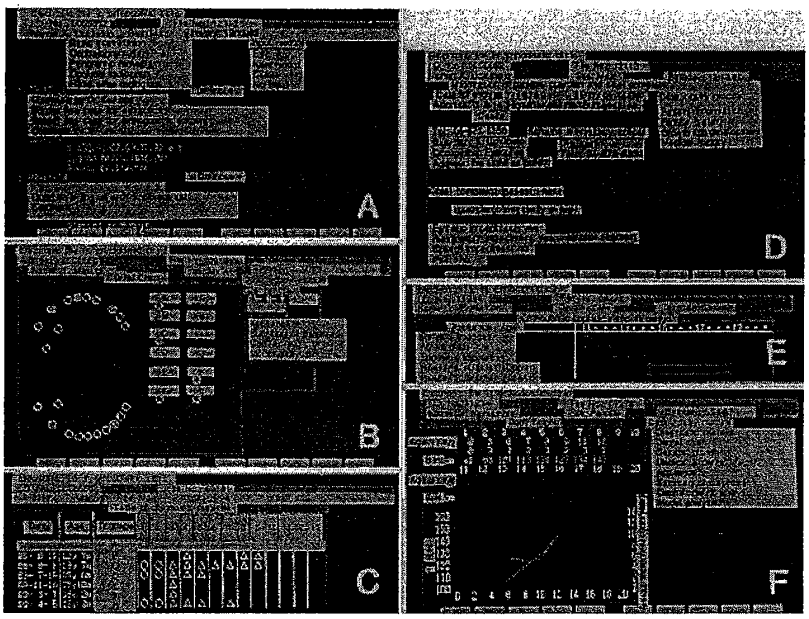


Fig. 5. Patient's electronic file shown on CRT display. Patient's name with Dental Hospital identification card number and orthodontic file number is shown at the top of each display. **A,** Treatment records. **B,** Dental chart, *A,* present tooth; *B,* congenitally missing tooth; *C,* impacted tooth; *D,* macrodontia; *E,* others; *F,* erupted tooth; *G,* other abnormal tooth; *H,* supernumerary tooth; *I,* microdontia; *J,* fusion tooth; *K,* extracted tooth; *L,* missing tooth. **C,** List of diagnostic materials obtained at various treatment stages (*A* through *G*), *1,* facial photograph; *2,* intraoral photograph; *3,* dental model; *4,* panoramic radiogram; *5,* lateral cephalogram at centric occlusion; *6,* lateral cephalogram at rest position; *7,* P-A cephalogram; *8,* occlusal radiogram; *9,* hand wrist radiogram; *10,* dental radiogram; *11,* TMJ radiogram (Schuller); *12,* TMJ radiogram (Grant-Lanting); *13,* functional examination. **D,** Family, medical and dental histories. **E,** List of orthodontic appliances used during treatment. **F,** Growth curve.

ClearCorrect Exhibit 1002, Page 2266 of 3373

Fig. 6

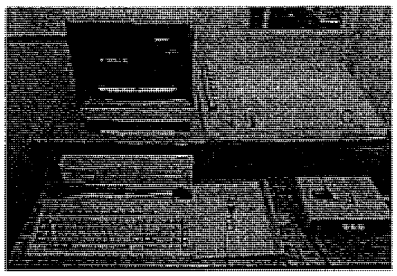


Fig. 6. Personal computer with peripheral devices for analyzing dental model and lateral cephalogram. *A,* Digital calipers; *B,* digitizer; *C,* plotter.

Fig. 7

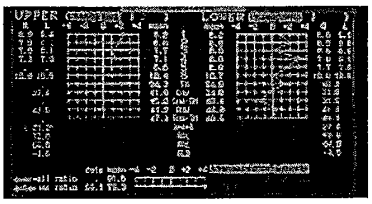


Fig. 7. Dental model analysis.

ClearCorrect Exhibit 1002, Page 2267 of 3373

Fig. 8a

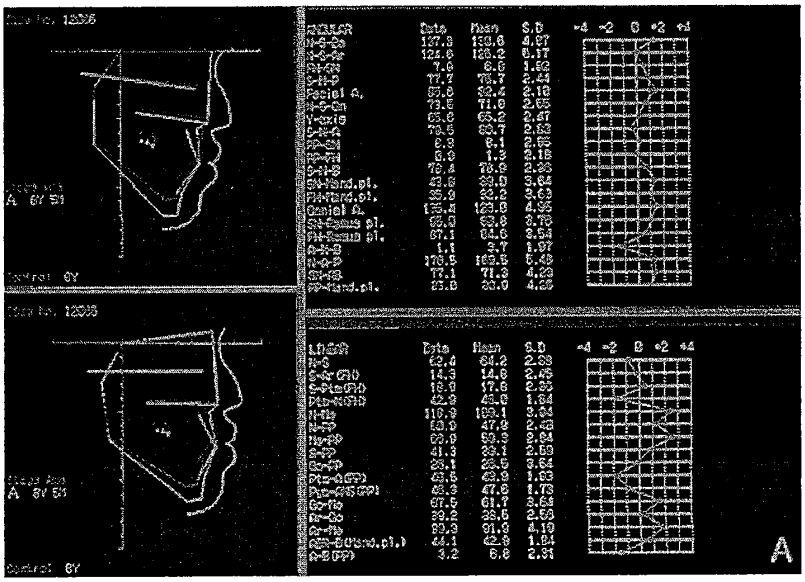


Fig. 8. Lateral cephalogram analyses. **A,** Analysis used in our department.

ClearCorrect Exhibit 1002, Page 2268 of 3373

Fig. 8b-d

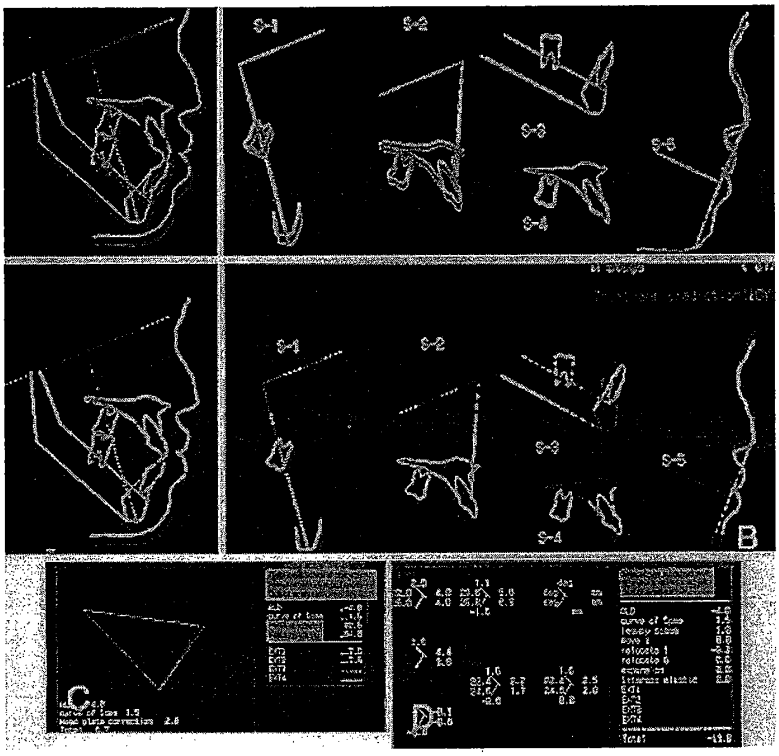


Fig. 8. (cont'd) **B,** Ricketts analysis. **C,** Tweed analysis. **D,** Steiner analysis.

ClearCorrect Exhibit 1002, Page 2269 of 3373

Fig. 9

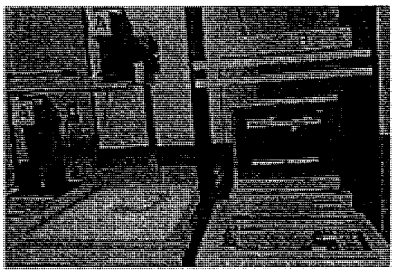


Fig. 9. *A,* CCD cameras (for slides and x-ray films), and *B,* image processor.

ClearCorrect Exhibit 1002, Page 2270 of 3373

Fig. 10a-d

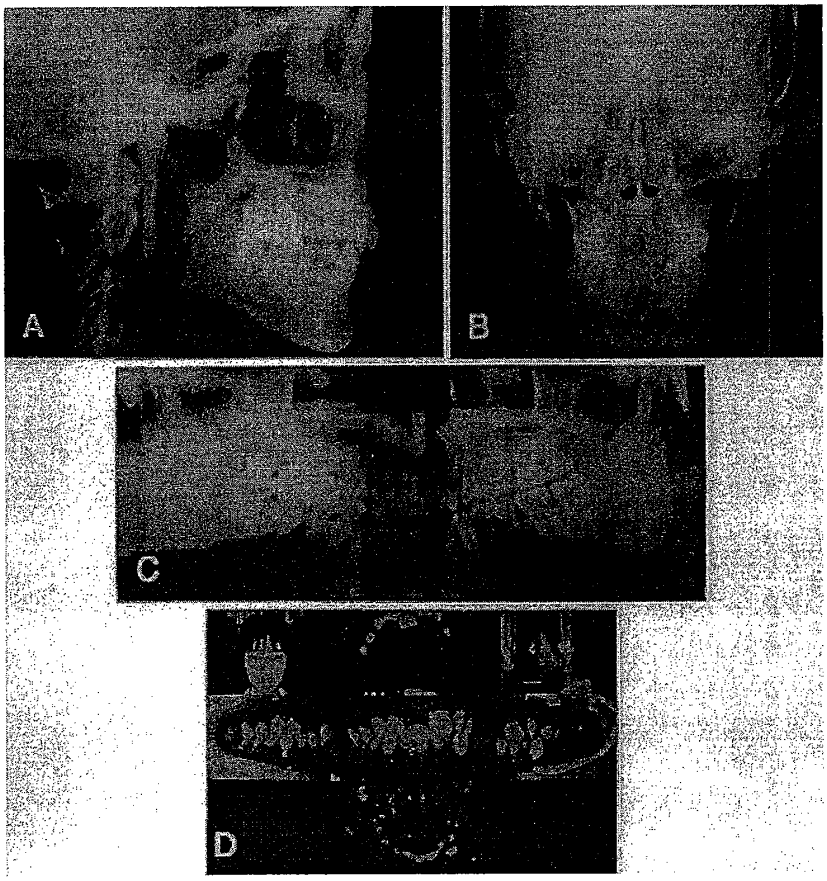


Fig. 10. Radiograms and color slides reviewed on the CRT display. **A**, Lateral cephalogram; **B**, P-A cephalogram; **C**, panoramic radiogram; **D**, facial and intraoral photographs taken at a stage.

ClearCorrect Exhibit 1002, Page 2271 of 3373

Fig. 10e

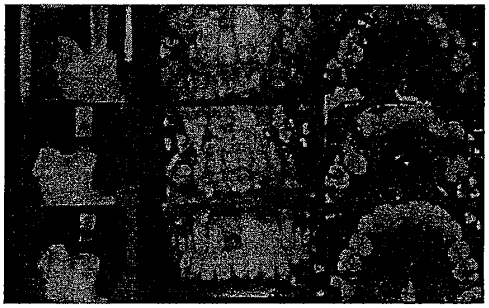


Fig. 10. (cont'd) **E,** facial and intraoral photographs taken at the three different stages during treatment.

Fig. 11

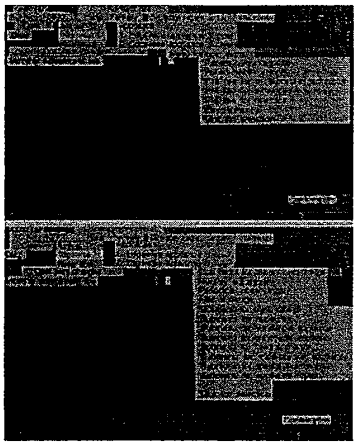


Fig. 11. Cost items for treatment fee. When one of main menus is selected *(upper),* its related cost items and submenus are shown for next selection *(lower).*

ClearCorrect Exhibit 1002, Page 2272 of 3373

Fig. 12

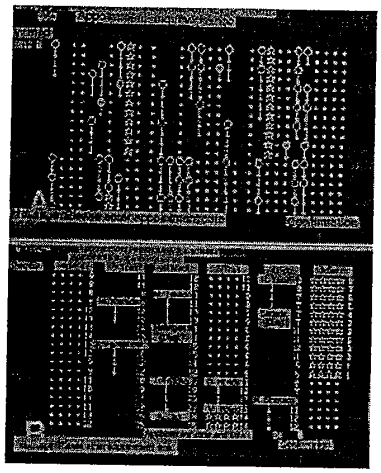


Fig. 12. Scheduled tables for a month (**A**) and a week (**B**); ••• and ✪ denote off day in the clinic.

ClearCorrect Exhibit 1002, Page 2273 of 3373

Three-Dimensional Computed Tomography in Maxillofacial Surgical Planning

Kurt P. Schellhas, MD; Mohammed El Deeb, DDS; Clyde H. Wilkes, MD, PhD; Richard K. Check, DDS; John W. Larsen, MD; Kenneth B. Heithoff, MD; Hollis M. Fritts, MD

• Fifty-four maxillofacial three-dimensional computed tomographic examinations were performed during a 12-month period for the purpose of surgical planning. Pathologic entities in the series included trauma, neoplasia, cleft palate, and other developmental anomalies. Computer-assisted mandibular disarticulation was performed routinely after each study to permit direct viewing of the mandible or maxilla in isolation. Three-dimensional computed tomography is a useful technique for maxillofacial surgical planning.

(*Arch Otolaryngol Head Neck Surg* 1988;114:438-442)

Three-dimensional computed tomography (CT) is a valuable technique for the planning of skeletal, plastic, and maxillofacial surgical procedures.[1-13] Anatomic measurements can be made from three-dimensional display images and manufactured life-sized models, and spatial relationships may be analyzed from desired perspectives.[7,8,10] Three-dimensional views provide key information to the radiologist and surgeon that may not be apparent on either conventional roentgenograms or axial CT images alone.

Accepted for publication Oct 31, 1987.

From the Center for Diagnostic Imaging, St Louis Park, Minn (Drs Schellhas, Heithoff, and Fritts); and the Department of Oral Surgery, University of Minnesota, School of Dentistry, Minneapolis (Dr El Deeb). Drs Wilkes, Check, and Larsen are in private practice in Minneapolis.

Read in part before the meeting of the American Cleft Palate Association, San Antonio, Tex, March 14, 1987.

Reprint requests to Center for Diagnostic Imaging, 5775 Wayzata Blvd, Suite 190, St Louis Park, MN 55416 (Dr Schellhas).

MATERIALS AND METHODS

Fifty-four maxillofacial three-dimensional CT studies (29 female and 25 male subjects, aged 6 to 59 years) were performed in 12 months on a spectrum of abnormalities, including the following: anomalous development (including clefts), 18 patients; trauma (mostly posttraumatic deformities), 12 patients; neoplasia, four patients; and infection/inflammation, four patients. Ten patients being evaluated for permanent dental implants were also studied. There were also six miscellaneous entities that were scanned. Computed tomographic examinations were performed on a fourth-generation CT scanner (GE 9800) using overlapping or consecutive (stacked) 1.5- and 3-mm-thick axial or coronal CT scans through the area of interest. Most patients with mandibular conditions were scanned in axial projection stopping at the inferior orbital rim, so as to exclude the eyes from direct radiation exposure. Patients were secured within the head holder with tape and sedated when necessary, to ensure a motion-free study.

Mandibular examinations were performed using overlapping 3-mm-thick axial images at 2-mm scan intervals. Consecutive (stacked) 1.5-mm-thickness scans were performed through the temporomandibular joints (TMJs). Cleft palates were scanned with either overlapping 3-mm-thickness scans or consecutive 1.5-mm-thick scans, depending on the size of the area of interest and patient limitations. Following each CT study, data were input to a three-dimensional processor (Dimensional Medicine Inc) for rendering of discrete voxel faces, later viewed in two dimensions on a specialized viewing apparatus (also Dimensional Medicine Inc). Two-dimensional roentgenographic images were routinely obtained in various projections and viewed by both radiologist and clinician.

Mandibular disarticulations were performed by three different specially trained radiologic technologists. Disarticulation required painstaking manual removal of specific anatomic areas from each two-dimensional axial image later processed into three-dimensional images.

RESULTS

Typical examination times ranged from ten minutes (for alveolar ridge examinations) to 30 minutes for a full mandible, including the TMJs. Twenty to 25 1.5-mm images were obtained for the alveolar ridge examinations, while up to 100 images were obtained for some of the full-face examinations.

ClearCorrect Exhibit 1002, Page 2274 of 3373

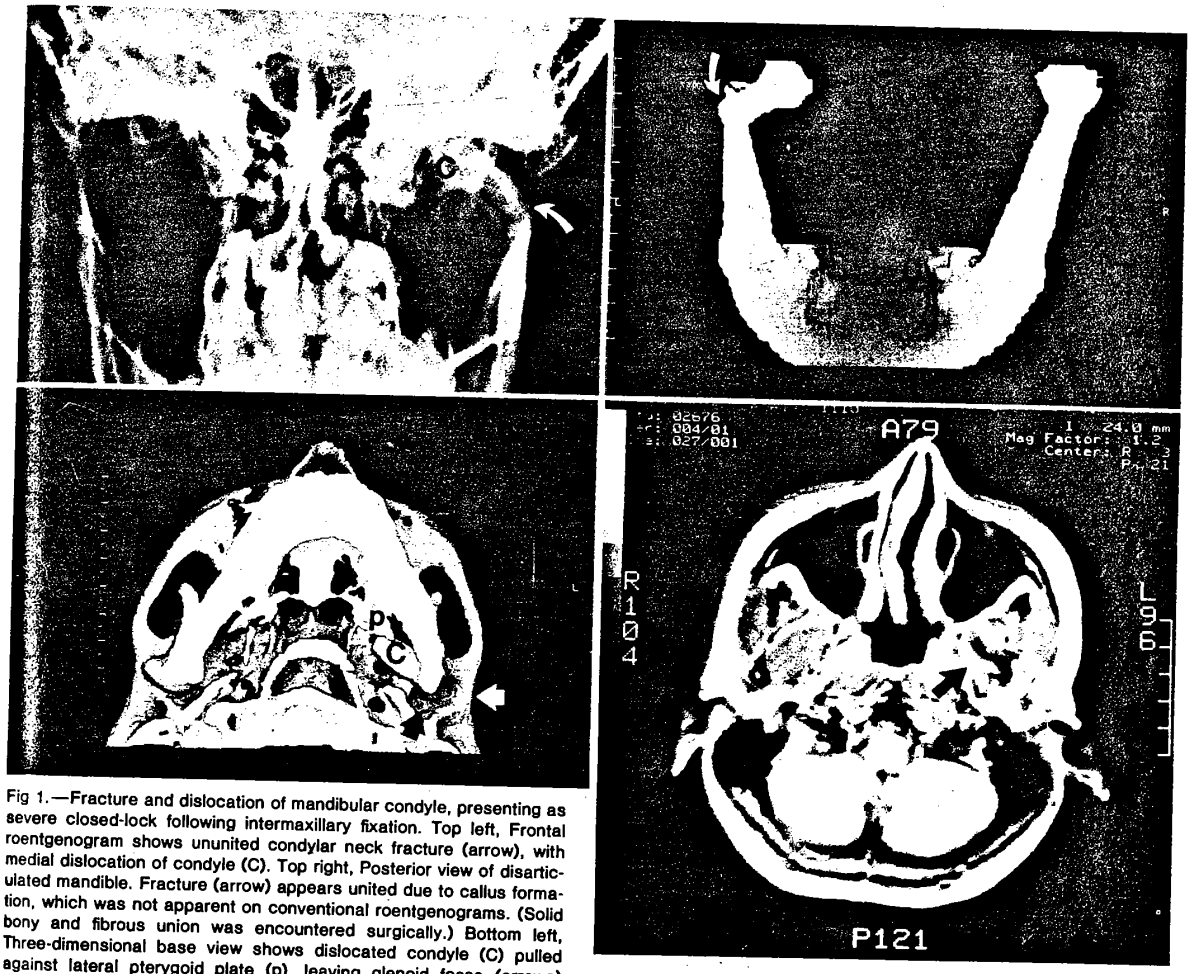


Fig 1.—Fracture and dislocation of mandibular condyle, presenting as severe closed-lock following intermaxillary fixation. Top left, Frontal roentgenogram shows ununited condylar neck fracture (arrow), with medial dislocation of condyle (C). Top right, Posterior view of disarticulated mandible. Fracture (arrow) appears united due to callus formation, which was not apparent on conventional roentgenograms. (Solid bony and fibrous union was encountered surgically.) Bottom left, Three-dimensional base view shows dislocated condyle (C) pulled against lateral pterygoid plate (p), leaving glenoid fossa (arrows) empty. Bottom right, Axial T_1-weighted (repetition time, 2000 ms; echo time, 20 ms) magnetic resonance image demonstrates normal signal within dislocated condyle (arrow), ruling out avascular necrosis.

COMMENT

Three-dimensional images are generated from data obtained during highly specialized CT examinations. Computed tomographic studies can be performed with any of the newer scanners, provided that certain scanning protocols are followed. It is vitally important to properly secure the patient within the head-holding device and use sedation if necessary to ensure lack of motion during examination. Employment of high-resolution thin-scan sections (1.5 to 3 mm) is equally important to ensure accuracy of the three-dimensional images. The high sensitivity of CT provides distinct advantages over conventional imaging techniques, particularly for detecting soft-tissue lesions and subtle calcifications, such as the early formation of callus (Fig 1). Three-dimensional images provide valuable information when planning major reconstructive procedures to correct traumatic or developmental defects (Figs 2 and 3).[7,13] Implanted surgical materials are particularly well detected with three-dimensional CT studies (Fig 4). Three-dimensional images are of particular value to the clinician, who may be uncomfortable analyzing multiple two-dimensional axial or coronal CT images. The ability to view an area of interest in three dimensions allows both clinician and radiologist to examine subtle points of anatomy in various perspectives and assess spatial relationships.

Computer-assisted disarticulation of key areas of interest has special application in mandibular and cleft palate surgery planning (Fig 5).[10] Mandibular disarticulation permits direct, multiplanar viewing of the

ClearCorrect Exhibit 1002, Page 2275 of 3373



Fig 2.—Severe posttraumatic facial deformity following self-inflicted gunshot wound. Large bony defect (arrows) accompanies soft-tissue injury.

mandible in isolation. Traumatic, developmental, inflammatory, and neoplastic mandibular lesions may be viewed and precisely assessed following disarticulation (Figs 1, 3, 6, and 7).[14,15] Life-sized visual images and models can be provided to permit precise measurement and the manufacture of anatomically correct prosthetic devices when needed. Cleft palates may be viewed directly after mandibular disarticulation and removal. Soft-tissue overlay techniques are continually improving and provide valuable information for soft-tissue reconstruction.

Recent advances in permanent dental implants have expanded the need and applications for three-dimensional imaging.[16] Life-sized images and manufactured models of the alveolar ridges may be provided with three-dimensional techniques, often eliminating the need for surgical procedures performed entirely for the purpose of obtaining intraoperative alveolar ridge impressions. In many circumstances, impressions can be taken from manufactured life-sized three-dimensional models of the alveolar ridges, thus permitting the assembly of anatomically correct permanent dental implants without requiring a diagnostic surgical procedure.

Overlapping 1.5-mm-thick images,

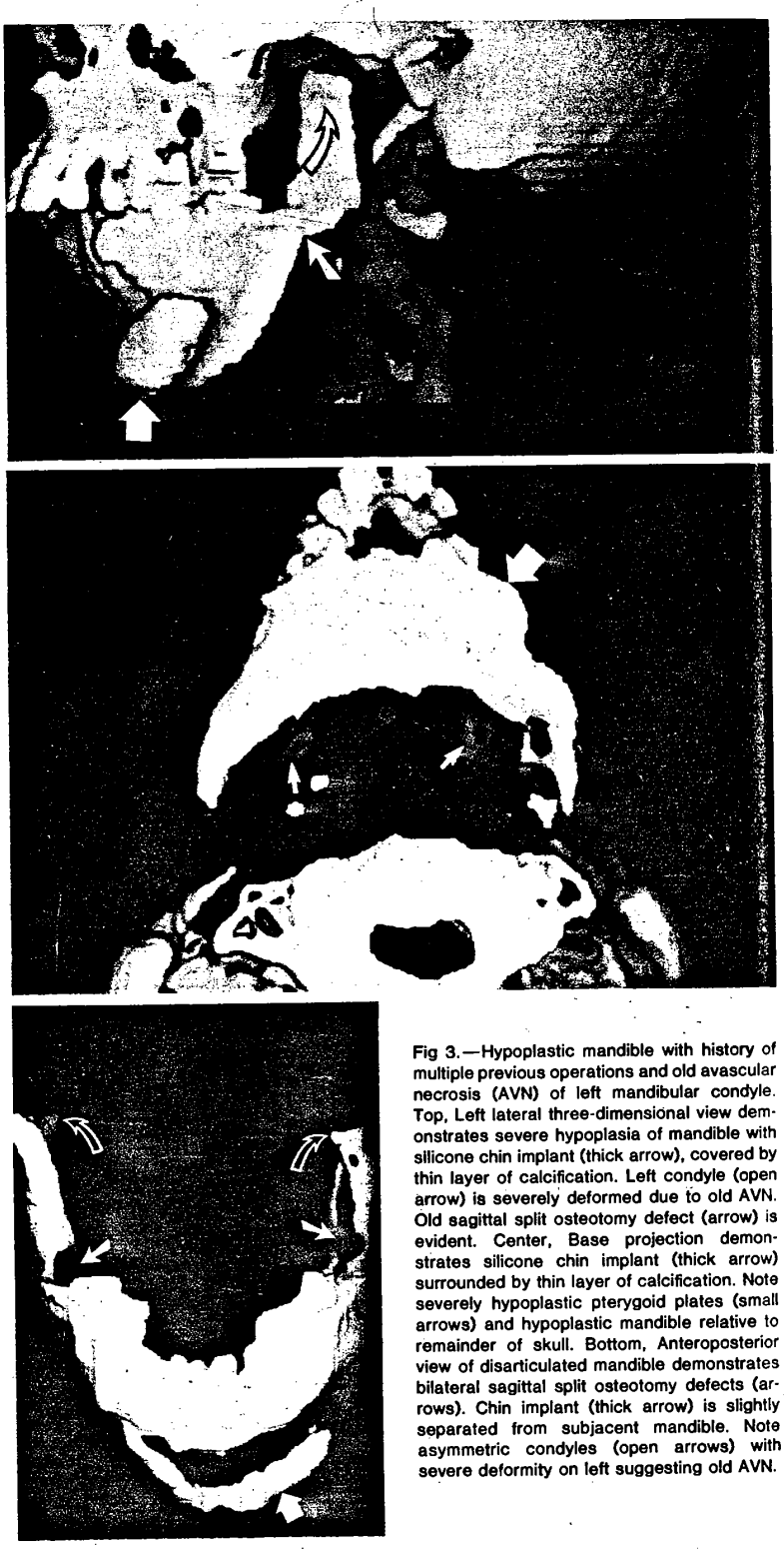


Fig 3.—Hypoplastic mandible with history of multiple previous operations and old avascular necrosis (AVN) of left mandibular condyle. Top, Left lateral three-dimensional view demonstrates severe hypoplasia of mandible with silicone chin implant (thick arrow), covered by thin layer of calcification. Left condyle (open arrow) is severely deformed due to old AVN. Old sagittal split osteotomy defect (arrow) is evident. Center, Base projection demonstrates silicone chin implant (thick arrow) surrounded by thin layer of calcification. Note severely hypoplastic pterygoid plates (small arrows) and hypoplastic mandible relative to remainder of skull. Bottom, Anteroposterior view of disarticulated mandible demonstrates bilateral sagittal split osteotomy defects (arrows). Chin implant (thick arrow) is slightly separated from subjacent mandible. Note asymmetric condyles (open arrows) with severe deformity on left suggesting old AVN.

ClearCorrect Exhibit 1002, Page 2276 of 3373



Fig 4.—Orbital encroachment by surgically implanted hydroxyapatite used for previous malar augmentation procedure. Frontal (left) and oblique (right) views demonstrate orbital encroachment due to surgically implanted hydroxyapatite (arrows).



Fig 5.—Facial cleft in 6-year-old boy. Frontal (left) and base (right) views of cleft following mandibular disarticulation and removal clearly demonstrate cleft (arrows in right).

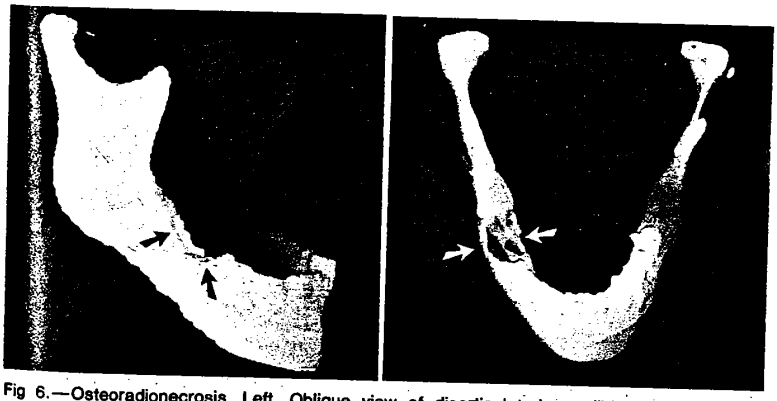


Fig 6.—Osteoradionecrosis. Left, Oblique view of disarticulated mandible shows irregular excavation (arrows) in alveolar ridge. Right, Irregular "dry socket" (arrows) is well seen from above.

scanned at 1-mm intervals, provide the highest two- and three-dimensional detail available. Such thin-section examinations must be limited, however, to small parts such as the TMJs or alveolar ridges, as it is simply not practical to scan larger areas in this fashion. Maximum tube heating occurs while performing the 1.5-mm-thick cuts, significantly prolonging examinations of this type. This precludes use of this technique in a full mandible examination. Gains in spatial resolution associated with the use of multiple 1.5-mm-thick cuts for large areas may be canceled by patient motion that commonly occurs

ClearCorrect Exhibit 1002, Page 2277 of 3373



Fig 7.—Ivory osteoma of mandible. Osteoma (arrows) is sharply defined and has broad base.

in examinations lasting over 30 minutes.[1] Each case must be assessed individually before deciding on scan axis, image thickness, and whether sedation will be required.

Some limitations to three-dimensional imaging exist. Volume averaging occurs in all CT studies and is directly proportional to scan thickness. This is of particular importance in three-dimensional studies, where volume-averaging errors can be compounded as the three-dimensional images are generated. The use of thin-section overlapping scans acts to minimize volume averaging on three-dimensional images (Fig 1).[4,13] It is common for closely approximated bony structures, such as degenerated TMJs, to appear fused with either two- or three-dimensional CT techniques due to partial volume averaging. Conventional roentgenograms and tomograms of the facial region are helpful for correlation with three-dimensional cases. Conventional roentgenographic techniques provide high spatial resolution of small parts that may be prone to three-dimensional volume-averaging artifact.

References

1. Vannier MW, Marsh JL, Warren JO: Three-dimensional CT reconstruction images for craniofacial surgical planning and evaluation. *Radiology* 1984;150:179-184.
2. Roberts D, Pettigrew J, Udupa J, et al: Three-dimensional imaging and display of the temporomandibular joint. *Oral Surg Oral Med Oral Pathol* 1984;58:461-474.
3. Roberts D, Pettigrew J, Ram C, et al: Radiographic techniques used to evaluate the temporomandibular joint: Computed tomography, three-dimensional imaging and nuclear magnetic resonance. *Anesth Prog* 1984;31:241-256.
4. Hemmy DC, Tessier PL: CT of dry skulls with craniofacial deformities: Accuracy of three-dimensional reconstruction. *Radiology* 1985; 157:113-116.
5. Vannier MW, Conroy GC, Marsh JL, et al: Three-dimensional cranial surface reconstruction using high-resolution computed tomography. *Am J Phys Anthropol* 1985;67:299-311.
6. Moaddab MB, Dumas AL, Chavoor AG, et al: Temporomandibular joint: Computed tomographic three-dimensional reconstruction. *Am J Orthod Dentofacial Orthop* 1985;88:342-352.
7. Jackson IT, Bite U: Three-dimensional computed tomographic scanning and major surgical reconstruction of the head and neck. *Mayo Clin Proc* 1986;61:546-555.
8. Cutting C, Bookstein FL, Grayson B, et al: Three-dimensional computer-assisted design of craniofacial surgical procedures: Optimization and interaction with cephalometric and CT-based models. *Plast Reconstr Surg* 1986;77:877-887.
9. Altman NR, Altman DH, Wolfe SA, et al: Three-dimensional CT reformation in children. *AJNR* 1986;146:1261-1267.
10. Hodgkinson PD, Rabey GP: Three-dimensional nasal morphology in adult bilateral cleft palate patients: A morphoanalytic study. *Br J Plast Surg* 1986;39:193-205.
11. Kursunogul S, Kaplan P, Resnick D, et al: Three-dimensional computed tomographic analysis of the normal temporomandibular joint. *J Oral Maxillofac Surg* 1986;44:257-259.
12. Dumas AL, Moaddab MB, Homayoun NH, et al: A three-dimensional developmental measurement of the temporomandibular joint. *J Craniomand Pract* 1986;4:22-35.
13. DeMarini DP, Steiner E, Poster RB, et al: Three-dimensional computed tomography in maxillofacial trauma. *Arch Otolaryngol Head Neck Surg* 1986;112:146-150.
14. Schellhas KP, Wilkes CH, Omlie MR, et al: Temporomandibular joint: MR imaging of internal derangements and postoperative changes. *AJNR* 1987;8:1093-1101. Also published in *AJR* 1988;150:381-389.
15. Schellhas KP, Wilkes CH, Omlie MR, et al: Temporomandibular joint imaging: Practical application of available technology. *Arch Otolaryngol Head Neck Surg* 1987;113:744-748.
16. Bellasamba RL, Brisante RF, Baumrind S: Three-dimensional radiographic study of the positional relationship of complete dentures: A pilot study. *J Prosthet Dent* 1986;55:625-628.

ClearCorrect Exhibit 1002, Page 2278 of 3373

CHAPTER 6

SCHROEDER et al., "Algorithms I," The Visualization Toolkit chapter 6-9.9 1996

Fundamental Algorithms

We have seen how to represent basic types of visualization data such as structured points and grids, unstructured grids, and polygonal data. This chapter explores methods to transform this data to and from these various representations, eventually generating graphics primitives that we can render. These methods are called *algorithms*, and are of special interest to those working in the field of visualization. Algorithms are the verbs that allow us to express our data in visual form. By combining these verbs appropriately, we can reduce complex data into simple, readily comprehensible sentences that are the power of data visualization.

6.1 Introduction

The algorithms that transform data are the heart of data visualization. To describe the various transformations available, we need to categorize algorithms according to the *structure* and *type* of transformation. By structure we mean the effects that transformation has on the topology and geometry of the dataset. By type we mean the type of dataset that the algorithm operates on.

Structural transformations can be classified in four ways, depending on how they affect the geometry, topology, and attributes of a dataset.

- *Geometric transformations* alter input geometry but do not change the topology of the dataset. For example, if we translate, rotate, and/or scale the

ClearCorrect Exhibit 1002, Page 2279 of 3373

points of a polygonal dataset, the topology does not change, but the point coordinates, and therefore the geometry, does.

- *Topological transformations* alter input topology but do not change geometry and attribute data. Converting a dataset type from polygonal data to unstructured grid data, or from structured points to unstructured grid, changes the topology but not the geometry. More often, however, the geometry changes whenever the topology does, so topological transformation is uncommon.
- *Attribute transformations* convert data attributes from one form to another, or create new attributes from the input data. The structure of the dataset remains unaffected. Computing vector magnitude or creating scalars based on elevation are data attribute transformations.
- *Combined transformations* change both dataset structure and attribute data. For example, computing contour lines or surfaces is a combined transformation.

We also may classify algorithms according to the type of data they operate on, or the type of data they generate. By type, we most often mean the type of attribute data, such as scalars or vectors. Typical categories include:

- *Scalar algorithms* operate on scalar data. For example, the generation of contour lines of temperature on a weather map.
- *Vector algorithms* operate on vector data. Showing oriented arrows of airflow (direction and magnitude) is an example of vector visualization.
- *Tensor algorithms* operate on tensor matrices. An example of a tensor algorithm is to show the components of stress or strain in a material using oriented icons.
- *Modelling algorithms* generate dataset topology or geometry, or surface normals or texture data. Modelling algorithms tend to be the catch-all category for many algorithms, since some do not fit neatly into any single category mentioned above. For example, generating glyphs oriented according to the vector direction and then scaled according to the scalar value, is a combined scalar/vector algorithm. For convenience we classify such an algorithm as a modelling algorithm, because it does not fit squarely into any other category.

Algorithms also can be classified according to the type of data they process. This is the most common scheme found in the visualization literature. However, this scheme is not without its problems. Often the categories overlap, resulting in confusion. For example, a category (not mentioned above) is *volume visualization*, which refers to the visualization of volume data (or in our terminology, structured points). This category was initially created to describe the visualization of scalar data arranged on a volume, but more recently, vector (and even tensor) data has been visualized on a volume. Hence, we have to qualify our

ClearCorrect Exhibit 1002, Page 2280 of 3373

techniques to *volume vector visualization*, or other potentially confusing combinations.

In the text that follows, we will use the attribute type classification scheme: scalar, vector, tensor, and modelling. In cases where the algorithms operate on a particular dataset type, we place them in the appropriate category according to our best judgment. Be forewarned, though, that alternative classification schemes do exist, and may be better suited to describing the true nature of the algorithm.

Generality Versus Efficiency

Most algorithms can be written specifically for a particular dataset type, or more generally, treating any dataset type. The advantage of a specific algorithm is that it is usually faster than a comparable general algorithm. (See "Other Data Abstractions" on page 130 where we discussed the trade-off between abstract and concrete forms.) An implementation of a specific algorithm also may be more memory efficient and its implementation may better reflect the relationship between the algorithm and the dataset type it operates on.

One example of this is contour surface creation. Algorithms for extracting contour surfaces were originally developed for volume data, mainly for medical applications. The regularity of volumes lends itself to efficient algorithms. However, the specialization of volume-based algorithms precludes their use for more general datasets such as structured or unstructured grids. Although the contour algorithms can be adapted to these other dataset types, they are less efficient than those for volume datasets.

Our presentation of algorithms favors the more general implementations. In some special cases we will describe performance improving techniques for particular dataset types. Refer to the bibliography at the end of each chapter for detailed descriptions of specialized algorithms.

6.2 Scalar Algorithms

Scalars are single data values associated with each point and/or cell of a dataset. (Recall that in the *Visualization Toolkit* we associate data with points.) Because scalar data is commonly found in real-world applications, and because scalar data is so easy to work with, there are many different algorithms to visualize it.

Color Mapping

Color mapping is a common scalar visualization technique that maps scalar data to colors, and displays the colors on the computer system. The scalar mapping is implemented by indexing into a *color lookup table*. Scalar values serve as indices into the lookup table.

The mapping proceeds as follows. The lookup table holds an array of colors (e.g., red, green, blue components or other comparable representations). Associ-

ClearCorrect Exhibit 1002, Page 2281 of 3373

$$s_i < \min, i = 0$$

$$s_i > \max, i = n - 1$$

$$i = n\left(\frac{s_i - \min}{\max - \min}\right)$$

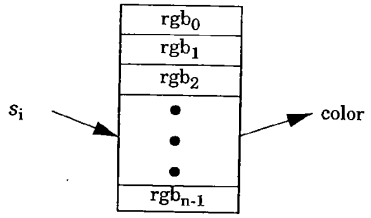


Figure 6–1 Mapping scalars to colors via a lookup table.

ated with the table is a minimum and maximum *scalar range (min, max)* into which the scalar values are mapped. Scalar values greater than the maximum range are clamped to the maximum color, scalar values less than the minimum range are clamped to the minimum color value. Then, for each scalar value s_i, the index i into the color table with n entries (and 0-offset) is given by Figure 6–1.

A more general form of the lookup table is called a *transfer function*. A transfer function is any expression that maps scalar value into a color specification. For example, Figure 6–2 maps scalar values into separate intensity values for the red, green, and blue color components. We can also use transfer functions to map scalar data into other information such as local transparency. (Transfer functions are discussed in more detail in "Transparency and Alpha Values" on page 212 and "Volume Rendering" on page 216.) A lookup table is a discrete sampling of a transfer function. We can create a lookup table from any transfer function by sampling the transfer function at a set of discrete points.

Color mapping is a one-dimensional visualization technique. It maps one piece of information (i.e., a scalar value) into a color specification. However, the display of color information is not limited to one-dimensional displays. Often we

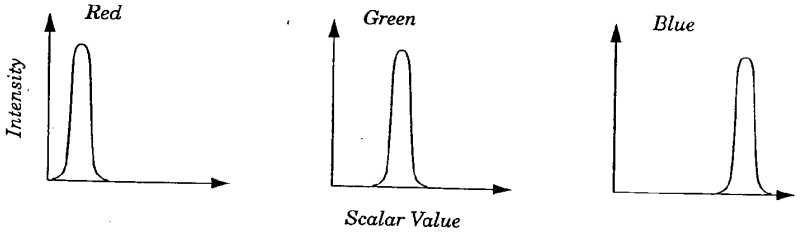
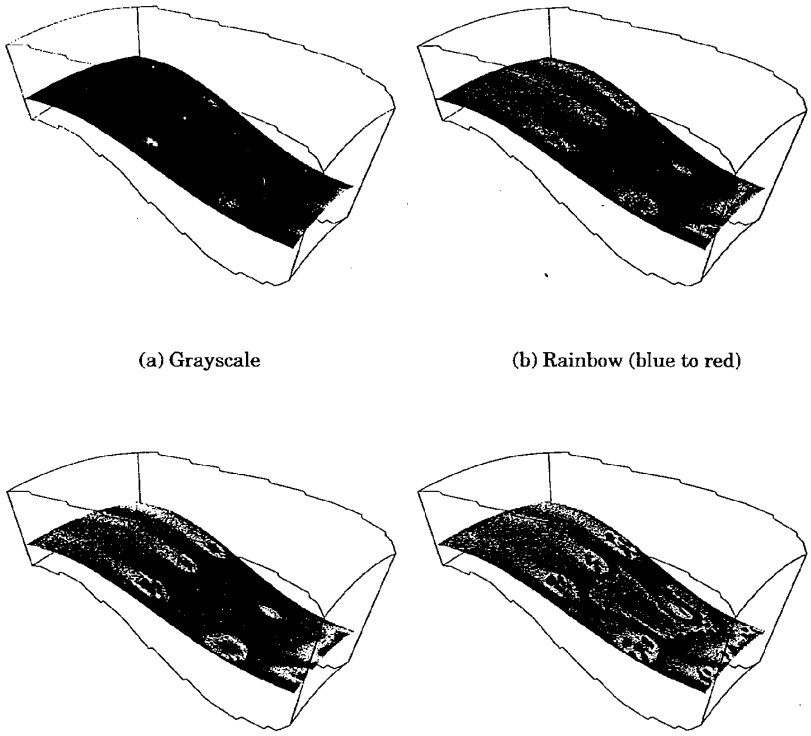


Figure 6–2 Transfer function for color components red, green, and blue as a function of scalar value.

ClearCorrect Exhibit 1002, Page 2282 of 3373



(a) Grayscale (b) Rainbow (blue to red)

(c) Rainbow (red to blue) (d) Large contrast

Figure 6–3 Flow density colored with different lookup tables: (a) Grayscale, (b) Rainbow (blue to red), (c) Rainbow (red to blue), (d) Large contrast (`rainbow.tcl`).

use color information mapped onto 1D, 2D, or 3D objects. This is a simple way to increase the information content of our visualizations.

The key to color mapping for scalar visualization is to choose the lookup table entries carefully. Figure **6–3** shows four different lookup tables used to visualize gas density as fluid flows through a combustion chamber. The first lookup table is grayscale. Grayscale tables often provide better structural detail to the eye. The other three images in Figure **6–3** use different color lookup

ClearCorrect Exhibit 1002, Page 2283 of 3373

tables. The second uses rainbow hues from blue to red. The third uses rainbow hues arranged from red to blue. The last table uses a table designed to enhance contrast. Careful use of colors can often enhance important features of a dataset. However, any type of lookup table can exaggerate unimportant details or create visual artifacts because of unforeseen interactions between data, color choice, and human physiology.

Designing lookup tables is as much art as it is science. From a practical point of view, tables should accentuate important features, while minimizing less important or extraneous details. It is also desirable to use palettes that inherently contain scaling information. For example, a color rainbow scale from blue to red is often used to represent temperature scale, since many people associate "blue" with cold temperatures, and "red" with hot temperatures. However, even this scale is problematic: a physicist would say that blue is hotter than red, since hotter objects emit more blue light (i.e., shorter wavelength) than red. Also, there is no need to limit ourselves to "linear" lookup tables. Even though the mapping of scalars into colors has been presented as a linear operation (Figure **6–1**), the table itself need not be linear. That is, tables can be designed to enhance small variations in scalar value using logarithmic or other schemes.

There is another element to visualization that is the artistic, or aesthetic, quality. Good visualizations represent a balance between effective communication of information and aesthetically pleasing presentation. While it is true in this day of mass media that information is often sacrificed for the sake of image, improving the comfort level and engaging the human observer more deeply in the presentation of data improves the effectiveness of communication.

Contouring

A natural extension to color mapping is *contouring*. When we see a surface colored with data values, the eye often separates similarly colored areas into distinct regions. When we contour data, we are effectively constructing the boundary between these regions. These boundaries correspond to contour lines (2D) or surfaces (3D) of constant scalar value.

Examples of 2D contour displays include weather maps annotated with lines of constant temperature (isotherms), or topological maps drawn with lines of constant elevation. Three-dimensional contours are called *isosurfaces*, and can be approximated by many polygonal primitives. Examples of isosurfaces include constant medical image intensity corresponding to body tissues such as skin, bone, or other organs. Other abstract isosurfaces such as surfaces of constant pressure or temperature in fluid flow also may be created.

Consider the 2D structured grid shown in Figure **6–4**. Scalar values are shown next to the points that define the grid. Contouring always begins by selecting a scalar value, or contour value, that corresponds to the contour lines or surfaces generated. To generate the contours, some form of interpolation must be used. This is because we have scalar values at a finite set of points in the dataset, and our contour value may lie between the point values. Since the most common interpolation technique is linear, we generate points on the contour sur-

ClearCorrect Exhibit 1002, Page 2284 of 3373

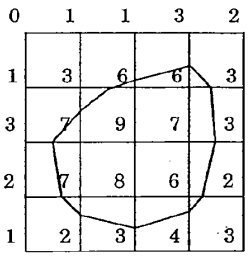


Figure 6–4 Contouring a 2D structured grid with contour line value = 5.

face by linear interpolation along the edges. If an edge has scalar values 10 and 0 at its two end points, and if we are trying to generate a contour line of value 5, then edge interpolation computes that the contour passes through the midpoint of the edge.

Once the points on cell edges are generated, we can connect these points into contours using a few different approaches. One approach detects an edge intersection (i.e., the contour passes through an edge) and then "tracks" this contour as it moves across cell boundaries. We know that if a contour edge enters a cell, it must exit a cell as well. The contour is tracked until it closes back on itself, or exits a dataset boundary. If it is known that only a single contour exists, then the process stops. Otherwise, every edge in the dataset must be checked to see whether other contour lines exist.

Another approach uses a divide and conquer technique, treating cells independently. This is the *marching squares* algorithm in 2D, and *marching cubes* [Lorensen87] in 3D. The basic assumption of these techniques is that a contour can only pass through a cell in a finite number of ways. A case table is constructed that enumerates all possible topological *states* of a cell, given combinations of scalar values at the cell points. The number of topological states depends on the number of cell vertices, and the number of inside / outside relationships a vertex can have with respect to the contour value. A vertex is considered inside a contour if its scalar value is larger than the scalar value of the contour line. Vertices with scalar values less than the contour value are said to be outside the contour. For example, if a cell has four vertices and each vertex can be either inside or outside the contour, there are $2^4 = 16$ possible ways that the contour passes through the cell. In the case table we are not interested in where the contour passes through the cell (e.g., geometric intersection), just how it passes through the cell (i.e., topology of the contour in the cell).

Figure 6–5 shows the sixteen combinations for a square cell. An index into the case table can be computed by encoding the state of each vertex as a binary digit. For 2D data represented on a rectangular grid, we can represent the 16 cases with 4 bit index. Once the proper case is selected, the location of the contour line / cell edge intersection can be calculated using interpolation. The algo-

ClearCorrect Exhibit 1002, Page 2285 of 3373

rithm processes a cell and then moves, or *marches to* the next cell. After all cells are visited, the contour will be completed. In summary, the marching algorithms proceed as follows:

1. Select a cell.
2. Calculate the inside / outside state of each vertex of the cell.
3. Create an index by storing the binary state of each vertex in a separate bit.
4. Use the index to look up the topological state of the cell in a case table.
5. Calculate the contour location (via interpolation) for each edge in the case table.

This procedure will construct independent geometric primitives in each cell. At the cell boundaries duplicate vertices and edges may be created. These duplicates can be eliminated by using a special coincident point-merging operation. Note that interpolation along each edge should be done in the same direction. If not, numerical round-off will likely cause points to be generated that are not precisely coincident, and will not merge properly.

There are advantages and disadvantages to both the edge-tracking and marching cubes approaches. The marching squares algorithm is easy to implement. This is particularly important when we extend the technique into three dimensions, where isosurface tracking becomes much more difficult. On the other hand, the algorithm creates disconnected line segments and points, and the required merging operation requires extra computation resources. The tracking algorithm can be implemented to generate a single polyline per contour line, avoiding the need to merge coincident points.

As mentioned previously, the 3D analogy of marching squares is marching cubes. Here, there are 256 different combinations of scalar value, given that there are eight points in a cubical cell (i.e., 2^8 combinations). Figure 6–6 shows these combinations reduced to 15 cases by using arguments of symmetry. We use combinations of rotation and mirroring to produce topologically equivalent cases.

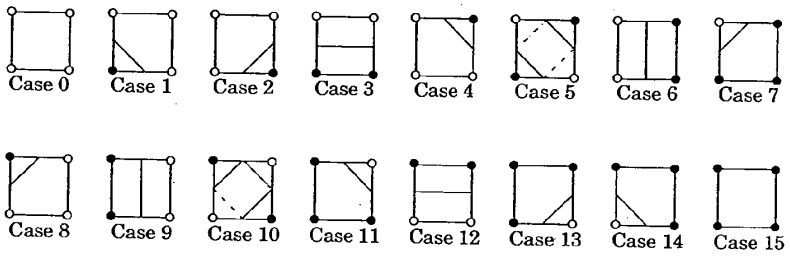


Figure 6–5 Sixteen different marching squares cases. Dark vertices indicate scalar value is above contour value. Cases 5 and 10 are ambiguous.

ClearCorrect Exhibit 1002, Page 2286 of 3373

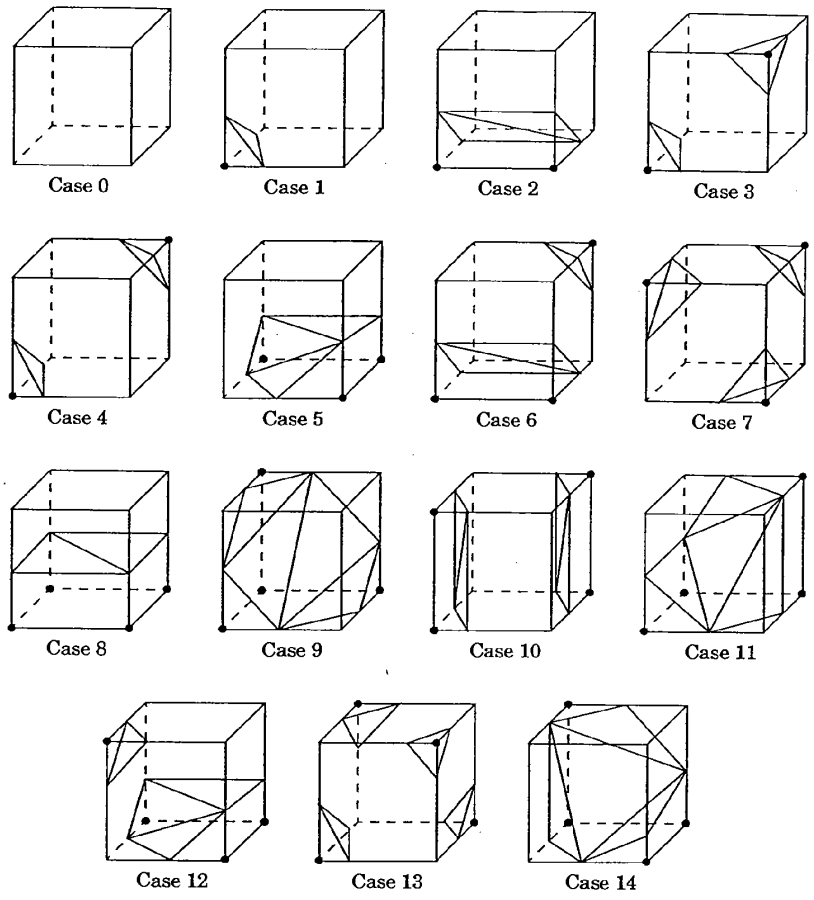


Figure 6–6 Marching cubes cases for 3D isosurface generation. The 256 possible cases have been reduced to 15 cases using symmetry. Dark vertices are greater than the selected isosurface value.

An important issue is *contouring ambiguity*. Careful observation of marching squares cases numbered 5 and 10 and marching cubes cases numbered 3, 6, 7, 10, 12, and 13 show that there are configurations where a cell can be contoured in more than one way. (This ambiguity also exists when using an edge tracking approach to contouring.) Contouring ambiguity arises on a 2D square or

ClearCorrect Exhibit 1002, Page 2287 of 3373

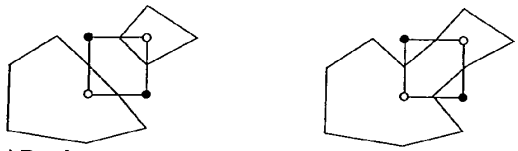


Figure 6–7 Choosing a particular contour case will break (a) or join (b) the current contour. Case shown is marching squares case 10.

the face of a 3D cube when adjacent edge points are in different states, but diagonal vertices are in the same state.

In two dimensions, contour ambiguity is simple to treat: for each ambiguous case we implement one of the two possible cases. The choice for a particular case is independent of all other choices. Depending on the choice, the contour may either extend or break the current contour as illustrated in Figure **6–7**. Either choice is acceptable since the resulting contour lines will be continuous and closed (or will end at the dataset boundary).

In three dimensions the problem is more complex. We cannot simply choose an ambiguous case independent of all other ambiguous cases. For example Figure **6–8** shows what happens if we carelessly implement two cases independent of one another. In this figure we have used the usual case 3 but replaced case 6 with its *complementary* case. Complementary cases are formed by exchanging the "dark" vertices with "light" vertices. (This is equivalent to swapping vertex scalar value from above the isosurface value to below the isosurface value, and vice versa.) The result of pairing these two cases is that a hole is left in the isosurface.

Several different approaches have been taken to remedy this problem. One approach tessellates the cubes with tetrahedron, and uses a *marching tetrahedra* technique. This works because the marching tetrahedra exhibit no ambiguous cases. Unfortunately, the marching tetrahedra algorithm generates isosurfaces consisting of more triangles, and the tessellation of a cube with tetrahedra requires making a choice regarding the orientation of the tetrahedra. This choice may result in artificial "bumps" in the isosurface because of interpolation along the face diagonals as shown in Figure **6–9**. Another approach evaluates the asymptotic behavior of the surface, and then chooses the cases to either join or break the contour. Nielson and Hamann [Nielson91] have developed a technique based on this approach they call the *asymptotic decider*. It is based on an analysis of the variation of the scalar variable across an ambiguous face. The analysis determines how the edges of isosurface polygons should be connected.

A simple and effective solution extends the original 15 marching cubes cases by adding additional complementary cases. These cases are designed to be compatible with neighboring cases and prevent the creation of holes in the isosurface. There are six complementary cases required, corresponding to the

ClearCorrect Exhibit 1002, Page 2288 of 3373

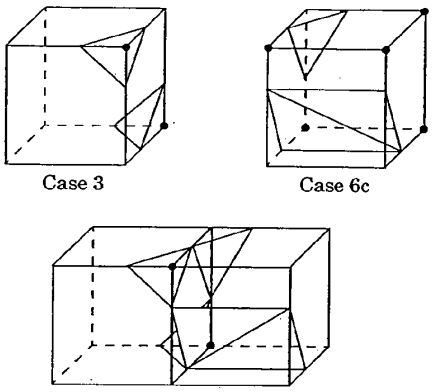


Figure 6–8 Arbitrarily choosing marching cubes cases leads to holes in the isosurface.

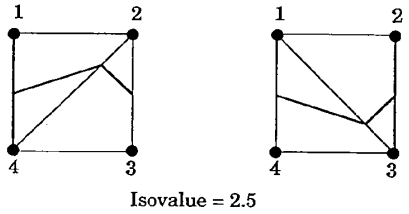


Figure 6–9 Using marching triangles or marching tetrahedra to resolve ambiguous cases on rectangular lattice (only face of cube is shown). Choice of diagonal orientation may result in "bumps" in contour surface. In 2D, diagonal orientation can be chosen arbitrarily, but in 3D diagonal is constrained by neighbor.

marching cubes cases 3, 6, 7, 10, 12, and 13. The complementary marching cubes cases are shown in Figure **6–10**.

We can extend the general approach of marching squares and marching cubes to other topological types. In **vtk** we use marching lines, triangles, and tetrahedra to contour cells of these types (or composite cells that are composed of these types). In addition, although we speak of regular types such as squares and cubes, marching cubes can be applied to any cell type topologically equivalent to a cube (e.g., hexahedron or noncubical voxel).

Figure **6–11** shows four applications of contouring. In Figure **6–11**(a) we see 2D contour lines of CT density value corresponding to different tissue types. These lines were generated using marching squares. Figure **6–11**(b) through

ClearCorrect Exhibit 1002, Page 2289 of 3373

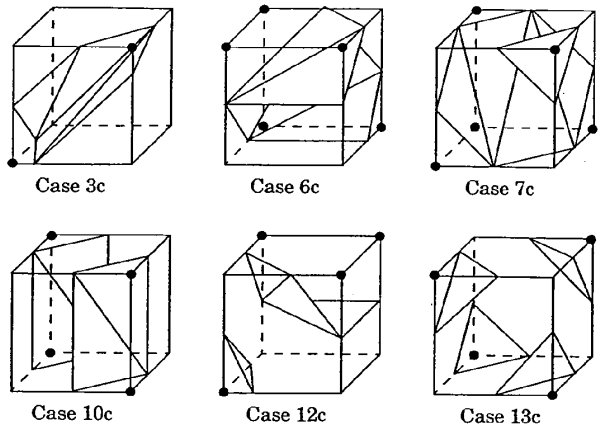


Figure 6–10 Marching cubes complementary cases.

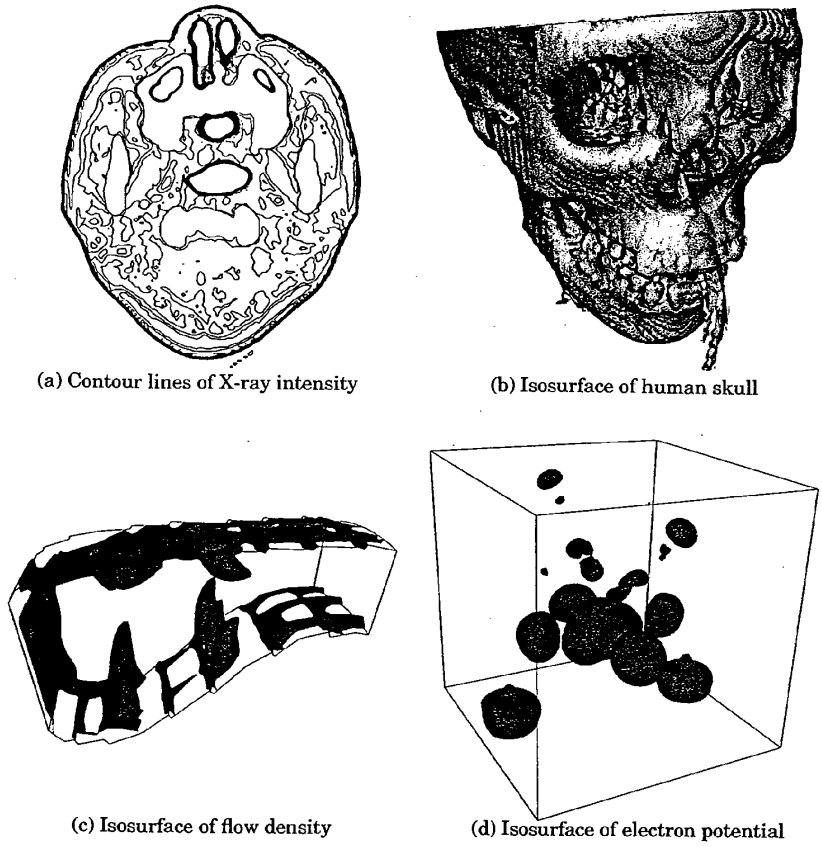
Figure **6–11**(d) are isosurfaces created by marching cubes. Figure **6–11**(b) is a surface of constant image intensity from a computed tomography (CT) X-ray imaging system. (Figure **6–11**(a) is a 2D subset of this data.) The intensity level corresponds to human bone. Figure **6–11**(c) is an isosurface of constant flow density. Figure **6–11**(d) is an isosurface of electron potential of an iron protein molecule. The image shown in Figure **6–11**(b) is immediately recognizable because of our familiarity with human anatomy. However, for those practitioners in the fields of computational fluid dynamics and molecular biology, Figure **6–11**(c) and Figure **6–11**(d) are equally familiar. As these examples show, methods for contouring are powerful yet general techniques for visualizing data from a variety of fields.

Scalar Generation

The two visualization techniques presented thus far, color mapping and contouring, are simple, effective methods to display scalar information. It is natural to turn to these techniques first when visualizing data. However, often our data is not in a form convenient to these techniques. The data may not be single-valued (i.e., a scalar), or it may be a mathematical or other complex relationship. That is part of the fun and creative challenge of visualization: We must tap our creative resources to convert data into a form we can visualize.

For example, consider terrain data. We assume that the data is x-y-z coordinates, where x and y represent the coordinates in the plane, and z represents the elevation above sea level. Our desired visualization is to color the terrain according to elevation. This requires creating a colormap — possibly using white for

ClearCorrect Exhibit 1002, Page 2290 of 3373



(a) Contour lines of X-ray intensity

(b) Isosurface of human skull

(c) Isosurface of flow density

(d) Isosurface of electron potential

Figure 6–11 Contouring examples. (a) Marching squares used to generate contour lines (`headSlic.tcl`); (b) Marching cubes surface of human bone (`headBone.tcl`); (c) Marching cubes surface of flow density (`combIso.tcl`); (d) Marching cubes surface of iron-protein (`ironPIso.tcl`).

high altitudes, blue for sea level and below, and various shades of green and brown corresponding to elevation between sea level and high altitude. We also need scalars to index into the colormap. The obvious choice here is to extract the z coordinate. That is, scalars are simply the z-coordinate value.

This example can be made more interesting by generalizing the problem. Although we could easily create a filter to extract the z-coordinate, we can create

ClearCorrect Exhibit 1002, Page 2291 of 3373

$$s_i = \frac{(p_i - p_l) \cdot (p_h - p_l)}{|p_h - p_l|^2}$$

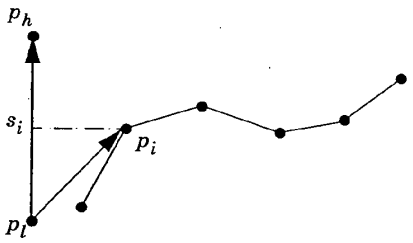




Figure 6–12 Computing scalars using normalized dot product. Bottom half of figure illustrates technique applied to terrain data from Honolulu, Hawaii (`hawaii.tcl`).

a filter that produces elevation scalar values where the elevation is measured along any axis. Given an oriented line starting at the (low) point p_l (e.g., sea level) and ending at the (high) point p_h (e.g., mountain top), we compute the elevation scalar s_i at point $p_i = (x_i, y_i, z_i)$ using the dot product as shown in Figure **6–12**. The scalar is normalized using the magnitude of the oriented line, and may be clamped between minimum and maximum scalar values (if necessary). The bottom half of this figure shows the results of applying this technique to a terrain model of Honolulu, Hawaii. A lookup table of 256 ranging from deep blue (water) to yellow-white (mountain top) is used to color map this figure.

Part of the creative practice of visualization is selecting the best technique for given data from the palette of available techniques. Often this requires creative mapping by the user of the visualization system. In particular, to use scalar visualization techniques we need only to create a relationship to generate a unique scalar value. Other examples of scalar mapping include an index value into a list of data, computing vector magnitude or matrix determinate, evaluating surface curvature, or determining distance between points. Scalar genera-

ClearCorrect Exhibit 1002, Page 2292 of 3373

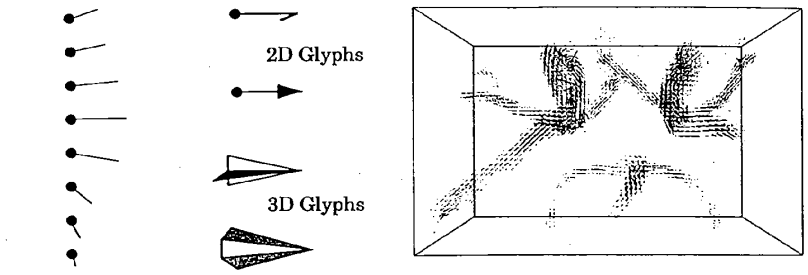


Figure 6–13 Vector visualization techniques: (a) oriented lines; (b) using oriented glyphs; (c) complex vector visualization (`complexV.tcl`).

tion, when coupled with color mapping or contouring, is a simple, yet effective, technique for visualizing many types of data.

6.3 Vector Algorithms

Vector data is a three-dimensional representation of direction and magnitude. Vector data often results from the study of fluid flow, or when examining derivatives (i.e., rate of change) of some quantity.

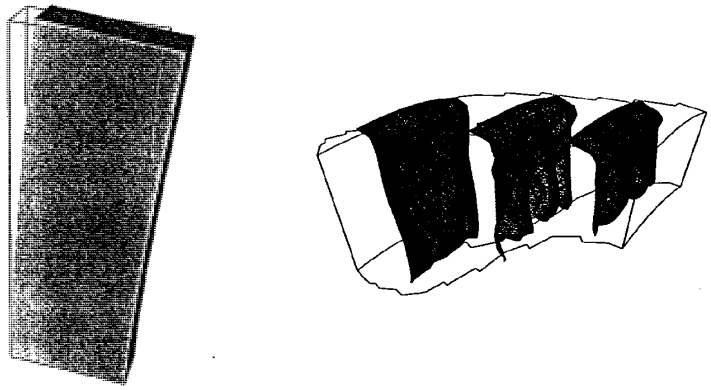
Hedgehogs and Oriented Glyphs

A natural vector visualization technique is to draw an oriented, scaled line for each vector (Figure **6–13**(a)). The line begins at the point with which the vector is associated and is oriented in the direction of the vector components (v_x, v_y, v_z). Typically, the resulting line must be scaled up or down to control the size of its visual representation. This technique is often referred to as a *hedgehog* because of the bristly result.

There are many variations of this technique (Figure **6–13**(b)). Arrows may be added to indicate the direction of the line. The lines may be colored according to vector magnitude, or some other scalar quantity (e.g., pressure or temperature). Also, instead of using a line, oriented "glyphs" can be used. By glyph we mean any 2D or 3D geometric representation such as an oriented triangle or cone.

Care should be used in applying these techniques. In 3D it is often difficult to understand the position and orientation of a vector because of its projection into a 2D image. Also, using large numbers of vectors can clutter the display to the point where the visualization becomes meaningless. Figure **6–13**(c) shows

ClearCorrect Exhibit 1002, Page 2293 of 3373



(a) Vibration of beam (b) Momentum profiles

Figure 6–14 Warping geometry to show vector field; (a) Beam displacement (`vib.tcl`); (b) Flow momentum (`velProf.tcl`).

167,000 3D vectors (using oriented and scaled lines) in the region of the human carotid artery. The larger vectors lie inside the arteries, the smaller vectors lie outside the arteries and are randomly oriented (measurement error) but small in magnitude. Clearly the details of the vector field are not discernible from this image.

Scaling glyphs also poses interesting problems. In what Tufte has termed a "visualization lie," [Tufte83] scaling a 2D or 3D glyph results in nonlinear differences in appearance. The surface area of an object increases with the square of its scale factor, so two vectors differing by a factor of two in magnitude may appear up to four times different based on surface area. Such scaling issues are common in data visualization, and great care must be taken to avoiding misleading viewers.

Warping

Vector data is often associated with "motion." The motion is in the form of velocity or displacement. An effective technique for displaying such vector data is to "warp" or deform geometry according to the vector field. For example, imagine representing the displacement of a structure under load by deforming the structure. Or if we are visualizing the flow of fluid, we can create a flow profile by distorting a straight line inserted perpendicular to the flow.

Figure **6–14** shows two examples of vector warping. In the first example the motion of a vibrating beam is shown. The original undeformed outline is shown in wireframe. The second example shows warped planes in a structured grid

ClearCorrect Exhibit 1002, Page 2294 of 3373

dataset. The planes are warped according to flow momentum. The relative back and forward flow are clearly visible in the deformation of the planes.

Typically, we must scale the vector field to control geometric distortion. Too small a distortion may not be visible, while too large a distortion can cause the structure to turn inside out or self-intersect. In such a case the viewer of the visualization is likely to lose context, and the visualization will become ineffective.

Displacement Plots

Vector displacement on the surface of an object can be visualized with displacement plots. A displacement plot shows the motion of an object in the direction perpendicular to its surface. The object motion is caused by an applied vector field. In a typical application the vector field is a displacement or strain field.

Vector displacement plots draw on the ideas in "Scalar Generation" on page 164. Vectors are converted to scalars by computing the dot product between the surface normal and vector at each point (Figure **6–15**(a)). If positive values result, the motion at the point is in the direction of the surface normal (i.e., positive displacement). Negative values indicate that the motion is opposite the surface normal (i.e., negative displacement).

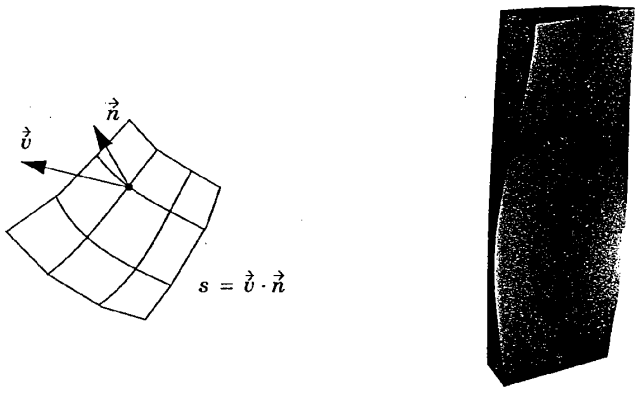
A useful application of this technique is the study of vibration. In vibration analysis, we are interested in the eigenvalues (i.e., natural resonant frequencies) and eigenvectors (i.e., mode shapes) of a structure. To understand mode shapes we can use displacement plots to indicate regions of motion. There are special regions in the structure where positive displacement changes to negative displacement. These are regions of zero displacement. When plotted on the surface of the structure, these regions appear as the so-called *modal* lines of vibration. The study of modal lines has long been an important visualization tool for understanding mode shapes.

Figure **6–15**(b) shows modal lines for a vibrating rectangular beam. The vibration mode in this figure is the second torsional mode, clearly indicated by the crossing modal lines. (The aliasing in the figure is because of the coarseness of the analysis mesh.) To create the figure we combined the procedure of Figure **6–15**(a) with a special lookup table. The lookup table was arranged with dark areas in the center (i.e., corresponds to zero dot product) and bright areas at the beginning and end of the table (corresponds to 1 or -1 dot product). As a result, regions of large normal displacement are bright and regions near the modal lines are dark.

Time Animation

Some of the techniques described so far can be thought of as moving a point or object over a small time step. The hedgehog line is an approximation of a point's

ClearCorrect Exhibit 1002, Page 2295 of 3373



(a) Scalar computation (b) Displacement plot

Figure 6–15 Vector displacement plots. (a) Vector converted to scalar via dot product computation; (b) Surface plot of vibrating plate. Dark areas show nodal lines. Bright areas show maximum motion (`dispPlot.tcl`).

motion over a time period whose duration is given by the scale factor. In other words, if velocity $\vec{V} = dx/dt$, then the displacement of a point is

$$dx = \vec{V}\,dt \tag{6-1}$$

This suggests an extension to our previous techniques: repeatedly displace points over many time steps. Figure **6–16** shows such an approach. Beginning with a sphere S centered about some point C, we move S repeatedly to generate the bubbles shown. The eye tends to trace out a path by connecting the bubbles, giving the observer a qualitative understanding of the fluid flow in that area. The bubbles may be displayed as an animation over time (giving the illusion of motion) or as a multiple exposure sequence (giving the appearance of a path).

Such an approach can be misused. For one thing, the velocity at a point is instantaneous. Once we move away from the point the velocity is likely to change. Using Equation **6-1** above assumes that the velocity is constant over the entire step. By taking large steps we are likely to jump over changes in the velocity. Using smaller steps we will end in a different position. Thus the choice of step size is a critical parameter in constructing accurate visualization of particle paths in a vector field.

ClearCorrect Exhibit 1002, Page 2296 of 3373

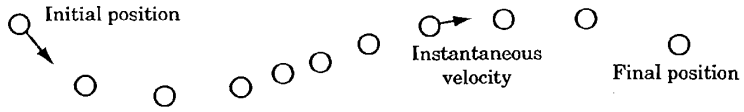


Figure 6–16 Time animation of a point C. Although the spacing between points varies, the time increment between each point is constant.

To evaluate Equation **6-1** we can express it as an integral:

$$\vec{x}(t) = \int_t \vec{V} dt \tag{6-2}$$

Although this form cannot be solved analytically for most real world data, its solution can be approximated using numerical integration techniques. Accurate numerical integration is a topic beyond the scope of this book, but it is known that the accuracy of the integration is a function of the step size dt. Since the path is an integration throughout the dataset, the accuracy of the cell interpolation functions, as well as the accuracy of the original vector data, plays an important role in realizing accurate solutions. No definitive study is yet available that relates cell size or interpolation function characteristics to visualization error. But the lesson is clear: the result of numerical integration must be examined carefully, especially in regions of large vector field gradient. However, as with many other visualization algorithms, the insight gained by using vector integration techniques is qualitatively beneficial, despite the unavoidable numerical errors.

The simplest form of numerical integration is Euler's method,

$$\vec{x}_{i+1} = \vec{x}_i + \vec{V}_i \Delta t \tag{6-3}$$

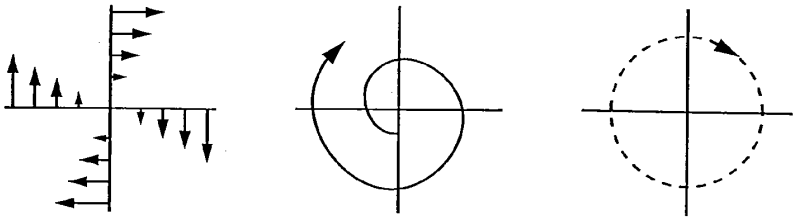
where the position at time $\vec{x}_{i+1}$ is the vector sum of the previous position plus the instantaneous velocity times the incremental time step Δt.

Euler's method has error on the order of $O(\Delta t^2)$, which is not accurate enough for some applications. One such example is shown in Figure **6–17**. The velocity field describes perfect rotation about a central point. Using Euler's method we find that we will always diverge and, instead of generating circles, will generate spirals instead.

In this text we will use the Runge-Kutta technique of order 2 [Conte72]. This is given by the expression

$$\vec{x}_{i+1} = \vec{x}_i + \frac{\Delta t}{2}(\vec{V}_i + \vec{V}_{i+1}) \tag{6-4}$$

ClearCorrect Exhibit 1002, Page 2297 of 3373



(a) Rotational vector field (b) Euler's method (c) Runge-Kutta

Figure 6–17 Euler's integration (b) and Runge-Kutta integration of order 2 (c) applied to uniform rotational vector field (a). Euler's method will always diverge.

where the velocity $\vec{V}_{i+1}$ is computed using Euler's method. The error of this method is $O(\Delta t^3)$. Compared to Euler's method, the Runge-Kutta technique allows us to take a larger integration step at the expense of one additional function evaluation. Generally this trade-off is beneficial, but like any numerical technique, the best method to use depends on the particular nature of the data. Higher-order techniques are also available, but generally not necessary, because the higher accuracy is countered by error in interpolation function or inherent in the data values. If you are interested in other integration formulas, please check the references at the end of the chapter.

One final note about accuracy concerns. The errors involved in either perception or computation of visualizations is an open research area. The discussion in the preceding paragraph is a good example of this. There we characterized the error in streamline integration using conventional numerical integration arguments. But there is a problem with this argument. In visualization applications, we are integrating across cells whose function values are continuous, but whose derivatives are not. As the streamline crosses the cell boundary, subtle effects may occur that are not treated by the standard numerical analysis. Thus the standard arguments need to be extended for visualization applications.

Integration formulas require repeated transformation from global to local coordinates. Consider moving a point through a dataset under the influence of a vector field. The first step is to identify the cell that contains the point. This operation is a search (see "Searching" on page 325), plus a conversion to local coordinates. Once the cell is found, then the next step is to compute the velocity at that point by interpolating the velocity from the cell points. The point is then incrementally repositioned (using the integration formula Equation **6-4**). The process is then repeated until the point exits the dataset or the distance or time traversed exceeds some specified value.

This process can be computationally demanding. There are two important steps we can take to improve performance.

- *Improving search procedures.* There are two distinct types of searches. Initially, the starting location of the particle must be determined by a global

ClearCorrect Exhibit 1002, Page 2298 of 3373

search procedure. Once the initial location of the point is determined in the dataset, an incremental search procedure can then be used. Incremental searching is efficient because the motion of the point is limited within a single cell, or at most across a cell boundary. Thus, the search space is greatly limited, and the incremental search is faster relative to the global search.

- *Coordinate transformation.* The cost of a coordinate transformation from global to local coordinates can be reduced if either of the following conditions are true: the local and global coordinate systems are identical with one another (or vary by x-y-z translation), or if the vector field is transformed from global space to local coordinate space. The structured point coordinate system is an example of parallel coordinates, and global to local coordinate transformation can be greatly accelerated. If the vector field is transformed into local coordinates (either as a preprocessing step or on a cell-by-cell basis), then the integration can proceed completely in local space. Once the integration path is computed, selected points along the path can be transformed into global space for the sake of visualization.

Streamlines

A natural extension of the previous time animation techniques is to connect the point position $\vec{x}(t)$ over many time steps. The result is a numerical approximation to a particle trace represented as a line.

Borrowing terminology from the study of fluid flow, we can define three related line representation schemes for vector fields.

- *Particle traces* are trajectories traced by fluid particles over time.
- *Streaklines* are the set of particle traces at a particular time t_i that have previously passed through a specified point x_i.
- *Streamlines* are integral curves along a curve s satisfying the equation

$$s = \int_{\bar{t}} \vec{V}\, ds, \text{ with } s = s(x, \bar{t}) \qquad \textbf{(6-5)}$$

for a particular time $\bar{t}$.

Streamlines, streaklines, and particle traces are equivalent to one another if the flow is steady. In time-varying flow, a given streamline exists only at one moment in time. Visualization systems generally provide facilities to compute particle traces. However, if time is fixed, the same facility can be used to compute streamlines. In general, we will use the term streamline to refer to the method of tracing trajectories in a vector field. Please bear in mind the differences in these representations if the flow is time-varying.

Figure **6–18** shows forty streamlines in a small kitchen. The room has two windows, a door (with air leakage), and a cooking area with a hot stove. The air leakage and temperature variation combine to produce air convection currents

ClearCorrect Exhibit 1002, Page 2299 of 3373

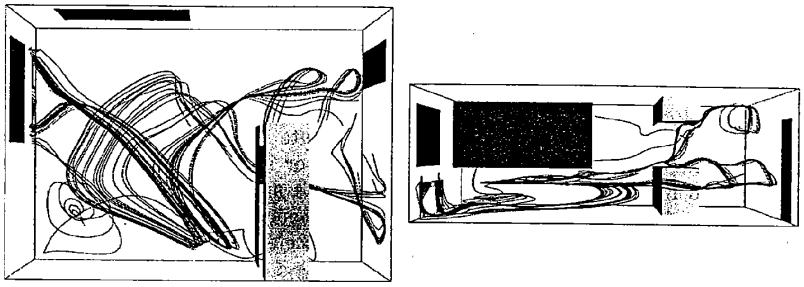


Figure 6–18 Flow velocity computed for a small kitchen (top and side view). Forty streamlines start along the rake positioned under the window. Some eventually travel over the hot stove and are convected upwards (`Kitchen.cxx`).

throughout the kitchen. The starting positions of the streamlines were defined by creating a *rake*, or curve (and its associated points). Here the rake was a straight line. These streamlines clearly show features of the flow field. By releasing many streamlines simultaneously we obtain even more information, as the eye tends to assemble nearby streamlines into a "global" understanding of flow field features.

Many enhancements of streamline visualization exist. Lines can be colored according to velocity magnitude to indicate speed of flow. Other scalar quantities such as temperature or pressure also may be used to color the lines. We also may create constant time dashed lines. Each dash represents a constant time increment. Thus, in areas of high velocity, the length of the dash will be greater relative to regions of lower velocity. These techniques are illustrated in Figure 6–19 for airflow around a blunt fin. This example consists of a wall with half a rounded fin projecting into the fluid flow. (Using arguments of symmetry, only half of the domain was modeled.) Twenty-five streamlines are released upstream of the fin. The boundary layer effects near the junction of the fin and wall are clearly evident from the streamlines. In this area, flow recirculation is apparent, as well as the reduced flow speed.

6.4 Tensor Algorithms

As we mentioned earlier, tensor visualization is an active area of research. However there are a few simple techniques that we can use to visualize 3×3 real symmetric tensors. Such tensors are used to describe the state of displacement or

ClearCorrect Exhibit 1002, Page 2300 of 3373

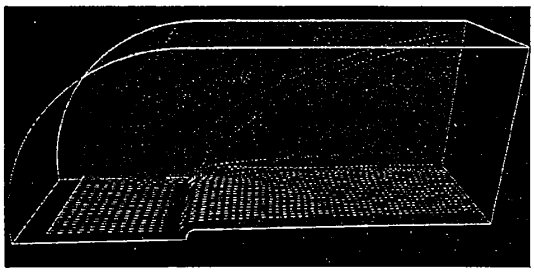


Figure 6–19 Dashed streamlines around a blunt fin. Each dash is a constant time increment. Fast moving particles create longer dashes than slower moving particles. The streamlines also are colored by flow density scalar (`bluntStr.cxx`).

$$\begin{bmatrix} \sigma_x & \tau_{xy} & \tau_{xz} \\ \tau_{yx} & \sigma_y & \tau_{yz} \\ \tau_{zx} & \tau_{zy} & \sigma_z \end{bmatrix}$$

(a) Stress tensor

$$\begin{bmatrix} \frac{\partial u}{\partial x} & \left(\frac{\partial u}{\partial y}+\frac{\partial v}{\partial z}\right) & \left(\frac{\partial u}{\partial z}+\frac{\partial w}{\partial x}\right) \\ \left(\frac{\partial u}{\partial y}+\frac{\partial v}{\partial z}\right) & \frac{\partial v}{\partial y} & \left(\frac{\partial v}{\partial z}+\frac{\partial w}{\partial y}\right) \\ \left(\frac{\partial u}{\partial z}+\frac{\partial w}{\partial x}\right) & \left(\frac{\partial v}{\partial z}+\frac{\partial w}{\partial y}\right) & \frac{\partial w}{\partial z} \end{bmatrix}$$

(b) Strain tensor

Figure 6–20 Stress and strain tensors. Normal stresses in the x-y-z coordinate directions indicated as $\sigma_x, \sigma_y, \sigma_z$, shear stresses indicated as τ_{ij}. Material displacement represented by u, v, w components.

stress in a 3D material. The stress and strain tensors for an elastic material are shown in Figure **6–20**.

In these tensors the diagonal coefficients are the so-called normal stresses and strains, and the off-diagonal terms are the shear stresses and strains. Normal stresses and strains act perpendicular to a specified surface, while shear stresses and strains act tangentially to the surface. Normal stress is either compression or tension, depending on the sign of the coefficient.

A 3×3 real symmetric matrix can be characterized by three vectors in 3D called the eigenvectors, and three numbers called the eigenvalues of the matrix. The eigenvectors form a 3D coordinate system whose axes are mutually perpen-

ClearCorrect Exhibit 1002, Page 2301 of 3373

dicular. In some applications, particularly the study of materials, these axes also are referred to as the principle axes of the tensor and are physically significant. For example, if the tensor is a stress tensor, then the principle axes are the directions of normal stress and no shear stress. Associated with each eigenvector is an eigenvalue. The eigenvalues are often physically significant as well. In the study of vibration, eigenvalues correspond to the resonant frequencies of a structure, and the eigenvectors are the associated mode shapes.

Mathematically we can represent eigenvalues and eigenvectors as follows. Given a matrix **A**, the eigenvector $\vec{x}$ and eigenvalue λ must satisfy the relation

$$A \cdot \vec{x} = \lambda \vec{x} \tag{6-6}$$

For Equation **6-6** to hold, the matrix determinate must satisfy

$$\det|A - \lambda I| = 0 \tag{6-7}$$

Expanding this equation yields a n^{th} degree polynomial in λ whose roots are the eigenvalues. Thus, there are always n eigenvalues, although they may not be distinct. In general, Equation **6-7** is not solved using polynomial root searching because of poor computational performance. (For matrices of order 3 root searching is acceptable because we can solve for the eigenvalues analytically.) Once we determine the eigenvalues, we can substitute each into Equation **6-7** to solve for the associated eigenvectors.

We can express the eigenvectors of the 3×3 system as

$$\vec{v}_i = \lambda_i \vec{e}_i, \text{ with } i = 1, 2, 3 \tag{6-8}$$

with $\vec{e}_i$ a unit vector in the direction of the eigenvalue, and λ_i the eigenvalues of the system. If we order eigenvalues such that

$$\lambda_1 \geq \lambda_2 \geq \lambda_3 \tag{6-9}$$

then we refer to the corresponding eigenvectors $\vec{v}_1$, $\vec{v}_2$, and $\vec{v}_3$ as the *major*, *medium*, and *minor* eigenvectors.

Tensor Ellipsoids

This leads us to the tensor ellipsoid technique for the visualization of real, symmetric 3×3 matrices. The first step is to extract eigenvalues and eigenvectors as described in the previous section. Since eigenvectors are known to be orthogonal, the eigenvectors form a local coordinate system. These axes can be taken as the *minor*, *medium*, and *major* axes of an ellipsoid. Thus, the shape and orientation of the ellipsoid represent the relative size of the eigenvalues and the orientation of the eigenvectors.

To form the ellipsoid we begin by positioning a sphere at the tensor location. The sphere is then rotated around its origin using the eigenvectors, which in the form of Equation **6-8** are direction cosines. The eigenvalues are used to scale the sphere. Using 4×4 transformation matrices and referring to

ClearCorrect Exhibit 1002, Page 2302 of 3373

Equation **3-6**, Equation **3-9**, and Equation **3-13**, we form the ellipsoid by transforming the sphere centered at the origin using the matrix T

$$T = T_T \cdot T_R \cdot T_S \quad \textbf{(6-10)}$$

(remember to read right-to-left). The eigenvectors can be directly plugged in to create the rotation matrix, while the point coordinates x-y-z and eigenvalues $\lambda_1 \geq \lambda_2 \geq \lambda_3$ are inserted into the translation and scaling matrices. A concatenation of these matrices forms the final transformation matrix T.

Figure **6–21**(a) depicts the tensor ellipsoid technique. In Figure **6–21**(b) we show this technique to visualize material stress near a point load on the surface of a semi-infinite domain. (This is the so-called Boussinesq's problem.) From Saada [Saada74] we have the analytic expression for the stress components in Cartesian coordinates shown in Figure **6–21**(c). Note that the z-direction is defined as the axis originating at the point of application of the force P. The variable ρ is the distance from the point of load application to a point x-y-z. The orientation of the x and y axes are in the plane perpendicular to the z axis. (The rotation in the plane of these axes is unimportant since the solution is symmetric around the z axis.) (The parameter ν is Poisson's ratio which is a property of the material. Poisson's ratio relates the lateral contraction of a material to axial elongation under a uniaxial stress condition. See [Saada74] or [Timoshenko70] for more information.)

In Figure **6–22** we visualize the analytical results of Boussinesq's problem from Saada. The left-hand portion of the figure shows the results by displaying the scaled and oriented principal axes of the stress tensor. (These are called *tensor axes*.) In the right-hand portion we use tensor ellipsoids to show the same result. Tensor ellipsoids and tensor axes are a form of *glyph* (see "Glyphs" on page 185) specialized to tensor visualization.

A certain amount of care must be taken to visualize this result since there is a stress singularity at the point of contact of the load. In a real application loads are applied over a small area and not at a single point. Also, plastic behavior prevents stress levels from exceeding a certain point. The results of the visualization, as with any computer process, are only as good as the underlying model.

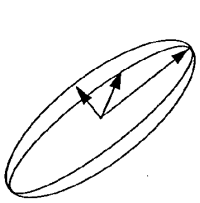
6.5 Modelling Algorithms

Modelling algorithms are the catch-all category for our taxonomy of visualization techniques. Modelling algorithms have one thing in common: They create or change dataset geometry or topology.

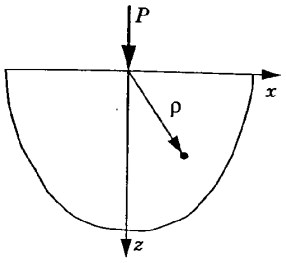
Source Objects

As we have seen in previous examples, source objects begin the visualization pipeline. Source objects are used to create geometry such as spheres, cones, or

ClearCorrect Exhibit 1002, Page 2303 of 3373



(a) Tensor ellipsoid



(b) Point load on semiinfinite domain

$$\sigma_x = -\frac{P}{2\pi\rho^2}\left(\frac{3zx^2}{\rho^3} - (1-2\nu)\left(\frac{z}{\rho} - \frac{\rho}{\rho+z} + \frac{x^2(2\rho+z)}{\rho(\rho+z)^2}\right)\right)$$

$$\sigma_y = -\frac{P}{2\pi\rho^2}\left(\frac{3zy^2}{\rho^3} - (1-2\nu)\left(\frac{z}{\rho} - \frac{\rho}{\rho+z} + \frac{y^2(2\rho+z)}{\rho(\rho+z)^2}\right)\right)$$

$$\sigma_z = -\frac{3Pz^3}{2\pi\rho^5}$$

$$\tau_{xy} = \tau_{yx} = -\frac{P}{2\pi\rho^2}\left(\frac{3xyz}{\rho^3} - (1-2\nu)\left(\frac{xy(2\rho+z)}{\rho(\rho+z)^2}\right)\right)$$

$$\tau_{xz} = \tau_{zx} = -\frac{3Pxz^2}{2\pi\rho^5}$$

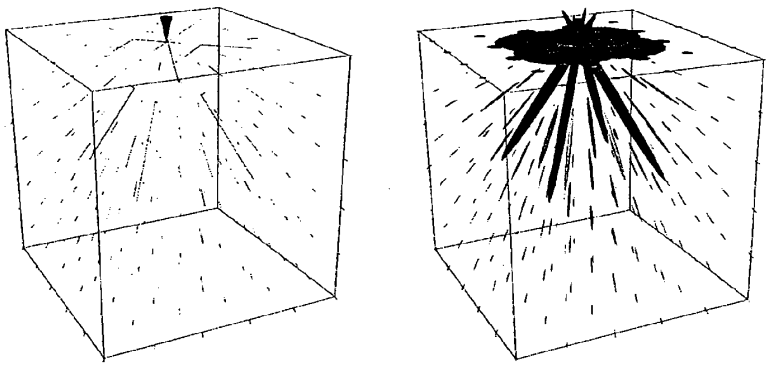
$$\tau_{yz} = \tau_{zy} = -\frac{3Pyz^2}{2\pi\rho^5}$$

c) Analytic solution

Figure 6–21 Tensor ellipsoids. (a) Ellipsoid oriented along eigenvalues (i.e., principle axes) of tensor; (b) Pictorial description of Boussinesq's problem; (c) Analytic results according to Saada.

cubes to support visualization context or are used to read in data files. Source objects also may be used to create dataset attributes. Some examples of source objects and their use are as follows.

ClearCorrect Exhibit 1002, Page 2304 of 3373



(a) Tensor axes (b) Tensor ellipsoids

Figure 6–22 Tensor visualization techniques; (a) Tensor axes (`TenAxes.tcl`); (b) Tensor ellipsoids (`TenEllip.tcl`).

Modelling Simple Geometry. Spheres, cones, cubes, and other simple geometric objects can be used alone or in combination to model geometry. Often we visualize real-world applications such as air flow in a room and need to show real-world objects such as furniture, windows, or doors. Real-world objects often can be represented using these simple geometric representations. These source objects generate their data procedurally. Alternatively, we may use reader objects to access geometric data defined in data files. These data files may contain more complex geometry such as that produced by a 3D CAD (Computer-Aided Design) system.

Supporting Geometry. During the visualization process we may use source objects to create supporting geometry. This may be as simple as three lines to represent a coordinate axis or as complex as tubes wrapped around line segments to thicken and enhance their appearance. Another common use is as supplemental input to objects such as streamlines or probe filters. These filters take a second input that defines a set of points. For streamlines, the points determine the initial positions for generating the streamlines. The probe filter uses the points as the position to compute attribute values such as scalars, vectors, or tensors.

Data Attribute Creation. Source objects can be used as procedures to create data attributes. For example, we can procedurally create textures and texture coordinates. Another use is to create scalar values over a uniform grid. If the scalar

ClearCorrect Exhibit 1002, Page 2305 of 3373

values are generated from a mathematical function, then we can use the visualization techniques described here to visualize the function. In fact, this leads us to a very important class of source objects: implicit functions.

Implicit Functions

Implicit functions are functions of the form

$$F(x, y, z) = c \tag{6-11}$$

where c is an arbitrary constant. Implicit functions have three important properties.

- *Simple geometric description.* Implicit functions are convenient tools to describe common geometric shapes. This includes planes, spheres, cylinders, cones, ellipsoids, and quadrics.
- *Region separation.* Implicit functions separate 3D Euclidean space into three distinct regions. These regions are inside, on, and outside the implicit function. These regions are defined as $F(x, y, z) < 0$, $F(x, y, z) = 0$, and $F(x, y, z) > 0$, respectively.
- *Scalar generation.* Implicit functions convert a position in space into a scalar value. That is, given an implicit function we can sample it at a point (x_i, y_i, z_i) to generate a scalar value c_i.

An example of an implicit function is the equation for a sphere of radius R

$$F(x, y, z) = x^2 + y^2 + z^2 - R^2 \tag{6-12}$$

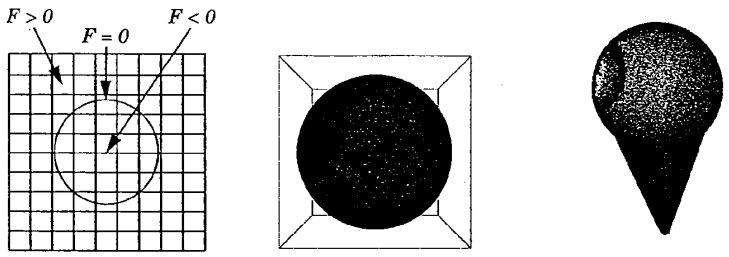
This simple relationship defines the three regions $F(x, y, z) = 0$ (on the surface of the sphere), $F(x, y, z) < 0$ (inside the sphere), and $F(x, y, z) > 0$ (outside the sphere). Any point may be classified inside, on, or outside the sphere simply by evaluating Equation **6-12**.

Implicit functions have a variety of uses. This includes geometric modelling, selecting data, and visualizing complex mathematical descriptions.

Modelling Objects. Implicit functions can be used alone or in combination to model geometric objects. For example, to model a surface described by an implicit function, we sample F on a dataset and generate an isosurface at a contour value c_i. The result is a polygonal representation of the function. Figure **6–23**(b) shows an isosurface for a sphere of radius=1 sampled on a volume. Note that we can choose nonzero contour values to generate a family of offset surfaces. This is useful for creating blending functions and other special effects.

Implicit functions can be combined to create complex objects using the boolean operators union, intersection, and difference. The union operation $F \cup G$

ClearCorrect Exhibit 1002, Page 2306 of 3373



(a) Sphere sampling (b) Isosurface of sphere (c) Boolean combinations

Figure 6–23 Sampling functions: (a) 2D depiction of sphere sampling; (b) Isosurface of sampled sphere; (c) Boolean combination of two spheres, a cone, and two planes. (One sphere intersects the other, the planes clip the cone.) (Refer to `sphere.tcl` and `iceCream.tcl`.)

between two functions $F(x, y, z)$ and $G(x, y, z)$ at a point (x_0, y_0, z_0) is the minimum value

$$F \cup G = min(F(x_0, y_0, z_0), G(x_0, y_0, z_0)) \quad \textbf{(6-13)}$$

The intersection between two implicit functions is given by

$$F \cap G = max(F(x_0, y_0, z_0), G(x_0, y_0, z_0)) \quad \textbf{(6-14)}$$

The difference of two implicit functions is given by

$$F - G = max(F(x_0, y_0, z_0), -G(x_0, y_0, z_0)) \quad \textbf{(6-15)}$$

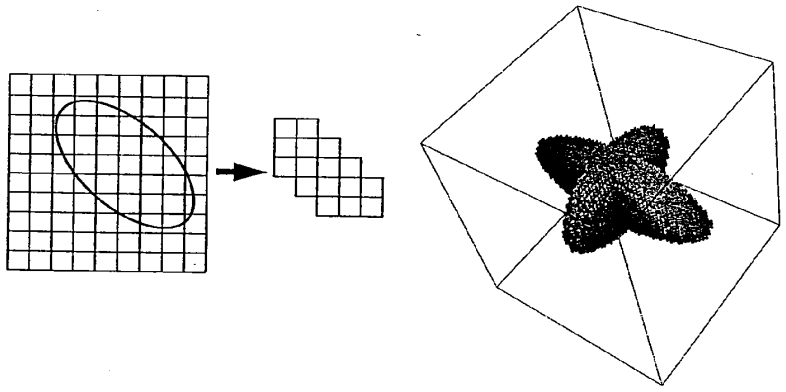
Figure **6–23**(c) shows a combination of simple implicit functions to create an ice-cream cone. The cone is created by clipping the (infinite) cone function with two planes. The ice cream is constructed by performing a difference operation on a larger sphere with a smaller offset sphere to create the "bite." The resulting surface was extracted using surface contouring with isosurface value 0.0.

Selecting Data. We can take advantage of the properties of implicit functions to select and cut data. In particular we will use the region separation property to select data. (We defer the discussion on cutting to "Cutting" on page 187.)

Selecting or extracting data with an implicit function means choosing cells and points (and associated attribute data) that lie within a particular region of the function. To determine whether a point *x-y-z* lies within a region, we simply evaluate the point and examine the sign of the result. A cell lies in a region if all its points lie in the region.

Figure **6–24**(a) shows a 2D implicit function, here an ellipse, used to select the data (i.e., points, cells, and data attributes) contained within it. Boolean com-

ClearCorrect Exhibit 1002, Page 2307 of 3373



(a) Selecting data with implicit function (b) Selecting data with boolean combination

Figure 6–24 Implicit functions used to select data: (a) 2D cells lying in ellipse are selected; (b) Two ellipsoids combined using the union operation used to select voxels from a volume. Voxels shrunk 50 percent (`extractD.tcl`).

binations also can be used to create complex selection regions as illustrated in Figure **6–24**(b). Here, two ellipses are used in combination to select voxels within a volume dataset. Note that extracting data often changes the structure of the dataset. In Figure **6–24** the input type is a structured points dataset, while the output type is an unstructured grid dataset.

Visualizing Mathematical Descriptions. Some functions, often discrete or probabilistic in nature, cannot be cast into the form of Equation **6-11**. However, by applying some creative thinking we can often generate scalar values that can be visualized. An interesting example of this is the so-called *strange attractor*.

Strange attractors arise in the study of nonlinear dynamics and chaotic systems. In these systems, the usual types of dynamic motion — equilibrium, periodic motion, or quasi-periodic motion — are not present. Instead, the system exhibits chaotic motion. The resulting behavior of the system can change radically as a result of small perturbations in its initial conditions.

A classical strange attractor was developed by Lorenz in 1963 [Lorenz63]. Lorenz developed a simple model for thermally induced fluid convection in the atmosphere. Convection causes rings of rotating fluid and can be developed from

ClearCorrect Exhibit 1002, Page 2308 of 3373

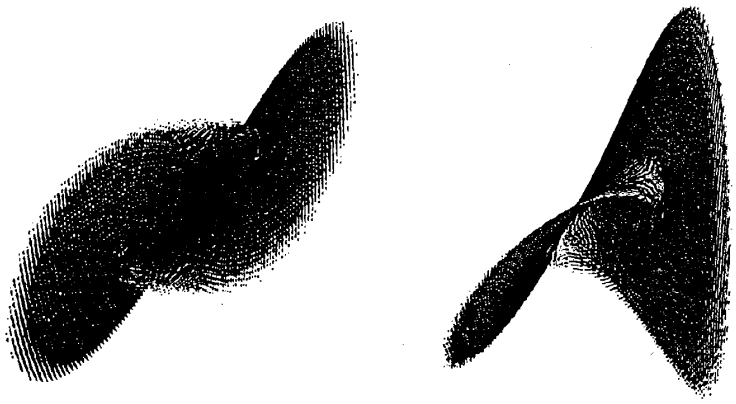


Figure 6–25 Visualizing a Lorenz strange attractor by integrating the Lorenz equations in a volume. The number of visits in each voxel is recorded as a scalar function. The surface is extracted via marching cubes using a visit value of 50. The number of integration steps is 10 million, in a volume of dimensions 200^3. The surface roughness is caused by the discrete nature of the evaluation function (`Lorenz.cxx`).

the general Navier-Stokes partial differential equations for fluid flow. The Lorenz equations can be expressed in nondimensional form as

$$\begin{aligned} \frac{dx}{dt} &= \sigma(y - x) \\ \frac{dy}{dt} &= \rho x - y - xz \\ \frac{dz}{dt} &= xy - \beta z \end{aligned} \tag{6-16}$$

where x is proportional to the fluid velocity in the fluid ring, y and z measure the fluid temperature in the plane of the ring, the parameters σ and ρ are related to the Prandtl number and Raleigh number, respectively, and β is a geometric factor.

Certainly these equations are not in the implicit form of Equation **6-11**, so how do we visualize them? Our solution is to treat the variables x, y, and z as the coordinates of a three-dimensional space, and integrate Equation **6-16** to generate the system "trajectory", that is, the state of the system through time. The integration is carried out within a volume and scalars are created by counting the number of times each voxel is visited. By integrating long enough, we can create a volume representing the "surface" of the strange attractor, Figure **6–25**. The surface of the strange attractor is extracted by using marching cubes and a scalar value specifying the number of visits in a voxel.

ClearCorrect Exhibit 1002, Page 2309 of 3373

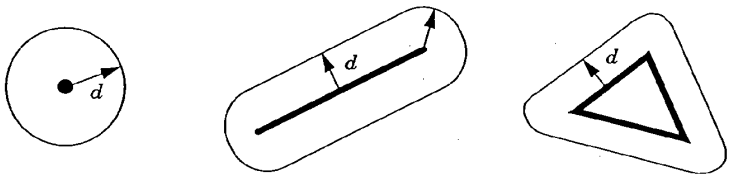


Figure 6–26 Distance functions to a point, line, and triangle.

Implicit Modelling

In the previous section we saw how implicit functions, or boolean combinations of implicit functions, could be used to model geometric objects. The basic approach is to evaluate these functions on a regular array of points, or volume, and then to generate scalar values at each point in the volume. Then either volume rendering (see "Volume Rendering" on page 216), or isosurface generation in combination with surface rendering, is used to display the model.

An extension of this approach, called implicit modeling, is similar to modeling with implicit functions. The difference lies in the fact that scalars are generated using a distance function instead of the usual implicit function. The distance function is computed as a Euclidean distance to a set of generating primitives such as points, lines, or polygons. For example, Figure **6–26** shows the distance functions to a point, line, and triangle. Because distance functions are well-behaved monotonic functions, we can define a series of offset surfaces by specifying different isosurface values, where the value is the distance to the generating primitive. The isosurfaces form approximations to the true offset surfaces, but using high volume resolution we can achieve satisfactory results.

Used alone the generating primitives are limited in their ability to model complex geometry. By using boolean combinations of the primitives, however, complex geometry can be easily modeled. The boolean operations union, intersection, and difference (Equation **6-13**, Equation **6-14**, and Equation **6-15**, respectively) are illustrated in Figure **6–27**. Figure **6–28** shows the application of implicit modeling to "thicken" the line segments in the text symbol "HELLO". The isosurface is generated on a $110 \times 40 \times 20$ volume at a distance offset of 0.25 units. The generating primitives were combined using the boolean union operator. Although Euclidean distance is always a nonnegative value, it is possible to use a signed distance function for objects that have an outside and an inside. A negative distance is the negated distance of a point inside the object to the surface of the object. Using a signed distance function allows us to create offset surfaces that are contained within the actual surface.

Another interesting feature of implicit modeling is that when isosurfaces are generated, more than one connected surface can result. These situations occur when the generating primitives form concave features. Figure **6–29** illus-

ClearCorrect Exhibit 1002, Page 2310 of 3373

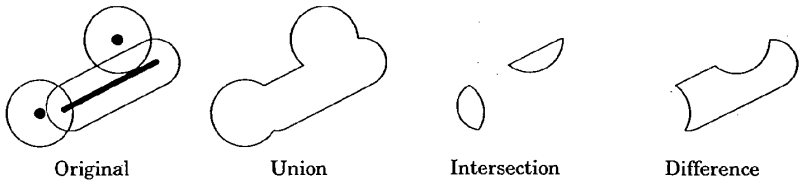


Figure 6–27 Boolean operations using points and lines as generating primitives.

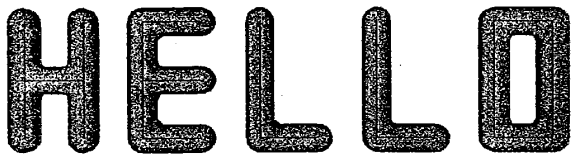


Figure 6–28 Implicit modelling used to thicken a stroked font. Original lines can be seen within the translucent implicit surface (`hello.tcl`).

trates this situation. If desired, multiple surfaces can be separated by using the connectivity algorithm described in "Connectivity" on page 377.

Glyphs

Glyphs, sometimes referred to as icons, are a versatile technique to visualize data of every type. A glyph is an "object" that is affected by its input data. This object may be geometry, a dataset, or a graphical image. The glyph may orient, scale, translate, deform, or somehow alter the appearance of the object in response to data. We have already seen a simple form of glyph: hedgehogs are lines that are oriented, translated and scaled according to the position and vector value of a point. A variation of this is to use oriented cones or arrows. (See "Hedgehogs and Oriented Glyphs" on page 167.)

More elaborate glyphs are possible. In one creative visualization technique Chernoff [Chernoff73] tied data values to an iconic representation of the human face. Eyebrows, nose, mouth, and other features were modified according to financial data values. This interesting technique built on the human capability to recognize facial expression. By tying appropriate data values to facial characteristics, rapid identification of important data points is possible.

ClearCorrect Exhibit 1002, Page 2311 of 3373

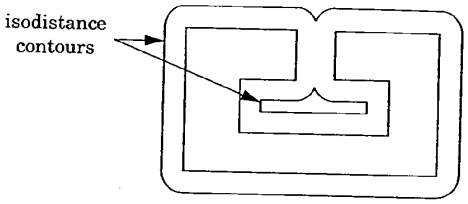


Figure 6–29 Concave features can result in multiple contour lines/surfaces.

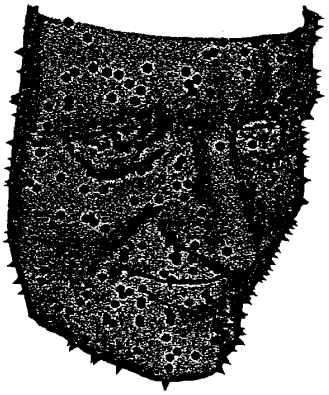


Figure 6–30 Glyphs indicate surface normals on model of human face. Glyph positions are randomly selected (`spikeF.tcl`).

In a sense, glyphs represent the fundamental result of the visualization process. Moreover, all the visualization techniques we present can be treated as concrete representations of an abstract glyph class. For example, while hedgehogs are an obvious manifestation of a vector glyph, isosurfaces can be considered a topologically two-dimensional glyph for scalar data. Delmarcelle and Hesselink [Delmarcelle95] have developed a unified framework for flow visualization based on types of glyphs. They classify glyphs according to one of three categories.

- *Elementary icons* represent their data across the extent of their spatial domain. For example, an oriented arrow can be used to represent surface normal.
- *Local icons* represent elementary information plus a local distribution of the values around the spatial domain. A surface normal vector colored by

ClearCorrect Exhibit 1002, Page 2312 of 3373

local curvature is one example of a local icon, since local data beyond the elementary information is encoded.

- *Global icons* show the structure of the complete dataset. An isosurface is an example of a global icon.

This classification scheme can be extended to other visualization techniques such as vector and tensor data, or even to nonvisual forms such as sound or tactile feedback. We have found this classification scheme to be helpful when designing visualizations or creating visualization techniques. Often it gives insight into ways of representing data that can be overlooked.

Figure **6–30** is an example of glyphing. Small 3D cones are oriented on a surface to indicate the direction of the surface normal. A similar approach could be used to show other surface properties such as curvature or anatomical keypoints.

Cutting

Often we want to cut through a dataset with a surface and then display the interpolated data values on the surface. We refer to this technique as *data cutting* or simply *cutting*. The data cutting operation requires two pieces of information: a definition for the surface and a dataset to cut. We will assume that the cutting surface is defined by an implicit function. A typical application of cutting is to slice through a dataset with a plane, and color map the scalar data and/or warp the plane according to vector value.

A property of implicit functions is to convert a position into a scalar value (see "Implicit Functions" on page 180). We can use this property in combination with a contouring algorithm (e.g., marching cubes) to generate cut surfaces. The basic idea is to generate scalars for each point of each cell of a dataset (using the implicit cut function), and then contour the surface value $F(x, y, z) = 0$.

The cutting algorithm proceeds as follows. For each cell, function values are generated by evaluating $F(x, y, z)$ for each cell point. If all the points evaluate positive or negative, then the surface does not cut the cell. However, if the points evaluate positive and negative, then the surface passes through the cell. We can use the cell contouring operation to generate the isosurface $F(x, y, z) = 0$. Data attribute values can then be computed by interpolating along cut edges.

Figure **6–31** illustrates a plane cut through a structured grid dataset. The plane passes through the center of the dataset with normal (–0.287, 0, 0.9579). For comparison purposes a portion of the grid geometry is also shown. The grid geometry is the grid surface k=9 (shown in wireframe). A benefit of cut surfaces is that we can view data on (nearly) arbitrary surfaces. Thus, the structure of the dataset does not constrain how we view the data.

We can easily make multiple planar cuts through a structured grid dataset by specifying multiple isovalues for the cutting algorithm. Figure **6–32** shows 100 cut planes generated perpendicular to the camera's view plane normal. Rendering the planes from back to front with an opacity of 0.05 produces a simulation of volume rendering. (See "Volume Rendering" on page 216.)

ClearCorrect Exhibit 1002, Page 2313 of 3373

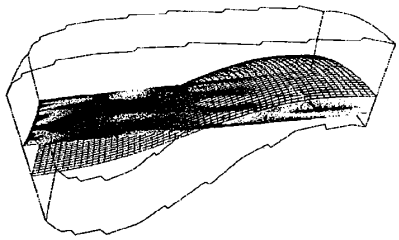


Figure 6–31 Cut through structured grid with plane. The cut plane is shown solid shaded. A computational plane of constant k value is shown in wireframe for comparison (`cut.tcl`).

This example illustrates that cutting the volumetric data in a structured grid dataset produced polygonal cells. Similarly, cutting polygonal data produces lines. Using a single plane equation, we can extract "contour lines" from a surface model defined with polygons. Figure **6–33** shows contours extracted from a surface model of the skin. At each vertex in the surface model we evaluate the equation of the plane $F(x, y, z) = c$ and store the value of the function as a scalar value. Cutting the data with 46 isovalues from 1.5 to 136.5 produces contour lines that are 3 units apart.

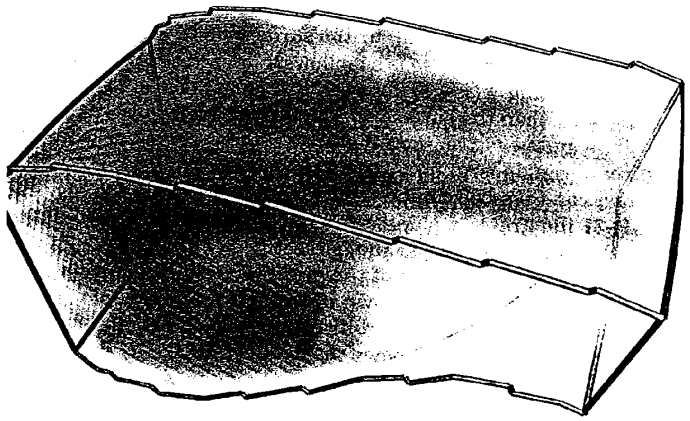


Figure 6–32 100 cut planes with opacity of 0.05. Rendered back to front to simulate volume rendering (`combVol.tcl`).

ClearCorrect Exhibit 1002, Page 2314 of 3373

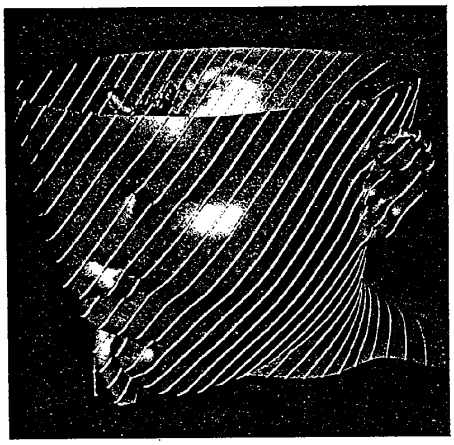


Figure 6–33 Cutting a surface model of the skin with a series of planes produces contour lines (`cutModel.tcl`). Lines are wrapped with tubes for visual clarity.

6.6 Putting It All Together

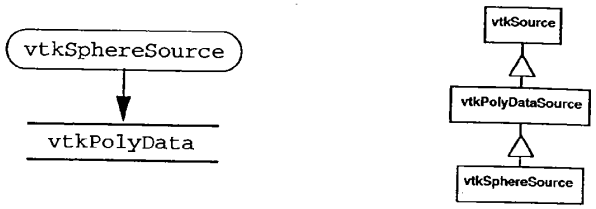
Process Object Design

Algorithms are implemented in the *Visualization Toolkit* as process objects. These objects may be either sources, filters, or mappers (See "The Visualization Pipeline" on page 88.) In this section we will describe how these objects are implemented.

Source Design. Source objects have no visualization data for input and one or more outputs, Figure **6–34**. To create a source object, inheritance is used to specify the type of dataset that the process object creates for output. Figure **6–34** illustrates this for the concrete source object `vtkSphereSource`. This class inherits from `vtkSource`, indicating that it is a source object, and `vtkPolyData`, indicating that it creates polygonal data on output.

The convenience object `vtkPolyDataSource` has been created to simplify subclass derivation. For example, `vtkBYUReader` is also of type `vtkPolyDataSource`. The major difference between `vtkSphereSource` and `vtkBYUReader` is the implementation of the virtual method `Execute()`. This method actually creates its output data. If you derive a source object you do not need to make it a subclass of any convenience object (e.g., `vtkPolyDataSource`) but you should

ClearCorrect Exhibit 1002, Page 2315 of 3373



(a) Functional model (b) Object model

Figure 6–34 Source object design. Example shown is a source object that creates a polygonal representation of a sphere.

are created, since no convenience classes exist expressly for derivation in this case.

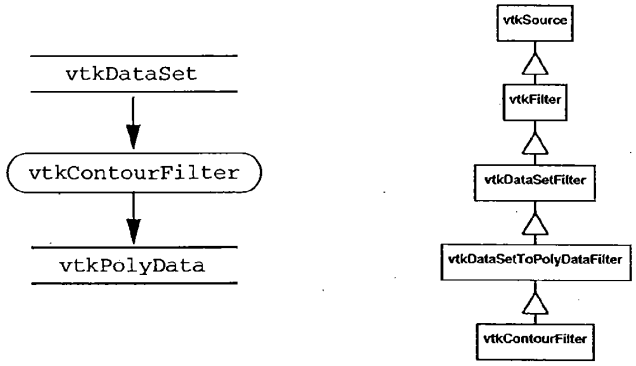
Filter Design. Filter objects have one or more inputs and one or more outputs as shown in Figure 6–35. (You may also refer to "Multiple Input / Output" on page 103.) To create a filter object, inheritance is used to specify the type of input and output data objects. Figure 6–35 illustrates this for the concrete source object `vtkContourFilter` (which implements marching cubes and other contouring techniques). It is worth examining this object diagram in detail since it is the basis for the architecture of the visualization pipeline.

The superclasses of `vtkContourFilter` are `vtkSource`, `vtkFilter`, `vtkDataSetFilter`, and `vtkDataSetToPolyDataFilter`. Although the inheritance of `vtkContourFilter` from `vtkSource` may be confusing at first glance, the meaning is this: the filter is a source of visualization data. Similarly, inheritance from `vtkFilter` means that `vtkContourFilter` has at least one input. The class `vtkDataSetFilter` specifies the type of data `vtkContourFilter` takes as input (i.e., a dataset), while `vtkDataSetToPolyDataFilter` specifies the type of output (i.e., polygonal data). Note that inheritance from `vtkDataSetFilter` and `vtkDataSetToPolyDataFilter` is optional – this functionality could be implemented directly in `vtkContourFilter`. These optional objects are simply convenience objects to make class derivation a little easier.

What is left for `vtkContourFilter` to implement is its `Execute()` method (as well as constructor, print method, and any other methods special to this class). Thus the primary difference between classes with equivalent inheritance hierarchies is the implementation of the `Execute()` method.

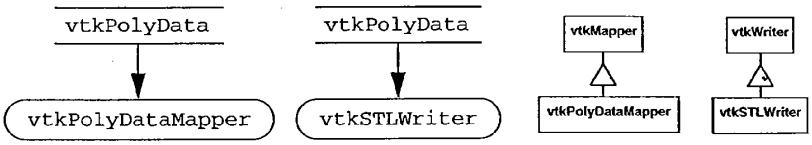
As we mentioned a moment ago, the class `vtkDataSetFilter` enforces filter input type with the type checking features of the C++ compiler. It accepts type `vtkDataSet` (or subclasses). Since `vtkDataSet` is a base class for all data types, this filter will accept any type as input. Specialized filters are derived from other classes. For example, filters that accept polygonal data are derived from

ClearCorrect Exhibit 1002, Page 2316 of 3373



(a) Functional model (b) Object model

Figure 6–35 Filter object design. The example shown is for an object that receives a general dataset as input and creates polygonal data on output.



(a) Functional models (b) Object models

Figure 6–36 Mapper object design. Graphics mapper shown (e.g., `vtkPolyDataMapper`) maps polygonal data through graphics library primitives. Writer shown (e.g., `vtkSTLWriter`) writes polygonal data to stereo lithography format.

`vtkPolyDataFilter`, and filters that accept structured point datasets are derived from `vtkStructuredPointsFilter`.

We encourage you to examine the source code carefully (included on the CD-ROM) for a few filter and source objects. The architecture is simple enough that you can grasp it quickly.

Mapper Design. Mapper objects have one or more inputs and no visualization data output, Figure **6–36**. Two different types of mappers are available in the *Visualization Toolkit*: graphics mappers and writers. Graphics mappers interface geometric structure and data attributes to the graphics library; writers write datasets to disk or other I/O devices.

ClearCorrect Exhibit 1002, Page 2317 of 3373

Since mappers take datasets as input, type enforcement is required. Each mapper implements this functionality directly. For example, both classes `vtkPolyDataMapper` and `vtkSTLWriter` implement a `SetInput()` method to enforce the input to be of type `vtkPolyData`. Other mappers and writers enforce input type as appropriate.

Although writers and mappers do not create visualization data, they both have methods similar to the `Execute()` method of the sources and filters. Each subclass of `vtkMapper` must implement the `Render()` method. This method is exchanged by the graphics system actors and its associated mappers during the rendering process. The effect of the method is to map its input dataset to the appropriate rendering library/system. Subclasses of the class `vtkWriter` must implement the `WriteData()` method. This method causes the writer to write its input dataset to disk (or other I/O device).

Color Maps

Color maps are created in the *Visualization Toolkit* using instances of the class `vtkLookupTable`. This class allows you to create a lookup table using HSVA (e.g., hue, saturation, value, and alpha opacity value) specification. Although we discussed the HSV color system in Chapter 3, we haven't yet defined alpha opacity. We shall do so in Chapter 7, but until then consider the alpha value to be the opacity of an object. Alpha values of one indicate that the object is opaque, while alpha values of zero indicate that the object is transparent.

The procedure for generating lookup table entries is to define pairs of values for HSVA. These pairs define a linear ramp for hue, saturation, value, and opacity. When the `Build()` method is invoked, these linear ramps are used to generate a table with the number of table entries requested. Alternatively, `vtkLookupTable` also enables you to load colors directly into the table. Thus, you build custom tables that cannot be simply expressed as linear ramps of HSVA values.

To demonstrate this procedure, we specify a starting and ending value for each of the components of HSVA, then we will create a rainbow lookup table from blue to red by using the following C++ code.

```
vtkLookupTable *lut=vtkLookupTable::New();
    lut->SetHueRange(0.6667, 0.0);
    lut->SetSaturationRange(1.0, 1.0);
    lut->SetValueRange(1.0, 1.0);
    lut->SetAlphaRange(1.0, 1.0);
    lut->SetNumberOfColors(256);
    lut->Build();
```

Since the default values for `SaturationRange`, `ValueRange`, `AlphaRange`, and the number of lookup table colors are (1,1), (1,1), (1,1), and 256, respectively, we can simplify this process to the following

ClearCorrect Exhibit 1002, Page 2318 of 3373

```
vtkLookupTable *lut=vtkLookupTable::New();
    lut->SetHueRange(0.6667, 0.0);
    lut->Build();
```

(The default values for HueRange are (0.0, 0.6667) — a red to blue color table.

To build a black and white lookup table of 256 entries we use

```
vtkLookupTable *lut=vtkLookupTable::New();
    lut->SetHueRange(0.0, 0.0);
    lut->SetSaturationRange(0.0, 0.0);
    lut->SetValueRange(0.0, 1.0)
```

In some cases you may want to specify colors directly. You can do this by specifying the number of colors, building the table, and then inserting new colors. When you insert colors, the RGBA color description system is used. For example, to create a lookup table of the three colors red, green, and blue, use the following C++ code.

```
vtkLookupTable *lut=vtkLookupTable::New();
    lut->SetNumberOfColors(3);
    lut->Build();
    lut->SetTableValue(0, 1.0, 0.0, 0.0, 1.0);
    lut->SetTableValue(0, 0.0, 1.0, 0.0, 1.0);
    lut->SetTableValue(0, 0.0, 0.0, 1.0, 1.0);
```

Lookup tables in the *Visualization Toolkit* are associated with the graphics mappers. Mappers will automatically create a red to blue lookup table if no table is specified, but if you want to create your own, use the `mapper->SetLookupTable(lut)` operation where `mapper` is an instance of `vtkMapper` or its subclasses.

A few final notes on using lookup tables.

- Mappers use their lookup table to map scalar values to colors. If no scalars are present, the mappers and their lookup tables do not control the color of the object. Instead the `vtkProperty` object associated with the `vtkActor` class does. Use the method `actor->GetProperty()->SetColor(r,g,b)` where `r`, `g`, and `b` are floating-point values specifying color.
- If you want to prevent scalars from coloring your object, use the method `mapper->ScalarVisibilityOff()` to turn off color mapping. Then the actor's color will control the color of the object.
- The scalar range (i.e., the range into which the colors are mapped) is specified with the mapper. Use the method `mapper->SetScalarRange(min, max)`.

You can also derive your own lookup table types. Look at `vtkLogLookupTable` for an example. This particular lookup table inherits from `vtkLookup-`

ClearCorrect Exhibit 1002, Page 2319 of 3373

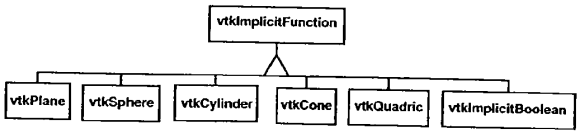


Figure 6–37 Inheritance hierarchy of `vtkImplicitFunction` and subclasses.

`Table`. It performs logarithmic mapping of scalar value to table entry, a useful capability when scalar values span many orders of magnitude.

Implicit Functions

As we have seen, implicit functions can be used for visualizing functions, creating geometry, and cutting or selecting datasets. **vtk** includes several implicit functions including a single plane (`vtkPlane`), multiple convex planes (`vtkPlanes`), spheres (`vtkSphere`), cones (`vtkCone`), cylinders (`vtkCylinder`), and the general quadric (`vtkQuadric`). The class `vtkImplicitBoolean` allows you to create boolean combinations of these implicit function primitives. Other implicit functions can be added to **vtk** by deriving from the abstract base class `vtkImplicitFunction`.

The existing inheritance hierarchy for implicit functions is shown in Figure 6–37. Subclasses of `vtkImplicitFunction` must implement the two methods `Evaluate()` and `Gradient()`. The method `Evaluate()` returns the value of the function at point (x,y,z), while the method `Gradient()` returns the gradient vector to the function at point (x,y,z).

Contouring

Scalar contouring is implemented in the *Visualization Toolkit* with `vtkContourFilter`. This filter object accepts as input any dataset type. Thus, `vtkContourFilter` treats every cell type and each cell type must provide a method for contouring itself.

Contouring in **vtk** is implemented using variations of the marching cubes algorithm presented earlier. That is, a contour case table is associated with each cell type, so each cell will generate contouring primitives as appropriate. For example, the tetrahedron cell type implements "marching tetrahedron" and creates triangle primitives, while the triangle cell type implements "marching triangles" and generates lines segments.

The implication of this arrangement is that `vtkContourFilter` will generate point, line, and surface contouring primitives depending on the combination of input cell types. Thus `vtkContourFilter` is completely general. We have created another contour filter, `vtkMarchingCubes`, that is specific to the dataset type structured points (in particular, 3D volumes). These two filters allow us to compare (at least for this one algorithm) the cost of generality.

ClearCorrect Exhibit 1002, Page 2320 of 3373



(a) Quarter resolution (b) Half resolution (c) Full resolution

Resolution	Specific (w/ normals)	General (no normals)	Factor	General (w/ normals)	Factor
64 x 64 x 93	1.000	2.889	2.889	7.131	7.131
128 x 128 x 93	5.058	11.810	2.330	23.260	4.600
256 x 256 x 93	37.169	51.620	1.390	87.230	2.350

Figure 6–38 The cost of generality. Isosurface generation of three volumes of different sizes are compared. The results show normalized execution times for two different implementations of the marching-cubes isosurface algorithm. The specialized filter is `vtkMarchingCubes`. The general algorithms are first `vtkContourFilter` and then in combination with `vtkPolyDataNormals`.

Recall from "Generality Versus Efficiency" on page 155 the issues regarding the trade-offs between general and specific algorithms. Figure **6–38** shows a comparison of CPU times for a volume dataset at $64 \times 64 \times 93$, $128 \times 128 \times 93$, and $256 \times 256 \times 93$ resolution. The volume is a CT dataset of a human head. Three cases were run. In the first case the `vtkMarchingCubes` object was used. The output of this filter is triangles plus point normals. In the second case `vtkContourFilter` was run. The output of this filter is just triangles. In the last case `vtkContourFilter` was combined with `vtkPolyDataNormals` (to generate point normals). The output of the combined filters is also triangles plus point normals.

The execution times are normalized to the smallest dataset using the `vtkMarchingCubes` object. The results are clear: The specific object outperforms the general object by a factor of 1.4 to 7, depending on data size and whether normals are computed. The larger differences occur on the smaller datasets. This is because the ratio of voxel cells containing the isosurface to the total number of voxels is larger for smaller datasets. (Generally the total number of voxels increases as the resolution cubed, while the voxels containing the isosurface increase as the resolution squared.) As a result, more voxels are processed in the

ClearCorrect Exhibit 1002, Page 2321 of 3373

smaller datasets relative to the total number of voxels than in the larger datasets. When the datasets become larger, more voxels are "empty" and are not processed.

Although these results do not represent all implementations or the behavior of other algorithms, they do point to the cost of generality. Of course, there is a cost to specialization as well. This cost is typically in programmer time, since the programmer must rewrite code to adapt to new circumstances and data. Like all trade-offs, resolution of this issue requires knowledge of the application.

An example use of `vtkContourFilter` is shown in Figure **6–39**. This example is taken from Figure **4–1**, which is a visualization of a quadric function. The class `vtkSampleFunction` samples the implicit quadric function using the `vtkQuadric` class. Although `vtkQuadric` does not participate in the pipeline in terms of data flow, it is used to define and evaluate the quadric function. It is possible to generate one or more isolines/isosurfaces simultaneously using `vtkContourFilter`. As Figure **6–39** shows, we use the `GenerateValues()` method to specify a scalar range, and the number of contours within this range (including the initial and final scalar values). `vtkContourFilter` generates duplicate vertices, so we can use `vtkCleanPolyData` to remove them. To improve the rendered appearance of the isosurface, we use `vtkPolyDataNormals` to create surface normals. (We describe surface normal generation in Chapter 9.)

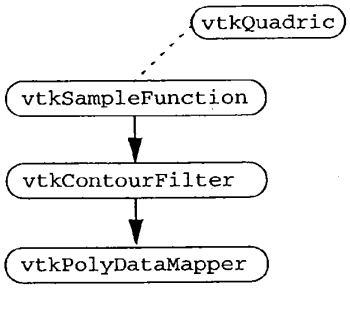
Cutting

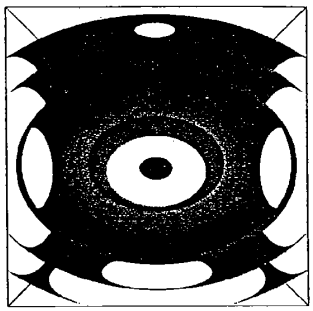
`vtkCutter` performs cutting of all **vtk** cell types. The `SetValue()` and `GenerateValues()` methods permit the user to specify which multiple scalar values to use for the cutting. `vtkCutter` requires an implicit function that will be evaluated at each point in the dataset. Then each cell is cut using the cell's `Contour` method. Any point attributes are interpolated to the resulting cut vertices. The sorting order for the generated polygonal data can be controlled with the `SortBy` method. The default sorting order, `SortByValue()`, processes cells in the inner loop for each contour value. `SortByCell()` processes the cutting value in the inner loop and produces polygonal data that is suitable for back-to-front rendering (see Figure **6–32**). (The sorting order is useful when rendering with opacity as discussed in Chapter 7.) Notice the similarity of this filter to the `vtkContourFilter`. Both of these objects contour datasets with multiple isovalues. `vtkCutter` uses an implicit function to calculate scalar values while `vtkContourFilter` uses the scalar data associated with the dataset's point data.

Glyphs

The `vtkGlyph3D` class provides a simple, yet powerful glyph capability in the *Visualization Toolkit*. `vtkGlyph3D` is an example of an object that takes multiple inputs (Figure **6–40**). One input, specified with the `SetInput()` method, defines a set of points and possible attribute data at those points. The second input, specified with the `SetSource()` method, defines a geometry to be copied to every point in the input dataset. The source is of type `vtkPolyData`. Hence, any

ClearCorrect Exhibit 1002, Page 2322 of 3373





```
// Define implicit function
vtkQuadric *quadric = vtkQuadric::New();
  quadric->SetCoefficients(.5,1,.2,0,.1,0,0,.2,0,0);
vtkSampleFunction *sample = vtkSampleFunction::New();
  sample->SetSampleDimensions(50,50,50);
  sample->SetImplicitFunction(quadric);
vtkContourFilter *contour = vtkContourFilter::New();
  contour->SetInput(sample->GetOutput());
  contour->GenerateValues(5,0,1.2);
vtkPolyDataMapper *contourMapper = vtkPolyDataMapper::New();
  contourMapper->SetInput(contour->GetOutput());
  contourMapper->SetScalarRange(0,1.2);
vtkActor *contourActor = vtkActor::New();
  contourActor->SetMapper(contourMapper);

// Create outline
vtkOutlineFilter *outline = vtkOutlineFilter::New();
  outline->SetInput(sample->GetOutput());
vtkPolyDataMapper *outlineMapper = vtkPolyDataMapper::New();
  outlineMapper->SetInput(outline->GetOutput());
vtkActor *outlineActor = vtkActor::New();
  outlineActor->SetMapper(outlineMapper);
  outlineActor->GetProperty()->SetColor(0,0,0);
```

Figure 6–39 Contouring quadric function. Pipeline topology, C++ code, and resulting image are shown (`contQuad.cxx`).

ClearCorrect Exhibit 1002, Page 2323 of 3373

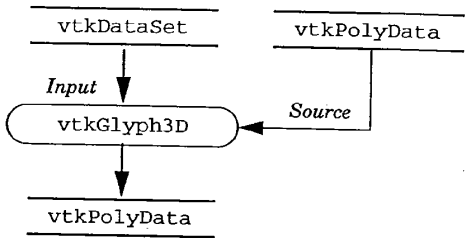


Figure 6–40 Data flow into and out of the `vtkGlyph3D` class.

filter, sequence of filters creating polygonal data, or a polygonal dataset may be used to describe the glyph's geometry.

The behavior of an instance of `vtkGlyph3D` depends on the nature of the input data and the value of its instance variables. Generally, the input `Source` geometry will be copied to each point of the `Input` dataset. The geometry will be aligned along the input vector data and scaled according to the magnitude of the vector or the scalar value. In some cases, the point normal is used rather than the vector. Also, scaling can be turned on or off.

We saw how to use `vtkGlyph3D` in the example given in Figure **4–14**. Cones were used as the glyph and were located at each point on the sphere, oriented along the sphere's surface normal.

Streamlines

Streamlines and particle motion require numerical integration to guide a point through the vector field. Vector visualization algorithms that we will see in later chapters also require numerical integration. As a result, we designed an object hierarchy that isolates the numerical integration process into a single base class. The base class is `vtkStreamer` and it is responsible for generating a particle path through a vector field of specified length (expressed as elapsed time). Each derived class of `vtkStreamer` takes advantage of this capability to move through the vector field but implements its own particular representational technique to depict particle motion. Streamlines (`vtkStreamLine`) draw connected lines while particle motion is shown by combining the output of `vtkStreamPoints` with the `vtkGlyph3D` object. Using `vtkGlyph3D` we can place spheres or oriented objects such as cones or arrows at points on the particle path created by `vtkStreamPoints`. The inheritance hierarchy for `vtkStreamer` and subclasses is shown in Figure **6–41**.

The integration method in `vtkStreamer` is implemented as a virtual function. Thus it can be overloaded as necessary. Possible reasons for overloading include implementing an integration technique of higher or lower accuracy, or creating a technique specialized to a particular dataset type. For example, the

ClearCorrect Exhibit 1002, Page 2324 of 3373

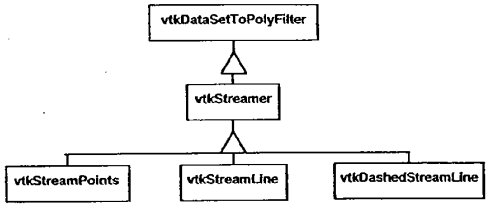


Figure 6–41 Inheritance hierarchy for `vtkStreamer` and subclasses.

search process in a volume is much faster than it is for other dataset types, therefore, highly efficient vector integration techniques can be constructed.

The vector integration technique in **vtk** will accommodate any cell type. Thus, integration through cells of any topological dimension is possible. If the cells are of topological dimension 2 or less, the integration process constrains particle motion to the surface (2D) or line (1D). The particle may only leave a cell by passing through the cell boundary, and traveling to a neighboring cell, or exiting the dataset.

Abstract Filters

Attribute transformations create or modify data attributes without changing the topology or geometry of a dataset. Hence filters that implement attribute transformation (e.g., `vtkElevationFilter`) can accept any dataset type as input, and may generate any dataset type on output. Unfortunately, because filters must specialize the particular type of data they output, at first glance it appears that filters that create general dataset types on output are not feasible. This is because the type `vtkDataSet` is an abstract type and must be specialized to allow instantiation.

Fortunately, there is a a solution to this dilemma. The solution is to use the "virtual constructor" `MakeObject()`. Although C++ does not allow virtual constructors, we can simulate it by creating a special virtual function that constructs a copy of the object that it is invoked on. For example, if this function is applied to a dataset instance of type `vtkPolyData`, the result will be a copy of that instance (Figure **6–42**). (Note that we use reference counting to make copies and avoid duplicating memory.) The virtual constructor function `MakeObject()` is implemented in a number of **vtk** classes including datasets and cells.

Using the virtual constructor we can construct filters that output abstract data types like `vtkDataSet`. We simply apply `MakeObject()` to the input of the filter. This will then return a pointer to a concrete object that is the output of the filter. The result is a general filter object that can accept any dataset type for input and creates the general `vtkDataSet` type as output. In **vtk**, this function-

ClearCorrect Exhibit 1002, Page 2325 of 3373

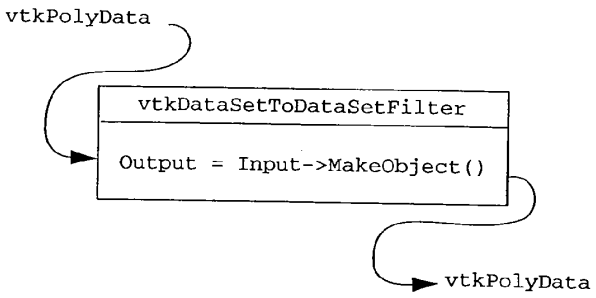


Figure 6–42 Depiction of data flow for abstract filter output. The output object type is the same as the input type.

ality has been implemented in the abstract class `vtkDataSetToDataSetFilter`.

There are other filters that implement variations of this delegation technique. The class `vtkPointSetToPointSetFilter` is similar to `vtkDataSetToDataSetFilter`. This class takes as input any dataset whose geometry is explicitly defined via an instance of `vtkPoints` (or subclass), and generates on output an object of the same type (i.e., `vtkPointSet`). The class `vtkMergeFilter` combines dataset structure and point attributes from one or more input datasets. For example, you can read multiple files and combine the geometry/topology from one file with different scalars, vectors, and normals from other files.

One difficulty using abstract filter types is that the output type may not match with the input type of a downstream filter. For example, the output of `vtkElevationFilter` is specified as `vtkDataSet` even though the input may be of type `vtkPolyData`, and we know from the previous discussion that the actual output type will be `vtkPolyData`. This difficulty is removed by using the filter `vtkCastToConcrete`, which allows you to run-time cast to the appropriate output type. In this case we would use the `GetPolyDataOutput()` from `vtkCastToConcrete`. After checking the validity of the cast, this method returns a dataset cast to `vtkPolyData`. Of course, this process requires that the input to `vtkCastToConcrete` be set before the output is requested.

Visualizing Blood Flow

In this example we'll combine a few different techniques to visualize blood flow in the human carotid arteries. Our data contains both vectors that represent the velocity of blood and scalars that are proportional to the magnitude of the velocity (i.e., speed).

We can provide context for the visualization by creating an isosurface of speed. This isosurface shows regions of fastest blood flow, and is similar to, but

ClearCorrect Exhibit 1002, Page 2326 of 3373

not the same as, the actual surface of the arteries. However, it provides us with a visual cue to the structure of the arteries.

The first vector visualization technique we'll use is to generate vector glyphs (Figure **6–43**). Unfortunately, we cannot just create glyphs at each point because of the number of points (over 167,000 points). To do so would result in a confusing mess, and the interactive speed would be poor. Instead, we'll use two filters to select a subset of the available points. These filters are `vtkThresholdPoints` and `vtkMaskPoints`.

`vtkThresholdPoints` allows us to extract points that satisfy a certain threshold criterion. In our example, we choose points whose speed is greater than a specified value. This eliminates a large number of points, since most points lie outside the arteries and have a small speed value.

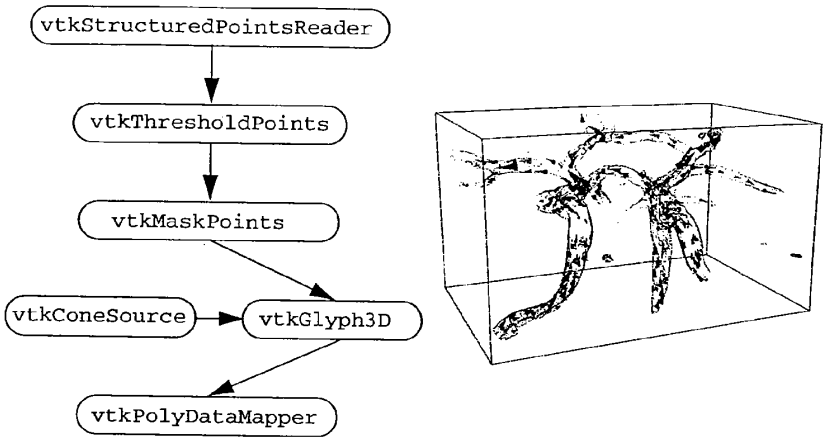
The filter `vtkMaskPoints` allows us to select a subset of the available points. We specify the subset with the `OnRatio` instance variable. This instance variable indicates that every `OnRatio` point is to be selected. Thus, if the `OnRatio` is equal to one, all points will be selected, and if the `OnRatio` is equal to ten, every tenth point will be selected. This selection can be either uniform or random. Random point selection is set using the `RandomModeOn()` and `RandomModeOff()` methods.

After selecting a subset of the original points, we can use the `vtkGlyph3D` filter in the usual way. A cone's orientation indicates blood flow direction, and its size and color correspond to the velocity magnitude. Figure **6–43** shows the pipeline, sample code, and a resulting image from this visualization. Note that we've implemented the example using the interpreted language Tcl. See Chapter 11 if you want more information about Tcl.

In the next part of this example we'll generate streamtubes of blood velocity. Again we use an isosurface of speed to provide us with context. The starting positions for the streamtubes were determined by experimenting with the data. Because of the way the data was measured and the resolution of the velocity field, many streamers travel outside the artery. This is because the boundary layer of the blood flow is not captured due to limitations in data resolution. Consequently, as the blood flows around curves, there is a component of the velocity field that directs the streamtube outside the artery. As a result it is hard to find starting positions for the streamtubes that yield interesting results. We use the source object `vtkPointSource` in combination with `vtkThresholdPoints` to work around this problem. `vtkPointSource` generates random points centered around a sphere of a specified radius. We need only find an approximate position for the starting points of the streamtubes and then generate a cloud of random seed points. `vtkThresholdPoints` is used to cull points that may be generated outside the regions of high flow velocity.

Figure **6–44** shows the pipeline, sample Tcl code, and a resulting image from the visualization. Notice that the isosurface is shown in wireframe. This provides context, yet allows us to see the streamtubes within the isosurface.

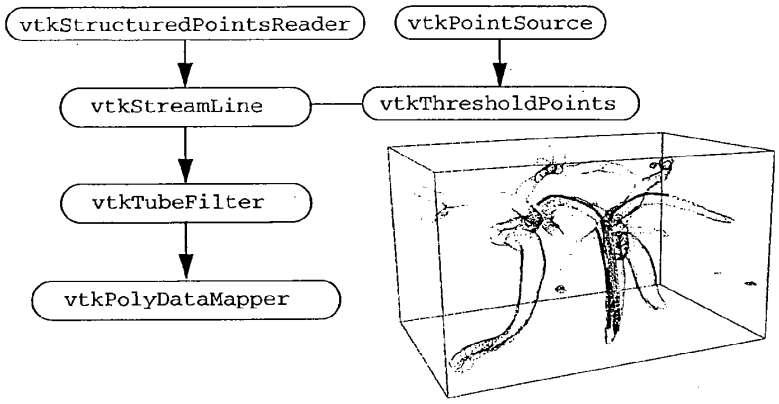
ClearCorrect Exhibit 1002, Page 2327 of 3373




```
vtkStructuredPointsReader reader
    reader SetFileName "../../../vtkdata/carotid.vtk"
    reader DebugOn
vtkThresholdPoints threshold
    threshold SetInput [reader GetOutput]
    threshold ThresholdByUpper 200
vtkMaskPoints mask
    mask SetInput [Threshold GetOutput]
    mask SetOnRatio 10
vtkConeSource cone
    cone SetResolution 3
    cone SetHeight 1
    cone SetRadius 0.25
vtkGlyph3D cones
    cones SetInput [mask GetOutput]
    cones SetSource [cone GetOutput]
    cones SetScaleFactor 0.005
    cones SetScaleModeToScaleByVector
vtkPolyDataMapper vecMapper
    vecMapper SetInput [cones GetOutput]
    vecMapper SetScalarRange 2 10
```

Figure 6–43 Visualizing blood flow in human carotid arteries. Cone glyphs indicate flow direction and magnitude. The code fragment shown is from the Tcl script `thrshldV.tcl` and shows creation of vector glyphs.

ClearCorrect Exhibit 1002, Page 2328 of 3373




```
vtkStructuredPointsReader reader
    reader SetFileName "../../../vtkdata/carotid.vtk"
vtkPointSource source
    source SetNumberOfPoints 25
    source SetCenter 133.1 116.3 5.0
    source SetRadius 2.0
vtkThresholdPoints threshold
    threshold SetInput [reader GetOutput]
    threshold ThresholdByUpper 275
vtkStreamLine streamers
    streamers SetInput [reader GetOutput]
    streamers SetSource [source GetOutput]
    streamers SetMaximumPropagationTime 100.0
    streamers SetIntegrationStepLength 0.2
    streamers SpeedScalarsOn
    streamers SetTerminalSpeed .1
vtkTubeFilter tubes
    tubes SetInput [streamers GetOutput]
    tubes SetRadius 0.3
    tubes SetNumberOfSides 6
    tubes SetVaryRadiusToVaryRadiusOff
vtkPolyDataMapper streamerMapper
    streamerMapper SetInput [tubes GetOutput]
    streamerMapper SetScalarRange 2 10
```

Figure 6–44 Visualizing blood flow in the human carotid arteries. Streamtubes of flow vectors (`streamV.tcl`).

ClearCorrect Exhibit 1002, Page 2329 of 3373

6.7 Chapter Summary

Visualization algorithms transform data from one form to another. These transformations can change or create new structure and/or attributes of a dataset. Structural transformations change either the topology or geometry of a dataset. Attribute transformations change dataset attributes such as scalars, vectors, normals, or texture coordinates.

Algorithms are classified according to the type of data they operate on. Scalar, vector, and tensor algorithms operate on scalar, vector, and tensor data, respectively. Modelling algorithms operate on dataset geometry or topology, texture coordinates, or normals. Modelling algorithms also may include complex techniques that may represent combinations of different data types.

Algorithms can be designed and implemented for general types of data or specialized for a specific type. General algorithms are typically less efficient than their specialized counterparts. Conversely, general algorithms are more flexible and do not require rewriting as new dataset types are introduced.

Important scalar algorithms include color mapping and contouring. Color maps are used to map scalar values to color values. Contouring algorithms create isosurfaces or isolines to indicate areas of constant scalar value.

Glyphs such as hedgehogs are useful for visualizing vector data. These techniques are limited by the number of glyphs that can be displayed at one time. Particle traces or streamlines are another important algorithm for vector field visualization. Collections of particle traces can convey something of the structure of a vector field.

Real, symmetric 3×3 tensors can be characterized by their eigenvalues and eigenvectors. Tensors can be visualized using tensor ellipsoids or oriented axes.

Implicit functions and sampling techniques can be used to make geometry, cut data, and visualize complex mathematical descriptions. Glyphs are objects whose appearance is associated with a particular data value. Glyphs are flexible and can be created to visualize a variety of data.

6.8 Bibliographic Notes

Color mapping is a widely studied topic in imaging, computer graphics, visualization, and human factors. References [Durrett87] [Ware88] [Rheingans92] provide samples of the available literature. You also may want to learn about the physiological and psychological effects of color on perception. The text by Wyszecki and Stiles [Wyszecki82] serves as an introductory reference.

Contouring is a widely studied technique in visualization because of its importance and popularity. Early techniques were developed for 2D data [Watson92]. Three dimensional techniques were developed initially as contour connecting methods [Fuchs77] — that is, given a series of 2D contours on evenly spaced planes, connect the contours to create a closed surface. Since the introduction of marching cubes, many other techniques have been implemented. (A

ClearCorrect Exhibit 1002, Page 2330 of 3373

few of these include [Nielson91] [Montani94] and [Durst88]). A particularly interesting reference is given by Livnat et al. [Livnat96]. They show a contouring method with the addition of a preprocessing step that generates isocontours in near optimal time.

Although we barely touched the topic, the study of chaos and chaotic vibrations is a delightfully interesting topic. Besides the original paper by Lorenz [Lorenz63], the book by Moon [Moon87] is a good place to start.

Two- and three-dimensional vector plots have been used by computer analysts for many years [Fuller80]. Streamlines and streamribbons also have been applied to the visualization of complex flows [Volpe89]. Good general references on vector visualization techniques are given in [Helman90] and [Richter90].

Tensor visualization techniques are relatively few in number. Most techniques are glyph oriented [Haber90] [deLeeuw93]. We will see a few more techniques in Chapter 9.

Blinn [Blinn82], Bloomental [Bloomenthal88] [Bloomenthal97] and Wyvill [Wyvill86] have been important contributors to implicit modeling. Implicit modeling is currently popular in computer graphics for modeling "soft" or "blobby" objects. These techniques are simple, powerful, and are becoming widely used for advanced computer graphics modeling.

6.9 References

[Abraham85]
R. H. Abraham and Christopher D. Shaw. *Dynamics The Geometry of Behavior.* Aerial Press, Santa Cruz, CA, 1985.

[Blinn82]
J. F. Blinn. "A Generalization of Algebraic Surface Drawing." *ACM Transactions on Graphics.* 1(3):235–256, July 1982.

[Bloomenthal88]
J. Bloomenthal. "Polygonization of Implicit Surfaces." *Computer Aided Geometric Design.* 5(4):341–355, November 1982.

[Bloomenthal97]
J. Bloomenthal, editor. *Introduction to Implicit Surfaces.* Morgan Kaufmann Publishers, Inc., San Francisco, CA., 1997.

[Chernoff73]
H. Chernoff. "Using Faces to Represent Pints in K-Dimensional Space Graphically." *J. American Statistical Association.* 68:361–368, 1973.

[Cline93]
H. Cline, W. Lorensen, and W. Schroeder. "3D Phase Contrast MRI of Cerebral Blood FLow and Surface Anatomy." *Journal of Computer Assisted Tomography.* 17(2):173–177, March/April 1993.

[Conte72]
S. D. Conte and C. de Boor. *Elementary Numerical Analysis.* McGraw-Hill Book Company, 1972.

ClearCorrect Exhibit 1002, Page 2331 of 3373

[deLeeuw93]
W. C. de Leeuw and J. J. van Wijk. "A Probe for Local Flow Field Visualization." In *Proceedings of Visualization '93*. pp. 39–45, IEEE Computer Society Press, Los Alamitos, CA, 1993.

[Delmarcelle95]
T. Delmarcelle and L. Hesselink. "A Unified Framework for Flow Visualization." In *Computer Visualization Graphics Techniques for Scientific and Engineering Analysis*. R. S. Gallagher, ed. CRC Press, Boca Raton, FL, 1995.

[Durrett87]
H. J. Durrett, ed. *Color and the Computer*. Academic Press, Boston, MA, 1987.

[Durst88]
M. J. Durst. "Additional Reference to Marching Cubes." *Computer Graphics*. 22(2):72–73, 1988.

[Fuchs77]
H. Fuchs, Z. M. Kedem, and S. P. Uselton. "Optimal Surface Reconstruction from Planar Contours." *Communications of the ACM*. 20(10):693–702, 1977.

[Fuller80]
A. J. Fuller and M.L.X. dosSantos. "Computer Generated Display of 3D Vector Fields." *Computer Aided Design*. 12(2):61–66, 1980.

[Haber90]
R. B. Haber and D. A. McNabb. "Visualization Idioms: A Conceptual Model to Scientific Visualization Systems." *Visualization in Scientific Computing*, G. M. Nielson, B. Shriver, L. J. Rosenblum, ed. IEEE Computer Society Press, pp. 61–73, 1990.

[Helman90]
J. Helman and L. Hesselink. "Representation and Display of Vector Field Topology in Fluid Flow Data Sets." *Visualization in Scientific Computing*. G. M. Nielson, B. Shriver, L. J. Rosenblum, eds. IEEE Computer Society Press, pp. 61–73, 1990.

[Livnat96]
Y. Livnat, H. W. Shen, C. R. Johnson. "A Near Optimal Isosurface Extraction Algorithm for Structured and Unstructured Grids." *IEEE Transactions on Visualization and Computer Graphics*. Vol. 2, No. 1, March 1996.

[Lorensen87]
W. E. Lorensen and H. E. Cline. "Marching Cubes: A High Resolution 3D Surface Construction Algorithm." *Computer Graphics*. 21(3):163–169, July 1987.

[Lorenz63]
E. N. Lorenz. "Deterministic Non-Periodic Flow." *Journal of Atmospheric Science*. 20:130–141, 1963.

[Montani94]
C. Montani, R. Scateni, and R. Scopigno. "A Modified Look-Up Table for Implicit Disambiguation of Marching Cubes." *Visual Computer*. (10):353–355, 1994.

[Moon87]
F. C. Moon. *Chaotic Vibrations*. Wiley-Interscience, New York, NY, 1987.

ClearCorrect Exhibit 1002, Page 2332 of 3373

[Nielson91]
G. M. Nielson and B. Hamann. "The Asymptotic Decider: Resolving the Ambiguity in Marching Cubes." In *Proceedings of Visualization '91*. pp. 83–91, IEEE Computer Society Press, Los Alamitos, CA, 1991.

[Rheingans92]
P. Rheingans. "Color, Change, and Control for Quantitative Data Display." In *Proceedings of Visualization '92*. pp. 252–259, IEEE Computer Society Press, Los Alamitos, CA, 1992.

[Richter90]
R. Richter, J. B. Vos, A. Bottaro, and S. Gavrilakis. "Visualization of Flow Simulations." *Scientific Visualization and Graphics Simulation*. D. Thalmann editor, pp. 161–171, John Wiley and Sons, 1990.

[Saada74]
A. S. Saada. *Elasticity Theory and Applications*. Pergamon Press, Inc., New York, NY, 1974.

[Timoshenko70]
S. P. Timoshenko and J. N. Goodier. *Theory of Elasticity, 3d Edition*. McGraw-Hill Book Company, New York, NY, 1970.

[Tufte83]
E. R. Tufte. *The Visual Display of Quantitative Information*. Graphics Press, Cheshire, CT, 1990.

[Volpe89]
G. Volpe. "Streamlines and Streamribbons in Aerodynamics." Technical Report AIAA-89-0140, 27th Aerospace Sciences Meeting, 1989.

[Ware88]
C. Ware. "Color Sequences for Univariate Maps: Theory, Experiments and Principles." *IEEE Computer Graphics and Applications*. 8(5):41–49, 1988.

[Watson92]
D. F. Watson. *Contouring: A Guide to the Analysis and Display of Spatial Data*. Pergamon Press, 1992.

[Wyszecki82]
G. Wyszecki and W. Stiles. *Color Science: Concepts and Methods, Quantitative Data and Formulae*. John Wiley and Sons, 1982.

[Wyvill86]
G. Wyvill, C. McPheeters, B. Wyvill. "Data Structure for Soft Objects." *Visual Computer*. 2(4):227–234, 1986.

6.10 Exercises

6.1 Sketch contour cases for marching triangles. How many cases are there?

6.2 Sketch contour cases for marching tetrahedron. How many cases are there?

6.3 A common visualization technique is to animate isosurface value. The procedure is to smoothly vary isosurface value over a specified range.
a) Create an animation sequence for the quadric example (Figure **4–1**).
b) Create an animation sequence for the head sequence (Figure **6–11**(b)).

ClearCorrect Exhibit 1002, Page 2333 of 3373

6.4 Marching cubes visits each cell during algorithm execution. Many of these cells do not contain the isosurface. Describe a technique to improve the performance of isosurface extraction by eliminating visits to cells not containing isosurface. (*Hint:* use a preprocessing step to analyze data. Assume that many isosurfaces will be extracted and that the preprocessing step will not count against execution time.)

6.5 Scan-line rasterization proceeds along horizontal spans in graphics hardware (see "Rasterization" on page 60). Interpolation of color occurs along horizontal spans as well.
a) Show how the orientation of a polygon affects interpolated color.
b) Discuss potential problems caused by orientation dependent viewing of visualizations.

6.6 Write a program to simulate beam vibration. Use the code associated with Figure **6–14**(a) as your starting point.

6.7 Using the filters `vtkStreamLine`, `vtkMaskPoints`, and `vtkGlyph3D`, create a visualization consisting of oriented glyphs along a streamline.

6.8 Visualize the following functions.
a) Scalar $S(x, y, z) = \sin(xy)$, for x,y between 0 and π .
b) The effective stress field (a scalar field) from Figure **6–21**.
c) The vector field described in the combustor data (i.e., `combq.bin` and `combxyz.bin`).

6.9 Tensor ellipsoids are based on an ellipsoidal glyph. Describe two other glyphs that you might use.

6.10 Write a source object to generate a polygonal representation of a torus.

6.11 Design a glyph to convey airplane heading, speed, and altitude, and proximity (i.e., distance) to other planes.

6.12 Morphing is a process to smoothly blend images (2D) or geometry (3D) between two known images or geometry. Using an implicit modeling approach, how would you morph a torus into a cube?

6.13 Describe a technique to visualize vector information by animating a color map. (*Hint:* By choosing a map carefully, you can give the illusion of motion across a surface.)

6.14 Isoline contours of different values are typically shown together in one image.
a) Describe the advantages and disadvantages of displaying isosurfaces simultaneously.
b) What two graphics properties might you adjust to improve the display of multiple isosurfaces?

6.15 Describe a parallel algorithm for marching cubes. Use a parallel architecture of your choice.

ClearCorrect Exhibit 1002, Page 2334 of 3373

6.16 Decomposition can greatly increase the speed of an operation.
a) Prove that 3D Gaussian smoothing can be decomposed into three 1D operations.
b) Give the complexity of the decomposed filter and the same filter implemented as a 3D convolution.
c) Under what conditions can constant smoothing be decomposed into 1D operations.

ClearCorrect Exhibit 1002, Page 2335 of 3373

CHAPTER 8

Advanced Data Representation

This chapter examines advanced topics in data representation. Topics include topological and geometric relationships and computational methods for cells and datasets.

8.1 Coordinate Systems

We will examine three different coordinate systems: the global, dataset, and structured coordinate systems. Figure 8–1 shows the relationship between the global and dataset coordinate systems, and depicts the structured coordinate system.

Global Coordinate System

The global coordinate system is a Cartesian, three-dimensional space. Each point is expressed as a triplet of values *(x,y,z)* along the *x*, *y*, and *z* axes. This is the same system that was described in Chapter 3 (see "Coordinate Systems" on page 49).

The global coordinate system is always used to specify dataset geometry (i.e., the point coordinates), and data attributes such as normals and vectors. We will use the word "position" to indicate that we are using global coordinates.

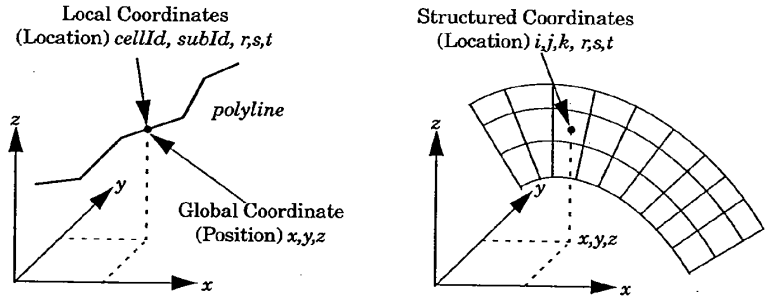


Figure 8–1 Local and global coordinate systems.

Dataset Coordinate System

The dataset, or local, coordinate system is based on combined topological and geometric coordinates. The topological coordinate is used to identify a particular cell (or possibly a subcell), and the geometric coordinate is used to identify a particular location within the cell. Together they uniquely specify a location in the dataset. Here we will use the word "location" to refer to local or dataset coordinates.

The topological coordinate is an "id": a unique, nonnegative integer number referring to either a dataset point or cell. For a composite cell, we use an additional "sub-id" to refer to a particular primary cell that composes the composite cell. The sub-id is also unique and nonnegative. The id and sub-id together select a particular primary cell.

To specify a location within the primary cell, we use geometric coordinates. These geometric coordinates, or *parametric coordinates*, are coordinates "natural" or canonical to the particular topology and dimension of a cell.

We can best explain local coordinates by referring to an example. If we consider the polyline cell type shown in Figure **8–1**, we can specify the position of a point by indicating 1) the polyline cell id, 2) the primary cell (i.e., line) sub-id and 3) the parametric coordinate of the line. Because the line is one-dimensional, the natural or parametric coordinate is based on the one-dimensional parameter r. Then any point *along* the line is given by a linear combination of the two end points of the line x_i and x_{i+1}

$$x(r) = (1-r)x_i + rx_{i+1} \qquad \textbf{(8-1)}$$

where the parametric coordinate r is constrained between (0,1). In this equation we are assuming that the sub-id is equal to i.

The number of parametric coordinates corresponds to the topological dimension of the cell. Three-dimensional cells will be characterized by the three

ClearCorrect Exhibit 1002, Page 2337 of 3373

parametric coordinates *(r, s, t)*. For cells of topological order less than three, we will ignore the last *(3 – n)* parametric coordinates, where n is the topological order of the cell. For convenience and consistency, we also will constrain each parametric coordinate to range between *(0,1)*.

Every cell type will have its own parametric coordinate system. Later in this chapter we will describe the parametric coordinate systems in detail. But first we will examine another coordinate system, the *structured coordinate system*.

Structured Coordinate System

Many dataset types are structured. This includes structured points and structured grids. Because of their inherent structure, they have their own natural coordinate system. This coordinate system is based on the *i-j-k* indexing scheme that we touched on in Chapter 5 (see "Structured Points" on page 128).

The structured coordinate system is a natural way to describe components of a structured dataset. By fixing some indices, and allowing the others to vary within a limited range, we can specify points, lines, surfaces, and volumes. For example, by fixing the i index $i = i_0$, and allowing the j and k indices to range between their minimum and maximum values, we specify a surface. If we fix three indices, we specify a point, if we fix two indices, we specify a line, and if we allow three indices to vary, we specify a volume (or sub-volume). The structured coordinate system is generally used to specify a *region of interest* (or ROI). The region of interest is an area that we want to visualize, or to operate on.

There is a simple relationship between the point and cell id of the dataset coordinate system and the structured coordinate system. To obtain a point id p_{id} given the indices (i_p, j_p, k_p) and dimensions (n_x, n_y, n_z) we use

$$p_{id} = i_p + j_p n_x + k_p n_x n_y \tag{8-2}$$

with $0 \le i_p < n_x$, $0 \le j_p < n_y$, $0 \le k_p < n_z$. (We can use this id to index into an array of points or point attribute data.) This equation implicitly assumes an ordering of the points in topological space. Points along the i axis vary fastest, followed by the j and then the k axes. A similar relationship exists for cell id's

$$cell_{id} = i_p + j_p(n_x - 1) + k_p(n_x - 1)(n_y - 1) \tag{8-3}$$

Here we've taken into account that there are one fewer cells along each topological axes than there are points.

8.2 Interpolation Functions

Computer visualization deals with discrete data. The data is either supplied at a finite number of points or created by sampling continuous data at a finite number of points. But we often need information at positions other than these discrete point locations. This may be for rendering or for subsampling the data

ClearCorrect Exhibit 1002, Page 2338 of 3373

during algorithm execution. We need to interpolate data from known points to some intermediate point using *interpolation functions*.

Interpolation functions relate the values at cell points to the interior of the cell. Thus, we assume that information is defined at cell points, and that we must interpolate from these points. We can express the result as a weighted average of the data values at each cell point.

General Form

To interpolate data from the cell points p_i to a point p that is inside the cell, we need three pieces of information:

1. the data values at each cell point,
2. the parametric coordinates of the point p within the cell, and
3. the cell type including interpolation functions.

Given this information, the interpolation functions are a linear combination of the data values at the cell points

$$d = \sum_{i=0}^{n-1} W_i \cdot d_i \tag{8-4}$$

where d is the data value at the interior cell location (r,s,t), d_i is the data value at the i^{th} cell point, and W_i is a weight at the i^{th} cell point. The interpolation weights are functions of the parametric coordinates $W_i = W(r,s,t)$. In addition, because we want $d = d_i$ when the interior point coincides with a cell point, we can place additional constraints on the weights

$$W_i = 1, W_j = 0 \text{ when } p = p_i \text{ and } i \neq j \tag{8-5}$$

We also desire the interpolated data value d to be no smaller than the minimum d_i and no larger than the maximum d_i. Thus the weights should also satisfy

$$\sum W_i = 1, \quad 0 \leq W_i \leq 1 \tag{8-6}$$

The interpolation functions are of a characteristic shape. They reach their maximum value $W_i = 1$ at cell point p_i, and are zero at all other points. Examining Equation **8-1**, we draw Figure **8–2** and see that each interpolation function has the shape of a peaked "hat," and that interpolation is a linear combination of these hat functions, scaled by the data value at each point.

Equation **8-4** is the general form for cell interpolation. It is used to interpolate any data value defined at the cell points to any other point within the cell. We have only to define the specific interpolation functions W_i for each cell type.

ClearCorrect Exhibit 1002, Page 2339 of 3373

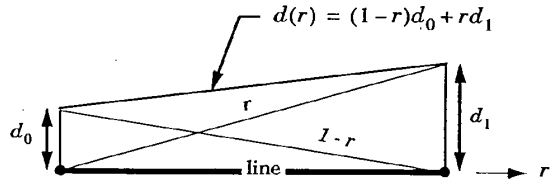


Figure 8–2 Interpolation is a linear combination of local interpolation functions. Interpolation functions are scaled by data values at cell points.

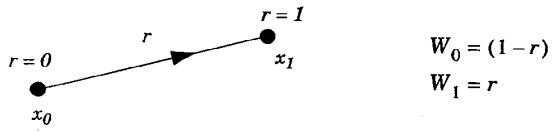


Figure 8–3 Parametric coordinate system and interpolation functions for a line.

Specific Forms

Each cell type has its own interpolation functions. The weights W_i are functions of the parametric coordinates r, s, and t. In this section we will define the parametric coordinate system and interpolation function for each primary cell type. Composite cells use the interpolation functions and parametric coordinates of their composing primary cells. The only difference in coordinate system specification between primary and composite cells is that composite cells use the additional sub-id to specify a particular primary cell.

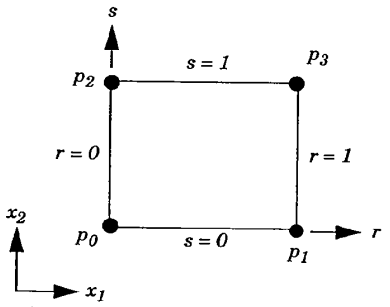
Vertex. Vertex cells do not require parametric coordinates or interpolation functions since they are zero-dimensional. The single weighting function is $W_0 = 1$.

Line. Figure 8–3 shows the parametric coordinate system and interpolation functions for a line. The line is described using the single parametric coordinate r.

Pixel. Figure 8–4 shows the parametric coordinate system and interpolation functions for a pixel cell type. The pixel is described using the two parametric coordinates (r,s). Note that the pixel edges are constrained to lie parallel to the global coordinate axes. These are often referred to as *bilinear interpolation* functions.

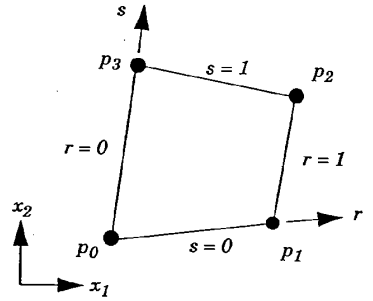
Quadrilateral. Figure 8–5 shows the parametric coordinate system and interpolation functions for a quadrilateral cell type. The quadrilateral is described using the two parametric coordinates (r,s).

ClearCorrect Exhibit 1002, Page 2340 of 3373



$$W_0 = (1-r)(1-s)$$
$$W_1 = r(1-s)$$
$$W_2 = (1-r)s$$
$$W_3 = rs$$

Figure 8–4 Parametric coordinate system and interpolation functions for a pixel.



$$W_0 = (1-r)(1-s)$$
$$W_1 = r(1-s)$$
$$W_2 = rs$$
$$W_3 = (1-r)s$$

Figure 8–5 Parametric coordinate system and interpolation functions for a quadrilateral.

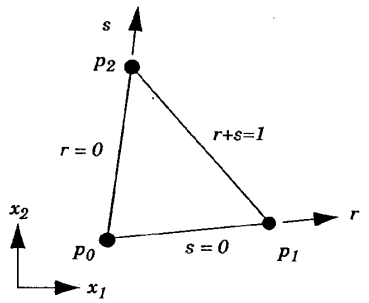
Triangle. Figure **8–6** shows the parametric coordinate system and interpolation functions for a triangle cell type. The triangle is characterized using the two parametric coordinates *(r,s)*.

Polygon. Figure **8–7** shows the parametric coordinate system and interpolation functions for a polygon cell type. The polygon is characterized using the two parametric coordinates *(r,s)*. The parametric coordinate system is defined by creating a rectangle oriented along the first edge of the polygon. The rectangle also must bound the polygon.

The polygon poses a special problem since we do not know how many vertices define the polygon. As a result, it is not possible to create general interpolation functions in the fashion of the previous functions we have seen. Instead, we use a function based on weighted distance squared from each polygon vertex.

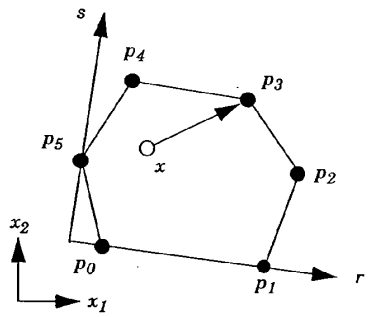
The weighted distance squared interpolation functions work well in practice. However, there are certain rare cases where points topologically distant

ClearCorrect Exhibit 1002, Page 2341 of 3373



$$W_0 = 1 - r - s$$
$$W_1 = r$$
$$W_2 = s$$

Figure 8–6 Parametric coordinate system and interpolation functions for a triangle.



$$W_i = \frac{\left(\frac{1}{r_i}\right)^2}{\sum\left(\frac{1}{r_i}\right)^2}$$

$$r_i = |p_i - x|$$

Figure 8–7 Parametric coordinate system and interpolation functions for a polygon.

from the interior of a polygon have an undue effect on the polygon interior (Figure **8–8**). These situations occur only if the polygon is concave and wraps around on itself.

Tetrahedron. Figure **8–9** shows the parametric coordinate system and interpolation functions for a tetrahedron cell type. The tetrahedron is described using the three parametric coordinates *(r,s,t)*.

Voxel. Figure **8–10** shows the parametric coordinate system and interpolation functions for a voxel cell type. The voxel is described using the three parametric coordinates *(r,s,t)*. Note that the voxel edges are constrained to lie parallel to the global coordinate axes. These are often referred to as *trilinear interpolation* functions.

ClearCorrect Exhibit 1002, Page 2342 of 3373

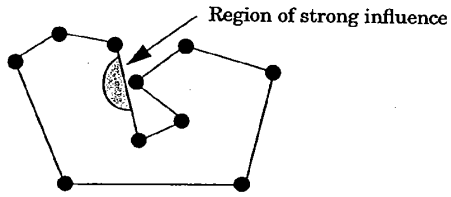
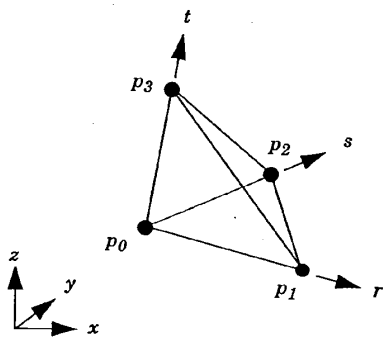
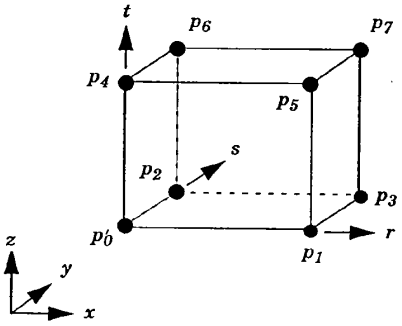


Figure 8–8 Potential problem with distance-based interpolation functions.



$$W_0 = 1 - r - s - t$$
$$W_1 = r$$
$$W_2 = s$$
$$W_3 = t$$

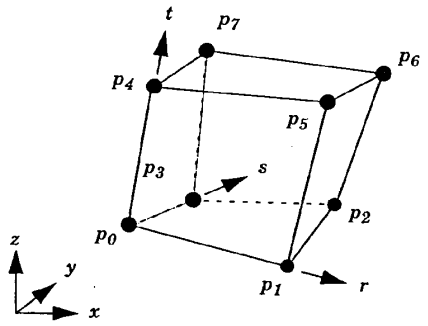
Figure 8–9 Parametric coordinate system and interpolation functions for a tetrahedron.



$$W_0 = (1-r)(1-s)(1-t)$$
$$W_1 = r(1-s)(1-t)$$
$$W_2 = (1-r)\,s(1-t)$$
$$W_3 = rs(1-t)$$
$$W_4 = (1-r)(1-s)t$$
$$W_5 = r(1-s)t$$
$$W_6 = (1-r)s\,t$$
$$W_7 = rst$$

Figure 8–10 Parametric coordinate system and interpolation functions for a voxel.

ClearCorrect Exhibit 1002, Page 2343 of 3373



$$W_0 = (1-r)(1-s)(1-t)$$
$$W_1 = r(1-s)(1-t)$$
$$W_2 = rs\,(1-t)$$
$$W_3 = (1-r)s(1-t)$$
$$W_4 = (1-r)(1-s)t$$
$$W_5 = r(1-s)t$$
$$W_6 = rst$$
$$W_7 = (1-r)st$$

Figure 8–11 Parametric coordinate system and interpolation functions for a hexahedron.

Hexahedron. Figure **8–11** shows the parametric coordinate system and interpolation functions for a hexahedron cell type. The hexahedron is described using the three parametric coordinates *(r,s,t)*.

8.3 Coordinate Transformation

Coordinate transformation is a common visualization operation. This may be either transformation from dataset coordinates to global coordinates, or global coordinates to dataset coordinates.

Dataset to Global Coordinates

Transforming between dataset coordinates and global coordinates is straightforward. We start by identifying a primary cell using the cell id and sub-id. Then the global coordinates are generated from the parametric coordinates by using the interpolation functions of Equation **8-4**. Given cell points $p_i = p_i(x_i, y_i, z_i)$ the global coordinate p is simply

$$p = \sum_{i=0}^{n-1} W_i(r_0, s_0, t_0)p_i \qquad \textbf{(8-7)}$$

where the interpolation weights W_i are evaluated at the parametric coordinate (r_0, s_0, t_0).

In the formulation presented here, we have used the same order interpolation functions for both data and cell geometry. (By order we mean the polynomial degree of the interpolating polynomials.) This is termed *iso-parametric* interpolation. It is possible to use different interpolation functions for geometry and data. *Super-parametric* interpolation is used when the order of the interpolation

ClearCorrect Exhibit 1002, Page 2344 of 3373

functions for geometry is greater than those used for data. *Sub-parametric* interpolation is used when the order of the interpolation functions for geometry is less than those used for data. Using different interpolation functions is commonly used in numerical analysis techniques such as the finite element method. We will always use the iso-parametric interpolation for visualization applications.

Global to Dataset Coordinates

Global to dataset coordinate transformations are expensive compared to dataset to global transformations. There are two reasons for this. First, we must identify the particular cell C_i that contains the global point p. Second, we must solve Equation **8-4** for the parametric coordinates of p.

To identify the cell C_i means doing some form of searching. A simple but inefficient approach is to visit every cell in a dataset and determine whether p lies inside any cell. If so, then we have found the correct cell and stop the search. Otherwise, we check the next cell in the list.

This simple technique is not fast enough for large data. Instead, we use accelerated search techniques. These are based on spatially organizing structures such as an octree or three-dimensional hash table. The idea is as follows: we create a number of "buckets," or data place holders, that are accessed by their location in global space. Inside each bucket we tag all the points or cells that are partially or completely inside the bucket. Then, to find a particular cell that contains point p, we find the bucket that contains p, and obtain all the cells associated with the bucket. We then evaluate inside/outside for this abbreviated cell list to find the single cell containing p. (See "Searching" on page 325 for a more detailed description.)

The second reason that global to dataset coordinate transformation is expensive is because we must solve the interpolation function for the parametric coordinates of p. Sometimes we can do this analytically, but in other cases we must solve for the parametric coordinates using numerical techniques.

Consider the interpolation functions for a line (Figure **8–2**). We can solve this equation exactly and find that

$$r = \frac{(x - x_0)}{(x_1 - x_0)} = \frac{(y - y_0)}{(y_1 - y_0)} = \frac{(z - z_0)}{(z_1 - z_0)} \qquad \textbf{(8-8)}$$

Similar relations exist for any cell whose interpolation functions are linear combinations of parametric coordinates. This includes vertices, lines, triangles, and tetrahedra. The quadrilateral and hexahedron interpolation functions are nonlinear because they are products of linear expressions for the parametric coordinates. As a result, we must resort to numerical techniques to compute global to dataset coordinate transformations. The interpolation functions for pixels and voxels are nonlinear as well, but because of their special orientation with respect to the x, y, and z coordinate axes, we can solve them exactly. (We will treat pixel and voxel types in greater depth in "Special Techniques for Structured Points" on page 329.)

ClearCorrect Exhibit 1002, Page 2345 of 3373

To solve the interpolation functions for parametric coordinates we must use nonlinear techniques for the solution of a system of equations. A simple and effective technique is Newton's method [Conte72].

To use Newton's method we begin by defining three functions for the known global coordinate $p = p(x,y,z)$ in terms of the interpolation functions $W_i = W_i(r,s,t)$

$$\begin{aligned} f(r,s,t) &= 0 = x - \sum W_i x_i \\ g(r,s,t) &= 0 = y - \sum W_i y_i \\ h(r,s,t) &= 0 = z - \sum W_i z_i \end{aligned} \tag{8-9}$$

and then, expanding the functions using a Taylor's series approximation,

$$\begin{aligned} f &= 0 = f_0 + \frac{\partial f}{\partial r}(r - r_0) + \frac{\partial f}{\partial s}(s - s_0) + \frac{\partial f}{\partial t}(t - t_0) + \ldots \\ g &= 0 = g_0 + \frac{\partial g}{\partial r}(r - r_0) + \frac{\partial g}{\partial s}(s - s_0) + \frac{\partial g}{\partial t}(t - t_0) + \ldots \\ h &= 0 = h_0 + \frac{\partial h}{\partial r}(r - r_0) + \frac{\partial h}{\partial s}(s - s_0) + \frac{\partial h}{\partial t}(t - t_0) + \ldots \end{aligned} \tag{8-10}$$

we can develop an iterative procedure to solve for the parametric coordinates. This yields the general form

$$\begin{bmatrix} r_{i+1} \\ s_{i+1} \\ t_{i+1} \end{bmatrix} = \begin{bmatrix} r_i \\ s_i \\ t_i \end{bmatrix} - \begin{bmatrix} \frac{\partial f}{\partial r} & \frac{\partial f}{\partial s} & \frac{\partial f}{\partial t} \\ \frac{\partial g}{\partial r} & \frac{\partial g}{\partial s} & \frac{\partial g}{\partial t} \\ \frac{\partial h}{\partial r} & \frac{\partial h}{\partial s} & \frac{\partial h}{\partial t} \end{bmatrix}^{-1} \begin{bmatrix} f_i \\ g_i \\ h_i \end{bmatrix} \tag{8-11}$$

Fortunately, Newton's method converges quadratically (if it converges) and the interpolation functions that we have presented here are well behaved. In practice, Equation **8-11** converges in just a few iterations.

8.4 Computing Derivatives

Interpolation functions enable us to compute data values at arbitrary locations within a cell. They also allow us to compute the rate of change, or derivatives, of data values. For example, given displacements at cell points we can compute cell strains and stresses — or, given pressure values, we can compute the pressure gradient at a specified location.

To introduce this process, we will begin by examining the simplest case:

ClearCorrect Exhibit 1002, Page 2346 of 3373

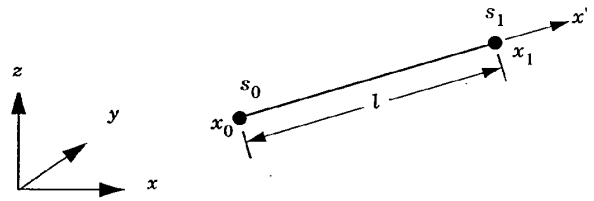


Figure 8–12 Computing derivatives in an 1D line cell.

computing derivatives in a 1D line (Figure **8–12**). Using geometric arguments, we can compute the derivatives in the r parametric space according to

$$\frac{ds}{dr} = \frac{(s_1 - s_0)}{1} = (s_1 - s_0) \tag{8-12}$$

where s_i is the data value at point i. In the local coordinate system x', which is parallel to the r coordinate system (that is, it lies along the vector $\vec{x}_1 - \vec{x}_0$), the derivative is

$$\frac{ds}{dx'} = \frac{(s_1 - s_0)}{l} \tag{8-13}$$

where l is the length of the line.

Another way to derive Equation **8-13** is to use the interpolation functions of Figure **8–3** and the chain rule for derivatives. The chain rule

$$\frac{d}{dr} = \frac{d}{dx'} \cdot \frac{d}{dr}x' \tag{8-14}$$

allows us to compute the derivative d/dx' using

$$\frac{d}{dx'} = \left(\frac{d}{dr}\right) \Big/ \frac{d}{dr}x' \tag{8-15}$$

With the interpolation functions we can compute the x' derivatives with respect to r as

$$\frac{d}{dr}x' = \frac{d}{dr}\left(\sum_{i=0}^{1} W_i \cdot x'_i\right) = -x_0' + x_1' = l \tag{8-16}$$

which, when combined with Equation **8-15** and Equation **8-12** for the s derivatives, yields Equation **8-13**.

One final step remains. The derivatives in the $\vec{x}$ coordinate system must be converted to the global x-y-z system. We can do this by creating a unit vector $\vec{v}$

ClearCorrect Exhibit 1002, Page 2347 of 3373

as

$$\vec{v} = \frac{(\vec{x}_1 - \vec{x}_0)}{|x_1 - x_0|} \tag{8-17}$$

where $\vec{x}_0$ and $\vec{x}_1$ are the locations of the two end points of the line. Then the derivatives in the x, y, and z directions can be computed by taking the dot products along the axes.

$$\begin{aligned}
\frac{ds}{dx} &= \left(\frac{s_1 - s_0}{l}\right)\vec{v} \cdot (1, 0, 0) \\
\frac{ds}{dy} &= \left(\frac{s_1 - s_0}{l}\right)\vec{v} \cdot (0, 1, 0) \\
\frac{ds}{dz} &= \left(\frac{s_1 - s_0}{l}\right)\vec{v} \cdot (0, 0, 1)
\end{aligned} \tag{8-18}$$

To summarize this process, derivatives are computed in the local r-s-t parametric space using cell interpolation. These are then transformed into a local $x' - y' - z'$ Cartesian system. Then, if the $x' - y' - z'$ system is not aligned with the global $x - y - z$ coordinate system, another transformation is required to generate the result.

We can generalize this process to three dimensions. From the chain rule for partial derivatives

$$\begin{aligned}
\frac{\partial}{\partial x} &= \frac{\partial}{\partial r}\frac{\partial r}{\partial x} + \frac{\partial}{\partial s}\frac{\partial s}{\partial x} + \frac{\partial}{\partial t}\frac{\partial t}{\partial x} \\
\frac{\partial}{\partial y} &= \frac{\partial}{\partial r}\frac{\partial r}{\partial y} + \frac{\partial}{\partial s}\frac{\partial s}{\partial y} + \frac{\partial}{\partial t}\frac{\partial t}{\partial y} \\
\frac{\partial}{\partial z} &= \frac{\partial}{\partial r}\frac{\partial r}{\partial z} + \frac{\partial}{\partial s}\frac{\partial s}{\partial z} + \frac{\partial}{\partial t}\frac{\partial t}{\partial z}
\end{aligned} \tag{8-19}$$

or after rearranging

$$\begin{bmatrix} \frac{\partial}{\partial r} \\ \frac{\partial}{\partial s} \\ \frac{\partial}{\partial t} \end{bmatrix} = \begin{bmatrix} \frac{\partial x}{\partial r} & \frac{\partial y}{\partial r} & \frac{\partial z}{\partial r} \\ \frac{\partial x}{\partial s} & \frac{\partial y}{\partial s} & \frac{\partial z}{\partial s} \\ \frac{\partial x}{\partial t} & \frac{\partial y}{\partial t} & \frac{\partial z}{\partial t} \end{bmatrix} \begin{bmatrix} \frac{\partial}{\partial x} \\ \frac{\partial}{\partial y} \\ \frac{\partial}{\partial z} \end{bmatrix} = J \begin{bmatrix} \frac{\partial}{\partial x} \\ \frac{\partial}{\partial y} \\ \frac{\partial}{\partial z} \end{bmatrix} \tag{8-20}$$

The 3×3 matrix J is called the Jacobian matrix, and it relates the parametric coordinate derivatives to the global coordinate derivatives. We can rewrite

ClearCorrect Exhibit 1002, Page 2348 of 3373

Equation **8-20** into more compact form

$$\frac{\partial}{\partial r_i} = J\frac{\partial}{\partial x_i} \tag{8-21}$$

and solve for the global derivatives by taking the inverse of the Jacobian matrix

$$\frac{\partial}{\partial x_i} = J^{-1}\frac{\partial}{\partial r_i} \tag{8-22}$$

The inverse of the Jacobian always exists as long as there is a one-to-one correspondence between the parametric and global coordinate systems. This means that for any *(r, s, t)* coordinate, there corresponds only one *(x, y, z)* coordinate. This holds true for any of the parametric coordinate systems presented here, as long as pathological conditions such as cell self-intersection or a cell folding in on itself are avoided. (An example of cell folding is when a quadrilateral becomes nonconvex.)

In our one-dimensional example, the derivatives along the line were constant. However, other interpolation functions (e.g., Figure **8–5**) may yield nonconstant derivatives. Here, the Jacobian is a function of position in the cell and must be evaluated at a particular *(r, s, t)* coordinate value.

8.5 Topological Operations

Many visualization algorithms require information about the topology of a cell or dataset. Operations that provide such information are called *topological operations*. Examples of these operations include obtaining the topological dimension of a cell, or accessing neighboring cells that share common edges or faces. We might use these operations to decide whether to render a cell (e.g., render only one-dimensional lines) or to propagate particles through a flow field (e.g., traversing cells across common boundaries).

Before proceeding we need to define some terms from topology. *Manifold topology* describes a region surrounding a point that is topologically connected. That is, a region around the point is topologically equivalent to a small "disk" (in two-dimensions) or "ball" (in three-dimensions). Topology that is not manifold is termed *nonmanifold*. Examples of manifold and nonmanifold geometry are shown in Figure **8–13**.

There are some simple rules we can use to decide whether a surface or region approximated with cells is manifold or nonmanifold. In two dimensions, if every edge of a two-dimensional cell is used by exactly one other cell, than the surface is locally manifold. In three dimensions, if every face of a three-dimensional cell is used by exactly one other cell, than the region is locally manifold.

We also will use the term *simplex* on some occasions. A simplex of dimension n is the convex region defined by a set of $n+1$ independent points. A vertex, line, triangle, and tetrahedron are simplices of dimension 0, 1, 2, and 3, respectively. These are shown in Figure **8–14**.

ClearCorrect Exhibit 1002, Page 2349 of 3373

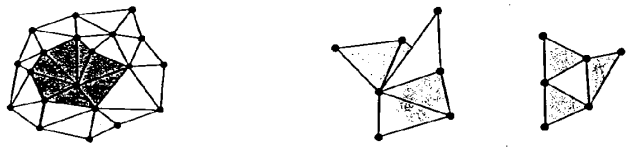


Figure 8–13 Manifold and nonmanifold surface topology. If the local neighborhood around a vertex is topologically a 2D disk (i.e., a small disk can be placed on the surface without tearing or overlapping), then the surface is manifold at that vertex.

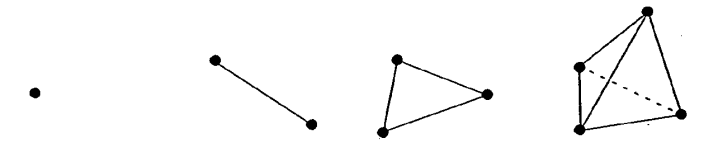


Figure 8–14 Simplices of dimension three and lower.

Cell Operations

Cell operations return information about the topology of a cell. Typically, we want to know the topological order of the cell or the topology of the cell boundary.

Given a cell C_i of topological dimension d, the cell is (implicitly) composed of boundary cells of topological order d-1 and lower. For example, a tetrahedron is composed of four two-dimensional triangles, six one-dimensional edges, and four zero-dimensional vertices. Cell operations return information about the number of boundary cells of a particular topological dimension, as well as the ordered list of points that define each bounding cell.

Another useful cell operation returns the closest boundary cell of dimension d-1 given the parametric coordinates of the cell. This operation ties the geometry to the topology of the cell, as compared to the parametric coordinate system, which ties the topology to the geometry. The closest boundary cell operation is implemented by partitioning each cell into various regions, as illustrated in Figure 8–15. To determine the closest boundary cell we need only to identify the parametric region that the point lies in, and then return the appropriate boundary cell.

Another useful cell operation is cell decomposition into simplices. Every cell can be decomposed into a collection of simplices. By doing so, and by operating on the simplex decomposition rather than the cell itself, we can create algorithms that are independent of cell type. For example, if we want to intersect two

ClearCorrect Exhibit 1002, Page 2350 of 3373

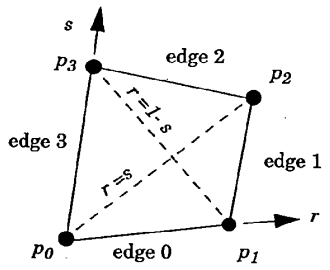


Figure 8–15 Closest boundary cell operation for quadrilateral cell.

datasets of varied cell type, without simplex decomposition we would have to create methods to intersect every possible combination of cells. With simplex decomposition, we can create a single intersection operation that operates on only the limited set of simplices. The significant advantage of this approach is that as new cells are added to the visualization system, only the cell object (including its method for simplex decomposition) must be implemented, and no other objects need be modified.

Dataset Operations

Dataset operations return information about the topology of a dataset or topological information about the adjacency of cells. Typical operations include determining the neighbors of a cell or returning a list of all cells that use a particular point.

We can formalize the adjacency operations by continuing the discussion of "Cell Types" on page 119. Adjacency methods are used to obtain information about the neighbors of a cell. A neighbor of a particular cell C_i is simply a cell that shares one or more points in common with C_i. A vertex neighbor is a neighbor that shares one or more vertices. An edge neighbor is a neighbor that shares one or more edges. A face neighbor is a cell that shares vertices that define one of the faces of the cell. Note that a face neighbor is also an edge neighbor, and an edge neighbor is also a vertex neighbor.

The adjacency operators are simple set operations. For a particular cell C_i defined by points

$$C_i = \{p_1, p_2, ..., p_n\} = P \tag{8-23}$$

and a point list $\bar{P} = (\bar{p}_1, \bar{p}_2, ..., \bar{p}_n)$ with $\bar{P} \subset P$, where $\bar{P}$ typically corresponds to the points defining a boundary cell of C_i; the neighbors of C_i are the adjacency set $A(\bar{C}, \bar{P})$. The adjacency set is simply the intersection of the use sets for each

ClearCorrect Exhibit 1002, Page 2351 of 3373

point, excluding the cell C_i.

$$A(C_i, \bar{P}) = \left(\bigcap_{i=1}^{n} U(\bar{p}_i) \right) - C_i \quad \textbf{(8-24)}$$

The adjacency set represents a variety of useful information. In a manifold object represented by a polyhedra, for example, each polygon must have exactly one edge neighbor for each of its edges. Edges that have no neighbors are boundary edges; edges that have more than one edge neighbor represent nonmanifold topology. Datasets that consist of three-dimensional cells (e.g., unstructured grids) are topologically consistent only if, for each cell, there is exactly one face neighbor for each face. Faces that have no neighbors are on the boundary of the dataset. More than one face neighbor implies that the neighbors are self-intersecting (in 3D space).

8.6 Searching

Searching is an operation to find the cell containing a specified point p, or to locate cells or points in a region surrounding p. Algorithms requiring this operation include streamline generation, where we need to find the starting location within a cell; probing, where the data values at a point are interpolated from the containing cell; or collision detection, where cells in a certain region must be evaluated for intersection. Sometimes (e.g., structured point datasets), searching is a simple operation because of the regularity of data. However, in less structured data, the searching operation is more complex.

To find the cell containing p, we can use the following naive search procedure. Traverse all cells in the dataset, finding the one (if any) that contains p. To determine whether a cell contains a point, the cell interpolation functions are evaluated for the parametric coordinates (r,s,t). If these coordinates lie within the cell, then p lies in the cell. The basic assumption here is that cells do not overlap, so that at most a single cell contains the given point p. To determine cells or points lying in the region surrounding p, we can traverse cells or points to see whether they lie within the region around p. For example, we can choose to define the region as a sphere centered at p. Then, if a point or the points composing a cell lie in the sphere, the point or cell is considered to be in the region surrounding p.

These naive procedures are unacceptable for all but the smallest datasets, since they are of order $O(n)$, where n is the number of cells or points. To improve the performance of searching, we need to introduce supplemental data structures to support spatial searching. Such structures are well-known and include MIP maps, octrees, kd-trees, and binary sphere trees (see "Bibliographic Notes" on page 350 at the end of this chapter).

The basic idea behind these spatial search structures is that the search space is subdivided into smaller parts, or buckets. Each bucket contains a list of the points or cells that lie within it. Buckets are organized in structured fashion

ClearCorrect Exhibit 1002, Page 2352 of 3373

so that constant or logarithmic time access to any bucket is possible. For example, if we assign a portion of 2D Euclidean space into a grid of n by m buckets, the location of p in a particular bucket can be determined with two subtractions and two divisions: a constant time access. Similarly, the location of p in a non-uniformly subdivided octree is determined in logarithmic time, since recursive insertion into octant children is required. Once the bucket is found, the search is then limited to the points or cells contained within it. In a properly designed spatial search structure, the number of points or cells in a bucket is a small portion of the total number of cells and less then a fixed value. Thus, the time to search within a bucket can be bounded by a fixed constant. The result is that introducing spatial search structures reduces search times to a maximum $O(log\ n)$, or better yet $O(n)$.

We have two options when applying spatial search structures. We may insert points into the search structure, or we may insert cells, depending on the application. There are advantages and disadvantages to both approaches. Inserting cells into buckets is not a trivial operation. In general, cells are arbitrarily oriented and shaped, and will not fit completely into a single bucket. As a result, cells often span multiple buckets. To reliably determine whether a cell is in a bucket requires geometric intersection tests, a costly operation. Another approach is to use the *bounding box* of a cell to decide which bucket(s) a cell belongs in. We only need to intersect the bounding box with a bucket to determine whether the cell may belong in the bucket. Unfortunately, even though this operation is generally fast, often cells are associated with buckets even though they may not actually lie inside them, wasting (in large models) memory resources and extra processing time.

Inserting points into a search structure is easier because points can be uniquely placed into a bucket. Inserting points also allows us to search for both points *and* cells. Cells can be found by using p to index into the appropriate bucket. The closest point(s) p_i to p are then located. Using the topological adjacency operator to retrieve the cells using points p_i, we can then search these cells for the cell containing p. This procedure must be used with caution, however, since the closest points may not be used by the cells containing p (Figure **8–16**).

8.7 Cell / Line Intersection

An important geometric operation is intersection of a line with a cell. This operation can be used to interactively select a cell from the rendering window, to perform ray-casting for rendering, or to geometrically query data.

In the *Visualization Toolkit* each cell must be capable of intersecting itself against a line. Figure **8–17** summarizes these operations for the nine primitive cell types supported by **vtk**. (Intersections on composite cells are implemented by intersecting each primitive cell in turn.)

Line/cell intersection for 0D, 1D, and 2D cells follows standard approaches. Intersection against 3D cells is difficult. This is because the surfaces of these cells are described parametrically and are not necessarily planar. For example, to

ClearCorrect Exhibit 1002, Page 2353 of 3373

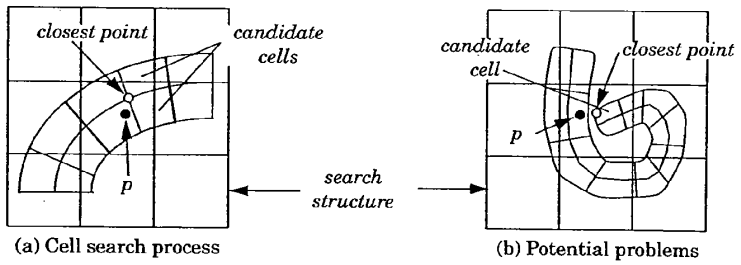


Figure 8–16 Using search structure (containing points) to find cells. (a) Points are associated with appropriate bucket. Point p is used to index into bucket, and closest point(s) p_i is found. Cells using p_i are evaluated for the cell containing p. (b) Sometimes closest points p_i are not used by cells containing p.

intersect a line with a tetrahedron, we can intersect the line against the four triangular faces of the tetrahedron. Hexahedron, however, may have nonplanar faces. Thus, we cannot intersect the line against six quadrilateral, planar faces. Instead, we use line/face intersection as an initial guess, and project the intersection point onto the surface of the cell. This produces an approximate result, but is accurate enough for most applications.

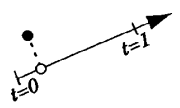
8.8 Scalars and Colors

There is a close correspondence between scalar data and colors. We saw this in "Color Mapping" on page 155, where we saw how to use a color table to map scalar values into a color specification (i.e., red, green, and blue, or *RGB*). There are cases, however, when we want to circumvent this mapping process. Such cases occur when color data is supplied instead of scalar data.

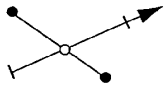
A common example occurs in imaging. Recall that an image is a regular, two-dimensional array of points. The points define pixels, which in turn form a two-dimensional structured points dataset. Images are frequently stored as a pair of dimensions along with data values. The data values may be one of black and white (e.g., a bitmap), grayscale, or color (e.g., a pixmap). Bitmaps and grayscale images can be directly cast into the form of single-values scalar data, and we can use our earlier approach. Pixmaps, however, consist of (at a minimum) three values per pixel of red, green, and blue. (Sometimes, a fourth alpha opacity value may also be included.) Thus, pixmaps cannot be directly cast into scalar form.

To accommodate color data, special types of scalar objects need to be created. Each class must act as if it were a scalar: that is, a request for data at a particular point must return a *single* scalar value. This allows us to use standard scalar visualization techniques such as contouring or warping. Thus a mapping

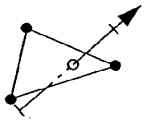
ClearCorrect Exhibit 1002, Page 2354 of 3373



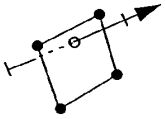
Vertex
- project point onto ray
- distance to line must be within tolerance
- t must lie between [0,1]



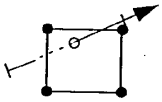
Line
- 3D line intersection
- distance between lines must be within tolerance
- s,t must lie between [0,1]



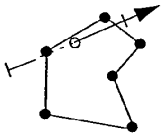
Triangle
- line/plane intersection
- intersection point must lie in triangle
- t must lie between [0,1]



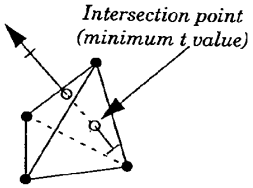
Quadrilateral
- line/plane intersection
- intersection point must lie in quadrilateral
- t must lie between [0,1]



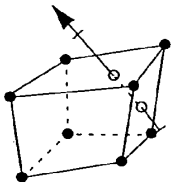
Pixel
- line/plane intersection
- intersection point must lie in pixel (uses efficient in/out test)
- t must lie between [0,1]



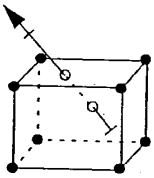
Polygon
- line/plane intersection
- intersection point must lie in polygon (uses ray casting for polygon in/out)
- t must lie between [0,1]



Tetrahedron
- intersect each (triangle) face
- t must lie between [0,1]



Hexahedron
- intersect each (quadrilateral) face
- since face may be non-planar, project previous result onto hexahedron surface
- t must lie between [0,1]



Voxel
- intersect each (pixel) face
- t must lie between [0,1]

Figure 8–17 Summary of line/cell intersection operations for nine primitive cell types. Line is assumed normalized in parametric coordinate t with $0 \le t \le 1$.

ClearCorrect Exhibit 1002, Page 2355 of 3373

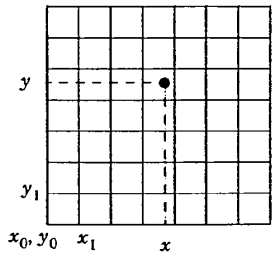


Figure 8–18 Structured point coordinate transformation.

from *RGB* or *RGBA* color coordinates to a single scalar value is required.

One simple mapping returns the *luminance* Y of a color. Given three components, *RGB*, the luminance is

$$Y = 0.30R + 0.59G + 0.11B \tag{8-25}$$

If the color includes transparency, *RGBA*, the luminance is

$$Y = A(0.30R + 0.59G + 0.11B) \tag{8-26}$$

Using this abstraction allows us to treat single-valued scalars and scalars consisting of multivalued colors the same. The end result is that we can mix both types of scalar data into our visualization networks.

8.9 Special Techniques for Structured Points

A significant attraction of the structured points dataset is the speed and simplicity of computation. In this section, we will explore specific techniques that exploit the special regular topology and geometry of structured point datasets.

Coordinate Transformation

Given a point p we can find the structured coordinates by performing three division operations (Figure **8–18**). Taking the integer `floor` function yields the structured coordinates. Taking the fractional part of the result yields the parametric coordinates of the cell. We can then use Equation **8-3** to convert to dataset coordinates.

Derivative Computation

Because the structured point dataset is oriented parallel to the coordinate x, y, and z axes, and because the spacing of points in each of these directions is regu-

ClearCorrect Exhibit 1002, Page 2356 of 3373

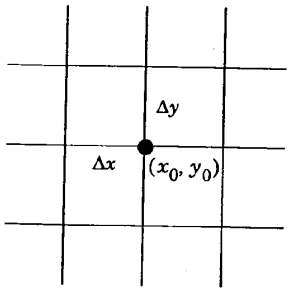


Figure 8–19 Using finite differences to compute derivatives on structured points dataset.

lar, finite difference schemes can be used to compute partial derivatives at the cell points. Referring to Figure **8–19**, we see that central differences can be used in each of the three directions according to

$$\begin{aligned} g_x &= \frac{d(x_0+\Delta x, y_0, z_0) - d(x_0-\Delta x, y_0, z_0)}{2\Delta x} \\ g_y &= \frac{d(x_0, y_0+\Delta y, z_0) - d(x_0, y_0-\Delta y, z_0)}{2\Delta y} \\ g_z &= \frac{d(x_0, y_0, z_0+\Delta z) - d(x_0, y_0, z_0-\Delta z)}{2\Delta z} \end{aligned} \tag{8-27}$$

(Note that at the boundary of the dataset, one-sided differences may be used.) We can use these equations to compute derivatives within the cell as well. We simply compute the derivatives at each cell point from Equation **8-27**, and then use the cell interpolation functions to compute the derivative at the point inside the cell.

Topology

Structured datasets lend themselves to efficient topological operations (i.e., both structured points and structured grids). Given a cell id, it is possible to determine vertex, edge, or face neighbors using simple constant time operations. First, given the cell id in a three-dimensional structured dataset, we use a combination of division and modulo arithmetic to compute the structured coordinates

$$\begin{aligned} i &= id \text{ modulo } (n_x - 1) \\ j &= (id/(n_x - 1)) \text{ modulo } (n_y - 1) \\ k &= id/((n_x - 1)(n_y - 1)) \end{aligned} \tag{8-28}$$

ClearCorrect Exhibit 1002, Page 2357 of 3373

Face neighbors are determined by incrementing one of the i, j, or k indices. Edge neighbors are determined by incrementing any two indices, while vertex neighbors are found by incrementing all three indices. Care must be taken while incrementing to insure that the indices fall in the range

$$\begin{aligned} 0 \le i < (n_x - 1) \\ 0 \le j < (n_y - 1) \\ 0 \le k < (n_z - 1) \end{aligned} \tag{8-29}$$

An attempt to index outside these ranges indicates that the neighbor in question does not exist.

Searching

Given a point $p = (x, y, z)$ we can determine the cell containing p by using the equations given in Figure **8–18.** These equations generate the structured coordinates *(i, j, k)*, which can then be converted to cell id (i.e., dataset coordinates) using Equation **8-3.**

To find the closest point to p, we compute the structured coordinates by rounding to the nearest integer value (instead of using the floor function). Thus,

$$\begin{aligned} i &= \text{int}((x - x_0)/(x_1 - x_0)) \\ j &= \text{int}((y - y_0)/(y_1 - y_0)) \\ k &= \text{int}((z - z_0)/(z_1 - z_0)) \end{aligned} \tag{8-30}$$

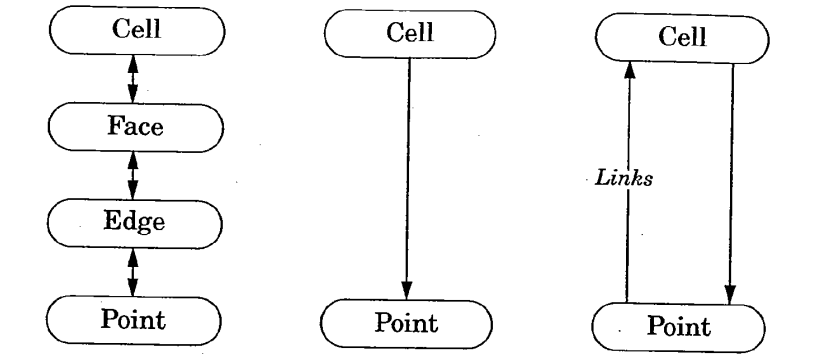
8.10 Putting It All Together

In this section we will finish our earlier description of an implementation for unstructured data. We also define a high-level, abstract interface for cells and datasets. This interface allows us to implement the general (i.e., dataset specific) algorithms in the *Visualization Toolkit*. We also describe implementations for color scalars, searching and picking, and conclude with a series of examples to demonstrate some of these concepts.

Unstructured Topology

In Chapter 5 we described data representations for the unstructured dataset types `vtkPolyData` and `vtkUnstructuredGrid`. Close examination of this data structure reveals that operations to retrieve topological adjacency are inefficient. In fact, to implement any operation to retrieve vertex, edge, or face neighbors requires a search of the cell array, resulting in *O(n)* time complexity. This is unacceptable for all but the smallest applications, since any algorithm travers-

ClearCorrect Exhibit 1002, Page 2358 of 3373



(a) Hierarchical topological structure

(b) Basic unstructured data representation

(c) Full unstructured data representation

Figure 8–20 Enhancing hierarchical unstructured data representation. (a) Conventional topological hierarchy for geometric model. (b) Basic unstructured data hierarchy. (c) Full unstructured data hierarchy. By introducing upward references from points to cells, the unstructured data hierarchy may be efficiently traversed in both directions, and is more compact than conventional topological hierarchies.

ing the cell array and retrieving adjacency information is at a minimum $O(n^2)$.

The reason for this inefficiency is that the data representation is a "downward" hierarchy (Figure **8–20**(b)). That is, given a cell we can quickly determine the topological features lower in the topological hierarchy such as faces, edges, and points. However, given a face, edge, or point we must search the cell array to determine the owning cells. To improve the efficiency of this data representation, we must introduce additional information into the hierarchy that allows "upward" hierarchy traversal (similar to that shown in Figure **8–20**(a)).

The solution to this problem is to extend the unstructured data structure with *cell links*. The cell links array is a list of lists of cells that use each point and corresponds to the upward links of Figure **8–20**(c). The cell links array transforms the hierarchical structure of Figure **5–10** into a ring structure. Cells reference their composing points, and points in turn reference the cells that use them. The full unstructured data structure is shown in Figure **8–21**.

The cell links array is in fact an implementation of the use sets of Equation **5-1**. We can use this equation to compute adjacency operation in constant time, if the maximum number of cells using a point is much smaller than the number of points in a dataset. To see this, we refer to Equation **8-24** and see that the adjacency operations consist of a finite number of set intersections. Each operation is an intersection of the link lists for each point. If the number of cells in each link list is "small," then the intersection operation can be bounded by a fixed constant in time, and the total operation can be considered a constant time operation.

ClearCorrect Exhibit 1002, Page 2359 of 3373

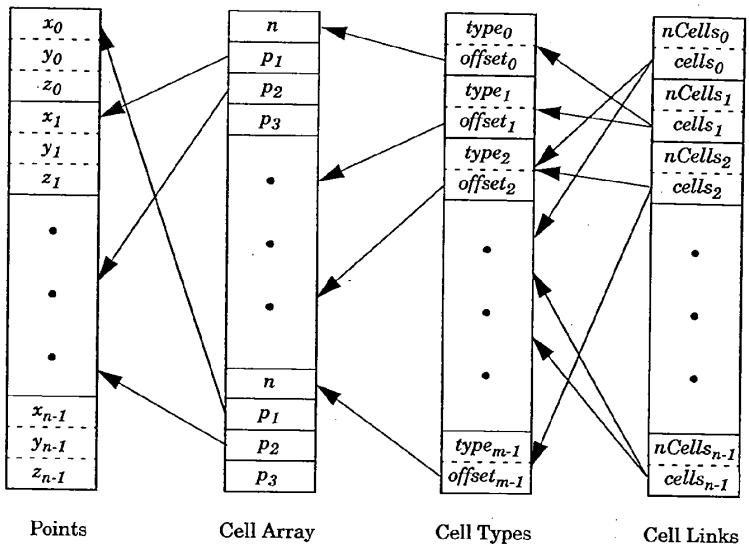


Figure 8–21 Complete unstructured data representation including link lists. There are m cells and n points. The n structures in the link list are lists of cells that use each vertex. Each link list is variable in length.

There are several important characteristics of this data representation.

- The cell links array is an extension of the basic unstructured data representation. As a result, we can defer the construction of the cell links until they are required. Often the cell links are never needed and require no computer resources to compute or store.
- Building the cell links is a linear $O(n)$ operation. Each cell is traversed and for every point that the cell uses, the list of using cells for that point is extended to include the current cell. Building the cell links is only needed once as an initialization step.
- The data representation is compact relative to other topology representation schemes (e.g., the winged-edge structure and the radial-edge structures [Baumgart74] [Weiler88]). These other data structures contain explicit representation of intermediate topology such as edges, loops, faces, or special adjacency information such as adjacent edges (winged-edge structure) or extensive "use" descriptions (radial-edge structure). The compactness of representation is particularly important for visualization, since the data size is typically large.

ClearCorrect Exhibit 1002, Page 2360 of 3373

The unstructured data structure in the *Visualization Toolkit* is implemented using the four classes `vtkPoints` (and subclasses), `vtkCellArray`, `vtkCellTypes`, and `vtkCellLinks`. The building of this data structure is incremental. At a minimum, the points and cells are represented using `vtkPoints` and `vtkCellArray`. If random access or extra type information is required, then the object `vtkCellTypes` is used. If adjacency information is required, an instance of the class `vtkCellLinks` is created. These operations are carried out behind the scenes, and generally do not require extra knowledge by the application programmer.

Abstract Interfaces

With the completion of Chapters 5 and 8, we can summarize the abstract interface for cells, datasets, and the point data attributes. These pseudo-code descriptions encapsulate the core functionality of the classes `vtkDataSet`, `vtkCell`, and `vtkPointData`, and their subclasses. All algorithms presented in this text can be implemented using combinations of these methods.

Dataset Abstraction. The dataset is the central data representation in **vtk**. Datasets are composed of one or more cells and points. Associated with the points are attribute data consisting of scalars, vectors, normals, texture coordinates, and user-defined data.

`type = GetDataType()`
Return the type of dataset (e.g., `vtkPolyData`, `vtkStructuredPoints`, `vtkStructuredGrid`, `vtkRectilinearGrid`, or `vtkUnstructuredGrid`).

`numPoints = GetNumberOfPoints()`
Return the number of points in the dataset.

`numCells = GetNumberOfCells()`
Return the number of cells in the dataset.

`GetPoint(ptId,x)`
Given a point id, return the *(x,y,z)* coordinates of the point.

`cell = GetCell(cellId)`
Given a cell id, return a pointer to a cell object.

`type = GetCellType(cellId)`
Return the type of the cell given by cell id.

`GetCellTypes(types)`
Return a list of types of cells that compose the dataset.

`cells = GetPointCells(ptId)`
Given a point id, return the cells that use this point.

ClearCorrect Exhibit 1002, Page 2361 of 3373

`GetCellPoints(cellId, ptIds)`
Given a cell id, return the point ids (e.g., connectivity list) defining the cell.

`GetCellNeighbors(cellId, ptIds, neighbors)`
Given a cell id and a list of points composing a boundary face of the cell, return the neighbors of that cell sharing the points.

`cellId = FindCell(x, cell, cellId, tol2, subId, pcoords, weights)`
Given a coordinate value x, an initial search cell defined by `cell` and `cellId`, and a tolerance measure (squared), return the cell id and sub-id of the cell containing the point and its interpolation function weights. The initial search cell is used to speed up the search process when the position x is known to be near the cell. If no cell is found, `cellId` < 0 is returned.

`pointData = GetPointData()`
Return a pointer to the object maintaining point attribute data. This includes scalars, vectors, normals, tensors, texture coordinates, and user-defined data.

`bounds = GetBounds()`
Get the bounding box of the dataset.

`length = GetLength()`
Return the length of the diagonal of the bounding box of the dataset.

`center = GetCenter()`
Get the center of the bounding box of the dataset.

`range = GetScalarRange()`
A convenience method to return the (minimum, maximum) range of the scalar attribute data associated with the dataset.

`dataSet = MakeObject()`
Make a copy of the current dataset. A "virtual" constructor. (Typically, reference counting methods are used to copy data.)

`CopyStructure(dataSet)`
Update the current structure definition (i.e., geometry and topology) with the supplied dataset.

Cell Abstraction. Cells are the atomic structures of **vtk**. Cells consist of a topology, defined by a sequence of ordered point ids, and a geometry, defined by point coordinates. The cell coordinate consists of a cell id, a subcell id, and a parametric coordinate. The subid specifies a primary cell that lies within a composite cell such as a triangle strip. Cell edges and faces are defined implicitly from the topology of the cell.

ClearCorrect Exhibit 1002, Page 2362 of 3373

`type = GetCellType()`
Return the type of the cell. Must be one of the twelve **vtk** cell types (or the empty cell type).

`dim = GetCellDimension()`
Return the topological definition of the cell.

`order = GetInterpolationOrder()`
Return the degree of the interpolating polynomial of the cell. (The twelve cell types are all degree 1; cells added in the future may be of higher-order.)

`numberPoints = GetNumberOfPoints()`
Return the number of points that define the cell.

`points = GetPoints()`
Return a list of point ids defining the cell.

`numberEdges = GetNumberOfEdges()`
Return the number of edges in the cell.

`edge = GetEdge(i)`
Given an edge id ($0 \leq i <$ numberEdges) return a pointer to a cell that represents an edge of the cell.

`numberFaces = GetNumberOfFaces()`
Return the number of faces in a cell.

`face = GetFace(i)`
Given an face id ($0 \leq i <$ numberFaces) return a pointer to a cell that represents a face of the cell.

`inOutStatus = CellBoundary(subId, pcoords, poindIds)`
Given a cell subid and parametric coordinates, return a list of point ids that define the closest boundary face of the cell. Also return whether the point is actually in the cell.

`inOutStatus = EvaluatePosition(x, closestPoint, subId, pcoords, weights, dist2)`
Given a point coordinate x, return the sub-id, parametric coordinates, and interpolation weights of the cell if x lies inside the cell. The position `closestPoint` is the closest point on the cell to x (may be the same) and `dist2` is the squared distance between them. The method returns an `inOutStatus` indicating whether x is *topologically* inside or outside the cell. That is, the point may satisfy parametric coordinate conditions but may lie off the surface of the cell (e.g., point lies above polygon). Use both `inOutStatus` and `dist2` to determine whether point is both topologically and geometrically in the cell.

ClearCorrect Exhibit 1002, Page 2363 of 3373

`EvaluateLocation(subId, pcoords, x, weights)`
Given a point location (i.e., sub-id and parametric coordinates), return the position `x` of the point and the interpolation weights.

`Contour(value, cellScalars, locator, verts, lines, polys, inputPointData, outputPointData)`
Given a contour value and scalar values at the cell points, generate contour primitives (vertices, lines, or polygons with associated points and attribute data values). The points are placed in a locator object (see "Searching" on page 331) which merges coincident points, and the attribute data values are interpolated (along the cell edge) from the `inputPointData` to the `outputPointData`.

`Clip(value, cellScalars, locator, cells, inputPointData, outputPointData, insideOut)`
Given a contour value and scalar values at the cell points, clip the cell to generate new cells of the same topological dimension as the original cell. The points are placed in a locator object (see "Searching" on page 331) which merges coincident points, and the attribute data values are interpolated (or copied) from the `inputPointData` to the `outputPointData`. The clipped cells are placed in the `cells` list.

`Derivatives(subId, pcoords, values, dim, derivs)`
Given a cell location (i.e., subid and parametric coordinates) and data values at the cell points, return `dim`*3 derivatives (i.e., corresponds to the x, y, and z directions times dimension of data).

`inOutStatus = IntersectWithLine(p1, p2, tol, t, x, pcoords, subId)`
Given a finite line defined by the two points `p1` and `p2` and an intersection tolerance, return the point of intersection `x`. The parametric coordinate `t` along the line and cell location at the point of intersection is also returned. Returns a nonzero if intersection occurs.

`Triangulate(index, ptIds, points)`
Decompose the cell into simplices of dimension equal to the topological cell dimension. The index is an integer that controls the triangulation if more than one triangulation is possible. The simplices are defined by an ordered list of point ids and their corresponding coordinates.

`bounds = GetBounds()`
Return the bounding box of the cell.

Point Attribute Abstraction. Point attribute data is information associated with the points of a cell/dataset. This information consists of scalars, vectors, normals, tensors, texture coordinates, and/or user-defined data. There is a one-to-one relationship between the points in a dataset and the attribute data. For example, scalar value at location 100 is associated with point id 100.

Many of the methods described below deal with moving data from the input

ClearCorrect Exhibit 1002, Page 2364 of 3373

to the output of a filter. Since the possibility exists that new types of attribute data could be added in the future, the details of moving data is hidden as much as possible (i.e., minimize the knowledge that the filter has about specific attribute types). Thus, generic functions like `CopyData()` allow for copying data from the input to the output without knowing what this data is.

`CopyScalarsOn() / CopyScalarsOff()`
Turn on/off boolean flag controlling copying of scalar data from input to output of filter.

`CopyVectorsOn() / CopyVectorsOff()`
Turn on/off boolean flag controlling copying of vector data from input to output of filter.

`CopyNormalsOn() / CopyNormalsOff()`
Turn on/off boolean flag controlling copying of normal data from input to output of filter.

`CopyTensorsOn() / CopyTensorsOff()`
Turn on/off boolean flag controlling copying of tensor data from input to output of filter.

`CopyTextureCoordsOn() / CopyTextureCoordsOff()`
Turn on/off boolean flag controlling copying of texture coordinates data from input to output of filter.

`CopyUserDefinedOn() / CopyUserDefinedOff()`
Turn on/off boolean flag controlling copying of user-defined data from input to output of filter.

`CopyAllOn() / CopyAllOff()`
Turn on/off all boolean flags controlling copying of data from input to output of filter.

`PassData(pointData)`
Transfer all point attribute data (`pointData`) to the output according to the copy flags listed previously.

`CopyAllocate(pointData)`
Initialize and allocate storage for point-by-point copy process.

`CopyData(pointData, fromId, toId)`
Given point data and a specific point id, copy the point attribute data (`pointData`) to the output point.

`InterpolateAllocate(pointData)`
Initialize and allocate storage for point-by-point interpolation process.

`InterpolatePoint(pointData, toId, ptIds, weights)`
Given input point data (`pointData`) and a list of points and their interpolation weights, interpolate data to the specified output point.

ClearCorrect Exhibit 1002, Page 2365 of 3373

`InterpolateEdge(pointData, toId, p1, p2, t)`
From an edge defined by the two points `p1` and `p2`, interpolate the `pointData` at the edge parametric coordinate `t` and copy the interpolated attribute data to the output point `ptId`.

`NullPoint(int ptId)`
Set the data value(s) of the specified output point id to a null value.

`SetScalars() / GetScalars()`
Set / return scalar data. The `GetScalars()` method may return a `NULL` value, in which case the scalars are not defined.

`SetVectors() / GetVectors()`
Set / return vector data. The `GetVectors()` method may return a `NULL` value, in which case the vectors are not defined.

`SetNormals() / GetNormals()`
Set / return normal data. The `GetNormals()` method may return a `NULL` value, in which case the normals are not defined.

`SetTensors() / GetTensors()`
Set / return tensor data. The `GetTensors()` method may return a `NULL` value, in which case the tensors are not defined.

`SetTextureCoords() / GetTextureCoords()`
Set / return texture coordinate data. The `GetTextureCoords()` method may return a `NULL` value, in which case the texture coordinates are not defined.

`SetUserDefined() / GetUserDefined()`
Set / return user-defined data. The `GetUserDefined()` method may return a `NULL` value, in which case user-defined data is not defined.

Traversing Intermediate Topology

The dataset abstraction implemented by **vtk** provides simple techniques to traverse points and cells. Sometimes we want to traverse intermediate topology such as edges or faces. For example, to identify boundary edges in a triangular mesh we must traverse each edge, counting the number of triangles that use each edge. (Recall that boundary edges are used by just one triangle.) Unfortunately, there is no obvious way to traverse edges. The same problem holds true if we want to traverse the faces of a dataset containing 3D cells.

A simple solution is to traverse each cell and then obtain the edges (or faces) that compose the cell. The problem with this approach is that edges and faces are generally used by more than one cell, resulting in multiple visits to the same face or edge. This may be acceptable in some algorithms, but usually we count on visiting each edge or face only once.

A better solution to this problem is to traverse each cell as before, but only process intermediate topology if the current cell has the smallest cell id. (The

ClearCorrect Exhibit 1002, Page 2366 of 3373

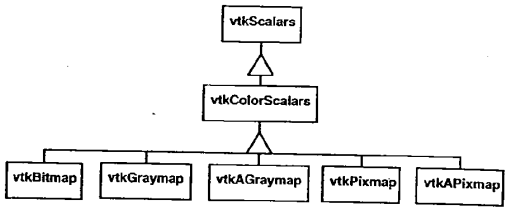


Figure 8–22 Color scalars object model.

current cell is the cell being visited in the traversal process.) To determine whether the current cell has the smallest cell id, we obtain all cells using the intermediate topology. This information can be obtained using the topological adjacency operators described earlier (e.g., Equation **8-24**).

To illustrate this process consider visiting the edges of a triangle mesh. We begin by visiting the first triangle, t, and then its edges. For each edge we determine the adjacent triangle(s) (if any) that use the edge. If the id of the adjacent triangle(s) is greater than triangle t's id, or there are no adjacent triangles, then we know to process the current edge. (Of course the first triangle will always have the smallest id — but this will change as the traversal proceeds.) We then continue traversing the triangle list for new t's. In this way all the edges of the mesh will be visited.

Color Scalar Data

Multivalued scalar data, or scalars represented by various color representations, are a special type in the *Visualization Toolkit*. These classes are of generic type `vtkColorScalars`, which is in turn a subclass of `vtkScalars` (Figure **8–22**).

`vtkColorScalars` is an abstract class that specifies a uniform interface to its concrete subclasses, as well as implementing the methods required by `vtkScalars`. Special features of this class are as follows.

- Subclasses of `vtkColorScalars` operate on color specification in the RGBA (i.e., red-green-blue-alpha transparency) format. The internal representation of data may be different, but must be converted to this form to satisfy the abstract interface. For example, `vtkGraymap`, which represents data as a single `unsigned char` value, converts its value to RGBA by setting its alpha value $\alpha = 1$ and each color component to the gray value $R = G = B =$ gray.
- To satisfy the abstract interface specified by `vtkScalars`, subclasses of `vtkColorScalars` must also be capable of converting their multivalued color values into a single value. Equation **8-25** and Equation **8-26** are used.
- Special methods provide information about the type of scalar, either `SingleValued` or `ColorScalar`, and the number of data values per scalar

ClearCorrect Exhibit 1002, Page 2367 of 3373

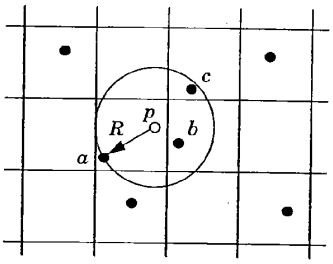


Figure 8–23 Determining closest point to p in `vtkPointLocator`. Initial search in bucket results in point a. Search must extend beyond local bucket as a function of search radius R, resulting in point b.

(i.e., `GetScalarType()` and `GetNumberOfValuesPerScalar()`). This information allows us to differentiate between general types of scalar and to perform special operations like texture mapping and writing data to disk.

- Every subclass of `vtkColorScalars` must be capable of returning an array of `unsigned char` values. The array consists of 1–4 values per scalar (depending on the number of values per scalar). This operation is used for high-performance texture and imaging operations.

Searching

The *Visualization Toolkit* provides two classes to perform searches for dataset points and cells. These are `vtkPointLocator` and `vtkCellLocator`. (Both of these classes are subclasses of `vtkLocator`, which is an abstract base class for spatial search objects.) `vtkPointLocator` is used to search for points and, if used with the topological dataset operator `GetPointCells()`, to search for cells as well. `vtkCellLocator` is used to search for cells.

`vtkPointLocator` is implemented as a regular grid of buckets (i.e., same topology and geometry as a structured point set). The number of buckets can be user-specified, or more conveniently, automatically computed based on the number of dataset points. On average, `vtkPointLocator` provides constant time access to points. However, in cases where the point distribution is not uniform, the number of points in a bucket may vary widely, giving $O(n)$ worst-case behavior. In practice this is rarely a problem, but adaptive spatial search structures (e.g., an octree) may sometimes be a better choice.

Determining closest point to a point p using `vtkPointLocator` (as well as other spatial search structures) is a three-step process. In the first step, the bucket containing p is found using the appropriate insertion scheme. (For `vtkPointLocator` this is three divisions to determine bucket indices (i, j, k).) Next, the list of points in this bucket is searched to determine the closest point. How-

ClearCorrect Exhibit 1002, Page 2368 of 3373

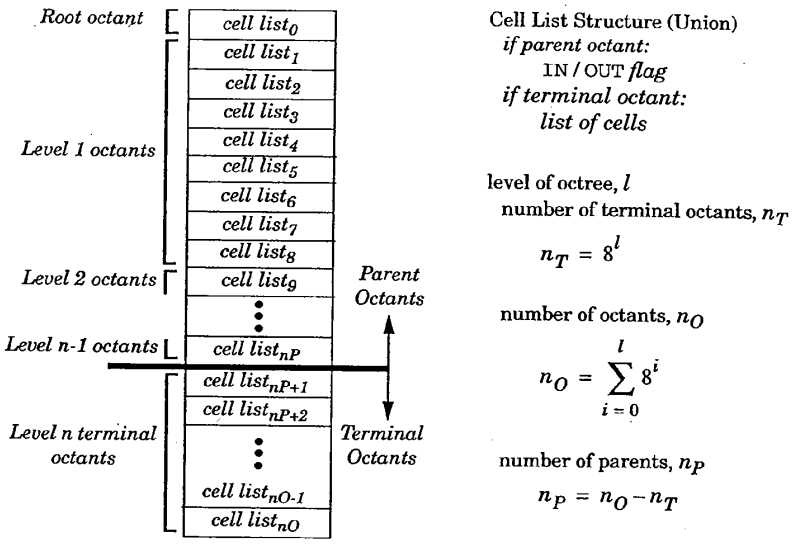


Figure 8–24 Structure of spatial search structure `vtkCellLocator`. The data structure represents a uniformly subdivided octree.

ever, as Figure **8–23** shows, this may not be the true closest point, since points in neighboring buckets may be closer. Consequently, a final search of neighboring buckets is necessary. The search distance is a function of the distance to the current closest point. Once all neighbors within this distance are searched, the closest point is returned.

`vtkCellLocator` is implemented as a uniformly subdivided octree with some peculiar characteristics (Figure **8–24**). Conventional octree representations use upward parent and downward children pointers to track parent and children octants. Besides the required list of entities (i.e., points or cells) in each octant, additional information about octant level, center, and size may also be maintained. This results in a flexible structure with significant overhead. The overhead is the memory resources to maintain pointers, plus the cost to allocate and delete memory.

In contrast, `vtkCellLocator` uses a single array to represent the octree. The array is divided into two parts. The first part contains a list of parent octants, ordered according to level and octant child number. In the second part are the terminal, or leaf octants. The terminal octants are ordered on a regular array of buckets, just the same as `vtkLocator`. The terminal octants contain a list of the entities inside the octant. The parent octants maintain a value indicating whether the octant is empty, or whether something is inside it. (Both types of information are represented in the same portion of the octant structure.)

ClearCorrect Exhibit 1002, Page 2369 of 3373

Because the octree is uniformly subdivided, parent-child relationships, as well as octant locations, can be computed quickly using simple division operations.

The advantage of this structure is that memory can be allocated and deleted quickly. In addition, insertion into the octree is exactly the same as with `vtkLocator`, and is simpler than conventional octrees. The parent octants provide quick culling capability, since their status (empty or nonempty) allows us to stop certain types of search operations. On the downside, because the octree is uniformly subdivided, this structure is wasteful of memory resources if the data is nonuniformly distributed.

Our experience with the search structures described here is that they work well for many types of visualization data. However, if your data is non-uniform, you may want to implement your own special search classes.

Picking

The *Visualization Toolkit* provides four classes to perform actor, point, cell, and world point picking. These are the classes `vtkPicker`, `vtkPointPicker`, `vtkCellPicker`, and `vtkWorldPointPicker`. These pickers vary in speed and functionality as described in the following.

The object `vtkPicker` intersects a ray defined from camera position to a screen (i.e., pixel coordinate) against the bounding box of all pickable and nontransparent actors. (An actor is pickable if its `Pickable` instance variable is true.) The result of the `vtkPicker` pick operation is to return a list of the actors whose bounding box is intersected. The actor closest to the camera position is also returned.

The object `vtkPointPicker` intersects the ray against the points defining each actor, and returns the point coordinate closest to the camera position, as well as the actor that the point belongs to. Since screen resolution prevents precise selection of a point, a tolerance around the ray must be specified. The tolerance is expressed as a fraction of the rendering window size. (Rendering window size is measured across the window diagonal.) Points must lie within this tolerance to be picked.

The object `vtkCellPicker` intersects the ray with the cells defining each actor, and returns the point of intersection, as well as the actor that the cell belongs to. If you are trying to select a unique actor, `vtkCellPicker` is the object to use because it performs surface (or cell) intersection. Picking actors using `vtkPicker` can yield undesirable results because of the overlap of bounding boxes; the same is true of `vtkPointPicker` because of tolerance problems. Unfortunately, `vtkCellPicker` is the slowest object of the three because of greater computational requirements.

The class `vtkWorldPointPicker` returns the *(x,y,z)* coordinate value of a pick in the rendering window. To determine this information, it combines the display *(x,y)* values with the *z*-buffer depth values. Of all the pickers it is the fastest, but it cannot determine the actual cell, point or actor that is selected. (Note: on some systems *z*-buffer operations are inoperative and this object will not function properly.)

ClearCorrect Exhibit 1002, Page 2370 of 3373

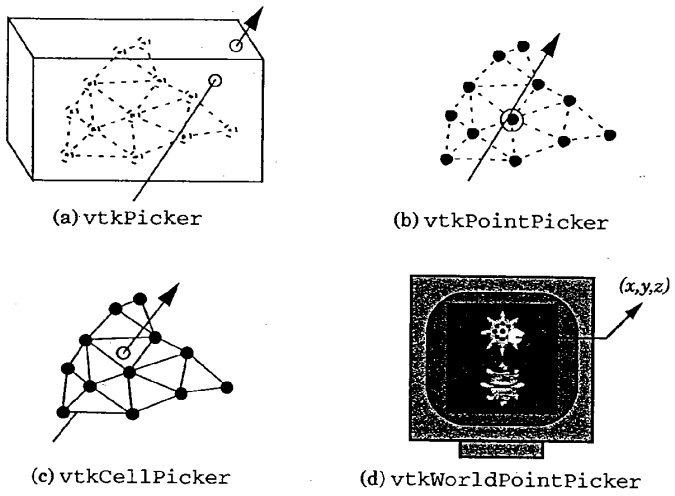


Figure 8–25 Summary of picking operations.

Figure 8–25 summarizes these four picking classes. Picking is built into the `vtkRenderWindowInteractor` class using the "p" key (see "Introducing vtkRenderWindowInteractor" on page 70). By default a `vtkCellPicker` is created, but you are free to specify your own picker type.

Examples

To conclude this section, we will examine how some of the dataset, cell, and point attribute operations are used. These operations tend to be used by class developers. You will not need to use them if you build applications by constructing visualization pipelines with existing filters.

Find Free Edges. In our first example we will take a peek inside the filter `vtkLinearExtrusionFilter`. This filter implements the following modelling operation. Given a polygonal mesh, extrude the mesh in a given direction, constructing a "skirt" or "walls" from the free edges. If the polygonal example is a single square, the result of this operation is a cube. Or, if the polygonal data consists of a single line, the result of the operation is a quadrilateral. A point will generate a line as shown in Figure 8–26(a).

Recall that free edges are edges used by only one polygon. We can determine this information using the dataset topology operation `GetCellEdgeNeighbors()`. We use Equation 8-24 and the two points defining the edge of the

ClearCorrect Exhibit 1002, Page 2371 of 3373

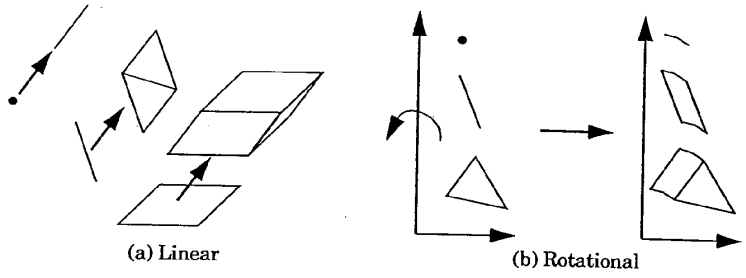


Figure 8–26 Depiction of linear and rotational extrusion.

polygon to determine the adjacency set (i.e., the polygons sharing this edge). If no other polygon uses this edge, then the edge is extruded to generate a triangle strip. The C++ pseudo code is as follows.

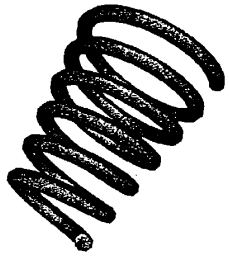
```
    for (cellId=0; cellId < numCells; cellId++)
      {
      cell = mesh.GetCell(cellId);
      if ((dim=cell->GetCellDimension()) == 0)
      //create lines from points
      else if ( dim == 1 )
      // create strips from lines
  else if ( dim == 2 ) // create strips from boundary edges
       {
       numEdges = cell->GetNumberOfEdges();
       for (i=0; i<numEdges; i++)
         {
         edge = cell->GetEdge(i);
         for (j=0; j<(edge->GetNumberOfPoints()-1); j++)
           {
           p1 = edge->PointIds.GetId(j);
           p2 = edge->PointIds.GetId(j+1);
           mesh.GetCellEdgeNeighbors(cellId, p1, p2, cellIds);
           if ( cellIds.GetNumberOfIds() < 1 )
            {
             //generate triangle strip
            }
           } //for each subedge
         } //for each edge
       } //for each polygon or triangle strip
     } //for each cell
```



(a) Linearly extruded fonts to show letter frequency in text (`alphaFreq.cxx`).



(b) Rotationally symmetric objects (`bottle.tcl`).



(c) Rotation in combination with linear displacement and radius variation (`spring.tcl`).

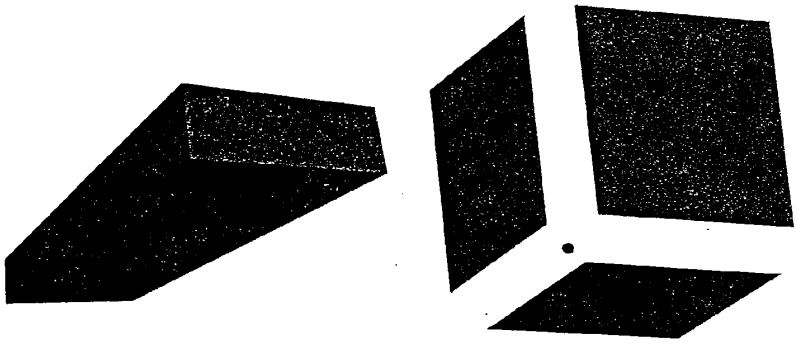
Figure 8–27 Models created using linear and rotational extrusion.

This same approach is used in the `vtkRotationalExtrusionFilter` (Figure **8–26**(b)). The difference between these two functions is that the type of motion is rotational as compared to linear (`vtkLinearExtrusionFilter`). These two filters can be used to perform some nifty modelling operations. Linear extrusion can be used to create bar charts with arbitrary cross sections, or to sweep out three-dimensional fonts. The rotational extrusion filter can be used to create rotationally symmetric objects such as bottles or wine glasses. Examples of these techniques are shown in Figure **8–27**.

Find Cells. In this example we combine picking and a topological operation to select cells sharing a common point. Specifically, we use `vtkPointPicker` and the topological dataset operation `GetPointCells()`. Figure **8–28** depicts this operation. We have also included a fragment of C++ code implementing this procedure. Note that this procedure will work for any dataset type, even if the geometry is implicitly defined (e.g., `vtkStructuredPoints`).

The most difficult part of this procedure is the picking process. The selec-

ClearCorrect Exhibit 1002, Page 2373 of 3373



(a) Original data (b) Selected cells

```
sphereActor->SetPosition(picker->GetPickPosition());

if ( picker->GetPointId() >= 0 )
  {
  cout << "Point id: " << picker->GetPointId() << "\n";
  cellsActor->VisibilityOn();
  plateActor->VisibilityOff();
  cells->Initialize();
  cells->Allocate(100);
  cells->SetPoints(plateOutput->GetPoints());

  plateOutput->GetPointCells(picker->GetPointId(), cellIds);
  for (i=0; i < cellIds.GetNumberOfIds(); i++)
    {
    cellId = cellIds.GetId(i);
    plateOutput->GetCellPoints(cellId, ptIds);
    cells->InsertNextCell(plateOutput->GetCellType(cellId), ptIds
    }
  }
else
  {
  cellsActor->VisibilityOff();
  plateActor->VisibilityOn();
  }
renWin->Render();
```

(c) C++ code (`pickCells.cxx`)

Figure 8–28 Selecting group of cells sharing a common point. (a) Original data. (b) Selected cells sharing point on corner. Cells shrunk for clarity. The small sphere indicates the selected point. (c) C++ code fragment in pick routine.

ClearCorrect Exhibit 1002, Page 2374 of 3373

tion point must be specified in pixel coordinates. The `vtkPointPicker` converts these coordinates into world and then dataset coordinates using the renderer in which the pick occurred. (The renderer uses the transformation matrix of its active camera to perform coordinate transformation.)

The picking process is conveniently managed in `vtkRenderWindowInteractor`. This object allows the specification of functions to execute just before picking and just after picking (i.e., `StartPickMethod()` and `EndPickMethod()`). Using this facility we can define a postpicking function to retrieve the point id and then execute the `GetPointCells()` operation. This process is shown in Figure **8–28**.

Point Probe. In this example we will show how to build a point probe using the dataset and cell operations described in this chapter. A point probe is defined as follows. Given a *(x,y,z)* point coordinate, find the cell coordinates (i.e., cell id, subcell id, and parametric coordinates) and the interpolation weights. Once the interpolation weights are found, we can then compute local data values at *(x,y,z)*.

The point probe is implemented using the dataset operation `FindCell()`. This method requires a point specified in global coordinates (our *(x,y,z)* value) and a tolerance. The tolerance is often necessary because of numerical precision or when picking near the surface of 3D cells, or on 0D, 1D, and 2D cells. The `FindCell()` operation returns the information we require, plus the interpolation weights of the cell containing our point probe. To determine the data value at our probe point, we need to retrieve the data values on the cell points. We can then use the interpolation functions of Equation **8-4** to determine the probe scalar value.

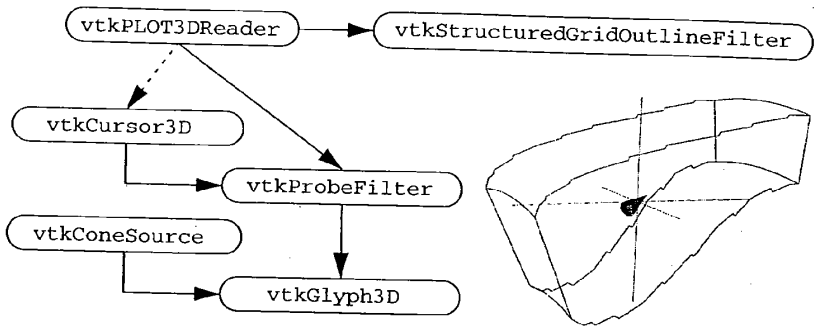
Figure **8–29** depicts this process and includes C++ code. In the example we use the combustor dataset with the objects `vtkCursor3D`, `vtkProbeFilter`, and `vtkGlyph3D`. The purpose of the cursor is to control the position of the probe point. The class `vtkProbeFilter` performs the probing operation just described. (This filter has been generalized so that it can handle more than one input point.) `vtkGlyph3D` is used to place an oriented, scaled cone at the cursor focal point. This gives us visual feedback about the scalar and vector quantities at the probe. Of course, we can extract numeric values and display them to the user if this is important.

8.11 Chapter Summary

Three important visualization coordinate systems are the world, dataset, and structured coordinate systems. The world coordinate system is an *x-y-z* Cartesian three-dimensional space. The dataset coordinate system consists of a cell id, subcell id, and parametric coordinates. The structured coordinate system consists of *(i,j,k)* integer indices into a rectangular topological domain.

Visualization data is generally in discrete form. Interpolation functions are used to obtain data at points between the known data values. Interpolation functions vary depending on the particular cell type. The form of the interpolation

ClearCorrect Exhibit 1002, Page 2375 of 3373




```
//
// Loop over all input points, interpolating source data
//
for (ptId=0; ptId < numPts; ptId++)
  {
  // Get the xyz coordinate of the point in the input dataset
  x = input->GetPoint(ptId);

  // Find the cell that contains xyz and get it
  cell = source->FindAndGetCell(x,NULL,-1,tol2,subId,pcoords,weights
  if (cell)
    {
    // Interpolate the point data
    outPD->InterpolatePoint(pd,ptId,&(cell->PointIds),weights);
    }
  else
    {
    outPD->NullPoint(ptId);
    }
  }
```

Figure 8–29 Creating a point probe. Visualization network shown in diagram above. C++ code shows inner loop of `vtkProbeFilter` and resulting image for combustor data (`probe.cxx`).

functions are weighting values located at each of the cells points. The interpolations functions form the basis for conversion from dataset to global coordinates and vice versa. The interpolation functions also are used to compute data derivatives.

Topological operators provide information about the topology of a cell or dataset. Obtaining neighboring cells to a particular cell is an important visualization operation. This operation can be used to determine whether cell boundaries are on the boundary of a dataset or to traverse datasets on a cell-by-cell basis.

ClearCorrect Exhibit 1002, Page 2376 of 3373

Because of the inherent regularity of structured point datasets, operations can be efficiently implemented compared to other dataset types. These operations include coordinate transformation, derivative computation, topological query, and searching.

8.12 Bibliographic Notes

Interpolation functions are employed in a number of numerical techniques. The finite element method, in particular, depends on interpolation functions. If you want more information about interpolation functions refer to the finite element references suggested below [Cook89] [Gallagher75] [Zienkiewicz87]. These texts also discuss derivative computation in the context of interpolation functions.

Basic topology references are available from a number of sources. Two good descriptions of topological data structures are available from Weiler [Weiler86] [Weiler88] and Baumgart [Baumgart74]. Weiler describes the radial-edge structure. This data structure can represent manifold and nonmanifold geometry. The winged-edge structure described by Baumgart is widely known. It is used to represent manifold geometry. Shephard [Shephard88] describes general finite element data structures — these are similar to visualization structures but with extra information related to analysis and geometric modelling.

There are extensive references regarding spatial search structures. Samet [Samet90] provides a general overview of some. Octrees were originally developed by Meagher [Meagher82] for 3D imaging. See [Williams83], [Bentley75], and [Quinlan94] for information about MIP maps, kd-trees, and binary sphere trees, respectively.

8.13 References

[Baumgart74]
B. G. Baumgart. "Geometric Modeling for Computer Vision." Ph.D. thesis, Stanford University, Palo Alto, CA, 1974.

[Bentley75]
J. L. Bentley. "Multidimensional Binary Search Trees Used for Associative Search." *Communications of the ACM*. 18(9):509–516, 1975.

[Conte72]
S. D. Conte and C. de Boor. *Elementary Numerical Analysis*. McGraw-Hill Book Company, 1972.

[Cook89]
R. D. Cook, D. S. Malkus, and M. E. Plesha. *Concepts and Applications of Finite Element Analysis*. John Wiley and Sons, New York, 1989.

[Gallagher75]
R. H. Gallagher. *Finite Element Analysis: Fundamentals*. Prentice Hall, Upper Saddle River, NJ, 1975.

ClearCorrect Exhibit 1002, Page 2377 of 3373

[Meagher82]
D. J. Meagher. "Efficient Synthetic Image Generation of Arbitrary 3D Objects." In *Proceedings of the IEEE Conference on Pattern Recognition and Image Processing*. pp. 473–478, 1982.

[Quinlan94]
S. Quinlan. "Efficient Distance Computation Between Non-Convex Objects." In *Proceedings of IEEE International Conference on Robotics and Automation*. 1994.

[Samet90]
H. Samet. *Design and Analysis of Spatial Data Structures*. Addison-Wesley, Reading, MA, 1990.

[Shephard88]
M. S. Shephard and P. M. Finnigan. "Toward Automatic Model Generation." *State-of-the-Art Surveys on Computational Mechanics*. A. K. Noor and J. T. Oden, eds., ASME, pp. 335–366, 1989.

[Weiler86]
K. J. Weiler. *Topological Structures for Geometric Modeling*. Ph.D. thesis, Rensselaer Polytechnic Institute, Troy, NY, May 1986.

[Weiler88]
K. J. Weiler. "The Radial-Edge Structure: A Topological Representation for Non-Manifold Geometric Boundary Representations." In M. J. Wozny, H. W. McLaughlin, and J. L. Encarnacao, eds., *Geometric Modeling for CAD Applications*. pp. 3–36, North Holland, 1988.

[Williams83]
L. Williams. "Pyramidal Parametrics." *Computer Graphics (SIGGRAPH '83)*. 17(3):1–11, 1983.

[Zienkiewicz87]
O. C. Zienkiewicz and R. L. Taylor. *The Finite Element Method — Vol. 1*. McGraw Hill Book Co., NY, 4th ed., 1987.

8.14 Exercises

8.1 Given a volume of dimensions $5 \times 10 \times 15$ with origin (1.0, 2.0,3.0) and voxel spacing (0.5, 0.5, 1.0).
a) Compute minimum point position.
b) Compute maximum point position.
c) For cell id 342, compute cell minimum point position and maximum point position.
d) What points (list ids) define cell id 342?
e) Given point specified in structured coordinates as $i, j, k = (3, 6, 4)$; $r, s, t = (0.1, 0.2, 0.5)$, compute global coordinates.
f) Given point id 342; compute global coordinates.

8.2 Compute global coordinates and interpolation weights for the points specified in dataset coordinates (refer to Figure **8–30**(a-d)).
a) Line with $r = 0.5$.

ClearCorrect Exhibit 1002, Page 2378 of 3373

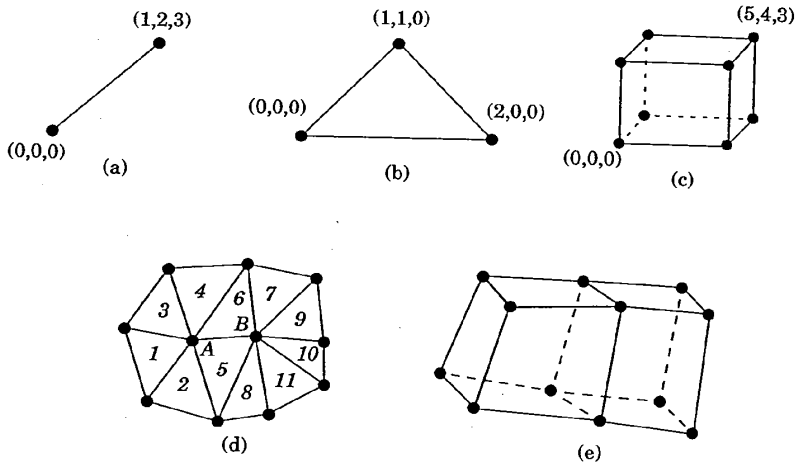


Figure 8–30 Exercise figures.

b) Triangle with $r, s = (0.25, 0.33)$.
c) Voxel with $r, s, t = (0.25, 0.33, 0.5)$.

8.3 Compute parametric coordinates for cells shown in Figure **8–30**(a–d).
a) Line with $x, y, z = (0.3, 0.6, 0.9)$.
b) Triangle with $x, y, z = (0.5, 0.25, 0.0)$.
c) Voxel with $x, y, z = (0.5, 0.4, 2.0)$.

8.4 Given the line shown in Figure **8–30**(a), if scalar data values are $(s_0, s_1) = (0.0, 0.25)$, what are the derivatives in the x, y, z directions?

8.5 Refer to Figure **8–30**(d) and let the numbers indicate cell ids and the letters indicate point ids.
a) List the cells using point A.
b) List the cells using point B.
c) List cells using edge (A, B). How does this list correspond to your answers in parts a) and b) above?

8.6 Refer to Figure **8–30**(e).
a) How many boundary faces are there?
b) How many "internal" faces?

8.7 Describe a procedure to intersect two finite lines. How does tolerance value come into play?

8.8 Describe a procedure to intersect a line and triangle. Are there special characteristics of a triangle that can be used to speed this operation?

ClearCorrect Exhibit 1002, Page 2379 of 3373

8.9 Compare memory requirements for the three unstructured grid data structures shown in Figure **8–20**. Assume that two cells use each face, four faces use each edge, and six edges use each vertex (i.e., a structured dataset).

8.10 Using the abstract cell and dataset interface, write a program to compute
a) number of points in a dataset,
b) number of cells in a dataset,
c) number of edges in a dataset,
d) number of faces in a dataset.

8.11 Given a volume of dimensions $5 \times 10 \times 15$.
a) How many internal faces are there (i.e. used by two voxels)?
b) How many boundary faces are there (i.e., used by one voxel)?

8.12 Write a general extrusion filter that sweeps an object along a path to construct a new surface. Assume that the path is defined by a sequence of transformation matrices. Can you think of a way to prevent self-intersection?

ClearCorrect Exhibit 1002, Page 2380 of 3373

CHAPTER 9

Advanced Algorithms

We return again to visualization algorithms. This chapter describes algorithms that are either more complex to implement, or less widely used for 3D visualization applications. We retain the classification of algorithms as either scalar, vector, tensor, or modelling algorithms.

9.1 Scalar Algorithms

As we have seen, scalar algorithms often involve mapping scalar values through a lookup table, or creating contour lines or surfaces. In this section, we examine another contouring algorithm, *dividing cubes*, which generates contour surfaces using dense point clouds. We also describe carpet plots. Carpet plots are not true 3D visualization techniques, but are widely used to visualize many types of scalar data. Finally, clipping is another important algorithm related to contouring, where cells are cut into pieces as a function of scalar value.

Dividing Cubes

Dividing cubes is a contouring algorithm similar to marching cubes [Cline88]. Unlike marching cubes, dividing cubes generates point primitives as compared to triangles (3D) or lines (2D). If the number of points on the contour surface is

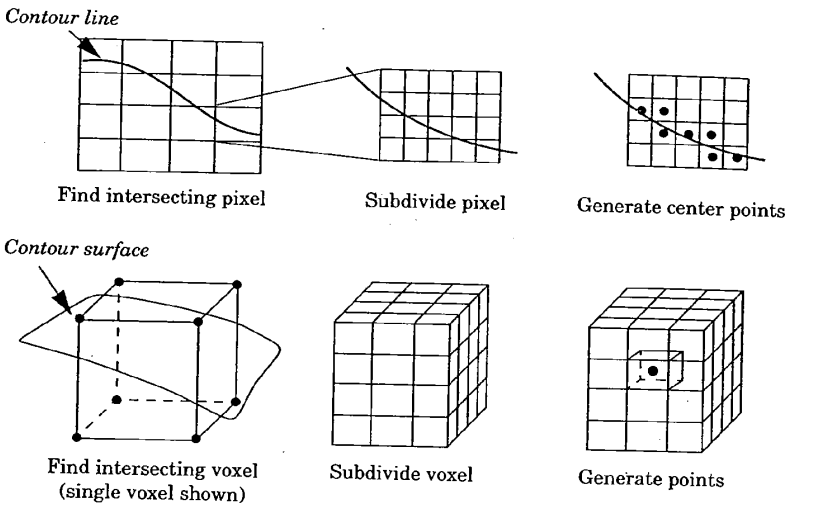


Figure 9–1 Overview of the dividing cubes algorithm. Voxels through which the contour passes are subdivided into subvoxels at less than screen resolution. If the contour passes through a subvoxel, a center point is generated.

large, the rendered appearance of the contour surface appears "solid." To achieve this solid appearance, the density of the points must be at or greater than screen resolution. (Also, the points must be rendered using the standard lighting and shading equations used in surface rendering.)

The motivation for dividing cubes is that rendering points is much faster than rendering polygons. This varies depending upon rendering hardware/software. Special purpose hardware has been developed to render shaded points at high speed. In other systems, greater attention has been placed on polygon rendering, and the rendering speed differences are not so great. Also, certain geometric operations such as clipping and merging data are simple operations with points. Comparable operations with polygons are much more difficult to implement.

One disadvantage of creating contours with dense point clouds is that magnification of the surface (via camera zooming, for example) reveals the disconnected nature of the surface. Thus, the point set must be constructed for maximum zoom, or constructed dynamically based on the relative relationship between the camera and contour.

Although dividing cubes was originally developed for volume datasets, it is possible to adapt the algorithm to other dataset types by subdividing in parametric coordinates. Our presentation assumes that we are working with volumes.

Figure **9–1** provides an overview of the dividing cubes algorithm. Like other

ClearCorrect Exhibit 1002, Page 2382 of 3373

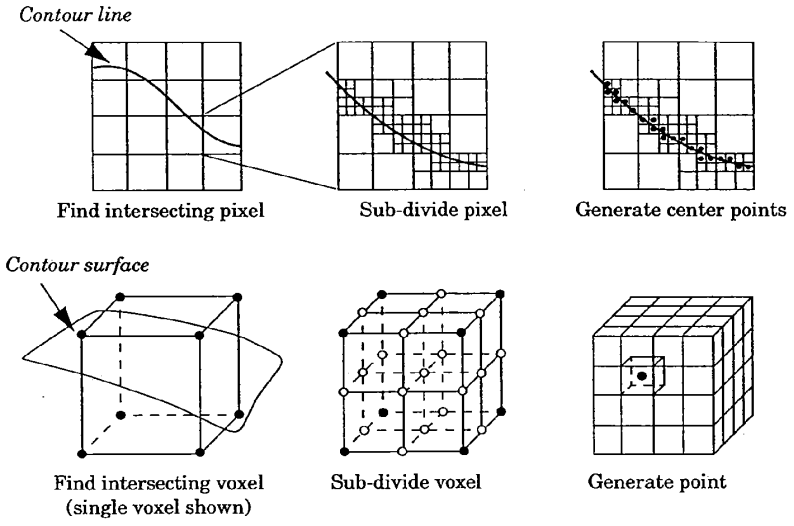


Figure 9–2 Recursive dividing cubes algorithm. Top half of figure shows algorithm depicted in two dimensions. Lower half depicts algorithm in three dimensions.

contouring algorithms, we first choose a contour value. We begin by visiting each voxel and select those through which the isosurface passes. (The isosurface passes through a voxel when there are scalar values both above and below the contour value.) We also compute the gradient at each voxel point for use in computing point normals.

After selecting a voxel that the isosurface passes through, the voxel is subdivided into a regular grid of $n_1 \times n_2 \times n_3$ subvoxels. The number of divisions is controlled by the width of a voxel w_i in combination with screen resolution R. The screen resolution is defined as the distance between adjacent pixels in world coordinates. We can express the number of divisions n_i along the coordinate axes x_i as

$$n_i = \frac{w_i}{R} \tag{9-1}$$

where the quotient is rounded up to the nearest integer. The scalar values at the subpoints are generated using the interpolation functions for a voxel (see Figure **8–10**). Then we determine whether the contour passes through each subvoxel. If it does, we simply generate a point at the center of the subvoxel and compute its normal using the standard interpolation functions.

An interesting variation on this algorithm is a recursive implementation as shown in Figure **9–2**. Instead of subdividing the voxel directly (i.e., procedurally)

ClearCorrect Exhibit 1002, Page 2383 of 3373

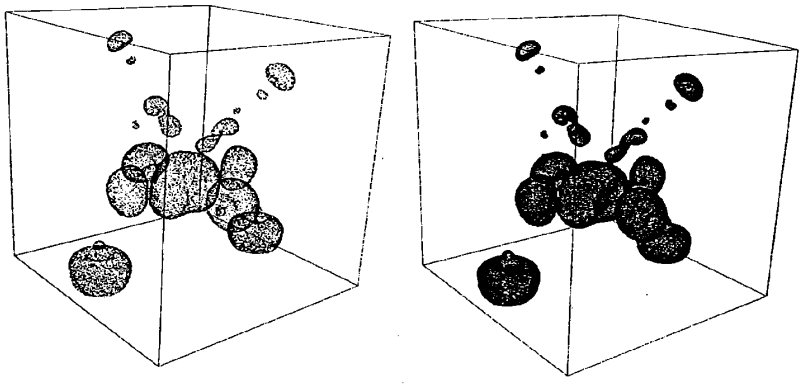


Figure 9–3 Examples of dividing cubes isosurface. The left image consists of 50,078 points, and the right image consists of 2,506,989 points (`dcubes.tcl`).

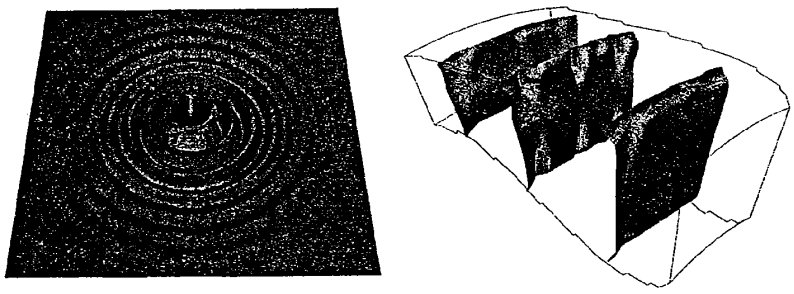
into a regular grid we recursively divide the voxel (similar to octree decomposition). The voxel is subdivided regularly creating eight subvoxels and 19 new points (12 midedge points, 6 midface points, and 1 midvoxel point). The scalar values at the new points are interpolated from the original voxel using the trilinear interpolation functions. The process repeats for each subvoxel if the isosurface passes through it. This process continues until the size of the subvoxel is less than or equal to screen resolution. In this case, a point is generated at the center of the subvoxel. The collection of all such points composes the dividing cubes' isosurface.

The advantage of the recursive implementation is that the subdivision process terminates prematurely in those regions of the voxel where the contour cannot pass. On the other hand, the recursive subdivision requires that the voxel subdivision occurs in powers of two. This can generate far more points than the procedural implementation.

Figure **9–3** shows two examples of dividing cubes isosurfaces. The contour surface on the left consists of 50,078 points. Because the points are not generated at display resolution, it is possible to see through the contour surface. The second contour surface on the right is composed of 2,506,989 points. The points are generated at display resolution, and as a result the contour surface appears solid.

As Figure **9–1** and Figure **9–2** show, the points generated by dividing cubes do not lie exactly on the contour surface. We can determine the maximum error by examining the size of the terminal subvoxels. Assume that a terminal subvoxel is a cube, and that the length of the side of the cube is given by l. Then the maximum error is half the length of the cube diagonal, or $l\sqrt{3}/2$.

ClearCorrect Exhibit 1002, Page 2384 of 3373



(a) Exponential cosine function (b) Flow energy

Figure 9–4 Carpet plots. (a) Visualization of an exponential cosine function. Function values are indicated by surface displacement. Colors indicate derivative values (`expCos.cxx`). (b) Carpet plot of combustor flow energy in a structured grid. Colors and plane displacement represent energy values (`warpComb.tcl`).

Carpet Plots

A common data form is a 2D structured point set with associated scalar data. *Carpet plots* can visualize data in this form. A carpet plot is created by warping a 2D surface in the direction of the surface normal (or possibly some user-defined direction). The amount of warping is controlled by the scalar value, possibly in combination with a scale factor. Carpet plots are similar to the vector displacement plots (see "Displacement Plots" on page 169).

Although carpet plots are typically applied to structured point data, they can be used to visualize datasets composed of 2D structured grids or 2D unstructured grids. In their basic form carpet plots can be used to visualize only three variables: two surface position coordinates and a scalar value. However, it is common to introduce another variable by using color mapping on the surface.

Figure **9–4** illustrates application of carpet plots. Figure **9–4**(a) shows the exponential cosine function centered at the origin with points located at radius r

$$F(r) = e^{-r}\cos(10r) \tag{9-2}$$

The function values are used to warp the surface while the function derivatives are used to color it.

Figure **9–4**(b) shows a carpet plot that visualizes flow energy in a structured grid. Both displacement and color are used to show the energy values. Although this figure is similar to Figure **6–14**(b) there are some important differences. Figure **6–14**(b) displays vector data whereas Figure **9–4**(b) displays scalar

ClearCorrect Exhibit 1002, Page 2385 of 3373

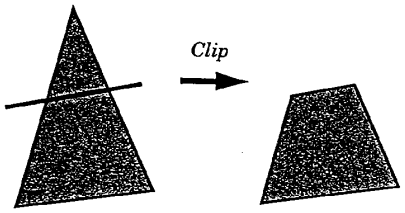


Figure 9–5 Clipping a triangle produces a polygon. The dark line represents an infinite plane.

data. Figure **9–4**(b) deforms the surface in the direction of surface normal (or possibly a user-defined direction). The vector data (i.e., vector orientation) controls the direction of deformation in Figure **6–14**(b).

Clipping With Scalar Fields

Clipping is a common graphics operation that limits the extent of a polygon so that it does not lie outside the view frustrum (See "Cameras" on page 46.) Figure **9–5** shows a triangle before and after clipping with an infinite plane. The clip operation transforms a polygon into a polygon. Clipping can also be a powerful modeling tool. Clipping part of a structure can reveal internal details of the surface or other parts contained within the surface. Objects can be split into pieces and the pieces can be individually moved and controlled.

We can do clipping with arbitrary implicit functions using a variation of the "marching" primitives discussed in "Contouring" on page 158. We illustrate the technique for triangles.

Recall that marching triangles transforms triangles into lines that approximate a scalar value called the isovalue. This is accomplished using the inside/outside relationship that each vertex has with respect to some scalar value. For our purposes here, we use a scalar value that represents the signed distance of the triangle vertex to a plane. This infinite plane, described by an implicit function of the form $F(x, y, z) = n_x x + n_y y + n_z z - d = 0$, partitions space into two infinite half spaces. All points with negative scalar values lie on one side of the plane and all with positive values lie on the other side. Figure **9–6** shows a finite plane represented by a grid of triangles. The thick line shows the infinite plane defined by $F(x,y,z) = x + y + z - c = 0$. The cut algorithm described in "Cutting" on page 187 creates a set of lines using the contour operations specific to each cell primitive. In this example, the triangle's contour operator extracts lines that lie on the intersection of the infinite plane and the triangles that comprise the finite plane. The contour operation for a triangle uses the eight cases shown in

ClearCorrect Exhibit 1002, Page 2386 of 3373

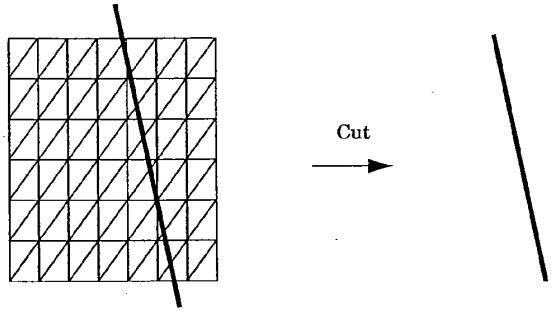


Figure 9–6 Cutting polygons produces lines (`cutPlane.tcl`).

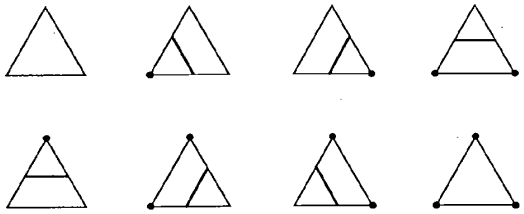


Figure 9–7 The eight cases for cutting (contouring) a triangle. Black dots show triangle vertices that are "inside" the scalar cutting region. Solid lines show the output of the cutting operation.

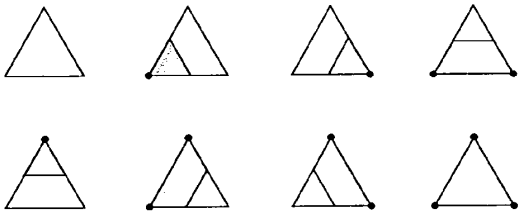


Figure 9–8 The eight cases for clipping a triangle. Black dots show triangle vertices that are "inside" the scalar clipping region. Shaded regions show the output of the clip operation.

Figure **9–7** to contour or "cut" each triangle appropriately.

Clipping transforms polygons into polygons. We do clipping with a modified case table for the triangle that outputs polygons shown in Figure **9–8**. In **vtk**, each polygonal data cell has a different case table to define the clip operation.

ClearCorrect Exhibit 1002, Page 2387 of 3373

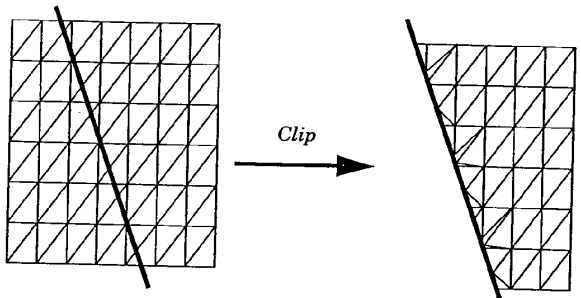


Figure 9–9 A plane of triangles clipped with a plane function (`clipPlane.tcl`).

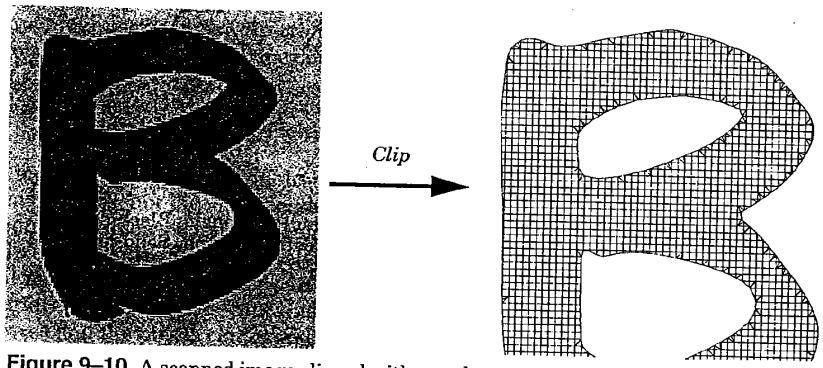


Figure 9–10 A scanned image clipped with a scalar value of 1/2 its maximum intensity produces a mixture of quadrilaterals and triangles (`createBFont.tcl`).

Applying the clip algorithm to the polygonal data in Figure **9–9** using the same scalar field generated with a plane equation produces a new set of triangles.

Formulating clipping using scalar fields permits more sophisticated operations. Clipping can use scalar data that is computed or scalar data that is part of a polygonal dataset's point attributes. Figure **9–10** shows a scanned image that is first converted to a quadrilateral mesh with vertex scalar values set to the scanned image intensity. Clipping this quadrilateral mesh with a value equal to 1/2 the maximum intensity of the scanned image produces a polygonal model show in Figure **9–10**.

ClearCorrect Exhibit 1002, Page 2388 of 3373

9.2 Vector Algorithms

In Chapter 6 we showed how to create simple vector glyphs and how to integrate particles through a vector field to create streamlines. In this section we extend these concepts to create streamribbons and streampolygons. In addition, we introduce the concept of vector field topology, and show how to characterize a vector field using topological constructs.

Streamribbons and Streamsurfaces

Streamlines depict particle paths in a vector field. By coloring these lines, or creating local glyphs (such as dashed lines or oriented cones), we can represent additional scalar and temporal information. However, these techniques can convey only elementary information about the vector field. Local information (e.g., flow rotation or derivatives) and global information (e.g., structure of a field such as vortex tubes) is not represented. Streamribbons and streamsurfaces are two techniques used to represent local and global information.

A natural extension of the streamline technique widens the line to create a ribbon. The ribbon can be constructed by generating two adjacent streamlines and then bridging the lines with a polygonal mesh. This technique works well as long as the streamlines remain relatively close to one another. If separation occurs, so that the streamlines diverge, the resulting ribbon will not accurately represent the flow, because we expect the surface of the ribbon to be everywhere tangent to the vector field (i.e., definition of streamline). The ruled surface connecting two widely separated streamlines does not generally satisfy this requirement.

The streamribbon provides information about important flow parameters: the vector vorticity and flow divergence. *Vorticity* $\vec{\omega}$ is the measure of rotation of the vector field, expressed as a vector quantity: a direction (axis of rotation) and magnitude (amount of rotation). *Streamwise vorticity* Ω is the projection of $\vec{\omega}$ along the instantaneous velocity vector, $\vec{v}$. Said another way, streamwise vorticity is the rotation of the vector field around the streamline defined as follows.

$$\Omega = \frac{\vec{v} \cdot \vec{\omega}}{|\vec{v}||\vec{\omega}|} \tag{9-3}$$

The amount of twisting of the streamribbon approximates the streamwise vorticity. Flow *divergence* is a measure of the "spread" of the flow. The changing width of the streamribbon is proportional to the cross-flow divergence of the flow.

A streamsurface is a collection of an infinite number of streamlines passing through a *base curve.* The base curve, or *rake,* defines the starting points for the streamlines. If the base curve is closed (e.g., a circle) the surface is closed and a streamtube results. Thus, streamribbons are specialized types of streamsurfaces with a narrow width compared to length.

Compared to vector icons or streamlines, streamsurfaces provide additional information about the structure of the vector field. Any point on the streamsur-

ClearCorrect Exhibit 1002, Page 2389 of 3373

face is tangent to the velocity vector. Consequently, taking an example from fluid flow, no fluid can pass through the surface. Streamtubes are then representations of constant mass flux. Streamsurfaces show vector field structure better than streamlines or vector glyphs because they do not require visual interpolation across icons.

Streamsurfaces can be computed by generating a set of streamlines from a user-specified rake. A polygonal mesh is then constructed by connecting adjacent streamlines. One difficulty with this approach is that local vector field divergence can cause streamlines to separate. Separation can introduce large errors into the surface, or possibly cause self-intersection, which is not physically possible.

Another approach to computing streamsurfaces has been taken by Hultquist [Hultquist92]. The streamsurface is a collection of streamribbons connected along their edges. In this approach, the computation of the streamlines and tiling of the streamsurface is carried out concurrently. This allows streamlines to be added or removed as the flow separates or converges. The tiling can also be controlled to prevent the generation of long, skinny triangles. The surface may also be "torn", i.e., ribbons separated, if the divergence of the flow becomes too high.

Stream Polygon

The techniques described so far provide approximate measures of vector field quantities such as streamwise vorticity and divergence. However, vector fields contain more information than these techniques can convey. As a result, other techniques have been devised to visualize this information. One such technique is the *stream polygon* [Schroeder91], which serves as the basis for a number of advanced vector and tensor visualization methods. The stream polygon is used to visualize local properties of strain, displacement, and rotation. We begin by describing the effects of a vector field on the local state of strain.

Nonuniform vector fields give rise to local deformation in the region where they occur. If the vector field is displacement in a physical medium such as a fluid or a solid, the deformation consists of local strain (i.e., local distortion) and rigid body motion. To mathematically describe the deformation, we examine a 3D vector $\vec{v} = (u, v, w)$ at a specified point $\vec{x} = (x, y, z)$. Using a first order Taylor's series expansion about $\vec{x}$, we can express the local deformation e_{ij} as

$$e_{ij} = \varepsilon_{ij} + \omega_{ij} \qquad \textbf{(9-4)}$$

where ε_{ij} is the local strain and ω_{ij} is the local rotation. Note that these variables are expressed as 3×3 tensors. (Compare this equation to that given in Figure **6–20**. Note that this equation and the following Equation **9-5** differ in their off-diagonal terms by a factor of 1/2. This is because Figure **6–20** expresses *engineering shear strain* which is used in the study of elasticity. Equation **9-5** expresses a tensor quantity and is mathematically consistent.)

The local strain is expressed as a combination of the partial derivatives at

ClearCorrect Exhibit 1002, Page 2390 of 3373

$\vec{x}$ as follows.

$$\varepsilon_{ij} = \begin{bmatrix} \dfrac{\partial u}{\partial x} & \dfrac{1}{2}\left(\dfrac{\partial u}{\partial y} + \dfrac{\partial v}{\partial x}\right) & \dfrac{1}{2}\left(\dfrac{\partial u}{\partial z} + \dfrac{\partial w}{\partial x}\right) \\ \dfrac{1}{2}\left(\dfrac{\partial u}{\partial y} + \dfrac{\partial v}{\partial x}\right) & \dfrac{\partial v}{\partial y} & \dfrac{1}{2}\left(\dfrac{\partial v}{\partial z} + \dfrac{\partial w}{\partial y}\right) \\ \dfrac{1}{2}\left(\dfrac{\partial u}{\partial z} + \dfrac{\partial w}{\partial x}\right) & \dfrac{1}{2}\left(\dfrac{\partial v}{\partial z} + \dfrac{\partial w}{\partial y}\right) & \dfrac{\partial w}{\partial z} \end{bmatrix} \tag{9-5}$$

The terms on the diagonal of ε_{ij} are the normal components of strain. The off-diagonal terms are the shear strain. The local rigid-body rotation is given by

$$\omega_{ij} = \begin{bmatrix} 0 & \dfrac{1}{2}\left(\dfrac{\partial u}{\partial y} - \dfrac{\partial v}{\partial x}\right) & \dfrac{1}{2}\left(\dfrac{\partial u}{\partial z} - \dfrac{\partial w}{\partial x}\right) \\ \dfrac{1}{2}\left(\dfrac{\partial v}{\partial x} - \dfrac{\partial u}{\partial y}\right) & 0 & \dfrac{1}{2}\left(\dfrac{\partial v}{\partial z} - \dfrac{\partial w}{\partial y}\right) \\ \dfrac{1}{2}\left(\dfrac{\partial w}{\partial x} - \dfrac{\partial u}{\partial z}\right) & \dfrac{1}{2}\left(\dfrac{\partial w}{\partial y} - \dfrac{\partial v}{\partial z}\right) & 0 \end{bmatrix} \tag{9-6}$$

Equation **9-6** can also be represented using tensor notation as

$$\omega_{ij} = -\frac{1}{2}\varepsilon_{ijk}\vec{\omega} \tag{9-7}$$

where $\vec{\omega}$ is the vorticity vector referred to in the previous section. The vorticity, or local rigid body rotation is then

$$\vec{\omega} = \begin{bmatrix} \dfrac{\partial w}{\partial y} - \dfrac{\partial v}{\partial z} \\ \dfrac{\partial u}{\partial z} - \dfrac{\partial w}{\partial x} \\ \dfrac{\partial v}{\partial x} - \dfrac{\partial u}{\partial y} \end{bmatrix} \tag{9-8}$$

For the reader unfamiliar with tensor notation, this presentation is certainly less than complete. However, the matrices in Equation **9-5** and Equation **9-6** directly translate into visual form, which will help clarify the concepts presented here. Referring to Figure **9–11**, the normal strain, shear strain, and rigid body motion create distinct deformation modes. These modes combine to produce the total deformation. Modes of normal strain cause compression or extension in the direction perpendicular to a surface, while shear strains cause angular distortions. These strains combined with rigid body rotation around an axis yield the total strain at a point.

The essence of the stream polygon technique is to show these modes of

ClearCorrect Exhibit 1002, Page 2391 of 3373

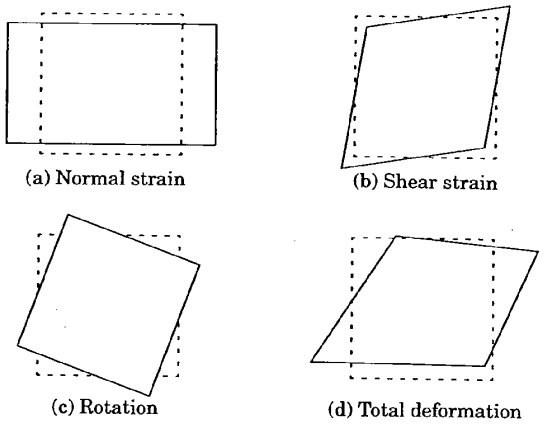


Figure 9–11 Components of local deformation due to vector field. Dotted line shows initially undeformed object.

deformation. A regular n-sided polygon (Figure 9–12) is placed into a vector field at a specified point and then deformed according to the local strain. The components of strain may be shown separately or in combination. The orientation of the normal of the polygon is arbitrary. However, it is convenient to align the normal with the local vector. Then the rigid body rotation about the vector is the streamwise vorticity, and the effects of normal and shear strain are in the plane perpendicular to a streamline passing through the point.

The stream polygon offers other interesting possibilities. The stream polygon may be swept along a trajectory, typically a streamline, to generate tubes. The radius of the tube r can be modified according to some scalar function. One application is to visualize fluid flow. In incompressible flow with no shear, the radius of the tube can vary according to the scalar function vector magnitude. Then the equation

$$r(\vec{v}) = r_{max}\sqrt{\frac{|\vec{v}_{min}|}{|\vec{v}|}} \tag{9-9}$$

represents an area of constant mass flow. As a result, the tube will thicken as the flow slows and narrow as the velocity increases. Each of the n sides of the tube can be colored with a different scalar function, although for visual clarity, at most, one or two functions should be used.

The streamtubes generated by the streampolygon and the streamtubes we described in the previous section are not the same. The streampolygon does not necessarily lie along a streamline. If it does, the streampolygon represents infor-

ClearCorrect Exhibit 1002, Page 2392 of 3373

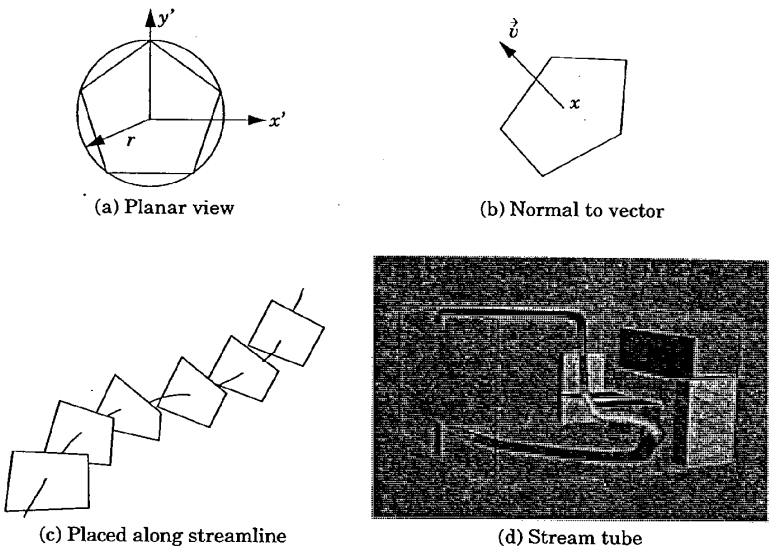


Figure 9–12 The stream polygon. (a) Planar view. (b) Aligned with vector. (c) Aligned along streamline. (d) Sweeping polygon to form tube (`officeTube.tcl`).

mation at a point, while the streamtube is an approximation constructed from multiple streamlines. Also, the radial variation in the tubes constructed from streampolygon sweeps do not necessarily relate to mass flow since the radius in a streampolygon can be tied to an arbitrary scalar variable.

Vector Field Topology

Vector fields have a complex structure characterized by special features called *critical points* [Globus91] [Helman91]. Critical points are locations in the vector field where the local vector magnitude goes to zero and the vector direction becomes undefined. At these points the vector field either converges or diverges, and/or local circulation around the point occurs.

Critical points lie in dataset cells where the u, v, and w components of the vector field each pass through zero. These points are located using an iterative search procedure such as the bi-section technique. Each iteration evaluates the cell interpolation function until the zero vector is found. Once a critical point is found, its local behavior is determined from the matrix of partial derivatives. This is because at the critical point the velocity is zero, and the vector field can

ClearCorrect Exhibit 1002, Page 2393 of 3373

be approximated by a first-order expansion of partial derivatives [Helman91]

$$\begin{aligned} u &\approx \frac{\partial u}{\partial x}dx + \frac{\partial u}{\partial y}dy + \frac{\partial u}{\partial z}dz \\ v &\approx \frac{\partial v}{\partial x}dx + \frac{\partial v}{\partial y}dy + \frac{\partial v}{\partial z}dz \\ w &\approx \frac{\partial w}{\partial x}dx + \frac{\partial w}{\partial y}dy + \frac{\partial w}{\partial z}dz \end{aligned} \tag{9-10}$$

The matrix of partial derivatives J can be written in vector notation as

$$\vec{u} = J d\vec{x} \text{ with } J = \begin{bmatrix} \frac{\partial u}{\partial x} & \frac{\partial u}{\partial y} & \frac{\partial u}{\partial z} \\ \frac{\partial v}{\partial x} & \frac{\partial v}{\partial y} & \frac{\partial v}{\partial z} \\ \frac{\partial w}{\partial x} & \frac{\partial w}{\partial y} & \frac{\partial w}{\partial z} \end{bmatrix} \tag{9-11}$$

and is referred to as the Jacobian. The behavior of the vector field in the vicinity of a critical point is characterized by the eigenvalues of J. The eigenvalues consist of an imaginary and real component. The imaginary component describes the rotation of the vector field around the critical point, while the real part describes the relative attraction or repulsion of the vector field to the critical point. In two dimensions the critical points are as shown in Figure **9–13**.

A number of visualization techniques have been developed to construct vector field topology from an analysis of critical points. These techniques provide a global understanding of the field, including points of *attachment* and *detachment* and field *vortices*. Using a fluid flow analogy, points of attachment and detachment occur on the surface of an object where the tangential component of the vector field goes to zero, and the flow is perpendicular to the surface. Thus, streamlines will begin or end at these points. There is no common definition for a vortex, but generally speaking, vortices are regions of relatively concentrated vorticity (e.g., flow rotation). The study of vortices is important because they represent areas of energy loss, or can have significant impact on downstream flow conditions (e.g., trailing vortices behind large aircraft).

One useful visualization technique creates vector field skeletons that divide the vector field into separate regions. Within each region, the vector field is topologically equivalent to uniform flow. These skeletons are created by locating critical points, and then connecting the critical points with streamlines. In 3D vector field analysis this technique can be applied to the surface of objects to locate lines of flow separation and attachment and other important flow features. Also, in general 3D flow, the regions of uniform flow are separated by surfaces, and creation of 3D flow skeletons is a current research topic.

Vortex visualization is another area of current research. One technique

ClearCorrect Exhibit 1002, Page 2394 of 3373

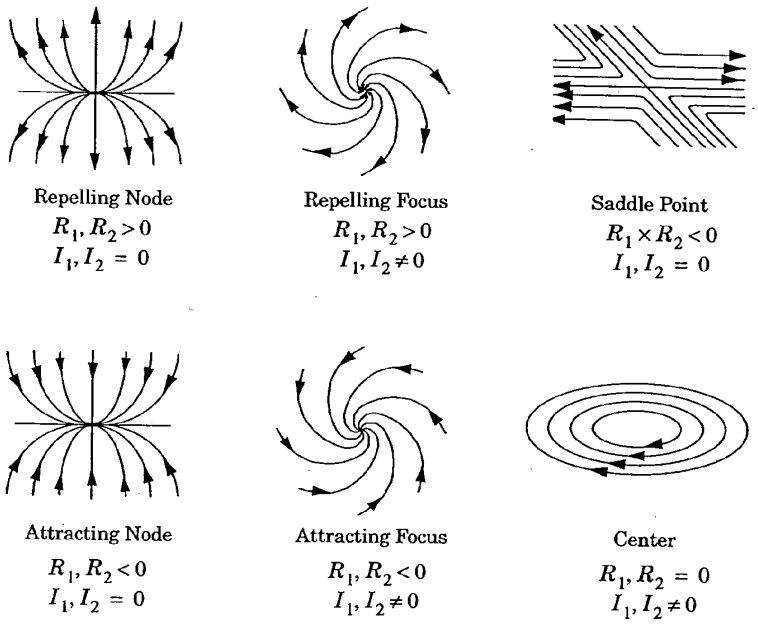


Figure 9–13 Critical points in two dimensions. The real part of the eigenvalues (R_1, R_2) of the matrix of first derivatives control the attraction or repulsion of the vector field. The imaginary part of the eigenvalues (I_1, I_2) controls the rotation.

computes the *helicity-density*

$$H_d = \vec{v} \cdot \vec{w} = |\vec{v}||\vec{w}| \cos\varphi \qquad \textbf{(9-12)}$$

This is a scalar function of the vector dot product between the vorticity and the local vector. Large positive values of H_d result in right-handed vortices, while large negative values indicate left-handed vortices. Helicity-density can be conveniently shown using isosurfaces, which gives an indication for the location and structure of a vortex.

9.3 Tensor Algorithms

In Chapter 6 we saw that 3×3 real symmetric tensors can be characterized by the eigenvalues and eigenvectors of the tensor. Recall that we can express the eigenvectors of the system as

ClearCorrect Exhibit 1002, Page 2395 of 3373



(a) Ellipse definition (b) Ellipse swept to create tube

Figure 9–14 Creation of hyperstreamlines. An ellipse is swept along a streamline of the eigenfield. Major/minor axes of the ellipse are controlled by the other two eigenvectors.

$$\vec{v}_i = \lambda_i e_i, \text{ with } i = 1, 2, 3 \qquad \textbf{(9-13)}$$

where e_i is a unit vector in the direction of the eigenvalue, and λ_i are the eigenvalues. Thus, we can decompose a 3×3 real symmetric tensor field into three vector fields, each field defined by one of the three eigenvectors described in Equation **9-13**. We call these vector fields *eigenfields*, since they are derived from the eigenvectors of the tensor field.

Decomposition of the tensor field in this fashion provides additional insight into visualizing 3×3 real symmetric tensors. We can directly use the vector field visualization techniques presented previously or use variations of them. One such technique is a novel extension of the streampolygon technique, the method of *hyperstreamlines*.

Hyperstreamlines

Hyperstreamlines are constructed by creating a streamline through one of the three eigenfields, and then sweeping a geometric primitive along the streamline [Delmarcelle93]. Typically, an ellipse is used as the geometric primitive, where the remaining two eigenvectors define the major and minor axes of the ellipse (Figure **9–14**). Sweeping the ellipse along the eigenfield streamline results in a tubular shape. Another useful generating geometric primitive is a cross. The length and orientation of the arms of the cross are controlled by two of the eigenvectors. Sweeping the cross results in a helical shape since the eigenvectors (and therefore cross arms) will rotate in some tensor fields.

Figure **9–15** shows an example of hyperstreamlines. The data is from a point load applied to a semi-infinite domain. Compare this figure to Figure **6–22** that used tensor ellipsoids to visualize the same data. Notice that there is less clutter and more information available from the hyperstreamline visualization.

ClearCorrect Exhibit 1002, Page 2396 of 3373

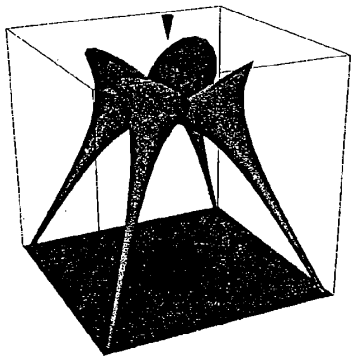


Figure 9–15 Example of hyperstreamlines (`Hyper.tcl`). The four hyperstreamlines shown are integrated along the minor principle stress axis. A plane (colored with a different lookup table) is also shown.

9.4 Modelling Algorithms

Visualizing Geometry

One of the most common applications of visualization is to view geometry. We may have a geometric representation of a part or complex assembly (perhaps designed on a CAD system) and want to view the part or assembly before it is manufactured. While viewing geometry is better addressed in a text on computer graphics, often there is dataset structure we wish to view in the same way. For example, we may want to see data mapped on a particular portion of the dataset, or view the structure of the dataset itself (e.g., view a finite element mesh).

Three-dimensional datasets have a surface and interior. Typically we want to visualize the surface of the dataset or perhaps a portion of the interior. (Note: volume rendering is a different matter — see "Volume Rendering" on page 216.) To visualize the dataset we must extract a portion of the dataset topology/geometry (and associated data) as some form of surface primitives such as polygons. If the surface of the dataset is opaque, we may also wish to eliminate occluded interior detail.

We have already seen how structured datasets, such as structured points or structured grids, have a natural *i-j-k* coordinate system that allow extraction of points, lines, and planes from the interior of the dataset (see "Structured Coordinate System" on page 311). For example, to extract the fifth *i*-plane from a struc-

ClearCorrect Exhibit 1002, Page 2397 of 3373

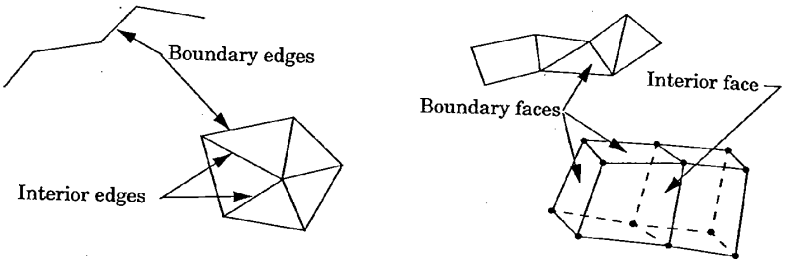


Figure 9–16 Boundary edges and faces.

tured grid of dimensions (i_m, j_m, k_m), we specify the data extents using $(4, 4, 0, (j_m - 1), 0, (k_m - 1))$ (assuming zero-offset addressing).

More generally, we can extract boundary edges and faces from a dataset. A boundary edge is an 1D cell type (e.g., line or polyline), or the edge of a 2D cell used by only that single cell. Similarly, a boundary face is a 2D cell type (e.g., polygon, triangle strip) or the face of a 3D cell used by only that single cell (Figure **9–16**). We can obtain this information using the topological operators of the previous chapter. Cells of dimensions two or less are extracted as is, while boundary edges and faces are determined by counting the number of cell neighbors for a particular topological boundary (i.e., edge or face neighbors). If there are no neighbors, the edge or face is a boundary edge or face, and is extracted.

Using these techniques we can view the structure of our dataset. However, there are also situations where we want more control in the selection of the data. We call this *data extraction*.

Data Extraction

Often we want to extract portions of data from a dataset. This may be because we want to reduce the size of the data, or because we are interested in visualizing only a portion of it.

Reducing dataset size is an important practical capability, because visualization data size can be huge. By reducing data size, reductions in computation and memory requirements can be realized. This results in better interactive response.

We also may need to reduce data size in order to visualize the important features of a large dataset. This can be used to reduce image clutter and improve the effectiveness of the visualization. Smaller data size also enables the visualization user to navigate through and inspect data more quickly relative to larger datasets. Next we describe two techniques to extract data. One is based on *geometry extraction*, and the other is based on *data thresholding*, or *thresholding*.

ClearCorrect Exhibit 1002, Page 2398 of 3373

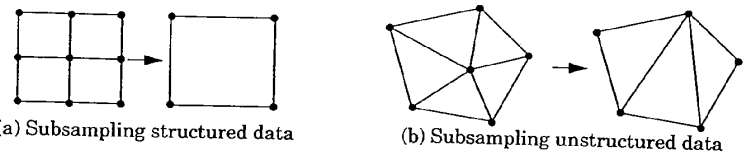


Figure 9–17 Subsampling data. (a) Structured data can be subsampled by choosing every *n*th point. (b) Subsampling unstructured data requires local retriangulation.

Geometry Extraction. Geometry extraction selects data based on geometric or topological characteristics. A common extraction technique selects a set of points and cells that lie within a specified range of ids. A typical example is selecting all cells having ids between 0–100, or all cells using point ids 250–500. Finite element analysts use this method frequently to isolate the visualization to just a few key regions.

Another useful technique called *spatial extraction*, selects dataset structure and associated data attributes lying within a specified region in space. For example, a point and radius can be used to select (or deselect) data within an enclosing sphere. Implicit functions are particularly useful tools for describing these regions. Points that evaluate negative are inside the region, while points outside the region evaluate positive; thus, cells whose points are all positive are outside the region, and cells whose points are all negative are inside the region.

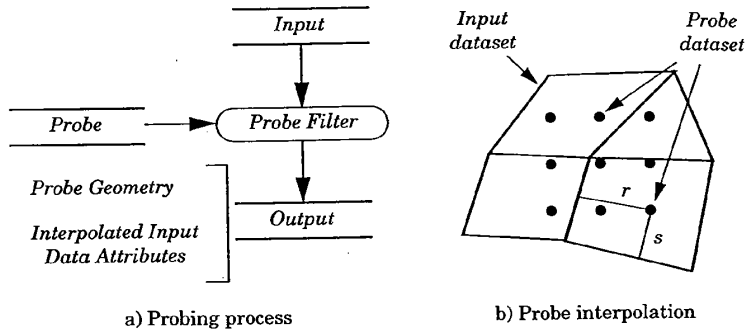
Subsampling (Figure **9–17**) is a method that reduces data size by selecting a subset of the original data. The subset is specified by choosing a parameter *n*, specifying that every *n*th data point is to be extracted. For example, in structured datasets such as structured points and grids, selecting every *n*th point produces the results shown in Figure **9–17**(a).

Subsampling modifies the topology of a dataset. When points or cells are not selected, this leaves a topological "hole." Dataset topology must be modified to fill the hole. In structured data, this is simply a uniform selection across the structured *i-j-k* coordinates. In unstructured data (Figure **9–17**(b)), the hole must be filled in by using triangulation or other complex tessellation schemes. Subsampling is not typically performed on unstructured data because of its inherent complexity.

A related technique is *data masking*. In data masking we select every *n*th cell that at a minimum leaves one or more topological "holes" in the dataset. Masking also may change the topology of the dataset, since partial selections of cells from structured datasets can only be represented using unstructured grids. Masking is typically used to improve interactive performance or to quickly process portions of data.

Thresholding. Thresholding extracts portions of a dataset data based on attribute values. For example, we may select all cells having a point with scalar

ClearCorrect Exhibit 1002, Page 2399 of 3373



a) Probing process

b) Probe interpolation

Figure 9–18 Probing data. The geometry of one dataset *(Probe)* is used to extract dataset attributes from another dataset *(Input)*.

value between (0,1) or all points having a velocity magnitude greater than 1.0.

Scalar thresholding is easily implemented. The threshold is either a single value that scalar values are greater than or less than, or a range of values. Cells or points whose associated scalar values satisfy the threshold criteria can be extracted. Other dataset attribute types such as vectors, normals, or tensors can be extracted in similar fashion by converting the type to a single scalar value. For example, vectors can be extracted using vector magnitude, and tensors using matrix determinate.

A problem with both geometry extraction and thresholding is that the approaches presented thus far extract "atomic" pieces of data, that is, a complete cell. Sometimes the cell may lie across the boundary of the threshold. In this case the cell must be clipped (see "Clipping With Scalar Fields" on page 360) and only a portion of the cell is extracted.

Probing

Probing obtains dataset attributes by sampling one dataset (the input) with a set of points (the probe) as shown in Figure **9–18**(a). Probing is also called "resampling." Examples include probing an input dataset with a sequence of points along a line, on a plane, or in a volume. The result of the probing is a new dataset (the output) with the topological and geometric structure of the probe dataset, and point attributes interpolated from the input dataset. Once the probing operation is completed, the output dataset can be visualized with any of the appropriate techniques described in this text.

Figure **9–18**(b) illustrates the details of the probing process. For every point in the probe dataset, the location in the input dataset (i.e., cell, subcell, and parametric coordinates) and interpolation weights are determined. Then the data

ClearCorrect Exhibit 1002, Page 2400 of 3373

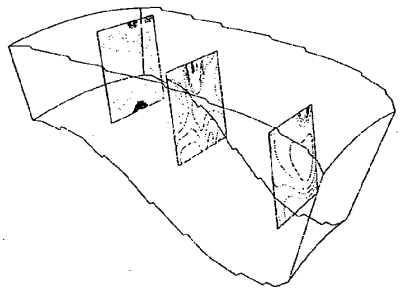


Figure 9–19 Probing data in a combustor. Probes are regular array of 50^2 points that are then passed through a contouring filter (`probeComb.tcl`).

values from the cell are interpolated to the probe point. Probe points that are outside the input dataset are assigned a nil (or appropriate) value. This process repeats for all points in the probe dataset.

Probing can be used to reduce data or to view data in a particular fashion.

- Data is reduced when the probe operation is limited to a subregion of the input dataset, or the number of probe points is less than the number of input points.
- Data can be viewed in a particular fashion by sampling on specially selected datasets. Using a probe dataset consisting of a line enables *x*-*y* plotting along a line, or using a plane allows surface color mapping or line contouring.

Probing must be used carefully or errors may be introduced. Under-sampling data in a region can miss important high-frequency information or localized data variations. Oversampling data, while not creating error, can give false confidence in the accuracy of the data. Thus the sampling frequency should have a similar density as the input dataset, or if higher density, the visualization should be carefully annotated as to the original data frequency.

One important application of probing converts irregular or unstructured data to structured form using a volume of appropriate resolution as a probe to sample the unstructured data. This is useful if we use volume rendering or other volume visualization techniques to view our data.

Figure **9–19** shows an example of three probes. The probes sample flow density in a structured grid. The output of the probes is passed through a contour filter to generate contour lines. As this figure illustrates, we can be selective with the location and extent of the probe, allowing us to focus on important regions in the data.

ClearCorrect Exhibit 1002, Page 2401 of 3373

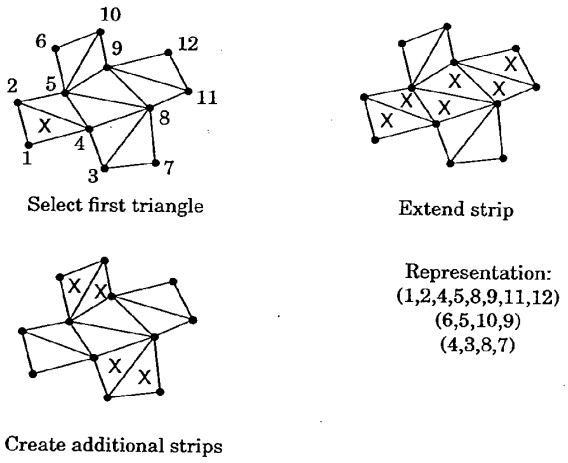


Figure 9–20 Creating triangle strips.

Triangle Strip Generation

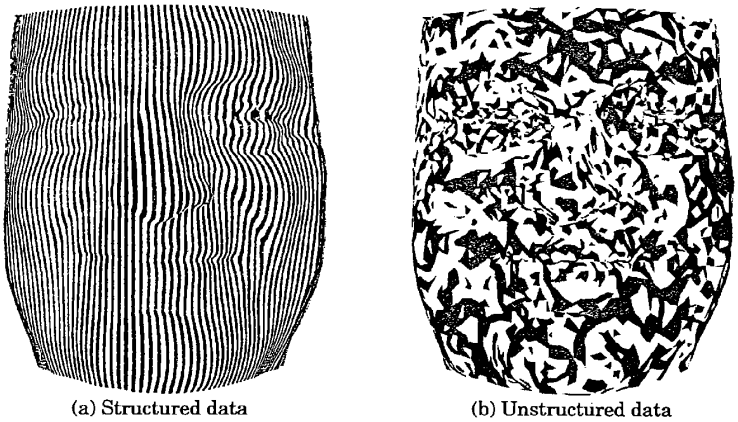
Triangle strips are compact representations of triangle polygons as described in "Triangle Strip" on page 121. Many rendering libraries include triangle strips as graphics primitives because they are a high-performance alternative to general polygon rendering.

Visualization and graphics data is often represented with triangles. Marching cubes, for example, generates thousands and potentially millions of triangles to represent an isosurface. To achieve greater performance in our visualizations, we can convert triangle polygons into triangle strips. Or, if data is represented using polygons, we can first triangulate the polygons and then create triangle strips.

A simple method to generate triangle strips uses greedy gathering of triangles into a strip (Figure **9–20**). The method proceeds as follows. An "unmarked" triangle is found to initialize the strip — unmarked triangles are triangles that have not yet been gathered into a triangle strip. Starting with the initial triangle, the strip may grow in one of three directions, corresponding to the three edges of the triangle. We choose to grow the strip in the direction of the first unmarked neighbor triangle we encounter. If there are no unmarked neighbors the triangle strip is complete; otherwise, the strip is extended by adding triangles to the list that satisfy triangle strip topology. The strip is grown until no unmarked neighbor can be found. Additional strips are then created using the same procedure until every triangle is marked.

The length of the triangle strips varies greatly depending on the structure

ClearCorrect Exhibit 1002, Page 2402 of 3373



(a) Structured data (b) Unstructured data

Figure 9–21 Triangle strip examples. (a) Structured triangle mesh consisting of 134 strips each of 390 triangles (`stripF.tcl`). (b) Unstructured triangle mesh consisting of 2227 strips of average length 3.94, longest strip 101 triangles. Images are generated by displaying every other triangle strip (`uStripeF.tcl`).

of the triangle mesh. Figure **9–21**(a) shows triangle strips each of 390 triangles in length from a dataset that was originally structured. Such a case is an exception: unstructured triangle meshes typically average about 5–6 triangles per strip (Figure **9–21**(b)). Even so, the memory savings are impressive. A triangle strip of length 6 requires 8 points to represent, while 8 triangles require 24 points, for a memory savings of 66.7 percent. Rendering speed may be greatly affected, too, depending upon the capabilities of the rendering system.

Connectivity

Intercell connectivity is a topological property of datasets. Cells are topologically connected when they share boundary features such as points, edges, or faces (Figure **9–22**). Connectivity is useful in a number of modeling applications, particularly when we want to separate out "parts" of a dataset.

One application of connectivity extracts a meaningful portion of an isosurface. If the isosurface is generated from measured data such as an MRI or CT scan, it likely contains "noise" or unimportant anatomical structure. Using connectivity algorithms, we can separate out the part of the isosurface that we desire, either by eliminating noise or undesirable anatomical structure. Figure **9–23** is an example where a 2D surface of interest (e.g., an isocontour) is extracted from a noisy signal.

Connectivity algorithms can be implemented using a recursive visit

ClearCorrect Exhibit 1002, Page 2403 of 3373

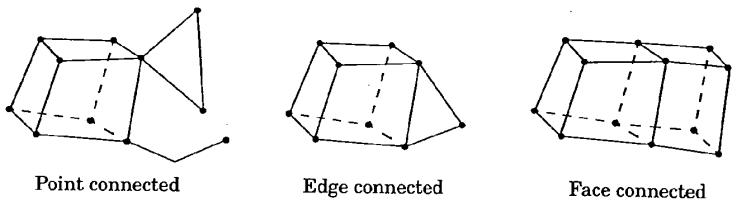


Figure 9–22 Connected cells.

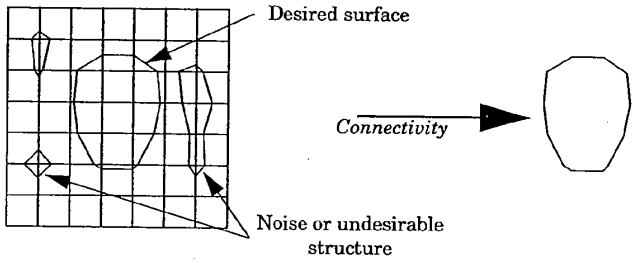


Figure 9–23 Extracting portion of isosurface of interest using connectivity.

method. We begin by choosing an arbitrary cell and mark it "visited". Then, depending upon the type of connectivity desired (i.e., point, edge, face), we gather the appropriate neighbors and mark them visited. This process repeats recursively until all connected cells are visited. We generally refer to such a set of connected cells as a connected "surface" even though the cells may be of a topological dimension other than two.

To identify additional connected surfaces we locate another unvisited cell and repeat the processes described previously. We continue to identify connected surfaces until every cell in the dataset is visited. As each connected surface is identified, it is assigned a surface number. We can use this number to specify the surfaces to extract or we can specify "seed" points or cells and extract the surfaces connected to them.

In some cases the recursion depth of the connectivity algorithm becomes larger than the computer system can manage. In this case, we can specify a maximum recursion depth. When this depth is exceeded, recursion is terminated and the current cells in the recursion are used as seeds to restart the recursion.

Polygon Normal Generation

Gouraud and Phong shading (see Chapter 3) can improve the appearance of rendered polygons. Both techniques require point normals. Unfortunately polygonal

ClearCorrect Exhibit 1002, Page 2404 of 3373

meshes do not always contain point normals, or data file formats may not support point normals. Examples include the marching cubes algorithm for general datasets (which typically will not generate surface normals) and the stereo lithography file format (does not support point normals). Figure **9–24**(a) shows a model defined from stereo-lithography format. The faceting of the model is clearly evident.

To address this situation we can compute surface normals from the polygonal mesh. A simple approach follows. First, polygon normals are computed around a common point. These normals are then averaged at the point, and the normal is renormalized (i.e., $|n| = 1$) and associated with the point. This approach works well under two conditions.

1. The orientation of all polygons surrounding the point are consistent as shown in Figure **9–24**(b). A polygon is oriented consistently if the order of defining polygon points is consistent with its edge neighbors. That is, if polygon p is defined by points *(1,2,3)*, then the polygon edge neighbor p_{23} must use the edge *(2,3)* in the direction *(3,2)*. If not consistent, then the average point normal may be zero or not accurately represent the orientation of the surface. This is because the polygon normal is computed from a cross product of the edges formed by its defining points.
2. The angular difference in surface normals between adjacent polygons is small. Otherwise, sharp corners or edges will have a washed out appearance when rendered, resulting in an unsatisfactory image (Figure **9–24**(c)).

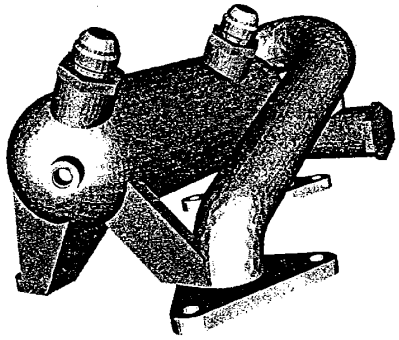
To avoid these problems we adopt a more complex polygon normal generation algorithm. This approach includes steps to insure that polygons are oriented consistently, and an edge-splitting scheme that duplicates points across sharp edges.

To orient edges consistently we use a recursive neighbor traversal. An initial polygon is selected and marked "consistent." For each edge neighbor of the initial polygon, the ordering of the neighbor polygon points is checked — if not consistent, the ordering is reversed. The neighbor polygon is then marked "consistent." This process repeats recursively for each edge neighbor until all neighbors are marked "consistent". In some cases there may be more than one connected surface, so that the process may have to be repeated until all polygons are visited.

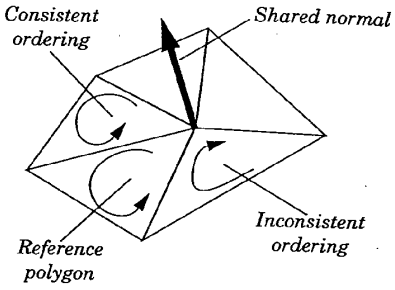
A similar traversal method splits sharp edges. A sharp edge is an edge shared by two polygons whose normals vary by a user-specified *feature angle*. The feature angle between two polygons is the angle between their normals (Figure **9–25**(a)). When sharp edges are encountered during the recursive traversal, the points along the edge are duplicated, effectively disconnecting the mesh along that edge (Figure **9–25**(b)). Then, when shared polygon normals are computed later in the process, contributions to the average normal across sharp edges is prevented.

On some computers limitations on recursion depth may become a problem. Polygonal surfaces can consist of millions of polygons, resulting in large recur-

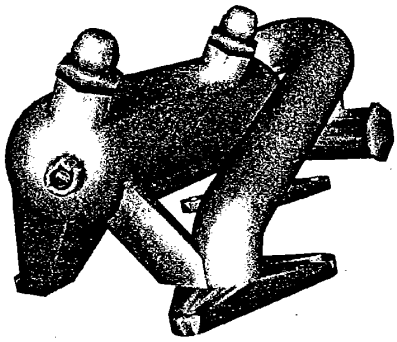
ClearCorrect Exhibit 1002, Page 2405 of 3373



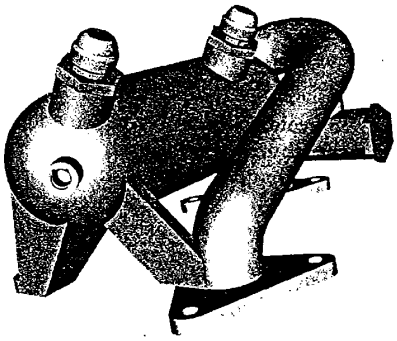
(a) Original faceted mode



(b) Normal computation



(c) Naive normal computation



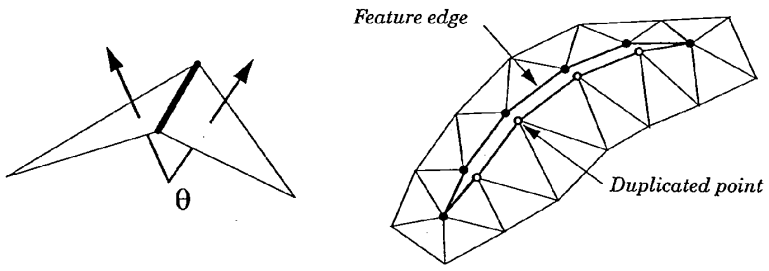
(d) Split-edge normal computation

Figure 9–24 Surface normal generation. (a) Faceted model without normals. (b) Polygons must be consistently oriented to accurately compute normals. (c) Sharp edges are poorly represented using shared normals as shown on the corners of this cube. (d) Normal generation with sharp edges split (`Normals.cxx`).

sion depth. As a result, the depth of recursion can be specified by the user. If recursion depth exceeds the specified value, the recursion halts and the polygons on the boundary of the recursion become seeds to begin the process again.

Figure **9–24**(d) shows the result of the advanced normal generation tech-

ClearCorrect Exhibit 1002, Page 2406 of 3373



a) Feature edge b) Exaggerated splitting of feature edge

Figure 9–25 Computing feature angles (a) and splitting edges (b).

nique with a feature angle of 60 degrees. Sharp edges are well defined and curved areas lack the faceting evident in the original model. The figure is shown with Gouraud shading.

Decimation

Various data compression techniques have been developed in response to large data size. The UNIX utilities `compress/uncompress` and the PC utility `zip` compress data files. The MPEG compression algorithm compresses video sequences. These techniques may be loss-less, meaning that no data is lost between the compression/decompression steps, or lossy, meaning that data is lost during compression. The utilities `compress/uncompress` and `zip` are loss-less, while MPEG is lossy.

In graphics, data compression techniques have been developed as well. The subsampling methods we saw earlier in this chapter are an example of simple data compression techniques for visualization data. Another emerging area of graphics data compression is polygon reduction techniques.

Polygon reduction techniques reduce the number of polygons required to model an object. The size of models, in terms of polygon count, has grown tremendously over the last few years. This is because many models are created using digital measuring devices such as laser scanners or satellites. These devices can generate data at tremendous rates. For example, a laser digitizer can generate on the order of 500,000 triangles in a 15-second scan. Visualization algorithms such as marching cubes also generate large numbers of polygons: one to three million triangles from a 512^3 volume is typical.

One polygon reduction technique is the decimation algorithm [Schroeder92a]. The goal of the decimation algorithm is to reduce the total number of triangles in a triangle mesh, preserving the original topology and forming a good approximation to the original geometry. A triangle mesh is a special form of a polygonal mesh, where each polygon is a triangle. If need be, a polygon mesh

ClearCorrect Exhibit 1002, Page 2407 of 3373

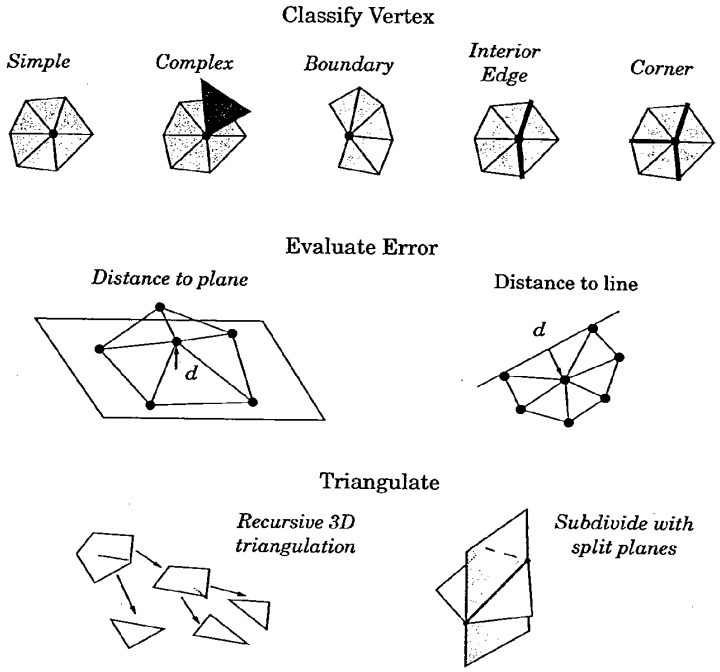


Figure 9–26 Overview of decimation algorithm.

can be converted to a triangle mesh using standard polygon triangulation methods.

Decimation is related to the subsampling technique for unstructured meshes described in Figure **9–17**(b). The differences are that

- decimation treats only triangle meshes not arbitrary unstructured grids;
- the choice of which points to delete is a function of a *decimation criterion*, a measure of the local error introduced by deleting a point; and
- the triangulation of the hole created by deleting the point is carried out in a way as to preserve edges or other important features.

Decimation proceeds by iteratively visiting each point in a triangle mesh. For each point, three basic steps are carried out (Figure **9–26**). The first step classifies the local geometry and topology in the neighborhood of the point. The classification yields one of the five categories shown in the figure: simple, boundary, complex, edge, and corner point. Based on this classification, the second step

ClearCorrect Exhibit 1002, Page 2408 of 3373

uses a local error measure (i.e., the decimation criterion) to determine whether the point can be deleted. If the criterion is satisfied, the third step deletes the point (along with associated triangles), and triangulates the resulting hole. A more detailed description of each of these steps and example applications follow.

Point Classification. The first step of the decimation algorithm characterizes the local geometry and topology for a given point. The outcome of classification determines whether the vertex is a potential candidate for deletion, and if it is, which criteria to use.

Each point may be assigned one of five possible classifications: simple, complex, boundary, interior edge, or corner vertex. Examples of each type are shown in Figure **9–26**.

A *simple point* is surrounded by a complete cycle of triangles, and each edge that uses the point is used by exactly two triangles. If the edge is not used by two triangles, or if the point is used by a triangle not in the cycle of triangles, then the point is *complex*. These are nonmanifold cases.

A point that is on the boundary of a mesh, that is, within a semicycle of triangles, is a *boundary point*.

A simple point can be further classified as an *interior edge* or *corner point*. These classifications are based on the local mesh geometry. If the surface normal angle between two adjacent triangles is greater than a specified *feature angle*, then a *feature edge* exists (see Figure **9–25**(a)). When a point is used by two feature edges, the point is an interior edge point. If one, three, or more feature edges use the point, the point is a *corner point*.

Complex and corner vertices are not deleted from the triangle mesh; all other vertices become candidates for deletion.

Decimation Criterion. Once we have a candidate point for deletion, we estimate the error that would result by deleting the point and then replacing it (and its associated triangles) with another triangulation. There are a number of possible error measures; but the simplest are based on distance measures of local planarity or local colinearity (Figure **9–26**).

In the local region surrounding a simple point, the mesh is considered nearly "flat," since there are by definition no feature edges. Hence, simple points use an error measure based on distance to plane. The plane passing through the local region can be computed either using a least-squares plane or by computing an area-averaged plane.

Points classified as boundary or interior edge are considered to lay on an edge, and use a distance to edge error measure. That is, we compute the distance that the candidate point is from the new edge formed during the triangulation process.

A point satisfies the decimation criterion d if its distance measure is less than d. The point can then be deleted. All triangles using the point are deleted as well, leaving a "hole" in the mesh. This hole is patched using a local triangulation process.

ClearCorrect Exhibit 1002, Page 2409 of 3373

Triangulation. After deleting a point, the resulting hole must be retriangulated. Although the hole, defined by a loop of edges, is topologically two dimensional, it is generally non-planar, and therefore general purpose 2D triangulation techniques cannot be used. Instead, we use a special recursive 3D divide-and-conquer technique to triangulate the loop.

Triangulation proceeds as follows. An initial split plane is chosen to divide the loop in half and create two subloops. If all the points in each subloop lie on opposite sides of the plane, then the split is a valid one. In addition, an *aspect ratio* check insures that the loop is not too long and skinny, thereby resulting in needle-like triangles. The aspect ratio is the ratio between the length of the split line to the minimum distance of a point in the subloop to the split plane. If the candidate split plane is not valid or does not satisfy the aspect ratio criterion, then another candidate split plane is evaluated. Once a split plane is found, then the subdivision of each subloop continues recursively until a subloop consists of three edges. In this case, the subloop generates a triangle and halts the recursion.

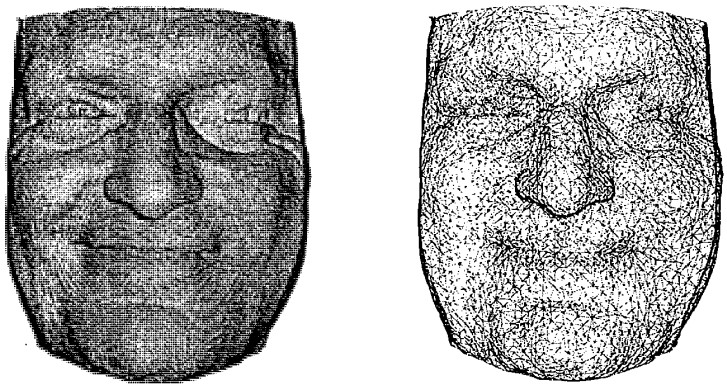
Occasionally, triangulation fails because no split plane can be found. In this case, the candidate point is not deleted and the mesh is left in its original state. This poses no problem to the algorithm and decimation continues by visiting the next point in the dataset.

Results. Typical compression rates for the decimation algorithm range from 2:1 to 100:1, with 10:1 a nominal figure for "large" (i.e., 10^5 triangles) datasets. The results vary greatly depending upon the type of data. CAD models typically reduce the least because these models have many sharp edges and other detailed features, and the CAD modellers usually produce minimal triangulations. Terrain data, especially if relatively flat regions are present, may reduce at rates of 100:1.

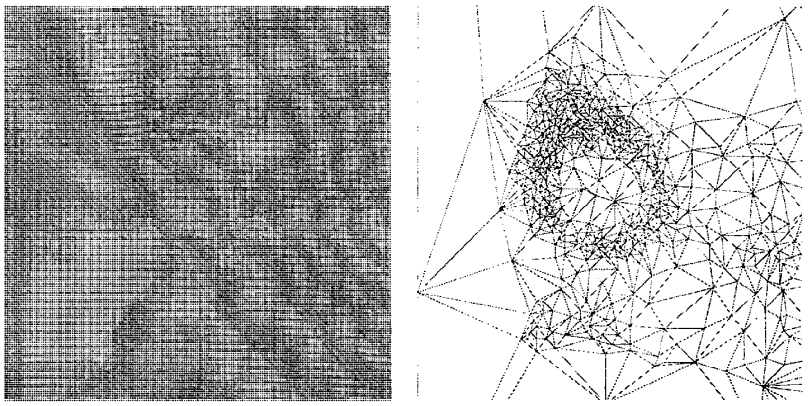
Figure **9–27** shows two applications of decimation to laser digitized data and to a terrain model of Honolulu, Hawaii. In both cases the reduction was on the order of 90 percent for a 10:1 compression ratio. Wireframe images are shown to accentuate the density of the polygonal meshes. The left-hand image in each pair is the original data; the right-hand image is the decimated mesh. Notice the gradations in the decimated mesh around features of high curvature. The advantage of decimation, as compared to subsampling techniques, is that the mesh is adaptively modified to retain more details in areas of high curvature.

Advanced Techniques. Polygon reduction is an active field of research. Many powerful algorithms beyond the decimation algorithm have been presented (see "Bibliographic Notes" on page 421). Although we cannot cover the field in its entirety in this section, there are two notable trends worth addressing. First, progressive schemes [Hoppe96] allow incremental transmission and reconstruction of triangle meshes — this is especially important for Web-based geometry visualization. Second, recent algorithms modify the topology of the mesh [He96] [Popovic97] [Schroeder97]. This feature is essential towards obtaining arbitrary levels of mesh reduction.

ClearCorrect Exhibit 1002, Page 2410 of 3373



(a) Decimation of laser digitizer data (`deciFran.tcl`).



(b) Decimation of terrain data (`deciHawa.tcl`).

Figure 9–27 Examples of decimation algorithm. Triangle meshes are shown in wireframe.

A *progressive mesh* is a series of triangle meshes M^i related by the operations

$$(\hat{M} = M^n) \rightarrow M^{n-1} \rightarrow \ldots \rightarrow M^1 \rightarrow M^0 \qquad \textbf{(9-14)}$$

where M and M^n represent the mesh at full resolution, and M^0 is a simplified base mesh. The critical characteristic of progressive meshes is that is possible to

ClearCorrect Exhibit 1002, Page 2411 of 3373

choose the mesh operations in such a way to make them invertible. Then the operations can be applied in reverse order (starting with the base mesh M^0)

$$M^0 \rightarrow M^1 \rightarrow \ldots \rightarrow M^{n-1} \rightarrow M^n \tag{9-15}$$

to obtain a mesh of desired reduction level (assuming that the reduction level is *less than* the base mesh M^0).

One such invertible operator is an edge collapse and its inverse is the edge split shown in Figure **9–28**(a). Each collapse of an interior mesh edge results in the elimination of two triangles (or one triangle if the collapsed vertex is on a boundary). The operation is represented by five values

$$\text{Edge Collapse/Split } (v_s, v_t, v_l, v_r, A) \tag{9-16}$$

where v_s is the vertex to collapse/split, v_t is the vertex being collapsed to / split from, and v_l and v_r are two additional vertices to the left and right of the split edge. These two vertices in conjunction with v_s and v_t define the two triangles deleted or added. A represents vertex attribute information, which at a minimum contains the coordinates x of the collapsed / split vertex v_s. (Note: in the context of the decimation algorithm, the edge collapse operator replaces the recursive triangulation process.)

While progressive meshes allow us to compactly store and transmit triangle meshes, the problem remains that the size of the base mesh is often larger than desired reduction level. Since in some applications we wish to realize *any* given level, we want the base mesh to contain no triangles

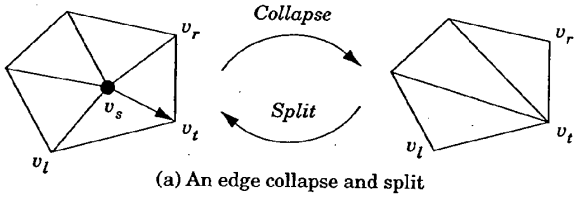
$$(\hat{M} = M^n) \rightarrow M^{n-1} \rightarrow \ldots \rightarrow M^1 \rightarrow (M^0 = M(V, \varnothing)) \tag{9-17}$$

(some vertices are necessary to initiate the edge split operations). To address this problem, the invertible edge collapse/split operator — which is topology preserving — is extended with a vertex split/merge operator. The vertex split/merge operator modifies the topology of the mesh and allows arbitrary levels of reduction.

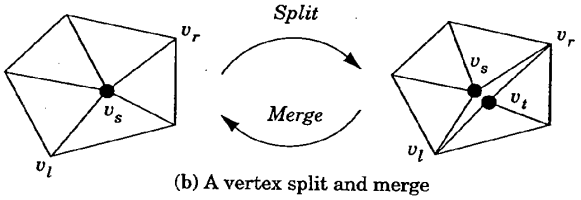
A mesh split occurs when we replace vertex v_s with vertex v_t in the connectivity list of one or more triangles that originally used vertex v_s (Figure **9–28**(b)). The new vertex v_t is given exactly the same coordinate value as v_s. Splits introduce a "crack" or "hole" into the mesh. We prefer not to split the mesh, but at high decimation rates this relieves topological constraint and enables further decimation. Splitting is only invoked when a valid edge collapse is not available, or when a vertex cannot be triangulated (e.g., a nonmanifold vertex). Once the split operation occurs, the vertices v_s and v_t are re-inserted into the priority queue.

Different splitting strategies are used depending on the classification of the vertex (Figure **9–28**(c)). Interior edge vertices are split along the feature edges, as are corner vertices. Nonmanifold vertices are split into separate manifold pieces. In any other type of vertex splitting occurs by arbitrarily separating the loop into two pieces. For example, if a simple vertex cannot be deleted because a

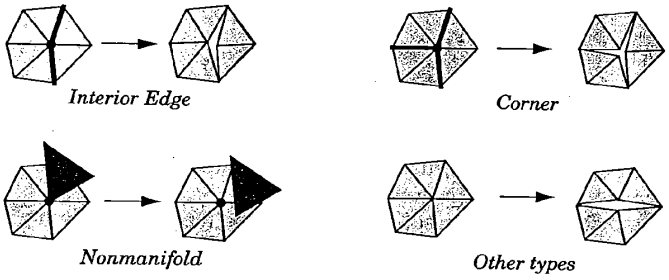
ClearCorrect Exhibit 1002, Page 2412 of 3373



(a) An edge collapse and split



(b) A vertex split and merge



(c) Vertex splits applied to various mesh features.Darker lines indicate feature edges.

Figure 9–28 Progressive mesh operators edge collapse/split and vertex split/merge.

valid edge collapse is not available, the loop of triangles will be arbitrarily divided in half (possibly in a recursive process).

Like the edge collapse/split, the vertex split/merge can also be represented as a compact operation. A vertex split/merge operation can be represented with four values

$$\text{Vertex Split/Merge } (v_s, v_t, v_l, v_r) \tag{9-18}$$

The vertices v_l and v_r define a sweep of triangles (from v_r to v_l) that are to be

ClearCorrect Exhibit 1002, Page 2413 of 3373

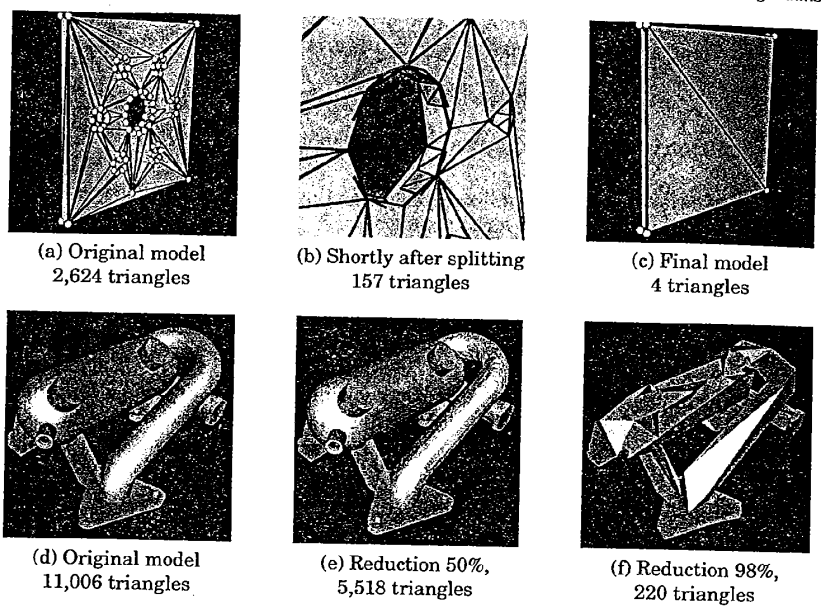


Figure 9–29 Results of topology modifying progressive mesh algorithm.

separated from the original vertex v_s (we adopt a counter-clockwise ordering convention to uniquely define the sweep of triangles).

Figure **9–29** shows the results of applying the topology modifying progressive mesh algorithm to two sets of data. In Figure **9–29**(a-c), a thin plate with holes is decimated (the darker lines show split edges). The middle image in the sequence shows the limits of topology on the algorithm. It is only when the topology of the mesh is allowed to be modified that the final level of reduction is possible. Figure **9–29**(d-f) shows the same algorithm applied to CAD data.

Mesh Smoothing

Mesh smoothing is a technique that adjusts the point coordinates of a dataset. The purpose of mesh smoothing is to improve the appearance of a mesh, and/or improve the shape of dataset cells. During smoothing the topology of the dataset is not modified, only the geometry. Applications of mesh smoothing include improving the appearance of isosurfaces, or as a modelling tool to remove surface noise. The appearance of models can be dramatically improved by applying mesh smoothing. Figure **9–30** is an example of smoothing applied to analytic surface (a semicylinder) with a random surface distortion (`smoothCyl.tcl`).

A simple, yet effective technique is Laplacian smoothing. The Laplacian

ClearCorrect Exhibit 1002, Page 2414 of 3373

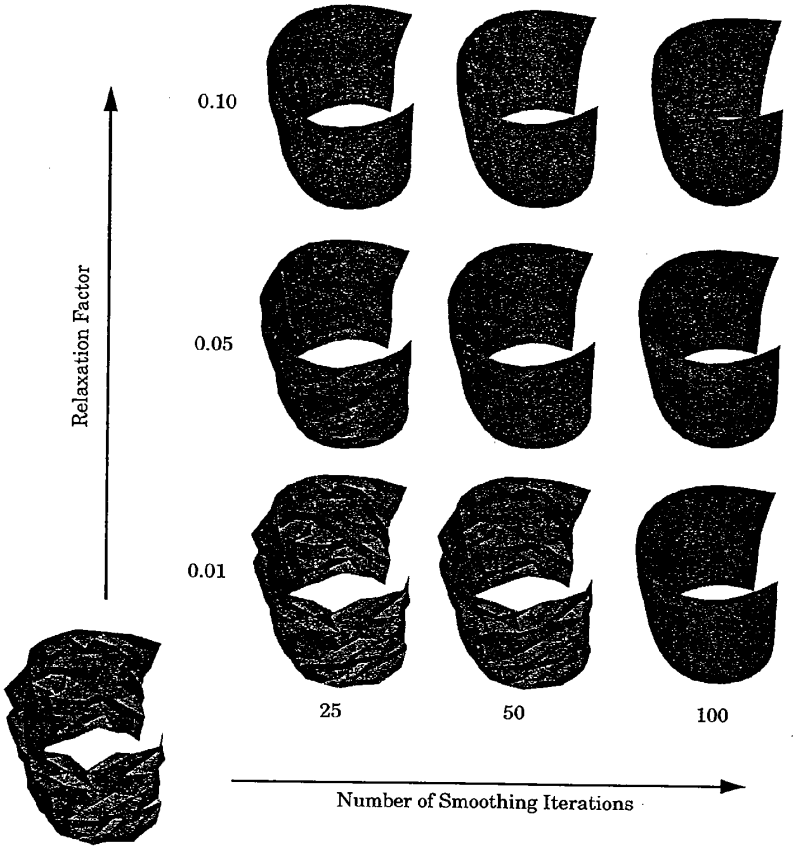


Figure 9–30 Mesh smoothing applied to a semicylinder. Lower left image is the original model. On the x-axis the number of smoothing iterations is modified. On the y-axis the relaxation factor is modified.

smoothing equation for a point p_i at position $\vec{x}_i$ is given by

$$\vec{x}_{i+1} = \vec{x}_i + \lambda \vec{V}_{ij} = \vec{x}_i + \lambda \sum (\vec{x}_j - \vec{x}_i) \quad \forall j{:}0 \le j < n \tag{9-19}$$

where $\vec{x}_{i+1}$ is the new coordinate position, and $\vec{x}_j$ are the positions of points p_j "connected" to p_i, and λ is a user-specified weight. Geometrically this relation is depicted in Figure **9–31**(a). Here the vertex p_i is connected to the surrounding points p_j via edges. The equation expresses that the new position $\vec{x}_{i+1}$ is offset

ClearCorrect Exhibit 1002, Page 2415 of 3373

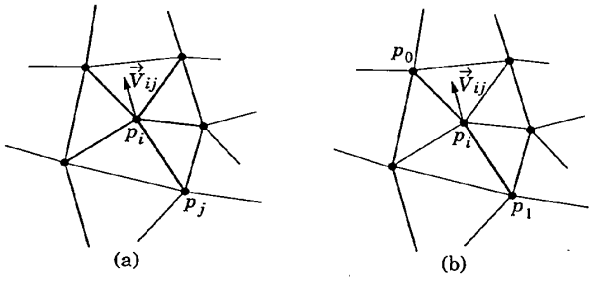


Figure 9–31 Mesh smoothing. (a) Motion of point. (b) Smoothing a point on an edge. Bold lines indicate connectivity.

from the original position $\vec{x}_i$ plus the average vector $\vec{V}_{ij}$ multiplied by λ. Typically, the factor λ is a small number (e.g., 0.01), and the process is executed repeatedly (e.g., 50-100 iterations). Notice that the overall effect of smoothing is to reduce the high frequency surface information. The algorithm will reduce surface curvature and tend to flatten the surface.

Besides adjusting the number of iterations and smoothing factor, smoothing can be controlled by modifying the connections between p_i and its surrounding points p_j. For example, if p_i lies along a fold or sharp edge in the mesh, we may want to only use the two edge end points to compute the smoothing vector $\vec{V}_{ij}$, limiting the motion of p_i along the edge (Figure **9–31**(b)). We can also anchor p_i to prevent any motion. Anchoring is useful for points that are located on "corners" or other special features such as nonmanifold attachments. One benefit of anchoring and controlling point connectivity is that we can limit the amount of shrinkage in the mesh. It also tends to produce better overall results. (In Figure **9–30** the boundary points of the surface are constrained to move along the boundary, while the points at sharp corners are anchored.)

Although Laplacian smoothing works well in most cases, there are applications of Laplacian smoothing that can badly damage the mesh. Large numbers of smoothing iterations, or large smoothing factors, can cause excessive shrinkage and surface distortion. Some objects, like spheres or the cylinder shown in Figure **9–30**, will lose volume with each iteration, and can even shrink to a point. In rare cases it is possible for the mesh to pull itself "inside-out." Situations like this occur when the average vector moves p_i across a mesh boundary, causing some of the attached triangles to overlap or intersect.

Mesh smoothing is particularly useful when creating models that do not require high accuracy. As we have seen, smoothing modifies point coordinates and, therefore, surface geometry. Use smoothing to improve the appearance of models, but characterize error carefully if you are going to measure from a smoothed surface. Alternatively, you may want to design your own smoothing algorithms that better fit the underlying data.

ClearCorrect Exhibit 1002, Page 2416 of 3373

Swept Volumes and Surfaces

Consider moving an object (e.g., your hand) over some path (e.g., raise your hand). How can we visualize this motion? The obvious answer is to form a time-animation sequence as the hand is moved. But what if we wish to statically represent the motion as well as the space that is traversed by the hand? Then we can use *swept surfaces* and *swept volumes*.

A swept volume is the volume of space occupied by an object as it moves through space along an arbitrary trajectory. A swept surface is the surface of the swept volume. Together, swept volumes and swept surfaces can statically represent the motion of objects.

Past efforts at creating swept surfaces and volumes have focused on analytical techniques. The mathematical representation of various 3D geometric primitives (e.g., lines, polygons, splines) was extended to include a fourth dimension of time (the path). Unfortunately, these approaches have never been practically successful, partly due to mathematical complexity and partly due to problem degeneracies.

Degeneracies occur when an n-dimensional object moves in such a way that its representation becomes $(n\text{-}1)$-dimensional. For example, moving a plane in the direction of its normal, sweeps out a 3D "cubical" volume. Sweeping the plane in a direction perpendicular to its normal, however, results in a degenerate condition, since the plane sweeps out a 2D "rectangle."

Instead of creating swept surfaces analytically, numerical approximation techniques can be used [Schroeder94]. Implicit modeling provides the basis for an effective technique to visualize object motion via swept surfaces and volumes. The technique is immune to degeneracies and can treat any geometric representation for which a distance function can be computed, such as the **vtk** cell types.

The technique to generate swept surfaces and volumes using an implicit modeling approach proceeds as follows. The geometric model, or part, and a path describing the parts motion, or sweep trajectory ST, must be defined. Then we use the following steps as depicted in Figure **9–32**.

1. Generate an implicit model from the part. This results in an implicit representation in the form of a volume. We call this the implicit model V_I.
2. Construct another volume, the workspace volume V_W, that strictly bounds V_I as it moves along the path ST. Then sweep V_I through V_W by moving in small steps, Δx, along ST. At each step, s, sample V_I with the workspace volume V_W. We use a boolean union operation to perform the sampling.
3. Extract isosurface, or offset surface(s) from V_W using a contouring algorithm such as marching cubes.
4. Step 3 may create multiple connected surfaces. If a single surface is desired, use connectivity to extract the single "largest" surface (in terms of number of triangles). This surface is an approximation to the swept surface, and the volume it encloses is an approximation to the swept volume.

ClearCorrect Exhibit 1002, Page 2417 of 3373

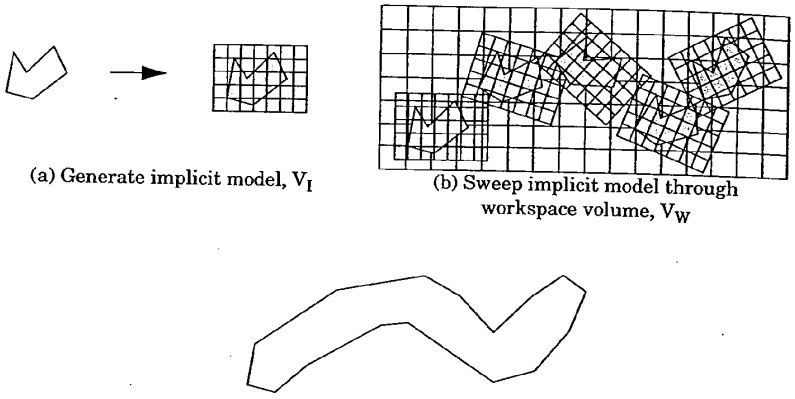


Figure 9–32 Overview of swept surface technique.

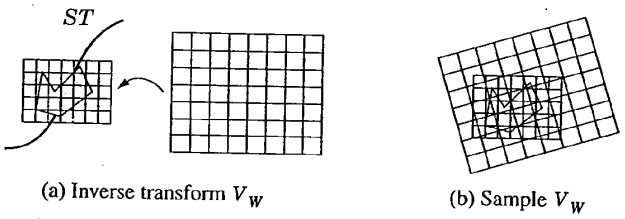
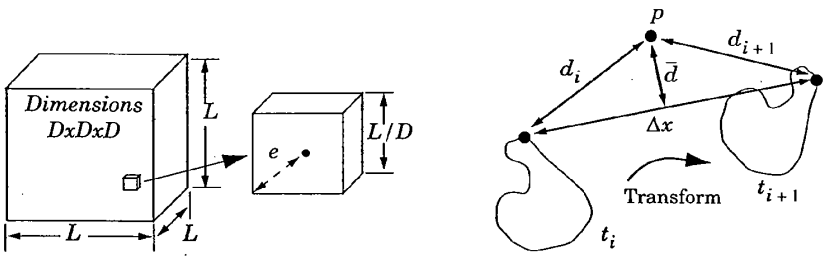


Figure 9–33 Generating workspace volume by sampling implicit volume.

There are a few points that require additional explanation. This algorithm uses two volumes, the implicit model and the workspace volume. Both are implicit models, but the workspace volume is used to accumulate the part as it moves along the sweep trajectory. In theory, the part could be sampled directly into the workspace volume to create the implicit model of the swept surface. Performance issues dictate that the implicit model is sampled into the workspace volume. This is because it is much faster to sample the implicit model of the part rather than the part itself, since computing the distance function from a part that may consist of tens of thousands of cells is relatively time-consuming, compared to sampling the implicit model V_I.

Sampling V_I is depicted in Figure **9–33**. The sweep trajectory is defined by

ClearCorrect Exhibit 1002, Page 2418 of 3373



(a) Sampling error (b) Stepping error

Figure 9–34 Computing sampling and stepping error.

a series of transformation matrices $ST = \{t_1, t_2, ..., t_m\}$. As the part moves along ST, interpolation is used to compute an inbetween transformation matrix t. Sampling is achieved by inverse transforming V_W into the local space of V_I using t. Then, similar to the probe operation described in "Probing" on page 374, the points of V_W are transformed by the inverse of the transformation matrix t^{-1}, and used to interpolate the distance values from the implicit model V_I.

Because we are dealing with an implicit modeling technique, parts with concave features can generate multiple surfaces. As discussed in "Connectivity" on page 377, the connectivity algorithm is used to separate out the swept surface. This final surface is an approximation to the actual swept surface, since we are sampling the actual geometric representation on an array of points (i.e., the implicit model), and then sampling the implicit model on another volume (i.e., the workspace volume). Also, stepping along the sweep trajectory generates errors proportional to the step size Δx.

These errors can be characterized as follows (Figure **9–34**). Given a voxel size L/D, where L is the edge length of the volume, and D is the dimension of the volume (assumed uniform for convenience), the maximum sampling error is

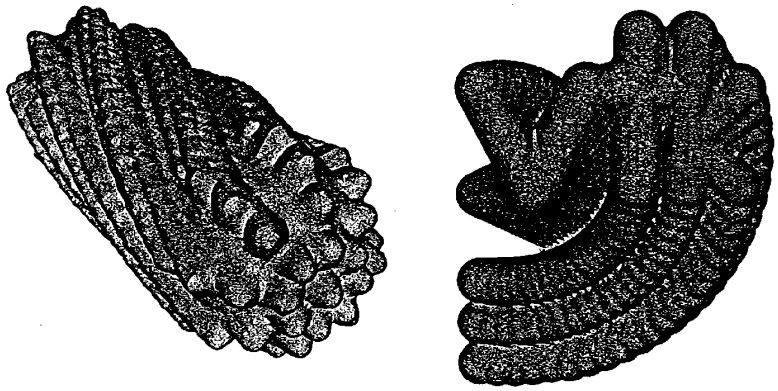
$$e \leq \frac{\sqrt{3}}{2}\left(\frac{L}{D}\right) \tag{9-20}$$

The error due to stepping, which includes both translation and rotational components, is bounded by $\Delta x/2$, where Δx is the maximum displacement of any point on the implicit model at any given translational step. Combining these terms for sampling both volumes and the error due to stepping, the total error is

$$e_{tot} \leq \frac{\sqrt{3}}{2}\left(\frac{L_I}{D_I} + \frac{L_W}{D_W}\right) + \frac{\Delta x}{2} \tag{9-21}$$

where the subscripts I and W refer to the implicit model and workspace volume, respectively.

ClearCorrect Exhibit 1002, Page 2419 of 3373



(a) Translated and rotated mace (b) Line-stroked "vtk"

Figure 9–35 Swept surfaces. (a) Swept mace sampled at 25 locations (`sweptMac.cxx`). (b) Swept vtk sampled at 21 locations (`sweptVtk.tcl`).

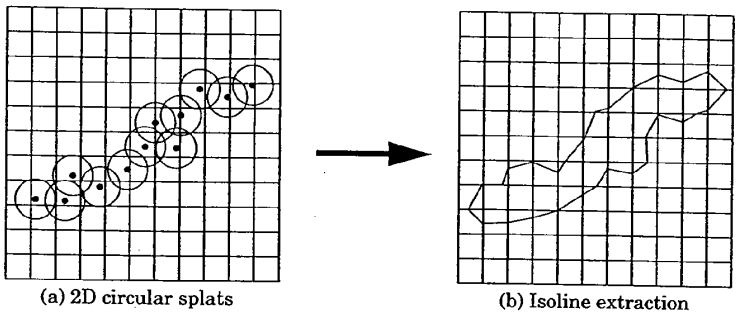
To show the application of this algorithm, we have generated swept surfaces for the letters "**vtk**" and the "mace" model as shown in Figure **9–35**. We have purposely chosen a step size to exaggerate the stepping error. Using more steps would smooth out the surface "bumps" due to stepping. Also, the appearance of the surface varies greatly with the selected isosurface value. Larger values give rounder, smoother surfaces. If you use small values near zero (assuming positive distance function) the surface may break up. To correct this you need to use a higher resolution workspace or compute negative distances. Negative distances are computed during the implicit modeling step by negating all points *inside* the original geometry. Negative distances allow us to use a zero isosurface value or to generate internal offset surfaces. Negative distances can only be computed for closed (i.e., manifold) objects.

Visualizing Unstructured Points

Unstructured point datasets consist of points at irregular positions in 3D space. The relationship between points is arbitrary. Examples of unstructured point datasets are visualizing temperature distribution from an array of (arbitrarily) placed thermocouples, or rainfall level measured at scattered positions over a geographic region.

Unlike structured points and grids, or even unstructured grids, unstructured point dataset have no topological component relating one point to another. For these reasons unstructured points are simple to represent but difficult to visualize. They are difficult to visualize because there is no inherent "structure"

ClearCorrect Exhibit 1002, Page 2420 of 3373



(a) 2D circular splats (b) Isoline extraction

Figure 9–36 Splatting techniques depicted in 2D. (a) Injecting points into structured point dataset (circular splats). (b) Visualizing structured point dataset via contouring.

to which we can apply our library of visualization techniques. Beyond just displaying points (possibly colored with scalar value, or using oriented vector glyphs) none of the techniques discussed thus far can be used. Thus, to visualize unstructured points we have to build structure to which we can apply our visualization techniques.

There are several approaches available to build topological structure given a random set of points. One common approach samples unstructured points with a structured point set, and then visualizes the data using standard volume or surface-based rendering techniques. Another approach creates n-dimensional triangulations from the unstructured points, thereby creating topological structure. These and other common techniques are described in the following sections.

Splatting Techniques. Splatting techniques build topological structure by sampling unstructured points with a structured point set (Figure **9–36**). The sampling is performed by creating special influence, or splatting, functions *SF(x,y,z)* that distribute the data value of each unstructured point over the surrounding region. To sample the unstructured points, each point is inserted into a structured point dataset *SP*, and the data values are distributed through *SP* using the splatting functions *SF(x,y,z)*. Once the topological structure is built, any structured point visualization technique can be used (including volume rendering).

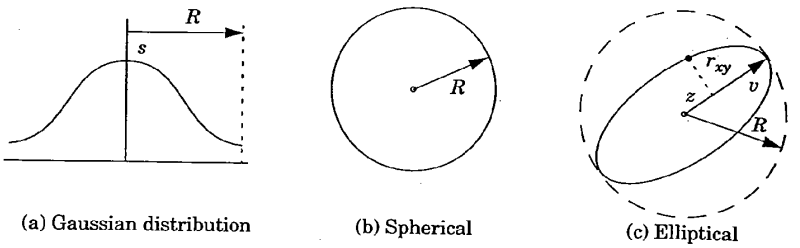
A common splatting function is a uniform Gaussian distribution centered at a point p_i. The function is conveniently cast into the form

$$SF(x, y, z) = se^{-f(r/R)^2} \tag{9-22}$$

where s is a scale factor that multiplies the exponential, f is the exponent scale factor $f \geq 0$, r is the distance between any point and the Gaussian center point (i.e., the splat point) $r = \|p - p_i\|$, and R is the radius of influence of the Gaussian, where $r \leq R$.

The Gaussian function (Figure **9–37**(a)) becomes a circle in cross section in

ClearCorrect Exhibit 1002, Page 2421 of 3373



(a) Gaussian distribution (b) Spherical (c) Elliptical

Figure 9–37 Gaussian splatting functions. (a) one-dimensional, (b) 2D spherical, and (c) 2D elliptical.

two dimensions (Figure **9–37**(b)) and a sphere in three dimensions. Since the value of the function is maximum when $r = 0$, the maximum value is given by the scale factor s. The parameter f controls the rate of decay of the splat. Scalar values can be used to set the value of s, so that relatively large scalar values create bigger splats than smaller values.

Splats may be accumulated using the standard implicit modeling boolean operations (Equation **6-13**, Equation **6-14**, and Equation **6-15**). That is, we may choose to form a union, intersection, or difference of the splats. The union and intersection operators are used most frequently.

Another interesting variation modifies the shape of the splat according to a vector quantity such as surface normal or vector data. Figure **9–37**(c) shows an example where the splat shape is elongated in the direction parallel to a vector. Thus, if we have a set of points and normals, we can create a polygonal surface by combining splatting with isosurface extraction.

To generate oriented splats, we modify Equation **9-22** by introducing an eccentricity factor E and the vector $\vec{v}$.

$$SF(x, y, z) = se^{-f\left(\frac{\left(\frac{r_{xy}}{E}\right)^2 + z^2}{R^2}\right)} \tag{9-23}$$

where z and r_{xy} are computed from

$$\begin{aligned} z &= \vec{v} \cdot (p - p_i), \text{ with } |\vec{v}| = 1 \\ r_{xy} &= r^2 - z^2 \end{aligned} \tag{9-24}$$

The parameter z is the distance along the vector $\vec{v}$, and the parameter r_{xy} is the distance perpendicular to v to the point p. The eccentricity factor controls the shape of the splat. A value $E = 1$ results in spherical splats, whereas $E > 1$ yields flattened splats and $E < 1$ yields elongated splats in the direction of the vector v.

ClearCorrect Exhibit 1002, Page 2422 of 3373

Figure 9–38(a) shows an elliptical splat with $E = 10$. (The splat surface is created by using isosurface extraction.) As expected, the splat is an ellipsoid. Figure 9–38(b) is an application of elliptical splatting used to reconstruct a surface from an unstructured set of points. The advantage of using an elliptical splat is that we can flatten the splat in the plane perpendicular to the point normal. This tends to bridge the space between the point samples. The surface itself is extracted using a standard isosurface extraction algorithm.

Interpolation Techniques. Interpolation techniques construct a function to smoothly interpolate a set of unstructured points. That is, given a set of n points $p_i = (x_i, y_i, z_i)$ and function values $F_i(p_i)$, a new function $F(p)$ is created that interpolates the points p_i. Once the interpolation function is constructed, we can build topological structure from the unstructured points by sampling $F(p)$ over a structured point dataset. We can then visualize the structured point dataset using the various techniques presented throughout the text.

Shepard's method is an inverse distance weighted interpolation technique [Wixom78]. The interpolation functions can be written

$$F(p) = \frac{\sum_{i=1}^{n} \frac{F_i}{|p - p_i|^2}}{\sum_{i=1}^{n} \frac{1}{|p - p_i|^2}} \tag{9-25}$$

where $F(p_i) = F_i$. Shepard's method is easy to implement, but has the undesirable property that limits its usefulness for most practical applications. The interpolation functions generate a local "flat spot" at each point p_i since the derivatives are zero

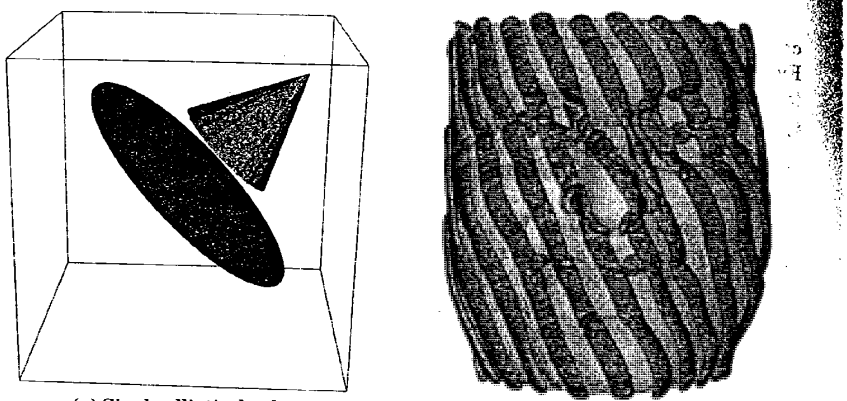
$$\frac{\partial F}{\partial x} = \frac{\partial F}{\partial y} = \frac{\partial F}{\partial z} = 0 \tag{9-26}$$

As a result, Shepard's method is overly constrained in the region around each point.

Shepard's method is an example of a basis function method. That is, the interpolation function *F(p)* consists of a sum of functions centered at each data point, p_i. Other basis function methods have been developed as described by Nielson [Nielson91]. They vary in localization of the basis functions and the sophistication of the interpolation function. Localization of basis functions means that their effect is isolated to a small region. Examples of more sophisticated basis functions include quadratic polynomials and cubic splines. Please see the references for more information.

Triangulation Techniques. Triangulation techniques build topology directly from unstructured points. The points are *triangulated* to create a topological structure

ClearCorrect Exhibit 1002, Page 2423 of 3373



(a) Single elliptical splat (b) Surface reconstruction

Figure 9–38 Elliptical splatting. (a) Single elliptical splat with eccentricity *E=10*. Cone shows orientation of vector (`singleSplat.cxx`). (b) Surface reconstructed using elliptical splats into 100^3 volume followed by isosurface extraction. Points regularly subsampled and overlayed on original mesh (`splatFace.tcl`).

consisting of n-dimensional simplices that completely bound the points and linear combinations of the points (the so-called *convex hull*). The result of triangulation is a set of triangles (2D) or tetrahedra (3D), depending upon the dimension of the input data [Lawson86].

An n-dimensional triangulation of a point set $P = (p_1, p_2, p_3, ..., p_n)$is a collection of n-dimensional simplices whose defining points lie in P. The simplices do not intersect one another and share only boundary features such as edges or faces. The Delaunay triangulation is a particularly important form [Bowyer81] [Watson81]. It has the property that the circumsphere of any n-dimensional simplex contains no other points of P except the $n+1$ defining points of the simplex (Figure **9–39**(a)).

The Delaunay triangulation has many interesting properties. In two dimensions, the Delaunay triangulation has been shown to be the optimal triangulation. That is, the minimum interior angle of a triangle in a Delaunay triangulation is greater than or equal to the minimum interior angle of any other possible triangulation. The Delaunay triangulation is the dual of the Dirichlet tessellation (Figure **9–39**(b)), another important construction in computational geometry. The Dirichlet tessellation, also known as the Voronoi tessellation, is a tiling of space where each tile represents the space closest to a point p_i. (The tiles are called Voronoi cells.) An n-dimensional Delaunay triangulation can be constructed from the Dirichlet tessellation by creating edges between Voronoi cells that share common $n-1$ boundaries (e.g., faces in 3D and edges in 2D). Conversely, the vertices of the Dirichlet tessellation are located at the circumcenters

ClearCorrect Exhibit 1002, Page 2424 of 3373

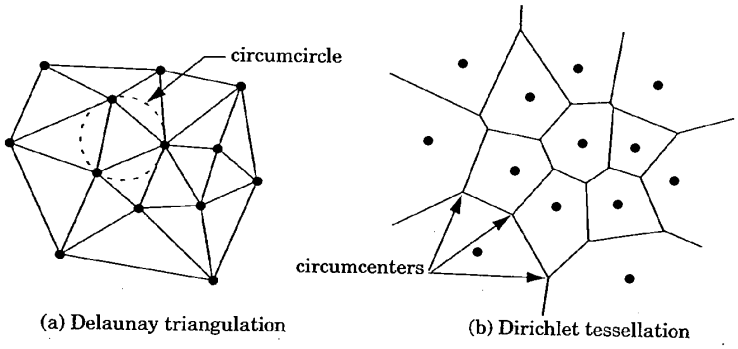


Figure 9–39 The Delaunay triangulation (a) and Dirichlet tessellation (b). The circumcircle of each triangle in a Delaunay triangulation contains no other points but the three vertices of the triangle. The region surrounding each point p_i in a Dirichlet tessellation is the set of points closest to p_i.

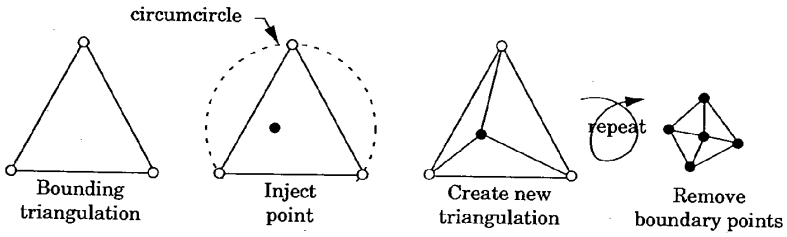


Figure 9–40 Computing the Delaunay triangulation using technique of Watson and Boyer. Points are injected into triangulation forming new Delaunay triangulations. In the final step, the initial bounding points are removed to reveal final triangulation.

of the Delaunay circumcircles.

The Delaunay triangulation can be computed using a variety of techniques. We describe a particularly elegant technique introduced independently by Watson [Watson81] and Bowyer [Bowyer81] (Figure **9–40**). The algorithm begins by constructing an initial Delaunay triangulation that strictly bounds the point set P, the so-called bounding triangulation. This bounding triangulation can be as simple as a single triangle (2D) or tetrahedron (3D). Then, each point of P is injected one by one into the current triangulation. If the injected point lies within the circumcircle of any simplex, then the simplex is deleted, leaving a "hole" in the triangulation. After deleting all simplices, the n–1 dimensional

ClearCorrect Exhibit 1002, Page 2425 of 3373

faces on the boundary of the hole, along with the injected point, are used to construct a modified triangulation. This is a Delaunay triangulation, and the process continues until all points are injected into the triangulation. The last step removes the simplices connecting the points forming the initial bounding triangulation to reveal the completed Delaunay triangulation.

This simplistic presentation of triangulation techniques has shown how to create topological structure from a set of unstructured points. We have ignored some difficult issues such as degeneracies and numerical problems. Degeneracies occur when points in a Delaunay triangulation lie in such a way that the triangulation is not unique. For example, the points lying at the vertices of a square, rectangle, or hexagon are degenerate because they can be triangulated in more than one way, where each triangulation is equivalent (in terms of Delaunay criterion) to the other. Numerical problems occur when we attempt to compute circumcenters, especially in higher-dimensional triangulations, or when simplices of poor aspect ratio are present.

Despite these problems, triangulation methods are a powerful tool for visualizing unstructured points. Once we convert the data into a triangulation (or in our terminology, an unstructured grid), we can directly visualize our data using standard unstructured grid techniques.

Hybrid Techniques. Recent work has focused on combining triangulation and basis function techniques for interpolating 2D bivariate data. The basic idea is as follows. A triangulation of P is constructed. Then an interpolating network of curves is defined over the edges of the triangulation. These curves are constructed with certain minimization properties of interpolating splines. Finally, the curve network is used to construct a series of triangular basis functions, or surface patches, that exhibit continuity in function value, and possibly higher order derivatives. (See [Nielson91] for more information.)

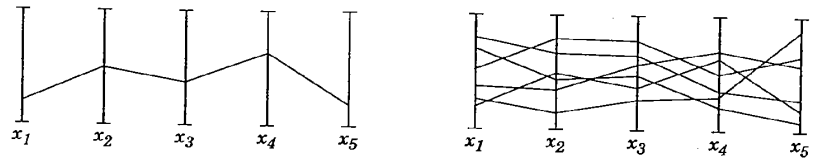
Multidimensional Visualization

The treatment of multidimensional datasets is an important data visualization issue. Each point in a dataset is described by an n-dimensional coordinate, where $n \geq 3$. Here we assume that each coordinate is an independent variable, and that we wish to visualize a single dependent variable. (Multidimensional visualization of vectors and tensors is an open research area.) An application of multidimensional data is financial visualization, where we might want to visualize return on investment as a function of interest rate, initial investment, investment period, and income, to name just a few possibilities.

There are two fundamental problems that we must address when applying multidimensional visualization. These are the problems of *projection* and *understanding*.

The problem of projection is that in using computer graphics we have two dimensions in which to present our data, or possibly three or four if we use specialized methods. Using 3D graphics we can give the illusion of three dimensions, or we can use stereo viewing techniques to achieve three dimensions. We can also

ClearCorrect Exhibit 1002, Page 2426 of 3373



(a) Plot of five-dimensional point (b) Plot of six points

Figure 9–41 Plotting a five-dimensional point using parallel coordinates. (a) plot of single point, (b) plot of many points.

use time as a fourth dimension by animating images. However, except for these limited situations, general n-dimensional data cannot be represented on a 2D computer screen.

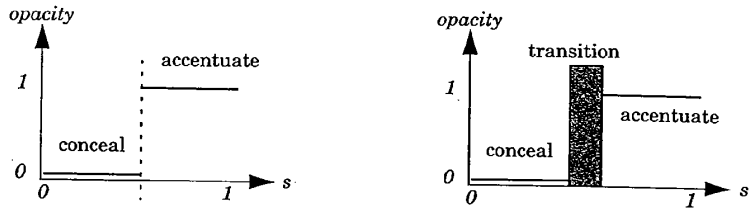
The problem of understanding is that humans do not easily comprehend more than three dimensions, or possibly three dimensions plus time. Thus, even if we could create a technique to display data of many dimensions, the difficulty in understanding the data would impair the usefulness of the technique.

Most multidimensional visualization techniques work with some form of dimension mapping, where n dimensions are mapped to three dimensions and then displayed with 3D computer graphics techniques. The mapping is achieved by fixing all variables except three, and then applying the visualization techniques described throughout the text to the resulting data. For maximum benefit, the process of fixing independent variables, mapping to three dimensions, and then generating visualization must be interactive. This improves the effectiveness of the visualization process, allowing the user to build an internal model of the data by manipulating different parts of the data.

One novel approach to multidimensional visualization has been proposed by Inselberg and Dimsdale [Inselberg87]. This approach uses *parallel coordinate systems*. Instead of plotting points on orthogonal axes, the i^{th} dimensional coordinate of each point is plotted along separate, parallel axes. This is shown in Figure **9–41** for a five-dimensional point. In parallel coordinate plots, points appear as lines. As a result, plots of n-dimensional points appear as sequences of line segments that may intersect or group to form complex fan patterns. In so doing, the human pattern recognition capability is engaged. Unfortunately, if the number of points becomes large, and the data is not strongly correlated, the resulting plots can become a solid mass of black, and any data trends are drowned in the visual display.

Another useful multivariable technique uses glyphs. This technique associates a portion of the glyph with each variable. Although glyphs cannot generally be designed for arbitrary n-dimensional data, in many applications we can create glyphs to convey the information we are interested in. Refer to "Glyphs" on page 185 for more information about glyphs.

ClearCorrect Exhibit 1002, Page 2427 of 3373



(a) Typical in/out map (b) Addition of transition region

Figure 9–42 1D texture map. (a) In/out map. (b) Addition of transition region to in/out map.

Texture Algorithms

Texturing is a common tool in computer graphics used to introduce detail without the high cost of graphics primitives. As we suggested in Chapter 7, texture mapping can also be used to visualize data. We explore a few techniques in the following sections.

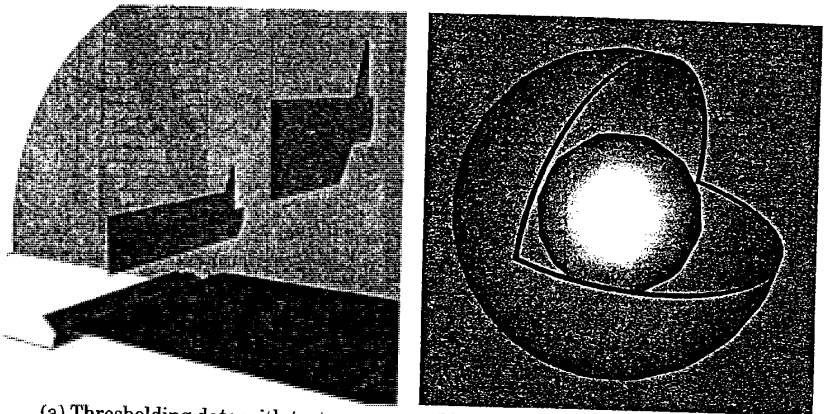
Texture Thresholding. We saw earlier how to threshold data based on scalar values (see "Thresholding" on page 373). We refer to this approach as *geometric thresholding* because structural components of a dataset (e.g., points and cells) are extracted based on data value. In contrast, we can use texture mapping techniques to achieve similar results. We call this technique *texture thresholding.*

Texture thresholding conceals features we do not want to see and accentuates features that we want to see. There are many variations on this theme. A feature can be concealed by making it transparent or translucent, by reducing its intensity, or using muted colors. A feature can be accentuated by making it opaque, increasing its intensity, or adding bright color. In the following paragraphs we describe a technique that combines intensity and transparency.

Texture thresholding requires two pieces of information: a texture map and an index into the map, or texture coordinate. In the simplest case we can devise a texture map that consists of two distinct regions as shown in Figure **9–42**(a). The first region is alternatively referred to as "conceal," "off," or "outside." The second region is referred to as "accentuate," "on," or "inside." (These different labels are used depending upon the particular application.) With this texture map in hand we can texture threshold by computing an appropriate texture coordinate. Areas that we wish to accentuate are assigned a coordinate to map into the "accentuate" portion of the texture map. Areas that we want to conceal are assigned a coordinate to map into the "conceal" portion of the texture map.

One texture threshold technique uses transparency. We can conceal a region by setting its alpha opacity value to zero (transparent), and accentuate it by setting the alpha value to one (opaque). Thus, the texture map consists of two

ClearCorrect Exhibit 1002, Page 2428 of 3373



(a) Thresholding data with texture

(b) Sphere cut with transparent texture

Figure 9–43 Examples of texture thresholding. (a) Using scalar threshold to show values of flow density on plane above value of 1.5 (`texThresh.tcl`). (b) Boolean combination of two planes to cut nested spheres (`tcutSph.cxx`).

regions: a concealed region with $\alpha = 0$ and an accentuated region with $\alpha = 1$. Of course, the effect can be softened by using intermediate alpha values to create translucent images.

An extension of this technique introduces a third region into the texture map: a transition region (Figure **9–42**(b)). The transition region is the region between the concealed and accentuated regions. We can use the transition region to draw a border around the accentuated region, further highlighting the region.

To construct the texture map we use *intensity-alpha,* or $I\alpha$ values. The intensity modulates the underlying color, while the alpha value controls transparency (as described previously). In the accentuated region, the intensity and opacity values are set high. In the concealed region, the intensity value can be set to any value (if $\alpha = 0$) or to a lower value (if $\alpha \neq 0$). The transition region can use various combinations of α and intensity. A nice combination produces a black, opaque transition region (i.e., $I = 0$ and $\alpha = 1$).

To visualize information with the thresholding technique, we must map data to texture coordinates. As we saw previously, we can use scalar values in combination with a threshold specification to map data into the concealed, transition, and accentuated regions of the texture map. Figure **9–43**(a) shows an example of texture thresholding applied to scalar data from a simulation of fluid flow. A scalar threshold s_T is set to show only data with scalar value greater than or equal to s_T.

Another useful texture thresholding application uses implicit functions to map point position to texture coordinate. This is similar in effect to geometric

ClearCorrect Exhibit 1002, Page 2429 of 3373

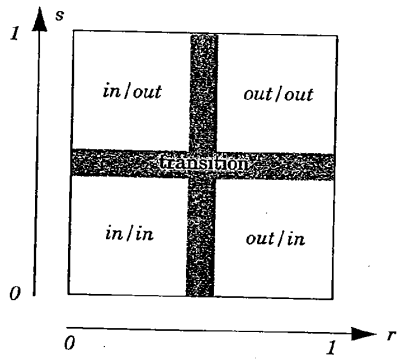


Figure 9–44 2D Boolean texture.

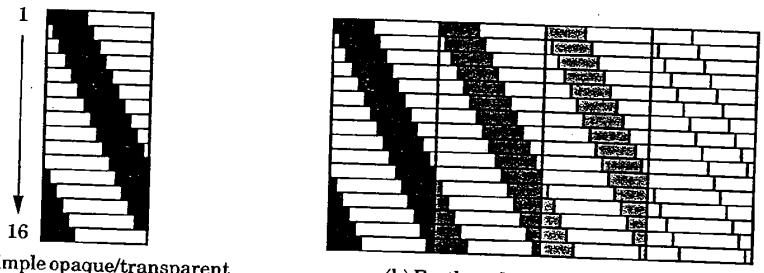
clipping (see "Clipping With Scalar Fields" on page 360). As we saw in "Implicit Functions" on page 180, implicit functions naturally map a (x, y, z) coordinate value into three regions: $F(x, y, z) < 0$, $F(x, y, z) = 0$, and $F(x, y, z) > 0$; or equivalently, the concealed, transition, and accentuated regions of the texture map. Using boolean combinations of implicit functions, we can create complex cuts of our data as illustrated in Figure **9–43**(b). This figure shows two nested spheres. The outer sphere is cut by a boolean combination of two planes to show the inner sphere.

Boolean Textures. Texture thresholding can be extended into higher dimensions. That is, 2D or 3D texture coordinates can be used to map two or three data variables into a texture map. One such technique is *boolean textures*, a method to clip geometry using a 2D texture map and two implicit functions [Lorensen93].

Boolean textures extend texture thresholding for geometric clipping from 1D to 2D. Instead of using a single implicit function to label regions "in" or "out", two implicit functions are used. This results in four different regions corresponding to all possible combinations of "in" and "out." The boolean texture map is modified to reflect this as shown in Figure **9–44**. As with 1D texture thresholding, transition regions can be created to separate the four regions.

The boolean texture map can be created with combinations of intensity and transparency values to achieve a variety of effects. By combining the four combinations of in/out (i.e., four regions of Figure **9–44**) with the two combinations of "conceal" and "accentuate," sixteen different boolean textures are possible. Figure **9–45**(a) illustrates these combinations expressed as boolean combinations of two implicit functions A and B. The "inside" of the implicit functions is indicated with subscript i, while the outside is indicated with subscript o. The boolean expressions indicate the regions that we wish to conceal, as shown by open circles. The darkened circles are the regions that are accentuated. We can see in Figure **9–45**(b) the effects of applying these different boolean textures to a

ClearCorrect Exhibit 1002, Page 2430 of 3373



(a) Simple opaque/transparent variation

(b) Feathered opaque/transparent variation

Figure 9–46 Texture maps for vector animation. Sixteen textures applied in succession create effect of motion along a vector. (a) Simple map. (b) Varying intensity "feathers" effect of motion.

sphere. The implicit functions in this figure are two elliptical cylinders sharing a common axis, and rotated 90 degrees from one another. In addition, transition regions have been defined with $I = 0$ to generate the dark cut edges shown. All 16 spheres share the same texture coordinates; only the texture map changes.

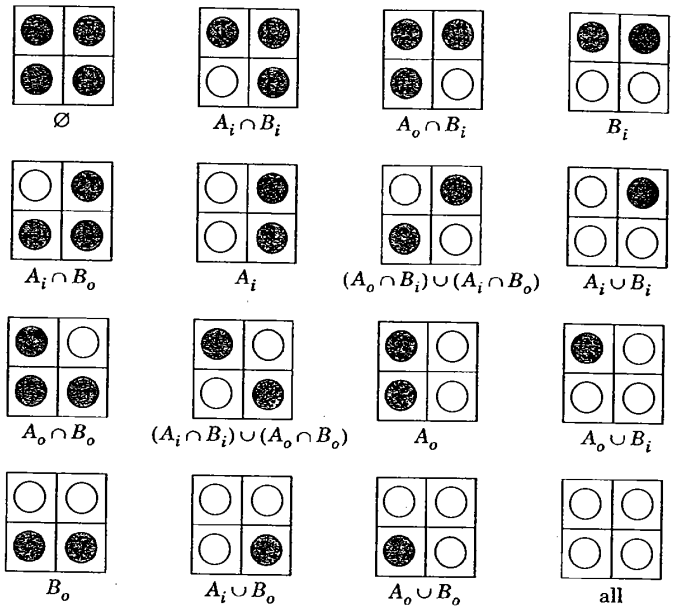
Texture Animation. Time-based animation techniques can illustrate motion or temporal data variations. This process often requires relatively large amounts of computer resource to read, process, and display the data. As a result, techniques to reduce computer resources are desirable when animating data.

Texture mapping can be used to animate certain types of data. In these techniques, the data is not regenerated frame by frame, instead a time-varying texture map is used to change the visual appearance of the data. An example of this approach is texture animation of vector fields [Yamrom95].

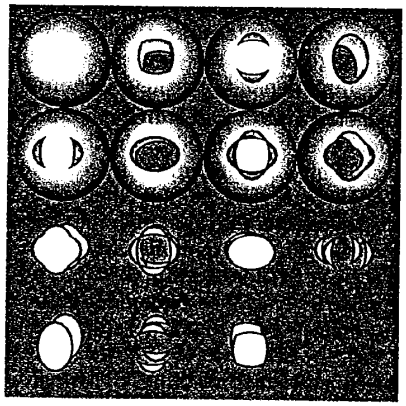
As we saw in "Hedgehogs and Oriented Glyphs" on page 167, vector fields can be represented as oriented and scaled lines. Texture animation can transform this static representational scheme into a dynamic representation. The key is to construct a series of 1D texture maps that when applied rapidly in sequence create the illusion of motion. Figure **9–46**(a) shows a series of sixteen such texture maps. The maps consist of intensity-alpha ($I\alpha$) values, A portion of the texture map is set fully opaque with full intensity ($I = 1, \quad \alpha = 1$). This is shown as the "dark" pattern in Figure **9–46**(a). The remainder of the map is set fully transparent with arbitrary intensity ($I = 1, \quad \alpha = 0$) shown as the "white" portion. As is evidenced by the figure, the sequence of 16 texture maps scanned top to bottom generate the appearance of motion from left to right. Notice also how the texture maps are designed to wrap around to form a continuous pattern.

Along with the 1D texture map, the texture coordinate s must also be generated — on a line this is straightforward. The line origin receives texture coordinate $s = 0$, while the line terminus receives texture coordinate value $s = 1$. Any intermediate points (if the vector is a polyline) are parameterized in monotonic

ClearCorrect Exhibit 1002, Page 2431 of 3373



(a) Combinations of 2D in/out textures



(b) Sixteen boolean textures (from above) applied to sphere (`quadricCut.cxx`)

Figure 9–45 Sixteen boolean textures. (a) Sixteen combinations of in/out. (b) Textures applied to sphere using two elliptical cylinder implicit functions.

ClearCorrect Exhibit 1002, Page 2432 of 3373

fashion in the interval (0,1). Texture coordinates need only be generated once. Only the texture map is varied to generate the vector animation.

Other effects are possible by modifying the texture map. Figure 9–46(b) shows a texture map with a repeating sequence of opaque/transparent regions. In each opaque region the intensity is gradually reduced from left to right. The result is that this tends to "feather" the appearance of the vector motion. The resulting image is more pleasing to the eye.

9.5 Putting It All Together

With the conclusion of this chapter we have provided an overview of the basics of data visualization. In this section we show you how to use some of the advanced algorithms as implemented in the *Visualization Toolkit*.

Dividing Cubes / Point Generation

Dividing cubes is implemented in **vtk** with the class `vtkDividingCubes`. It has been specialized to operate with structured point datasets. Besides specifying the contour value, you must specify a separation distance between points (using the method `SetDistance()`). If you desire a solid appearance, pick a distance that is less than or equal to display resolution.

The separation distance controls the accuracy of point generation. It is possible to generate points that appear to form a solid surface when rendered, but are not accurately located on the contour surface. Although this usually is not an issue when viewing contour surfaces, if the accuracy of the point positions is important, the distance value must be set smaller. However, this can result in huge numbers of points. To reduce the number of points, you can use the `SetIncrement()` method, which specifies that every nth point is to be generated. Using this approach, you can obtain good accuracy and control the total number of points. An example where point positions are important is when the points are used to locate glyphs or as seed points for streamline generation.

The *Visualization Toolkit* provides other point generation techniques. The source object `vtkPointSource` generates a user-specified number of points within a spherical region. The point positions are random within the sphere. (Note that there is a natural tendency for higher point density near the center of the sphere because the points are randomly generated along the radius and spherical angles ϕ and θ.)

Figure 9–47 is an example use of `vtkPointSource` to generate streamlines. The dataset is a structured grid of dimensions $21 \times 20 \times 20$ with flow velocity and a scalar pressure field. The dataset is a CFD simulation of flow in a small office. As this picture shows, there are a couple of bookcases, desks, a window, and an inlet and outlet for the ventilation system. On one of the desks is a small, intense heat source (e.g., a cigarette). In the left image 25 streamlines are started near the inlet using a `vtkPointSource` point generator. The second image shows what happens when we move the point source slightly to the left.

ClearCorrect Exhibit 1002, Page 2433 of 3373

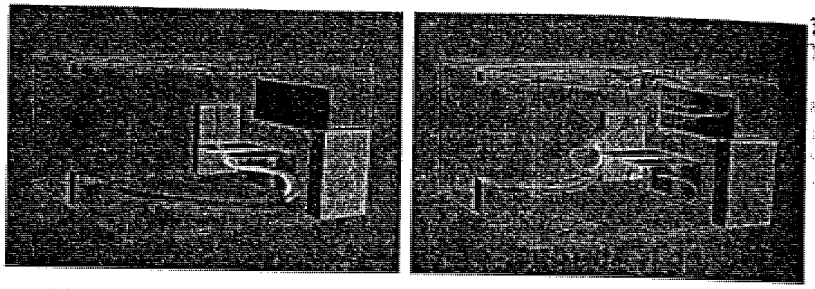


Figure 9–47 Using random point seeds to create streamlines (`office.tcl`).

By adjusting a single parameter (e.g., the center of the point source) it is possible to quickly explore our simulation data.

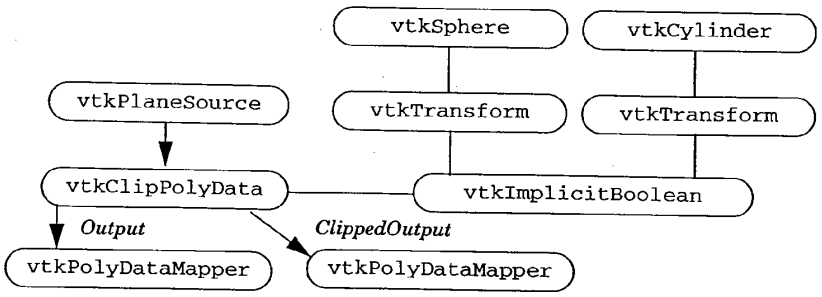
Another convenient object for point generation is the class `vtkEdgePoints`. `vtkEdgePoints` generates points on an isosurface. The points are generated by locating cell edges whose points are both above and below the isosurface value. Linear interpolation is used to generate the point. Since `vtkEdgePoints` operates on any cell type, this filter's input type is any dataset type (e.g., `vtkDataSet`). Unlike `vtkDividingCubes` this filter will not typically generate dense point clouds that appear solid.

Clipping with Scalar Fields

Clipping is implemented in `vtkClipPolyData`. Each polygonal data primitive implements the operation in its `Clip()` method using cases tables derived in a manner similar to that of triangles described on Page 360. `vtkClipPolyData` has methods to control whether an implicit function provides the scalar data or whether the dataset's scalar data will be used. `ComputeScalarDataOn()` uses the implicit function and `ComputeScalarDataOff()` uses the dataset's scalar data. Two output polygonal datasets are produced. These are accessed with `GetOutput()` and `GetClippedOutput()` methods. `GetOutput()` returns the polygonal data that is "inside" the clipping region while `GetClippedOutput()` returns polygonal data that is "outside" the region. (Note that `GenerateClippedOutputOn()` must be enabled if you are to get the clipped output.) The meaning of inside and outside can be reversed using the `InsideOutOn()` method. Figure **9–48** shows a plane of quadrilaterals clipped with a boolean implicit function.

Currently **vtk** supports clipping for all polygonal data cell types (vertices, polyvertices, line, polylines, polygons and triangle strips). Derivation of the cases for volumetric cell types like hexahedra are complex and require more research.

ClearCorrect Exhibit 1002, Page 2434 of 3373




```
vtkPlaneSource plane
  plane SetResolution 25 25
  plane SetOrigin -1 -1 0
  plane SetPoint1 1 -1 0
  plane SetPoint2 -1 1 0
vtkTransform trSphere
  trSphere Identity
  trSphere Translate .4 -.4 0
  trSphere Inverse
vtkSphere sphere
  sphere SetTransform trSphere
  sphere SetRadius .5
vtkTransform trCylinder
  trCylinder Identity
  trCylinder Translate -.4 .4 0
  trCylinder RotateZ 30
  trCylinder RotateY 60
  trCylinder RotateX 90
  trCylinder Inverse
vtkCylinder cylinder
  cylinder SetTransform trCylinder
  cylinder SetRadius .3
vtkImplicitBoolean boolean
  boolean AddFunction cylinder
  boolean AddFunction sphere
vtkClipPolyData clipper
  clipper SetInput [plane GetOutput]
  clipper SetClipFunction boolean
  clipper GenerateClippedOutputOn
  clipper GenerateClipScalarsOn
  clipper SetValue 0
```

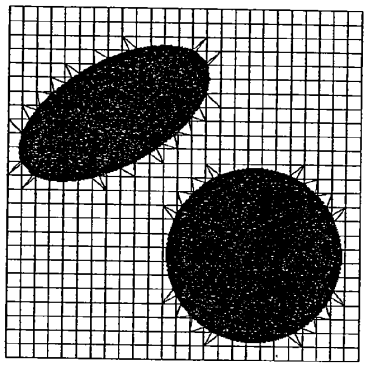


Figure 9–48 A plane clipped with a sphere and an ellipse. The two transforms place each implicit function into the appropriate position. Two outputs are generated by the clipper. (`clipSphCyl.tcl`).

ClearCorrect Exhibit 1002, Page 2435 of 3373

Swept Volumes and Surfaces

Swept surfaces can be applied in two interesting ways. First, they can be used as a modelling tool to create unusual shapes and forms. In this sense, swept surfaces are an advanced implicit modelling technique. Second, swept surfaces can be used to statically represent object motion. This is an important visualization technique in itself and has many important applications. One of these applications is design for maintainability.

When a complex mechanical system like a car engine is designed, it is important to design proper access to critical engine components. These components, like spark plugs, require higher levels of service and maintenance. It is important that these components can be easily reached by a mechanic. We've read horror stories of how it is necessary to remove an engine to change a spark plug. Insuring ready access to critical engine parts prevents situations like this from occurring.

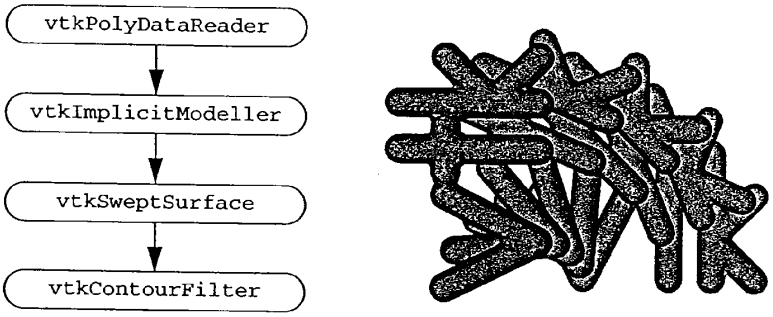
Swept surface can assist in the design of part access. We simply define a path to remove the part (early in the design process), and then generate a swept surface. This surface (sometimes referred to as a maintenance access solid or MAS) is then placed back into the CAD system. From this point on, the design of surrounding components such as fuel lines or wiring harnesses must avoid the MAS. As long as the MAS is not violated, the part can be removed. If the MAS is violated, a reevaluation of the removal path or redesign of the part or surrounding components is necessary.

Figure **9–49** shows how to create a swept surface from a simple geometric representation. The geometry is simply a line-stroked **vtk**. The next step is to define a motion path. This path is defined by creating a list of transformation matrices. Linear interpolation is used to generate intermediate points along the path if necessary.

In Figure **9–49** we also see the basic procedure to construct the swept surface. First, we must construct an implicit representation of the part by using `vtkImplictModeller`. This is then provided as input to `vtkSweptSurface`. It is important that the resolution of the implicit model is greater than or equal to that of `vtkSweptSurface`. This will minimize errors when we construct the surface. A bounding box surrounding the part and its motion can be defined, or it will be computed automatically. For proper results, this box must strictly contain the part as its moves. We also can set the number of interpolation steps, or allow this to be computed automatically as well. In the figure, we have chosen a small number to better illustrate the stepping of the algorithm.

Once `vtkSweptSurface` executes, we extract the swept surface using an isosurfacing algorithm. The isosurface value is an offset distance; thus we can create surfaces that take into account geometry tolerance. (This is particularly important if we are designing mechanical systems.) The implementation of the implicit modeller in **vtk** uses a positive distance function; so the isosurface value should always be positive. To create swept surfaces of zero and negative value requires a modification to the implicit modeller.

ClearCorrect Exhibit 1002, Page 2436 of 3373




```
# ingest data file
vtkPolyDataReader reader
  reader SetFileName "../../../vtkdata/vtk.vtk"

# create implicit model of vtk
vtkImplicitModeller imp
  imp SetInput [reader GetOutput]
  imp SetSampleDimensions 50 50 40
  imp SetMaximumDistance 0.25

# create swept surface
vtkTransformCollection transforms
vtkTransform t1
  t1 Identity
vtkTransform t2
  t2 Translate 0 0 2.5
  t2 RotateZ 90.0
transforms AddItem t1
transforms AddItem t2

vtkSweptSurface sweptSurfaceFilter
  sweptSurfaceFilter SetInput [imp GetOutput]
  sweptSurfaceFilter SetTransforms transforms
  sweptSurfaceFilter SetSampleDimensions 50 50 40
  sweptSurfaceFilter SetModelBounds -4.0  6.0  -1.0  6.0  -1.0
  sweptSurfaceFilter SetMaximumNumberOfInterpolationSteps 20

vtkContourFilter iso
  iso SetInput [sweptSurfaceFilter GetOutput]
  iso SetValue 0 0.33
```

Figure 9–49 Generating swept surface from line-stroked "vtk" (`sweptVtk.tcl`).

ClearCorrect Exhibit 1002, Page 2437 of 3373

Multidimensional Visualization

An important characteristic of multidimensional datasets is that they cannot be categorized according to any of the types defined in the *Visualization Toolkit*. This implies that source objects interfacing with multidimensional data are responsible for converting the data they interface with into one of the types defined in **vtk**. This can be a difficult process, requiring you to write interface code.

Other visualization systems treat this problem differently. In these systems a dataset type is defined that can represent multidimensional data. This dataset type is essentially an n-dimensional matrix. Additional filters are defined that allow the user to extract pieces of the dataset and assemble them into a more conventional dataset type, such as a volume or structured grid. After mapping the data from multidimensional form to conventional form, standard visualization techniques can be applied. (Future implementations of **vtk** may include this functionality. At the current time you must map multidimensional data into a known **vtk** form.)

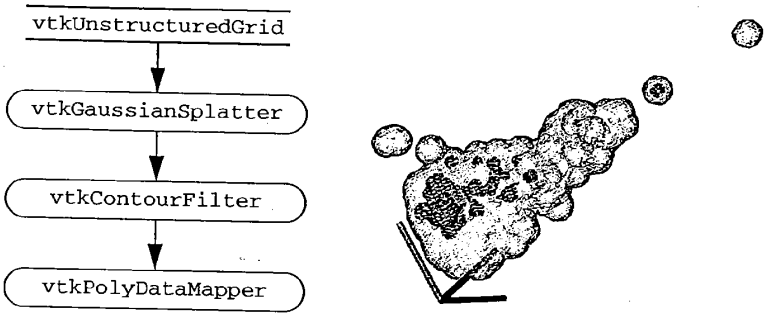
To demonstrate these ideas we will refer to Figure **9–50**. This is an example of multidimensional financial data. The data reflects parameters associated with monetary loans. In the file `financial.txt` there are six different variables: `TIME_LATE`, `MONTHLY_PAYMENT`, `UNPAID_PRINCIPLE`, `LOAN_AMOUNT`, `INTEREST_RATE`, and `MONTHLY_INCOME`. (Note: this is simulated data, don't make financial decisions based upon this!)

We will use Gaussian splatting to visualize this data (see "Splatting Techniques" on page 395). Our first step is to choose dependent and independent variables. This choice is essentially a mapping from multidimensional data into an unstructured point dataset. In this example we will choose `MONTHLY_PAYMENT`, `INTEREST_RATE`, and `LOAN_AMOUNT` as our (x, y, z) point coordinates, and `TIME_LATE` as a scalar value. This maps four of six variables. For now we will ignore the other two variables.

We use `vtkGaussianSplatter` to perform the splatting operation (i.e., conversion from unstructured points to volume dataset). This is followed by an isosurface extraction. We splat the data two times. The first time we splat the entire population. This is to show context and appears as gray/wireframe in the figure. The second time we splat the data and scale it by the value of `TIME_LATE`. As a result, only payments that are late contribute to the second isosurface.

The results of this visualization are interesting. First, we see that there is a strong correlation between the two independent variables `MONTHLY_PAYMENT` and `LOAN_AMOUNT`. (This is more evident when viewing the data interactively.) We see that the data falls roughly on a plane at a 45 degree angle between these two axes. With a little reflection this is evident: the monthly payment is strongly a function of loan amount (as well as interest rate and payment period). Second, we see that there is a clustering of delinquent accounts within the total population. The cluster tends to grow with larger interest rates and shrink with smaller monthly payments and loan amounts. Although the relationship with interest rate is expected, the clustering towards smaller monthly payments is not. Thus

ClearCorrect Exhibit 1002, Page 2438 of 3373




```
// construct pipeline for delinquent population
vtkGaussianSplatter *lateSplatter = vtkGaussianSplatter::New();
  lateSplatter->SetInput(dataSet);
  lateSplatter->SetSampleDimensions(50,50,50);
  lateSplatter->SetRadius(0.05);
  lateSplatter->SetScaleFactor(0.005);
  lateSplatter->DebugOn();

vtkContourFilter *lateSurface = vtkContourFilter::New();
  lateSurface->SetInput(lateSplatter->GetOutput());
  lateSurface->SetValue(0,0.01);
  lateSurface->DebugOn();

vtkPolyDataMapper *lateMapper = vtkPolyDataMapper::New();
  lateMapper->SetInput(lateSurface->GetOutput());
  lateMapper->ScalarVisibilityOff();

vtkActor *lateActor = vtkActor::New();
  lateActor->SetMapper(lateMapper);
  lateActor->GetProperty()->SetColor(1.0,0.0,0.0);
```

Figure 9–50 Visualization of multidimensional financial data. Visualization network, output image, and sample C++ code are shown (`finance.cxx`). The gray/wireframe surface represents the total data population. The dark surface represents data points delinquent on loan payment.

ClearCorrect Exhibit 1002, Page 2439 of 3373

our visualization has provided a clue into the data. Further exploration into the data may reveal the reason(s), or we may perform additional data analysis and acquisition to understand the phenomena.

One important note about multidimensional visualization. Because we tend to combine variables in odd ways (e.g., the use of MONTHLY_PAYMENT, INTEREST_RATE, and LOAN_AMOUNT as *(x, y, z)* coordinates), normalization of the data is usually required. To normalize data we simply adjust data values to lie between (0,1). Otherwise our data can be badly skewed and result in poor visualizations.

Connectivity

Many useful visualization algorithms often borrow from other fields. Topological connectivity analysis is one such technique. This technique is best categorized as a method in computational geometry, but serves many useful purposes in computer graphics and visualization.

To illustrate the application of connectivity analysis, we will use an MRI dataset generated by Janet MacFall at the Center for In Vivo Microscopy at Duke University. The dataset is a volume of dimensions 256^3 and is included on the CD-ROM. The data is of the root system of a small pine tree. Using the class `vtkSliceCubes`, an implementation of marching cubes for large volumes, we generate an initial isosurface represented by 351,118 triangles. (We have placed the file `pine_root.tri` on CD-ROM. This is a faster way of manipulating this data. If you have a large enough computer you can process the volume directly with `vtkVolume16Reader` and `vtkMarchingCubes`.)

Figure **9–51**(a) shows the initial dataset. Notice that there are many small, disconnected isosurfaces due to noise and isolated moisture in the data. We use `vtkConnectivityFilter` to remove these small, disconnected surfaces. Figure **9–51**(b) shows the result of applying the filter. Over 50,000 triangles were removed, leaving 299,480 triangles.

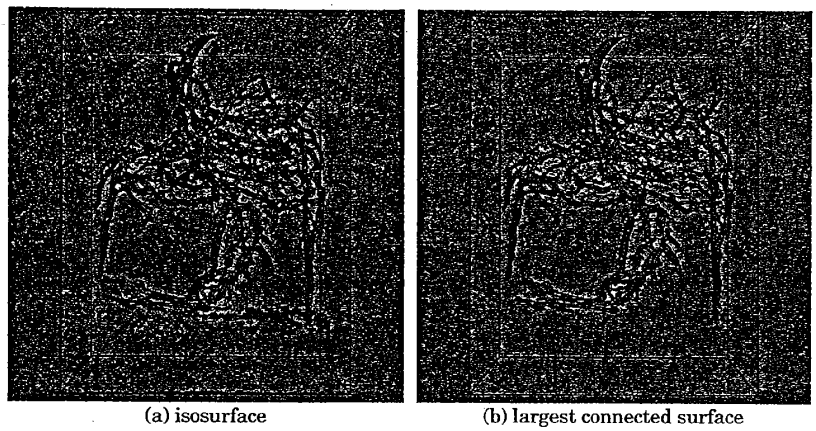
The `vtkConnectivityFilter` is a general filter taking datasets as input, and generating an unstructured grid as output. It functions by extracting cells that are connected at points (i.e., share common points). In this example the single largest surface is extracted. It is also possible to specify cell ids and point ids and extract surfaces connected to these.

Decimation

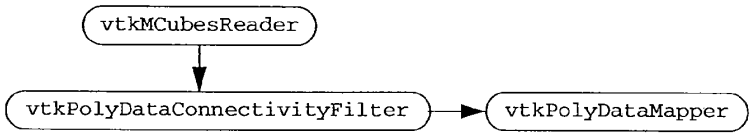
Decimation is a 3D data compression technique for surfaces represented as triangle meshes. We use it most often to improve rendering interactive response for large models.

Figure **9–52** shows the application of decimation to the data from the pine root example. The original model of 351,118 triangles is reduced to 81,111 triangles using a combination of decimation and connectivity. The decimation parameters are fairly conservative. Here we see a reduction of approximately 55 percent.

ClearCorrect Exhibit 1002, Page 2440 of 3373



(a) isosurface (b) largest connected surface




```
vtkMCubesReader reader
   reader SetFileName "../../../vtkdata/pineRoot/pine_root.tri"
vtkPolyDataConnectivityFilter connect
    connect SetInput [reader GetOutput]
    connect SetExtractionModeToLargestRegion
vtkPolyDataMapper isoMapper
    isoMapper SetInput [connect GetOutput]
    isoMapper ScalarVisibilityOff
vtkActor isoActor
    isoActor SetMapper isoMapper
    eval [isoActor GetProperty] SetColor $raw_sienna

vtkOutlineFilter outline
    outline SetInput [reader GetOutput]
vtkPolyDataMapper outlineMapper
    outlineMapper SetInput [outline GetOutput]
vtkActor outlineActor
    outlineActor SetMapper outlineMapper
```

Figure 9–51 Applying connectivity filter to remove noisy isosurfaces (`connPineRoot.tcl`). Data is from 256^3 volume data of the root system of a pine tree.

ClearCorrect Exhibit 1002, Page 2441 of 3373

The most common parameters to adjust in the `vtkDecimate` filter are the `TargetReduction`, `InitialError`, `ErrorIncrement`, `MaximumIterations`, and `InitialFeatureAngle`. `TargetReduction` specifies the compression factor (numbers closer to one represent higher compression). Because of topological, decimation criterion, aspect ratio, and feature angle constraints this reduction may not be realized (i.e., `TargetReduction` is a desired goal, not a guaranteed output). The `InitialError` and `ErrorIncrement` control the decimation criterion. As the filter starts, the decimation criterion is set to `InitialError`. Then, for each iteration the decimation criterion is incremented by `ErrorIncrement`. The algorithm terminates when either the target reduction is achieved, or the number of iterations reaches `MaximumIterations`. The `InitialFeatureAngle` is used to compute feature edges. Smaller angles force the algorithm to retain more surface detail.

Other important parameters are the `AspectRatio` and `MaximumSubIterations`. `AspectRatio` controls the triangulation process. All triangles must satisfy this criterion or the vertex will not be deleted during decimation. A sub-iteration is an iteration where the decimation criterion is not incremented. This can be used to coalesce triangles during rapid rates of decimation. `MaximumSubIterations` controls the number of sub-iterations. This parameter is typically set to two.

Texture Clipping

Texture mapping is a powerful visualization technique. Besides adding detail to images with minimal effort, we can perform important viewing and modelling operations. One of these operations is clipping data to view internal structure.

Figure **9–53** is an example of texture clipping using a transparent texture map. The motor show consists of five complex parts, some of which are hidden by the outer casing. To see the inside of the motor, we define an implicit clipping function. This function is simply the intersection of two planes to form a clipping "corner." The object `vtkImplicitTextureCoords` is used in combination with this implicit function to generate texture coordinates. These objects are then rendered with the appropriate texture map and the internal parts of the motor can be seen.

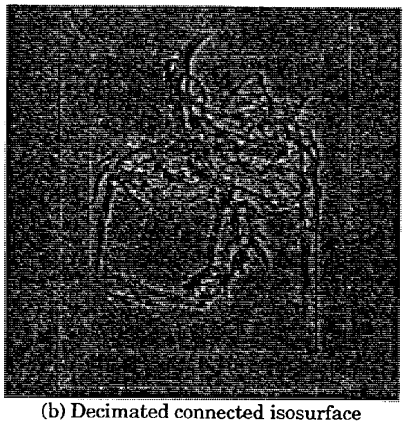
The texture map consists of three regions (as described previously in the chapter). The concealed region is transparent. The transition region is opaque but with a black (zero intensity) color. The highlighted region is full intensity and opaque. As can be seen from Figure **9–53**, the boundaries appear as black borders giving a nice visual effect.

The importance of texture techniques is that we can change the appearance of objects and even perform modelling operations like clipping with little effort. We need only change the texture map. This process is much faster relative to the alternative approach of geometric modelling. Also, hardware support of texture is becoming common. Thus the rendering rate remains high despite the apparent increase in visual complexity.

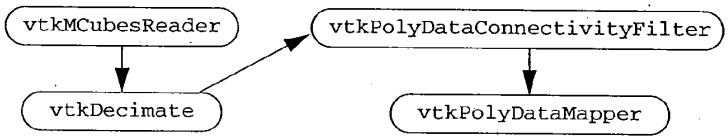
ClearCorrect Exhibit 1002, Page 2442 of 3373



(a) Connected isosurface



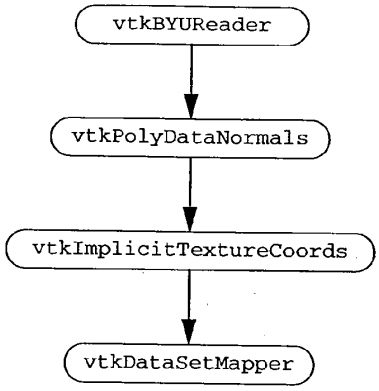
(b) Decimated connected isosurface

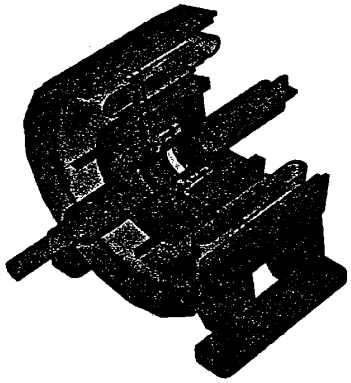



```
vtkMCubesReader reader
    reader SetFileName "../../../vtkdata/pineRoot/pine_root.tri"
     reader FlipNormalsOff
     reader DebugOn
vtkDecimate deci
     deci SetInput [reader GetOutput]
     deci SetTargetReduction 0.9
     deci SetAspectRatio 20
     deci SetInitialError 0.0005
     deci SetErrorIncrement 0.001
     deci SetMaximumIterations 6
     deci SetInitialFeatureAngle 30
vtkPolyDataConnectivityFilter connect
     connect SetInput [deci GetOutput]
     connect SetExtractionModeToLargestRegion
vtkPolyDataMapper isoMapper
     isoMapper SetInput [connect GetOutput]
     isoMapper ScalarVisibilityOff
```

Figure 9–52 Applying connectivity and decimation filters to remove noisy isosurfaces and reduce data size (`deciPineRoot.tcl`). Data is from 256^3 volume data of the root system of a pine tree.

ClearCorrect Exhibit 1002, Page 2443 of 3373





```
# texture
vtkStructuredPointsReader texReader
    texReader SetFileName "../../../vtkdata/texThres.vtk"
vtkTexture texture
    texture SetInput [texReader GetOutput]
    texture InterpolateOff
    texture RepeatOff

# read motor parts...each part colored separately
#
vtkBYUReader byu
    byu SetGeometryFileName "../../../vtkdata/motor.g"
    byu SetPartNumber 1
vtkPolyDataNormals normals
    normals SetInput [byu GetOutput]
vtkImplicitTextureCoords tex1
    tex1 SetInput [normals GetOutput]
    tex1 SetRFunction planes
vtkDataSetMapper byuMapper
    byuMapper SetInput [tex1 GetOutput]
vtkActor byuActor
    byuActor SetMapper byuMapper
    byuActor SetTexture texture
    eval [byuActor GetProperty] SetColor $cold_grey

# other parts follow...
```

Figure 9–53 Texture cut used to reveal internal structure of a motor. Two cut planes are used in combination with transparent texture (`motor.tcl`).

ClearCorrect Exhibit 1002, Page 2444 of 3373

Delaunay Triangulation

Delaunay triangulation is used to construct topology from unstructured point data. In two dimensions we generate triangles (i.e., an unstructured grid or polygonal dataset) while in three dimensions we generate tetrahedra (i.e., an unstructured grid). Typical examples of structured points include points measured in space, or a dimensional subset of multidimensional data.

In the example of Figure 9–54 we show how to create a 2D Delaunay triangulation from a field of points. The points are created by generating random x and y coordinate values in the interval [0, 1], and setting the z-value to a constant value (i.e., the points lie in an x-y plane). The points are then triangulated, and tubes and sphere glyphs are used to highlight the resulting points and edges of the triangulation.

One important concern regarding Delaunay triangulations is that the process is numerically sensitive. Creating triangles with poor aspect ratio (e.g., slivers) can cause the algorithm to break down. If you have a large number of points to triangulate, you may want to consider randomizing the point order. This approach tends to generate triangles with better aspect ratio and give better results. You may also want to consider other implementations of Delaunay triangulation that are more numerically robust. See [Edelsbrunner94] for an example.

9.6 Chapter Summary

Dividing cubes is a scalar contouring operation that generates points rather than surface primitives such as lines or polygons. Dense point clouds appear solid because of the limited resolution of computer images.

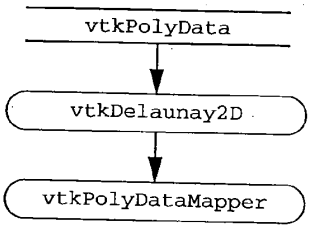
Vector fields have a complex structure. This structure can be visualized using streamribbons, streamsurfaces, and streampolygons. The topology of a vector field can be characterized by connecting critical points with streamlines.

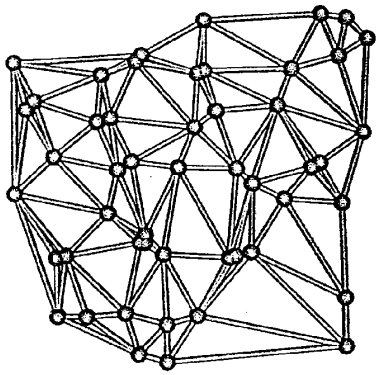
Tensor fields consist of three orthogonal vector fields. The vector fields are the major, medium, and minor eigenvectors of the tensor field. Hyperstreamlines can be used to visualize tensor fields.

Dataset topology operations generate triangle strips, extract connected surfaces, and compute surface normals. Decimation is a polygon reduction algorithm that reduces the number of triangles in a triangle mesh. Implicit modelling techniques can be used to construct swept surfaces and volumes. Unstructured points are easy to represent but difficult to visualize. Splatting, interpolation, and triangulation techniques are available to construct structure for unstructured points. Multivariate visualization is required for data of dimension four and higher. Data must be mapped to three dimensions before standard visualization techniques can be used. Parallel coordinates techniques are also available to visualize multivariate data.

Modelling algorithms extract geometric structure from data, reduce the complexity of the data or create geometry. Spatial extraction selects dataset

ClearCorrect Exhibit 1002, Page 2445 of 3373





```
# create some points
vtkMath math
vtkFloatPoints points
for {set i 0} {$i<50} {incr i 1} {
    eval points InsertPoint $i [math Random 0 1] \
                               [math Random 0 1] 0.0
}

vtkPolyData profile
    profile SetPoints points

# triangulate them
vtkDelaunay2D del
    del SetInput profile
    del SetTolerance 0.001
vtkPolyDataMapper mapMesh
    mapMesh SetInput [del GetOutput]
```

Figure 9–54 Two-dimensional Delaunay triangulation of a random set of points. Points and edges are shown highlighted with sphere glyphs and tubes (`DelMesh.tcl`). Only the pipeline to generate triangulation is shown.

structure and associated data attributes lying within a specified region in space. Subsampling reduces data by selecting every nth data point. A related technique, data masking, selects every nth cell. Subsets of a dataset can also be selected using thresholding, which selects cells or points that lie within a range of scalar values. Probing resamples data at a set of points. The probe produces a dataset that has the topology of the probe with data values from the probed dataset. Generating triangle strips can reduce storage requirements and improve rendering speeds on some systems. If a dataset has multiple disjoint structures, a connectivity algorithm can uniquely identify the separate structures. For polygonal data that does not have vertex normals defined, normal generation algorithms can compute these values that are suitable for interpolation

ClearCorrect Exhibit 1002, Page 2446 of 3373

by Gouraud or Phong shading. Decimation, another data reduction technique, removes triangles in "flat" regions and fills the resulting gaps with new triangles. Unstructured points present a challenge because the data does not have topology. Splatting represents each point in the data with a structured point set and accumulates these splats using implicit modelling techniques. Triangulation techniques build topology directly from the unstructured points.

Multidimensional visualization techniques focus on data that has many scalar data values for each point. Parallel coordinates is an interesting approach that plots the scalar values for a data point along a parallel axis. The observer looks for trends and relationships between the lines that represent each point's data.

Texture algorithms use texture coordinates and texture maps to select or highlight portions of a dataset. Texture thresholding assigns texture coordinates based on a scalar value. The scalar value and texture map determine how a cell or portion of a cell is rendered. Boolean textures extend this concept to 2D and 3D. Careful design of a boolean texture map permits the "clipping" of geometry with combinations of implicit surfaces. Texture can also be used to animate vector fields.

9.7 Bibliographic Notes

Dividing cubes is an interesting algorithm because of the possibilities it suggests [Cline88]. Point primitives are extremely simple to render and manipulate. This simplicity can be used to advantage to build accelerated graphics boards, perform 3D editing, or build parallel visualization algorithms.

Many plotting and visualization systems use carpet plots extensively. Carpet plots are relatively easy to represent and render. Often 2D plotting techniques are used (i.e., lighting and perspective effects ignored). Check [Wang90] for additional information on rendering carpet plots.

In recent years a number of powerful vector visualization techniques have emerged. These techniques include streamsurfaces [Hultquist92], streampolygons [Schroeder91], vector field topology [Helman91] [Globus91], streamballs [Brill94], and vorticity visualization [Banks94]. The streamballs technique is a recent technique that combines techniques from implicit modeling. You may also wish to see references [Crawfis92] [vanWijk93] and [Max94]. These describe volume rendering and other advanced techniques for vector visualization, topics not well covered in this text.

Some abstract yet beautiful visualization images are due to Delmarcelle and Hesselink [Delmarcelle93]. Their rendering of hyperstreamlines reflect the underlying beauty and complexity of tensor fields.

Polygon reduction is a relatively new field of study. SIGGRAPH '92 marked a flurry of interest with the publication of two papers on this topic [Schroeder92a] [Turk92]. Since then a number of valuable techniques have been published. One of the best techniques, in terms of quality of results, is given by [Hoppe93], although it is limited in time and space because it is based on formal

ClearCorrect Exhibit 1002, Page 2447 of 3373

optimization techniques. Other interesting methods include [Hinker93] and [Rossignac93]. A promising area of research is multiresolution analysis, where wavelet decomposition is used to build multiple levels of detail in a model [Eck95]. The most recent work in this field stresses progressive transmission of 3D triangle meshes [Hoppe96], improved error measures [Garland97], and algorithms that modify mesh topology [Popovic97] [Schroeder97].

Triangle strip generation is an effective technique for achieving dramatic improvements in rendering speed and reductions in data handling. The reference by [Evans96] describes other triangle strip generation algorithms as well as presenting some of the most effective techniques to date.

The use of texture for visualization is relatively unexploited. This has been due in part to lack of texture support in most graphics software and hardware. This is now changing, as more vendors support texture and software systems (such as OpenGL) that provide an API for texture. Important references here include the boolean textures [Lorensen93] and surface convolution techniques [Cabral93] [Stalling95].

Unstructured or unorganized point visualization is likely to play a prominent role in visualization as the field matures and more complex data is encountered. Nielson et al. have presented important work in this field [Nielson91].

Multidimensional visualization is another important focus of visualization research [Bergeron89] [Mihalisin90]. Much real-world data is both unstructured and multidimensional. This includes financial databases, marketing statistics, and multidimensional optimization. Addressing this type of data is important to achieve future advances in understanding and application. Feiner [Feiner90] has presented a simple projection method combined with virtual reality techniques. [Inselberg87] has introduced parallel coordinates. These techniques have been shown to be powerful for many types of visual analysis.

9.8 References

[Banks94]

D. C. Banks and B. A. Singer. "Vortex Tubes in Turbulent Flows: Identification, Representation, Reconstruction." In *Proceedings of Visualization '94*. pp. 132–139, IEEE Computer Society Press, Los Alamitos, CA, 1994.

[Bergeron89]

R. D. Bergeron and G. Grinstein. "A Reference Model for the Visualization of Multidimensional Data." In *Proceedings Eurographics '89*. pp. 393–399, North Holland, Amsterdam, 1989.

[Bowyer81]

A. Bowyer. "Computing Dirichlet Tessellations." *The Computer Journal*. 24(2):162–166, 1981.

[Brill94]

M. Brill, H. Hagen, H-C. Rodrian, W. Djatschin, S. V. Klimenko. "Streamball Techniques for Flow Visualization." In *Proceedings of Visualization '94*. pp. 225–231, IEEE Computer Society Press, Los Alamitos, CA, 1994.

ClearCorrect Exhibit 1002, Page 2448 of 3373

[Cabral93]
B. Cabral and L. Leedom. "Imaging Vector Fields Using Line Integral Convolution." In *Proceedings of SIGGRAPH '93*, pp. 263–270, Addison-Wesley, Reading, MA, 1993.

[Cline88]
H. E. Cline, W. E. Lorensen, S. Ludke, C. R. Crawford, and B. C. Teeter, "Two Algorithms for the Three-Dimensional Construction of Tomograms." *Medical Physics*. 15(3):320–327, June 1988.

[Crawfis92]
R, Crawfis and N. Max. "Direct Volume Visualization of Three Dimensional Vector Fields." In *Proceedings 1992 Workshop on Volume Visualization*. pp. 55–60, ACM Siggraph, New York, 1992.

[Delmarcelle93]
T. Delmarcelle and L. Hesselink. "Visualizing Second-Order Tensor Fields with Hyperstreamlines." *IEEE Computer Graphics and Applications*. 13(4):25–33, 1993.

[Eck95]
M. Eck, T. DeRose, T. Duchamp, H. Hoppe, M. Lounsbery, W. Stuetzle. "Multiresolution Analysis of Arbitrary Meshes." In *Proceedings SIGGRAPH '95*. pp. 173–182, Addison-Wesley, Reading, MA, August 1995.

[Edelsbrunner94]
H. Edelsbrunner and E. P. Mucke. "Three-dimensional alpha shapes." *ACM Transactions on Graphics*. 13:43–72, 1994.

[Evans96]
F. Evans, S. Skiena, A. Varshney. "Optimizing Triangle Strips for Fast Rendering." In *Proceedings of Visualization '96*. pp. 319–326, IEEE Computer Society Press, Los Alamitos, CA, 1996.

[Feiner90]
S. Feiner and C. Beshers. "Worlds within Worlds: Metaphors for Exploring *n*-Dimensional Virtual Worlds." In *Proceedings UIST'90* (ACM Symp. on User Interface Software). pp. 76–83, October, 1990.

[Garland97]
M. Garland and P. Heckbert. "Surface Simplification Using Quadric Error Metrics." In *Proceedings SIGGRAPH '97*. pp. 209–216, The Association for Computing Machinery, New York, August 1997.

[Globus91]
A. Globus, C. Levit, and T. Lasinski. "A Tool for Visualizing the Topology of Three-Dimensional Vector Fields." In *Proceedings of Visualization '91*. pp. 33–40, IEEE Computer Society Press, Los Alamitos, CA, 1991.

[He96]
T. He, L. Hong, A. Varshney, S. Wang. "Controlled Topology Simplification." *IEEE Transactions on Visualization and Computer Graphics*. 2(2):171–184, June 1996.

[Helman91]
J. L. Helman and L. Hesselink. "Visualization of Vector Field Topology in Fluid Flows." *IEEE Computer Graphics and Applications*. 11(3):36–46, 1991.

ClearCorrect Exhibit 1002, Page 2449 of 3373

[Hinker93]
P. Hinker and C. Hansen. "Geometric Optimization." In *Proceedings of Visualization '93*. pp. 189–195, IEEE Computer Society Press, Los Alamitos, CA, October 1993.

[Hoppe93]
H. Hoppe, T. DeRose, T. Duchamp, J. McDonald, W. Stuetzle. "Mesh Optimization." In *Proceedings of SIGGRAPH '93*. pp. 19–26, August 1993.

[Hoppe96]
H. Hoppe. "Progressive Meshes." In *Proceedings SIGGRAPH '96*. pp. 96–108, The Association for Computing Machinery, New York, August 1996.

[Hultquist92]
J. P. M. Hultquist. "Constructing Stream Surfaces in Steady 3-D Vector Fields." In *Proceedings of Visualization '92*. pp. 171–178, IEEE Computer Society Press, Los Alamitos, CA, 1992.

[Inselberg87]
A. Inselberg and B. Dimsdale. "Parallel Coordinates for Visualizing Multi-Dimensional Geometry." In *Computer Graphics 1987 (Proceedings of CG International '87)*. pp. 25–44, Springer-Verlag, 1987.

[Lawson86]
C. L. Lawson. "Properties of n-Dimensional Triangulations." *Computer-Aided Geometric Design*. 3:231–246, 1986.

[Lorensen93]
W. Lorensen. "Geometric Clipping with Boolean Textures." in *Proceedings of Visualization '93*. pp. 268–274, IEEE Computer Society Press, Los Alamitos, CA, Press, October 1993.

[Max94]
N. Max, R. Crawfis, C. Grant. "Visualizing 3D Vector Fields Near Contour Surfaces." In *Proceedings of Visualization '94*. pp. 248–255, IEEE Computer Society Press, Los Alamitos, CA, 1994.

[Mihalisin90]
T. Mihalisin, E. Gawlinski, J. Timlin, and J. Schwegler. "Visualizing a Scalar Field on an n-Dimensional Lattice." In *Proceedings of Visualization '90*. pp. 255–262, IEEE Computer Society Press, Los Alamitos, CA, October 1990.

[Nielson91]
G. M. Nielson, T. A. Foley, B. Hamann, D. Lane. "Visualizing and Modeling Scattered Multivariate Data." *IEEE Computer Graphics and Applications*. 11(3):47–55, 1991.

[Popovic97]
J. Popovic and H. Hoppe. "Progressive Simplicial Complexes." In *Proceedings SIGGRAPH '97*. pp. 217–224, The Association. for Computing Machinery, New York, August 1997.

[Rossignac93]
J. Rossignac and P. Borrel. "Multi-Resolution 3D Approximations for Rendering Complex Scenes." In *Modeling in Computer Graphics: Methods and Applications*. B. Falcidieno and T. Kunii, eds., pp. 455–465, Springer-Verlag Berlin, 1993.

ClearCorrect Exhibit 1002, Page 2450 of 3373

[Schroeder91]
W. Schroeder, C. Volpe, and W. Lorensen. "The Stream Polygon: A Technique for 3D Vector Field Visualization." In *Proceedings of Visualization '91*. pp. 126–132, IEEE Computer Society Press, Los Alamitos, CA, October 1991.

[Schroeder92a]
W. Schroeder, J. Zarge, and W. Lorensen. "Decimation of Triangle Meshes." *Computer Graphics (SIGGRAPH '92)*. 26(2):65–70, August 1992.

[Schroeder92b]
W. Schroeder, W. Lorensen, G. Montanaro, and C. Volpe. "Visage: An Object-Oriented Scientific Visualization System." In *Proceedings of Visualization '92*. pp. 219–226, IEEE Computer Society Press, Los Alamitos, CA, October 1992.

[Schroeder94]
W. Schroeder, W. Lorensen, and S. Linthicum, "Implicit Modeling of Swept Surfaces and Volumes." In *Proceedings of Visualization '94*. pp. 40–45, IEEE Computer Society Press, Los Alamitos, CA, October 1994.

[Schroeder97]
W. Schroeder. "A Topology Modifying Progressive Decimation Algorithm." In *Proceedings of Visualization '97*. IEEE Computer Society Press, Los Alamitos, CA, October 1997.

[Stalling95]
D. Stalling and H-C. Hege. "Fast and Independent Line Integral Convolution." In *Proceedings of SIGGRAPH '95*. pp. 249–256, Addison-Wesley, Reading, MA, 1995.

[Turk92]
G. Turk. "Re-Tiling of Polygonal Surfaces." *Computer Graphics (SIGGRAPH '92)*. 26(2):55–64, July 1992.

[vanWijk93]
J. J. van Wijk. "Flow Visualization with Surface Particles." *IEEE Computer Graphics and Applications*. 13(4):18–24, 1993.

[Wang90]
S-L C. Wang and J. Staudhammer. "Visibility Determination on Projected Grid Surfaces." *IEEE Computer Graphics and Applications*. 10(4):36–43, 1990.

[Watson81]
D. F. Watson. "Computing the n-Dimensional Delaunay Tessellation with Application to Voronoi Polytopes." *The Computer Journal*. 24(2):167–172, 1981.

[Wixom78]
J. Wixom and W. J. Gordon. "On Shepard's Method of Metric Interpolation to Scattered Bivariate and Multivariate Data." *Math. Comp*. 32:253–264, 1978.

[Yamrom95]
B. Yamrom and K. M. Martin. "Vector Field Animation with Texture Maps." *IEEE Computer Graphics and Applications*. 15(2):22–24, 1995.

9.9 Exercises

9.1 Describe an approach to adapt dividing cubes to other 3D cell types. Can your method be adapted to 1D and 2D cells?

ClearCorrect Exhibit 1002, Page 2451 of 3373

9.2 Discuss the advantages and disadvantages of representing surfaces with points versus polygons.

9.3 Streamribbons can be constructed by either i) connecting two adjacent streamlines with a surface, or ii) placing a ribbon on the streamline and orienting the surface according to streamwise vorticity vector. Discuss the differences in the resulting visualization.

9.4 Write the following programs to visualize velocity flow in the combustor.
a) Use `vtkProbeFilter` and `vtkHedgeHog`.
b) Use `vtkProbeFilter` and `vtkStreamLine`.
c) Use `vtkProbeFilter` and `vtkWarpVector`.
d) Use `vtkProbeFilter` and `vtkVectorNorm`.
e) Use `vtkProbeFilter` and `vtkVectorDot`.

9.5 Describe a method to extract geometry using an arbitrary dataset. (That is, extract geometry that lies within the culling dataset.) (*Hint:* how would you evaluate in/out of points?)

9.6 The filter `vtkPolyDataNormals` is often used in combination with the filters `vtkSmoothPolyData` and `vtkContourFilter` to generate smooth isosurfaces.
a) Write a class to combine these three filters into one filter. Can you eliminate intermediate storage?
b) How much error does `vtkSmoothPolyData` introduce into the isosurface? Can you think of a way to limit the error?
c) What is the difference between the surface normals created by `vtkMarchingCubes` and `vtkPolyDataNormals`?

9.7 Assume that we have a database consisting of interest rate R, monthly payment P, monthly income I, and days payment is late L.
a) If R, P, I are all sampled regularly, how would you visualize this data?
b) If all data is irregularly sampled, list three methods to visualize it.

9.8 Why do you think triangle strips are often faster to render than general polygons?

9.9 The normal generation technique described in this chapter creates consistently oriented surface normals.
a) Do the normals point inside or outside of a closed surface?
b) Describe a technique to orient normals so that they point out of a closed surface.
c) Can surface normals be used to eliminate visible triangles prior to rendering? (*Hint:* what is the relationship between camera view and surface normal?)

9.10 Describe a technique to partially threshold a cell (i.e., to cut a cell as necessary to satisfy threshold criterion). Can an approach similar to marching cubes be used?

ClearCorrect Exhibit 1002, Page 2452 of 3373

9.11 The class `vtkRendererSource` allows us to use the rendered image as a texture map (or structured points dataset). Write a program to construct iterated textures, that is textures that consist of repeated images. Can the same image be generated using texture coordinates?

9.12 Describe how you would modify the decimation algorithm to treat general polygons.

9.13 Several examples in the text (e.g., `deciFran.tcl` and `deciHawa.tcl`) use the class `vtkDecimate`. Modify these examples to use the topology modifying progressive decimation algorithm (implemented in `vtkDecimatePro`). How much greater reduction can you achieve?

ClearCorrect Exhibit 1002, Page 2453 of 3373

Minimizing finishing problems with the mini-positioner

Douglas J. Shilliday, D.D.S.
Columbus, Ohio

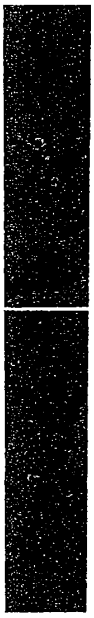
The desire to provide more patients with a controlling and finishing appliance that is readily available, easily adaptable, and inexpensive has led to the development of the flexible, preformed mini-positioner (Fig. 1). This positioner, when used after fixed appliances are removed, enhances the level and alignment of the maxillary and mandibular anterior teeth, maintains or improves the interarch relationship, and aids in closure of spaces left by the appliances. As the mini-positioner covers only the six maxillary and six mandibular anterior teeth, it cannot perform all the duties of a "full-coverage" tooth positioner. It can complement it, however, by controlling arch length and corrected rotations while the full-coverage positioner is being fabricated.

The minimal cost of the mini-positioner allows it to be used for a relatively short period of time and then discarded in favor of a conventional retainer or a full-coverage tooth positioner, although it is also durable enough to be continued as a retainer in itself. This has proved effective, especially in cases that originally exhibited a deep bite. As the mini-positioner covers only the anterior teeth, the posterior teeth are allowed to "self-equilibrate," the bite is prevented from deepening, and the vertical dimension is prevented from decreasing (Fig. 2).

Fitting of the mini-positioner is uncomplicated, as there need be only two sizes: "plus" and "minus." The size refers to whether the mesiodistal width of one maxillary central incisor of the treated case is more than 9 mm. (plus) or less than 9 mm. (minus). This versatility is possible because the mini-positioner provides tooth-receiving areas or slots rather than individual tooth-receiving sockets. The slots are designed so that the smaller tooth-receiving areas for the maxillary lateral incisors will not impinge on the larger canine or central incisor teeth and so that the mandibular incisor-receiving area will not impinge on the larger mandibular canines. Yet it still contacts each tooth on the labial, lingual, and incisal surfaces in an ideal arch and interarch relation.

If the mini-positioner is to be used as an interim control between fixed

Fig. 1. Th



A

C

Fig. 2. A
Mini-posi

applianc
be worn
sufficien
sive fre
bite har
and rel
is worn
during

ClearCorrect Exhibit 1002, Page 2454 of 3373

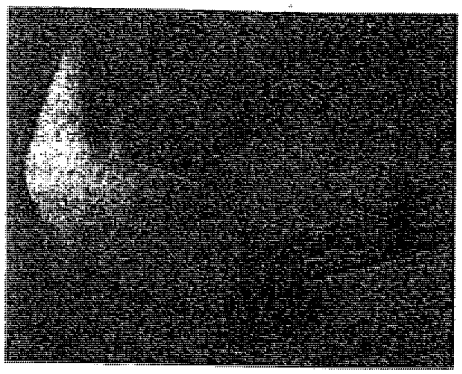


Fig. 1. The mini-positioner.

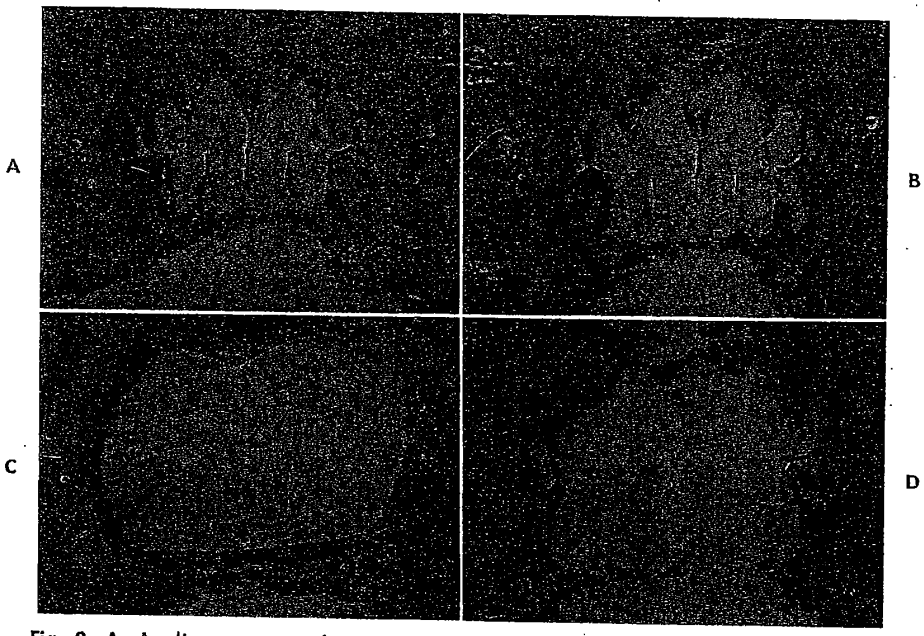


Fig. 2. A, Appliances removed, except for molar bands left on. B, Elastics in place. C, Mini-positioner fitted. D, One month after removal of fixed appliance.

appliance removal and placement of a full-coverage tooth positioner, it should be worn at night and 4 hours during the day (10 to 15 minutes at a time is sufficient). At this time, the mini-positioner is altered only to eliminate excessive frenum or gingival impingement. It is not necessary for the patient to bite hard into the mini-positioner to get the desired results; he can just close and relax. The patient should be told that the first two or three nights it is worn, the mini-positioner will probably come out but that if he wears it during the day as prescribed, retaining it at night will become routine. Patient

ClearCorrect Exhibit 1002, Page 2455 of 3373

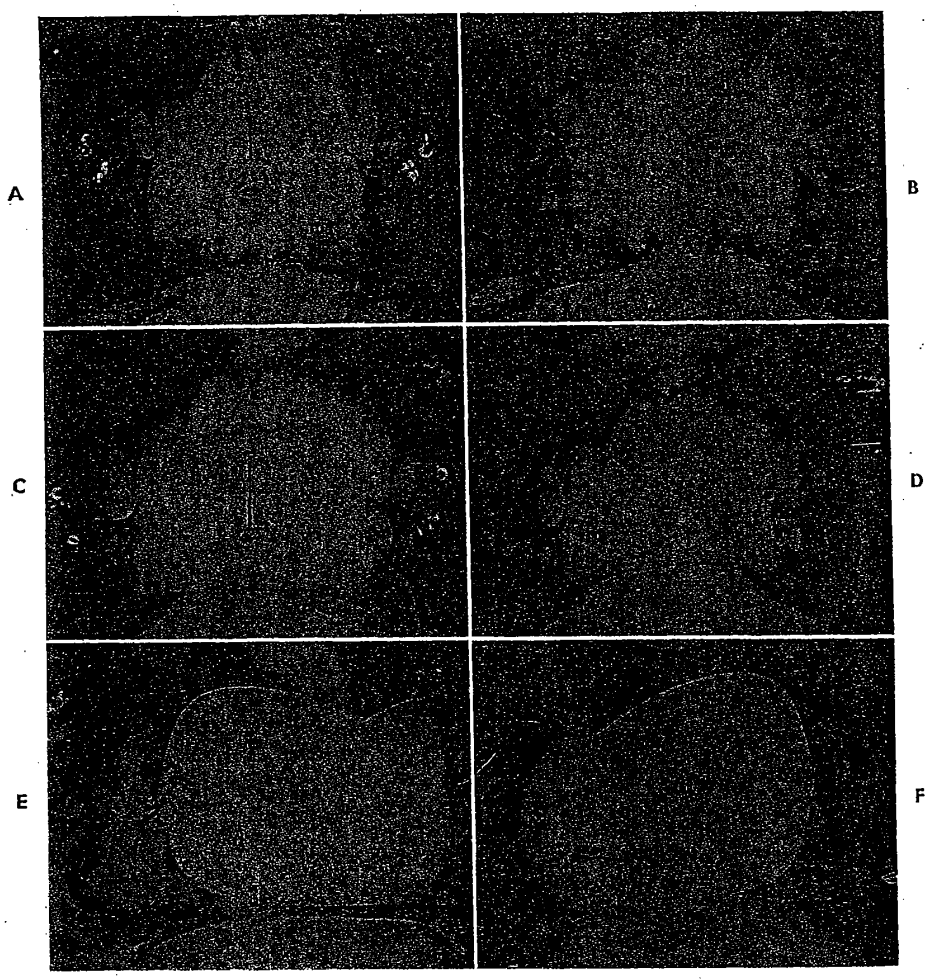


Fig. 3. A, Appliences removed except molar bands for elastic attachment. B, One month after appliance removal. C, Appliance removed except for molar bands for elastic attachment. D, One month after appliance removal. E and F, Mini-positioner after having been softened in hot tap water.

acceptance and the ability to wear the mini-positioner have proved to be excellent.

If the mini-positioner is to be worn between fixed appliance removal and the placement of conventional Hawley retainers and lingual holding arches, the four first molar bands may be left in place (Figs. 2 and 3) and retainer impressions may be taken 4 to 12 weeks later. The molar bands are used to fasten ¾ inch light elastics from molar to molar on the maxillary and mandibular arches to aid in closing spaces left by the fixed appliances. Occasionally,

three 3/16
incisors, o
central an
these smal
finds it ne
these spac
achieved i
structed w
is instruct
with daytii

If the
week peric
placed in
teeth. Tw
close enoug
The mini-p

The mi
minor rot
in correcti
recting an
trolling la
tector in c

Summary

The mi
that involv
treated cas
ers and ful

16 East 1

ClearCorrect Exhibit 1002, Page 2456 of 3373

three 3/16 inch light elastics are worn—one around the two maxillary central incisors, one around one central and lateral incisor, and one around the other central and lateral incisor. The patient is instructed to keep careful track of these small elastics. All elastics are worn 24 hours a day unless the patient finds it necessary to remove them while wearing the mini-positioner. Usually these spaces are closed in 2 to 4 weeks, and final leveling and alignment are achieved in 4 to 12 weeks. Impressions are then taken and retainers are constructed with the patient under full control at all times. Again the patient is instructed to wear the mini-positioner 4 hours during the day and all night, with daytime wearing gradually reduced after the first 4 weeks (Fig. 3).

If the mini-positioner is to be used as a retaining appliance after the 12-week period, it should be softened in hot tap water for 5 to 10 seconds and placed in the patient's mouth. He is then told to close on the posterior teeth. Two or three softenings may be required to get the posterior teeth close enough together so that they will not overerupt during the retention period. The mini-positioner is then worn at night only.

The mini-positioner has also been found to be effective (1) in correcting minor rotations in untreated cases that provide sufficient arch length, (2) in correcting treated cases that have started some slight relapse, (3) in correcting anterior cross-bites where there is sufficient arch length, (4) in controlling lateral tongue-thrust and thumb-sucking, and (5) as a mouth protector in contact sports.

Summary

The mini-positioner provides the orthodontist with a treatment adjunct that involves a minimum of time and cost. In controlling and finishing the treated case, it removes the urgency for construction and placement of retainers and full-coverage tooth positioners.

16 East Henderson Rd.

ClearCorrect Exhibit 1002, Page 2457 of 3373

Electronic Acknowledgement Receipt	
EFS ID:	38190593
Application Number:	16723706
International Application Number:	
Confirmation Number:	1026
Title of Invention:	AUTOMATED TREATMENT STAGING FOR TEETH
First Named Inventor/Applicant Name:	Ian Kitching
Customer Number:	107046
Filer:	Charles C. Hagadorn III/John Macalagay
Filer Authorized By:	Charles C. Hagadorn III
Attorney Docket Number:	22773-774.305
Receipt Date:	02-JAN-2020
Filing Date:	
Time Stamp:	19:38:38
Application Type:	Utility under 35 USC 111(a)

Payment information:

Submitted with Payment	no

File Listing:

Document Number	Document Description	File Name	File Size(Bytes)/ Message Digest	Multi Part /.zip	Pages (if appl.)
1	Non Patent Literature	Z-GOTTLIEB-JCO-INTERVIEWS-390.PDF	1456775 f8c93557b086e3aee8785a8d5aa74ce5d4b37f4d	no	21
Warnings:					

Information:					
2	Non Patent Literature	Z-GRAYSON-NEW-METHODS-1990.PDF	417056 ea1bc1df1bdca491660fa5573423e1d1adc806b5	no	3
Warnings:					
Information:					
3	Non Patent Literature	Z-GUESS-COMPUTER-TREATMENT-262.PDF	1132027 27b5f0ebeb878777c564331c016739377a028175	no	11
Warnings:					
Information:					
4	Non Patent Literature	Z-HEAVEN-COMPUTER-BASED-17.PDF	796720 3f97abf36236ee767d29370a23b097478485e5cd	no	3
Warnings:					
Information:					
5	Non Patent Literature	Z-HIGHBEAM-SIMULATING-STRESS-1996.PDF	140183 c10a4548ad43902dd7ffc898b642687a63b58e85	no	2
Warnings:					
Information:					
6	Non Patent Literature	Z-HIKAGE-INTEGRATED-ORTHODONTIC-248.PDF	2799512 61fa540c68cfd9c5031e0ed68836b0b4d6c9fc06	no	56
Warnings:					
Information:					
7	Non Patent Literature	Z-HOFFMAN-ROLE-OF-375.PDF	4616306 0097a93ab4ab42fa0f7da4eef39b837de6a59eee	no	23
Warnings:					
Information:					
8	Non Patent Literature	Z-HOJJATIE-THREE-DIMENSIONAL-1157.PDF	572590 e8e8f04e6191be80b820eb8222b0af8f0be0f269	no	10
Warnings:					
Information:					

9	Non Patent Literature	Z-HUCKINS-CAD-CAM-96.PDF	98055 3bc1b326bacd3b8def27813e0b6e7ec68648ce86	no	1
Warnings:					
Information:					
10	Non Patent Literature	Z-IMPORTANT-TIP-ABOUT-WEARING-1998.PDF	46522 340a2832fe869b21695cc4662c61b3a8fe5b3df6	no	1
Warnings:					
Information:					
11	Non Patent Literature	Z-JCO-INTERVIEWS-459-1994.PDF	789378 eb8cc6cdb5a807d275aff43995351e05fb98a4e1	no	14
Warnings:					
Information:					
12	Non Patent Literature	Z-JCO-INTERVIEWS-819-1983.PDF	1195122 24c006982a08e971fb69e1d665185d3c2c13c78f	no	19
Warnings:					
Information:					
13	Non Patent Literature	Z-JERROLD-THE-PROBLEM-478.PDF	247348 213460c6855c8b07584675786249eb1a9d4b0cd5	no	5
Warnings:					
Information:					
14	Non Patent Literature	Z-JONES-AN-ASSESSMENT-85.PDF	493613 e009d93ddc7c6e776651de4e4cef902144f91261	no	10
Warnings:					
Information:					
15	Non Patent Literature	Z-JP-FABER-COMPUTERIZED-INTERACTIVE-36.PDF	465810 139652252abf4b216de00c6d1ecdd548dd957a7e	no	6
Warnings:					
Information:					

16	Non Patent Literature	Z-KAMADA-CASE-REPORTS-11.PDF	642704 0333ab43190df705129d4b06e6d881f2b7caf4b0	no	20
Warnings:					
Information:					
17	Non Patent Literature	Z-KAMADA-CONSTRUCTION-OF-1982.PDF	856658 d28516253841da77323d15300fbbc0565fb1d546	no	28
Warnings:					
Information:					
18	Non Patent Literature	Z-KANAZAWA-THREE-DIMENSIONAL-1298.PDF	473549 8b4e653af57a0fd53fcbd21c7fe33ee8e6069b71	no	6
Warnings:					
Information:					
19	Non Patent Literature	Z-KESLING-THE-PHILOSOPHY-297.PDF	373829 fdcd21b043f3daf4df3d8cedf987333f939e5d0b	no	6
Warnings:					
Information:					
20	Non Patent Literature	Z-KESLING-COORDINATING-THE-285.PDF	492258 1f1cc962bcf019aa013e6e360f14929f1bd5a46a	no	8
Warnings:					
Information:					
21	Non Patent Literature	Z-KLEEMAN-THE-SPEED-673.PDF	920375 07b8b512ca1666a5c26df2826836b548a6dbe7b4	no	8
Warnings:					
Information:					
22	Non Patent Literature	Z-KOCHANEK-INTERPOLATING-SPLINES-33.PDF	640437 77af1aff1d1c0e24fc3d60e715ade91d42d635cd	no	9
Warnings:					
Information:					

23	Non Patent Literature	Z-KUNII-ARTICULATION-SIMULATION-181.PDF	709919 8488f62405d5670e0ced1a36020caef1d84829d3	no	8
Warnings:					
Information:					
24	Non Patent Literature	Z-KURODA-THREE-DIMENSIONAL-365.PDF	531182 e66065bdaea56b0ee4953cf100571c908e637a09	no	5
Warnings:					
Information:					
25	Non Patent Literature	Z-LAURENDEAU-A-COMPUTER-VISION-453.PDF	499672 53462babf653afe4a83458868d556955110a44c2	no	9
Warnings:					
Information:					
26	Non Patent Literature	Z-LEINFELDER-A-NEW-703.PDF	508063 e776fb6e5a7454cf74fb17ae7b1dcf95d3f82242	no	5
Warnings:					
Information:					
27	Non Patent Literature	Z-MANETTI-COMPUTER-AIDED-370.PDF	1687370 6009829137fa3e27079c72fcfd94212ae7fd2a62	no	8
Warnings:					
Information:					
28	Non Patent Literature	Z-MCCANN-INSIDE-THE-286.PDF	904121 f775a5baaaef6dd7aa3dd709e64ec5dba78cf946	no	9
Warnings:					
Information:					
29	Non Patent Literature	Z-MCNAMARA-INVISIBLE-RETAINERS-570.PDF	407944 bf0ebc18a99eba68c8f15486195871316f41e3e7	no	11
Warnings:					
Information:					

30	Non Patent Literature	Z-MCNAMARA-ORTHODONTIC-AND-347.PDF	3226062 3382eb655e5a3baf0e7255a107f6e0f6a771cd32	no	11
Warnings:					
Information:					
31	Non Patent Literature	Z-MOERMANN-COMPUTER-MACHINED-763.PDF	189931 a77edf1e2d2d4662a93f444408103dd956b69997	no	1
Warnings:					
Information:					
32	Non Patent Literature	Z-MOLES-CORRECTING-MILD-2002.PDF	548699 f7321a4804e8105aaea9d421ae311ecc5e9d37f6	no	2
Warnings:					
Information:					
33	Non Patent Literature	Z-MORMANN-MARGINALE-ADAPTION-1118.PDF	863951 360844e1504dc76f0ae34b2495b1cabc83a355a2	no	7
Warnings:					
Information:					
34	Non Patent Literature	Z-NAHOUM-THE-VACUUM-385.PDF	939672 1775cb4ea30de6e0a90ae17fb8c658e539cd7cb6	no	6
Warnings:					
Information:					
35	Non Patent Literature	Z-NASH-CEREC-CAD-22.PDF	768064 377dba4f0649b089bd258176f8727d2f7739fdfe	no	4
Warnings:					
Information:					
36	Non Patent Literature	Z-NISHIYAMA-A-NEW-93.PDF	333417 5365902a382260cdb332ff1d1306371daedbefa9	no	11
Warnings:					
Information:					

37	Non Patent Literature	Z-PAUL-DIGITAL-DOCUMENTATION-2415.PDF	331473 68c49e09b9b8bd681642f52084c19610e34e30af	no	5
Warnings:					
Information:					
38	Non Patent Literature	Z-PINKHAM-FOOLISH-CONCEPT-1989.PDF	319351 bd70ff64f1e8f99a127c469efb05c7ef4ff77587	no	3
Warnings:					
Information:					
39	Non Patent Literature	Z-PINKHAM-INVENTORS-CAD-1990.PDF	358948 63d0f3695636e91279b1a7fea3c5c9c66953da6f	no	3
Warnings:					
Information:					
40	Non Patent Literature	Z-PONITZ-INVISIBLE-RETAINERS-266.PDF	7027538 4b3bf2b405cc7aae25736077e374e897ec671345	no	7
Warnings:					
Information:					
41	Non Patent Literature	Z-PROCERA-RESEARCH-PROJECTS-1993.PDF	1374466 f8f711a24932ca9dc09f534844799f7b7c44f2c5	no	23
Warnings:					
Information:					
42	Non Patent Literature	Z-PROFFIT-CONTEMPORARY-ORTHODONTICS-470.PDF	7046676 55157d1ee9f6032eef11017014ecab95ac0977ab	no	66
Warnings:					
Information:					
43	Non Patent Literature	Z-RAINTREE-ESSIX-1997.PDF	202656 0bdad28f9217347ad4c948b6c6b5e12b97870f7e	no	7
Warnings:					
Information:					

44	Non Patent Literature	Z-REDMOND-CLINICAL-IMPLICATIONS-240.PDF	201923 a02546a8944f3785d3e9533064d32cefac20b4d2	no	3
Warnings:					
Information:					
45	Non Patent Literature	Z-REKOW-CAD-CAM-314.PDF	417444 9412c95ee9d02032bb48964f6c9cd300ac146362	no	5
Warnings:					
Information:					
46	Non Patent Literature	REKOW-CAD-CAM-314-318.PDF	438353 6df74fe2e7796ef7e9032e34208f085063e538f0	no	5
Warnings:					
Information:					
47	Non Patent Literature	Z-REKOW-COMPARISON-OF-344.PDF	137970 a2076efcb2bc05afff343e1174486be1d0d1b80e	no	2
Warnings:					
Information:					
48	Non Patent Literature	Z-REKOW-A-REVIEW-25.PDF	704188 85de7db6c599f36e43f29d216e5c93577ecef2aa	no	9
Warnings:					
Information:					
49	Non Patent Literature	Z-REKOW-CAD-CAM-287.PDF	616058 b05c2dfc6b543cdf4d571959747401203371f80f3	no	3
Warnings:					
Information:					
50	Non Patent Literature	Z-REKOW-COMPUTER-AIDED-512.PDF	206660 197c120e6676f898347e3324cc69293c7c1db83b	no	6
Warnings:					
Information:					

51	Non Patent Literature	Z-REKOW-DENTAL-CAD-43.PDF	1405103 415d80eeb9c022c3ff99c29b6b3f8b74961caf14	no	6
Warnings:					
Information:					
52	Non Patent Literature	Z-REKOW-FEASIBILITY-OF-1988.PDF	8757565 7b6df8e204824f80669aa569ee3b77f112843588	no	250
Warnings:					
Information:					
53	Non Patent Literature	Z-RICHMOND-THE-DEVELOPMENT-53.PDF	280562 0d0cf72c40bfd84a161d8a907eb40832d7f25864	no	3
Warnings:					
Information:					
54	Non Patent Literature	Z-RICHMOND-THE-DEVELOPMENT-125.PDF	1601545 d360e217f62d960481f4e850bd9b8c6fcb929732	no	15
Warnings:					
Information:					
55	Non Patent Literature	Z-RICHMOND-RECORDING-THE-199.PDF	585444 3953b7732a14747952acf49e8d0958efa2f26474	no	8
Warnings:					
Information:					
56	Non Patent Literature	Z-RUDGE-DENTAL-ARCH-279.PDF	467984 e790b39ac8b0473a4bc59f453418f4fc24af1f7d	no	7
Warnings:					
Information:					
57	Non Patent Literature	Z-SAKUDA-INTEGRATED-INFORMATION-210.PDF	1275068 a50292226ce8970f4cbb53d30870e9141c68d6ea	no	20
Warnings:					
Information:					

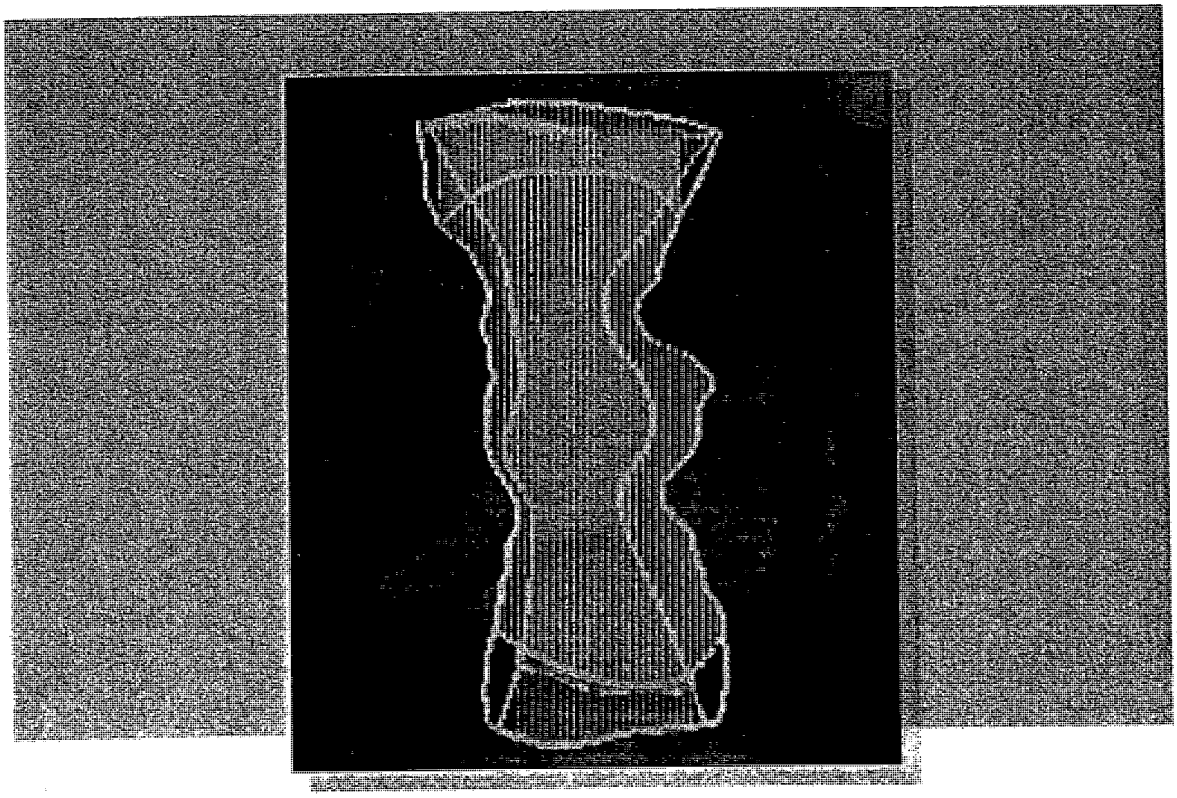
58	Non Patent Literature	Z-SCHELLHAS-THREE-DIMENSIONAL-438.PDF	588239 dfe96034ed5128782e350df3db87ac1ce4b9ca9b	no	5
Warnings:					
Information:					
59	Non Patent Literature	Z-SCHROEDER-THE-VISUAL-1998.PDF	7795772 21380687ffa5a5c09f6e8037f36f1d5802d1eaa0	no	175
Warnings:					
Information:					
60	Non Patent Literature	Z-SHILLIDAY-MINIMIZING-FINISHING-596.PDF	411143 be0344b01889dc8f564aa86acd2cbd07af648f02	no	4
Warnings:					
Information:					
		Total Files Size (in bytes):	74337023		

This Acknowledgement Receipt evidences receipt on the noted date by the USPTO of the indicated documents, characterized by the applicant, and including page counts, where applicable. It serves as evidence of receipt similar to a Post Card, as described in MPEP 503.

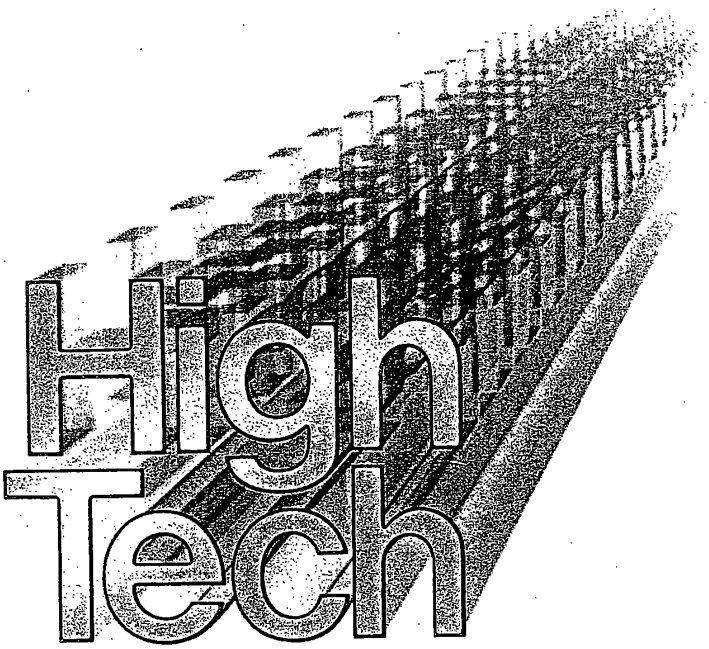
New Applications Under 35 U.S.C. 111
If a new application is being filed and the application includes the necessary components for a filing date (see 37 CFR 1.53(b)-(d) and MPEP 506), a Filing Receipt (37 CFR 1.54) will be issued in due course and the date shown on this Acknowledgement Receipt will establish the filing date of the application.
National Stage of an International Application under 35 U.S.C. 371
If a timely submission to enter the national stage of an international application is compliant with the conditions of 35 U.S.C. 371 and other applicable requirements a Form PCT/DO/EO/903 indicating acceptance of the application as a national stage submission under 35 U.S.C. 371 will be issued in addition to the Filing Receipt, in due course.
New International Application Filed with the USPTO as a Receiving Office
If a new international application is being filed and the international application includes the necessary components for an international filing date (see PCT Article 11 and MPEP 1810), a Notification of the International Application Number and of the International Filing Date (Form PCT/RO/105) will be issued in due course, subject to prescriptions concerning national security, and the date shown on this Acknowledgement Receipt will establish the international filing date of the application.

SIEMENS

CEREC – Computer-Reconstruction



High Tech
in der Zahnmedizin



in der Zahnmedizin

Ein revolutionäres optisches Abtastverfahren ersetzt den herkömmlichen Abdruck. In Bruchteilen einer Sekunde liefert die CEREC®-Mundkamera eine dreidimensionale Abbildung der Zahnpräparation. Unter Verwendung dieses „optischen Abdrucks" wird das Inlay mit Computerhilfe direkt am Bildschirm konstruiert. Vor den Augen des Patienten fertigt die vollautomatische Schleifmaschine in wenigen Minuten die gewünschte Füllung.

Dabei wird Dentalkeramik höchster Qualität verwendet, wie sie nur im industriellen Fertigungsprozeß herstellbar ist.

Das neue CEREC-System eröffnet die faszinierende Möglichkeit, ästhetisch anspruchsvolle, keramische Restaurationen in einem Zug zu präparieren und einzusetzen.

CEREC bietet, was viele Patienten wünschen: Natürlich wirkende Füllungen im Seitenzahnbereich

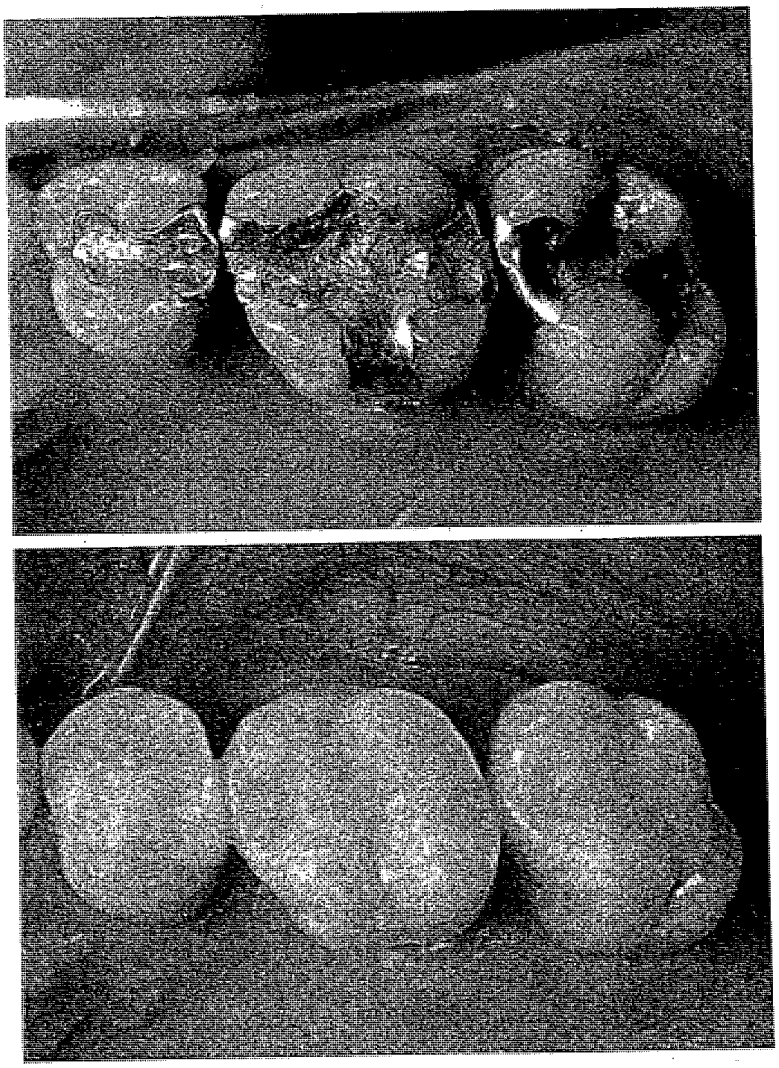
Amalgam, Gold- oder Kunststoff – keines dieser Materialien erfüllt alle Forderungen, die eigentlich an Restaurationen im Seitenzahnbereich zu stellen sind.

Für den Patienten können ästhetische Gesichtspunkte im Vordergrund stehen. Für den Zahnarzt aber sind auch die anderen Materialeigenschaften, etwa die Dauerhaftigkeit und die Biokompatibilität, von entscheidender Wichtigkeit.

Beim CEREC-System wird das Inlay aus einem industriell vorgefertigten Dentalkeramik-Block geschliffen. Der kontrollierte Herstellungsprozeß dieses Materialkörpers bietet höchste Fehlerfreiheit und Homogenität des Gefüges.

Durch Anwendung der adhäsiven Befestigungstechnik ist ein perfekter Randschluß erreichbar.

Das Ergebnis:
Natürliche Ästhetik und Farbanpassung durch schmelzähnliche Eigenfarbe und Transluzenz bei optimaler Material-Qualität.



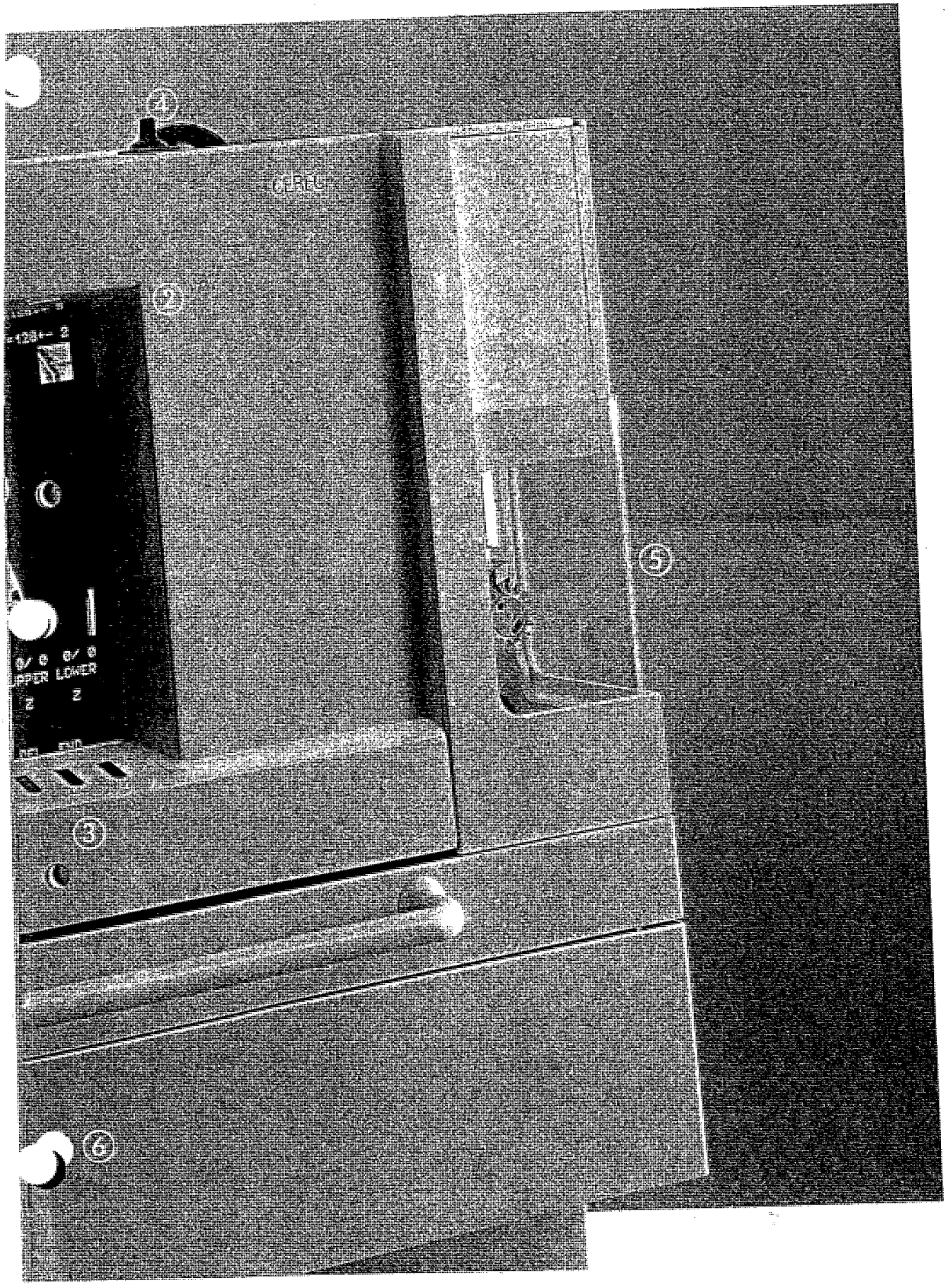
CEREC-Inlays nach zweijähriger Tragzeit im Mund.

Die CEREC-Einheit

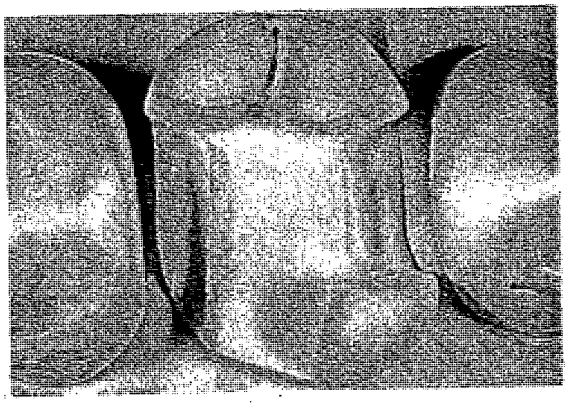
Optische Abdrucknahme, Konstruktion am Bildschirm und Herstellung der Inlays sind in einem Gerät integriert.

① CEREC-Mundkamera
② Bildschirm
③ Tastatur
④ Zeichenkugel
⑤ Schleifkammer
⑥ Materialschublade

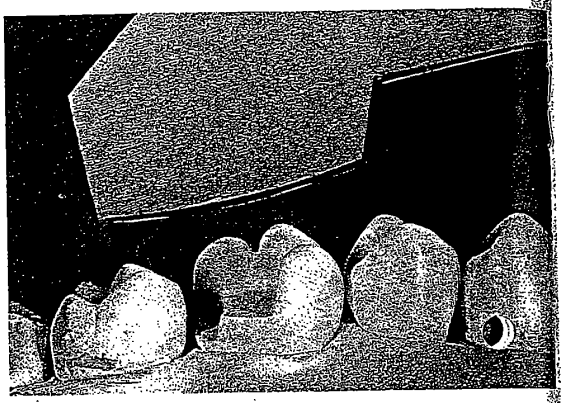



4
CERES
2
3
5
6

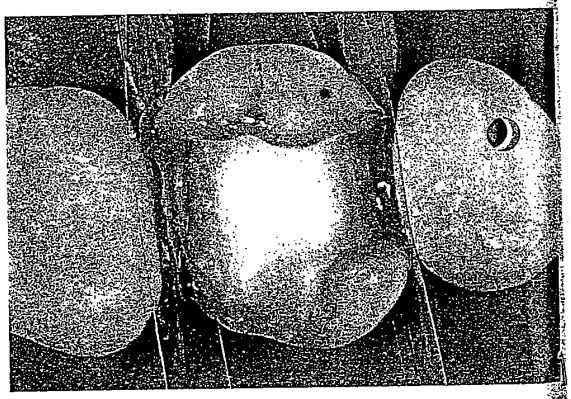
Schritt für Schritt zur ästhetischen Vollendung



1 Zur Vorbereitung der optischen Abdrucknahme wird Kontrastpuder aufgesprayt.

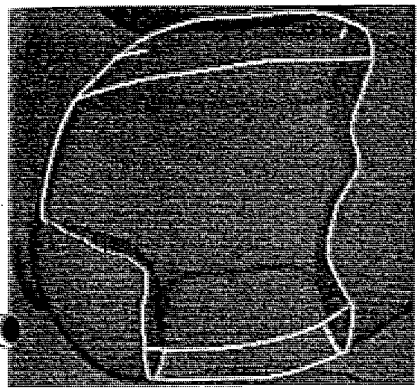


2 Der Kamerakopf wird mit dem Objektiv über der Kavität positioniert und abgestützt. Durch die Bedienung des Fußpedals wird der optische Abdruck ausgelöst.

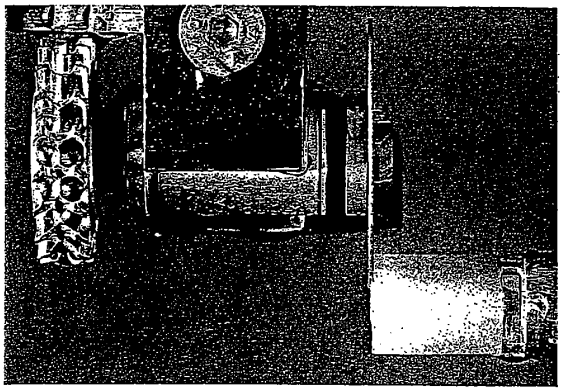


6 Die CEREC-Restaurationen werden adhäsiv eingesetzt. Alle zugänglichen Schmelzränder werden mit Ätzgel sorgfältig beschichtet und ca. 15 - 30 Sekunden geätzt.

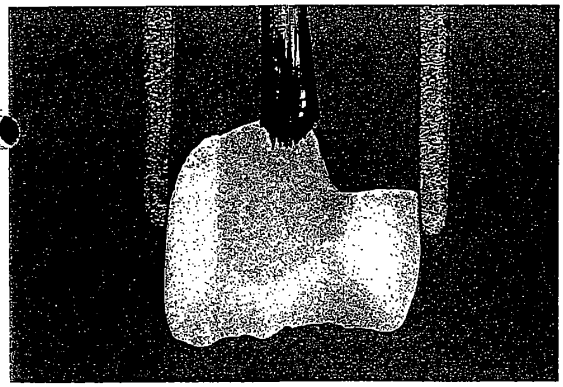
ClearCorrect Exhibit 1002, Page 2473 of 3373



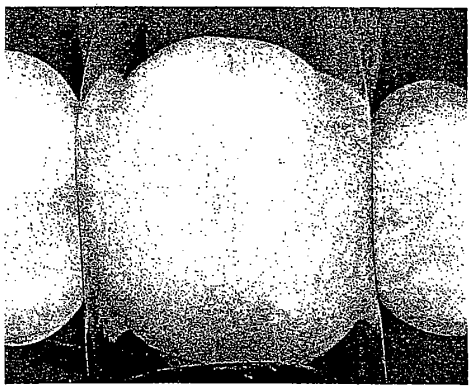
3 Das Inlay wird am Bildschirm durch Einzeichnen von Rahmenlinien mit Computerunterstützung konstruiert. Dabei werden die Approximalflächen mit den Kontaktpunkten synthetisch aufgebaut.



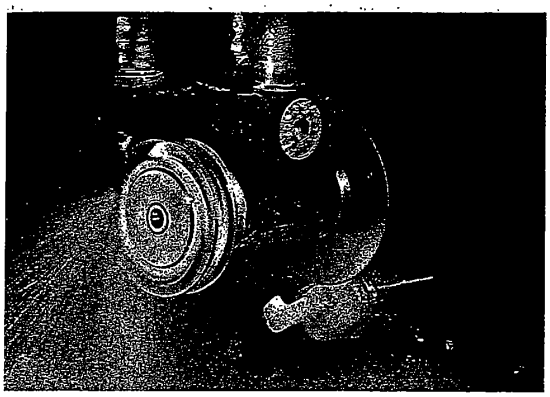
4 Der CEREC-Block, aus homogener, praktisch fehlerfreier Dentalkeramik wird nach Farbe und Größe ausgewählt und in den Halter eingesetzt.



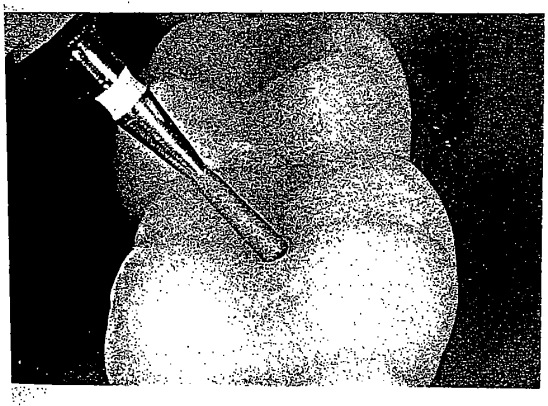
7 Das CEREC-Inlay selbst wird ebenfalls mit einem speziellen Keramik-Ätzmittel behandelt und anschließend silanisiert.



8 Das Inlay wird mit seitenzahntauglichem Composite-Material unter Verwendung von Bonding-Agent eingesetzt. Die Aushärtung erfolgt mit der Licht-Polymerisationslampe. Empfehlungswert sind Composite-Materialien, die zusätzlich über ein chemisches Härtungssystem verfügen.



5 Computergesteuert wird das Inlay von der Schleifeinrichtung in wenigen Minuten vollautomatisch aus dem CEREC-Block herausgefräst.

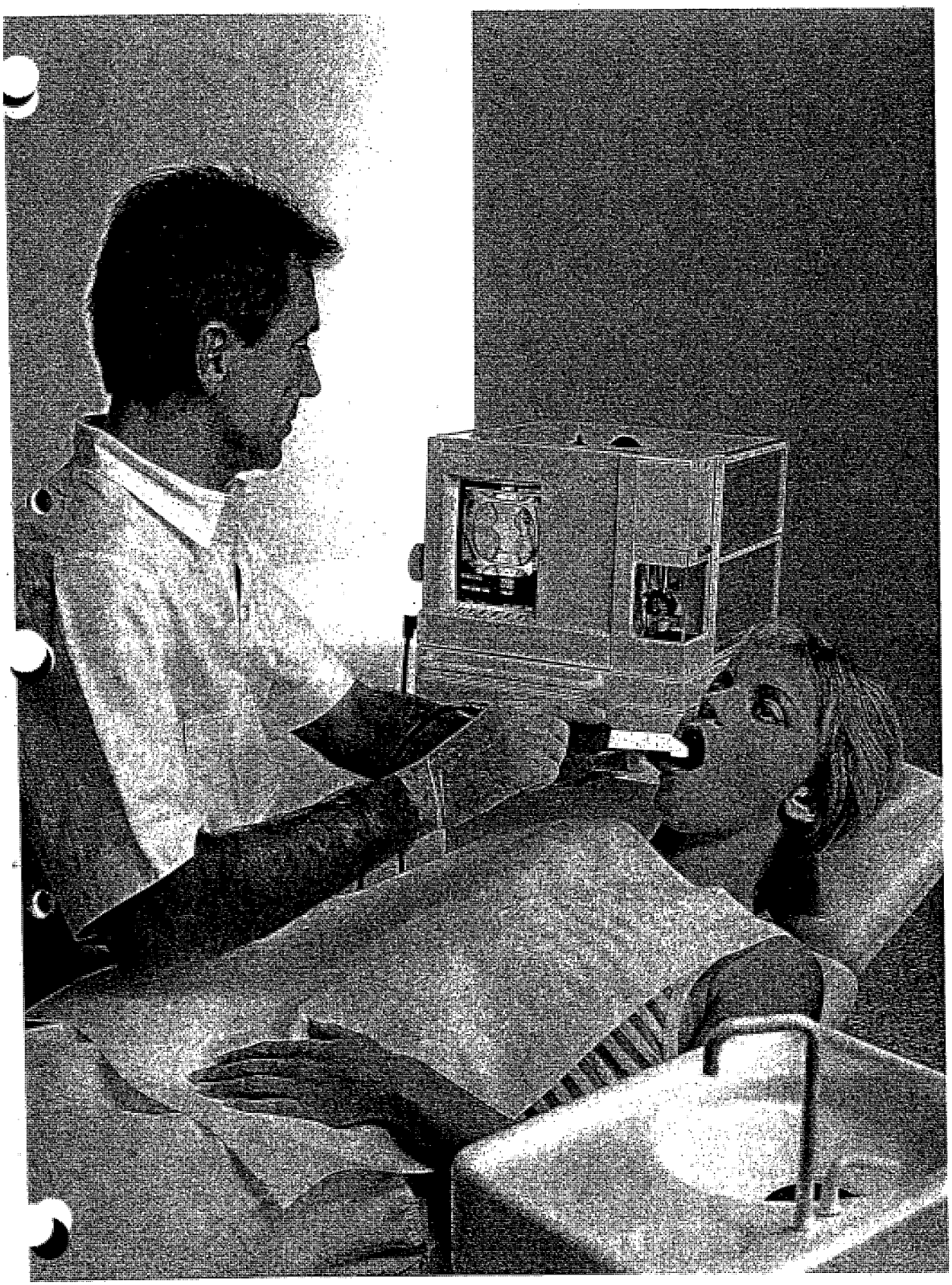


9 Die Konturierung wird mit Konturierdiamanten (40 µm Korngröße) und die Feinausarbeitung mit Finierdiamanten (15 µm Korngröße) durchgeführt. Die Oberflächenqualität hängt von der anschließenden sorgfältigen Politur mit flexiblen Disks ab.



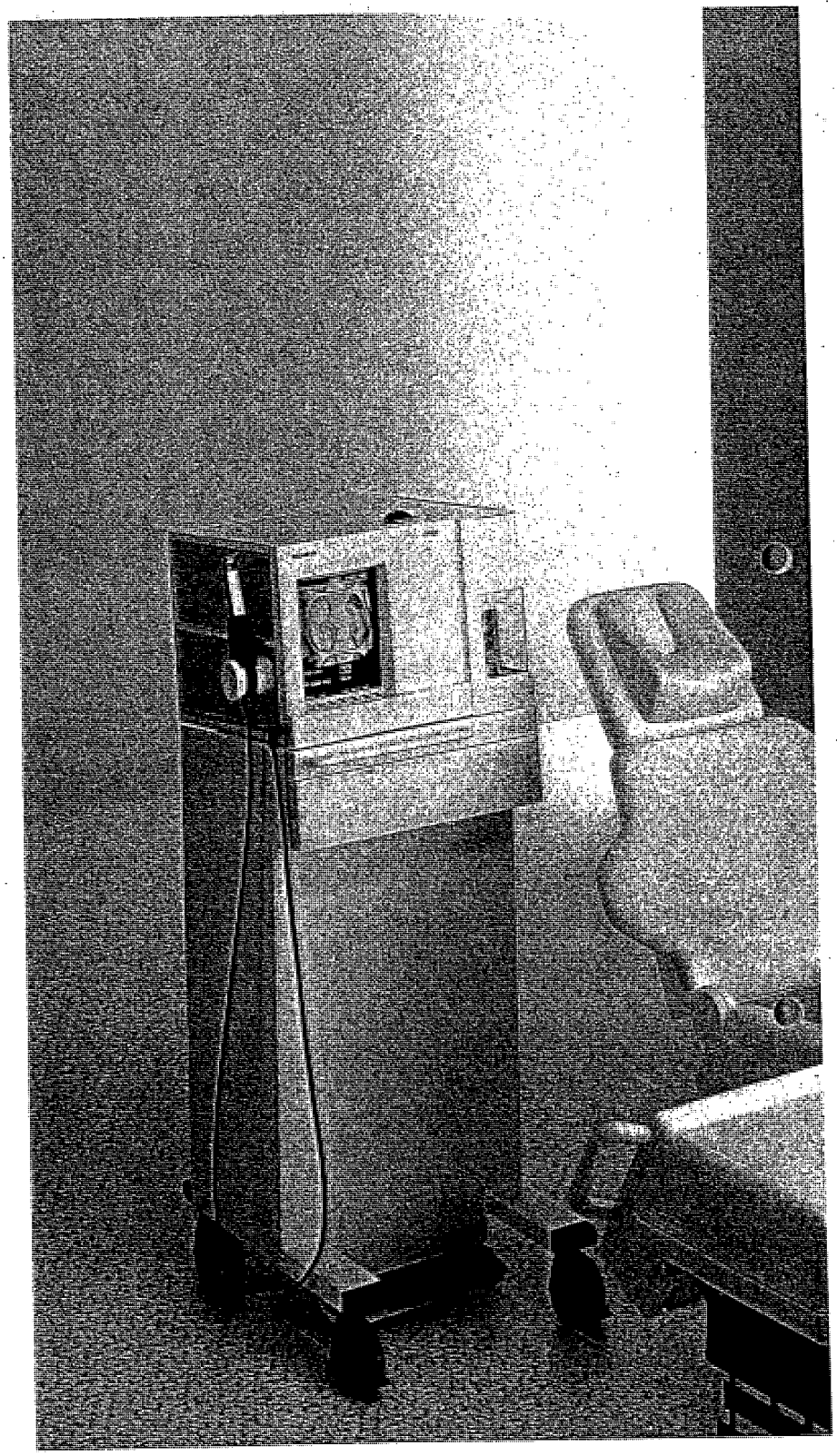
10 Das Resultat: Ein CEREC-Inlay von natürlicher Ästhetik.

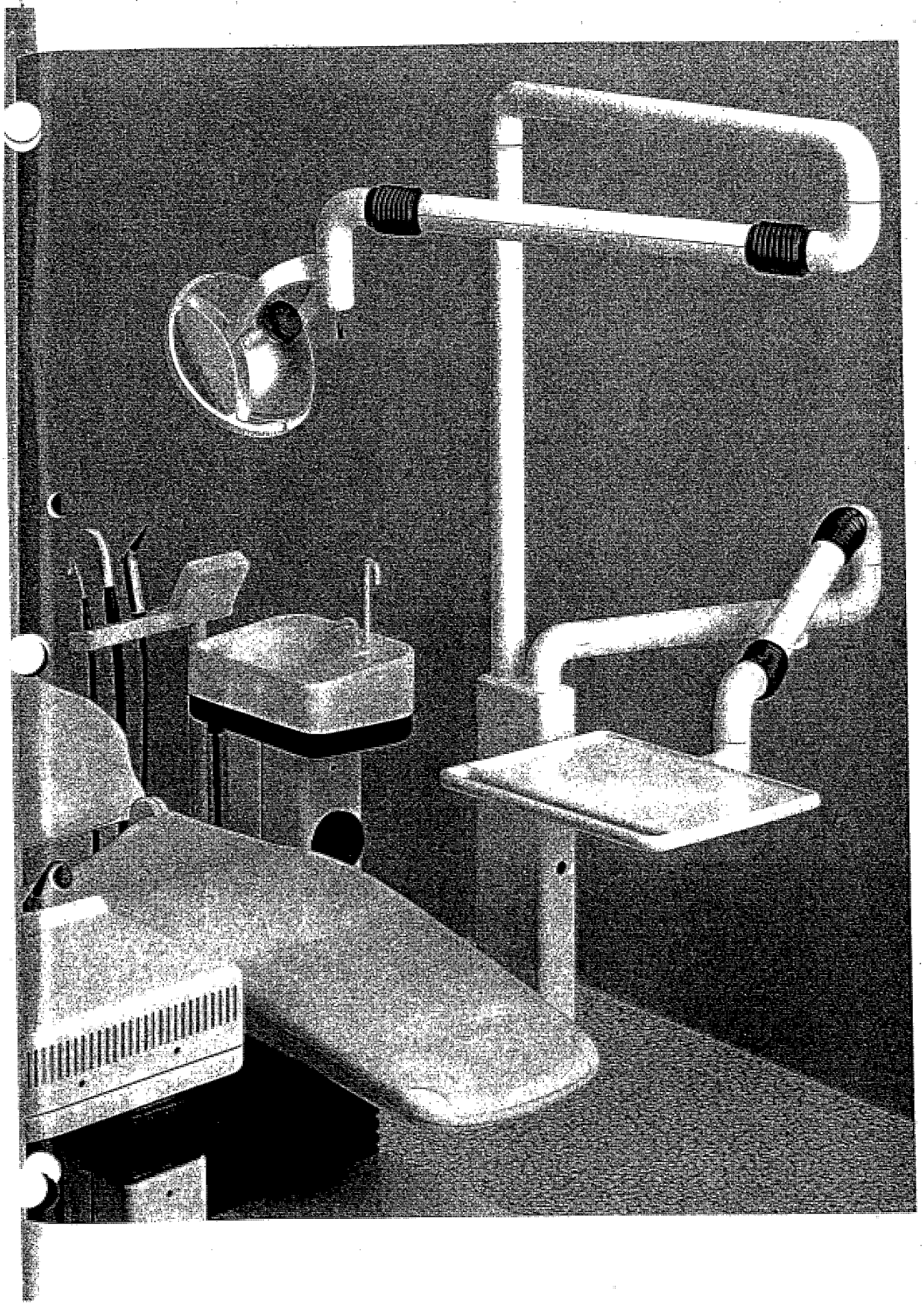
ClearCorrect Exhibit 1002, Page 2475 of 3373



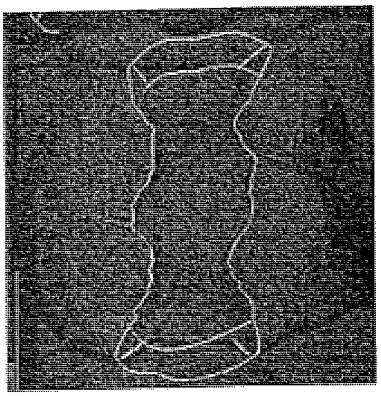
SIRONA® M mit CEREC-Einheit

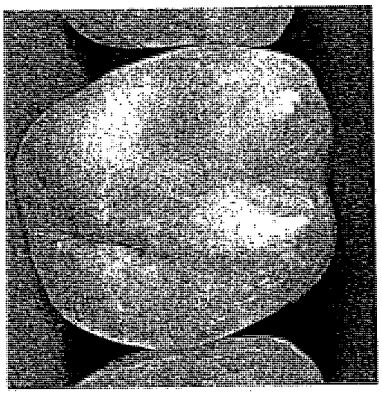
Ein Behandlungsplatz, dessen zukunftweisende Technologie und praktische Anwendbarkeit dem anspruchsvollen Zahnarzt völlig neue Perspektiven eröffnet.





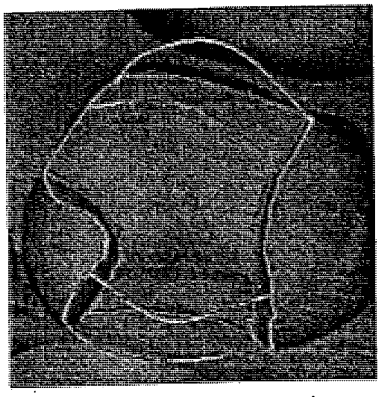
Das CEREC-System und seine Anwendungsgebiete

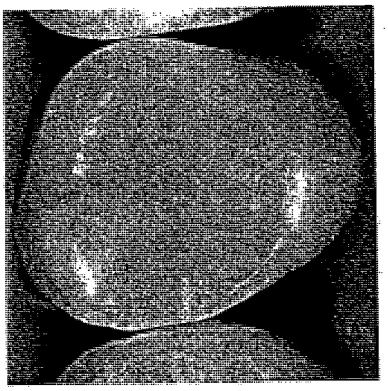




Inlays

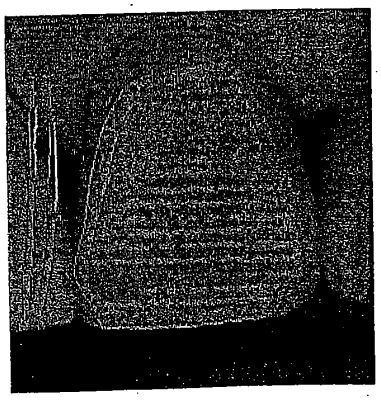
Occlusal und mehrflächig.

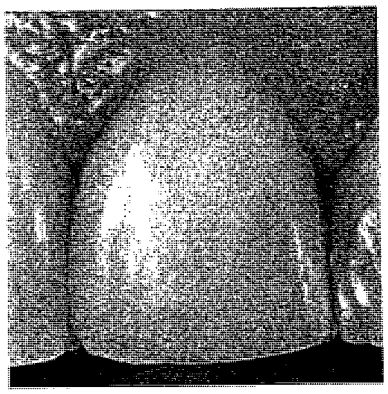




Onlays

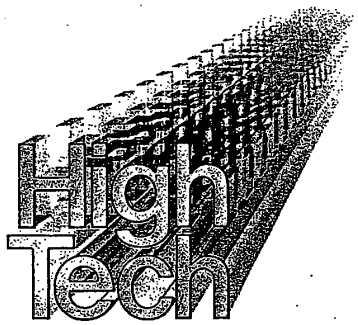
Mit dem Ersatz bzw. der Überdeckung von einem oder mehreren Höckern.





Schalenverblendungen

Im Frontzahnbereich.

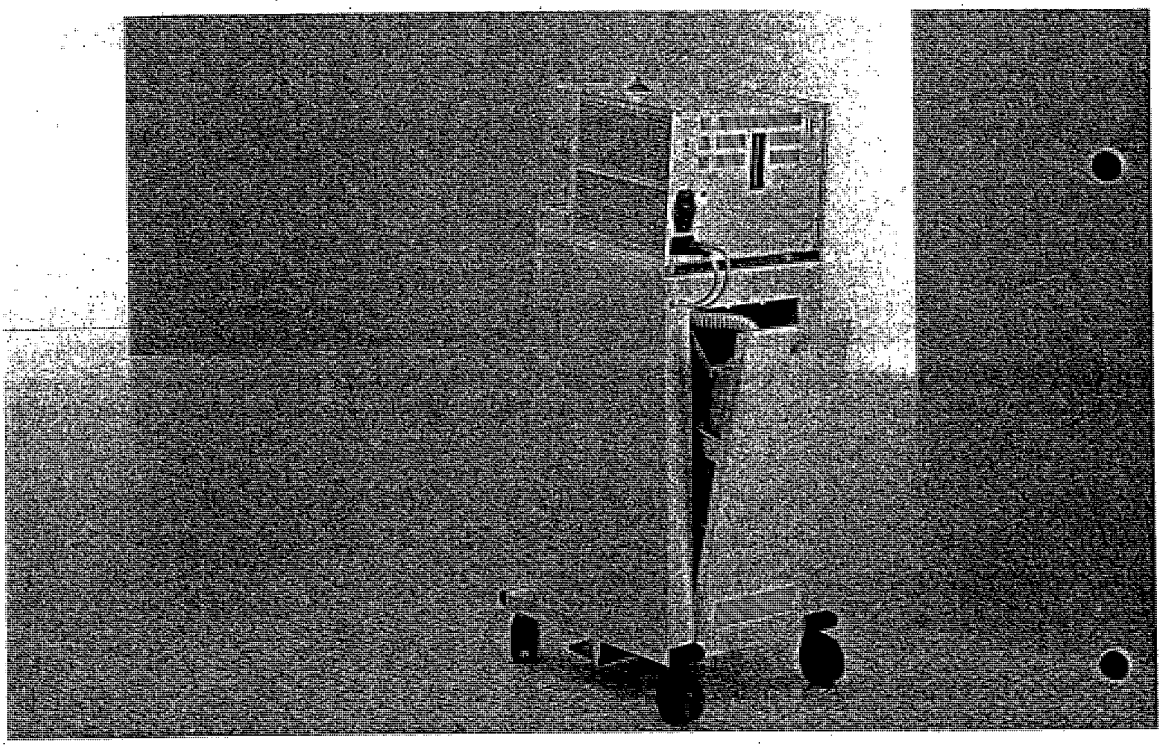


in der Zahnmedizin

Das CEREC-System stellt hohe Anforderungen an das dreidimensionale Vorstellungsvermögen des Behandlers.

Um das Verfahren zu erlernen, ist die Teilnahme an einem zwei- bis dreitägigen Ausbildungskurs unerläßlich.

Diese Mühe lohnt sich, denn erst die detaillierte Kenntnis der technischen Voraussetzungen erschließt die faszinierende volle Nutzung des Systems.



Die CEREC-Einheit ist von externen Wasseranschlüssen völlig unabhängig. Sie ist so beweglich, daß sie leicht in jeden Behandlungsraum gefahren werden kann.

Siemens Aktiengesellschaft
Bereich Medizinische Technik
Geschäftsbereich Dental
Fabrikstraße 31, D-6140 Bensheim

Änderungen infolge technischer Weiterentwicklung behalten wir uns vor.

Best.-Nr. A19100-M41-A471
Printed in the Federal Republic of Germany
4392 WS 098810

JCO-Online Copyright 2005 - VOLUME 26 : NUMBER 6 : PAGES (369-372) 1992

THE READERS' CORNER

PETER M. SINCLAIR, DDS, MSD

This month's topics are positioner appliances and employee embezzlement.

1. In what percentage of your cases do you use a positioner appliance?

Although 77% of the respondents said they used positioners, more than two-thirds of these did so infrequently (fewer than 5% of their cases). The remaining one-third of the positioner users were equally divided between those who prescribed them in about 20% of their cases and those who used them more than 75% of the time.

What are your indications for use of a positioner appliance ?

The primary indication was a high degree of patient cooperation throughout treatment. The major clinical indications listed were open bites, the need for detailing and settling of the posterior occlusion, and cases where treatment had to be discontinued early.

What are your instructions to the patient?

Patient instructions varied widely among the respondents, but the most popular protocol was full-time wear for 48 hours (often over a weekend following a Friday debonding), then nighttime wear plus four hours per day. Other commonly mentioned regimes were nighttime and four hours per day, with no full-time break-in period, and a gradual reduction in daytime wear while continuing at night.

For how long do you generally have a patient wear a positioner?

About half of the clinicians usually asked for two to three months of positioner wear. Fewer respondents prescribed positioners for two to three weeks or three to six months, and even fewer for six to 18 months.

How much correction do you expect from a positioner?

The most common reply was "minimal" (more than 60% of the positioner users). The remaining users also had limited expectations, often expecting 1-2mm of correction.

Do you find patient cooperation a problem ?

More than 70% of the readers felt that cooperation with positioner wear was a significant problem. This was particularly true for those who prescribed positioners for extended periods. All the respondents who did not experience cooperation problems stated that they carefully screened patients before selecting them for positioner wear.

ClearCorrect Exhibit 1002, Page 2482 of 3373

Have you observed any adverse effects from use of a positioner?

Half of the clinicians reported observing some adverse effects. The principal problem cited was muscle tightness and discomfort, particularly in patients with TMJ dysfunction. Another major concern was that if the positioner did not prevent the eruption of the terminal molar, this tooth could overerupt and produce an anterior open bite upon removal of the positioner.

Do you use different colors of positioner material? Do you find color to be a motivating factor in terms of patient cooperation?

The vast majority of the readers did not use colored positioners and did not believe they provided motivation. A few felt that clear positioners provided the greatest incentive for patient wear.

Do you routinely prescribe airholes?

More than 90% of the respondents said they used airholes. Many added, however, that these holes were too small to have any effect on breathing, and that they placed them primarily for the patients' peace of mind.

Have you used Elastodontics? With what success?

Only about one-fourth of the orthodontists had used Elastodontics. They reported a variety of success rates, ranging from "poor" to "some success" to "good results".

Specific comments included:

- "I use positioners especially for those cases that don't lend themselves to finishing elastics, such as multiple missing teeth."
- "I use positioners on patients who have been cooperative during treatment. With positioners being as expensive as they are, I am reluctant to throw good money after bad."
- "I use them to detail or seat the occlusion if cooperation has been a problem, the patient has been in treatment for a long time, and I'm concerned about decay, etc."
- "Cooperation is better than with functional appliances and worse than with headgear."

2. Have you ever had a staff member embezzle money from you ?

Six of the 46 respondents (13%) reported incidents of embezzlement. Most of the others added the caveat, "not to my knowledge".

If so, what position did the staff member hold?

In five of the six cases, the employee involved was in a front-desk or business position. The sixth was a chairside assistant who had been taking money to the bank.

ClearCorrect Exhibit 1002, Page 2483 of 3373

What amount was embezzled?

The amounts ranged from $200 to more than $10,000, with most between $1,000 and $5,000.

How was it done and how did you find out?

Most of the techniques involved cashing isolated patient checks or depositing them into the employee's own account. These were eventually picked up either by one of the check writers, who noticed the wrong account number or the forged signature on a canceled check, or by another staff member balancing the deposits when the embezzler was on sick leave.

In one case, the embezzler was altering the day sheets. In another, the employee was pocketing cash payments without crediting them to the patient, while depositing only checks; this was discovered when patients began to question their balances.

Was your bookkeeping done manually or by computer?

All six of the victimized practices were using manual bookkeeping, and most of them recommended changing to a computerized system.

What advice do you have for others?

Suggestions included hiring trustworthy people (such as the orthodontist's spouse) to do the bookkeeping, double- and triple-checking the books each day, making daily deposits, notating checks and cash separately, and having two staff members reconcile the day sheets. Other advice was to have more than one person familiar with the payment system and never to take anything for granted.

Respondents also recommended that the orthodontist always look at the day sheets and fully understand the office accounting system. Finally, they advised keeping temptations to a minimum--a good reason to have computerized bookkeeping.

If you have not had any embezzlement in your practice, are there any steps that you think have prevented or discouraged embezzlement?

Responses to this question included:

- "My wife works in the office; she makes all entries into accounts receivable and does the accounts payable."
- "Paying attention to the office statistics related to starts, charges, and daily receipts, as well as a good cash management system."
- "We utilize multiple personnel to handle payments. A computer-entered data system involves separate individuals running the day sheet and making adjustments. A daily record of any adjustments is placed on the doctor's desk."
- "My accountant visits monthly to verify services rendered, receipts, deposits, and income."
- "One person receives the funds and a second enters and totals daily receipts."
- "I review, sign, and date the financial sheets every day. Any alterations are handwritten by the

ClearCorrect Exhibit 1002, Page 2484 of 3373

financial secretary and discussed with me daily. "

- "All bank deposits are made by myself or my wife. All bank statements and canceled checks come to my home address. The accounts are checked and balanced by our bookkeeper, who does not post checks or cash. Unannounced spot-check audits are done by the accountant approximately every 18 months."
- "The doctor signs all checks and makes all deposits. The doctor signs cash slips for cash payments and keeps any cash until the deposit is made. The doctor reviews the ledger card of every finished case as part of the final records review. The doctor does not 'steal' from the office by taking home supplies such as pens, paper products, soft drinks, etc., that belong to the office. The doctor expects the staff to uphold the same standard."
- "We rotate our staff in money-handling positions and have an outside accountant do the books monthly."
- "Every payment receives a receipt. If any entries are made on the ledger cards without a receipt, something is wrong."
- "Even with our sophisticated computer security levels, I don't think we can fully prevent it. Hiring quality staff would seem most important."

JCO wishes to thank the following contributors to this month's column:

Drs. Richard S. Arnstine and Bernard H. Friedman, Shaker Heights, OH
Dr. Daniel M. Auter, Johnson City, TN
Dr. Maurice J. Belden, Presque Isle, ME
Dr. Milton D. Berkman, Scarsdale, NY
Dr. Jackie Berkowitz, Columbus, OH
Dr. James D. Bettinger, Artesia, CA
Dr. Richard E. Boyd, Columbia, SC
Dr. H.I. Bussa, Alief, TX
Dr. George D'Louhy, Santa Rosa, CA
Dr. John R. Davis, Pocatello, ID
Drs. Ralph DeDomenico and Mark David Lively, Tampa, FL
Dr. Walker C. Dorsett, Jr., Arcadia, CA
Dr. Ken H. Farrar, Marietta, GA
Dr. Thomas C. Field, Gainesville, GA
Dr. Robert S. Fields, Stamford, CT
Dr. Alan K. Fulks, Iron Mountain, MI
Dr. Ronald L. Gallerano, Houston, TX
Drs. Michael F. Gannon and Todd A. Curtis, Crystal Lake, IL
Dr. C. William Groesch, Springfield, IL
Dr. Dennis E. Halford, Sugar Land, TX
Dr. Chester S. Handelman, Chicago, IL
Dr. Jene Jordan, High Point, NC
Dr. James I. Heslop, Lancaster, PA
Dr. Michael P. Kerr, Howell, MI
Drs. Christopher K. and Peter C. Kesling and R. Thomas Rocke, Westville, IN
Drs. Leonard M. Kessler, Thomas F. Morganstern, and Gary M. Wiser, Freehold, NJ
Dr. Earle A. King, Wexford, PA
Dr. Jay R. Morgner, Imperial Beach, CA
Drs. Richard W. Mullen and Jerold R. Shapiro, Pompton Lakes, NJ
Dr. Thomas D. Murphy, Duluth, MN

ClearCorrect Exhibit 1002, Page 2485 of 3373

Dr. Herbert Nachtrab, South Weymouth, MA
Dr. John D. Nolan, Jr., New Orleans, LA
Dr. Patrick M. Ohlenforst, Irving, TX
Dr. Candland L. Olsen, Bountiful, UT
Dr. John Oubre, Lafayette, LA
Dr. Roy E. Parle, Simi Valley, CA
Dr. Richard M. Port, Vernon Hills, IL
Dr. William W. Robinson, Sherman, TX
Drs. John H. Rogers, Terry L. Duncan, and James K. Dillehay, Wichita, KS
Dr. Donald P. Rollofson, Elk Grove, CA
Dr. Barry Rosenberg, West Hartford, CT
Dr. Mark J. Schpero, New Haven, CT
Dr. David W. Warren, Miami, FL
Dr. Sheldon S. Watnick, Allen Park, MI
Drs. Joseph A. Wells, William A. Mitchell, and Richard F. Hewitt, Greenville, SC
Dr. David C. Wertz, Dubuque, IA □

ClearCorrect Exhibit 1002, Page 2486 of 3373

CEREC 3D

Manuel utilisateur

Version 2.0 Français



The Dental Company sirona

ALN121423

Copyright

© Sirona Dental Systems GmbH 2003. Tous droits réservés

Les informations contenues dans le présent manuel peuvent être modifiées sans préavis particulier.

Le logiciel ainsi que la documentation correspondante sont protégés par des droits d'auteurs. Il doit donc être traité comme tout autre matériel protégé.

Hormis pour un usage personnel, toute personne qui transfère le contenu du présent manuel sur bande magnétique, disquette ou sur tout autre support sans l'autorisation écrite de la société Sirona Dental Systems GmbH commet un délit puni par la loi.

Marque

Microsoft® et Windows NT® sont des marques déposées.

Windows™ est une marque de Microsoft Corporation.

Pentium® est une marque déposée.

Toutes les autres marques sont la propriété de leur possesseur respectif.

Composants d'autres fabricants

Le logiciel CEREC utilise des composants des fabricants indiqués ci-après :

Zlib :

© 1995-2000 Jean-loup Gailly, Mark Adler et Greg Roelofs

PaintLib :

© 1996-2000 Ulrich von Zadow

LibTiff :

© 1988-1997 Sam Leffler

© 1991-1997 Silicon Graphics, Inc.

LeadTools :

© 1991-2000 LEAD Technologies, Inc.

ALN121424

ClearCorrect Exhibit 1002, Page 2488 of 3373

Sommaire

1 **Introduction** 5
- 1.1 A propos de CEREC 3D 6
- 1.2 Utilisation du manuel 7
- 1.3 Autres formats de manuel 9

2 **Logiciel** 10
- 2.1 Conditions requises pour l'installation 11
- 2.2 Installation du logiciel 12
- 2.3 Désinstallation du logiciel 13
- 2.4 Protection contre la copie (clé électronique) 14

3 **Interface utilisateur** 16
- 3.1 Description de l'interface utilisateur 16
- 3.2 Barre d'icônes 17
- 3.3 Fenêtre View 18
- 3.4 Fenêtre Design 22
- 3.5 Fenêtre Cut 30
- 3.6 Barre d'état 31
- 3.7 Fenêtre de construction (Viewer 3D) 32
- 3.8 Barre de menus 34
- 3.9 Menu Restauration 35
- 3.10 Menu Construction 39
- 3.11 Menu Réglages 42
- 3.12 Menu Fenêtre 50
- 3.13 Menu "?" 53

4 **Empreinte optique** 54
- 4.1 Prises d'empreintes avec la caméra 3D 55
- 4.2 Enregistrements avec le scanner 62
- 4.3 Champs d'images 63
- 4.4 Catalogue d'images 64

5 **Construction** 66
- 5.1 Masquage de zones d'image 67
- 5.2 Indication du bord de la préparation 68
- 5.3 Redéfinition de l'axe d'introduction 71
- 5.4 Effacer et corriger des zones d'images de champs d'images 72

6 **Usinage** 74
- 6.1 Prévisualisation Simulation d'usinage 75
- 6.2 Démarrer le processus d'usinage 76

ALN121425

ClearCorrect Exhibit 1002, Page 2489 of 3373

Sommaire

7 Gérer/archiver les données 78

8 Types de restaurations et procédés de construction 81
8.1 Créer nouvelle restauration 82
8.2 Vue d'ensemble des types de restaurations et des procédés de construction 83
8.3 Procédé de construction Base de données dentaire 84
8.4 Procédé de construction Corrélation 86
8.5 Assainissement de l'arcade dentaire 89

9 Fixation adhésive de restaurations CEREC 90

10 CEREC 3D Messages 91
10.1 Informations 92
10.2 Avertissements 93
10.3 Messages de défaut 94

11 Liaison à la gestion du cabinet 97
11.1 Interface de paramètres 98
11.2 Interface SIDA 100
11.3 Interface OpenDenta 101

12 Conseils et astuces 102
12.1 Screenshot (Photo d'écran) / Image TIF 103
12.2 Indications techniques 104
12.3 Questions fréquentes 107

13 Glossaire 108

ALN121426

ClearCorrect Exhibit 1002, Page 2490 of 3373

Introduction

Dans ce chapitre

Ce chapitre est subdivisé en plusieurs paragraphes :

- „A propos de CEREC 3D" page 6
- „Utilisation du manuel" page 7
- „Autres formats de manuel" page 9

ALN121427

ClearCorrect Exhibit 1002, Page 2491 of 3373

1 Introduction

1.1 A propos de CEREC 3D

Chère cliente, cher client

Nous vous remercions de l'achat du CEREC® 3 / CEREC *Scan* de Sirona.

Cet appareil permet la fabrication assistée par ordinateur de restaurations céramiques à partir d'un matériau céramique (CEramic REConstruction) imitant l'aspect naturel des dents.

Le présent manuel fait partie de l'étendue de la livraison Gardez-le toujours à portée de main.

Afin de maîtriser parfaitement le fonctionnement de l'appareil, exercez-vous sur le modèle à partir des exemples décrits.

Afin d'éviter tout risque de dommages matériels et corporels, veuillez également tenir compte des consignes de sécurité.

Afin de pouvoir bénéficier de la garantie, nous vous prions de compléter intégralement le document joint **Protocole d'installation/fiche de garantie** dès la réception de l'appareil et de l'envoyer au numéro de fax indiqué.

Votre

équipe CEREC

ALN121428

ClearCorrect Exhibit 1002, Page 2492 of 3373

1.2 Utilisation du manuel

Présentation

Le manuel se présente sous forme d'une colonne d'images à gauche et d'une colonne de texte à droite.

Lorsqu'il n'y a pas d'image, un titre latéral dans la colonne de gauche sert à faciliter la navigation.

ATTENTION
signale les indications de sécurité à respecter impérativement.

REMARQUE
signale les informations supplémentaires, les indications et les conseils & astuces.

Conventions

Les conventions suivantes sont utilisées dans le présent manuel :

Tableau 1: Conventions

Exemple	Signification
1., 2., 3., ...	vous demande d'exécuter une tâche dans l'ordre indiqué.
■	indique les énumérations.
A, B, C, ...	indique une référence à un graphique (figure).
Ecriture en gras	Elle indique les points importants.
Ecriture en gras et en italique	Elle indique les éléments que vous pouvez sélectionner sur l'interface CEREC 3D (p. ex. menus, boutons et icônes)
Réglages/Configuration/ Schéma dentaire...	Sélectionnez *Schéma dentaire...* dans le sous-menu *Configuration* du menu *Réglages*.
"Guillemets"	Ils indiquent les noms de chapitres, les renvois, etc.
Cliquer	Appuyer une fois sur la touche de gauche de la souris - ou sur la touche d'entrée sur l'unité de prise d'empreinte - et relâcher la touche.

ALN121429

ClearCorrect Exhibit 1002, Page 2493 of 3373

Tableau 1: Conventions

Exemple	Signification
Double-clic	Appuyer deux fois de suite rapidement sur la touche de gauche de la souris - ou sur la touche d'entrée sur l'unité de prise d'empreinte - et relâcher la touche.
Saisie d'un point	Appuyer sur la touche de gauche de la souris et la maintenir enfoncée.
En cas d'enregistrement avec caméra 3D : Actionner la pédale	Même fonction que : actionnement de la touche d'entrée sur l'unité de prise d'empreinte ou de la touche de gauche de la souris.

ALN121430

ClearCorrect Exhibit 1002, Page 2494 of 3373

1.3 Autres formats de manuel

Format html

Le Manuel utilisateur en format html se trouve sur le CD de documentation joint. Ce format axé écran convient bien pour la recherche de termes p. ex. dans l'index ou le sommaire.

Vous pouvez appeler ce manuel via l'Aide (Aide en ligne).

Format pdf

Le Manuel utilisateur en format pdf se trouve sur le CD de documentation joint.

Ce format axé page convient parfaitement à l'impression des pages voulues.

ClearCorrect Exhibit 1002, Page 2495 of 3373

2 Logiciel

Dans ce chapitre

Dans ce chapitre, vous trouverez les informations suivantes :

- „Conditions requises pour l'installation" page 11
- „Installation du logiciel" page 12
- „Désinstallation du logiciel" page 13
- „Protection contre la copie (clé électronique)" page 14

ALN121432

ClearCorrect Exhibit 1002, Page 2496 of 3373

2.1 Conditions requises pour l'installation

(uniquement CEREC *Scan*)

Equipement du PC

Pour l'installation, vous devez disposer d'un PC compatible IBM et présentant l'équipement suivant :

- PC : ≥ Pentium® 4
- Système d'exploitation : Windows 2000 (Service Pack 1), Windows XP
- Internet Explorer : ≥ 5.0
- Carte graphique 3D avec accélérateur matériel : ≥ 64 MB GeForce2
- Résolution de l'écran : 1024 x 768 Pixel, True Color
- Mémoire RAM : ≥ 512 Mo
- Disque dur : ≥ 40 Go
- Interface parallèle (imprimante) (25 points)
- Une interface série libre (9 points, RS-232, COM1 ou COM 2)
- Lecteur de CD-/DVD

ALN121433

ClearCorrect Exhibit 1002, Page 2497 of 3373

2.2 Installation du logiciel

⚠ATTENTION
Pour l'installation du logiciel sur un PC, vous devez disposer de droits d'administrateur !

Effectuer l'installation

1. Insérez le CD CEREC dans le lecteur de CD/DVD.

Le programme d'installation démarre automatiquement.

2. Dans le cas contraire, lancer le fichier *Setup.exe* dans le répertoire principal du CD.
3. Sélectionnez la langue de l'installation.

Le contrat de licence apparaît ensuite.

4. Si vous acceptez le contrat de licence, le programme continue l'installation.

Installation standard ou installation personnalisée

Vous pouvez ensuite choisir entre l'installation standard et une installation personnalisée.

- Lors de l'installation standard, CEREC 3, SIROCAM (et Zoomer) et CEREC 3D sont installés dans la langue d'installation choisie. Si une caméra 3D (uniquement utilisable pour CEREC 3) est présente, les composants de la caméra sont également installés.
- Dans le cas d'une installation personnalisée, vous pouvez sélectionner une autre langue pour le logiciel CEREC à installer.

1. Après avoir opté pour l'un des deux types d'installation, cliquez sur le bouton correspondant.
2. Au terme de l'installation, vous pouvez afficher le fichier *Readme*. Ce fichier contient les informations les plus actuelles sur le logiciel CEREC.

⚠ATTENTION
Au terme de l'installation du nouveau logiciel, il faut transférer le nouveau programme d'usinage dans l'unité d'usinage (voir notice d'utilisation de l'unité d'usinage).

ALN121434

ClearCorrect Exhibit 1002, Page 2498 of 3373

2.3 Désinstallation du logiciel

1. Pour désinstaller le logiciel, cliquez sur ***Démarrer/ Programmes/CEREC/Désinstallation.***

Durant la désinstallation, le programme vous demande si vous voulez effacer les données patient ou les entrées dans la base de données d'enregistrement (entre autres, les données de calibrage).

2. Selon votre choix, cliquez sur le bouton *Oui* ou *Non*.

Le logiciel est désinstallé.

ALN121435

ClearCorrect Exhibit 1002, Page 2499 of 3373

2.4 Protection contre la copie (clé électronique)

Introduction

La possibilité d'usinage d'une restauration dépend de la clé électronique disponible et de l'identification de l'unité d'usinage utilisée.

Clé électronique

clé CEREC 3D

Raccorder la clé électronique

1. Monter la clé électronique sur l'interface parallèle de l'unité d'usinage ou du PC.
2. Vous pouvez ensuite monter plusieurs clés l'une sur l'autre ou brancher p. ex. une imprimante.

Sans clé électronique

Sans clé électronique, il est possible de concevoir et d'enregistrer toutes les restaurations. Pour l'usinage, vous devez disposer de la clé CEREC 3D.

ALN121436

ClearCorrect Exhibit 1002, Page 2500 of 3373

3 Interface utilisateur

Dans ce chapitre

Dans ce chapitre, vous trouverez les informations suivantes :

- „Description de l'interface utilisateur" page 16
- „Barre d'icônes" page 17
- „Fenêtre View" page 18
- „Fenêtre Design" page 22
- „Fenêtre Cut" page 30
- „Barre d'état" page 31
- „Fenêtre de construction (Viewer 3D)" page 32
- „Barre de menus" page 34
- „Menu Restauration" page 35
- „Menu Construction" page 39
- „Menu Réglages" page 42
- „Menu Fenêtre" page 50
- „Menu "?"" page 53

ALN121437

ClearCorrect Exhibit 1002, Page 2501 of 3373

3.1 Description de l'interface utilisateur

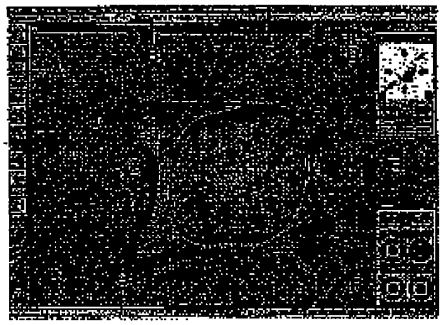


Fig. 3-1 Menu principal

CEREC 3D met à votre disposition une interface utilisateur structurée en menus et qui vous permettra de mesurer des cavités, de concevoir les restaurations voulues et de les usiner ensuite.

Les affichages à l'écran vous guident à travers les étapes de la conception et vous donnent toujours une vue d'ensemble de l'étape de programme en cours d'exécution.

Le menu principale se compose de :

- A: Barre d'icônes,
- B: Barre de menus,
- C: Titre de la fenêtre de programme,
- D: Fenêtre View,
- E: Croix de coordonnées,
- F: Fenêtre Design,
- G: Barre d'état,
- H: Echelle (1 mm)
- I: Fenêtre de construction (Viewer 3D)

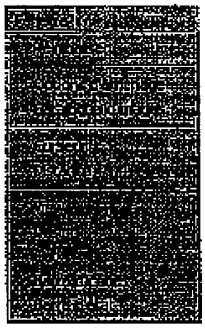


Fig. 3-2 Fenêtres/Barres affichées, Cut désactivé

REMARQUE

Vous pouvez afficher ou masquer les fenêtres/barres suivantes :

- View
- Design
- Cut
- Barre d'icônes
- Barre d'état

ALN121438

ClearCorrect Exhibit 1002, Page 2502 of 3373

3.2 Barre d'icônes

Vous pouvez afficher ou masquer la *barre d'icônes* via l'option de menu *Fenêtre/barre d'icônes*.

Les fonctions inactives sont représentées en gris, p. ex. explorer/enregistrer antagoniste/enregistrement occlusion.

Description des symboles/icônes



Créer nouvelle restauration



Charger restauration



Enregistrer restauration



Explorer/enregistrer dent préparée (préparation)



Explorer/enregistrer dent non préparée (Occlusion)



Explorer/enregistrer antagoniste/enregistrement occlusion



Avancer d'une étape de construction (suivant)



Reculer d'une étape de construction (retour)



Démarrer le processus d'usinage

Il est possible de prendre la *barre d'icônes* avec la souris et de la positionner librement sur l'écran. Elle peut être positionnée au bord à gauche, à droite, en haut ou en bas (comme d'habitude sous Windows).

ALN121439

ClearCorrect Exhibit 1002, Page 2503 of 3373

3.3 Fenêtre View

Introduction

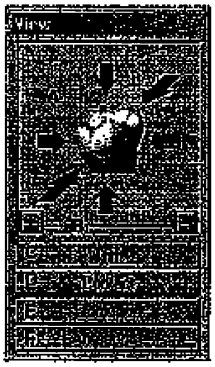
Vous pouvez afficher ou masquer cette fenêtre via l'option de menu *Fenêtre/ View*.

Les fonctions inactives sont représentées en gris, p. ex. Antagoniste.

Vous pouvez prendre la fenêtre avec la souris au niveau du bandeau supérieur et la positionner à volonté sur l'écran. Lorsque vous activez *Fenêtre/Réinitialiser*, la fenêtre retourne à sa position initiale (bord droit de l'écran).

Dans ce paragraphe

Ce paragraphe décrit les fonctions suivantes :



- A: Vuee standard
- B: Outil Zoom
- C: Afficher/Masquer les dents voisines (Trim)
- D: Afficher/Masquer les contact avec la dent voisine (Contact)
- E: Afficher/Masquer occlusion (Occlusion)
- F: Afficher/Masquer antagoniste

3.3.1 Vues standard



Fig. 3-9 Vues standard

Les objets affichés dans la fenêtre de construction peuvent être observés sous six angles différents en cliquant sur les flèches existantes :

- mésial
- distal
- buccal/labial
- lingual
- cervical
- occlusal/incisive

Lorsque vous déplacez le pointeur de la souris sur l'une de ces flèches, le sens de la vue est indiqué.

Lorsque vous cliquez sur la flèche, l'objet tourne pour se placer sous l'angle considéré.

ALN121440

ClearCorrect Exhibit 1002, Page 2504 of 3373

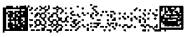


Fig. 3-4 Outil Zoom

3.3.2 Outil Zoom

Les objets affichés dans la fenêtre de construction peuvent être agrandis ou réduits comme suit :

- pas à pas, en cliquant sur "+" (agrandir) ou "–" (réduire)
- en continu, en maintenant enfoncé la touche "+" (agrandir) ou "–" (réduire)



Fig. 3-5 Bouton Trim

3.3.3 Afficher/Masquer les dents voisines (Trim)

Un clic sur le bouton *Trim* permet de masquer les dents voisines.

Si certaines parties des dents voisines sont gênantes lors de l'entrée du bord de préparation, il est possible de découper les parties gênantes. De plus, vous pouvez masquer des parties de l'image après l'enregistrement (voir „Masquage de zones d'image" page 67).

Un nouveau clic sur le bouton *Trim* permet d'afficher à nouveau les dents voisines.



Fig. 3-6 Bouton Contact

3.3.4 Afficher/Masquer les contact avec la dent voisine (Contact)

Un clic sur le bouton *Contact* permet d'afficher/masquer le contact avec la dent voisine.

REMARQUE

Afin de mieux évaluer la surface de contact, vous pouvez masquer les dents voisines à l'aide du bouton Trim .

Lorsque vous actionnez le bouton *Contact*, un schéma de couleurs apparaît au niveau des surfaces de contact. La signification des couleurs est la suivante :

- bleu : distance 0-1 mm
  surface plus réduite – distance plus importante
- vert : pénétration 0-50 µm
- jaune : pénétration 50-100µm
- rouge : pénétration >100µm

Avec les outils de *Design Scale*, *Shape* ou *Drop*, vous pouvez agencer les surfaces de contact selon vos souhaits.

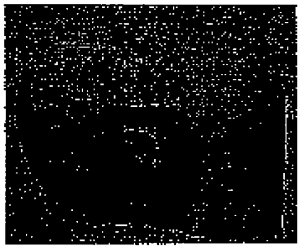


Fig. 3-7 Surface de contact

ALN121441

ClearCorrect Exhibit 1002, Page 2505 of 3373

3.3.5 Afficher/Masquer occlusion (Occlusion)

Lorsqu'il existe un Champs d'images de l'occlusion, il est possible de l'afficher ou de le masquer à l'aide de ce bouton.



Fig. 3-8 Bouton Occlusion

3.3.6 Afficher/Masquer antagoniste

Un clic sur le bouton ***Antagonist*** permet d'afficher/masquer la fenêtre ***Antagonist*** (Fig. 3-10).



Fig. 3-9 Bouton Antagoniste

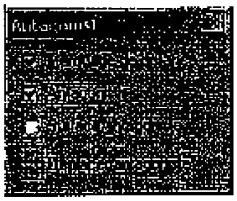


Fig. 3-10 Fenêtre Antagoniste

Dans cette fenêtre, vous pouvez activer ou désactiver les éléments suivants :

- ***Marquage de distance***
- ***Antagonist***
- ***Surface antagoniste***

Marquage de distance

Lorsque le ***Marquage de distance*** est activé, il apparaît sur la restauration un schéma de couleur dont la signification est la suivante :

- bleu : distance 0-1 mm
  surface plus réduite – distance plus importante
- vert : pénétration 0-50 µm
- jaune : pénétration 50-100 µm
- rouge : pénétration >100 µm

Avec les outils de ***Design Scale***, ***Shape*** ou ***Drop***, vous pouvez adapter la distance.



Fig. 3-11 Marquage de la distance

ALN121442

ClearCorrect Exhibit 1002, Page 2506 of 3373

Antagonist

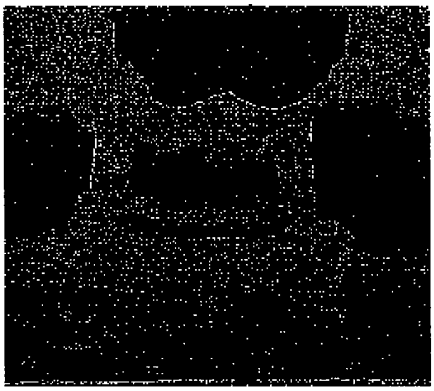


Fig. 3-12 Antagoniste/enregistrement occlusion affiché

Lorsque ***Antagonist*** est activé, l'enregistrement centré de l'occlusion apparaît au-dessus de la restauration.

Un clic sur le bouton à côté de ***Déplacer antagoniste*** (Fig. 3-10) permet de faire monter ou descendre l'enregistrement de l'occlusion. Le fait de relever l'enregistrement de l'occlusion permet d'avoir une meilleure vue sur la surface occlusale.

Vous pouvez examiner la restauration sous tous les angles et l'adapter à l'aide des ***outils de design***.

Surface antagoniste



Fig. 3-13 Surface antagoniste affichée

Lorsque ***Surface antagoniste*** est activée, la surface de mastication de l'antagoniste/l'enregistrement de l'occlusion devient visible au-dessus de la restauration.

Un clic sur le bouton à côté de ***Déplacer antagoniste*** (Fig. 3-10) permet de faire monter ou descendre l'enregistrement de l'occlusion. Le fait de relever l'enregistrement de l'occlusion permet d'avoir une meilleure vue sur la surface occlusale.

Vous pouvez examiner la restauration sous tous les angles et l'adapter à l'aide des ***outils de design***.

ALN121443

ClearCorrect Exhibit 1002, Page 2507 of 3373

3.4 Fenêtre Design

Introduction

Vous pouvez afficher ou masquer cette fenêtre via l'option de menu *Fenêtre/Design*.

Les fonctions inactives sont représentées en gris, p. ex. *Position*.

Vous pouvez prendre la fenêtre avec la souris au niveau du bandeau supérieur et la positionner à volonté sur l'écran.

Lorsque vous activez *Fenêtre/Réinitialiser*, la fenêtre retourne à sa position initiale (bord droit de l'écran).

Dans ce paragraphe

Ce paragraphe décrit les *outils de design* suivants :

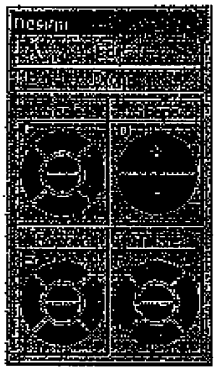




Fig. 3-14 Bouton Edit

- A: „Outil d'édition (Edit)" page 22
- B: „Gouttes de cire (Drop)" page 24
- C: „Outil Echelle (Scale)" page 24
- D: „Outil Surfaces de forme libre (Shape)" page 26
- E: „Outil de positionnement (Position)" page 28
- F: „Outil de rotation (Rotate)" page 29

3.4.1 Outil d'édition (Edit)

Un clic sur l'outil *Edit* permet d'activer/désactiver la fonction d'édition.

ALN121444

ClearCorrect Exhibit 1002, Page 2508 of 3373



Fig. 3-15 Fonction d'édition

La fonction d'édition peut être utilisée sur toutes les lignes de construction. Les lignes de construction sont automatiquement affichées et sont codées par des couleurs différentes.

Tableau 2: Couleurs des lignes de construction

Ligne de construction	Couleur
Bord de la préparation	bleu
Ligne de contact proximal	rose
Ligne de copie	vert
Crêtes marginale, ligne labiolinguale	turquoise
Fissure, arête de coupe	vert

L'édition n'agit que dans le plan d'observation.

Editer ligne de construction

1. Cliquez sur le bouton *Edit*.
2. Double-cliquez sur une ligne de construction pour placer le premier point de la ligne de correction.
3. Cliquez pour placer d'autres points de la ligne de correction

> ***REMARQUE***
> *La touche de droite de la souris permet d'effacer le dernier clic.*

4. Terminer la ligne de correction :
   - **Ligne fermée** (p. ex. équateur de couronne)
     Double-cliquez sur la ligne de construction
   - **Ligne ouverte** (p. ex. ligne de fissure)
     Double-cliquez sur la nouvelle extrémité de ligne voulue.



> ***REMARQUE***
> *Avec l'icône **Annuler**, vous pouvez annuler la dernière modification du tracé de la ligne.*

> ***REMARQUE***
> *Si vous voulez modifier la liaison au bord de préparation (point rouge), saisissez le point avec la touche de gauche de la souris et déplacez-le le long du bord de la préparation.*

ALN121445

ClearCorrect Exhibit 1002, Page 2509 of 3373

3.4.2 Gouttes de cire (Drop)



Fig. 3-16 Bouton Drop

Un clic sur le bouton *Drop* permet d'activer la fonction Gouttes de cire.

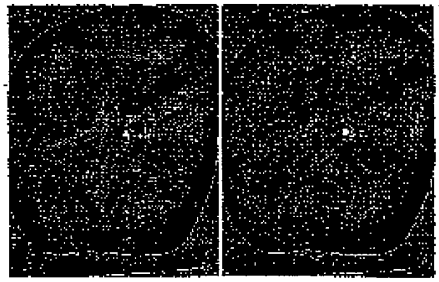


Fig. 3-17 Appliquez du matériau et lissez-le

Cette fonction vous permet de déposer du matériau goutte à goutte (Fig. 3-17, à gauche).

La barre d'espacement sur le clavier permet de passer à la fonction Lisser. Le curseur prend la forme d'une main avec laquelle, la touche gauche de la souris enfoncée, vous pouvez lisser localement la surface (Fig. 3-17, à droite).

3.4.3 Outil Echelle (Scale)



Un clic sur l'outil *Scale* permet d'activer/désactiver la fonction de mise à l'échelle. Cette fonction vous permet de déformer une zone sélectionnée.



Fig. 3-18 Moitié de restauration mésiale sélectionnée

Sélectionnez tout d'abord la zone à mettre à l'échelle en cliquant sur une ligne.

Tableau 3: Sélectionner la zone à mettre à l'échelle

Zone à sélectionner	Cliquez sur ...
Moitié de restauration ... **linguale/buccale/ mésiale/distale**	**Bord de la préparation** ... **lingual/buccal/mésial/ distal**
Zone entre bord de la préparation et crête marginale ... **linguale/buccale/ mésiale/distale**	Ligne de contact proximal .... **linguale/buccale/ mésiale/distale**

ALN121446

ClearCorrect Exhibit 1002, Page 2510 of 3373

Tableau 3: Sélectionner la zone à mettre à l'échelle

Zone à sélectionner	Cliquez sur
Zone au-dessus de l'équateur... linguale/buccale/ mésiale/distale	Crêtes marginales ... linguales/buccales/ mésiales/distales
Zone occlusale	Ligne de fissure
Cuspide	Bille de couleur turquoise sur les crêtes marginales

REMARQUE

Lors de la sélection du bord de préparation, de la ligne de contact proximal et des crêtes marginales, la touche de fonction F7 permet d'étendre la sélection à la deuxième moitié de la zone sélectionnée.
Un nouvel actionnement de F7 permet de revenir à la sélection de la zone initiale.



Fig. 3-19 Mise à l'échelle de la zone sélectionnée



Une fois que vous avez sélectionné une zone, vous pouvez la modifier :

- pas à pas, en cliquant sur un segment du cercle (p. ex. buccal)
- en continu, en maintenant enfoncé un segment du cercle (p. ex. buccal)



Pour quitter l'outil de mise à l'échelle, cliquez sur le bandeau marqué *Scale*.

ALN121447

ClearCorrect Exhibit 1002, Page 2511 of 3373

3.4.4 Outil Surfaces de forme libre (Shape)



Avec l'outil *Shape*, vous pouvez lisser les surfaces et déposer ou retirer du matériau :

- le long d'une ligne ouverte ou
- au sein d'une surface fermée

Apport de matériau le long d'une ligne ouverte

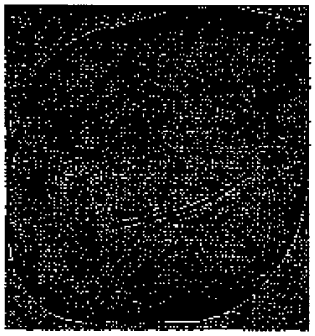


Fig. 3-20 Ligne ouverte



1. Commencez à dessiner une ligne en double-cliquant sur la restauration.
2. En cliquant, tracez la ligne voulue le long de laquelle vous voulez déposer ou retirer du matériau.

REMARQUE

Certains points isolés peuvent aussi se trouver sur la dent résiduelle, mais le point de départ et le point d'arrivée doivent se trouver sur la restauration.

3. Terminez votre ligne par un double-clic.
4. Vous pouvez faire monter (+) ou descendre (-) la ligne :

- pas à pas,
  en cliquant sur les demi-cercles *Shape* "+" ou "-"
- en continu,
  en maintenant enfoncés les demi-cercles "+" ou "-"

ALN121448

ClearCorrect Exhibit 1002, Page 2512 of 3373

Apport de matériau au sein d'une surface fermée

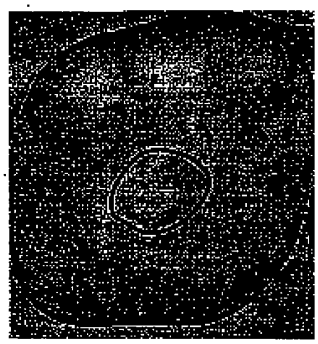


Fig. 3-21 Surface fermée



1. Commencez à dessiner une ligne en double-cliquant sur la restauration.
2. En cliquant, tracez la surface voulue à l'intérieur de laquelle vous voulez déposer ou retirer du matériau.

REMARQUE

Certains points isolés peuvent aussi se trouver sur la dent résiduelle, mais le point de départ et le point d'arrivée doivent se trouver sur la restauration.

3. Terminez la ligne par un double-clic sur le point de départ.
4. La zone au sein de la surface est activée, vous pouvez déposer du matériau (+) ou en retirer (-) :
   - pas à pas,
     en cliquant sur les demi-cercles ***Shape*** "+" ou "-"
   - en continu,
     en maintenant enfoncés les demi-cercles "+" ou "-"

Lisser la surface

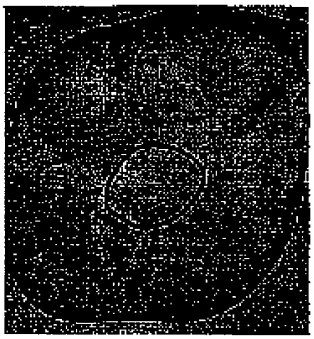


Fig. 3-22 Lisser la surface fermée



Avec l'outil ***Shape***, vous pouvez également lisser une surface préalablement définie.

1. Commencez à dessiner une ligne en double-cliquant sur la restauration.
2. En cliquant, tracez la surface voulue à l'intérieur de laquelle vous voulez effectuer le lissage.

REMARQUE

Certains points isolés peuvent aussi se trouver sur la dent résiduelle, mais le point de départ et le point d'arrivée doivent se trouver sur la restauration.

3. Terminez la ligne par un double-clic sur le point de départ.
4. Activez le lissage à l'aide de la barre d'espacement (A, Fig. 3-22).

La zone au sein de la surface est lissée.



Pour quitter l'outil ***Shape***, cliquez sur le bandeau marqué ***Shape***.

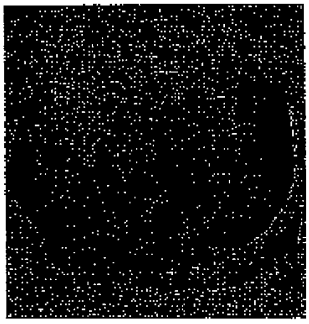
ALN121449

ClearCorrect Exhibit 1002, Page 2513 of 3373

3.4.5 Outil de positionnement (Position)



Un clic sur l'outil *Position* permet d'activer/désactiver la fonction de positionnement.





Cette fonction permet de décaler l'ensemble de la restauration dans les sens suivants :

- mésio-distal
- buccal-lingual
- occlusal-cervical

Le positionnement de la restauration peut s'effectuer de deux manières :

- pas à pas, en cliquant sur un segment du cercle
- en continu, en maintenant enfoncé un segment du cercle

Fig. 3-23 Positionner la restauration



Pour quitter l'outil de positionnement, cliquez sur le bandeau marqué ***Position***.

ALN121450

ClearCorrect Exhibit 1002, Page 2514 of 3373

3.4.6 Outil de rotation (Rotate)



Un clic sur l'outil *Rotate* permet d'activer la fonction de rotation.





Cette fonction permet de faire tourner l'ensemble de la restauration autour des axes suivants :

- mésio-distal
- buccal-lingual
- occlusal-cervical

La rotation de la restauration peut s'effectuer de deux manières :

- pas à pas, en cliquant sur un segment du cercle
- en continu, en maintenant enfoncé un segment du cercle

Fig. 3-24 Tourner la restauration



Pour quitter l'outil de rotation, cliquez sur le bandeau marqué *Rotate*.

ALN121451

ClearCorrect Exhibit 1002, Page 2515 of 3373

3.5 Fenêtre Cut

Vous pouvez afficher ou masquer la fenêtre *Cut* via l'option de menu *Fenêtre/Cut*.

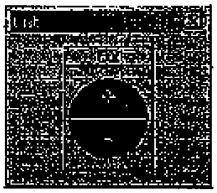


Fig. 3-25 Fenêtre de coupe (Cut)

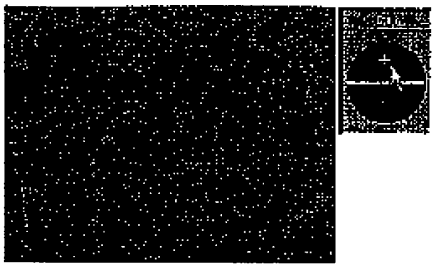


Fig. 3-26 Plan de coupe

Un clic sur l'outil *Cut* permet de tracer un plan de coupe à travers la restauration et la préparation. Le plan de coupe est parallèle au plan de l'écran. Le déplacement parallèle du plan de coupe peut s'effectuer de deux manières :

- pas à pas, en cliquant sur les demi-cercles *Cut* "+" ou "-"
- en continu, en maintenant enfoncé un demi-cercle



Pour quitter l'outil *Cut*, cliquez sur le bandeau marqué *Cut*.

Fermez la fenêtre *Cut* en cliquant sur x (Fermer) ou sur *Fenêtre/Cut*.

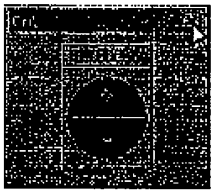


Fig. 3-27 Fermer la fenêtre Cut

ALN121452

ClearCorrect Exhibit 1002, Page 2516 of 3373

3.6 Barre d'état



Fig. 3-28 Barre d'état

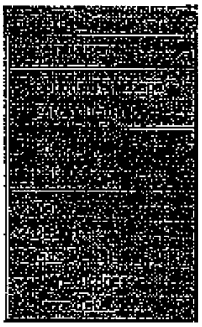


Fig. 3-29 Barre d'état affichée

REMARQUE

La barre d'état peut être affichée ou masquée via l'option de menu Fenêtre/Barre d'état.

La barre d'état vous donne des informations actuelles sur :

- A: les étapes de travail à effectuer,
- B: l'activité de l'unité d'usinage,
- C: lorsque la restauration et la préparation sont affichées, sur l'épaisseur de la céramique à l'endroit où se trouve le pointeur de la souris,
- D: la hauteur de fissure minimale,
- E: la hauteur de la préparation / occlusion à l'endroit où se trouve le pointeur de la souris.

ALN121453

ClearCorrect Exhibit 1002, Page 2517 of 3373

3.7 Fenêtre de construction (Viewer 3D)



Fig. 3-30 Viewer 3D.

CEREC 3D comporte une fenêtre principale (Viewer 3D-) pour la visualisation et la construction d'une restauration en 3D.

Une fois que tous les champs d'images ont été enregistrés, le Viewer 3D s'ouvre. Le temps qui s'écoule jusqu'à l'affichage du Viewer dépend du nombre de champs d'images et du nombre d'enregistrements individuels.

Dans la fenêtre de construction, vous pouvez effectuer les fonctions suivantes :

- visualiser les champs d'images de la préparation, de l'occlusion et des antagonistes et visualiser la restauration soit de manière isolée, soit dans n'importe quelle combinaison,
- redéfinir l'Axe d'introduction,
- masquer une zone d'image en introduisant une ligne ouverte dans le sens mésial et distal,
- indiquer le bord de la préparation,
- voir immédiatement les résultats obtenus lors de l'utilisation d'un outil (p. ex. éditer, mettre à l'échelle...)
- évaluer la pièce à usiner dans la simulation d'usinage avant l'usinage proprement dit,
- faire tourner les objets à volonté.

  A cet effet, maintenez enfoncée la touche gauche de la souris et déplacez la souris dans le sens voulu.

  Afin de faciliter l'orientation, le sens est indiqué (p. ex. mésial, lingual, ...).

Les objets sont représentés de manière centrée. Vous pouvez modifier la position des objets avec la touche droite de la souris en la maintenant enfoncée.

3.7.1 Echelle

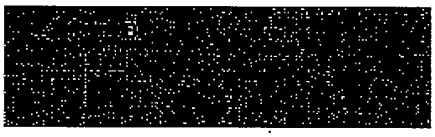


Fig. 3-31 Echelle

L'échelle s'affiche dans l'angle inférieur gauche du Viewer. La distance entre A et B correspond à 1 mm.

L'affichage de la graduation varie en fonction de l'agrandissement ou de la réduction de l'objet.

ALN121454

ClearCorrect Exhibit 1002, Page 2518 of 3373



Fig. 9-32 Croix de coordonnées

3.7.2 Croix de coordonnées

La croix de coordonnées vous indique dans quel sens l'objet est orienté sur l'écran. Les trois flèches indiquent les sens suivants :

- rouge : buccal
- vert : mésial
- bleu : occlusal

ALN121455

ClearCorrect Exhibit 1002, Page 2519 of 3373



Fig. 3-33 Barre de menus

3.6 Barre de menus

La barre de menus au bord supérieur de la fenêtre permet d'appeler d'autres fonctions de programme qui ne sont pas accessibles à partir des barres d'outils.

Il existe les menus suivants :

- Menu Restauration
- Menu Construction
- Menu Réglages
- Menu Fenêtre
- Menu "?"

REMARQUE

Les fonctions des options de menu peuvent aussi, en partie, être appelées via des raccourcis clavier indiqués dans l'option de menu ou via les symboles/icônes correspondants dans la barre d'outils.

ALN121456

ClearCorrect Exhibit 1002, Page 2520 of 3373

3.9 Menu Restauration

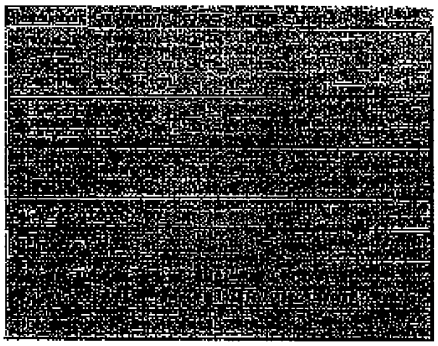


Fig. 3-34 Menu : Restauration

Le menu ***Restauration*** permet ...

- d'ouvrir une fenêtre pour une nouvelle restauration ***Restauration/Nouveau...*** ou ***Ctrl+N***
- charger une restauration existante ***Restauration/Charger...*** ou ***Ctrl+O***
- effacer une restauration ***Restauration/Supprimer...***
- enregistrer une restauration ***Restauration/Enregistrer...*** ou ***Ctrl+S***
- enregistrer une restauration sous un nouveau nom ou l'affecter à un autre patient ***Restauration/Enregistrer sous...***
- exporter une restauration ***Restauration/Export...***
- importer une restauration ***Restauration/Import...***
- ***Gérer les données patient...***
- Envoyer les données de la restauration par e-mail ***Restauration/Envoyer à ...***
- ouvrir la restauration précédente ou
- quitter l'application. ***Restauration/Quitter***

ALN121457

ClearCorrect Exhibit 1002, Page 2521 of 3373

Export

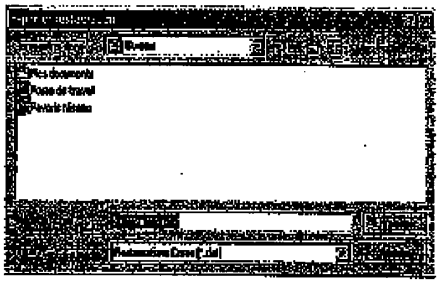


Fig. 3-35 Exporter restauration

Si une restauration est ouverte, cette dernière peut être sauvegardée sous forme comprimée à n'importe quel endroit sur l'un des lecteurs du PC (disques durs, lecteurs de disquettes et lecteurs de CD). A cet effet, une boîte de dialogue Windows standard s'affiche.

La restauration peut être enregistrée sous un nom quelconque, mais le type de fichier doit être "*.cdr" !

Import

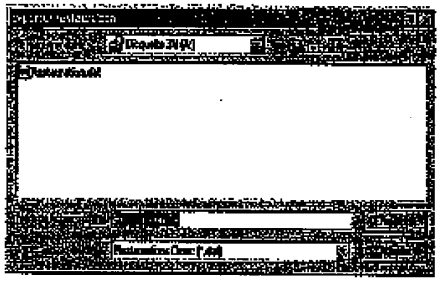


Fig. 3-36 Importer restauration

L'option de menu *Restauration / Import* ouvre une boîte de dialogue Windows standard permettant de chercher des restaurations CEREC comprimées dans tous les lecteurs (disques dure, lecteurs de disquettes et lecteurs de CD) du PC Si le fichier sélectionné (*.cdr ou *.dat) est une restauration CEREC, cette dernière s'ouvre. Dans le cas contraire, l'ouverture est refusée et un message d'erreur s'affiche.

ALN121458

ClearCorrect Exhibit 1002, Page 2522 of 3373

Gérer les données patient

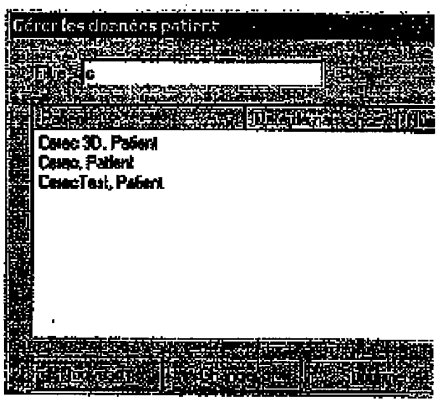


Fig. 3-37 Gérer les données patient

La gestion des données patient CEREC peut être appelée sous ***Restauration / Gérer les données patient.*** L'écran affiche une boîte de dialogue contenant pour l'essentiel une liste de tous les patients. Elle affiche non seulement le nom et le prénom, mais aussi la date de naissance et le numéro de fiche.

Le champ d'entrée ***Filtre*** permet d'agencer la liste avec plus de clarté en entrant un nom, un prénom ou les premières lettres.

Exemple :

Si vous tapez dans le champ d'entrée ***Filtre*** la lettre "c", l'écran affiche une liste de tous les patients dont le nom ou le prénom commence par la lettre "c".

Gérer les données patient Nouveau/Charger



Fig. 3-38 Modifier les données patient

Lors de la création d'un nouveau patient (bouton ***Nouveau***) et pour ***Charger*** les données d'un patient sélectionné, l'écran affiche un masque de saisie.

En double-cliquant sur un patient (ou en sélectionnant un patient et en actionnant le bouton ***Charger***), le programme affiche les données à modifier.

Tapez le ***nom, le prénom, la date de naissance**** et/ou un ***numéro de s.s.***.

* La ***date de naissance*** doit être indiquée conformément à la convention de saisie nationale réglée dans Windows : au format ***JJ.MM.AAAA*** (p. ex. : 27.03.1964) ou ***MM/JJ/AAAA*** (p. ex. : 03/27/1964).

Dans la structure des données CEREC, un patient est clairement identifié par l'une des deux entrées suivantes :

- ***nom, prénom et date de naissance***

ou

- ***numéro de s.s.***

Si la base de données est connectée, le ***nom, le prénom*** et la ***date de naissance*** doivent être mentionnés; l'indication du ***numéro de s.s.*** est optionnelle.

ALN121459

ClearCorrect Exhibit 1002, Page 2523 of 3373

Gérer les données patient Supprimer

La gestion des données patient permet en outre d'effacer un patient. Si des images CEREC ou des images vidéo sont encore affectées à un patient, le programme affiche un avertissement permettant d'interrompre le procédé d'effacement.

ATTENTION

Si l'ordre d'effacement est confirmé, ces images sont alors perdues.

Des patients auxquels des images RX sont affectées ne peuvent pas être effacés.

Les patients qui ont été entrés dans la base de données via l'interface SLIDA (Voir „Interface SLIDA" à partir de la page 100.) peuvent être effacés, mais pas modifiés, car la gestion de leurs données s'effectue exclusivement hors de l'application CEREC ; la base de données ne contient que des copies des données patient, pas les données originales.

En cas de sélection d'une nouvelle restauration (via la barre d'outils ou le menu Restauration), l'écran affiche tout d'abord un dialogue très similaire à la gestion des patient (Voir „Créer nouvelle restauration" à partir de la page 82.). Les données patient ne peuvent être ni modifiées, ni effacées.

ALN121460

ClearCorrect Exhibit 1002, Page 2524 of 3373

3.10 Menu Construction

Les étapes de construction pour la restauration d'une dent se déroulant dans un ordre bien défini.

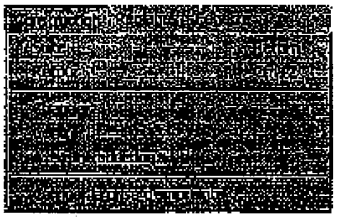


Fig. 3-89 Menu : Construction

Le menu ***Construction*** permet ...



- de passer à l'étape de construction suivante à exécuter
  Construction/Suite ou ***Return***



- retour à la dernière étape de construction
  Construction/Retour ou ***Ctrl+Z***
- modifier le type de restauration, le procédé de construction, et/ou la dent de la restauration ouverte.
  Construction/Changer
- redéfinir le ***centre***
  Construction/Centrer ...
- redéfinir ***l'axe d'introduction ...***
- ***Corriger la prise d'empreinte...***

3.10.1 Construction : Changer

L'option de menu ***Changer*** vous permet de changer le type de restauration, le procédé de construction et/ou la dent de la restauration ouverte.

A l'aide de cette fonction, vous pouvez également utiliser des restaurations de manière virtuelle, p. ex. dans le cadre de l'Assainissement de l'arcade dentaire.

ALN121461

ClearCorrect Exhibit 1002, Page 2525 of 3373

3.10.2 Construction : Centrer...

L'option de menu *Centrer* vous permet d'ouvrir la fenêtre *Centre*. Dans cette fenêtre, vous pouvez définir comme centre la préparation avec laquelle vous voulez continuer à travailler. Cette fonction est particulièrement précieuse dans le cadre de l'Assainissement de l'arcade dentaire.

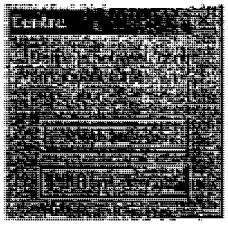


Fig. 3-40 Construction : Centre

Définir le centre

1. Sélectionnez *Construction/Centrer*.
   La fenêtre *Centre* s'ouvre (Fig. 3-40).
2. Cliquez sur la préparation à traiter (Fig. 3-41).
3. Cliquez sur le bouton *Fixer* (Fig. 3-40).

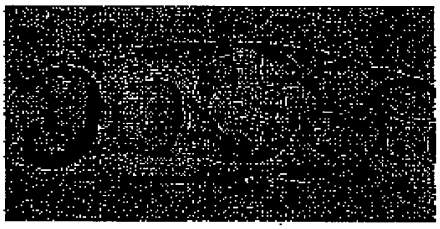


Fig. 3-41 Définir un nouveau centre



Fig. 3-42 Définir un nouveau centre

La préparation est représentée au milieu du Viewer et la fenêtre *Centre* se ferme.

Si vous voulez définir une autre préparation comme centre :

4. Sélectionnez *Construction/Centrer*.
5. Cliquez sur le bouton *Réinitialiser* (Fig. 3-40).
6. Répétez les étapes 2 et 3.

ALN121462

ClearCorrect Exhibit 1002, Page 2526 of 3373

3.10.3 Construction : Axe d'introduction ...

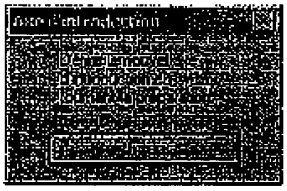


Fig. 3-43 Construction : Axe d'introduction

A l'aide de cette fonction, vous pouvez redéfinir le sens de la vision sur la préparation ainsi que le sens d'usinage (voir„Redéfinition de l'axe d'introduction" page 71).

3.10.4 Construction : Corriger la prise d'empreinte

Cette fonction vous permet d'éliminer des artefacts et de découper des informations de bordure gênantes, p. ex. en cas d'enregistrements provenant des champs d'images des antagonistes ou de l'occlusion (voir „Effacer et corriger des zones d'images de champs d'images" page 72).

ALN121463

ClearCorrect Exhibit 1002, Page 2527 of 3373

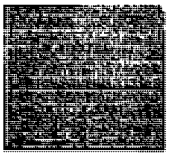


Fig. 3-44 Menu : Réglages

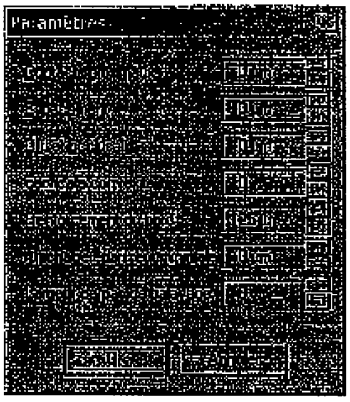


Fig. 3-45 Option de menu : Paramètres

3.11 Menu Réglages

Le menu Réglages permet d'adapter et de modifier les options de menu suivantes :

- Paramètres
- Instruments
- Configuration
- Calibrage

3.11.1 Réglages : Paramètres

Avant l'exécution d'une restauration, certains réglages sont nécessaires pour le processus d'usinage/de construction.

Vous pouvez effectuer ces réglages via l'option de menu ***Réglages/Paramètres....***

REMARQUE
L'appareil a été réglé de manière optimale durant son contrôle final en usine.

Vous pouvez contrôler les paramètres suivants et les modifier en cas de besoin :

- Contacts proximaux
- Espacement
- Offset occlusal
- Convexité cervicale
- Renforcement du bord
- Affichage épaisseur minimale
- Largeur de pas de balayage

ALN121464

ClearCorrect Exhibit 1002, Page 2528 of 3373

Paramètre : Contacts proximaux

Le logiciel CEREC 3D détermine automatiquement les contacts proximaux. Cette étape est exécutée avant que l'équateur ne soit affiché. Vous avez ainsi la possibilité d'évaluer le résultat et de le modifier si nécessaire.

REMARQUE

Si la dent voisine est à plus de 1mm (p. ex. dent voisine préparée), aucun contact ne sera réalisé.

Le réglage du paramètre *Contacts proximaux* agit sur les restaurations Inlay et Onlay. Dans le cas des restaurations de couronnes, les contacts proximaux doivent être systématiquement contrôlés et adaptés manuellement.

Si vous êtes d'avis que les contacts proposés par le logiciel sont régulièrement trop forts ou trop faibles, vous pouvez modifier le réglage à votre convenance via le menu ***Réglages/Paramètres.***

Si vous réglez une valeur plus élevée dans la fenêtre de saisie ***Contacts proximaux***, une quantité supérieure de matériau sera donc déposée au niveau des points de contact. Il est possible de faire varier l'épaisseur des points de contact par incréments de 25µm entre -200µm et 200µm.

REMARQUE

Ce réglage agit uniquement sur des propositions de lignes. Une modification de ce réglage n'est effective qu'après un nouveau calcul de l'équateur.

REMARQUE

Les points de contact proximaux sont déterminés par le logiciel par analyse de vos données de mesure. Une mauvaise qualité des données de mesure peut provoquer des propositions insuffisantes en terme de points de contact.

Le réglage du paramètre *Contacts proximaux* n'a aucune influence sur la construction de structures de couronnes ou de bridge.

ALN121465

ClearCorrect Exhibit 1002, Page 2529 of 3373

Paramètre : Espacement



Fig. 3-46 Espacement (représentation exagérée)

L'application vous permet de ménager, à dessein, dans la fenêtre de saisie Espacement, la place nécessaire pour la fixation adhésive de la couronne ou du inlay.

Plus vous augmentez ce paramètre, plus l'espace est important. Le réglage peut être modifié par incréments de 10µm entre - 100µm et 100µm.

REMARQUE

Le réglage influe sur le calcul de la restauration.

Paramètre : Décalage occlusal

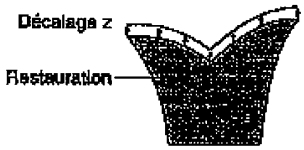


Fig. 3-47 Augmenter le décalage occlusal (représentation exagérée)

Si vous constatez que toutes vos restaurations présentent une quantité trop faible ou trop élevée de matériau dans le sens occlusal, ce paramètre vous permet de compenser cette différence.

Le décalage occlusal peut être modifié par incréments de 25µm entre -500µm et 500µm.

REMARQUE

Le réglage n'influe que lors de l'usinage de la restauration. Son effet n'est pas visible sur la prévisualisation d'usinage.

Le réglage du paramètre ***Décalage occlusal*** n'a aucune influence sur la construction de structures de couronnes ou de bridge.

Paramètre : Convexité cervicale

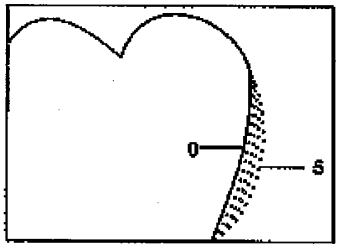


Fig. 3-48 Convexité (représentation exagérée)

Ce paramètre permet de modifier la courbure en-dessous de l'équateur.

ATTENTION

Si vous réglez une valeur trop importante pour ce paramètre, la surface peut dépasser latéralement au-dessus de l'équateur.

La ***convexité*** peut se régler par incréments de 1 entre 0 et 5.

ALN121466

ClearCorrect Exhibit 1002, Page 2530 of 3373

Paramètre : Renforcement du bord



Fig. 3-49 Renforcement du bord (représentation exagérée)

Avant l'usinage, le bord de la restauration est augmenté de la valeur de l'épaisseur réglée.

Le *renforcement du bord* peut être modifié par incréments de 25µm entre 0µm et 200µm.

Paramètre : Affichage épaisseur minimale

Ce paramètre sert au réglage des repères rouges dans la prévisualisation d'usinage. Si l'épaisseur de matière est inférieure à la valeur réglée, la surface est repérée en rouge.

Le paramètre *affichage épaisseur minimale* peut être modifié par incréments de 25µm entre 0µm et 1000µm.

Paramètre : Largeur de pas de balayage (uniquement CEREC *Scan*)

Si vous utilisez le scanner laser (option) pour réaliser l'empreinte optique, vous pouvez régler la résolution via le paramètre *Largeur de pas de balayage*.

La résolution peut se régler par incréments de 1 entre 3 et 15. Plus la valeur réglée pour le pas de balayage est faible, plus le balayage dure longtemps, mais plus le jeu de données de l'empreinte optique est précis.

ALN121467

ClearCorrect Exhibit 1002, Page 2531 of 3373

3.11.2 Réglages : Instruments

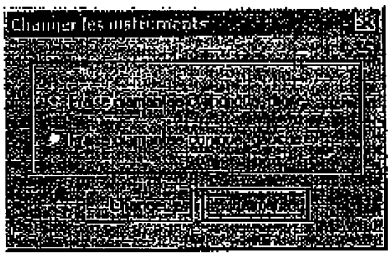


Fig. 3-50 Option de menu : Instruments

L'option de menu ***Instruments*** permet de changer les instruments (fraises diamantées) (voir chapitre "Changer les instruments" dans la notice d'utilisation de l'unité d'usinage).

3.11.3 Réglages : Configuration

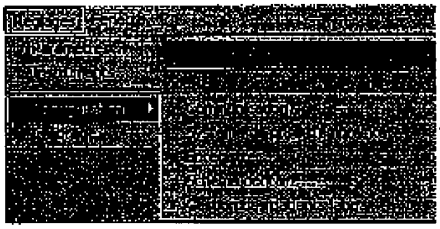


Fig. 3-51 Option de menu : Configuration

Cette option de menu permet de contrôler et de modifier les configurations réglées en usine.

- Communication
- Système de prise d'empreinte
- Enregistrer
- Schéma dentaire
- Gestion des patients labo

Configuration : Communication

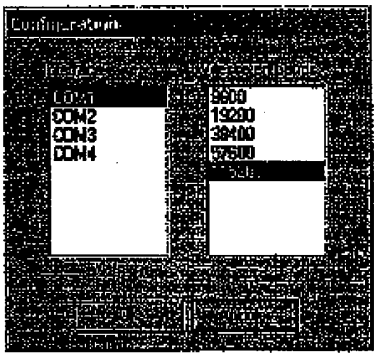


Fig. 3-52 Configuration : Communication

L'option de menu ***Réglages / Configuration / Communication ...*** vous permet de définir l'interface avec l'unité d'usinage (COM1 ..., vitesse de transmission 115200, ...).

ALN121468

ClearCorrect Exhibit 1002, Page 2532 of 3373

Configuration : Système de prise d'empreinte

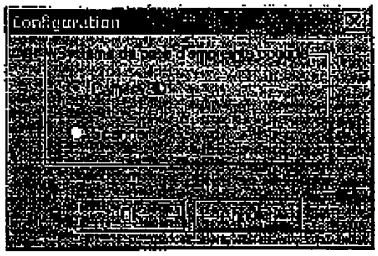


Fig. 3-53 Configuration : Système de prise d'empreinte

L'option de menu ***Réglages / Configuration / Système de prise d'empreinte ...*** vous permet de sélectionner la *caméra 3D* (si elle est installée) ou le *scanner*.

Configuration : Enregistrer

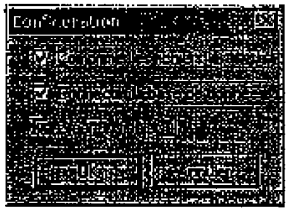


Fig. 3-54 Configuration : Enregistrer

L'option de menu ***Réglages / Configuration / Enregistrer ...*** vous permet de sélectionner les options suivantes :

- ***Comprimer les fichiers***
  Les données sont enregistrées sous forme comprimée.
- ***Connecter la base de données***
  Une base de données SIRONA existante sera utilisée pour les données patient et les images.

REMARQUE
Lorsqu'une base de données est connectée, les images seront toujours créées au format TIF.
Le réglage "Créer un fichier TIF ne peut être désélectionné.

- ***Créer un fichier TIF***
  Le programme génère des images TIF.

Configuration : Schéma dentaire

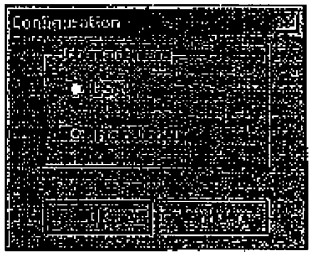


Fig. 3-55 Configuration : Schéma dentaire

L'option de menu ***Réglages / Configuration / Schéma dentaire ...*** vous permet de sélectionner le schéma dentaire US ou international.

ALN121469

ClearCorrect Exhibit 1002, Page 2533 of 3373

Configuration : Gestion des patients Labo

Lorsque la case se trouvant devant *Gestion des patients labo* est cochée, les dialogues d'entrée ci-après sont alors activés pour le technicien dentaire.

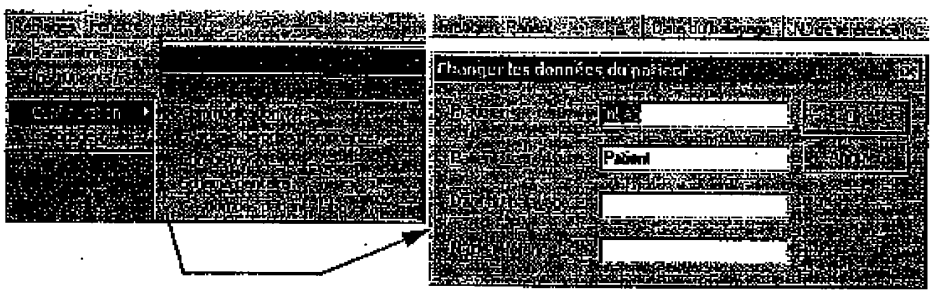


Fig. 3-66 Case cochée

Les données suivantes peuvent être de nouveau modifiées ou saisies :

- *Praticien,*
- *Patient,*
- *Date du balayage,*
- *N° de référence.*

Lorsque la case se trouvant devant *Gestion des patients labo* n'est PAS cochée, les dialogues d'entrée ci-après sont alors activés pour le technicien dentaire.

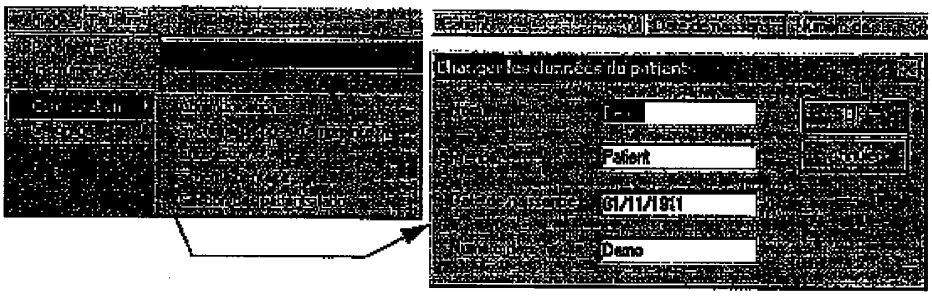


Fig. 3-67 Case NON cochée

Les données suivantes peuvent être modifiées ou saisies :

- *Nom,*
- *Prénom,*
- *Date de naissance,*
- *Numéro de s.s.*

ALN121470

ClearCorrect Exhibit 1002, Page 2534 of 3373

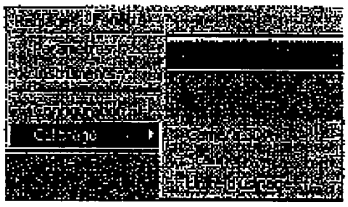


Fig. 3-58 Réglages : Calibrage

3.11.4 Réglages : Calibrage

L'option de menu ***Calibrage*** vous permet ...

- de calibrer la ***caméra 3D***;
  la caméra 3D doit être sélectionnée comme système de prise d'empreinte (voir chapitre "Calibrage de la caméra 3D" dans la notice d'utilisation pour l'unité de prise d'empreinte).

ATTENTION
Pour le calibrage de la caméra 3D, le set de calibrage 3D est nécessaire.
Le set de calibrage 3D ne doit pas être poudré.

- calibrer le ***scanner*** (voir chapitre "Calibrer le scanner" dans la notice d'utilisation de l'unité d'usinage).
- calibrer ***l'unité d'usinage*** (voir chapitre "Calibrer l'unité d'usinage" dans la notice d'utilisation de l'unité d'usinage).

ALN121471

ClearCorrect Exhibit 1002, Page 2535 of 3373

3.12 Menu Fenêtre

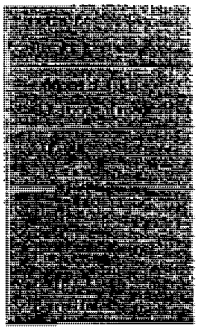


Fig. 3-59 Menu : Fenêtre

Le menu ***Fenêtre*** vous permet de régler l'agencement des différentes fenêtres de visualisation sur l'écran ainsi que d'actualiser le contenu de l'écran.

Pour la représentation des fenêtres à l'écran, vous pouvez appeler le réglage de base
Fenêtre/Réinitialiser

Pour l'évaluation et le traitement, vous disposer des vues ou des fenêtres suivantes :

- Options d'affichage
- Catalogue d'images
- Curseur
- Distance
- Fenêtre View
- Fenêtre Design
- Fenêtre Cut
- Barre d'icônes
- Barre d'état

REMARQUE
Les fenêtres/barres affichées sont cochées au niveau de l'option de menu.

Fenêtre : Options d'affichage

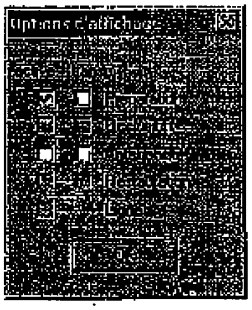


Fig. 3-60 Fenêtre : Options d'affichage

La fenêtre ***Options d'affichage*** présente l'état actuel de l'affichage en 3D, cet état pouvant être modifié de manière individuelle.

- Case cochée sous ***active*** – l'objet est visible
- Case NON cochée sous ***active*** – l'objet n'est pas visible
- Case cochée sous ***transp.*** – l'objet est représenté en transparence

ALN121472

ClearCorrect Exhibit 1002, Page 2536 of 3373